CRC REVIVALS

Intermediate-Energy Nuclear Physics

A. S. Iljinov, M. V. Kazarnovsky,
E. Ya. Paryev

CRC Press
Taylor & Francis Group

Intermediate-Energy Nuclear Physics

A. S. Iljinov
M. V. Kazarnovsky
E. Ya. Paryev

Institute for Nuclear Research of the
Academy of Sciences of Russia
Moscow, Russia

CRC Press
Taylor & Francis Group
Boca Raton London New York

CRC Press is an imprint of the
Taylor & Francis Group, an **informa** business

First published 1994 by CRC Press
Taylor & Francis Group
6000 Broken Sound Parkway NW, Suite 300
Boca Raton, FL 33487-2742

Reissued 2018 by CRC Press

© 1994 by CRC Press, Inc.
CRC Press is an imprint of Taylor & Francis Group, an Informa business

No claim to original U.S. Government works

This book contains information obtained from authentic and highly regarded sources. Reasonable efforts have been made to publish reliable data and information, but the author and publisher cannot assume responsibility for the validity of all materials or the consequences of their use. The authors and publishers have attempted to trace the copyright holders of all material reproduced in this publication and apologize to copyright holders if permission to publish in this form has not been obtained. If any copyright material has not been acknowledged please write and let us know so we may rectify in any future reprint.

Except as permitted under U.S. Copyright Law, no part of this book may be reprinted, reproduced, transmitted, or utilized in any form by any electronic, mechanical, or other means, now known or hereafter invented, including photocopying, microfilming, and recording, or in any information storage or retrieval system, without written permission from the publishers.

For permission to photocopy or use material electronically from this work, please access www.copyright.com (http://www.copyright.com/) or contact the Copyright Clearance Center, Inc. (CCC), 222 Rosewood Drive, Danvers, MA 01923, 978-750-8400. CCC is a not-for-profit organization that provides licenses and registration for a variety of users. For organizations that have been granted a photocopy license by the CCC, a separate system of payment has been arranged.

Trademark Notice: Product or corporate names may be trademarks or registered trademarks, and are used only for identification and explanation without intent to infringe.

Library of Congress Cataloging-in-Publication Data

Il'inov, A. S., 1944-
Intermediate-energy nuclear physics/A.S. Iljinov, M.V. Kazarnovsky, E. Ya. Paryev.
p. cm.
Includes bibliographical references and index.
ISBN 0-8493-4827-7
1. Nuclear reactions. 2. Hardron Interactions. I. Kazarnovskii,
M. V. II. Par'ev, E. IA. III. Title.
Qc794.144 1993
539.7'5--dc20 93-9456

A Library of Congress record exists under LC control number: 93009456

Publisher's Note
The publisher has gone to great lengths to ensure the quality of this reprint but points out that some imperfections in the original copies may be apparent.

Disclaimer
The publisher has made every effort to trace copyright holders and welcomes correspondence from those they have been unable to contact.

ISBN 13: 978-1-315-89470-6 (hbk)
ISBN 13: 978-1-351-07380-6 (ebk)

Visit the Taylor & Francis Web site at http://www.taylorandfrancis.com and the
CRC Press Web site at http://www.crcpress.com

PREFACE

During the last two decades, qualitatively new high-intensity proton accelerators up to 1 GeV with mean current of about 1 mA have been created. These are the so-called "meson facilities". The "kaon facilities", i.e., high-intensity proton accelerators which produce particles with energies of several tens GeV, are currently being constructed. As a result of the interaction of such protons with various targets, intensive secondary beams of neutrons, pions, kaons, antinucleons and other particles, as well as radionuclides, are generated. All such particles are usually called intermediate-energy particles and their interaction with nuclei is referred to as intermediate-energy nuclear reactions.

The high intensity of beams of intermediate-energy particles makes it possible to carry out experimental investigations of their interaction with nuclei with a high degree of statistical reliability. Owing to the considerable advances made in instrument design and the methods used for registering the products of nuclear reactions and computerization of the experimental procedure, the possibilities to obtain, process, and analyze a large body of experimental data have grown considerably. All this ensures a rapid influx of data (and a significantly higher order of accuracy) on nuclear reactions in the intermediate-energy range. A large body of such information has been accumulated so far.

In turn, these developments have given impetus to intensive theoretical studies in this field, especially to the study of deep inelastic processes, such as branched nucleonic-mesonic cascade and break-up of highly-excited nuclei, which are characteristic of the energy range under consideration. On the other hand, the entire body of this information has not been systematized. **Our monograph aims at filling this gap.**

In this connection, it should be emphasized that intermediate-energy nuclear physics has two peculiar features which make it a separate line of scientific investigation.

Indeed, nuclear reactions in the domain of low energies have, as a rule, a relatively small number of open channels (with the only exception being that of fission of heavy nuclei). Therefore, the exclusive experimental and corresponding theoretical investigation of a reaction is quite possible and often realized in practice. As the energy increases, new channels readily open and, in particular, channels involving the emission of an every-increasing number of particles. In this case, complete, exclusive experimental investigation of a reaction involves considerable difficulties and, finally, becomes practically impossible in spite of the previously mentioned achievements of the experimental technique. This is just the case in the domain of intermediate energies. This is the **first peculiarity** that distinguishes this energy range.

The **second peculiarity** is associated with specific features of the theoretical description of nuclear reactions in this energy range. In this instance a statistical approach must be used to describe such a complicated and branched nuclear process involving a large number of different states of the system at the same energy. Moreover, in this energy range the wavelength of an incident hadron is small as

compared to the separation between nucleons in a nucleus; its energy is large as compared to the mutual interaction energy and the kinetic energy of intranuclear nucleons. Therefore, to describe the behavior of intermediate-energy particles in a nucleus we can use simplified approaches (such as semiclassical, eikonal, and other approximations) which are characteristic of this energy range.

The monograph is devoted mainly to the interaction of hadrons with nuclei which leads to the excitation of a large number of degrees of freedom in a nucleus and, as a result, to the emission of several particles during an intranuclear cascade and subsequent decay of a highly-excited residual nucleus. These processes are described on the basis of a unified approach which reflects the peculiar features of intermediate-energy nuclear physics as outlined. Namely, the stage of an intranuclear cascade and the characteristics (distributions over the number of protons and neutrons, over the excitation energy, etc.) of a residual nucleus are treated by the method of classical (more precisely, semiclassical) kinetic equations, whereas the decay of a residual nucleus is described within the framework of a statistical model. The methods and results of the calculation of probabilities of various processes initiated by intermediate-energy hadrons in nuclei and experimental data are set forth and discussed. The possibility of obtaining information on the structure and properties of nuclei, in particular on the properties of highly-excited nuclear matter, by comparing the experimental data with the theoretical results is analyzed. Special attention is paid to new issues, like analytic methods for solution of kinetic equations describing the cascade. In particular, the exclusive description of an intranuclear cascade on the basis of the Liouville equation is given for the first time, to our knowledge, in Chapter 1. Other new areas of attention are nuclear absorption of hadrons from bound states of hadronic atoms, interaction of antinucleons with nuclei, multifragmentation of highly-excited residual nuclei, and polarization phenomena. These also have not been previously discussed in detail in the current literature.

The study of the interaction between nuclei, which is closely related to the previously mentioned issues, is a separate, large problem which is extensively studied in the literature. Therefore, we shall not dwell on this problem here. However, a peculiar nature of physics of hadron-nucleus interactions which bridges the gap between low-energy nuclear and heavy-ions physics will be demonstrated.

This range of issues can be useful in the analysis of problems associated with the evolution of the early (hot) universe, neutron stars and supernovas, and in solving a number of applied problems (e.g., the problems associated with the afterburning of radioactive waste in nuclear energy installations and with electronuclear breeding of energy).

In conclusion, the authors would like to express their thanks to Andrei R. Isaakian who worked laboriously and skillfully to present this book in English. Additionally, A. S. Iljinov is grateful to his co-authors, V. S. Barashenkov, A. S. Botvina, E. A. Cherepanov, S. E. Chigrinov, F. G. Gereghi, Ye. S. Golubeva, K. K. Gudima, S. G. Mashnik, M. V. Mebel, I. N. Mishustin, V. I. Nazaruk, I. A. Pshenichnov, N. M. Sobolevsky, and V. D. Toneev, with whom he developed models of nuclear reactions, for helpful discussions and fruitful collaboration.

THE AUTHORS

A. S. Iljinov, Ph.D., is a head of the radioisotope laboratory at the Institute for Nuclear Research of the Academy of Sciences of Russia. He has been associated with the institute since 1974. This site is the Moscow meson facility. Prior to 1970 he was associated with the Joint Institute for Nuclear Research, Dubna. He received his first doctoral degree in physics in 1971 while working at the Laboratory of Theoretical Physics of the Joint Institute for Nuclear Research, Dubna. He received his second doctoral degree in 1985 while at the Institute for Nuclear Research.

His current interests focus on the theory of nuclear reaction. Together with his colleagues he has formulated the optical-cascade model of nuclear absorption of stopped pions and antiprotons and has also developed the statistical model of multi-fragmentation of nuclei by intermediate energy particles. He has also participated in the discovery and study of the cold fusion of two nuclei which has been used in the synthesis of chemical elements 106 through 109. In 1984 he proposed the use of the Moscow meson facilty for production of high intensity radioactive nuclear beams.

Dr. Iljinov is the author or co-author of 140 scientific articles. He is co-author, along with Professor G. N. Flerov, of *On the Way to Super-Elements* (Pedagogics Publishers, Moscow, 1982) which has been translated into several languages, and of the handbook of *Production of Radionuclides of Intermediate Energies* (Landolt-Bornstein, Vol. 13, Springer-Verlag, Berlin, 1991).

M. V. Kazarnovsky, Ph.D., is the head of one of the theoretical laboratories of the Institute for Nuclear Research of the Russian Academy of Sciences and has been associated with the institute since 1970. He is also a Professor at the Moscow Physical-Technical Institute, where he is a lecturer in nuclear physics. Prior to 1970 he was associated with the Lebedev Physical Institute of the Academy of Sciences of the U.S.S.R. He received his first doctoral degree in 1955, a second doctoral degree in 1971, and the title of professor in 1987.

Dr. Kazarnovsky is the author or co-author of more than 120 scientific works and two monographs, primarily on the following topics: the theory of non-stationary neutron transport, the theory of nuclear reactions at intermediate energies, and the physics of ultracold nuetrons.

E. Ya. Paryev, Ph.D., is a senior scientist at the Institute for Nuclear Research of the Academy of Sciences of Russia and has been associated with the institute since 1974. He received his doctoral degree in 1985; the subject of his thesis was the application of the kinetic equations method in theory of nucleon-nucleus reactions at intermediate energies.

Together with Professor M. V. Kazarnovsky, he has developed, on the basis of these equations, the new analytic approach for the description of inclusive intermediate-energy nucleon-nucleus reactions, which take into account the spin dependence of the NN-interaction and quantum-mechanical effects at the initial state of this reaction as well.

He has also worked out various problems in the field of applied nuclear physics: transport of neutrons, charged particles in solids, and radiation protection of high-current accelerators. His current focus of interest is on the theory of production of various mesons ($K^{\pm}$, η, ω) in the nucleon-nucleon and nucleon-nucleus collisions at different energies.

Dr. Paryev has published 40 scientific papers and has presented reports at a variety of international conferences.

TABLE OF CONTENTS

INTRODUCTION 1

I. Notation 1

II. Classification of Cross-Sections of NRs 2

III. Quantum Formulation of Collision Problem 5
- A. Reaction Channels 5
- B. Transition Probabilities and S-Matrix 6
- C. S-Matrix and Cross-Sections—Scattering Amplitude 8
- D. Quantum-Mechanical Models of NRs 10

IV. Statistical Description of Dynamical Many-Particle Systems 14
- A. Phase Density and Liouville Equation 14
- B. Density Matrix—Quantum Liouville-von Neumann Equation 16
- C. Wigner Probability Function 18

References 19

Chapter 1
INTRANUCLEAR CASCADE MODEL 21

I. Formulation of the Problem and Basic Assumptions 21
- A. Prolegomena 21
- B. Basic Assumptions of the INC-Model 22

II. Exclusive Description of the INC 23
- A. Phase Density and Hamiltonian of the INC-Model 23
- B. A Streaming and a Collision Term 24
- C. Incorporation of the Pauli Exclusion Principle in the Collision Term 27
- D. Formulation of the Equation, the Initial, and the Boundary Conditions 28
- E. Integral Forms of the Liouville Equation 29
- F. Solution of the Integral Liouville Equation in the Form of the von Neumann Series 32
- G. "Macroapproximation" 33

III. Inclusive Description of the INC 35
- A. Boltzmann-Uehling-Uhlenbeck Equation 35
- B. Linearization of the BUU-Equation 37

IV. Characteristics of NRs 39
A. Preliminary Remarks 39
B. Total Cross-Section of Inelastic Interaction 41
C. Topological and Exclusive Cross-Sections 42
D. Inclusive Cross-Sections 43
E. Distribution of Nuclei Produced in the Cascade Over the Number of Neutrons and Protons, Excitation Energy, Momentum, and Angular Momentum 43

V. Taking Account of Quantum Effects in the INC-Model 44
A. Density Matrix—Quantum Liouville-von Neumann Equation 44
B. Transformation of the Liouville-von Neumann Equation to the Form Close to the Classical One 45
C. Validity Conditions of the INC-Model 48

VI. Conclusions 51

References 53

Chapter 2
METHODS FOR SOLUTION OF THE SYSTEM OF KINETIC EQUATIONS OF THE INTRANUCLEAR CASCADE MODEL 55

I. Analytic Methods of Solution 55
A. Cross-Section of Inelastic Interaction and Quasifree Nucleons 55
B. Quantum-Mechanical Calculation of a Quasifree Component of the Inclusive Cross-Section 60
C. Solution of the System of KEs for Cascade Nucleons in the Small-Angle Approximation—the Domain of Relatively High Energies of Secondary Nucleons 64
D. Solution of the System of KEs for Cascade Nucleons in the P_1-Approximation—the Domain of Low Energies of Secondary Nucleons 70
E. Nucleonic Cascade at Low Energies 75
1. Cross-Section for Production of Quasifree and Cascade Nucleons at Low Energies 75
2. Pre-Equilibrium Models of NRs at Low Energies 80

II. Solution of the System of KEs of the INC-Model by Means of the Monte Carlo Technique 83
A. Standard Monte Carlo INC-Model 84
1. General Scheme of the Monte Carlo Simulation of INCs 84

2. Model of a Target Nucleus 86
3. Characteristics of an Incident Particle Inside a T-Nucleus 87
4. Search of a Partner and an Interaction Point 88
5. Calculation of an Elementary Interaction 88
6. Cut-Off Energy 91
7. Characteristics of an R-Nucleus 92
B. Trawling Effect in the INC 93

III. Conclusions 95

References 96

Chapter 3
DECAY AND PROPERTIES OF HIGHLY EXCITED NUCLEI 99

I. Decay of a C-Nucleus with Zero Angular Momentum 99
A. Basic Tenets of Statistical Model of Decay of a C-Nucleus 99
B. Level Density of Highly Excited Nuclei 101
C. Effect of a High Excitation of a Nucleus on its Structure 106
1. Disappearance of Shell Effects at High Values of the Excitation Energy 106
2. Changes in Macroscopic Properties of a Nucleus Caused by an Increase in its Excitation Energy 111

II. Decay of a C-Nucleus with High Angular Momentum 115
A. Basic Relations of Semiclassical Model 115
B. The Effect of a High Value of the Angular Momentum on the Properties of a Nucleus 117

III. General Pattern of Decay of a Highly Excited Nucleus and Methods Used in Calculation of the Evaporation Cascade 118

IV. Analysis of Data Concerned with the Properties and Decay of Excited C-Nuclei 122
A. Statistical Properties of C-Nuclei Produced in Reactions with Low-Energy Particles 122
B. Decay of C-Nuclei Produced in Heavy-Ion-Induced Reactions 128

V. Explosive Decay of Hot Nuclei 130
A. Fermi Breakup of Light Nuclei 132

B. Multifragment Breakup of Medium-Weight Nuclei 136
1. Statistical Model of Multifragmentation 137
2. Basic Properties of Multifragmentation 139
3. Simulation of Multifragment Disintegration 143
4. Difference in Characteristics of the Evaporation and the Multifragment Decay 146

VI. Conclusions 150

References 152

Chapter 4
ANALYSIS OF THE INTERACTION OF NUCLEONS AND LIGHTEST NUCLEI WITH NUCLEI ON THE BASIS OF THE INC-MODEL 155

I. Inclusive Cross-Sections for Production of Secondary Nucleons 155
A. Energy Spectra and Average Multiplicities of Secondary Nucleons 155
B. Double Differential Cross-Sections for Production of Secondary Protons 158

II. Polarization Effects in Inclusive Nucleon-Nucleus Reactions at Intermediate Energies 163
A. Inclusive Polarization Characteristics of NA-Reactions 164
B. The System of KEs for the Functions Φ_α^ν and its Solution for Quasifree Nucleons 165
C. Solution of the System of Equations for Cascade Nucleons 168
D. Analyzing Power in the Reaction A (**p**,p′)X 171

III. Production of Particles in Proton-Nucleus Collisions 173
A. Production of Pions in Proton-Nucleus Interactions 174
1. System of KEs for Intranuclear Nucleonic-Mesonic Cascade 174
2. General Scheme of Solution of the System of KEs for Intranuclear Nucleonic-Mesonic Cascade 175
3. Inclusive Cross-sections for Pion Production—Comparison with Experimental Data 179
B. Production of K^+-Mesons in Proton-Nucleus Interactions 183
1. Inclusive Cross-Sections for Production of K^+-Mesons in pp-Collisions 185

2. Production of K^+-Mesons in Proton-Nucleus Collisions at Various Energies 187
C. Production of Antiprotons in Proton-Nucleus Interactions 195

IV. Trawling Effect 199
A. Manifestation of the Trawling Effect in pA-Interaction 199
B. Effect of Resonance Production 204
C. Manifestation of the Trawling Effect in Reactions Initiated by Lightest Nuclei (d, t, and α) 206

V. Conclusions 207

References 210

Chapter 5
INELASTIC PION-NUCLEUS INTERACTION 215

I. Absorption of Stopped π^- - Mesons by Nuclei 215
A. Optical + Cascade Model of Pion Absorption from Mesoatomic States by Nuclei 215
1. General Pattern of the Process 215
2. Radial Dependence of the Probability of Absorption of a Pion by a Nucleus 216
3. Mechanism for Absorption of a Pion by a Nucleus 220
4. Method of Calculation 221
B. Analysis of Experimental Data 222
1. Energy Spectra of Particles 222
2. Correlations Between Emitted Particles 227
3. Excitation Energy of R-Nuclei and Isotope Yield 230
4. Angular Momentum of R-Nuclei and Excitation of High-Spin Isomeric States 232
5. Momentum of an R-nucleus 237

II. Inelastic Pion-Nucleus Interactions at the Energies Lower than 300 MeV 239
A. Optical + Cascade Model for Inelastic π A-Interaction 240
1. Mean Free Path of a Pion in Nuclear Matter 241
2. Potential Energy of a Pion in a Nucleus 243
3. General Scheme of the Calculation 244
B. Comparison with Experimental Data 245

III. Conclusions 249

References 252

Chapter 6
ANNIHILATION OF ANTINUCLEONS ON NUCLEI 255

I. Models of Antinucleon-Nucleus Annihilation Based on the Mechanism of the Intranuclear Cascade 255
A. Optical + Cascade Model for the Absorption of Antiprotons by Nuclei from a Bound States of a $\bar{p}$-Atom 255
B. Cascade Model of Deep Inelastic Interactions of Intermediate-Energy Antinucleons with Nuclei 259

II. Incoherent Multipion-Nucleus Interaction 263
A. Characteristics of Emitted Particles 263
B. Characteristics of R-Nuclei 271

III. Interaction of Mesonic Resonances with Nuclei 277
A. Production of Mesonic Resonances in $\bar{N}$N-Annihilation 278
B. Interaction of η- and ω-Mesons with Nucleons 279
C. INC-Model with Mesonic Resonances 282
D. Production of η- and ω-Mesons in $\bar{N}$A-Annihilation 283
E. Near Threshold Production of η- and ω-Mesons by Protons and Pions on Nuclei 287

IV. Conclusions 292

References 293

Chapter 7
FISSION AND MULTIFRAGMENTATION OF NUCLEI BY INTERMEDIATE-ENERGY PARTICLES 297

I. Fission of Nuclei 297
A. Probability of Fission of Nuclei by Intermediate-Energy Particles 298
B. Mass-Energy Distribution of Fission Fragments 309
1. Diffusion Model of Formation of Distribution of Fragments Produced as a Result of Fission of Highly Excited C-Nuclei 310
2. Empirical Approximations of Fragment Distributions in the Case of Fission of C-Nuclei with Low Excitation 319

3. Analysis of Experimental Data on the Formation of Fragments of Fission of Nuclei by Intermediate - Energy Particles 324

II. Multifragmentation 333
A. Cascade-Fragmentation-Evaporation Model 334
B. Ensemble of Hot R-Nuclei 335
C. Analysis of Experimental Data on the Production of Nuclear Fragments by Intermediate-Energy Particles 338

III. Conclusions 350

References 351

INDEX 355

Taylor & Francis
Taylor & Francis Group
http://taylorandfrancis.com

INTRODUCTION

We shall first introduce the notations used throughout this book and recall certain concepts and facts from various fields of physics which form the basis of subsequent analysis.

I. NOTATION

The following general notation is used in this book. Three-dimensional vectors are denoted by bold italics, e.g., $\boldsymbol{r}, \boldsymbol{p}$; two-dimensional vectors (in particular, vectors of unit length) are denoted by bold Greek letters, e.g., $\boldsymbol{\Omega}$, $\boldsymbol{\beta}$; six-dimensional vectors in the phase space of coordinates and momenta are denoted by bold small letters, e.g., $\mathbf{x}$; sets of coordinates and/or momenta of arbitrary dimensionality are denoted by bold capitals, e.g., $\mathbf{X}$; relativistic four-dimensional vectors are denoted by light-face small italics with "hats" over them; their time component is denoted by zero in the superscript, e.g., $\hat{p} = (p^0, \boldsymbol{p})$.

Operators are denoted by bold, italic, and capital Latin, Greek, and Gothic letters with "hats" over them, e.g., $\hat{\boldsymbol{H}}$, $\hat{\boldsymbol{P}}$, $\hat{\mathfrak{T}}$.

Integrals over the entire space in which any vectors ($\mathbf{r}$, $\boldsymbol{\omega}$, $\mathbf{x}$, etc.) are defined by the symbol $\int$ and the differentials of these vectors. The multiplicity of an integral is determined by the dimensionality of the corresponding vector space, e.g., $\int d\boldsymbol{r}\, d\boldsymbol{\omega}\ldots$is a five-dimensional integral, and $\int d\mathbf{X}\ldots$the integral is preserved over the entire set of variables $\mathbf{X}$. The standard notation is preserved for integrals in other limits.

The dimensionalities of Dirac delta-functions can be seen from the dimensionalities of their arguments and are not, therefore, indicated, e.g., $\delta(R\text{-}r)$ is a one-dimensional, $\delta(\boldsymbol{\omega}\text{-}\boldsymbol{\omega}_0)$ a two dimensional, $\delta(\boldsymbol{R}\text{-}\boldsymbol{r})$ a three-dimensional, and $\delta(\mathbf{x}\text{-}\mathbf{y})$ a six-dimensional δ-function.

Formulas, figures, and tables are numbered in serial order separately within each chapter.

The following abbreviations are used throughout this work:

CFE-model	cascade-fragmentation-evaporation model
C-nucleus	compound nucleus
INC	intranuclear cascade
INC-model	model of intranuclear cascade
INCT-model	model of intranuclear cascade with trawling
KE	kinetic equation
l.s.	laboratory system of coordinates
NR	nuclear reaction
OC-model	optical + cascade model
R-nucleus	residual nucleus
c.m.s.	center-of-mass system of coordinates
T-nucleus	target nucleus

We do not give abbreviations here if they are not used in more than two chapters. In this case, they are explained in the chapters.

II. CLASSIFICATION OF CROSS-SECTIONS OF NRS

Let us consider an experimental situation typical for the study of interaction of particles with nuclei, especially at intermediate energies. A beam of particles, for example, from an accelerator, with a fluence n particles/cm^2 impinges on a stationary (in l.s.) target, for instance, a sample containing N nuclei under investigation. As a result of this interaction, Δn particles leave the beam, while the products of the corresponding processes caused by the interaction fly out in various directions. Let us denote an incident particle and a nucleus under investigation by the symbols a and A, respectively. Then the following processes are possible:

a + A	a + A	elastic scattering
	a* + A	scattering with an excitation of the a particle
	a + A*	scattering with an excitation of the nucleus
	a* + A*	scattering in which both the particle and the nucleus are excited
	a′ + A′	reaction involving the production of a new particle and a new nucleus
	a′ + a″ + A′	reaction involving the production of two new particles and a new nucleus

(1)

and so on. Each of these processes will be called an NR.

As a rule, NRs proceeding in the form of a direct process do not last longer than 10^{-21} - 10^{-22}s. Therefore, their evolution in time has eluded experimental observations so far. Only the final result of such reactions can be registered. Essentially all observable quantities characterizing NRs can be expressed in terms of corresponding cross-sections (in the general case of the interaction of particles and nuclei with non-zero spins, in terms of polarization characteristics as well). The same holds true for the formation of a C-nucleus in the case of NRs proceeding through such states. Thus, the information on NRs can be essentially always represented in the form of cross-sections.

Let us recall the definitions of certain cross-sections which are of particular interest for the subsequent analysis. Let incident particles be monoenergetic and monodirectional, their momentum being $\boldsymbol{p}_0$ and kinetic energy ϵ_0 in the l.s. The momenta and energies of outgoing particles in the l.s. are $\boldsymbol{p}$ and ϵ, respectively. The same quantities in the c.m.s. will be labeled by asterisks over them, e.g., $\overset{*}{\epsilon}_0$, $\overset{*}{\boldsymbol{p}}$, etc.

The total cross-section is defined as

$$\sigma^{tot}_{a+A} = \lim_{n,N\to\infty} \Delta n/Nn. \tag{2}$$

(The target is assumed to be thin enough so that we can disregard the effect of perturbation of a beam passing through it upon the result of the interaction of incident particles with T-nuclei.)

The differential elastic scattering cross-section is defined as

$$\frac{d\sigma^{el}_{a+A}}{d\Omega} = \lim_{n,N\to\infty} \frac{1}{nN} \frac{\delta n_a}{\delta\Omega} \tag{3}$$

where δn_a is the number of particles of the type a diverging in a small element $\delta\Omega$ of a solid angle under the condition that the internal quantum state of an incident particle and that of a scattering nucleus remain unchanged.

The total elastic scattering cross-section is defined as

$$\sigma^{el}_{a+A} = \int d\,\Omega\, \frac{d\sigma^{el}_{a+A}}{d\Omega} = \int d\,\overset{*}{\Omega}\, \frac{d\sigma^{el}_{a+A}}{d\overset{*}{\Omega}} \tag{4}$$

where $d\sigma^{el}_{a+A}/d\overset{*}{\Omega}$ is the differential elastic scattering cross-section in the c.m.s., and $d\overset{*}{\Omega}$ the element of a solid angle in the c.m.s.

The cross-section of inelastic interaction (the reaction cross-section) is defined as

$$\sigma^{in}_{a+A} = \sigma^{tot}_{a+A} - \sigma^{el}_{a+A} \tag{5}$$

The exclusive cross-section of the reaction $a + A \to \sum_{1\le j\le k} \sum_{1\le i\le m_k} b_j(\boldsymbol{p}_{ji}) + B$, i.e., of an NR in which m_1 particles of the type b_1, with the momenta $\boldsymbol{p}_{11},\ldots,\boldsymbol{p}_{1m_1},\ldots$, m_k particles of the type b_k with the momenta $\boldsymbol{p}_{k1},\ldots,\boldsymbol{p}_{km_k}$, and an R-nucleus B (whose composition is determined by a given set m_j, b_j) are produced, is defined as

$$\begin{aligned}&\frac{d^{3M}\sigma^{excl}(a + A \to m_1,b_1;\, m_2,b_2;\, \ldots;\, m_k,b_k)}{d\boldsymbol{p}_{11}\ldots d\boldsymbol{p}_{1m_1}\ldots d\boldsymbol{p}_{k1}\ldots d\boldsymbol{p}_{km_k}} = \\ &\frac{1}{m_1!\ldots m_k!} \lim_{n,N\to\infty} \frac{1}{nN} \frac{\delta n_1(b_1)}{\delta\boldsymbol{p}_{11}} \ldots \frac{\delta n_{m_1}(b_1)}{\delta\boldsymbol{p}_{1m_1}} \ldots \frac{\delta n_1(b_k)}{\delta\boldsymbol{p}_{k_1}} \ldots \frac{\delta n_{m_k}(b_k)}{\delta\boldsymbol{p}_{km_k}}\end{aligned} \tag{6}$$

Here $\delta n_i(b_j)$ is the number of particles of the type b_j emitted (in coincidence) from a target in a small interval $\delta\boldsymbol{p}_{ji}(1 \le i \le m_j)$ of momenta, and $M = m_i + m_2 + \ldots + m_k$. Such NRs include the reactions of the type (p,2p) and (p,pn), which are widely used for the investigation of the shell structure of a nucleus.

Rigorously speaking, the exclusive description of an NR implies the fixation of kinematic characteristics and internal states of all reaction products, including γ-quanta from transitions of all products of an NR to the ground state. It is obviously

impossible to experimentally investigate deep-inelastic hadron-nucleus interaction at intermediate energies with such completeness. By a theoretical exclusive description of an NR, we mean the fixation of characteristics of all particles incorporated in a given model and of an given model of an R-nucleus*.

The topological cross-section of the reaction $a + A \rightarrow m_1 b_1 + \ldots + m_k b_k + B$ is defined as

$$\sigma(a + A \rightarrow m_1 b_1 + \ldots + m_k b_k) = \int d\boldsymbol{p}_{11} \ldots d\boldsymbol{p}_{ji} \ldots d\boldsymbol{p}_{km_k} \frac{d^{3M}\sigma^{excl}(a + A \rightarrow m_1, b_1; \ldots)}{d\boldsymbol{p}_{11} \ldots d\boldsymbol{p}_{ji} \ldots d\boldsymbol{p}_{km_k}} . \tag{7}$$

The quantity σ^{in}_{a+A} is obviously the sum of topological cross-sections of all possible reactions involving the particle a and the nucleus A.

The inclusive differential cross-section of the reaction $a + A \rightarrow b + X$ is defined as

$$\frac{d\sigma(a + A \rightarrow b + X)}{d\boldsymbol{p}_b} = \lim_{n,N\rightarrow\infty} \frac{1}{nN} \frac{\delta n_b}{\delta \boldsymbol{p}_b} \tag{8}$$

where δn_b is the total number of particles of the type b emitted from a target in a small interval $\delta \boldsymbol{p}_b$ of momenta, irrespective of the formation of any other products of the reaction $a + A$ (denoted by the symbol X). The following obvious relation is valid

$$\frac{d\sigma(a + A \rightarrow b + X)}{d\boldsymbol{p}_b} = \sum_{[m_1,b_1;\ldots;m_k,b_k]} \sum_{1\le j\le k} \delta_{b_j b} \times \sum_{1\le i\le m_j} \int [1 \le j' \le k \; 1 \le i' \le m_k \; d\boldsymbol{p}_{j'i'}] \; \delta(\boldsymbol{p}_b - \boldsymbol{p}_{ji}) \times \frac{d^{3M}\sigma(a + A \rightarrow m_1, b_1; \ldots)}{d\boldsymbol{p}_{11} \ldots d\boldsymbol{p}_{ji} \ldots d\boldsymbol{p}_{km_k}} . \tag{9}$$

Here the symbol $\sum_{[m_1,b_1;\ldots;m_k,b_k]}$ implies summation over all possible combinations $m_1 b_1;\ldots;m_k,b_k$, for all possible k, and $\delta_{b_j b} = 1$, if the particles b_j and b are identical and $\delta_{b_j b} = 0$ in the opposite case.

The relativistically invariant quantity $E_b \frac{d\sigma(a + A \rightarrow b + X)}{d\boldsymbol{p}_b}$ (E_b is the total energy of the b-particle) is called the inclusive invariant cross-section for production

* For instance, nucleons, pions, and hard γ-quanta, as well as the products of decay of a highly-excited R-nucleus, including nucleons, light nuclei, and fission fragments, are usually incorporated in the INC-model, whereas γ-quanta emitted as a result of transitions between lowest discrete levels of an R-nucleus are not considered.

of particles of the type b. It is convenient to describe the production of new particles with the help of this quantity (see Chapter 4).

The total inclusive cross-section of the reaction $a + A \rightarrow b + X$ is defined as

$$\sigma(a + A \rightarrow b + X) = \int dp_b \frac{d\sigma(a + A \rightarrow b + X)}{dp_b} = \sum_{[m_1,b_1;\ \ldots\ ;\ m_k b_k]} \sum_{1 \le j \le k} \delta_{b_j b} m_j\, \sigma(a + A \rightarrow m_1,b_1; \ldots ; m_k,b_k). \tag{10}$$

It is obvious that σ $(a + A \rightarrow b + X)$ can be either smaller or larger than σ^{in}_{a+A}.

The multiplicity of particles of the type b in the reaction $a + A \rightarrow b + X$ is defined as

$$\overline{m}(a + A \rightarrow b + X) = \frac{1}{\sigma^{in}_{a+A}}\, \sigma(a + A \rightarrow b + X). \tag{11}$$

Intermediate forms, which are sometimes called "semi-inclusive" or "semi-exclusive," are also widely used for description of NRs at intermediate energies, since the inclusive description often does not carry sufficient information. In addition to topological cross-sections, such forms include functions of all kinds of correlations of the emission of particles with respect to the composition, energy and angles, e.g., the function of the energy-angle correlation of the emission of two nucleons used to separate the contribution of a quasifree knockout of nucleons.

III. QUANTUM FORMULATION OF COLLISION PROBLEM

A. REACTION CHANNELS

Consider a collision of two complex (in the general case) particles. Let us assume that they were at a large distance from one another at the initial instant $t = t_i < 0$ and did not interact. Later on (at $t \approx 0$), they approach one another and enter into interaction as a result of which one of the processes listed in formula (1) can take place. Then the products diverge and at $t \geqslant t_f > 0$ their interaction becomes negligibly small. Let, further, $\hat{H}$ be the total Hamiltonian of such a system. It can be represented in the form

$$\hat{H} = \hat{H}_0 + \hat{V} = \hat{H}'_0 + \hat{V}' \tag{12}$$

where $\hat{H}_0$ and $\hat{V}$ ($\hat{H}'_0$ and $\hat{V}'$) are the Hamiltonian of free particles and the operator of their interaction in the initial (final) state, respectively. Let us denote the complete

orthonormalized set of eigenfunctions* and eigenvalues of the operator $\hat{H}_0$ ($\hat{H}'_0$) by χ_a and ϵ_a (χ'_b and ϵ'_b), i.e.,

$$\hat{H}_0\,\chi_a = \epsilon_a\chi_a, \qquad \hat{H}'_0\chi'_b = \epsilon'_b\chi'_b. \tag{13}$$

Here a (b) is the set of all quantum numbers of the system in the initial (final) state. It includes discrete values, characterizing internal states of particles, and their momenta. Let the initial (final) state of the system be described by the wave packet, which would assume the form $\phi'_{\bar{a}}$ ($\phi_{\bar{b}}$) at $t=0$, if $\hat{V}$ ($\hat{V}'$) was equal zero identically; $\phi_{\bar{a}}$ ($\phi'_{\bar{b}}$) representing a superposition of the functions χ_a (χ'_b) corresponding to the set of values** of a (b) lying in the narrow interval around $\bar{a}$ ($\bar{b}$). The problem lies in the evaluation of the transition probability $P\,(\bar{a} \rightarrow \bar{b})\,\Delta\bar{b}$ from the initial reaction channel (the initial state vector $\Psi^{(+)}_{\bar{a}}$ at $t \lesssim t_i$) to one of the final reaction channels (the final state vectors $\Psi^{(-)}_{\bar{b}}$ at $t \gtrsim t_f$) defined by the interval $\Delta\bar{b}$ of quantum numbers.

It should be emphasized that separation of $\hat{H}$ into $\hat{H}_0$ and $\hat{V}$, and $\hat{H}'_0$ and $\hat{V}'$ reflects the characteristics of experimental apparatus. The apparatus "prepares" the system in the initial state $\phi_{\bar{a}}$. For instance, in the case of an NR considered in Section II, when a beam of particles a with exactly defined momentum $\boldsymbol{p}_0$ falls upon a target, containing A-nuclei, from an accelerator, the apparatus can, at least in principle, ensure the fixation of all discrete quantum numbers characterizing internal states of particles a and nuclei A. On the other hand, the registering system of the apparatus can allow us (at least in principle) to fix all discrete quantum numbers characterizing internal states of the interaction products (e.g., the products belonging to one of the channels listed on the right-hand side of Formula 1) and to measure their momenta after the divergence ($t \gtrsim t_f$) to a sufficient accuracy, i.e., to isolate the reaction products described by a certain final state vector.

B. TRANSITION PROBABILITIES AND S-MATRIX

In accordance with general principles of quantum theory, the probability $P\,(\bar{a} \rightarrow \bar{b})\,\Delta\bar{b}$ can be represented in the form

$$P\,(\bar{a} \rightarrow \bar{b})\,\Delta\bar{b} = \sum_{\Delta\bar{b}} |\langle\Psi^{(-)}_{\bar{b}}(t)|\Psi^{(+)}_{\bar{a}}(t)\rangle|^2 \tag{14}$$

* In accordance with the terminology accepted in the physical literature, the functions χ (and hence ϕ as well) will be called the state vectors. It is also assumed that they are defined in a certain Hilbert space, even when they are not normalized in the rigorous mathematical sense. The scalar product of two such vectors (e.g., χ_a and $\chi_{a'}$) will be denoted by the symbol $\langle\chi_{a'}|\chi_a\rangle$, i.e., their orthonormalization means that

$$\langle\chi_{a'}|\chi_a\rangle = \delta_{aa'}, \qquad \langle\chi'_b|\chi'_b\rangle = \delta_{bb'}$$

where $\delta_{aa'}$ ($\delta_{bb'}$) is the product of Kronecker δ-symbols, corresponding to all discrete values of the set a (b), and of δ-functions of their values in a continuum.

** To be more precise, the values of their components in a continuum, in particular, of particle momenta.

where the symbol $\Sigma_{\Delta\bar{b}}$ implies summation over all states in the interval $\Delta\bar{b}$ and $\Psi_{\bar{a}}^{(+)}(t)$ and $\Psi_{\bar{b}}^{(-)}(t)$ are the time-dependent wave functions (normalized to unity) of the system under consideration (i.e., the solutions of the time-dependent Schrödinger equation $i\,\frac{\partial\Psi}{\partial t} = \hat{H}\,\Psi$), chosen in a such a way that $\Psi_{\bar{a}}^{(+)}(t_i)$ coincides with the initial and $\Psi_{\bar{b}}^{(-)}(t_f)$ with the final state vector, i.e.,*

$$\Psi_{\bar{a}}^{(+)}(t_i) = e^{-i\hat{H}_0 t_i}\Phi_{\bar{a}}, \qquad \Psi_{\bar{b}}^{(-)}(t_f) = e^{-i\hat{H}_0' t_f}\Phi_{\bar{b}}'. \tag{15}$$

Expression (14) does not depend on t. Indeed, from Equation (15) we have

$$\Psi_{\bar{a}}^{(+)}(t) = e^{-i\hat{H}(t_i - t)}\, e^{-i\hat{H}_0 t_i}\Phi_{\bar{a}}, \qquad \Psi_{\bar{b}}^{(-)}(t) = e^{i\hat{H}(t_f - t)}\, e^{-i\hat{H}_0' t_f}\Phi_{\bar{b}}' \tag{16}$$

and for the scalar product $\langle\Psi_{\bar{b}}^{(-)}(t)|\Psi_{\bar{a}}^{(+)}(t)\rangle$ we obtain

$$\begin{aligned}\langle\Psi_{\bar{b}}^{(-)}(t)|\Psi_{\bar{a}}^{(+)}(t)\rangle &= \langle e^{i\hat{H}(t_f - t)}\, e^{-i\hat{H}_0' t_f}\Phi_{\bar{b}}'|e^{-i\hat{H}(t - t_i)}\, e^{-i\hat{H}_0 t_i}\Phi_{\bar{a}}\rangle = \\ &\langle\Phi_{\bar{b}}'|e^{i\hat{H}_0' t_f}\, e^{-i\hat{H}(t_f - t_i)}\, e^{-i\hat{H}_0 t_i}\Phi_{\bar{a}}\rangle.\end{aligned} \tag{17}$$

Bearing in mind that at $t \lesssim t_i$ the results of the action of the operators $\hat{H}$ and $\hat{H}_0$ on $\phi_{\bar{a}}$ coincide with one another (at $t \gtrsim t_f$, the same holds true for the operators $\hat{H}$ and $\hat{H}_0'$ as applied to the state vector $\phi_{\bar{b}}'$) and introducing the well-known Heisenberg S-matrix

$$\hat{S} = \lim_{\substack{t_i \to -\infty \\ t_f \to +\infty}} e^{i\hat{H}_0' t_f}\, e^{-i\hat{H}(t_f - t_i)}\, e^{-i\hat{H}_0 t_i} \tag{18}$$

(which represents a time-independent unitary operator), we finally get

$$P(\bar{a} \to \bar{b})\Delta\bar{b} = \textstyle\sum_{\Delta\bar{b}}|\langle\Phi_{\bar{b}}'|\hat{S}\Phi_{\bar{a}}\rangle|^2. \tag{19}$$

Thus, if the initial state of a system is prepared at the instant t_i long before the commencement of the particle interaction, and the registration of products of the interaction takes place considerably later than its completion, the quantum-mechanical calculation of probabilities of various transitions as a result of this interaction is reduced to the calculation of time-independent elements $\langle<\phi_{\bar{b}}'|\hat{S}\phi_{\bar{a}}\rangle$

* Here we have taken into account the fact that, given the wave function $\Psi'(t)$ of a system, described by a certain Hamiltonian $\hat{H}'$, at $t = t_o$, we can write it in the form

$$\Psi'(t) = e^{-i\hat{H}'(t - t_o)}\,\Psi'(t_o)$$

at any other instant t. From here on and to the end of Section III, we use, for the sake of brevity, the system of units in which the Plank constant $\hbar = 1$.

of S-matrix. This condition can be almost always satisfied in experimental studies of single collisions. The total energy and momentum are almost always conserved in such collisions as well (the Heisenberg uncertainty principle does not prevent them from being measured to a sufficient accuracy). However, in the microscopic treatment of a chain of consecutive collisions, these conditions may be violated for some time intervals and free paths of particles between collisions (see also Chapter 1).

C. S-MATRIX AND CROSS-SECTIONS—SCATTERING AMPLITUDE

It is obvious that the matrix elements $\langle \phi'_{\bar{b}} | \hat{S} \phi_{\bar{a}} \rangle$ must be practically equal to $\langle \chi'_b | \hat{S} \chi_a \rangle$, because this is the physical requirement imposed upon the wave packet $\phi_{\bar{a}}$ ($\phi'_{\bar{b}}$) as a superposition of χ_a (χ'_b) with a set of quantum numbers $\bar{a}$ ($\bar{b}$) close to a (b). Therefore, the probability $P(\bar{a} \rightarrow \bar{b}) \Delta\bar{b}$ can be calculated directly for transition between χ_a an χ'_b. Thus, the S-matrix formalism allows us to go over from the solution Ψ (t) of the time-dependent Schrödinger equation to the state vectors Ψ (ϵ) with a definite value of the energy ϵ, i.e., to the Fourier transform of Ψ(t) with respect to t which represents the solution of the time-independent Schrödinger equation $\hat{H}\psi = \epsilon\psi$. This turns out to be possible owing to the fact that S-matrix does not depend on t and gives the same result acting on Ψ(t) and on its Fourier transform $\psi(\epsilon)$. With the help of simple formal transformations we can represent the solution (which is reduced to χ_a for $\hat{V}=0$ and to χ'_b for $\hat{V}'=0$) of the time-independent Schrödinger equation in the following symbolic form

$$\psi^{(+)}(\epsilon) = \left\{1 + \frac{1}{\epsilon - \hat{H} + i0}\hat{V}\right\}\chi_a\psi^{(-)}(\epsilon) = \left\{1 + \frac{1}{\epsilon - \hat{H} - i0}\hat{V}'\right\}\chi'_b . \quad (20)$$

Hence, taking into account the energy-momentum conservation law, we readily obtain

$$\langle \chi'_b | \hat{S} \chi_a \rangle = \delta_{ab} - 2\pi i \delta(\epsilon_a - \epsilon'_b) \langle \chi'_b | \hat{\mathcal{T}} \chi_a \rangle = \quad (21a)$$

$$\delta_{ab} - 2\pi i \delta(\epsilon_a - \epsilon'_b)\delta(\boldsymbol{p}_a - \boldsymbol{p}'_b)\, T_{ba}. \quad (21b)$$

Here $\boldsymbol{p}_a$ and $\boldsymbol{p}_b$ are the total momenta of the system before and after the collision respectively,

$$\hat{\mathcal{T}} = \hat{V} + \hat{V}' \frac{1}{\epsilon_a - \hat{H} + i0} \hat{V} \quad (22)$$

is the so-called scattering matrix, and T_{ba} the reduced scattering matrix (it is defined only on the "momentum" shell $\boldsymbol{p}_a = \boldsymbol{p}_b$. It is just the matrix $\hat{\mathcal{T}}$ that describes the variation of the state upon a collision, because $\langle \chi'_b | \hat{S} \chi_a \rangle = \delta_{ab}$, if $\hat{\mathcal{T}} = 0$, and particles do not interact.

Since the cross-sections are time-independent characteristics of collisions (see Section II), they describe the processes in which the energy and momentum are conserved. Hence, the cross-sections can be expressed in terms of the matrix elements T_{ba}. Namely, bearing in mind the definition (Equation 6) and taking into account Equations 19 and 21b, we obtain the following expressions for the exclusive cross-section for the transition from the state χ_a to the states χ_b' whose sets of quantum numbers belong to a narrow interval Δ b:

$$\delta\sigma(a \to b) = \frac{(2\pi)^4}{v_{rel}} \sum_{\Delta b} \delta(\epsilon_a - \epsilon_b') \, \delta(\boldsymbol{p}_a - \boldsymbol{p}_b') |T_{ba}|^2 = \tag{23a}$$

$$\frac{(2\pi)^4}{v_{rel}} \delta(\epsilon_a - \epsilon_b') \delta(\boldsymbol{p}_a - \boldsymbol{p}_b') |T_{ba}|^2 \delta \boldsymbol{p}_{11}^b \ldots \delta \boldsymbol{p}_{km_k}^b \delta \boldsymbol{p}_r^b. \tag{23b}$$

Here $\boldsymbol{p}_r^b$ is the momentum of an R-nucleus, v_{rel} the relative velocity of colliding particles defined as

$$v_{rel} = \{(\boldsymbol{v}_1 - \boldsymbol{v}_2)^2 - [\boldsymbol{v}_1 \times \boldsymbol{v}_2]^2/c^2\}^{1/2} \approx |\boldsymbol{v}_1 - \boldsymbol{v}_2| \tag{24}$$

and $\boldsymbol{v}_i$ the velocity of the i-th particle before the collision (i = 1,2). As we go over from Equation 23a to 23b, we must take into account the fact that discrete quantum numbers characterizing internal states of outgoing particles can be fixed and that Δb is the product $\delta \boldsymbol{p}_{11}^b, \ldots, \delta \boldsymbol{p}_{km_k}^b = \delta \boldsymbol{p}_r^b$ of the intervals of momenta of outgoing particles, including the momentum of an R-nucleus.

Thus, the problem is reduced to the solution of the time-independent Schrödinger equation, because we are to find the function, $\psi^{(\pm)}(\epsilon)$ defined by Equation 20. To this end we must prescribe the boundary condition. In the general form, its formulation is rather cumbersome. In the case of the process involving only two particles in the final state, it has the following form in the c.m.s. for all open channels, i.e., the channels for which the energy-momentum conservation law does not prohibit the divergence of particles:

$$\psi \underset{r\to\infty}{\to} \varphi_\alpha \left\{ e^{i\overset{*}{\boldsymbol{p}}\boldsymbol{r}} + \frac{1}{r} f^{el}(a \to b) e^{i\overset{*}{p}_\alpha r} \right\} + \frac{1}{r} \sum_{\beta \neq \alpha} f^{in}(a \to b) \varphi_\beta' e^{i\overset{*}{p}_\beta r}. \tag{25}$$

Here mutual arrangement of the particles, i.e., the positions of their centers of mass relative to one another, is described by the vector $\boldsymbol{r}$ both before and after the act of their interaction, φ_α (φ_β') is the product of wave functions (characterized by the set of quantum numbers α (β)) of internal motion of particles in the initial (final) state, $\overset{*}{\boldsymbol{p}}_0$ and $\overset{*}{\boldsymbol{p}}$ are the momenta of relative motion of incident and outgoing particles (satisfying the energy-momentum conservation law) in the c.m.s. respectively, $f^{el}(a \to b)$ and $f^{in}(a \to b)$ the amplitudes of elastic and inelastic interaction of particles respectively, and $a \equiv \alpha$, $\overset{*}{\boldsymbol{p}}_0$ ($b \equiv \beta$, $\overset{*}{\boldsymbol{p}}_\beta$) is the complete set of quantum

numbers of a system before (after) the collision (in the case of an elastic collision $\overset{*}{p}_\alpha = \overset{*}{p}_0$ and $b \equiv \alpha$, $\overset{*}{\boldsymbol{p}}_\alpha$). For closed reaction channels (in which the divergence of particles is prohibited by the energy conservation law) the wave function decreases exponentially with increasing distance between the particles. The elements of the matrix $\hat{\mathcal{T}}$ taken between the state vectors of noninteracting particles

$$\chi_a = \varphi_\alpha e^{i\overset{*}{\boldsymbol{p}}_0 r} \quad \text{and} \quad \chi_b' = \varphi_\beta' e^{i\overset{*}{\boldsymbol{p}}_0 r} \tag{26}$$

are expressed in terms of the amplitudes $f^{el(in)}$ in the form

$$\langle \chi_b' | \hat{\mathcal{T}} \chi_a \rangle = -\frac{2\pi}{\mu} f^{el(in)}(a \to b) \tag{27}$$

where μ is the reduced mass of colliding particles. Hence, the cross-section of corresponding processes in the c.m.s. has the form

$$\frac{d\sigma^{el(in)}(a \to b)}{d\overset{*}{\boldsymbol{p}}_\beta} = \frac{1}{\overset{*}{p}_0 \mu} |f^{el(in)}(a \to b)|^2 \delta(\overset{*}{\epsilon}_a - \overset{*}{\epsilon}_b') \tag{28}$$

Obviously, the same result follows from the direct analysis of particle fluxes described by the time-independent Schrödinger equation. General problems of quantum theory of collisions are considered in detail, e.g., in the monographs of Goldberger and Watson[1] and Newton.[2]

D. QUANTUM-MECHANICAL MODELS OF NRS

We do not know forces acting between free nucleons in sufficient detail. It is also unknown to what extent the properties of intranuclear nucleons differ from those of free ones. Moreover, mathematical difficulties encountered in solving the Schrödinger equation for a system of a large number of strongly interacting particles are formidable. These difficulties increase rapidly with increasing excitation energy, especially when the reaction channels with the emission of three or more particles open. Therefore, various models describing a nucleus before, during, and after the collision, and the interaction of an incident particle with a nucleus phenomenologically or within the framework of approximate microscopic schemes, are widely used in the theory of NRs.[3-6] Here we shall succinctly recall basic concepts of only two of them, since they will be used in ensuing chapters.

To describe elastic scattering of particles by nuclei and to calculate the total interaction cross-section, the optical model is widely used. According to this model, the action of a nucleus upon an incident particle is replaced by a phenomenological complex-valued local potential (the optical potential) of the form

$$U(\boldsymbol{r}) = V(\boldsymbol{r}) + iW(\boldsymbol{r}) \tag{29}$$

where V and W are the real-valued functions of coordinates. As a result, the problem is reduced to the solution of the Schrödinger equation for one particle

$$-\frac{1}{2\mu}\Delta\psi + U\psi = \overset{*}{\epsilon}\psi \tag{30}$$

with the boundary condition in which the wave function of a nucleus is omitted for the sake of brevity (see Equation 25)

$$\psi \underset{r\to\infty}{\longrightarrow} e^{i\overset{*}{p}_0 r} + \frac{1}{r} f^{el}(\overset{*}{\vartheta})\, e^{i\overset{*}{p}_0 r} \tag{31}$$

where $\overset{*}{\vartheta}$ is the scattering angle in the c.m.s. In so doing, the scattering amplitude $f^{el}(\overset{*}{\vartheta})$ is determined, and through it the cross-section of elastic scattering (to the element $d\overset{*}{\Omega}$ of a solid angle) in accordance with Equation 28:

$$d\sigma^{el}(\overset{*}{\vartheta}) = |f^{el}(\overset{*}{\vartheta})|^2\, d\overset{*}{\Omega}. \tag{32}$$

The presence of an imaginary part iW (recall that $W \leqslant 0$, since in the opposite case the number of particles in the elastic channel increases with time) in the potential leads to the "absorption" of particles, which has the meaning of the escape of particles from the elastic channel to various inelastic ones. The fact that the potential $U(\boldsymbol{r})$ is a complex-valued function leads to an increase in the imaginary part of the scattering amplitude at $\overset{*}{\vartheta} = 0$. The latter is connected with the total interaction cross-section σ^{tot} through the so-called unitary relation ("the optical theorem")

$$\mathrm{Im} f^{el}(0) = p_0\, \sigma^{tot}/4\pi. \tag{33}$$

In the domain of intermediate-energies under consideration (e.g., at $\epsilon_0 \gtrsim 100$ MeV for an NA-interaction), the de Broglie wavelength $\lambda\!\!\!^{-}$ of an incident particle is small as compared to the radius R of a nucleus, and its kinetic energy is large as compared to the depth of the potential well ($\overset{*}{\epsilon}_0 \gg U$). In this case, the eikonal (diffraction) approximation is valid. It is based upon the assumption that the momentum $\boldsymbol{p}$ of the particle within the nucleus is close to its initial value $\boldsymbol{p}_0$. This allows us to disregard its squared deviation from $\boldsymbol{p}_0$ and to find the solution of Equation 30 in the closed form:

$$\psi = \exp\left\{ i\left[\overset{*}{\boldsymbol{p}}_0 \boldsymbol{r} - \frac{\mu}{\overset{*}{p}_0}\int_{-\infty}^{z} dz' U(\boldsymbol{\beta} + z'\overset{*}{\boldsymbol{p}}_0/\overset{*}{p}_0)\right]\right\}. \tag{34}$$

Here $\boldsymbol{\beta}$ and z are the components of the vector $\boldsymbol{r}$ perpendicular and along the vector $\boldsymbol{p}_0$, respectively. The scattering amplitude is given by the relations

$$f^{el}(\overset{*}{p}_0 \to \overset{*}{p}) = -\frac{\mu}{2\pi}\int d\boldsymbol{r} e^{-i\overset{*}{p}\boldsymbol{r}}\, U(\boldsymbol{r})\psi(\boldsymbol{r}) = \frac{i\overset{*}{p}}{2\pi}\int d\boldsymbol{\beta} e^{i\boldsymbol{\kappa}\boldsymbol{\beta}}\{i - e^{i\chi(\boldsymbol{\beta})}\}, \quad (35)$$

$$\chi(\boldsymbol{\beta}) = -\frac{\mu}{\overset{*}{p}_0}\int dz U(\boldsymbol{\beta} + z\overset{*}{p}_0/\overset{*}{p}_0) \quad (36)$$

where $\boldsymbol{\kappa} = \overset{*}{p}\text{-}\overset{*}{p}_0$ is the two-dimensional, which is perpendicular to $\overset{*}{p}_0$. Substituting Equation 35 in Equation 32, we obtain the differential cross-section of elastic scattering in the eikonal approximation. The function $\chi(\boldsymbol{\beta})$ is called eikonal and represents an increment of the phase acquired by the ψ-function of a particle upon its passage through the nucleus. The function

$$\Gamma(\boldsymbol{\beta}) = 1 - e^{i\chi(\boldsymbol{\beta})} \quad (37)$$

connected with scattering amplitude through the two-dimensional Fourier transformation

$$f^{el}(\boldsymbol{\varkappa}) = \frac{i\overset{*}{p}_0}{2\pi}\int d\boldsymbol{\beta} e^{i\boldsymbol{\varkappa}\boldsymbol{\beta}}\,\Gamma(\boldsymbol{\beta}), \quad (38a)$$

$$\Gamma(\boldsymbol{\beta}) = -\frac{i}{2\pi\overset{*}{p}_0}\int d\boldsymbol{\varkappa} e^{-i\boldsymbol{\varkappa}\boldsymbol{\beta}} f^{el}(\boldsymbol{\varkappa}) \quad (38b)$$

is called the profile function of the interaction. It can be seen, that, in the eikonal approximation, particles undergoing elastic scattering are almost completely concentrated in a narrow interval of angles $\overset{*}{\vartheta} \lesssim \lambda\!\!\!^{-}/R$.

Within the framework of the optical model, it is possible to choose a phenomenological potential which makes it possible to satisfactorily describe elastic scattering of nucleons on nuclei and σ^{tot} for all energies up to several hundred MeV*. As new experimental data become available, the form and parameters of phenomenological potentials of interaction between nuclei and pions, kaons, antinucleons, and other particles are subjected to refinement (see also Chapter 4).

In the domain of intermediate energies, a quasifree knockout of nucleons from a nucleus is one of the principal inelastic processes in NA-interactions. This is a process in which an incident nucleon, upon entering a nucleus, collides with one of intranuclear nucleons, transfers a certain amount of its energy and momentum to it, and then both nucleons move in the nucleus and, if they do not undergo new

* At higher energies, we can go over from the eikonal approximation to the Glauber-Sitenko approximation in a natural way. According to the latter, the eikonal χ represents the result of summation of all phases acquired by the $\bar{\bar{\psi}}$-function as the particle passes by each intranuclear nucleon. This makes it possible to describe elastic scattering and the total cross-section of the interaction between hadrons and nuclei for practically all energies.

collisions, can leave the nucleus. According to Equation 23b, the expression for the exclusive differential cross-section of this process in the l.s. can be written in the form

$$\frac{d^9\sigma(N \to 2N)}{dp_1 dp_2 dp_r} = \frac{(2\pi)^4}{v_{rel}} \delta(\epsilon_0 - \epsilon_1 - \epsilon_2 - \epsilon_r + \Delta\epsilon_b)\delta(p_0 - p_1 - p_2 - p_r)|T_{ba}|^2 \tag{39}$$

where ϵ_i and p_i are the kinetic energy and momentum of the i-th outgoing nucleon respectively, ϵ_r and p_r the same quantities for an R-nucleus, and $\Delta\epsilon_b$ is the difference between the binding energy of a T-nucleus and that of an R-nucleus (the latter can be in excited state). The distorted wave impulse approximation (DWIA) allows one to calculate the matrix elements T_{ba} to a reasonably good accuracy. According to this approximation, the intranuclear motion of the primary nucleon and that of the secondaries is treated within the framework of the optical model, whereas the matrix $\hat{\mathcal{T}}_{NN}$ describing the NN-scattering within a nucleus is taken the same as for collisions of free nucleons. If in this case the energy of the primary nucleon and the energies of both secondaries are large as compared to the depth of the optical potential and their wavelengths are small as compared to the radius of a nucleus, then their motion before and after the collision can be described in the eikonal approximation. Moreover, effects associated with antisymmetrization of the wave function in the initial and the final state turn out to be inessential in this case. The replacement of the matrix $\hat{\mathcal{T}}_{NN}$ by the free matrix makes it possible to express its matrix elements taken between the wave functions of colliding nucleons in terms of their vacuum-scattering amplitude. As a result, after the integration over the momentum of an R-nucleus, we can represent Equation 39 in the form

$$\frac{d^6\sigma(N \to 2N)}{dp_1 dp_2} = \frac{1}{p_1} \delta[\epsilon_0 - \epsilon_1 - \epsilon_2 - p_r^2/2M_{A-1} + \Delta\epsilon_b] \frac{d\sigma_{NN}^{el}}{d\Omega_1}|g_\alpha(p_r)|^2, \tag{40}$$

$$g_\alpha(p_r) = \frac{1}{(2\pi)^{3/2}} \int dr e^{-ip_r r} \varphi_\alpha(r) D_0(r) D_1(r) D_2(r), \tag{41}$$

$$D_0(r) = \exp\left\{ -i \frac{\epsilon_0 + m_N c^2}{p_0 c^2} \int_{-\infty}^{0} V_0(r + z' p_0/p_0) dz' \right\}, \tag{42}$$

$$D_j(r) = \exp\left\{ -i \frac{\epsilon_j + m_N c^2}{p_j c^2} \int_{0}^{\infty} V_j(r + z' p_j/p_j) dz' \right\}, \quad j = 1, 2 \tag{43}$$

where $p_r = p_0 - p_1 - p_2$, $d\sigma_{NN}^{el}/d\Omega_1$ is the differential cross-section of the elastic NN-scattering with the emission of one nucleon along the vector Ω_1, M_{A-1} the mass

of an R-nucleus, $\varphi_\alpha(r)$ the wave function of an intranuclear nucleon before the collision (α is the set of quantum numbers characterizing this wave function), D_0 and D_j are the factors taking into account the deviation of the wave functions of an incident and a scattered nucleon in a nucleus from plane waves, and V_0 and V_j potentials acting on these nucleons.[7]

Integrating Equation 40 over the momenta of one of the nucleons, setting $D_j = 1$ for it and summing over all nucleons of a definite type, we can obtain inclusive differential cross-section for a quasifree knockout of nucleons of a given type from a nucleus as it is, in particular, done in Section IB in Chapter 2.

IV. STATISTICAL DESCRIPTION OF DYNAMICAL MANY-PARTICLE SYSTEMS

A statistical description of classical dynamical many-particle systems can be given in terms of the phase density ρ_c. The density matrix ρ_q and the Wigner probability function $\hat{\rho}_w$ associated with it are its quantum-mechanical analogues. Let us recall basic properties of these quantities.

A. PHASE DENSITY AND LIOUVILLE EQUATION

Consider statistical ensemble of systems containing N particles. Let $\boldsymbol{r}_j$ be the coordinates of the j-th particle, $\boldsymbol{p}_j$ its momentum, $\boldsymbol{x}_j = (\boldsymbol{r}_j, \boldsymbol{p}_j)$ its point in the six-dimensional phase space, and $\mathbf{X} = (\ldots, \mathbf{x}_j, \ldots)$ the set of all points $\mathbf{x}_j$. The point $\mathbf{X}$ in the 6N-dimensional phase space determines completely the state of the system. By definition, the phase density is the probability density to find the system at the point $\mathbf{X}$ at the instant t. In other words, the quantity

$$\begin{aligned}\rho_c(\mathbf{X},t)d\mathbf{X} &\equiv \rho_c(\ldots, \mathbf{x}_j, \ldots;t) \prod_{1\le j\le N} d\mathbf{x}_j \equiv \\ &\rho_c(\ldots;\boldsymbol{r}_j,\boldsymbol{p}_j;\ldots;t) \prod_{1\le j\le N} d\boldsymbol{r}_j d\boldsymbol{p}_j\end{aligned} \tag{44}$$

is the probability that, at the instant t, each j-th particle is situated in the element $d\mathbf{x}_j$ centered near the point $\mathbf{x}_j$ of its six-dimensional phase space, and

$$\int d\mathbf{X}\rho_c(\mathbf{X},t) = 1 \tag{45}$$

where the integral is taken over the entire 6N-dimensional space of the values of the variable $\mathbf{X}$ on which ρ_c is defined. Since in classical mechanics any dynamical quantity F is a function of the state of a system (in general, of time as well), i.e., $F = F(\mathbf{X},t)$, its average (over the ensemble) value at the instant t is expressed in terms of ρ_c:

$$\langle F\rangle_t = \int d\mathbf{X}\rho_c(\mathbf{X},t)F(\mathbf{X},t). \tag{46}$$

Let the classical Hamiltonian of the system have the form

$$H = \sum_{i \le j \le N} p_j^2/2m_j + \frac{1}{2} \sum_{1 \le (j' \ne j) \le N} V_{jj'}(|\boldsymbol{r}_j - \boldsymbol{r}_{j'}|) \tag{47}$$

where m_j is the mass of the j-th particle and $V_{jj'}$ the potential describing the interaction between the j-th and the j′-th particle. Then, the time evolution of the state of the system is determined by the canonical equations of the form

$$\frac{d\boldsymbol{r}_j}{dt} \equiv \boldsymbol{v}_j = \frac{\partial H}{\partial \mathbf{p}_j} = \frac{\boldsymbol{p}_j}{m_j}, \qquad \frac{d\boldsymbol{p}_j}{dt} = -\frac{\partial H}{\partial \boldsymbol{r}_j} = -\sum_{\substack{1 \le j' \le N \\ j' \ne j}} \frac{\partial V_{jj'}(|\boldsymbol{r}_j - \mathbf{r}_{j'}|)}{\partial \boldsymbol{r}_j}. \tag{48}$$

The phase density satisfies the continuity equation

$$\frac{\partial \rho_c}{\partial t} + \sum_{i \le j \le N} \sum_{i \le k \le 3} \left[\frac{\partial}{\partial r_{jk}} \left(\frac{dr_{jk}}{dt} \rho_c \right) + \frac{\partial}{\partial p_{jk}} \left(\frac{dp_{jk}}{dt} \rho_c \right) \right] = 0 \tag{49}$$

(here r_{jk} and p_{jk} are the projections of the vectors $\boldsymbol{r}_j$ and $\boldsymbol{p}_j$ onto the k-th coordinate axis). In view of canonical Equations 48 and 49 can be written in the form

$$\frac{\partial \rho_c}{\partial t} = [H, \rho_c] \tag{50}$$

where

$$[A,B] \equiv \sum_{i \le j \le N} \left(\frac{\partial A}{\partial \boldsymbol{r}_j} \frac{\partial B}{\partial \boldsymbol{p}_j} - \frac{\partial A}{\partial \boldsymbol{p}_j} \frac{\partial B}{\partial \boldsymbol{r}_j} \right) \tag{51}$$

are the Poisson brackets (classical) for arbitrary functions A and B of the points of the phase space. Equation 50 is known as the Liouville equation*. It is first order with respect to t and linear. The first implies that, if ρ_c is known at a certain instant $t = t_o$, then for a given boundary condition (Equation 50) defines uniquely ρ_c at all subsequent instants. It follows here from, in particular, that the normalization

* In accordance with the terminology accepted in the physical literature, the functions χ (and hence ϕ as well) will be called the state vectors. It is also assumed that they are defined in a certain Hilbert space, even when they are not normalized in the rigorous mathematical sense. The scalar product of two such vectors (e.g., χ_a and $\chi_{a'}$) will be denoted by the symbol $\langle \chi_{a'} | \chi_a \rangle$, i.e., their orthonormalization means that

$$\langle \chi_{a'} | \chi_a \rangle = \delta_{aa'}, \qquad \langle \chi_b' | \chi_b' \rangle = \delta_{bb'}$$

where $\delta_{aa'}$ ($\delta_{bb'}$) is the product of Kronecker δ-symbols, corresponding to all discrete values of the set a (b), and of δ-functions of their values in a continuum.

of ρ_c does not depend on t, namely, if Equation 45 is satisfied at a certain $t = t_o$, then it remains valid at all other instants of time. The linearity of Equation 50 implies that the phase density satisfies the principle of superposition.

Canonical Equations 48 form the characteristic system of the Liouville Equation 50. In this sense, Equations 48 and 50 are equivalent to one another. In conclusion, let us reduce Equation 50 to a form which is more convenient for us. In accordance with Equation 48, we get

$$\frac{\partial \rho_c}{\partial t} = \sum_{1 \le (j' \ne j) \le N} \frac{\partial \rho_c}{\partial \boldsymbol{p}_j} \frac{\partial V_{jj'}(|\boldsymbol{r}_j - \boldsymbol{r}_{j'}|)}{\partial \boldsymbol{r}_j} - \sum_{1 \le j \le N} \boldsymbol{v}_j \frac{\partial \rho_c}{\partial \boldsymbol{r}_j}. \tag{52}$$

The problems associated with the Hamiltonian formalism and the Liouville equation are described in detail in many textbooks on classical mechanics. Goldstein[8] is of special note in this connection. In Chapter 1, we shall set forth the INC-model on the basis of the formalism of the phase density and the Liouville equation.

B. DENSITY MATRIX—QUANTUM LIOUVILLE-VON NEUMANN EQUATION

Unlike the case of classical physics, the state of a quantal system is characterized by a wave function which is treated as a vector in a certain Hilbert space, whereas a dynamical quantity is a linear operator acting upon this vector. A wave function depends on the set of independent commuting (i.e., simultaneously measurable) dynamic variables which determine a quantal system. In the case of statistical ensemble of systems containing N particles, it is convenient to choose this set in the form $\mathbf{R} = (\boldsymbol{r}_1, \ldots, \boldsymbol{r}_N)$ (for the sake of simplicity, we consider the particles as spinless objects), i.e., the number of independent variables is equal to 3N. Let us choose a certain "basic" complete orthonormalized set $\Phi_n(\mathbf{R}) \equiv |\Phi_n\rangle$ of state vectors of the system. The domain of the set of quantum numbers n may contain both discrete and continuous part. Hence*

$$\langle \phi_n | \phi_{n'} \rangle \equiv \int d\mathbf{R} \phi_n^* (\mathbf{R}) \phi_{n'}(\mathbf{R}) = \delta_{nn'} \tag{53}$$

To be more specific, we shall assume that $\Phi_n(\boldsymbol{R})$ are the eigenfunctions of a certain Hamiltonian $\hat{\boldsymbol{H}}'$ which correspond to eigenvalues E_n:

$$\hat{\boldsymbol{H}}' \phi_n(\mathbf{R}) = E_n \phi_n(\mathbf{R}). \tag{54}$$

* Equations 49 and 50 are various formulations of the Liouville theorem which reads that the phase volume of the system obeying canonical equations does not depend on time. Hence

$$\frac{d\rho_c}{dt} \equiv \frac{\partial \rho_c}{\partial t} + [\rho_c, H] = 0.$$

A quantal system is said to be in a pure state $\psi(\mathbf{R}) \equiv |\psi\rangle$ if it can be completely described by a single wave function $\psi(\mathbf{R})$, i.e., $\psi(\mathbf{R})$ contains maximum information on the system and allows one to uniquely predict the results of a "complete experiment". If the ensemble of systems under consideration is "prepared" by mixing a set of ensembles of systems, being in different quantum states $\psi_j(\mathbf{R}) = |\psi_j\rangle$ with statistical weights g_j ($\Sigma_j g_j = 1$), then the system is said to be in a mixed state. All essential information on physical properties of such systems, i.e., information which can be obtained in their experimental investigation, is contained in the density matrix*

$$\hat{\rho}_q(\mathbf{R},\mathbf{R}') = \sum_j g_j \psi_j(\mathbf{R})\psi_j^*(\mathbf{R}') = \sum_n \sum_{n'} \rho_{nn'} |\phi_n\rangle\langle\phi_{n'}|, \tag{55}$$

$$\rho_{nn'} = \sum_j a_{jn} a_{jn'}^* g_j \tag{56}$$

where a_{jn} are the coefficients of the expansion of ψ_j in the set of the functions ϕ_n:

$$\psi_j(\mathbf{R}) = \sum_n a_{jn}\phi_n(\mathbf{R}), \qquad a_{jn} = \langle\phi_n|\psi_j\rangle. \tag{57}$$

(Here the symbols Σ_j and Σ_n imply summation over a discrete and integration over a continuous part of the spectra of the values of j and n respectively.) The states ψ_j must be normalized ($\langle\psi_j|\psi_j\rangle = 1$), but not necessarily orthogonal to one another.

The probability of finding the system in a certain state ψ is expressed in terms of the density matrix in the form

$$G(\psi) = \langle\psi|\hat{\rho}_q\psi\rangle \tag{58}$$

In particular, the probability of finding the system in the state Φ_n is equal to ρ_{nn}. The density matrix must be obviously normalized to unity:

$$\mathrm{Tr}(\hat{\rho}_q) \equiv \sum_n \rho_{nn} = 1. \tag{59}$$

The average value of any dynamic quantity $\hat{F}$ is expressed in terms of the density matrix as follows:

$$\langle F\rangle = \sum_j g_j \langle\psi_j|\hat{F}|\psi_j\rangle = \sum_{n,n'} \langle\phi_{n'}|\hat{F}|\phi_n\rangle = \mathrm{Tr}(\hat{\rho}_q\hat{F}). \tag{60}$$

The time evolution of the density matrix is determined by the so-called Liouville-von Neumann equation:

$$\frac{\partial\hat{\rho}_q(\mathbf{R},\mathbf{R}',t)}{\partial t} = \frac{i}{\hbar}\left[\hat{\rho}_q,\hat{H}\right] \equiv \frac{i}{\hbar}\{\hat{H}(\mathbf{R}')\hat{\rho}_q(\mathbf{R},\mathbf{R}',t) - \hat{H}(\mathbf{R})\hat{\rho}_q(\mathbf{R},\mathbf{R}',t)\} \tag{61}$$

* Quantity 55 is often called the density operator, whereas by the density matrix (in the Φ_n-representation) is meant only the matrix $\rho_{nn'}$ (see Blum[9]).

which immediately follows from Equation 55, since the functions $\psi_j(\mathbf{R},t)$ satisfy the time-dependent Schrödinger equation $i\hbar \frac{\partial \psi_j}{\partial t} = \hat{H}\,\psi_j$, where $\hat{H}$ is the Hamiltonian of the system. If $\hat{\rho}_q$ is preset at a certain instant t, then Equation 61 determines it uniquely at all subsequent instants.

Thus, in what is concerned with the states of the system and dynamic quantities the density matrix plays the same role in quantum theory as the phase density in classical physics. A detailed presentation of the theory and applications of the density matrix and the Liouville-von Neumann equation can be found in References 9 to 12.

C. WIGNER PROBABILITY FUNCTION

The form of the Liouville-von Neumann equation which is most similar to the classical form is obtained, if we go over to the so-called Wigner probability function (WPF)[13]. Let us briefly recall the definition and properties of this quantity, using the system which is characterized by a set of n independent coordinates x_j and which is in the pure state, $\psi(x_1, \ldots, x_n)$, as an example. To give a statistical description of such a system, Wigner has proposed to use the function

$$P(x_1, \ldots, x_n; p_1, \ldots, p_n) = \frac{1}{(\pi\hbar)^n} \int dy_1 \ldots dy_n \exp\{2i(p_1y_1 + \ldots + p_ny_n)/\hbar\} \times \psi^*(x_1 + y_1, \ldots, x_n\, y_n)\, \psi(x_1 - y_1, \ldots, x_n - y_n) \tag{62}$$

which he has defined as "the probability function of the simultaneous values of $\ldots, x_j, \ldots$ for the coordinates and $\ldots p_j, \ldots$, for the momenta". The WPF has the following important properties:

1. $P(\ldots, x_j, \ldots; \ldots, p_j, \ldots)$ is always a real-valued function, although it is not always positive.
2. The integral of P over all momenta gives a correct expression for the probability function of the simultaneous values of $\ldots, x_j, \ldots$ for the coordinates:

$$\int dp_1 \ldots dp_n\, P(\ldots, x_j, \ldots; \ldots, p_j, \ldots) = |\psi(\ldots, x_j, \ldots)|^2. \tag{63}$$

3. The integral of P overall coordinates gives a correct expression for the probability function of the simultaneous values $\ldots, p_j, \ldots$ for the momenta:

$$\int dx_1 \ldots dx_n\, P(\ldots, x_j, \ldots; \ldots p_j, \ldots) = \left| \int \ldots dx_j \ldots \psi(\ldots, x_j, \ldots) \exp\left\{ -\frac{i}{\hbar}\left(\ldots + p_jx_j + \ldots \right)\right\}\right|^2. \tag{64}$$

4. For arbitrary functions $f(\ldots, x_j, \ldots)$ and $g(\ldots, p_j, \ldots)$, the expression

$$\langle f + g \rangle = \int \ldots dx_j dp_j \ldots P(\ldots, x_j, \ldots; \ldots, p_j, \ldots) \times [f(\ldots, x_j, \ldots) + g(\ldots, p_j, \ldots)] \tag{65}$$

represents the average value of the sum $f + g$.

Rigorously speaking, the WPF cannot be interpreted as the probability of the simultaneous measurement of coordinates and momenta, since it can assume negative values. However, this reflects the fact that, according to quantum mechanics, a simultaneous measurement of a coordinate and a momentum, conjugate to it, is restricted by the Heisenberg uncertainty principle. As for the evaluation of average values which are really admissible by the quantum-mechanical restrictions, the WPF seems to be the optimum quantum-mechanical analogue of ρ_c. The equation describing its time evolution has the form which is especially similar to the classical form. We shall present and discuss this equation in Chapter 1, Section V, where we consider the case in which the quantum-mechanical Hamiltonian is an analogue of Hamiltonian 47 and we shall use the formalism of the WPF for the analysis of the validity conditions and for the substantiation of a classical approach to the INC-model based upon the phase density and the Liouville equation. The WPF is widely used in solving various problems of quantum statistical mechanics (see References 10 and 11).

REFERENCES

1. **Goldberger, M. L. and Watson, K. M.,** *Collision Theory,* John Wiley & Sons, New York, 1964.
2. **Newton, R. G.,** *Scattering Theory of Waves and Particles,* McGraw-Hill, New York, 1966.
3. **Bohr, A. and Mottelson, B. R.,** *Nuclear Structure,* Vol. 1, W. A. Benjamin Inc., New York, 1969.
4. **Bohr, A. and Mottelson, B. R.,** *Nuclear Structure,* Vol. 2, W. A. Benjamin Inc., New York, 1974.
5. **Satchler, G. R.,** *Direct Nuclear Reactions,* Clarendon Press, Oxford, 1983.
6. **Sitenko, A. G.,** *Theory of Nuclear Reactions* (in Russian), Energoatomizdat, Moscow, 1983.
7. **Jacob, G. and Maris, Th. A. J.,** Quasi-Free Scattering and Nuclear Structure *Rev. Mod. Phys.,* 38, 121, 1966. Also, 45, 6, 1973.
8. **Goldstein, H.,** *Classical Mechanics,* Addison-Wesley, Cambridge, Mass., 1953.
9. **Blum, K.,** *Density Matrix: Theory and Application,* Plenum Press, New York, 1981.
10. **Balescu, R.,** *Equilibrium and Nonequilibrium Statistical Mechanics* Vol. 1, Wiley-Interscience, New York, 1975.
11. **Balescu, R.,** *Equilibrium and Nonequilibrium Statistical Mechanics,* Vol. 2, Wiley-Interscience, New York, 1975.
12. **Kadanoff, L. P. and Baym, G.,** *Quantum Statistical Mechanics,* W. A. Benjamin Inc., New York, 1962.
13. **Wigner, E.,** On the Quantum Correction for Thermodynamic Equilibrium, *Phys. Rev.,* 40, 749, 1932.

Taylor & Francis
Taylor & Francis Group
http://taylorandfrancis.com

Chapter 1

INTRANUCLEAR CASCADE MODEL

I. FORMULATION OF THE PROBLEM AND BASIC ASSUMPTIONS

A. PROLEGOMENA

We have already mentioned in the Introduction that an attempt to describe intermediate-energy NRs, involving a large number of particles, on the basis of quantum-mechanical approaches often encounters difficulties and sometimes may turn out to be practically impossible. Therefore, the INC-model, which reposes upon a classical (more precisely, a semiclassical) microscopic description of a collision between a particle and a nucleus, is widely used.

According to this model, which was for the first time proposed by Serber[1] and Goldberger[2], an NR initiated by a fast particle proceeds in the following way: The particle moves along the classical trajectory. Upon entering a nucleus treated as a system of nucleons in a potential well with a predetermined momentum and coordinate distribution (see below), it can collide with one of the nucleons. Particles produced in this collision also move along their classical trajectories and, in their turn, can also collide with intranuclear nucleons or with one another, and so on. When particles, thus produced, reach the boundary* of the nucleus, they can leave it (if their energy is high enough). These particles form the products of the NR.

Let us consider qualitatively the basic features of this process. At its initial stage, collisions of a fast incident particle and "excited"** nucleons with intranuclear nucleons, which are in their initial states, take place in the main, the cross-sections of these collisions being close to the free ones. Approaching the boundary of the nucleus, they leave it, forming the products of the reaction with the energy $\gtrsim$ 10–20 MeV. This stage of the process will be called a cascade. At this stage, each of excited nucleons undergoes a small number of collisions in a nucleus (one-two collisions in light nuclei and two-four collisions in heavy ones). Accordingly, the time of its evolution, $\tau_{cas} \sim R/\bar{v} \sim 10^{-23} - 10^{-22}$s ($\bar{v}$ is the mean velocity of an excited nucleon), is small, too.

When such fast nucleons leave a nucleus, several excited nucleons with relatively low energies (rigorously speaking, these are quasiparticles rather than nucleons) and holes corresponding to nucleons knocked out of initial nucleon states remain in it. Moving in the nucleus, these excited nucleons and holes reach its boundary. They are reflected from it, as a rule, and continue to move in the nucleus, exchanging their energy with one another and with other nucleons. To leave the nucleus with a noticeable probability, such a nucleon must acquire a corresponding energy. This may happen in collisions with a hole or another excited nucleon, but

* By the boundary of a nucleus we mean a sphere of a radius R beyond which the strong interaction of an incident and outgoing particles with intranuclear nucleons can be disregarded.

** Nucleons knocked out of their initial states (determined by the wave function of a nucleus in the ground state) and moving along definite trajectories in the nucleus will be called excited nucleons.

not always. In collisions with unexcited nucleons, the excited ones only lose their energy. Hence, the mean time τ_{eq} of the nucleon (mainly neutron) emission is considerably larger at this stage* than at the initial stage. This process is called a pre-equilibrium emission. At this stage, not only nucleons, but also other particles (γ-quanta and light fragments, d,t,α, etc.) can be emitted with a noticeable probability. It should be noted that, if the energy of an incident particle is not very high $\lesssim$ 50-80 MeV), the outlined cascade process may not take place, and then a pre-equilibrium emission becomes initial (and sometimes the only) stage of the reaction. Thus, pre-equilibrium emission can be regarded as a separate process. This is discussed in detail in a number of monographs and reviews cited in Section IE.2 in Chapter 2.

At the stage of pre-equilibrium emission, collisions of nucleons lead, as a rule, to a redistribution of energy over an ever widening set of degrees of freedom of the nucleus. As a result, the energy distribution of nucleons approaches the equilibrium one. The probability that a nucleon accumulates the energy sufficient for its escape from the nucleus decreases progressively, and the process of the particle emission gradually takes on the features of evaporation. Emission of particles by a nucleus at this evaporation stage can be treated as a decay of excited resonance nuclear states, i.e., of compound nuclei (C-nuclei). In cases when their mean level widths are sufficiently large and the mean level spacings are small, so that the levels overlap, a statistical approach is valid.

As well as pre-equilibrium emission (and even to a greater extent) evaporation may be the only process, if the energy of an incident particle is sufficiently small. Therefore, basic features of the evaporation of particles from C-nuclei have been studied in detail in the literature and are set forth in a number of monographs devoted to NRs. However, considerable progress has recently been made in the study of properties of highly-excited C-nuclei and of a mechanism of their decay. This is concerned, above all, with the phenomenon of the thermal damping of shell effects and with the behavior of nuclei with limiting high values of the excitation energy comparable to the total binding energy of a nucleus (see Chapter 3).

B. BASIC ASSUMPTIONS OF THE INC-MODEL

Mathematical formulation of the INC-model can be based on the two following assumptions:

1. Motion of all particles involved in the cascade obeys the laws of classical mechanics.
2. During the development of the cascade separate collisions of a pair of particles take place in the domain whose dimensions are small, as compared to the mean free path of a particle in nuclear matter, and the duration of the collision is small as compared to the mean time interval between subsequent collisions. Therefore, any collision can be considered as instantaneous and localized at a point. The problem of the validity range of these assumptions will be

* According to the estimates obtained in Reference 3, $\tau_{eq} \sim (5 - 10)\ \tau_{cas}$, see also Chapter 3.

discussed in Section VC. Now we shall give a formulation of the model. For the sake of simplicity, we shall confine ourselves to the case when an incident particle is a nucleon and disregard the meson production in NN-collisions. This is a satisfactory approximation, if the kinetic energy of an incident particle ϵ_0 satisfies the condition $\epsilon_0 \lesssim 300$ MeV. A generalization to the case of other incident particles is straight forward, but calls for a more cumbersome formalism. Moreover, in this chapter, we shall disregard the effects associated with the existence of the spin of nucleons (these effects will be discussed in Chapter 4).

II. EXCLUSIVE DESCRIPTION OF THE INC*

A. PHASE DENSITY AND HAMILTONIAN OF THE INC-MODEL

The point at which an incident particle enters a nucleus and positions and momenta of nucleons in the nucleus are random variables. Therefore, to describe the cascade we shall use a statistical approach.

Let us consider the statistical ensemble comprising the following systems: a nucleus consisting of A nucleons (Z protons and N = A - Z neutrons) and the (A + 1)-th nucleon colliding with the nucleus.

According to the concepts of classical mechanics, the state of such a system is determined by the values of the coordinate $\boldsymbol{r}_j$ and the momentum $\boldsymbol{p}_j$ of each nucleon. Let us denote the set of coordinates and momenta of all nucleons by $\mathbf{X} = (\mathbf{x}_1, \ldots, \mathbf{x}_{A+1})$, where $\mathbf{x}_j = (\boldsymbol{r}_j, \boldsymbol{p}_j)$. In what follows the set $\mathbf{X}$, for sake of brevity, will be referred to as the point $\mathbf{X}$ (in the $6(A+1)$-dimensional phase space) and the set $\mathbf{x}_j$ as the point $\mathbf{x}_j$. The set of variables consisting of $\mathbf{X}$ and the time t will be called the point $\mathbf{X}$,t (for the j-th nucleon this is the point $\mathbf{x}_j$,t).

Let $\rho_c(\mathbf{X},t)$ be the phase density of the system, i.e., the probability density to find it at the point $\mathbf{X}$,t. An account of the principal properties of the phase density is given in Section IVA of the Introduction. Namely, ρ_c is normalized to unity, its normalization being independent of t. An average value of any dynamic quantity F characterizing the system can be expressed in terms of ρ_c (see Equation 46 in the Introduction). In particular, cross-sections of any (both inclusive and exclusive ones) processes, distributions of residual nuclei (R-nuclei) over the number of protons and neutrons, over the excitation energy, momenta, angular momenta, and other polarization characteristics are expressed in terms of ρ_c.

The time evolution of ρ_c is determined by the Liouville equation (Equations 50 or 52 in the Introduction) which represents a first-order linear partial differential equation. Specific form of this equation and that of its characteristic system, i.e., the canonical equations (Equation 48 in the Introduction), are defined by the form of the Hamiltonian. In the case of the system of A+1 interacting "spinless"

* To our knowledge, a consistent mathematical formulation of the exclusive description of NRs on the basis of the INC-model within the framework of classical concepts has not been given yet in scientific literature. Therefore, we shall describe it in sufficient detail in spite of the fact that the expressions used in this procedure are rather cumbersome.

nucleons under consideration, the Hamiltonian has the form (Equation 47, Introduction) with $N = A + 1$. However, the actual interaction $V_{jj'}(|\boldsymbol{r}_{j'} - \boldsymbol{r}_j|)$ of the j-th and the j'-th nucleon is the sum of a sharp short-range repulsive term $V^{sh}_{jj'}$ and a long-range attractive term $V^{\ell}_{jj'}$ slowly decreasing with increasing distance between nucleons. Owing to the presence of the long-range part $V_{jj'}$ the interaction of a given nucleon with the other nucleons manifests itself over the entire volume of the nucleus. This fact seems to contradict Assumption 2 of the model. However, to a good approximation, each separate nucleon (the j-th one) may be thought of as undergoing the effect of other nucleons (the j'-th ones) in the form of certain effective field $V_j(\boldsymbol{r}_j)$ which is practically independent of their specific coordinates. In accordance with this, the Hamiltonian of the INC-model can be represented in the form

$$H = H_0 + V,\ H_0 = \sum_{1 \le j \le A+1} H_j,\ H_j = T_j + V_j,\ V = \frac{1}{2} \sum_{1 \le (j' \ne j) \le A+1} V^{sh}_{jj'} \quad (1)$$

where H_0 describes the motion of nucleons without collisions, V is their interaction which results in collisions and T_j the kinetic energy of the j-th nucleon. Separation of the NN-interaction $V_{jj'}$ into $V^{\ell}_{jj'}$ and $V^{sh}_{jj'}$ with a subsequent their reduction to the effective field V_j and residual short-range interaction V is a rather good approximation, and it is extensively used in theoretical nuclear physics (see, for example, References 4 and 5). However, to construct a tallying INC-model, we must carry out such a separation in a self-consistent manner and take into account adequately both the motion of free nucleons in the field V_j and their collisions caused by the short-range part of the interaction. The problems arising in connection with this procedure will be discussed briefly in section VC.

The field V_j is often sought on the basis of phenomenological considerations. For example, the potential of the Skyrme type[6]

$$V_j(\boldsymbol{r}) = -A\rho + B\rho^{\gamma} \quad (2)$$

is widely used. Here ρ is the nucleon density at point $\boldsymbol{r}$ and A, B and γ are positive constants. The term proportional to ρ^{γ} ($\gamma > 1$) is introduced to prevent the collapse of the nucleus. This is important for the analysis of heavy ion collisions (see, for example, Reference 7). It is, however, obvious that the potential V_j (2) is a functional of the phase density. This leads to its dependence on time and to the nonlinearity of the Liouville equation. While calculating the NA-interaction, one can consider V_j as independent of ρ_c and use it in the form obtained, for example, within the framework of the optical model (e.g., Reference 4).

B. A STREAMING AND A COLLISION TERM

According to Equation 1 the Liouville equation (Equation 52, Introduction) can be written in the form

$$\frac{\partial \rho_c}{\partial t} = S + C, \quad (3)$$

$$S = \sum_{1\le j\le A+1} \left[\frac{\partial V_j(\boldsymbol{r}_j)}{\partial \boldsymbol{r}_j} \frac{\partial \rho_c}{\partial \boldsymbol{p}_j} - \frac{d\boldsymbol{r}_j}{dt} \frac{\partial \rho_c}{\partial \boldsymbol{r}_j} \right], \tag{4}$$

$$C = \frac{1}{2} \sum_{1\le (j'\ne j)\le A+1} \left\langle \frac{\partial V_{sh}^{j'j}(|\boldsymbol{r}_{j'} - \boldsymbol{r}_j|)}{\partial \boldsymbol{r}_j} \left(\frac{2\rho_c}{\partial \boldsymbol{p}_j} - \frac{\partial \rho_c}{\partial \boldsymbol{p}_{j'}} \right) \right\rangle_{\boldsymbol{r}_j = \boldsymbol{r}_{j'}}. \tag{5}$$

Here the symbol $<\ldots>_{\boldsymbol{r}_j=\boldsymbol{r}_{j'}}$ means an average taken over a "macroscopically small volume". This volume, say, this is a sphere of a radius a, is such that a is considerably smaller than distances at which ρ_c changes noticeably. On the other hand, this volume must be "microscopically large", namely $a \gg \sqrt{\sigma_{jj'}^{tot}}$, where $\sigma_{jj'}^{tot}$ is the total cross-section for the collision of the j-th and the j′-th nucleon, in order to reflect the random nature of such a collision. The sum S will be called a streaming term and the sum C a collision term. The streaming term describes a continuous variation of coordinates and momenta of particles of the system between collisions. This variation is determined by the Hamiltonian H_0. As was noticed above, the change in the phase density corresponding to it can be expressed in terms of the solution of canonical equations:

$$\boldsymbol{v}_j \equiv \frac{d\boldsymbol{r}_j}{dt} = \frac{\partial T_j}{\partial \boldsymbol{p}_j}, \qquad \frac{d\boldsymbol{p}_j}{dt} = -\frac{\partial V_j}{\partial \boldsymbol{r}_j} \tag{6}$$

which directly follow from Equation 48, Introduction, and Equation 1. Indeed, let the points $\mathbf{X}(t_0)$, t_0 and $\mathbf{X}$, t lie on the same trajectory of the system of particles in the fields V_j (in other words, they belong to the same partial solution of these equations). Then $\mathbf{X}(t_0)$ can be treated as a function of $\mathbf{X}$,t and t_0 (its dependence on $\mathbf{X}$ and t is not indicated for the sake of brevity). Let, further, $\Gamma(\mathbf{X}_0, t_0 \to \mathbf{X}, t)$ be the propagator of the system which gives the probability to find the system at the point $\mathbf{X}$, t, if it was at the point $\mathbf{X}_0$,t_0 (i.e., this is the Green function of the equation defined by Equations 3 and 4 with C=0). It satisfies the equation

$$\frac{\partial \Gamma}{\partial t} + \sum_{1\le j\le A+1} \left(\boldsymbol{v}_j \frac{\partial \Gamma}{\partial \boldsymbol{r}_j} - \frac{\partial V_j}{\partial \boldsymbol{r}_j} \frac{\partial \Gamma}{\partial \boldsymbol{p}_j} \right) = \delta(t - t_0)\, \delta(\mathbf{X} - \mathbf{X}_0). \tag{7}$$

For $t < t_0$, Γ equal to zero (for the boundary condition, see Section D) and has the form

$$\Gamma(\mathbf{X}_0, t_0 \to \mathbf{X}, t) = \Theta(t - t_0)\, \delta[\mathbf{X}_0 - \mathbf{X}(t_0)] \tag{8}$$

where $\Theta(z) = (z + |z|)/2|z|$, i.e., it depends on $\mathbf{X}$ and t only through the function $\mathbf{X}(t_0)$. Hence, if $\rho_c(\mathbf{X}, t_0)$ is the phase density at the instant t_0 than in the absence of collisions it becomes

$$\rho_c(\mathbf{X}, t) = \int d\mathbf{X}_0 \rho_c(\mathbf{X}_0, t_0)\, \Gamma(\mathbf{X}_0, t_0 \to \mathbf{X}, t) = \rho_c\, [\mathbf{X}(t_0), t_0] \tag{9}$$

at the instant t (the phase density is conserved along the trajectory of the system).

It should be noted that equation defined by Equations 3 and 4 with $C=0$ representing a classical analogue of a quantum model of independent particles in the time-dependent (in the general case) potential field. If this potential is chosen to be a self-consistent field, then we obtain a classical analogue of the time-dependent Hartree-Fock model. The same model is applicable to the description of the initial (ground) state of the nucleus as well. It is evident that in this case both the potential and the phase density $\rho_N^0(\mathbf{X}^A)$ ($\mathbf{X}^A = (\mathbf{x}_1,\ldots,\mathbf{x}_A)$) of a nucleus do not depend on t (the time-independent Hartree-Fock model). Namely

$$\rho_N^0(\mathbf{X}^A) = \hat{P}_{N,Z} \prod_{1\le j\le A} \rho_j^0(\boldsymbol{X}_j) \tag{10}$$

where $\rho_j^0(\mathbf{X}_j)$ is the probability density to find the j-th nucleon at the point $\mathbf{x}_j$ normalized to unity and $\hat{P}_{N,Z}$ the symmetrization operator (which preserves the normalization) with respect to the permutation of arbitrary pairs of identical particles taken from N neutrons and/or Z protons.

The collision term is the sum of terms which describe the result of the collision between the j-th and the j′-th nucleon (within a "macroscopically small volume"). It is assumed that an "instantaneous" sudden jump in the momenta of colliding nucleons takes place, as a result, without any change in their coordinates. Such a collision does not affect the motion of other nucleons. The phase density decreases, if the momenta of colliding nucleons belong to the set $\mathbf{X} = (\ldots;\boldsymbol{r}_j,\boldsymbol{p}_j;\ldots;\boldsymbol{r}_{j'},\boldsymbol{p}_{j'};\ldots)$ (after the collision they will have values differing from the initial ones). However, it increases if their momenta $\boldsymbol{p}'_j \neq \boldsymbol{p}_j$ and $\boldsymbol{p}'_{j'} \neq \boldsymbol{p}_{j'}$ and fall into a vicinity of the values $\boldsymbol{p}_j$, $\boldsymbol{p}_{j'}$ after the collision, while all other nucleons had (and, of course, preserved) the values of coordinates and momenta belonging to the set $\mathbf{X}$.

Let $w_{jj'}(\boldsymbol{p}_j,\boldsymbol{p}_{j'} \to \boldsymbol{p}'_j,\boldsymbol{p}'_{j'})\,d\boldsymbol{p}'_j\,d\boldsymbol{p}'_{j'}$ be the probability (per unit time) of such an elastic collision of the j-th nucleon with the momentum $\boldsymbol{p}_j$ and the j′-th nucleon with the momentum $\boldsymbol{p}_{j'}$ which are situated in the unit volume that their momenta fall into the intervals $d\boldsymbol{p}'_j$ and $d\boldsymbol{p}'_{j'}$ in the vicinity of $\boldsymbol{p}'_j$ and $\boldsymbol{p}'_{j'}$, respectively, as a result, and the next relation is satisfied

$$w_{jj'}(\boldsymbol{p}_j,\boldsymbol{p}_{j'} \to \boldsymbol{p}'_j,\boldsymbol{p}'_{j'}) = w_{jj'}(\boldsymbol{p}'_j,\boldsymbol{p}'_{j'} \to \boldsymbol{p}_j,\boldsymbol{p}_{j'}). \tag{11}$$

Then we get

$$\left\langle \frac{\partial V_{jj'}^{sh}}{\partial \boldsymbol{r}_j}\left(\frac{\partial \rho_c}{\partial \boldsymbol{p}_j} - \frac{\partial \rho_c}{\partial \boldsymbol{p}_{j'}}\right)\right\rangle_{\boldsymbol{r}_j = \boldsymbol{r}_{j'}} = \delta_a(\boldsymbol{r}_j - \boldsymbol{r}_{j'}) \int d\boldsymbol{p}'_j d\boldsymbol{p}'_{j'} w_{jj'}(\boldsymbol{p}_j,\boldsymbol{p}_{j'} \to \boldsymbol{p}'_j,\boldsymbol{p}'_{j'}) \times \\ \times \{\rho_c[\mathbf{X}(\boldsymbol{p}'_j,\boldsymbol{p}'_{j'}),t] - \rho_c(\mathbf{X},t)\} \tag{12}$$

where $\mathbf{X}(\boldsymbol{p}'_j,\boldsymbol{p}'_{j'})$ is the set $\mathbf{X}$ in which the quantities $\boldsymbol{p}_j$ and $\boldsymbol{p}_{j'}$ are replaced by $\boldsymbol{p}'_j$ and $\boldsymbol{p}'_{j'}$, respectively, and $\delta_a(\mathbf{r})$ the three-dimensional Dirac* "δ-function in the macroscopic meaning." In accordance with the aforesaid, it can be chosen in the form

$$\delta_a(\mathbf{r}) = \frac{3}{4\pi a^3}\,\Theta\,(a - r) \tag{13}$$

where a is the "macroscopically small size". However, $a \gg \sqrt{\sigma_{jj'}^{tot}}$, i.e., $(\sigma_{jj'}^{tot})^{3/2}\,\delta_a(\boldsymbol{r}) \ll 1$. Being multiplied by ρ_c and integrated over $\boldsymbol{r}$ the function $\delta_a(\boldsymbol{r})$ defined by Equation 13 reveals the properties of the ordinary δ-function.

If collisions of nucleons in nuclear matter are believed to proceed in the same way as those of the free ones, then the probability $w_{jj'}$ can be expressed in terms of the corresponding differential scattering cross-section $d\sigma_{jj'}^{cl}/d\overset{*}{\boldsymbol{\Omega}}$ in the c.m.s. and of the components of the four-momentum (in the l.s.). Namely, taking account of relativistic kinematics, we obtain

$$w_{jj'}\,(\boldsymbol{p}_j,\boldsymbol{p}_{j'} \to \boldsymbol{p}'_j,\boldsymbol{p}'_{j'}) = c\,\frac{1}{p_j^0 p_{j'}^0 p_j^{0'} p_{j'}^{0'}}\,(\hat{p}_j + \hat{p}_{j'})^2\,\delta(\hat{p}_j + \hat{p}'_j - \hat{p}'_{j'})\,\frac{d\sigma_{jj'}^{cl}}{d\overset{*}{\boldsymbol{\Omega}}}. \tag{14}$$

(c is the velocity of light).

C. INCORPORATION OF THE PAULI EXCLUSION PRINCIPLE IN THE COLLISION TERM

Equation 12 is based on purely classical concepts, and does not take into account quantum-mechanical effects, in particular, the Pauli exclusion principle, which rules out the possibility of finding more than one fermion in a single quantum state (integrals in Equation 12 are taken over the entire space of momenta). We can take into account this important effect by formally introducing the so-called Pauli-blocking factors into the integrand of Equation 12. As a result, we obtain

$$\begin{aligned}\left\langle \frac{\partial V_{jj'}^{sh}}{\partial \boldsymbol{r}_j}\left(\frac{\partial \rho_c}{\partial \boldsymbol{p}_j} - \frac{\partial \rho_c}{\partial \boldsymbol{p}_{j'}}\right)\right\rangle_{\boldsymbol{r}_j = \boldsymbol{r}_{j'}} &= \delta_a(\boldsymbol{r}_j - \boldsymbol{r}_{j'}) \times \\ &\times \int d\boldsymbol{p}'_j d\boldsymbol{p}'_{j'} w_{jj'}(\boldsymbol{p}_j,\boldsymbol{p}_{j'} \to \boldsymbol{p}'_j,\boldsymbol{p}'_{j'}) \times \\ &\times \{\rho_c[\mathbf{X}(\boldsymbol{p}'_j,\boldsymbol{p}'_{j'}),t](1 - f_j)(1 - f_{j'}) - \rho_c(\mathbf{X},t)(1 - f'_j)(1 - f'_{j'})\}\end{aligned} \tag{15}$$

where, for the sake of brevity, we have introduced the notation $f_j \equiv f(\alpha_j,\boldsymbol{r}_j,\boldsymbol{p}_j,t)$, $f'_j \equiv f(\alpha_j,\boldsymbol{r}_j,\boldsymbol{p}_j,t)$ and $f(\alpha,\boldsymbol{r},\boldsymbol{p},t)$ is the single-particle phase-space distribution function of α-nucleons (α is the doubled projection of the isotopic spin of a nucleon, i.e., $\alpha = 1$ for protons and $\alpha = -1$ for neutrons) which determines the nonvacancy of the elementary cell of the phase space with respect to the α-nucleon. The function $f(\alpha,\boldsymbol{r},\boldsymbol{p},t)$ is defined by the relation

$$f(\alpha,\boldsymbol{r},\boldsymbol{p},t) = \frac{1}{2}\,(2\pi\hbar)^3 \sum_{1\le j\le A+1} \delta_{\alpha_j\alpha} \int d\mathbf{X}\rho_c(\mathbf{X},t)\,\delta(\boldsymbol{r}_j - \boldsymbol{r})\,\delta(\boldsymbol{p}_j - \boldsymbol{p}) \tag{16}$$

It is obvious that such an approach is an eclectic one by nature and calls for a substantiation.

The introduction of the Pauli-blocking factors into Equation 12 violates the linearity of the Liouville equation. To avoid this difficulty, the function $f(\alpha,\boldsymbol{r},\boldsymbol{p},t)$ appearing in them is replaced by $f(\alpha,\boldsymbol{r},\boldsymbol{p},0)$, i.e., by the distribution function of nucleons in a nucleus before a collision. In this procedure, a nucleus is treated as an ideal local completely degenerate Fermi gas of nucleons in the effective potential well $V_\alpha(\boldsymbol{r})$. In accordance with this we have

$$f(\alpha,\boldsymbol{r},\boldsymbol{p},0) = \Theta[p_{F,\alpha}(\boldsymbol{r}) - p] \tag{17}$$

where $p_{F,\alpha}(\boldsymbol{r}) = \sqrt{2m_N E_{F,\alpha}(\boldsymbol{r})}$ is the Fermi momentum for α-nucleons at the $\boldsymbol{r}$ (m_N is the nucleon mass and $E_{F,\alpha}(\boldsymbol{r})$ the Fermi energy at this point). It should be recalled that $p_{F,\alpha}(\boldsymbol{r})$ is connected with the density $\rho_\alpha(\boldsymbol{r})$ of the α-nucleons at the point $\boldsymbol{r}$ normalized to $f(\alpha)$ through the relation

$$\rho_\alpha(\boldsymbol{r}) = \frac{1}{4\pi^3\hbar^3}\int d\boldsymbol{p}\Theta[p_{F,\alpha}(\boldsymbol{r}) - p] = \frac{1}{3\pi^2\hbar_3}p^3_{F,\alpha}(\boldsymbol{r}) \tag{18}$$

(for protons $f(\alpha) \equiv f(1) = Z$ and for neutrons $f(\alpha) \equiv f(-1) = N$).

D. FORMULATION OF THE EQUATION, THE INITIAL, AND THE BOUNDARY CONDITIONS

Taking into account Equations 3 to 5, and 15, we can write the equation for ρ_c in the form

$$\begin{aligned}\frac{\partial\rho_c}{\partial t} + \sum_{1\le j\le A+1}\left(\boldsymbol{v}_j\frac{\partial\rho_c}{\partial\boldsymbol{r}_j} - \frac{\partial V_j}{\partial\boldsymbol{r}_j}\frac{\partial\rho_c}{\partial\boldsymbol{p}_j}\right) &= \frac{1}{2}\sum_{1\le(j'\ne j)\le A+1}\delta_a(\boldsymbol{r}_j - \boldsymbol{r}_{j'})\\ &\int d\boldsymbol{p}'_j d\boldsymbol{p}'_{j'}\, w_{jj'}(\boldsymbol{p}_j,\boldsymbol{p}'_j \to \boldsymbol{p}'_j,\boldsymbol{p}'_{j'}) \times\\ &\times\{\rho_c[\mathbf{X}(\boldsymbol{p}'_j,\boldsymbol{p}'_{j'}),t](1 - f_j)(1 - f_{j'}) - \rho_c(\mathbf{X},t)(1 - f'_j)(1 - f'_{j'})\}.\end{aligned} \tag{19}$$

Given the initial and the boundary condition, its solution is unique. We shall choose these conditions as follows.

The initial condition will be used in the form

$$\rho_c(\mathbf{X},0) = \rho^0_N(\mathbf{X}^A)\rho_p(\mathbf{x}_{A+1},0) \tag{20}$$

where $\rho^0_N(\mathbf{X}^A)$ and $\rho_p(\mathbf{x}_{A+1},0)$ are the phase density of a nucleus in the ground state and that of an incident nucleon before the collision (at the instant $t = 0$), respectively. The quantity $\rho^0_N(\mathbf{X}^A)$ is determined by Formula 10 in which within the framework of the degenerate nucleon Fermi gas model $\rho^0_j(\mathbf{x}_j)$ has the form

$$\rho^0_j(\mathbf{x}_j) = \frac{2}{(2\pi\hbar)^3 f(\alpha_j)}\Theta[p_{F,\alpha}(\boldsymbol{r}_j) - p_j]. \tag{21}$$

The phase density of an incident (with the momentum p_0) nucleon before the collision is written in the form

$$\rho_p(x_{A+1},0) = \frac{1}{\pi}\int d\omega_0\, \Theta(-\omega_0 p_0)\, \delta(p_0 - p_{A+1})\, \delta(R_0 - r_{A+1})\, \frac{|\omega_0 p_0|}{p_0} \equiv \tag{22a}$$

$$\frac{1}{\pi R^2}\, \Theta(-r_{A+1}p_{A+1})\, \delta(p_{A+1} - p_0)\, \delta(r_{A+1} - R)\, \frac{|r_{A+1}p_0|}{Rp_0} \tag{22b}$$

where $R_0 = \omega_0 R$ ($|\omega_0| \equiv 1$) is the radius vector of a point lying on the boundary of the nucleus, and the origin of coordinates is chosen in its center of mass. Such a form corresponds to the case when a nucleon falls upon a nucleus with equal probability within the disc of a radius R.

In accordance with the aforesaid (see Section IIA) we shall formulate the boundary condition in the following form: for $t > 0$

$$\rho_c(X,t) = 0, \text{ if } r_j = R \text{ and } r_j p_j < 0 \text{ for any j.} \tag{23}$$

E. INTEGRAL FORMS OF THE LIOUVILLE EQUATION

Equation 19 can be recast in various forms of a purely integral equation. Below we shall give two of them. To this end we shall write Equation 19 in the form

$$\hat{L}_i\, \rho_c(X,t) = \int dX' \rho_c(X',t)\, Q_i(X' \to X,t). \tag{24}$$

The following expressions present two versions ($i = 1,2$) of the operator $\hat{L}_i$ and the kernel $Q_i(X' \to X,t)$:

$$\hat{L}_1 = \frac{\partial}{\partial t} + \sum_{1\le j\le A+1} \left(v_j \frac{\partial}{\partial r_j} - \frac{\partial V_j}{\partial r_j}\frac{\partial}{\partial p_j}\right), \tag{25a}$$

$$\hat{L}_2 = \hat{L}_1 + W(X,t), \tag{25b}$$

$$Q_1(X' \to X,t) = Q_2(X' \to X,t) - W(X',t)\, \delta(X' - X), \tag{26a}$$

$$Q_2(X' \to X,t) = \frac{1}{2}\sum_{1\le(j'\ne j)\le A+1} \widetilde{w}_{jj'}(t,X' \to X). \tag{26b}$$

Here the following notation is introduced:

$$W(X,t) = \frac{1}{2}\sum_{1\le(j'\ne j)\le A+1} \widetilde{W}_{jj'}(t,X). \tag{27}$$

$$\widetilde{w}_{jj'}(t,X) = \delta_a(r_j - r_{j'}) \int dp'_j dp'_{j'} w_{jj'}(p_j,p_{j'} \to p'_j,p'_{j'})(1 - f'_j)(1 - f'_{j'}), \tag{28}$$

$$\widetilde{w}_{jj'}(t,\mathbf{X}' \to \mathbf{X}) = \delta_a(\boldsymbol{r}_j - \boldsymbol{r}_{j'})\, w_{jj'}(\boldsymbol{p}'_j,\boldsymbol{p}'_{j'} \to \boldsymbol{p}_j,\boldsymbol{p}_{j'})(1 - f_j)(1 - f_{j'}) \times \tag{29}$$

$$\delta(\boldsymbol{r}_j - \boldsymbol{r}'_j)\, \delta(\boldsymbol{r}_{j'} - \boldsymbol{r}'_{j'}) \prod_{\substack{1 \le i \le A+1 \\ i \ne j,j'}} \delta(\mathbf{x}_i - \mathbf{x}'_i).$$

Suppose that we know the inverse operator $\hat{L}_i^{-1}$ which is the solution of the equation

$$\hat{L}_i\, \Gamma^i = \delta(t - t_0)\, \delta(\mathbf{X} - \mathbf{X}_0) \tag{30}$$

satisfying the condition $\Gamma^i = 0$ for $t < t_0$ and the boundary condition in the form in Equation 23 for $t > t_0$. Then, considering the right-hand side of Equation 24 as a "source", we can easily reduce it to the form

$$\rho_c(\mathbf{X},t) = \rho_0^i(\mathbf{X},t) + \int_0^t dt_0 \int d\mathbf{X}_0 \rho_c(\mathbf{X}_0,t_0)\, \widetilde{Q}_i(\mathbf{X}_0,t_0 \to \mathbf{X},t), \tag{31}$$

$$\rho_0^i(\mathbf{X},t) = \int d\mathbf{X}_0 \rho_c(\mathbf{X}_0,0)\, \Gamma^i(\mathbf{X}_0,0 \to \mathbf{X},t), \tag{32}$$

$$\widetilde{Q}_i(\mathbf{X}_0,t_0 \to \mathbf{X},t) = \int d\mathbf{X}' Q_i(\mathbf{X}_0 \to \mathbf{X}',t_0)\, \Gamma^i(\mathbf{X}',t_0 \to \mathbf{X},t). \tag{33}$$

It is seen from comparison of Equations 25a and 30 with Equation 7 that Γ^1 coincides with Γ determined by the relation in Equation 8. The solution of Equation 30 for Γ^2 has the form

$$\Gamma^2(\mathbf{X}_0,t_0 \to \mathbf{X},t) = \exp\{-\int_{t_0}^t dt' W[\mathbf{X}(t'),t']\}\, \Gamma^1(\mathbf{X}_0,t_0 \to \mathbf{X},t). \tag{34}$$

This can be readily verified by a direct substitution.

Let us consider these expressions. Both Γ^1 $(\mathbf{X}_0,t_0 \to \mathbf{X},t)$, and Γ^2 $(\mathbf{X}_0,t_0 \to \mathbf{X},t)$ are the propagators of the system which describe its evolution from the point $\mathbf{X}_0,t_0$ to the point $\mathbf{X},t$ without collisions. However, the expression for Γ^1 is obtained under the assumption that collisions are excluded in the system during the time interval between t_0 and t, whereas Γ^2 takes into account the fact that the probability of such collisions differs from zero. According to Equation 27 its normalization is given by the expression

$$\exp\left\{-\int_{t_0}^t dt'\, W[\mathbf{X}(t'),t']\right\} = \prod_{1 \le (j' \ne j) \le A+1} \exp\left\{-\frac{1}{2}\int_{t_0}^t dt' \widetilde{W}_{jj'}[t',\mathbf{X}(t')]\right\} \tag{35}$$

i.e., it is equal to the product of the probabilities of avoiding the collision between every pair of nucleons (the j-th and the j'-th ones) during this time interval. In particular, taking into account the fact that intranuclear nucleons do not collide

with one another, if the nucleus is in the ground state (i.e., $\widetilde{W}_{jj'} = 0$ for $t = 0$ and $j,j' \leq A$), by virtue of Equation 28, we obtain

$$\Gamma^2(\mathbf{X}_0,0 \rightarrow \mathbf{X},t) = \Gamma^1(\mathbf{X}_0,0 \rightarrow \mathbf{X},t), \tag{36}$$

$$\exp\left\{ - \sum_{1 \leq j \leq A} \int_0^t dt' \delta_a[\boldsymbol{r}_{j0} - \boldsymbol{r}_{A+1}(t')] \, W_{jA+1} \, [\boldsymbol{p}_j, \boldsymbol{x}_{A+1}(t')] \right\},$$

$$W_{jA+1}(\boldsymbol{p}_j, \boldsymbol{x}_{A+1}) = \int d\boldsymbol{p}'_j d\boldsymbol{p}'_{A+1} \times \tag{37}$$

$$w_{jA+1} \, (\boldsymbol{p}_i, \boldsymbol{p}_{A+1} \rightarrow \boldsymbol{p}'_j, \boldsymbol{p}'_{A+1})(1 - f'_j)(1 - f'_{A+1}).$$

The functions ρ_0^i represent the phase densities of the system under the consideration that nucleons do not collide. The quantity ρ_0^1 is normalized to unity, i.e., it describes the system under the assumption that not a single collision has taken place in the system during the time interval (0,t). Since $\Gamma^1 = \Gamma$, then according to Equation 8 it has the form (compare to Equation 9):

$$\rho_0^1(\mathbf{X},t) = \rho_N^0 \, (\mathbf{X}^A) \rho_p[\mathbf{x}_{A+1}(0),0]. \tag{38}$$

By virtue of Equations 8, 10, and 34, ρ_0^2 can be written in the form

$$\rho_0^2(\mathbf{X},t) = \rho_0^1(\mathbf{X},t) \exp\left\{ - \sum_{1 \leq j \leq A} \int d\boldsymbol{p}_j \times \right. \tag{39}$$

$$\left. \int_0^t dt' \rho_j^0[\boldsymbol{r}_{A+1}(t'), \boldsymbol{p}_j] \, W_{jA+1}[\boldsymbol{p}_j, \mathbf{x}_{A+1}(t')] \right\}.$$

This expression is obtained with allowance for collisions and represents the collisionless part of the total phase density. The remaining part of ρ_c is formed as a result of collisions and equal to the second term on the right-hand side of Equation 31 at $i = 2$. The physical meaning of the expression which describes this part of ρ_c is quite clear: it is obvious that the probability of a collision at the point $\mathbf{X}_0,t_0$ is proportional to $\rho_c(\mathbf{X}_0,t_0)$. The quantity $Q_2(\mathbf{X}_0 \rightarrow \mathbf{X}',t_0)$ which according to Equation 33 appears in $\widetilde{Q}_2$ determines both the coefficient of proportionality and the probability of the transition $\mathbf{X}_0 \rightarrow \mathbf{X}'$ (its dependence on t is determined by the time dependence of the Pauli-blocking factors). The phase density $\rho_c(\mathbf{X}',t_0)$ formed as a result is "led" by the propagator Γ^2 in a predetermined way along the trajectory up to the point $\mathbf{X},t$, the length of this path and consequently the duration of the time interval (t_0,t) being a random variable. The integral on the right-hand side of Equation 31 sums up the probabilities for coming to the point $\mathbf{X},t$ from all possible "initial" points $\mathbf{X}_0,t_0$.

At $i = 1$, the second term in Equation 31 includes both the phase density which arises as a result of the nucleon collisions and the decrease of its collisionless

part. The integral of this term over **X** is equal to zero, because the integral of Q_1 $(\mathbf{X}_0 \rightarrow \mathbf{X}',t)$ over $\mathbf{X}'$ is equal to zero. Interpretation of this term is less obvious.

It can be easily verified that both solutions of Equation 31 obtained in this section satisfy our initial and boundary conditions.

Finally, it should be noted that the integral over $\mathbf{X}'$ in Equation 33 can be easily evaluated, but the resultant expression is rather cumbersome.

F. SOLUTION OF THE INTEGRAL LIOUVILLE EQUATION IN THE FORM OF THE VON NEUMANN SERIES

The solution of Equation 31 can be represented in the form of the von Neumann series:

$$\rho_c(\mathbf{X},t) = \rho_0^i(\mathbf{X},t) + \int_0^t dt_0 \int d\mathbf{X}_0 \rho_0^i(\mathbf{X}_0,t_0)\, G_i(\mathbf{X}_0,t_0 \rightarrow \mathbf{X},t) \tag{40}$$

where the resolvent kernel is given by the expressions

$$G_i(\mathbf{X}_0,t_0 \rightarrow \mathbf{X},t) = \sum_{1 \le n < \infty} G_n^i(\mathbf{X}_0,t_0 \rightarrow \mathbf{X},t), \tag{41}$$

$$G_1^i(\mathbf{X}_0,t_0 \rightarrow \mathbf{X},t) \equiv \widetilde{Q}_i(\mathbf{X}_0,t_0 \rightarrow \mathbf{X},t), \tag{41a}$$

$$G_n^i(\mathbf{X}_0,t_0 \rightarrow \mathbf{X},t) = \int_{t_0}^t dt' \int d\mathbf{X}' \widetilde{Q}_i(\mathbf{X}_0,t_0 \rightarrow \mathbf{X}',t') \times \tag{41b}$$

$$G_{n-1}^i(\mathbf{X}',t' \rightarrow \mathbf{X},t),\ n \ge 2.$$

Substituting ρ_0^i in the form of Equations 38 or 39 and $\widetilde{Q}_i$ in the form of Equation 33 (where Q_i are defined by Equations 26a and 26b, $\Gamma^1 = \Gamma$ by Equation 8, and Γ^2 by Equations 8, 34, 35, and 28) in these expressions, we obtain two series (which correspond to $i = 1,2$) for the calculation of ρ_c. It can be shown that in the cases which we are interested in (within the framework of the INC-model) these series converge to a solution which always exists and is unique.

The following features of these series should be noted. If $i = 1$, integrals of the kernel in Equation 33 and all its iterations over **X** are equal to zero. Therefore, any number of terms of this series preserves the normalization of the phase density. In the case corresponding to $i = 2$, the integral of a finite number n of terms of the series in Equations 40 and 41 over **X** is always smaller than unity and tends monotonically to unity for $n \rightarrow \infty$. All terms of this series are positive and have clear physical meaning: as was already mentioned, the first term (ρ_0^2) describes an incident nucleon which does not undergo collisions, the second term (the result of the first iteration) describes the states of the motion of nucleons in a nucleus, which arises after a collision between an incident nucleon and one of intranuclear nucleons; the third term of the series (the second iteration) describes the result of the collision involving one of nucleons formed at the previous stage, and so on. Thus, this series represents an expansion of the phase density in "series in the number of collisions"

or in "series in the generations" of particles participating in the cascade. Such an apt interpretation of each term of this series allows us to simulate it by means of the Monte Carlo technique in quite a natural way.

Within the framework of one or another physical model, the probability of collision $Q_2(X_0 \rightarrow X', t_0)$ and the propagator Γ^2 $(X',t_0 \rightarrow X,t)$ are simulated, and a sampling of chains of consecutive segments of the trajectory of the system is carried out. At each successive step, the point X in Q_2 and the lengths of the segments between collisions are random variables for a given point X_0 determined at the previous step. For this reason, the largest part of calculations of exclusive characteristics of the INC by means of the Monte Carlo technique actually represents the evaluation of this series within the framework of one or another approximation.

G. "MACROAPPROXIMATION"

As has been mentioned, the Liouville equation can be considerably simplified if the following approximations are used: 1) the initial state of a nucleus is described by the Thomas-Fermi model, i.e., by Formulas 10 and 21; 2) the dependence of the Pauli-blocking factors on time is disregarded, and it is assumed that they are described by the Thomas-Fermi model as well, i.e., the function f occurring in them has the form of Equation 17.

These approximations seem quite natural in the case of heavy nuclei, namely, when the number of excited nucleons, i.e., nucleons with $p_j > p_{F,\alpha}(r_j)$ (see Section IA), is significantly small than A. Under this condition we can also disregard the collisions between excited nucleons with one another. Moreover, we can disregard the effect of a change in the phase density of unexcited nucleons during the development of the cascade on the probability of collisions of excited nucleons with unexcited ones, i.e., deem that, for an arbitrary number of excited nucleons, collisions of each of them with unexcited ones proceed in the same way as in a nucleus which is in the ground state. This means that a nucleus can be treated as a system containing a "macroscopically large" number of nucleons. Therefore, such an approximation will be called a "macroapproximation". It will be shown in Chapters 2 and 4 (see also Reference 8) that, for sufficiently large values of A ($A \gtrsim 10$), such an approximation leads to reasonable results in a number of cases which are of practical importance. However, it does not take into account the conservation of the baryon number in NRs, and if A is small, it can lead to a possibility of a process in which the number of nucleons leaving the nucleus is larger than A. We shall discuss one possibility for the refinement of this approximation (namely, the incorporation of the "trawling effect") in Chapters 2 and 4.

The calculation of the cascade is considerably simplified within the framework of the macroapproximation. The use of this approximation allows one to calculate the distribution over the excitation energy, momentum, and angular momentum of the R-nucleus as well. Therefore, the so-called standard Monte Carlo model of the INC which is described in Chapter 2, Section IIA is based upon it. It is realized in the form of various codes and extensively used for exclusive calculations of the cascade.

Let us consider the integral form of the cascade Equation 31 at $i=2$ in the macroapproximation. According to this approximation the phase density of unexcited nulceons does not vary and, in the total phase density ρ_c, it appears as a constant factor of the form (see Equations 10 and 21):

$$\rho_N^0(\mathbf{X}^A) = \frac{1}{(4\pi^3\hbar^3)^A}\left\{\prod_{1\le j\le N}\frac{1}{N}\Theta[p_{F,-1}(\boldsymbol{r}_j) - p_j]\right\} \times \left\{\prod_{N+1\le j\le A}\frac{1}{Z}\Theta[p_{F,1}(\boldsymbol{r}_j) - p_j]\right\}. \tag{42}$$

(Here, as above, nucleons are neutrons for $j \leqslant N$ and protons for $j \geqslant N+1$). We shall omit it for the sake of brevity and consider only the phase density of excited nucleons which will be denoted by the symbol ρ_c^* $(\mathbf{X},t)$ (here $\mathbf{X}$ is, of course, the set of $\mathbf{x}_j$ which refers only to excited nucleons). Hence, $\rho_c = \rho_c^*\,\rho_N^0$ and in accordance with Equations 22a and 37–39 the equation for ρ_c^* has the form

$$\begin{aligned}\rho_c^*(\mathbf{X},t) &= \frac{|\boldsymbol{p}_0\boldsymbol{r}_{A+1}(0)|}{\pi p_0 R}\Theta[-\boldsymbol{p}_0\boldsymbol{r}_{A+1}(0)]\,\delta[\boldsymbol{R} - \boldsymbol{r}_{A+1}(0)] \times \\ &\delta[\boldsymbol{p}_0 - \boldsymbol{p}_{A+1}(0)]\exp\{-W_{A+1}(0;\boldsymbol{x}_{A+1},t)\} + \\ &+ \int_0^t dt_0 \int d\mathbf{X}_0\rho_c^*(\mathbf{X}_0,t_0)\,Q^*(\mathbf{X}_0,t_0 \to \mathbf{X},t)\end{aligned} \tag{43}$$

where

$$\begin{aligned}W_{A+1}(t_0;\boldsymbol{x}_{A+1},t) &= \frac{1}{4\pi^3\hbar^3}\sum_{\alpha=\pm1}\int_{t_0}^t dt' \int d\boldsymbol{p}d\boldsymbol{p}'d\boldsymbol{p}'_{A+1} \times \\ &w_{\alpha A+1}\,[\boldsymbol{p},\boldsymbol{p}_{A+1}(t') \to \boldsymbol{p}',\boldsymbol{p}'_{A+1}] \times \Theta\{p_{F,\alpha}[\boldsymbol{r}_{A+1}(t')] - p\} \\ &\Theta\{p' - p_{F,\alpha}[\boldsymbol{r}_{A+1}(t')]\}\,\Theta\{p_{A+1} - p_{F,\alpha_{A+1}}[\boldsymbol{r}_{A+1}(t')]\}\end{aligned} \tag{44}$$

(to emphasize the fact that w_{jA+1} depends only on α of the j-th nucleon we have replaced the symbol w_{jA+1} by $w_{\alpha A+1}$). According to Equations 8, 26b, 29, 33, and 36 the kernel Q^* can be represented as the sum of terms each of which describes the collisions of one excited j-th nucleon with unexcited ones, whereas all other excited nucleons (the i-th ones, $i\neq j$) are spectators and continue to move along their former trajectories, i.e.,

$$Q^*(\mathbf{X}_0,t_0 \to \mathbf{X},t) = \sum_j Q_j^*(\mathbf{x}_{j0},t_0 \to \mathbf{x}_j,\mathbf{x}_{j'};t)\prod_{i\neq j,j'}\Gamma_i^*(\mathbf{x}_{i0},t_0 \to \mathbf{x}_i,t). \tag{45}$$

Here we have taken into account that each such collision generates a new excited nucleon (denoted by j′);

$$\Gamma_i^*(\mathbf{x}_{i0},t_0 \to \mathbf{x}_i,t) = \Theta(t - t_0)\,\delta[\mathbf{x}_{i0} - \mathbf{x}_i(t_0)]\,\exp\{-\,W_i(t_0;\mathbf{x}_i,t)\} \tag{46}$$

where $W_i(t_0;\mathbf{x}_i,t)$ is determined by Equation 44 in which the subscript $A+1$ must be replaced by i. Finally, Q_j^* can be written in the form

$$\begin{aligned} Q_j^*(\mathbf{x}_{i0},t_0 \to \mathbf{x}_j,\mathbf{x}_{j'};t) = {} & \frac{1}{4\pi^3\hbar^3}\sum_{\alpha=\pm 1}\int d\boldsymbol{p}\,d\boldsymbol{p}'\,d\boldsymbol{p}_j' \times \\ & \times\ \Theta\{p_{F,\alpha}[\boldsymbol{r}_j(t_0)] - p\}\,w_{j\alpha}(\boldsymbol{p}_{j0},\boldsymbol{p} \to \boldsymbol{p}_j',\boldsymbol{p}') \cdot \\ & \cdot\ \Theta\{p_j' - p_{F,\alpha j}[\boldsymbol{r}_j(t_0)]\}\,\Theta\{p' - p_{F,\alpha}[\boldsymbol{r}_j(t_0)]\} \times \\ & \times\ \Gamma_j^*[\boldsymbol{r}_j(t_0),\boldsymbol{p}_j',t_0 \to \mathbf{x}_i,t]\,\Gamma_{j'}^*[\boldsymbol{r}_j(t_0),\boldsymbol{p}',t_0 \to \mathbf{x}_{j'},t] \end{aligned} \tag{47}$$

(as well as in Equation 44 we have replaced here $w_{jj'}$ by $w_{j\alpha}$ where $\alpha \equiv \alpha_{j'}$).

Although the expressions obtained are cumbersome, their physical meaning is rather simple. Everything which has been said in Section E about the similar terms of Equation 31 at $i=2$ is applicable to these expressions, with the difference that ρ_c^* describes the behavior of only excited nucleons.

The solution of Equation 43, as well as that of 31 can be written in the form of the von Neumann series, which in the present case represents the solution of the system of equations for many-particle distribution function of nucleons in the process of the development of the INC.[9] It is seen from the analysis performed what approximations are to be used to obtain it within the framework of purely classical concepts. We shall not write down the expressions for the terms of this series, because they are rather cumbersome. It should be noted, however, that their calculation by means of the Monte Carlo technique, outlined in Section F, turns out to be not very complicated, because only the motion of excited nucleon is traced in this approach, whereas the medium in which they move and the law of their scattering remain unchanged*.

III. INCLUSIVE DESCRIPTION OF THE INC

A. BOLTZMANN-UEHLING-UHLENBECK EQUATION

In solving a number of problems associated with the analysis of the INC, it is not necessary to determine ρ_c as a function of all its variables. For instance, we have already demonstrated within the framework of the macroapproximation that it is sufficient to consider only the behavior of excited nucleons. This considerably simplifies the calculations. However, an advancement of paramount importance along these lines can be made in the calculation of inclusive characteristics of NRs.

* This procedure allows one, of course, to determine the coordinates and momenta of nucleons knocked out of their initial states as well, and hence, the energy, the momentum, and the angular momentum of holes in the distribution of nucleons below the Fermi energy (see Chapters 2 and 4).

These characteristics are completely determined by the single-particle phase densities $\Psi_\alpha(\mathbf{x},t)$ of protons ($\alpha = 1$) and neutrons ($\alpha = -1$). They, in their turn, are proportional to the single-particle distribution functions of α-nucleons in the phase space (see Equation 16)

$$\Psi_\alpha(\mathbf{x},t) = \frac{1}{4\pi^3\hbar^3} f(\alpha,\mathbf{x},t) \tag{48}$$

and have the meaning of the number of α-nucleons in a unit volume of the six-dimensional phase space in the vicinity of the point $\mathbf{x} = (\mathbf{r},\mathbf{p})$ at the instant t.

Consider, first, the equation for $f(\alpha,\mathbf{x},t)$. To obtain it, let us multiply both sides of Equation 19 by $4\pi^3\hbar^3\,\delta_{\alpha_j\alpha}\,\delta(\mathbf{x}_j-\mathbf{x})$, integrate it over $\mathbf{X}$ and sum over j. As a result we get

$$\begin{aligned}\left(\frac{\partial}{\partial t} + \mathbf{v}\frac{\partial}{\partial \boldsymbol{r}} - \frac{\partial V_\alpha}{\partial \boldsymbol{r}}\frac{\partial}{\partial \boldsymbol{p}}\right) f_\alpha &= \frac{1}{4\pi^3\hbar^3}\sum_{\alpha'=\pm 1}\int d\boldsymbol{p}'d\boldsymbol{p}''d\boldsymbol{p}''' \times \\ &\times \{w_{\alpha\alpha'}(\boldsymbol{p}',\boldsymbol{p}'' \to \boldsymbol{p},\boldsymbol{p}'')\, f'_\alpha f''_{\alpha'}(1 - f_\alpha)(1 - f'''_{\alpha\alpha'}) - \\ &w_{\alpha\alpha'}(\boldsymbol{p},\boldsymbol{p}''' \to \boldsymbol{p}',\boldsymbol{p}'')f_\alpha f'''_{\alpha\alpha'}(1 - f'_\alpha)(1 - f''_{\alpha'})\}\end{aligned} \tag{49}$$

where the following notation is introduced: $f_\alpha \equiv f(\alpha,\boldsymbol{r},\boldsymbol{p},t)$, $f'_\alpha \equiv f(\alpha,\boldsymbol{r},\boldsymbol{p}',t)$, etc., and $w_{\alpha\alpha'} = w_{\alpha_j\alpha_j'}$, as well. Assuming that an α_0-nucleon impinges on a nucleus, by virtue of Equations 16, 20, 21, and 22a, we get for the initial condition

$$\begin{aligned}f(\alpha,\mathbf{x},0) = 4\pi^2\hbar^3\delta_{\alpha\alpha_0}\int d\boldsymbol{\omega}_0 \frac{|\boldsymbol{\omega}_0\boldsymbol{p}_0|}{p_0}\,\Theta(-\,\boldsymbol{\omega}_0\boldsymbol{p}_0) \times \\ \times\, \delta(\boldsymbol{p}_0 - \boldsymbol{p})\,\delta(\mathbf{R}_0 - \boldsymbol{r}) + \Theta[p_{F,\alpha}(\boldsymbol{r}) - p]\end{aligned} \tag{50}$$

and from Equation 23 we obtain for the boundary condition

$$f(\alpha,\boldsymbol{R},\boldsymbol{p},t) = 0 \quad \text{for} \quad \boldsymbol{R}\boldsymbol{p} < 0 \text{ for any } \alpha \text{ and } t > 0. \tag{51}$$

Equation 49 is known as the Boltzmann-Uehling-Uhlenbeck equation (BUU-equation). It was proposed by Uehling and Uhlenbeck[10] as a generalization of the Boltzmann equation, which takes into account the Pauli exclusion principle. The BUU-equation is extensively used in quantum statistical mechanics. In recent years, a great number of papers* devoted to various aspects of the application of this equation to the theory of NRs at intermediate and high energies (however, mainly to the case of the heavy ion interactions) have been published. Deprived of the possibility of even listing them, we would like to cite several reviews[13-17] in which

* In these papers, it is often called the Boltzmann equation,[7] the Vlasov-Uehling-Uhlenbeck equation,[11] the Landau-Vlasov equation,[12] etc.

special attention has been paid to the derivation and discussion of this equation. We shall return to this issue in section 5C.

Similar to Equation 19, the BUU-equation can be reduced to a purely integral equation (only of the type of Equation 31 at $i = 1$, since its collision term is essentially nonlinear in f).

B. LINEARIZATION OF THE BUU-EQUATION

The BUU-equation is linearized within framework of macroapproximation (see Section IIG). Let us recall that in this approximation the interaction of excited nucleons with one another and with holes in the distribution of unexcited nucleons, as well as the interaction of holes with one another, is neglected. Hence, if instead of f, we shall introduce the function

$$\varphi(\alpha,\mathbf{x},t) = \Theta[p - p_{F,\alpha}(\boldsymbol{r})]\, f(\alpha,\mathbf{x},t) + \Theta[p_{F,\alpha}(\boldsymbol{r}) - p][1 - f(\alpha,\mathbf{x},t)] \quad (52)$$

(which has the meaning of the distribution function of nucleons for $p > p_{F,\alpha}$ and that of holes for $p < p_{F,\alpha}$), then according to this approximation the collision term is linear in φ. Hence, in this approximation, we can consider the behavior of not only excited nucleons, but also of holes in the distribution of unexcited nucleons (confining ourselves, however, only to the processes of the degradation of energy of separate excited nucleons and holes). However, to avoid cumbersome expressions we shall consider here, as well as in Section IIG, only excited nucleons. Discarding the terms of the second and higher orders in f for excited nucleons and neglecting the existence of the holes below the Fermi energy in Equation 49, we obtain the following linear system of kinetic equations (KEs) for the function f_α:

$$\begin{aligned}
&\left(\frac{\partial}{\partial t} + v\frac{\partial}{\partial \boldsymbol{r}} - \frac{\partial V_\alpha}{\partial \boldsymbol{r}}\frac{\partial}{\partial \boldsymbol{p}}\right) f_\alpha = \frac{1}{4\pi^3\hbar^3}\int d\boldsymbol{p}'d\boldsymbol{p}''d\boldsymbol{p}''' \times \\
&\times f'_\alpha[2w_{\alpha\alpha}(\boldsymbol{p}',\boldsymbol{p}'' \to \boldsymbol{p},\boldsymbol{p}''')\,\Theta(p_{F,\alpha} - p'')\,\Theta(p''' - p_{F,\alpha}) + w_{\alpha-\alpha}(\boldsymbol{p}',\boldsymbol{p}'' \to \boldsymbol{p},\boldsymbol{p}''') \times \\
&\times \Theta(p_{F,-\alpha} - p'')\,\Theta(p''' - p_{F,-\alpha})] + f'_{-\alpha}w_{-\alpha\alpha}(\boldsymbol{p}'',\boldsymbol{p}' \to \boldsymbol{p},\boldsymbol{p}''') \cdot \\
&\times \Theta(p_{F,\alpha} - p'')\,\Theta(p''' - p_{F,\alpha}) - f_\alpha \sum_{\alpha'=\pm 1} w_{\alpha\alpha'}(\boldsymbol{p},\boldsymbol{p}''' \to \boldsymbol{p}',\boldsymbol{p}'') \\
&\times \Theta(p_{F,\alpha'} - p''')\,\Theta(p' - p_{F,\alpha})\,\Theta(p'' - p_{F,\alpha'})
\end{aligned} \quad (53)$$

with the initial condition (see Equation 50)

$$f(\alpha,\mathbf{x},0) = 4\pi^2\hbar^3\delta_{\alpha\alpha_0}\int d\boldsymbol{\omega}_0\Theta(-\boldsymbol{\omega}_0,\boldsymbol{p}_0)\frac{|\boldsymbol{\omega}_0\boldsymbol{p}_0|}{p_0}\,\delta(\boldsymbol{p}_0 - \boldsymbol{p})\,\delta(\boldsymbol{R}_0 - \boldsymbol{r}) \quad (54)$$

and the boundary condition in the form of Equation 51 (to simplify the notation the explicit dependence of the Fermi momenta on coordinates is omitted here and in subsequent Equations 58 and 59).

In the Introduction (see also the next section) we have already mentioned that only various cross-sections, i.e., the characteristics of the cascade integrated over time, can be compared with experimental data. These cross-sections are expressed in terms of the integrals of ρ_c or f_α over t from $t=0$ to the instant τ_{cas} which corresponds to the situation when the cascade stage is already completed, and the pre-equilibrium stage has not yet begun. However, as we noted above, the description of the pre-equilibrium stage within the framework of the macroapproximation is not correct. In accordance with this we can set $\tau_{cas} = \infty$. To derive the system of KEs for the single-particle distribution functions integrated over time let us integrate Equation 53 over t from 0 to ∞. As a result, using the kinetic energy of particles E and the unit vector $\mathbf{\Omega} = \boldsymbol{p}/p$ oriented along the direction of motion as independent variables instead of their momenta, for the functions

$$\Phi_\alpha(\boldsymbol{r},E,\mathbf{\Omega}) \equiv \frac{R^2 v}{4\pi^2\hbar^3}\frac{d\boldsymbol{p}}{dEd\mathbf{\Omega}}\int_0^\infty dt f(\alpha,x,t) \tag{55}$$

we get the system of KEs

$$\begin{aligned}\left[\mathbf{\Omega}\frac{\partial}{\partial \boldsymbol{r}} - E\frac{\partial V_\alpha}{\partial \boldsymbol{r}}\mathbf{\Omega}\frac{\partial}{\partial E}\frac{1}{E} + \mu_\alpha(\boldsymbol{r},E)\right]\Phi_\alpha(\boldsymbol{r},E,\mathbf{\Omega}) &= \int d\mathbf{\Omega}'\int_E^{E_0(r)} dE' \\ \times\ [\Phi_\alpha(\boldsymbol{r},E',\mathbf{\Omega}')K_{\alpha\to\alpha}(\boldsymbol{r};\ E',\mathbf{\Omega}' \to E,\mathbf{\Omega}) &+ \Phi_{-\alpha}(\boldsymbol{r},E',\mathbf{\Omega}') \times \\ \times\ K_{-\alpha\to\alpha}(\boldsymbol{r};\ E',\mathbf{\Omega}' \to E,\mathbf{\Omega}] &+ \delta_{\alpha\alpha_0}\delta(E-\epsilon_0)\,\delta(\mathbf{\Omega}-\mathbf{\Omega}_0)\,\delta(z-z_0)\end{aligned} \tag{56}$$

with the boundary condition

$$\phi_\alpha(\boldsymbol{R},E,\boldsymbol{\omega}) = 0 \qquad \text{for} \qquad \mathbf{\Omega}\boldsymbol{R} < 0. \tag{57}$$

Here $E_0(\boldsymbol{r}) = \epsilon_o - V_{\alpha_0}(\boldsymbol{r})$ is the kinetic energy of a primary nucleon at the point $\boldsymbol{r}$ inside the nucleus (ϵ_0 is its kinetic energy outside the nucleus), z and z_o are the projections of the vectors $\boldsymbol{r}$ and $\boldsymbol{R}_0$ onto the direction $\mathbf{\Omega}_0$ of the motion of an incident nucleon, and

$$\begin{aligned}\mu_\alpha(\boldsymbol{r},E) &= \frac{1}{4\pi^3\hbar^3 v}\sum_{\alpha'=\pm 1}\int d\boldsymbol{p}'d\boldsymbol{p}''d\boldsymbol{p}'''w_{\alpha\alpha'}(\boldsymbol{p},\boldsymbol{p}''' \to \boldsymbol{p}',\boldsymbol{p}'') \times \\ &\times\ \Theta(p_{F,\alpha'} - p''')\,\Theta(p' - p_{F,\alpha})\,\Theta(p'' - p_{F,\alpha'}), \\ \times\ K_{\alpha\to\alpha}(\boldsymbol{r}_j E',\mathbf{\Omega}' \to E,\mathbf{\Omega}) &= \frac{1}{4\pi^3\hbar^3 v'}\frac{d\boldsymbol{p}}{dEd\mathbf{\Omega}}\int d\boldsymbol{p}'d\boldsymbol{p}''' \\ &\times\ [2w_{\alpha\alpha}(\boldsymbol{p}',\boldsymbol{p}'' \to \boldsymbol{p},\boldsymbol{p}''')\,\Theta(p_{F,\alpha} - p'')\,\Theta(p''' - p_{F,\alpha}) + \\ &w_{\alpha-\alpha}(\boldsymbol{p}',\boldsymbol{p}'' \to \boldsymbol{p},\boldsymbol{p}''')\,\Theta(p_{F,\alpha} - p'')\,\Theta(p''' - p_{F,\alpha})],\end{aligned} \tag{58}$$

$$K_{-\alpha\to\alpha}(r;\, E',\Omega' \to E,\Omega) = \frac{1}{4\pi^3\hbar^3 v'}\frac{dp}{dEd\Omega}\int dp''dp''' \times$$
$$\times\, w_{-\alpha\alpha}(p'',p' \to p,p''')\, \Theta(p_{F,\alpha} - p'')\, \Theta(p''' - p_{F,-\alpha\alpha})\,. \tag{59}$$

In Chapter 2 we shall use these formula to carry out analytic calculations of inclusive cross-sections of nucleon-nuclear reactions.

IV. CHARACTERISTICS OF NRS

A. PRELIMINARY REMARKS

It has already been mentioned that a branched inelastic process initiated by an intermediate-energy particle splits into three stages: the fast cascade stage proceeding during a time interval τ_{cas}, the stage of pre-equilibrium emission which lasts during $\tau_{eq} \approx (5\text{-}10)\tau_{cas}$, and the evaporation stage, whose duration is larger by several orders of magnitude. In experiments, it is presently impossible to separate these processes in time (except possibly for the final evaporation stage). The measurable quantities are various cross-sections which are expressed in terms of the integrals of the fluxes of outgoing particles over time. However, the fluxes of particles formed at different stages of an NR can be distinguished by their energy and angular distributions. The cascade stage is characterized by high-energy nucleons flying mostly forward. Nucleons of the pre-equilibrium stage have considerably lower energies and their angular distribution is close to the isotropic distribution. The same holds true to even a greater extent for evaporating nucleons. Since the analysis of various stages of the process calls for different approaches, it is expedient to represent the expressions for the cross-sections in terms of integrals over appropriate time intervals. Thus, in the expressions for the cross-sections given below, the cascade is characterized by the time interval from $t_i = 0$ to $t_f = \tau_{cas}$ (in the macroapproximation $t_i = 0$ and $t_f = \infty$) and the pre-equilibrium stage by the interval ($t_i = \tau_{cas}$ $t_f = \tau_{eq}$). The INC-model offers one of the possibilities for description of the latter stage as well (see Section IE in Chapter 2). Formally, evaporation takes place in the interval from $t_i = \tau_{eq}$ to $t_f = \infty$. However, the INC-model is inapplicable for its description.

The expressions for the cross-sections can be derived, if we take into account the fact that by definition the probability of the event in which the j-th particle with the momentum $\boldsymbol{p}$ lying in the interval $d\boldsymbol{p}$ of the momentum space crosses the unit surface area perpendicular to the unit vector $\boldsymbol{\omega}$ at the point $\boldsymbol{R}$ during the time interval dt is equal to

$$dP_t(j) = dt\,d\boldsymbol{p}\int d\mathbf{X}\, \rho_c\,(\mathbf{X},t)\, \delta(\boldsymbol{r}_j - \boldsymbol{R})\, \delta(\boldsymbol{p}_j - \boldsymbol{p})\, \frac{|\boldsymbol{\omega p}|}{m_N}. \tag{60}$$

In the subsequent analysis, it is convenient to make use of the quantities

$$\bar{\rho}(\mathbf{x}_j,\mathbf{x}_{j'}, \ldots; j_1, \ldots, j_n; t) = \int \left\{ \prod_{\substack{1 \le i \le A+1 \\ i \ne j, j', \ldots, j_1, \ldots, j_n}} d\mathbf{x}_i \Theta(R - r_i) \right\} \times \\ \times d\mathbf{x}_{j_1} \ldots d\mathbf{x}_{j_n} \rho_c(\mathbf{X},t) \tag{61}$$

which have the meaning of the phase density of the j-th, j′-th,...nucleons under the condition that at the instant t the location of the j_1-th,..., j_n-th nucleons is uncertain, whereas the remaining nucleons are inside the nucleus *a priori*. In particular, $\bar{\rho}$ (j_1,..., j_n;t) (integration is carried out over the coordinates and momenta of all nucleons) is the probability of the state in which at the instant t all nucleons, excepts for the j_1-th,..., and j_n-th, are inside the nucleus, and the coordinates of the remaining ones are arbitrary. Hence $\bar{\rho}$ (t) is the probability of the state in which all nucleons are inside the nucleus. The probability of the event in which by the instant t one and only one j-th nucleon has left a nucleus is expressed in terms of these quantities in the form

$$P_t(j) = \bar{\rho}(j;t) - \bar{\rho}(t). \tag{62a}$$

The probability of the event that only j-th and j′-th nucleons have left a nucleus by the instant t is given by

$$P_t(j,j') = \bar{\rho}(j,j';t) - P_t(j) - P_t(j') - \bar{\rho}(t) = \\ \bar{\rho}(j,j';t) - \bar{\rho}(j;t) - \bar{\rho}(j';t) + \bar{\rho}(t) \tag{62b}$$

and so on. The quantities $\bar{\rho}(j_1,\ldots, j_n;t)$, in their turn, can be expressed in terms of the integrals of the flux densities of nucleons through the surface of the nucleus and, finally, in terms of $\bar{\rho}$ ($\mathbf{x}_j,\mathbf{x}_j'$,...;$j_1$,..., j_n;t). Namely, according to Equation 52 in the Introduction we get

$$\frac{\partial}{\partial t} \bar{\rho}(j_1, \ldots, j_n;t) = - \sum_{\substack{1 \le j \le A+1 \\ j \ne j1, \ldots, jn}} \int \left\{ \prod_{\substack{1 \le i \le A+1 \\ i \ne j1, \ldots, jn}} d\mathbf{x}_i \Theta(R - r_i) \right\} \times \\ \times d\mathbf{x}_{j_1} \ldots d\mathbf{x}_{jn} \left(\boldsymbol{v}_j \frac{\partial \rho_c}{\partial \boldsymbol{r}_j} - \frac{\partial V_j}{\partial \boldsymbol{r}_j} \frac{\partial \rho_c}{\partial \boldsymbol{p}_j} \right). \tag{63}$$

Here the integrals of the second term in round brackets vanish after the integration over $\boldsymbol{p}_j$. The same holds true for the first term after the integration over $\boldsymbol{r}_j$, if j coincides with one of the values j_1,...,j_n. Taking into account the condition that, $\bar{\rho}(j_1,\ldots, j_n;0) = 1$, transforming the volume integral into the surface one and integrating over time, for the remaining terms of the sum we obtain

$$\bar{\rho}(j_1, \ldots, j_n;t) = 1 - R^2 \sum_{\substack{1\le j\le A+1\\ i\ne j_1,\ldots,j_n}} \int dp_j d\omega(v_j\omega_j) \times \\ \times \int_0^t dt'\bar{\rho}(\boldsymbol{R},\boldsymbol{p}_j;j_1, \ldots, j_n;t') \tag{64}$$

($\omega = \boldsymbol{R}/R$). The function $\bar{\rho}$ $(\boldsymbol{R},\boldsymbol{p}_j;j_1,\ldots, j_n;t)$, in its turn, can be represented here in terms of the flux densities of nucleons with the help of the relation

$$\left(\frac{\partial}{\partial t} + v_j \frac{\partial}{\partial \boldsymbol{r}_j} - \frac{\partial V_j}{\partial \boldsymbol{r}_j}\frac{\partial}{\partial \boldsymbol{p}_j}\right) \bar{\rho}(\mathbf{x}_j;j_1, \ldots, j_n;t) = \\ \sum_{\substack{1\le i\le A+1\\ i\ne j,j_1,\ldots,j_n}} \int d\omega dp_i(\omega v_i)\, \bar{\rho}(\mathbf{x}_j,\mathbf{x}_i;j_1, \ldots, j_n;t)_{r_i=R} \tag{65}$$

and so on. This allows us to relate the partial probabilities of the escape of the nucleons P_t (j), $P_t(j,j')$, etc., to differential momentum distributions, and to the coordinates of the escape points.

Thus, the cross-sections of various processes and characteristics of NRs associated with them can be expressed in terms of the quantities $\bar{\rho}$. Below we shall give the expressions for some of them which are of practical interest.

B. TOTAL CROSS-SECTION OF INELASTIC INTERACTION

Within the framework of the outlined approach the expression for the total cross-section of inelastic NA-interaction in accordance with Equation 2 of the Introduction can be represented in the form

$$\sigma^{in} = R^2 \int d\omega_0 \Theta(-\omega_0 p_0) \frac{|\omega_0 p_0|}{p_0} P_{\alpha_0}(\boldsymbol{R}_0,\boldsymbol{p}_0) \tag{66}$$

where $P_{\alpha_0}(\boldsymbol{R}_0,\boldsymbol{p}_0)$ is the probability of the event in which an α-nucleon which has entered the nucleus at the point $\boldsymbol{R}_0$ with the momentum $\boldsymbol{p}_0$ undergoes a collision earlier than reaches the boundary of the nucleus again and $\boldsymbol{\omega}_0 = \boldsymbol{R}_0/R$. Hence taking into account Equation 43, we readily obtain

$$P_{\alpha_0}(\boldsymbol{R}_0,\boldsymbol{p}_0) = 1 - \exp\{-W_{A+1}[0;\boldsymbol{R}(\boldsymbol{R}_0,\boldsymbol{p}_0), \boldsymbol{p}(\boldsymbol{R}_0,\boldsymbol{p}_0), \tau(\boldsymbol{R}_0,\boldsymbol{p}_0)]\} \tag{67}$$

where $\boldsymbol{R}(\boldsymbol{R}_0,\boldsymbol{p}_0)$ is the point on the nucleus boundary at which this nucleon would leave the nucleus, if it had not experienced the collision, $\boldsymbol{p}$ $(\boldsymbol{R}_0,\boldsymbol{p}_0)$ the value of its momentum at the instant of its escape and $\tau(\boldsymbol{R}_0,\boldsymbol{p}_0)$ the time during which it passes through the nucleus. To evaluate the function W_{A+1} one can make use of Equation 44.

On the other hand the quantity σ^{in} can be measured in experiments and/or calculated by quantum-mechanical methods outlined in the Introduction. Since the

calculation of σ^{in} by classical methods is often incorrect, it is sometimes expedient to use experimental data or results of quantum-mechanical calculations for the total cross-section of inelastic interaction and to treat Equation 66 as a normalization coefficient in calculations of partial cross-sections of separate processes. However this circumstance is not taken into account in Equations 68 through 73 which are presented below.

C. TOPOLOGICAL AND EXCLUSIVE CROSS-SECTIONS

The partial cross-section of the escape of only one j-th nucleon during a time interval (t_i,t_f) can be represented in the form (here and in what follows the dependence of cross-sections on t_i and t_f, as well as the composition of initial and/or final participants of the NR, is omitted for the sake of simplicity if it does not lead to misunderstanding)

$$\sigma(j) = \pi R^2[P_{t_f}(j) - P_{t_i}(j)] \tag{68}$$

According to Equations 60, 62a, and 64, the double differential cross-section of this process has the form

$$\begin{aligned} \frac{d\sigma(j)}{d\boldsymbol{p}_j} &= \pi R^4 \int_{t_i}^{t_f} dt \left[1 - \sum_{1\le(j'\neq j)\le A+1} \gamma_t(t',j) \right] \times \\ &\int d\boldsymbol{\omega}(\boldsymbol{v}_j\boldsymbol{\omega})\bar{\rho}(\boldsymbol{R},\boldsymbol{p}_j;t) \\ \gamma_t(j',j) &= \frac{1}{\int d\boldsymbol{p}_j d\boldsymbol{\omega}(\boldsymbol{v}_j\boldsymbol{\omega})\bar{\rho}(\boldsymbol{R},\boldsymbol{p}_j;t)} \times \\ &\int d\boldsymbol{p}_{j'} d\boldsymbol{\omega}'(\boldsymbol{v}_{j'}\boldsymbol{\omega}'_j)[\bar{\rho}(\boldsymbol{R}',\boldsymbol{p}_j;t) - \bar{\rho}(\boldsymbol{R}',\boldsymbol{p}_{j'};t)] \end{aligned} \tag{69}$$

The topological $\sigma(\alpha)$ and the exclusive $d\sigma^{excl}(\alpha)/d\boldsymbol{p}$ cross-section of the escape of one α-nucleon are obtained by means of the appropriate summation of these expressions

$$\sigma(\alpha) = \sum_{1\le j\le A+1} \delta_{\alpha\alpha_j}\sigma(j), \quad \frac{d\sigma^{excl}(\alpha)}{d\boldsymbol{p}} = \sum_{1\le j\le A+1} \delta_{\alpha\alpha_j} \frac{d\sigma(j)}{d\boldsymbol{p}_j}\bigg|_{\boldsymbol{p}_j = \boldsymbol{p}} \tag{70}$$

The partial cross-section of the escape of two (the j-th and the j′-th nucleon) and only two nucleons is given by

$$\sigma(j,j') = \pi R^2[P_{t_f}(j,j') - P_{t_i}(j,j')] \tag{71}$$

where $P_t\,(j,j')$ is determined by Equation 62b.

The topological cross-sections for the escape of two nucleons of the same type $\sigma(\alpha,\alpha)$ and that for nucleons of different types $\sigma(\alpha,-\alpha)$ are defined by the formula

$$\sigma(\alpha, \pm \alpha) = \frac{1}{2} \sum_{1 \le (j' \ne j) \le A+1} \delta_{\alpha\alpha_j} \delta_{\pm\alpha\alpha_{j'}} \sigma(j,j') \tag{72}$$

Using Relation 65 two times, we can obtain the corresponding exclusive cross-sections for the escape of two nucleons. However, these expressions are very cumbersome, and for this reason we do not write them down explicitly. In a similar way, we can find the expressions for more complex cross-sections as well and obtain the correlation characteristics of NRs which are expressed in terms of appropriate cross-sections.

D. INCLUSIVE CROSS-SECTIONS

According to Equations 16, 48, and 60 the inclusive differential cross-section for the escape of α-nucleons is expressed in terms of the flux density $\nu\Psi_\alpha(\boldsymbol{x},t)$ of such nucleons. As follows from its definition (see Section II of the Introduction), this cross-section can be represented in the form

$$\frac{d\sigma_\alpha}{d\boldsymbol{p}} = \pi R^4 \int d\omega(\omega\nu)\, \Theta(\omega\nu) \int_{t_i}^{t_f} dt\, \Psi_\alpha(\boldsymbol{R},\boldsymbol{p},t) \tag{73}$$

In the macroapproximation, going over from the momenta of secondary nucleons to the variables which are more widely used, namely the energy ϵ and the direction $\boldsymbol{\Omega}$ of the escape of a nucleons, according to Equations 55 and 73 we get

$$\frac{d\sigma_\alpha}{d\epsilon d\boldsymbol{\Omega}} = R^2 \int d\omega(\omega\boldsymbol{\Omega})\, \Theta(\omega\boldsymbol{\Omega})\, \Phi_\alpha(\boldsymbol{R},\epsilon,\boldsymbol{\Omega}). \tag{73a}$$

The inclusive partial cross-section $\sigma(\alpha)$ for the escape of α-nucleons is equal to integrals of these expressions over momenta (energies and angles) of outgoing nucleons.

Finally, according to Section II in the Introduction, the average multiplicity of α-nucleons can be found as the ratio $\sigma_\alpha/\sigma^{in}$.

E. DISTRIBUTION OF NUCLEI PRODUCED IN THE CASCADE OVER THE NUMBER OF NEUTRONS AND PROTONS, EXCITATION ENERGY, MOMENTUM, AND ANGULAR MOMENTUM

Knowing the exclusive (and topological) cross-sections of various NRs, we can determine the distributions* of R-nuclei over the number of protons Z and neutrons

* As well as the cross-sections of the processes considered above, these quantities depend, of course, on the energy and the type of an incident nucleon and the number of neutrons and protons in a target nucleus (T-nucleus). However, for the sake of simplicity, it is not indicated in the formulas we present here.

N, over the recoil momentum $\boldsymbol{p}_r$, and over the excitation energy E* which are denoted by P(Z,N), P($\boldsymbol{p}_r$) and P (E*) respectively. The following obvious relations are valid:

$$
\begin{aligned}
P(Z,N) &= \sigma(Z,N)/\sigma^{in}, \\
P(\boldsymbol{p}_r) &= \frac{1}{\sigma^{in}} \sum_{\{n\}} \int d\boldsymbol{p}_1 \ldots d\boldsymbol{p}_n \frac{d^{3n}\sigma(\boldsymbol{p}_1,\ldots,\boldsymbol{p}_n)}{d\boldsymbol{p}_1 \ldots d\boldsymbol{p}_n} \delta(\boldsymbol{p}_0 - \boldsymbol{p}_r - \sum_{1\le k\le n} \boldsymbol{p}_k), \\
P(E^*) &= \frac{1}{\sigma^{in}} \sum_{\{n\}} \int d\boldsymbol{p}_1 \ldots d\boldsymbol{p}_n \frac{d^{3n}\sigma(\boldsymbol{p}_1,\ldots,\boldsymbol{p}_n)}{d\boldsymbol{p}_1 \ldots d\boldsymbol{p}_n} \times \\
&\times \delta\left[\epsilon_0 - E^* - E_{bt} + E_b - \epsilon(\boldsymbol{p}_r) - \sum_{1\le k\le n} \epsilon_{\alpha_k}(\boldsymbol{p}_k)\right].
\end{aligned}
\tag{74}
$$

Here σ (Z,N) is the topological cross-section for production of an R-nucleus containing Z protons and N neutrons, the symbol {n} denotes an arbitrary set of reaction channels with the escape of n nucleons, $d^{3n}\sigma\ (\boldsymbol{p}_i,\ldots,\boldsymbol{p}_n)/d\boldsymbol{p}_1\ldots d\boldsymbol{p}_n$ is the exclusive differential cross-section for the escape of nucleons with the momenta $\boldsymbol{p}_1,\ldots,\boldsymbol{p}_n$ respectively, $\epsilon_{\alpha_k}(p_k)$ the kinetic energy of the nucleon of the type α_k which leaves the nucleus with the momentum $\boldsymbol{p}_k$, $\epsilon(\boldsymbol{p}_r)$ the recoil energy of an R-nucleus with the momentum $\boldsymbol{p}_r = \boldsymbol{p}_0 - \sum_{i\le k\le n} \boldsymbol{p}_k$ and E_{bt} and E_b are the binding energies of a T-nucleus and an R-nucleus in the ground state, respectively.

Distribution P ($\boldsymbol{I}$) of R-nuclei over the values of the angular momentum $\boldsymbol{I}$ can be obtained similarly to their momentum distribution, if we shall use Equation 61 as a starting point and take into account the fact that at $\boldsymbol{r}_j = \boldsymbol{R}_{j'}$, $\boldsymbol{r}_j, = \boldsymbol{R}_{j'},\ldots$ these expressions describe the flux densities of outgoing nucleons as functions of momenta $\boldsymbol{p}_j,\boldsymbol{p}_{j'},\ldots$ and coordinates $\boldsymbol{R}_j,\boldsymbol{R}_{j'},\ldots$ of the points of escape. Hence, being multiplied by $\delta(\boldsymbol{l}_j - [\boldsymbol{R}_j \times \boldsymbol{p}_j])$ and integrated over $\boldsymbol{R}_j$ and $\boldsymbol{p}_j$, they determine the probability of the escape of the j-th nucleon with the angular momentum $\boldsymbol{l}_j$. However, we must be aware of the inconsistency of such an approach, which, being purely classical, cannot correctly take into account the effects associated with the existence of the spin of a T-nucleus and of outgoing nucleons.

V. TAKING ACCOUNT OF QUANTUM EFFECTS IN THE INC-MODEL

A. DENSITY MATRIX—QUANTUM LIOUVILLE-VON NEUMANN EQUATION

So far we considered the INC within the framework of classical concepts. Quantum effects were partially taken into account with help of ad hoc assumptions introduced artificially: 1) the initial distribution of nucleons in a nucleus over coordinates and momenta is stationary and described by a quantum mechanical model of noninteracting particles (usually by the local Fermi gas model); and 2) final states of nucleons colliding in a nucleus with one another obey the constraints imposed by the Pauli exclusion principle. In the present section we shall demonstrate

that results obtained above can be derived on the basis of the quantum-mechanical formulation of the problem of the NA-collision within the framework of certain approximations,. We shall also discuss the validity range of these approximations and the possibility of taking into account corrections.

The quantum analogue of the phase density is the density matrix $\hat{\rho}_q(\mathbf{R},\mathbf{R}',t)$, where $\mathbf{R}$ is the set of independent commuting dynamical variables characterizing the system (see Section IVB in the Introduction). In the case under consideration, $\mathbf{R} \equiv (\boldsymbol{r}_1,\ldots, \boldsymbol{r}_{A+1})$ is the set of the variables $\boldsymbol{r}_1,\ldots, \boldsymbol{r}_{A+1}$ (we disregard the effects associated with the spin of nucleons). It has been pointed out in the Introduction (see Equation 55 there) that, if at the instant t the probability of finding the system in the state characterized by the wave function $\Psi_n(\mathbf{R},t)$ (normalized to unity) is equal to g_n, the density matrix can be represented in the form

$$\hat{\rho}_q(\mathbf{R},\mathbf{R}',t) = \sum_n g_n \Psi_n(\mathbf{R},t) \Psi_n^*(\mathbf{R}',t), \qquad \sum_n g_n = 1. \tag{75}$$

Here the domain of the values of n can contain both a discrete and a continuous part. In the latter case, the symbol Σ_n has the meaning of an appropriate integral.

Basic properties of $\hat{\rho}_q$ are described in the Introduction. As well as in the classical approach, average values of quantum-mechanical dynamical quantities are expressed in terms of $\hat{\rho}_q$ (see Equation 60 in the Introduction). The density matrix satisfies the Liouville-von Neumann Equation 61 in the Introduction, which uniquely determines its time evolution, if the value of the density matrix is preset at a certain initial instant.

B. TRANSFORMATION OF THE LIOUVILLE-VON NEUMANN EQUATION TO THE FORM CLOSE TO THE CLASSICAL ONE

It has already been mentioned that the similarity between the classical and the quantum-statistical approach to the description of dynamical systems is manifested with utmost clarity, if the Wigner probability function (WPF; see Section IV.C in the Introduction) is used. To go over to it we shall write Equation 61 of the Introduction with regard for Equation 75 in the following form:

$$\frac{\partial \hat{\rho}_q}{\partial t} = \frac{i}{\hbar} \sum_n g_n \{\Psi_n(\mathbf{R},t)\hat{H}(\mathbf{R}') \Psi_n^*(\mathbf{R}',t) - \Psi_n^*(\mathbf{R}',t) \hat{H}(\mathbf{R}) \Psi_n(\mathbf{R},t)\}. \tag{76}$$

Let here $\hat{H}$ be a quantum-mechanical analogue of the Hamiltonian 47 of the Introduction for the system of A + 1 spinless nucleons under consideration, i.e., it has the form

$$\hat{H}(\mathbf{R}) = - \sum_{i\le j\le A+1} \frac{\hbar^2}{2m_N} \frac{\partial^2}{\partial \boldsymbol{r}_j^2} + \frac{1}{2} \sum_{1\le (j'\ne j)\le A+1} V_{jj'}(|\boldsymbol{r}_j - \boldsymbol{r}_{j'}|). \tag{77}$$

Then according to Equation 62 in the Introduction, the WPF is expressed for it in terms $\hat{\rho}_q(\mathbf{R},\mathbf{R}',t)$ in the form

$$\rho_w(\mathbf{X},t) = \frac{1}{(\pi,\hbar)^{3(A+1)}} \int dy_1 \ldots dy_{A+1} \times$$
$$\times \exp\left\{\frac{2i}{\hbar}(\boldsymbol{p}_1 \boldsymbol{y}_1 + \ldots + \boldsymbol{p}_{A+1}\boldsymbol{y}_{A+1})\right\} \times \tag{78}$$
$$\times \hat{\rho}_q(\boldsymbol{r}_1 - \boldsymbol{y}_1, \ldots, \boldsymbol{r}_{A+1}\boldsymbol{y}_{A+1} - ;\boldsymbol{r}_1 + \boldsymbol{y}_1, \ldots, \boldsymbol{r}_{A+1} + \boldsymbol{y}_{A+1};t).$$

Here, as in Section IIA, $\mathbf{X} = (\ldots,\mathbf{X}_j,\ldots)$ is the set of coordinates and momenta of all particles. The equation for the WPF is obtained after the substitution of $\boldsymbol{r}_j \pm \boldsymbol{y}_j$ for $\boldsymbol{r}'_j$ (+) and $\boldsymbol{r}_j$ (−) in Equation 76, multiplication of the resultant equation by $(\pi\hbar)^{-3(A+1)} \exp[2i(\ldots + \boldsymbol{p}_j\boldsymbol{y}_j + \ldots)/\hbar]$ and integration over all $\boldsymbol{y}_j$. As a result we get

$$\frac{\partial}{\partial t}\rho_w(\mathbf{X},t) = I_1 + I_2, \tag{79}$$

$$I_1 = \sum_n g_n \frac{1}{(\pi\hbar)^{3(A+1)}} \int \ldots dy_j \ldots \exp\left[\frac{2i}{\hbar}(\ldots + \boldsymbol{p}_j\boldsymbol{y}_j + \ldots)\right] \times$$
$$\times \sum_{1\le j\le A+1} \frac{i\hbar}{2m_N}\left\{\Psi^*(\ldots, \boldsymbol{r}_j + \boldsymbol{y}_j, \ldots;t) \cdot \frac{\partial^2}{\partial \boldsymbol{r}_j^2}\Psi(\ldots, \boldsymbol{r}_j - \boldsymbol{y}_j, \ldots;t)\right. \tag{80}$$
$$\left. - \Psi(\ldots, \boldsymbol{r}_j - \boldsymbol{y}_j, \ldots;t)\frac{\partial}{\partial^2 \boldsymbol{r}_j}\Psi^*_n(\ldots, \boldsymbol{r}_j + \boldsymbol{y}_j, \ldots;t)\right\},$$

$$I_2 = \sum_n g_n \frac{i}{\hbar(\pi\hbar)^{3(A+1)}} \int \ldots dy_j \ldots \exp\left[\frac{2i}{\hbar}(\ldots + \boldsymbol{p}_j\boldsymbol{y}_j + \ldots)\right] \times$$
$$\times \Psi^*_n(\ldots, \boldsymbol{r}_j + \boldsymbol{y}_j, \ldots;t)\,\Psi(\ldots, \boldsymbol{r}_j - \boldsymbol{y}_j, \ldots;t) \cdot \times \tag{81}$$
$$\frac{1}{2}\sum_{1\le(j'\ne j)\le A+1} \times \{V_{jj'}(\boldsymbol{r}_j + \boldsymbol{y}_j - \boldsymbol{r}_{j'} - \boldsymbol{y}_{j'}) - V_{jj'}(\boldsymbol{r}_j - \boldsymbol{y}_j - \boldsymbol{r}_{j'} + \boldsymbol{y}_{j'})\}$$

Carrying out the integration by parts in Equation 80, we can reduce the integral I_1 to the form

$$I_1 = -\sum_{1\le j\le A+1} \frac{\boldsymbol{p}_j}{m_N}\frac{\partial \rho_w}{\partial \boldsymbol{r}_j} \tag{82}$$

which coincides with the second sum in Equation 52 in the Introduction. The integral I_2 is reduced to the expression coinciding with the first sum in that equation in the limiting case $\hbar \to 0$. This can be demonstrated by expanding the terms in the braces in the integrand of the expression in Equation 81 in the Taylor series in the components of $\boldsymbol{y}_i$. Indeed, the first nonvanishing term of such an expansion coincides with the first sum in Equation 52 in the Introduction (if we set $\rho_c = \rho_w$). The discarded terms are proportional to $\hbar^2$, to third derivatives of ρ_w with respect to

the components of momenta and of $V_{jj'}$ with respect to coordinates, and to the derivatives of higher orders. Thus, Equation 79 is reduced to the classical Liouville equation under the condition that $V_{jj'}$ varies only slightly at the distances of the order of the wavelength of interacting particles, the role of ρ_c being played by ρ_W.

However the actual NN-interaction contains sharply varying short-range parts for which this condition is not satisfied. Therefore, as well as in the classical case (see Section IIA), we separate this part ($V^{sh}_{jj'}$) from the potential in Equation 77 in the form of V. We shall deem that the remaining long-range parts $V^{\ell}_{jj'}$ add up to give the effective fields $V_j(\boldsymbol{r}_j)$, which are slowly varying functions of coordinates of the j-th nucleon, so that for them Equation 81 is reduced to a good accuracy to the second sum in Equation 52 in the Introduction. Thus, the terms of the Hamiltonian (Equation 77) corresponding to the kinetic energy and to the long-range part of the NN-potential form the quantity coinciding with the streaming term in Equation 3 as well as in the case corresponding to the validity range of classical physics. As for the collision term, it is determined by the integral

$$\begin{aligned} I_2 = {} & \frac{i}{\hbar}\frac{1}{(\pi\hbar)^{3(A+1)}}\sum\nolimits_n g_n \int \ldots d\boldsymbol{y}_j \ldots \exp\left[\frac{2i}{\hbar}(\ldots + \boldsymbol{p}_j\boldsymbol{y}_j + \ldots)\right] \times \\ & \times \Psi^*_n(\ldots, \boldsymbol{r}_j + \boldsymbol{y}_j, \ldots, \boldsymbol{r}_{j'} + \boldsymbol{y}_{j'}, \ldots; t) \times \\ & \cdot \frac{1}{2}\sum_{1\le(j'\ne j)\le A+1}\{V^{sh}_{\alpha_j\alpha_{j'}}(\boldsymbol{r}_j + \boldsymbol{y}_j - \boldsymbol{r}_{j'} - \boldsymbol{y}_{j'}) - V^{sh}_{\alpha_j\alpha_{j'}}(\boldsymbol{r}_j - \boldsymbol{y}_j - \boldsymbol{r}_{j'} + \boldsymbol{y}_{j'})\} \cdot \\ & \times \Psi(\ldots, \boldsymbol{r}_j - \boldsymbol{y}_j, \ldots, \boldsymbol{r}_{j'} - \boldsymbol{y}_{j'}, \ldots; t) \end{aligned} \tag{83}$$

It was shown by Wigner[18], that this term can be recast into the form that bears even closer resemblance to the classical collision term. Namely, as applied to our case, we get

$$\begin{aligned} I_2 = {} & \frac{1}{\pi^3\hbar^4}\sum_{1\le(j'\ne j)\le A+1}\int d\boldsymbol{p}'_j d\boldsymbol{p}'_{j'} U_{jj'}(\boldsymbol{p}'_j - \boldsymbol{p}_j, \boldsymbol{p}'_{j'} - \boldsymbol{p}_{j'}, \boldsymbol{r}_{j'} - \boldsymbol{r}_j)\rho_W[X(\boldsymbol{p}'_j, \boldsymbol{p}'_{j'}), t], \\ U_{jj'}(\boldsymbol{q}, \boldsymbol{q}', \boldsymbol{r}) = {} & \delta(\boldsymbol{q} + \boldsymbol{q}')\int d\boldsymbol{y} V^{sh}_{\alpha_j\alpha_{j'}}(\boldsymbol{r} + \boldsymbol{y})\sin\left[\frac{2}{\hbar}\boldsymbol{y}(\boldsymbol{q}' - \boldsymbol{q})\right] \end{aligned} \tag{84}$$

(compare with Equation 12). This makes it possible to obtain the equation for ρ_W in the closed form.

It has been pointed out in Section I that the INC-model is based on the assumption that a collision of a pair of particles takes place in the domain whose dimensions are small, as compared to the mean free path L of nucleons in a nucleus, and the collision time is small, as compared to the time interval τ between subsequent collisions. If these assumptions are satisfied, we can believe that within the framework of classical concepts collisions of particles in a nucleus proceed in the same way as those of free ones. It is obvious, however, that, if quantum mechanical effects are taken into account, this assumption is valid only if the condition $L \gg \hbar/\Delta p$, $\tau \gg \hbar/\Delta E$, where Δp and ΔE are the mean momentum and energy transferred in a collision, is satisfied. Then we can treat collisions in a manner similar to that

employed in Section II, but considering it within the framework of quantum mechanics, e.g., by means of the methods outlined in the Introduction (see Section IIID). A consistent approach based on the method of the BBGKY-hierarchy which is widely used in quantum statistical mechanics leads to the same result, and the same is true for the use of Equation 84.[19]

C. VALIDITY CONDITIONS OF THE INC-MODEL

The mean distance δ between nucleons in a nucleus is about 1.2-1.3 fm. the effective radius r_{int} of the strong interaction is the same order of magnitude. On the other hand, owing to the Pauli exclusion principle the mean free path L of nucleons with the energy of several tens or hundreds of MeV in a nucleus is sufficiently large ($L \approx 3$ fm at $E = 50$ MeV) and varies only slightly with energy. The de Broglie wavelength $\lambda\!\!\!^{-}$ of such nucleons is small ($\lambda\!\!\!^{-} \approx 0.6$ fm for $E = 50$ MeV). Therefore, one may hope that, for a cascade initiated by nucleons whose energy lies in this range, the validity conditions of the INC-model are satisfied reasonably well. However, as the energy of nucleons increases, the processes involving other particles, primarily pions, begin to play a more prominent role, and there arises a problem of validity of the INC-model for such more complex processes.

This problem will be briefly discussed in the end of this section. Here we shall restrict our consideration to a purely nucleonic cascade, since there are certain unsettled points even in this case. Indeed, we have demonstrated that the cascade can be described by quantum-mechanical methods with the help of the WPF, which under reasonable assumptions satisfies the equation having the form close to the classical one. However, the following questions have not yet been elucidated: 1) the error of approximations used in the derivation of the streaming term from Equation 81; 2) the initial condition for the equation for ρ_W; and 3) the specific form of the collision term for collisions inside a nucleus. Let us consider these issues at greater length.

The nuclear field V_α affects the motion of particles mainly near the boundary of a nucleus. Therefore, in the NA-interactions at intermediate energies, it can be manifested noticeably in two ways: 1) in the elastic scattering of an incident particle and (to a lesser extent) in a quasifree knockout of fast nucleons from a nucleus, when a prominent role is played by the interference of waves scattered by different points of the boundary; and 2) in the spectra of secondary nucleons of relatively low energies when their wavelength outside the nucleus becomes comparable to an effective size characterizing the diffuseness of the nuclear surface (e.g., to the parameter of diffuseness in the optical potential). A consistent analysis of the interference effects at the initial stage of the cascade is possible on the basis of the OC-model.[20,21]

According to this model the elastic passage of an incident particle through a nucleus (i.e., the process in which quantum-mechanical effects are conspicuous) and, if required, transitions to certain inelastic channels are described within the framework of quantum mechanics, e.g., with the help of the optical model or the Glauber-Sitenko model (see Sec. III.D in the Introduction). An escape from these channels is related to the "sources" of the subsequent classical cascade through

the unitary relations. In Chapters 2 and 4 we shall demonstrate that even a approximate quantum-mechanical treatment of the first collision between an incident and a intranuclear nucleon noticeably improves the agreement of the cascade calculations with experimental data. This is associated with a more rigorous calculation of the results of the first collision experienced by an incident particle in a nucleus. An additional improvement may be because effects caused by quantum uncertainties in the transferred energy and momentum are masked, and because the sources of the classical cascade are averaged over the distribution of products of the first collision.

The following method if often used to improve the calculations of the spectra of secondary nucleons in the domain of low energies. The INC-model calculations is carried out only for the nucleons whose energy is higher than a certain value (called the "cut-off energy" $E_{cut\ off}$). When the escape of such nucleons is completed, an excited R-nucleus is formed which contains several excited nucleons and holes in the distribution of unexcited nucleons. A subsequent emission of nucleons by this nucleus is treated on the basis of the pre-equilibrium and/or the evaporation model. Such an approach is realized, in particular, in the Monte Carlo scheme outlined in Chapter 2, Section II. It should be emphasized that the resultant distributions of secondary nucleons calculated by this technique depend only slightly on the value of $E_{cut\ off}$.[22] In conclusion, it should be noted that corrections to the streaming term can be estimated directly through evaluation of the subsequent nonvanishing terms of expansion of the integral in Equation 81 in y_i or from Equation 84.

The problem of the initial condition for the equation for the WPF has been considered in a series of interesting papers of Remler and Sathe.[23-25] A consistent approach to this problem is that the result of the transformation in Equation 62 in the Introduction as applied to the initial wave packets (Section IIIA in the Introduction) can be taken as the initial value of ρ_W. Or taking into account the fact that it is sufficient to know only the integrals of ρ_c (and hence of ρ_W as well) over time to calculate the cross-sections, we can abandon the idea to consider the temporal dependence of ρ_W and go over to the stationary equation for the WPF with an appropriately formulated boundary condition (which can be obtained by applying Transformation 62 in the Introduction to Equation 25 there.) In the latter case, the problem can be solved within the framework of the OC-model as well, i.e., we seek the solution of the stationary equation for ρ_W with the above-mentioned sources and the boundary condition corresponding to the absence of the nucleon flux from the outside to the nucleus ($\rho_W = 0$ for $\boldsymbol{pr} < 0, r > R$).

A correct evaluation of the collision term (the integral in Equations 83 or 84) presents more severe difficulties. In the analysis given above, the effect of nuclear matter on collisions of nucleons in a nucleus was taken into account only through the introduction of the Pauli-blocking factors into the collision term. However, this does not exhaust the role played by nuclear matter. The point is that the cross-sections for collisions of two nucleons placed in nuclear matter must differ from the vacuum cross-sections for the following reasons:

1) Owing to the separation of the long-range part of the NN-interaction, which is included in the mean field, the two-nucleon potential that causes the collision of nucleons in nuclear matter differs from the vacuum one. In particular, this potential differs noticeably from zero at considerably shorter distances between nucleons.[4,26]
2) The presence of surrounding nucleons distorts the wave functions of colliding particles. This also affects the nature of their collision.
3) The nucleons in a nucleus can differ noticeably by its structure from the free ones, e.g., their constituent quarks can be partially incorporated into non-nucleonic complexes, such as isobars, multi-quark bags, etc.
4) Since the mean free path and the mean time between collisions of nucleons are not sufficiently large, the energy-momentum conservation law is obeyed only approximately in every separate collision, e.g., an uncertainty of the energy can be as large as 10MeV.[9]

In addition to this range of problems, there exist also the problems generated by relativistic effects which influence the form of the collision term as well. Apart from pure kinematics,* these effects are associated with creation of new particles, both real and virtual ones, and with the retardation of the interaction.[28] In particular, peculiarities of the virtual production of pions and Δ-isobars in nuclear matter[29] apparently may result in a noticeable deviation of the NN-interaction in a nucleus from the vacuum one. As the energy increases, the manifestation of the retardation of the interaction becomes more and more pronounced. In particular, it can result in a decrease in the probability of subsequent collisions between intranuclear nucleons and fast secondary particles produced in the same nucleus, since the time (and, correspondingly, the length) of their production is larger than that for the slow ones by a factor of $1/\sqrt{1-\beta^2}$. If their velocity is close to c ($1 - \beta \ll 1$), they can be produced even after the escape from the nucleus.[28]

In recent years, many papers have been devoted to the solution of these problems.[11-17] However, the detailed discussion of these papers is far beyond the scope of our work. Therefore, in addition to the papers[7,9,11,12] already cited, we shall mention here one version of the INC-model which is intensively developed nowadays. It is based on the Walecka model[30-31] in which the nucleus is described by methods of quantum-field theory. To be more specific, the field of nucleons (with the mass m_N) which interact through the field of scalar mesons (with the mass m_B) and the field vector mesons (with the mass m_V) is considered in this model. Under certain assumptions it has been found that the problem of evaluation of these fields is reduced to the solution of the equation for the corresponding WPF. However so far this approach was used mainly for the description of heavy ion collisions.[16]

On the whole, it should be emphasized that the range of problems associated with the collision term in nuclear matter is very complicated and far from being solved. Among them, the problems associated with the first collision of an incident

* A detailed presentation of the relativistic Kinetic theory as applied to rarified systems is given in the monograph.[27]

particle in a nucleus (in particular, certain relativistic effects) seem to be treatable on the basis of the OC-model.

Real pion production in NN-collisions noticeably affects the development of the INC even for the energy of an incident nucleon $\gtrsim$ 400 MeV. As the energy of an incident particle increases, the production of new particles plays a more and more prominent role. A formal generalization of the Liouville equation (Equation 19) to the case of production of new particles, as well as to that of their absorption and decay, involves no difficulties. However, every new type of particles creates the same problems as those enumerated above. In a number of cases, the validity of the INC-model turns out to be open to question. For example, the mean free path of a pion with the energy lying in the interval 100-200 MeV in a nucleus is small as compared to its de Broglie wavelength (see Chapter 2, Section II). The potential of the interaction between a particle and a nucleus is often unknown. In Chapters 4-7, we shall consider specific cases which are of paramount importance for intermediate energy nuclear physics.

VI. CONCLUSIONS

The INC-model treats the NR initiated by a fast particle in the following way. A nucleus is considered as a system of nucleons in a potential well with a given distribution over momenta and coordinates. Upon entering a nucleus, an incident particle can collide with one of the nucleons. Particles produced in this collision can also collide with intranuclear nucleons or with one another, and so on. Between collision, particles move along their classical trajectories. On reaching the boundary of the nucleus, they can leave it, thus forming the products of the NR. The model is based upon the assumption that a separate collision of any pair of particles takes place in the domain whose dimensions are small as compared to the mean free path of particles in nuclear matter, and its duration is smaller than the mean time between their collisions. This assumption is approximately satisfied because the actual NN-interaction in a nucleus can be divided into two components, a long-range and a short-range one. The first component gives, in the main, the contribution to the effective potential field V_j, which acts on a separate j-th nucleon and which depends only slightly on the details of the behavior of other nucleons. The second component V is responsible for collisions of particles in a nucleus. Under these assumptions the model allows one to obtain mathematically rigorous exclusive description of the INC by introduction of the concept of the phase density ρ_c for the system in question (an incident particle + nucleus), i.e., the probability density to find given values of coordinates and momenta of all particles. The phase density satisfies the Liouville equation (or KE). This equation describes the time evolution of ρ_c caused both by the motion of particles along their trajectories in the fields V_j between collisions (the streaming term of the KE) and by an instantaneous change in the momenta of particles because of their collisions under the action of the short-range part of the NN-interaction.

Since this equation is of the first order with respect to t, it uniquely defines ρ_c for all $t > t_0$, if ρ_c is preset at the initial instant of time $t = t_0$. For not very high

energies of colliding particles the Pauli exclusion principle, which imposes a constraint upon nucleon final states, plays an important role. This effect can be taken into account approximately by formal introduction of the Pauli-blocking factors into the collision term of the KE. The equation for ρ_c can be recast into various forms of a purely integral equation the solution of which can be expressed in terms of the von Neuman series. Owing to the clear physical meaning of its terms, one version of such a series, namely the "series in the number of collisions" or the "series in the generations" of particles involved in the cascade, is especially convenient for a simulation of a cascade by means of the Monte Carlo technique. The most parts of the calculations of exclusive characteristics of the cascade by this method is reduced actually to the evaluation of just this series within the framework of one or another approximation. This permits considerably simplifying the calculations. One of such approximations is the macroapproximation according to which the violation of the distribution of intranuclear nucleons over coordinates and momenta and collisions of excited cascade nucleons with one another during the development of the cascade is neglected.

To determine inclusive characteristics of the cascade (e.g., the differential of partial inclusive cross-sections for production of nucleons of one or another type) it is sufficient to calculate only the single-particle phase densities Ψ_α of protons and neutrons ($\alpha = \pm 1$) instead of ρ_c depending on the coordinates and momenta of all particles involved in the cascade. If the conditions which ensure the validity of the INC-model are satisfied, then the closed equation of the Boltzmann type can be obtained for Ψ_α. With allowance for the Pauli exclusion principle it assumes the form of the BUU-equation. Unlike the Liouville equation it is essentially nonlinear even if the constraints imposed by the Pauli exclusion principle are disregarded. The BUU-equation can be linearized in the macroapproximation and reduced to the form convenient for analytic calculations.

Characteristics of the intranuclear-cascade process accessible for experimental investigations are expressed in terms of various cross-sections which, in their turn, are represented in the form of integrals of ρ_c (or Ψ_α) over time.

The results cited above were obtained on the basis of the classical approach. A quantum-mechanical formalism close to a classical one uses the Wigner probability function ρ_W instead of ρ_c. It can be shown that the expression for the streaming term in the quantum analogue of the Liouville equation for ρ_W differs only slightly from the classical one. The distinctions in the collision term can be caused both by the distinctions between the NN-interaction in vacuum and in nuclear matter and by quantum-mechanical kinematic effects associated, y, with an uncertainty of the change in the energy-momentum during subsequent collisions of nucleons in a nucleus.

REFERENCES

1. **Serber, R.**, Nuclear Reactions at High Energies, *Phys. Rev.*, 72, 1114, 1947.
2. **Goldberger, M.**, The Interaction of High Energy Neutrons and Heavy Nuclei, *Phys. Rev.*, 74, 1269, 1948.
3. **Bunakov, V. E.**, Master Equations in the Nuclear Reaction Theory, *Part. Nucl.*, 11, 1285, 1980.
4. **Bohr, A. and Mottelson, B. R.**, *Nuclear Structure, Vol. 1, Single-Particle motion.* W. A. Benjamin Inc., New York, 1969.
5. **Bohr, A. and Mottelson, B. R.**, *Nuclear Structure, Vol. 2, Nuclear Deformations.* W. A. Benjamin Inc., New York, 1974.
6. **Skyrme, T. H. R.**, The Effective Nuclear Potential, *Nucl. Phys.*, 9, 615, 1958/59.
7. **Bertsch, G. R., Kruse, H., and Das Gupta, S.**, Boltzmann Equation for Heavy Ion Collisions, *Phys. Rev. C*, 29, 673, 1984.
8. **Barashenkov, V. S., Iljinov, A. S., Sobolevsky, N. M., and Toneev, V. D.**, Interactions of Particles and Nuclei of High and Superhigh Energies with Nuclei, *Usp. (Sov. Phys.)*, 16, 31, 1973.
9. **Bunakov, V. E. and Matvejev, G. V.**, The Physical and Mathematical Foundations of the Intranuclear Cascade Model Algorithm, *Z. Phys. A*, 322, 511, 1985.
10. **Uehling, E. A. and Uhlenbeck, G. E.**, Transport Phenomena in Einstein-Bose and Fermi-Dirac Gases. I. *Phys. Rev.*, 43, 552, 1933.
11. **Ko, C. M. and Li, Q.**, Relativistic Vlasov-Uehling-Uhlenbeck Model for Heavy-Ion Collisions. *Phys. Rev. C*, 37, 2270, 1988.
12. **Gregoire, C., Remand, B., Sebille, F., Vinet, L., and Raffray, Y.**, Semi-classical Dynamics of Heavy-Ion Reactions, *Nucl. Phys. A*, 465, 317, 1987.
13. **Ter Haar, B. and Malfliet, R.**, Nucleons, Mesons and Deltas in Nuclear Matter: A Relativistic Dirac-Brueckner Approach, *Phys. Rep.*, 149, 207, 1987.
14. **Bertsch, G. F. and Das Gupta, S.**, A Guide to Microscopic Models for Intermediate Energy Heavy Ion Collisions, *Phys. Rep.* 160, 191, 1988.
15. **Botermans, W. and Malfliet, R.**, Quantum Transport Theory of Nuclear Matter, *Phys. Rep.* 198, 115, 1990.
16. **Cassing, W., Metag, V., Mosel, U., and Niita, K.**, Production of Energetic Particles in Heavy-Ion Collisions, *Phys. Rep.* 188, 363, 1990.
17. **Nesterov, M. M. and Tarasov, N. A.**, Semiclassical Approach to the Description of Nuclear Reactions with Fast Particles, *Phys. Rep.* 185, 171, 1990.
18. **Wigner, E.**, On the Quantum Correction for Thermodynamic Equilibrium, *Phys. Rev.* 40, 749, 1932.
19. **Yang, Bo-jun. and Yao, Shu-guang**, Kinetic Equation of Nuclear Gas, *Phys. Rev. C*, 36, 667, 1987.
20. **Kazarnovskii, M. V. and Paryev, E. Ya.**, Unified Optical + Cascade Model of Nuclear Reactions at Intermediate Energies [in Russian], *Izv. Akad. Nauk Kaz SSR, Ser. Phys.-Mat.* N4, 28, 1983.
21. **Iljinov, A. S., Kazarnovskii, M. V., and Matushko, V. L.**, Optical + Cascade Model for the Interaction of Antinucleons with Nuclei. *Program of Experimental Investigations at the Meson Facility of INR AN SSSR* [in Russian], *Proceedings of Vth seminar*, 294, Moscow, 1987.
22. **Barashenkov, V. S. and Toneev, V. D.**, *Interaction of High Energy Particles and Nuclei with Atomic Nuclei* [in Russian], Atomizdat, Moscow, 1972.
23. **Remler, E. A. and Sathe, A. P.**, Quasi-Classical Scattering Theory and Bound State Production Processes, *Ann. Phys.* 91, 295, 1975.
24. **Remler, E. A.**, Use of the Wigner Representation in Scattering Problems, *Ann Phys.* 95, 455, 1975.
25. **Rembler, E. A.**, Intranuclear Transport Theory, *Ann. Phys.* 113, 326, 1979.
26. **Bethe, H. A.**, Theory of Nuclear Matter. *Annu. Rev. Nucl. Sci.*, 21, 93, 1971.

27. **De Groot, S. R., van Leeuwen, W. A., and van Weert, Ch. G.,** *Relativistic Kinetic Theory: Principles and Applications,* North-Holland, Amsterdam, 1980.
28. **Nicolaev, N. N.,** Quark Interactions in Collisions of High Energy Leptons, Photons and Hadrons with Atomic Nuclei, *Usp. Fiz. Nauk,* 134, 369, 1981.
29. **Ericson, T. and Weise, W.,** *Pions and Nuclei,* Clarendon Press, Oxford, 1988.
30. **Walecka, J. D.,** A Theory of Highly Condensed Matter, *Ann. Phys.* (N.Y.), 83, 491, 1974.
31. **Serot, B. D. and Walecka, J. D.,** The Relativistic Nuclear Many-Body Problem, *Advances in Nuclear Physics,* Vol. 16, Negele, J. W. and Vogt, E., Eds., Plenum Press, New York, 1986.

Chapter 2

METHODS FOR SOLUTION OF THE SYSTEM OF KINETIC EQUATIONS OF THE INTRANUCLEAR CASCADE MODEL

In Chapter 1, the system of kinetic equations (KEs) describing the intranuclear cascade was presented. Now we shall consider in detail the methods used for solution of this system of equations.

I. ANALYTIC METHODS OF SOLUTION

In this section, we shall consider various approximate methods used for solution of the system of the linear KEs (Equation 56, Chapter 1) for single-particle distribution functions Φ_α integrated over time (recall that these functions describe the nucleonic cascade). On the basis of solutions obtained we shall derive expressions for inclusive cross-sections for production of secondary nucleons and set forth the method which allows one to take into account the contribution of quantum-mechanical effects to these cross-sections as well.

A. CROSS-SECTION OF INELASTIC INTERACTION AND QUASIFREE NUCLEONS

The system of KEs for the functions Φ_α can be solved by the iteration method*. Within the framework of this technique, the flux of primary nucleons $\Phi_\alpha^{(0)}$ is described by the solution of Equation 56, Chapter 1, without the integral term on the right-hand side. The distribution of the nucleons of the first generation produced in a collision of a primary nucleon with unexcited intranuclear nucleons is obtained as a result of the substitution of $\Phi_\alpha^{(0)}$ in the integral term of this system of KEs (this is the first iteration). In accordance with the accepted terminology[1,2] such nucleons will be called quasifree nucleons. Subsequent iterations of the system describe distributions of nucleons of higher generations. Such nucleons will be called cascade nucleons.[2]

The function $\Phi_\alpha^{(0)}$ defines the cross-section σ^{in} of inelastic interaction through the relation (Equation 66, Chapter 1). According to Equation 73a in Chapter 1 the remainder of the function Φ_α describes the double differential cross-section for the production of nucleons of the α type. On the basis of the above line of reasoning, it is convenient to represent it in the form**

$$\frac{d^2\sigma_{\alpha_0\alpha}}{d\epsilon d\Omega} = \frac{d^2\sigma^{(q)}_{\alpha_0\alpha}}{d\epsilon d\Omega} + \frac{d^2\sigma^{(c)}_{\alpha_0\alpha}}{d\epsilon d\Omega}, \tag{1}$$

* As a matter of fact, this is reduced to the evaluation of the terms of the von Neumann series of type as in Equations 40 and 41 in Chapter 1 integrated over time.

** To emphasize the dependence of the cross-section on the type of the primary α_0 and the secondary α nucleon, the symbol $\alpha_0\alpha$ is written here and in what follows as an explicit subscript in the expression for the cross-section.

where ϵ is the energy of the nucleon emitted from a nucleus and the superscripts q and c denote the quasifree and the cascade component of the cross-section, respectively. The quasifree component of the cross-section is most sensitive to the details of the energy and the angular dependence of the kernel $K_{\alpha\to\alpha(-\alpha\to\alpha)}(\mathbf{r}; E',\boldsymbol{\Omega}'\to E,\boldsymbol{\Omega})$ and to the initial conditions, since any subsequent collision results in a smearing of the function Φ_α with respect to these variables and in loss of memory in this function about initial conditions. Therefore, it is desirable to evaluate it to as high accuracy as possible. This will be done in the present section. The distribution of cascade nucleons will be sought within the framework of more crude approximations (see Sections C-E). While evaluating both components of the cross-section (Equation 1), we shall disregard, for the sake of simplicity, the deflection of the trajectory of a nucleon with $p > p_{F,\alpha}$ under the action of the effective nuclear potential field $V_\alpha{}^2$. Then, it can be shown[3] that the cross-section for the production of quasifree nucleons has the form[2,4]

$$\begin{aligned}\frac{d^2\sigma^{(q)}_{\alpha_0\alpha}}{d\epsilon d\boldsymbol{\Omega}} = \int d\mathbf{r}\ \varphi_{\alpha_0}\,[\Lambda(\mathbf{r}, -\boldsymbol{\Omega}_0),E_0(\mathbf{r});\mathbf{r},\boldsymbol{\Omega}_0]\ \times \\ \varphi_\alpha\,[\Lambda(\mathbf{r},\boldsymbol{\Omega}),E(\mathbf{R});\mathbf{R},\boldsymbol{\Omega}]\ \times \\ [\delta_{\alpha\alpha_0}K_{\alpha\to\alpha}\,(\mathbf{r};E_0(\mathbf{r}),\boldsymbol{\Omega}_0 \to E(\mathbf{r}),\boldsymbol{\Omega}) + \\ \delta_{-\alpha\alpha_0}K_{-\alpha\to\alpha}(\mathbf{r};E_0(\mathbf{r}),\boldsymbol{\Omega}_0 \to E(\mathbf{r}),\boldsymbol{\Omega})]\end{aligned} \tag{2}$$

$$\begin{aligned}\varphi_\alpha[a,b(\mathbf{r});\mathbf{r},\boldsymbol{\Omega}] = \exp\left\{-\int_0^a \mu_\alpha[\mathbf{r} - x'\boldsymbol{\Omega},b(\mathbf{r} - x'\boldsymbol{\Omega}]dx'\right\}; \\ E_0(\mathbf{r}) = \epsilon_0 - V_{\alpha_0}(\mathbf{r}),\ E(\mathbf{r}) = \epsilon - V_\alpha(\mathbf{r}).\end{aligned} \tag{3}$$

Here $\Lambda\,(r,\boldsymbol{\Omega})$ is the distance from the point $\mathbf{r}$ to the boundary of a nucleus measured along the vector $\boldsymbol{\Omega}$.

The cross-section of an inelastic interaction of a nucleon with a nucleus is determined by the expression Equation 66 in Chapter 1 where

$$P_{\alpha_0}(\mathbf{R}_0,\mathbf{p}_0) = 1 - \varphi_{\alpha_0}\,[\Lambda(\mathbf{R}, -\boldsymbol{\Omega}_0),E_0(\mathbf{R});\mathbf{R},\boldsymbol{\Omega}_0]. \tag{4}$$

In the case of a uniform nucleus of a radius $R = r_0A^{1/3}$, we obtain[5,6]

$$\sigma^{in} = \pi R^2\left\{1 - \frac{1}{2a_0^2}[1 - (1 + 2a_0)e^{-2a_0}]\right\},\ a_0 = \mu_{\alpha_0}(E_0)R. \tag{5}$$

Let us now find the cross-section for quasifree scattering of nucleons 2. Substituting the expression 14, Chapter 1 for the function w in the relations 59, Chapter 1 and neglecting, for the sake of simplicity, the dependence of $d\sigma^{el}_{\alpha\alpha(\alpha-\alpha,-\alpha\alpha)}/d\overset{*}{\boldsymbol{\Omega}}$

on the momentum $\mathbf{p}''$* and the difference in the Fermi energies of protons and neutrons as well, we obtain[2]

$$\mathbf{K}_{\alpha\to\alpha}(\mathbf{r};E',\boldsymbol{\Omega}' \to E,\boldsymbol{\Omega}) = \left[2\rho_\alpha(\mathbf{r})\frac{d\sigma^{el}_{\alpha\alpha}(E',\overset{*}{\vartheta})}{d\overset{*}{\boldsymbol{\Omega}}} + \rho_{-\alpha}(\mathbf{r})\frac{d\sigma^{el}_{\alpha-\alpha}(E',\overset{*}{\vartheta})}{d\overset{*}{\boldsymbol{\Omega}}}\right] \times$$
$$K_q(E',\boldsymbol{\Omega}' \to E,\boldsymbol{\Omega}),$$

$$K_{-\alpha\to\alpha}(\mathbf{r};E',\boldsymbol{\Omega}' \to E,\boldsymbol{\Omega}) = \rho_\alpha(r)\frac{d\sigma^{el}_{-\alpha\alpha}(E',\overset{*}{\tilde{\vartheta}})}{d\overset{*}{\boldsymbol{\Omega}}} K_q(E',\boldsymbol{\Omega}' \to E,\boldsymbol{\Omega}) \times \quad (6)$$

$$K_q(E',\boldsymbol{\Omega}' \to E,\boldsymbol{\Omega}) = \frac{3\Theta(1-2\tilde{z})}{2E'\omega\sqrt{E_F}}\,\Theta(E'-E) \times$$
$$\Theta(\varkappa)\left[\varkappa - \left(\varkappa - \frac{E'-E}{E_F}\right)\Theta\left(\varkappa - \frac{E'-E}{E_F}\right)\right], \quad (7)$$

$$\omega = |\boldsymbol{\Omega}/\sqrt{\tilde{\nu}} - \boldsymbol{\Omega}'/\sqrt{\tilde{\nu}'}|,\ \tilde{\nu} = E(1+E/2M),\ M = m_N c^2, \quad (8)$$
$$\varkappa = 1 - 2\left(\boldsymbol{\Omega}'\boldsymbol{\Omega} - \frac{E}{E'}\sqrt{\frac{\tilde{\nu}'}{\tilde{\nu}}}\right)^2\left[\omega^2 E_F(1-\tilde{z}+\sqrt{1-2\tilde{z}})\right]^{-1},$$

$$\tilde{z} = (E'-E)\left(\boldsymbol{\Omega}'\boldsymbol{\Omega} - \frac{E}{E'}\sqrt{\frac{\tilde{\nu}'}{\tilde{\nu}}}\right)\left[M\omega^2\sqrt{\tilde{\nu}\tilde{\nu}'}\right]^{-1}, \quad (9)$$
$$E_F = \frac{1}{2}\left[E_{F,p} + E_{F,n}\right].$$

Here $\rho_\alpha(\mathbf{r})$ is the mean density of nucleons in a nucleus of the α type at the point $\mathbf{r}$, and $\overset{*}{\vartheta}$ and $\overset{*}{\tilde{\vartheta}}$ are the scattering angles of nucleons in the center-of-mass system(c.m.s.) for the collisions $\alpha,\mathbf{p}'$; $\gamma,\mathbf{p}'' \to \alpha,\mathbf{p};\gamma,\mathbf{p}'''$ ($\gamma = \alpha,-\alpha$) and $\alpha,\mathbf{p}'';-\alpha,\mathbf{p}' \to \alpha,\mathbf{p};-\alpha,\mathbf{p}'''$ respectively. In nonrelativistic approximation, but when the condition $E',E \gg E_F$ is satisfied, the function K_q assumes the most simple form

$$K_q \simeq K_{oq} = \frac{2}{E'}\,\delta\left(\boldsymbol{\Omega}'\boldsymbol{\Omega} - \sqrt{\frac{E}{E'}}\right), \quad (10)$$

* Being valid for $p' \gg p_F$ this is a rather good approximation even at $p' \sim p_F^7$.

i.e. it coincides with the indicatrix of scattering on a free quiescent nucleon. Making use of nonrelativistic expression for the function w and disregarding the anisotropy of the NN-scattering in the c.m.s. we obtain, in accordance with 1.58, Chapter 1 the following expression for μ_α[2,7]

$$\mu_\alpha(\mathbf{r},E) = [\rho_\alpha(\mathbf{r})\sigma^{el}_{\alpha\alpha}(E) + \rho_{-\alpha}(\mathbf{r})\sigma^{el}_{\alpha-\alpha}(E)] \cdot \tilde{y}\left(\frac{E_F}{E}\right), \tag{11}$$

$$\tilde{y}(\tilde{x}) = \begin{cases} 1 - \frac{7}{5}\tilde{x} & \text{for } \tilde{x} \le 0.5 \\ 1 - \frac{7}{5}\tilde{x} + \frac{2}{5}\tilde{x}\,(2 - \frac{1}{\tilde{x}})^{5/2} & \text{for } \tilde{x} > 0.5, \end{cases} \tag{12}$$

where $\sigma^{el}_{\alpha\alpha(\alpha-\alpha)}$ are the total free cross-sections of the elastic $\alpha\alpha(\alpha\text{-}\alpha)$-scattering, and $\tilde{y}(\tilde{x})$ is the Pauli blocking factor for these scattering cross-sections in nuclear medium. Calculations taking into account the relativistic effects lead to practically the same result in the energy range under consideration. As for the isotropy of scattering, the pp-scattering is practically isotropic in the c.m.s. for $\epsilon_0 \lesssim 500$ MeV[1,8], whereas the anisotropy of the pn-scattering is effectively smoothed off owing to the Pauli exclusion principle (which prohibits the scattering at small angles). Hence, in the first approximation, it can be disregarded in the calculation of the quantity μ_α. According to Equations 6-9 and 11, the expression 2 for the cross-section of the quasifree scattering of nucleons calculated within the framework of the model of a uniform nucleus under the condition that

$$V_{\alpha_0} \equiv V_\alpha = V_N = -[E_F + B_N] \tag{13}$$

(where B_N is the mean energy of the separation of a nucleon with the minimum binding energy) has the form[2]

$$\frac{d^2\sigma^{(q)}_{\alpha_0\alpha}}{d\epsilon d\Omega} = \sum\nolimits_{\alpha_0\alpha}(E_0)K_q(E_0,\Omega_0 \to E,\Omega)\, I^{(q)}(\vartheta), \tag{14}$$

$$\sum\nolimits_{\alpha_0\alpha}(E_0) = \delta_{\alpha\alpha_0}\left[2f(\alpha)\frac{d\sigma^{el}_{\alpha\alpha}(E_0,\overset{*}{\vartheta})}{d\overset{*}{\Omega}} + f(-\alpha)\frac{d\sigma^{el}_{\alpha-\alpha}(E_0,\overset{*}{\vartheta})}{d\overset{*}{\Omega}}\right] + \delta_{-\alpha\alpha_0}f(\alpha)\frac{d\sigma^{el}_{-\alpha\alpha}(E_0,\overset{*}{\tilde{\vartheta}})}{d\overset{*}{\Omega}}. \tag{15}$$

$$I^{(q)}(\vartheta) = \frac{3}{4\pi R^2}\int_{-R}^{R} dz_1 \iint_{x_1^2+y_1^2 \le R^2 - z_1^2} dx_1 dy_1 \times \exp[-\mu_{\alpha_0}(E_0)\Lambda(\mathbf{r},-\Omega_0) - \mu_\alpha(E)\Lambda(\mathbf{r},\Omega)], \tag{16}$$

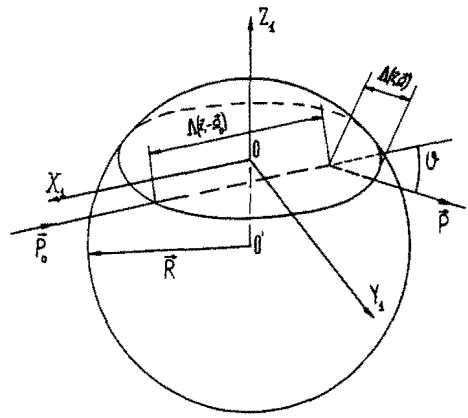

FIGURE 1. This represents a scheme of quasifree scattering of a primary nucleon with the momentum $\mathbf{p}_0$ on an intranuclear nucleon.

$$\Lambda(\mathbf{r}, -\boldsymbol{\Omega}_0) = (R^2 - z_1^2 - y_1^2)^{1/2} - x_1,\ \Lambda(\mathbf{r}, \boldsymbol{\Omega}) = x_1 \cos\vartheta - y_1 \sin\vartheta + [R^2 - z_1^2 - (x_1 \sin\vartheta + y_1 \cos\vartheta)^2]^{1/2},\ \vartheta = \cos^{-1}(\boldsymbol{\Omega}_0 \boldsymbol{\Omega}) \tag{17}$$

(for notation, see Figure 1). Here f(1) = Z, f(-1) = N, and

$$I^{(q)}(0°) = \frac{3}{(a_1 - a_2)a_2^2}\left\{1 - (1 + a_2)e^{-a_2} - \left(\frac{a_2}{a_1}\right)^2 [1 - (1 + a_1)e^{-a_1}]\right\} \tag{18}$$

$$I^{(q)}(180°) = \frac{3}{a_+^3}\left[\frac{a_+^2}{2} - 1 + (1 + a_+)e^{-a_+}\right]; \tag{19}$$

$$a_1 = 2\mu_\alpha(E)R,\quad a_2 = 2\mu_{\alpha_0}(E_0)R,\quad a_+ = a_1 + a_2 \tag{20}$$

Taking into account a weak dependence of μ_α (E) on the energy[7], at $\alpha_0 = \alpha$ we can obtain[2]

$$I^{(q)}(\vartheta) = I_0^{(q)} + I_1^{(q)} \sin^2(\vartheta/2) + \ldots, \tag{21}$$

$$I_0^{(q)} = \frac{6}{\tilde{a}^3}\left[1 - e^{-\tilde{a}} \sum_{m=0}^{2} \frac{\tilde{a}^m}{m!}\right], \tag{22}$$

$$I_1^{(q)} = (1 - e^{-\tilde{a}})\,\tilde{a} + e^{-\tilde{a}} - 2I_0^{(q)}, \tag{23}$$

$$\tilde{a} = \frac{3}{2\pi R^2}[f(\alpha_0)\sigma_{11}^{\text{eff}} + f(-\alpha_0)\sigma_{1-1}^{\text{eff}}], \tag{24}$$

where $\sigma^{\text{eff}}_{11(1\text{-}1)}$ is the value of $\sigma^{\text{el}}_{11(1\text{-}1)}(E)\ \tilde{y}\left(\frac{E_F}{E}\right)$ averaged over the energy. It is often sufficient to confine oneself to the following form of averaging[2]:

$$\sigma^{\text{eff}}_{11(1-1)} = \frac{1}{2}\left[\sigma^{\text{el}}_{11(1-1)}(E_0)\tilde{y}\left(\frac{E_F}{E_0}\right) + \sigma^{\text{el}}_{11(1-1)}(E)\tilde{y}\left(\frac{E_F}{E}\right)\right]. \tag{25}$$

Calculations have demonstrated[2] that the formula 21 is sufficiently accurate practically for all $\vartheta \lesssim 60^0$.

In the case of a nucleus with a diffuse boundary, the expression 2 for $\alpha_0 = \alpha$ and small ϑ can be approximately written in the form[2]

$$\begin{aligned}\frac{d^2\sigma^{(q)}_{\alpha_0\alpha}}{d\epsilon d\Omega} &= 2\pi\int_0^\infty b_\perp db_\perp \int_{-\infty}^{\infty} dz\rho(r)\sum_{\alpha_0\alpha}(\epsilon_0 - V_N(r)) \times \\ &K_q(\epsilon_0 - V_N(r), \Omega_0 \to \epsilon - V_N(r), \Omega) \times \\ &\times \exp\left\{-\int_{-\infty}^{\infty}\rho(r')\,[f(\alpha_0)\,\sigma^{\text{eff}}_{11}(r') + f(-\alpha_0)\,\sigma^{\text{eff}}_{1-1}(r')]dz'\right\}; \\ &r = (b_\perp^2 + z^2)^{1/2}, \quad r' = (b_\perp^2 + z'^2)^{1/2},\end{aligned} \tag{26}$$

where $\rho(r)$ is the density of intranuclear nucleons at the point r normalized to unity. In the case when N = Z, the formulas in 21 and 26 are valid for an arbitrary combination of the quantities α_0 and α. Comparison with the Monte Carlo calculation of the intranuclear cascade (see Section II) has shown that the expression 26 describes sufficiently well the double differential distributions of quasifree nucleons up to the angles of about 40^0-50^0. A discrepancy in the low-energy part of the spectrum (see Figure 2) has been observed for larger values of the angle.

B. QUANTUM-MECHANICAL CALCULATION OF A QUASIFREE COMPONENT OF THE INCLUSIVE CROSS-SECTION

For energies of incident nucleons higher than 100 MeV (for which $\lambda\!\!\!^{-} \lesssim 0.5$ fm, i.e., considerably smaller than the radius of a nucleus and the mean free path, $L \sim 2 \div 3$ fm, of a nucleon in nuclear matter), quantum-mechanical effects exert most strong influence on the initial stage of a reaction. For instance, the elastic scattering of a nucleon on a nucleus is caused, in the main, by quantum-mechanical effects. It can be expected that diffraction and interference in the incident and the scattered wave and the quantization of the energy levels of a nucleus (especially in the case of the 1p-shell nuclei) manifest themselves noticeably during the first collision of an incident nucleon with one of intranuclear nucleons, i.e., in the quasifree scattering. The expressions of 2, 14, and 26 for the quasifree component

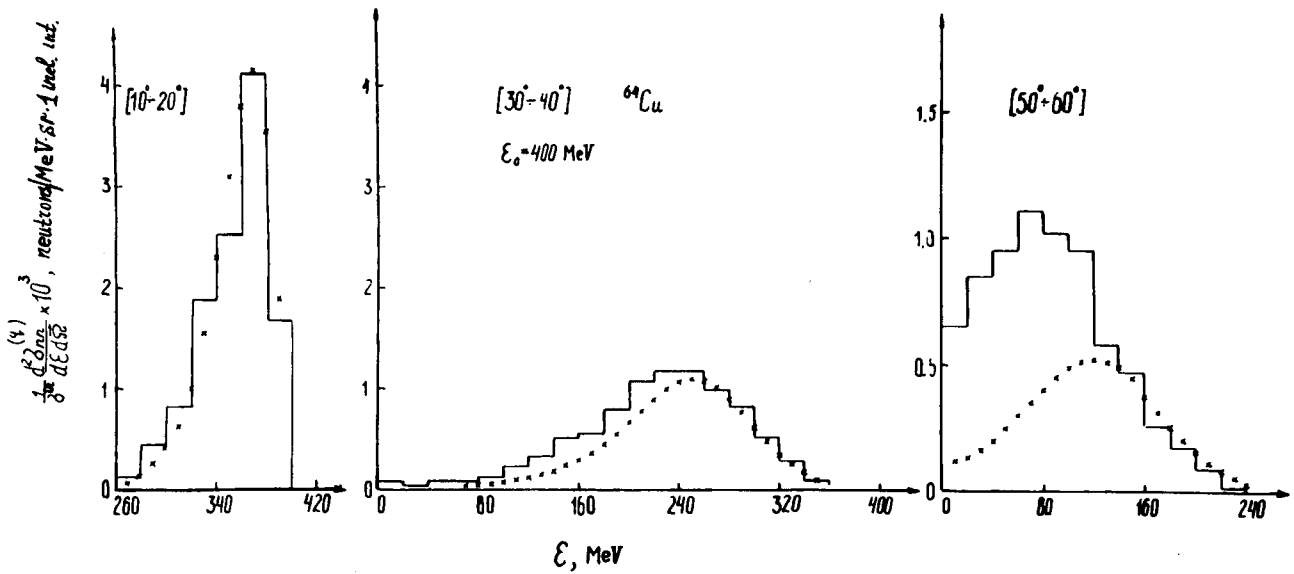

FIGURE 2. Here are double differential distributions of quasifree neutrons produced in the interaction of 400 MeV neutrons with ^{64}Cu nuclei as functions of the energy of secondary neutrons. The data shown in this figure are averaged over the angular intervals 10°-20°, 30°-40° and 50°-60°. Histograms correspond to the calculation by the Monte Carlo method and the crosses to analytic calculation.

of the inclusive cross-section obtained on the basis of the solution of the semiclassical system of KEs 56, Chapter 1 within the framework of a model which considers a nucleus as a local Fermi gas of nucleons do not take into account these effects. This can lead to errors, if these expressions are used for calculation of double differential cross-sections for production of secondary nucleons in the domain of the peak corresponding to the quasifree scattering (see Chapter 4). Hence, in a number of cases, it is necessary to resort to quantum-mechanical calculations to obtain the correct value of the cross-section $d^2\sigma^{(q)}_{\alpha o\alpha}/d\epsilon d\Omega$[9]. On the other hand, the contribution coming from subsequent collisions can be determined on the basis of the analytic solution of the system of KEs (Equation 56, Chapter 1). The sum of these expressions is considered as the double differential cross-section for production of nucleons of the α type 1 (a similar method has been used by Bunakov and Matvejev[10]).

To carry out quantum-mechanical calculation of double differential distributions $d^2\sigma^{(q)}_{\alpha o\alpha}/d\epsilon d\Omega$ of quasifree nucleons in the $A(\alpha_0,\alpha)X$ reaction in this range of energy of primary nucleons, we shall use the distorted-wave impulse approximation (DWIA).[9] For the sake of simplicity, we shall confine ourselves to the case of even-even nuclei of the 1p-shell, that is, ^{12}C and ^{16}O, and shall not take into account polarization effects in the nucleon-nucleon collisions. As a result, using the single-particle shell model for the wave functions of bound nucleon states in a T-nucleus we can represent the quantity $d^2\sigma^{(q)}_{\alpha o\alpha}/d\epsilon d\Omega$ in the following form[11] (see also Equation 39-43 in the Introduction):

$$\frac{d^2\sigma^{(q)}_{\alpha o\alpha}}{d\epsilon d\Omega} = \int_{4\pi} d\Omega' \int_0^\infty d\epsilon' \frac{d^4\sigma^{(q)}_{\alpha o\alpha}}{d\epsilon d\Omega d\epsilon' d\Omega'},$$

$$= \frac{4}{(\hbar c)^2}\frac{k}{k_0}\sum_{nlj}\frac{k'\bar{E}_0^2}{E_t}\left[\delta_{\alpha\alpha_0}\left(2\frac{d\sigma^{el}_{\alpha\alpha}}{d\overset{*}{\Omega}} + \frac{d\sigma^{el}_{\alpha-\alpha}}{d\overset{*}{\Omega}}\right) + \delta_{\alpha\alpha_0}\frac{d\sigma^{el}_{\alpha\alpha}}{d\overset{*}{\Omega}}\right] \times \tag{27}$$

$$\frac{N_{nlj}}{(2l+1)}\sum_{m_e=-l}|g'_{nlm_l}(\mathbf{k}_t)|^2\,\delta(\epsilon_0 - \epsilon - \epsilon' - |E_{nlj}|),$$

$$\mathbf{k}_t = \mathbf{k} + \mathbf{k}' - \mathbf{k}_0,\ E_t = (\hbar^2c^2k_t^2 + M^2)^{1/2},\ \bar{E}_0^2 = \tag{28}$$

$$\frac{1}{4}[(\epsilon + \epsilon' + 2M)^2 - \hbar^2c^2(\mathbf{k} + \mathbf{k}')^2],\ M = m_Nc^2$$

Here $\mathbf{k}_0$,$\mathbf{k}_0$, and $\mathbf{k}'$ are the wave vectors of the primary, the quasifree and the recoil nucleon, respectively; N_{nlj} is the number of nucleons of one type on the nuclear shell with the quantum numbers {n,l,j} and the energy E_{nlj} ($N_{101/2} = 2$ for $1s_{1/2}$-shell and $N_{113/2} = 4$ for $1p_{3/2}$-shell in ^{12}C), and ϵ' the kinetic energy of the recoil nucleon. Finally,

$$g'_{nlm_l}(k_t) = \frac{1}{(2\pi)^{3/2}} \int d\mathbf{r} e^{-i\mathbf{k}_t\mathbf{r}} \chi_{nlm_l}(\mathbf{r}) D_0(\mathbf{r}) D_1(\mathbf{r}) \tag{29}$$

where $\chi_{nlm_l}(\mathbf{r}) = \chi_{nl}(r) Y_{lm_l}(\mathbf{\Omega}_r)$ (Y_{lm_l} is the spherical harmonic) is the single-particle wave function of an intranuclear nucleon in the $\{n,l,m_l,j\}$ state normalized to unity, and the factors $D_i(\mathbf{r})(i = 0,1)$ describe the distortions of the wave functions of the incident ($i = 0$) and the quasifree ($i = 1$) nucleon. It should be noted that, in contrast to our case, the quantity $g'_{nlm_l}(\mathbf{k}_t)$, which determines the cross-sections for the (p,2p) and (p,pn) reactions, contains the factor $D_2(\mathbf{r})$ describing the distortion of the wave function of the second knocked-out nucleon. In the eikonal approximation which is valid for high-energy particles the factors D_0 and D_1 have the form[11]

$$D_0(\mathbf{r}) = \exp\left\{-i\frac{(\epsilon_0 + M)}{\hbar^2 c^2 k_0} \int_{-\infty}^{0} V_0(\mathbf{r} + \mathbf{\Omega}_0 z')dz'\right\}, \quad \mathbf{\Omega}_0 = \frac{\mathbf{k}_0}{k_0}$$

$$D_1(\mathbf{r}) = \exp\left\{-i\frac{(\epsilon + M)}{\hbar^2 c^2 k} \int_{0}^{\infty} V_1(\mathbf{r} + \mathbf{\Omega} z')dz'\right\}, \quad \mathbf{\Omega} = \frac{\mathbf{k}}{k} \tag{30}$$

where $V_i(\mathbf{r})$ is the corresponding optical potential. While calculating the radial wave functions χ_{nl} we shall neglect, for the sake of simplicity, the spin-orbit interaction. Then, within the framework of the harmonic-oscillator model with potential $V(r) = -V_0 + \frac{1}{2} m_N \tilde{\omega}^2 r^2$ we obtain the following expression for the 1s- and 1p-shells of the ^{12}C and ^{16}O nuclei[11]

$$\chi_{nl}(r) \equiv \chi_{1l}(r) = \pi^{-1/4} \tilde{\alpha}^{3/2} \sqrt{\frac{2^{l+2}}{(2l+1)!!}} (\tilde{\alpha} r)^l \exp\left[-\frac{1}{2}(\tilde{\alpha} r)^2\right],$$
$$\tilde{\alpha} = \sqrt{\frac{m_N \tilde{\omega}}{\hbar}}. \tag{31}$$

Let us use the Gaussian form[11] for the optical potential of the incident and quasifree nucleon

$$V_0(\mathbf{r}) = [U_1(\epsilon_0) + iU_2(\epsilon_0)]e^{-r^2/\tilde{b}_0^2}, \quad V_1(\mathbf{r}) = [U_1(\epsilon) + iU_2(\epsilon)]e^{-r^2/\tilde{b}_0^2} \tag{32}$$

and, for the sake of simplicity, disregard the difference between the quantities $(\epsilon + M)U_2(\epsilon)/\hbar^2 c^2 k$ and $(\epsilon + M)U_1(\epsilon)/\hbar^2 c^2 k$ for the incident and quasifree nucleon, replacing them by their average values. Then making use of Equations 30 and 31 and taking into account the fact that for small angles

$$D_0(\mathbf{r})D_1(\mathbf{r}) = \exp\{-\sqrt{\pi}\,\tilde{b}_0\,U\,e^{-b_\perp^2/\tilde{b}_0^2}\},\quad U = \frac{1}{2\hbar^2c^2}\times$$
$$\left\{-\left[\frac{(\epsilon_0+M)\,U_2(\epsilon_0)}{k_0}+\frac{(\epsilon+M)\,U_2(\epsilon)}{k}\right]+\right. \tag{33}$$
$$\left. i\left[\frac{(\epsilon_0+M)\,U_1(\epsilon_0)}{k_0}+\frac{(\epsilon+M)\,U_1(\epsilon)}{k}\right]\right\}$$

(where $b_\perp$ is the distance from the z-axis which passes through the center of the nucleus in the direction of the vector $\mathbf{\Omega}_0$), after some algebra we obtain[11]

$$g'_{100}(\mathbf{k}_t) = \frac{\tilde{\alpha}^{1/2}}{\pi^{3/4}}F(\mathbf{k}_t,1),\quad g'_{110}(\mathbf{k}_t) = -i\sqrt{\frac{2}{\tilde{\alpha}}}\frac{(\mathbf{k}_t\mathbf{\Omega}_0)}{\pi^{3/4}}F(\mathbf{k}_t,1)$$
$$g'_{11\pm1}(\mathbf{k}_t) = \pm i\,\frac{\tilde{\alpha}^{3/2}|\mathbf{k}_t^\perp|}{\pi^{3/4}}F(\mathbf{k}_t,2); \tag{34}$$

$$F(\mathbf{k}_t,n) = \exp\left\{-\frac{(\mathbf{k}_t\mathbf{\Omega}_0)^2}{2\tilde{\alpha}^2}\right\}\sum_{m=0}^{\infty}\frac{(-\sqrt{\pi}\,\tilde{b}_0U)^m\exp\{-|\mathbf{k}_t^\perp|^2/(2\tilde{\alpha}^2+4m/\tilde{b}_0^2)\}}{m!(\tilde{\alpha}^2+2m/\tilde{b}_0^2)^n}, \tag{35}$$
$$\mathbf{k}_t^\perp = \mathbf{k}_t - (\mathbf{k}_t\mathbf{\Omega}_0)\mathbf{\Omega}_0.$$

Well-known[12] expressions for momentum distributions $g_s(\mathbf{k}_t)$ and $g_p(\mathbf{k}_t)$ of nuclear nucleons, which are at the 1s- and the 1p-shell, respectively, can be derived from the formulas 34 and 35. Setting in them $U = 0$, we obtain

$$g_s(\mathbf{k}) \equiv |g'_{100}(\mathbf{k}_t)|^2\Big/_{U=0} = \frac{1}{\pi^{3/2}\tilde{\alpha}^3}e^{-k_t^2/\tilde{\alpha}^2},$$

$$g_p(\mathbf{k}_t) \equiv \frac{1}{3}\sum_{m'=-1}^{1}|g'_{11m'}(\mathbf{k}_t)|^2\Big/_{U=0} = \frac{2k_t^2}{3\pi^{3/2}\tilde{\alpha}^5}e^{-k_t^2/\tilde{\alpha}^2}. \tag{36}$$

C. SOLUTION OF THE SYSTEM OF KES FOR CASCADE NUCLEONS IN THE SMALL-ANGLE APPROXIMATION—THE DOMAIN OF RELATIVELY HIGH ENERGIES OF SECONDARY NUCLEONS

Let us seek the solution of the system of KEs 56, Chapter 1, which describes the nucleonic cascade in a nucleus, in the form of an expansion in powers of a small parameter* $\beta = (N\text{-}Z)/A$

$$\Phi_\alpha(\mathbf{r},E,\mathbf{\Omega}) = \sum_{j=0}^{\infty}\Phi_\alpha^{(j)}(\mathbf{r},E,\mathbf{\Omega})\beta^j. \tag{37}$$

* The main contribution to this expansion comes from the terms with $j = 0$ and $j = 1$.[11]

Moreover, we shall disregard the anisotropy of the differential cross-sections of the elastic NN-scattering the c.m.s. in the expressions 6 (such an approximation does not lead to large errors[2,11] in the energy range under consideration, i.e., when the energy ϵ_0 varies within the range of about several hundred MeV).

Then taking into account a weak dependence of the quantity $\sigma^{el}_{\alpha\alpha(\alpha-\alpha)}(E)$ $\tilde{y}(E_F/E)$ in 11 on the energy, for the functions $\Phi^{(j)}_{\pm}$ defined as

$$\Phi^{(j)}_{+} = \Phi^{(j)}_{\alpha} + \Phi^{(j)}_{-\alpha}, \quad \Phi^{(j)}_{-} = \alpha(\Phi^{(j)}_{\alpha} - \Phi^{(j)}_{-\alpha}), \quad j = 0,1,2,\ldots, \tag{38}$$

we can reduce Equation 56, Chapter 1, to the following system* of recurrence equations which have the identical form:[11]

$$\begin{aligned}
&[\boldsymbol{\Omega}\nabla + \tilde{\mu}\rho(\mathbf{r})]\, \Phi^{(j)}_{\pm}(\mathbf{r},E,\boldsymbol{\Omega}) = \tilde{\mu}\rho(\mathbf{r})\, \Delta_{\pm} \int d\boldsymbol{\Omega}' \int_{E}^{E_0} dE' \Phi^{(j)}_{\pm}(r,E',\Omega') \times \\
&\tilde{K}_q(E',\boldsymbol{\Omega}' \to E,\boldsymbol{\Omega}) + \tilde{\mu}\, \frac{(1-\gamma)}{(1+\gamma)}\, \rho(\mathbf{r}) \times \\
&\Big[\Phi^{(j-1)}_{\pm}(\mathbf{r},E,\boldsymbol{\Omega}) - \tilde{\Delta}_{\pm} \int d\boldsymbol{\Omega}' \int_{E}^{E_0} dE'\, \Phi^{(j-1)}_{\pm}(r,E,'\Omega') \times \\
&\tilde{K}_q(E',\Omega' \to E,\Omega)\Big] + \delta_{j0}\delta_{\pm}\, \delta(E - E_0)\, \delta(\boldsymbol{\Omega} - \boldsymbol{\Omega}_0)\, \delta(z - z_0),
\end{aligned} \tag{39}$$

where

$$\Phi^{(j)}_{\pm}(\mathbf{R},E,\boldsymbol{\Omega}) = 0 \quad \text{for} \quad \boldsymbol{\Omega}\,\mathbf{R} < 0, \quad \Phi^{(-1)}_{\pm} \equiv 0; \tag{40}$$

$$\tilde{K}_q(E',\boldsymbol{\Omega}' \to E,\boldsymbol{\Omega}) = [4\pi\tilde{y}(E_F/E')]^{-1} K_q(E',\boldsymbol{\Omega}' \to E,\boldsymbol{\Omega}), \tag{41}$$

$$\tilde{\mu} = (A/2)(\sigma^{eff}_{11} + \sigma^{eff}_{1-1}), \quad A = N + Z, \quad \gamma = \sigma^{eff}_{1-1}/\sigma^{eff}_{11}, \tag{42}$$

$$\Delta_{+} = 2, \Delta_{-} = 2/(1+\gamma), \tilde{\Delta}_{+} = 2, \tilde{\Delta}_{-} = 2/(1-\gamma), \delta_{+} = 1,\ \delta_{-} = \alpha_0 \tag{43}$$

and the quantities ρ (**r**) and $\sigma^{eff}_{11(1\cdot1)}$ are defined in Section A.

Let us consider the solution Equation 39 for relatively high values of the energy: $E_0/2 \le E \le E_0$. Since for these values of the energy the main contribution comes

* Here and in what follows we shall seek the solution of this system of KEs for the cascade nucleons, disregarding the dependence of the Fermi energy E_F on the coordinate.[11] This implies that the potential V_N is constant for $r < R$ and vanishes abruptly at $r = R$. Hence, the intranuclear cascade is initiated by a nucleon produced in the vicinity of the point $\mathbf{R}_0$ inside the nucleus with the energy $E_0 = \epsilon_0 - V_N$.

from the nucleons which are scattered at small angles, we shall seek the solution of Equation 39 in the small-angle approximation,[3,11] i.e., under the assumption that the directions of nucleon momenta in the nucleus differ only slightly from the initial one ($\boldsymbol{\Omega} \simeq \boldsymbol{\Omega}_0 + \boldsymbol{\vartheta}, \boldsymbol{\Omega}' = \boldsymbol{\Omega}_0 + \boldsymbol{\vartheta}', \boldsymbol{\Omega}_0\boldsymbol{\vartheta} = \boldsymbol{\Omega}_0\boldsymbol{\vartheta}' = 0; |\boldsymbol{\vartheta}|, |\boldsymbol{\vartheta}'| << 1$), and that they move almost along the straight line. In accordance with this

$$\widetilde{K}_q(E', \boldsymbol{\Omega}' \to E, \boldsymbol{\Omega}) \equiv \widetilde{K}_q(E' \to E, \boldsymbol{\Omega}'\boldsymbol{\Omega}) = \widetilde{K}_q(E' \to E, |\boldsymbol{\vartheta} - \boldsymbol{\vartheta}'|^2) \quad (44)$$

and we can seek the solution of Equation 39 for a spherical nucleus in the "plane geometry" separately for each chord of the form $\mathbf{r}(z) = \mathbf{R}_0 + (z - z_0)\boldsymbol{\Omega}_0$ intersecting the nucleus, replacing $\boldsymbol{\Omega}\nabla\Phi^{(j)}_{\pm}$ by $d\Phi^{(j)}_{\pm}/dz$. Introducing the new variable $\widetilde{t}$ connected with z through the relation

$$\widetilde{t} = \int_{z_0}^{z} \rho[\mathbf{R}_0 + (z' - z_0)\,\boldsymbol{\Omega}_0]dz' \quad (45)$$

and disregarding the influence exerted by relativistic effects and by the Fermi motion on the scattering of an excited nucleon on an unexcited one*, with the help of the Mellin transformation with respect to E and the Fourier transformation with respect to $\boldsymbol{\vartheta}$ we can introduce the functions

$$\Phi^{(j)}_{\pm}(\widetilde{t}, \eta, \boldsymbol{\xi}) = \int_0^{E_0} dE \left[\frac{E}{E_0}\right]^{\eta - 1} \int d\boldsymbol{\vartheta} e^{-i\boldsymbol{\xi}\boldsymbol{\vartheta}}\, \Phi^{(j)}_{\pm}(\widetilde{t}, E, \boldsymbol{\vartheta}) \quad (46)$$

For them after some algebra, we obtain the equation

$$\left[\frac{d}{d\widetilde{t}} + p_{\pm}\right] \Phi^{(j)}_{\pm}(\widetilde{t}, \eta, \boldsymbol{\xi}) = T^{(j)}_{\pm}(\widetilde{t}, \eta, \boldsymbol{\xi}) \quad (47)$$

with the boundary condition

$$\Phi^{(j)}_{\pm}(\widetilde{t}, \eta, \boldsymbol{\xi}) \Big/ \widetilde{t} = \begin{matrix} = 0 \\ -0 \end{matrix} \quad (48)$$

where

$$p_{\pm} = \widetilde{\mu}[1 - \Delta_{\pm}\widetilde{K}_q(\eta, \boldsymbol{\xi})],\ T^{(j)}_{\pm}(\widetilde{t}, \eta, \boldsymbol{\xi}) = \widetilde{\mu}\,\frac{(1 - \gamma)}{(1 + \gamma)} \times$$

* In this case, $\widetilde{K}_q(E', \boldsymbol{\Omega}' \to E, \boldsymbol{\Omega}) = (1/2\pi E')\,\delta(\boldsymbol{\Omega}'\boldsymbol{\Omega} - \sqrt{E/E'})$ (see the expression 10). The effect of the Fermi motion on the distributions of nucleons of the first and the second generation will be taken into account below.

$$[1 - \widetilde{\Delta}_{\pm}\widetilde{K}_q(\eta,\xi)]\ \Phi_{\mp}^{(j-1)}(\widetilde{t},\eta,\xi) + \delta_{j0}\delta_{\pm}\delta(\widetilde{t}),\ \widetilde{K}_q(\eta,\xi) = \tag{49}$$

$$\int d\vartheta e^{-i\xi\vartheta} \int_0^{E'} dE\left(\frac{E}{E'}\right)^{\eta-1} \widetilde{K}_q(E',\Omega' \to E,\Omega) = \frac{1}{\eta} e^{-\xi^2/4\eta}.$$

The solution of this equation has the form

$$\Phi_{\pm}^{(j)}(\widetilde{t},\eta,\xi) = \delta_{j0}\delta_{\pm}\Theta(\widetilde{t})e^{-p\pm\widetilde{t}} + \widetilde{\mu}\frac{(1-\gamma)}{(1+\gamma)} \times$$

$$[1 - \widetilde{\Delta}_{\pm}\widetilde{K}_q(\eta,\xi)]\ e^{-p\pm\widetilde{t}} \times \tag{50}$$

$$\int_{-0}^{\widetilde{t}} d\widetilde{t}'e^{p\pm\widetilde{t}'}\ \Phi_{\mp}^{(j-1)}(\widetilde{t}',\eta,\xi),\ j = 0,1,2\ldots,$$

$$\Theta(x) = (x + |x|)/2|x|.$$

Finally, applying the inverse transformations of Mellin and Fourier to the expression 50 according to the relation

$$\Phi_{\pm}^{(j)}(\widetilde{t},E,\vartheta) = \frac{1}{(2\pi)^3 iE_0}\int_{\sigma-i\infty}^{\sigma+i\infty} d\eta e^{\eta\ln(E_0/E)}\int d\xi e^{i\xi\vartheta}\ \Phi_{\pm}^{(j)}(\widetilde{t},\eta,\xi) \tag{51}$$

and confining ourselves to the terms with $j=0$ and $j=1$ in the expansion 37, we obtain[11]

$$\Phi_{\alpha}(\widetilde{t},E,\vartheta) = \delta_{\alpha\alpha_0}\frac{1}{2\pi}\delta(E - E_0)\ \delta\left(\frac{\vartheta^2}{2}\right)\ \Theta(\widetilde{t}) \times$$

$$\exp\left\{-\left[f(\alpha)\sigma_{11}^{el}(E_0) + f(-\alpha)\ \sigma_{1-1}^{el}(E_0)\right]\widetilde{y}\left(\frac{E_F}{E_0}\right)\widetilde{t}\right\} + \delta_{\alpha\alpha_0} \times$$

$$\left\{\frac{f(\alpha)}{A}L_1(\widetilde{t},E,\vartheta,0) + \frac{f(-\alpha)}{A}L_1(\widetilde{t},E,\vartheta,\gamma) + \alpha\beta\left(1 - \frac{1}{\gamma}\right) \times\right. \tag{52}$$

$$\left.[L_1(\widetilde{t},E,\vartheta,0) - L_1(\widetilde{t},E,\vartheta,\gamma) - L_2(\widetilde{t},E,\vartheta,0) + L_2(\widetilde{t},E,\vartheta,\gamma)]\right\} +$$

$$\delta_{-\alpha\alpha_0}\cdot\frac{f(\alpha)}{A}[L_1(\widetilde{t},E,\vartheta,0) - L_1(\widetilde{t},E,\vartheta,\gamma)],$$

where $f(\alpha) = Z$ at $\alpha = 1$ and $f(\alpha) = N$ at $\alpha = -1$, and the functions L_1, L_2 are defined by the relations

$$L_1(\tilde{t},E,\vartheta,\gamma) = \frac{\Theta(\tilde{t})\cdot 2\tilde{\mu}\,\tilde{t}\,e^{-\tilde{\mu}\tilde{t}}}{\pi E_0(1+\gamma)}\,\delta\left(\ln\frac{E_0}{E} - \vartheta^2\right) + \frac{1}{E_0}K_c(\tilde{t},E_0 \to E,\vartheta,\gamma,0), \tag{53}$$

$$L_2(\tilde{t},E,\vartheta,\gamma) = \frac{\Theta(\tilde{t})e^{-\tilde{\mu}\tilde{t}}}{\pi E_0}\left[\frac{\tilde{\mu}\,\tilde{t}}{1+\gamma}\right]^2\delta\left(\ln\frac{E_0}{E} - \vartheta^2\right) + \frac{1}{2E_0}K_c(\tilde{t},E_0 \to E,\vartheta,\gamma,1). \tag{54}$$

$$K_c(\tilde{t},E_0 \to E,\vartheta,\gamma,n) = \frac{\Theta(\tilde{t})e^{-\tilde{\mu}\tilde{t}}}{\pi}\sum_{m=2}^{\infty}\left[\frac{2\tilde{\mu}\,\tilde{t}}{1+\gamma}\right]^{m+n} \times \left(\ln\frac{E_0}{E} - \frac{\vartheta^2}{m}\right)^{m-2}\Theta\left(\ln\frac{E_0}{E} - \frac{\vartheta^2}{m}\right)[m(m-2)!\,(m+n)!]^{-1}. \tag{55}$$

The first term in Equation 52 describes the flux of primary nucleons. The first terms in L_1 and L_2 describe the distributions of nucleons of the first generation, i.e., of quasifree nucleons. The remainder terms in these functions describe the distributions of nucleons of the second (with $m = 2$) and higher generations, i.e., of cascade nucleons. We have found the contribution of quasifree nucleons to $\Phi_\alpha(\tilde{t},E,\vartheta)$ disregarding the Fermi motion of nuclear nucleons. Since this is a rather crude approximation, we shall substract it and add an "exact" (following from the solution of KEs 39) expression for this term Φ_α instead. This procedure is reduced to the substitution of the factor

$$\tilde{K}_q(E_0,\Omega_0 \to E,\Omega) \quad \text{for} \quad (1/\pi E_0)\,\delta\left(\ln\frac{E_0}{E} - \vartheta^2\right) \tag{56}$$

in the first terms of the functions L_1 and L_2. Similarly replacing these terms by the expression 27, 28 calculated in the DWIA, we shall take into account a correction for quantum-mechanical effects at the initial stage of the cascade.

To take into account the effect of the Fermi motion of the intranuclear nucleons in the distributions of the second-generation nucleons it is necessary to replace

$$(1/2\pi E_0)\,\Theta\left(\ln\frac{E_0}{E} - \frac{\vartheta^2}{2}\right) \text{ by } \int d\Omega' \int_E^{E_0} dE'\,\tilde{K}_q(E_0,\Omega_0 \to E',\Omega') \times \tilde{K}_q(E',\Omega' \to E,\Omega) \tag{57}$$

in the terms of the expressions for $L_{1,2}(\tilde{t},E,\vartheta,\gamma)$ corresponding to $m = 2$. The methods which allow one to take into account approximately the effect of the Fermi

motion in the distributions of the higher-generation nucleons will be considered in Section E.

Using the formulas 73a in Chapter 1 and Equations 52-56 for the double differential distribution $d^2\sigma_{\alpha_0\alpha}/d\epsilon d\Omega$ of secondary nucleons of the type α, we obtain the expression[11]

$$\frac{d^2\sigma_{\alpha_0\alpha}}{d\epsilon d\Omega} = \delta_{\alpha\alpha_0}\left\{\frac{f(\alpha)}{A} L_1(\epsilon,\vartheta,0) + \frac{f(-\alpha)}{A} L_1(\epsilon,\vartheta,\gamma) + \alpha\beta\left(1 - \frac{1}{\gamma}\right) \times \right.$$
$$\left. [L_1(\epsilon,\vartheta,0) - L_1(\epsilon,\vartheta,\gamma) - L_2(\epsilon,\vartheta,0) + L_2(\epsilon,\vartheta,\gamma)]\right\} + \tag{58}$$
$$\delta_{-\alpha\alpha_0}\frac{f(\alpha)}{A}[L_1(\epsilon,\vartheta,0) - L_1(\epsilon,\vartheta,\gamma)],$$

where

$$L_1(\epsilon,\vartheta,\gamma) \equiv 2\pi\int_0^\infty b_\perp db_\perp L_\perp(\tilde{t}(b_1),\epsilon - V_N,\vartheta,\gamma) = \frac{2\tilde{\mu}}{(1+\gamma)}\pi I_1 \times$$
$$\tilde{K}_q(E_0,\Omega_0 \to E,\Omega) + \frac{1}{E_0}K_c(E_0 \to E,\vartheta,\gamma,0), \tag{59}$$

$$L_2(\epsilon,\vartheta,\gamma) \equiv 2\pi\int_0^\infty b_\perp db_\perp L_2(\tilde{t}(b_\perp),\epsilon - V_N,\vartheta,\gamma) =$$
$$\left(\frac{\tilde{\mu}}{1+\gamma}\right)^2 \pi I_2\,\tilde{K}_q(E_0,\Omega_0 \to E,\Omega) + \frac{1}{2E_0}K_c(E_0 \to E,\vartheta,\gamma,1), \tag{60}$$

$$K_c(E_0 \to E,\vartheta,\gamma,n) = \sum_{m=2}^{\infty}\left[\frac{2\tilde{\mu}}{1+\gamma}\right]^{m+n}\cdot I_{m+n}\cdot\left(\ln\frac{E_0}{E} - \frac{\vartheta^2}{m}\right)^{m-2} \times$$
$$\Theta\left(\ln\frac{E_0}{E} - \frac{\vartheta^2}{m}\right)[m(m-2)!\,(m+n)!]^{-1}, \tag{61}$$

$$I_k = \int_0^\infty db_\perp^2\ \exp[-\tilde{\mu}\tilde{t}(b_\perp)]\,\tilde{t}^k(b_\perp), \quad \tilde{t}(b_\perp) = \int_{-\infty}^{+\infty}\rho(\sqrt{b_\perp^2 + z^2})\,dz;$$
$$E_0 = \epsilon_0 - V_N, \qquad E = \epsilon - V_N. \tag{62}$$

In the case of a nucleus of a radius R with a uniform distribution of the nucleon density, the expression 62 is reduced to

$$I_k = \frac{8\pi^2}{9}\frac{(k+1)!\,R^6}{\tilde{\mu}^{K+2}}\left[1 - e^{-(3\tilde{\mu}/2\pi R^2)}\sum_{m=0}^{k+1}\frac{(3\tilde{\mu}/2\pi R^2)^m}{m!}\right], \tag{63}$$

whereas for the Gaussian distribution of the nucleon density in a nucleus ($\rho(\mathbf{r}) = \rho_0 e^{-b_0 r^2}$) it assumes the form

$$I_k = \frac{(k-1)!}{b_0 \tilde{\mu}^k}\left[1 - e^{-(\tilde{\mu} b_0/\pi)} \sum_{m=0}^{k-1} \frac{(\tilde{\mu} b_0/\pi)^m}{m!}\right]. \tag{64}$$

If we use a more accurate semiclassical expression from Section A, or a quantum-mechanical one from Section B as a quasifree component $d^2\sigma^{(q)}_{\alpha_0\alpha}/d\epsilon d\Omega$ of the cross-section $d^2\sigma_{\alpha_0\alpha}/d\epsilon d\Omega$ for production of secondary nucleons, then the cascade component $d^2\sigma^{(c)}_{\alpha_0\alpha}/d\epsilon d\Omega$ of this cross-section is described by the formulas 58-60 in which only the second terms of the functions $L_1(\epsilon,\vartheta,\gamma)$ and $L_2(\epsilon,\vartheta,\gamma)$ must be retained. Integrating Equation 58 over the angle ϑ, we readily obtain the corresponding expression for the cross-section $d\sigma_{\alpha_0\alpha}/d\epsilon$ of production of secondary nucleons differentiated with respect to the energy.

D. SOLUTION OF THE SYSTEM OF KES FOR CASCADE NUCLEONS IN THE P_1-APPROXIMATION—THE DOMAIN OF LOW ENERGIES OF SECONDARY NUCLEONS

It has already been mentioned that the angular and the energy distribution of cascade nucleons in the domain of low energies (as compared to the initial energy) is noticeably smeared. Hence, its convolution with the indicatrix $\tilde{K}_q$ is hardly sensitive to the details of the structure of the latter. Therefore, we shall use the substitution of $(1/2\pi E')\ \delta(\Omega'\Omega - \sqrt{E/E'})$ for $\tilde{K}_q$ which was indicated above (see Section C). In addition to this, we confine ourselves, for the sake of simplicity, to the case N = Z* and to the model of a uniform nucleus. Then the system of KEs 39 for the functions

$$\Phi_+ = \Phi_+^{(0)}, \quad \Phi_- = \alpha_0 \Phi_-^{(0)} \tag{65}$$

is reduced to two independent equations which have the identical form

$$[\Omega\nabla + \mu]\ \Phi_\pm(\mathbf{r},E,\Omega) = \mu_\pm \int d\Omega' \int_E^{E_0} \frac{dE'}{E'}\ \delta\left(\Omega'\Omega - \sqrt{\frac{E'}{E}}\right) \times \Phi_\pm(\mathbf{r},E',\Omega') + S_\pm(\mathbf{r},E,\Omega). \tag{66}$$

The boundary condition for this equation has the form

$$\Phi_\pm(\mathbf{R},E,\Omega) = 0 \quad \text{for } \Omega\mathbf{R} < 0. \tag{67}$$

* This assumption is valid for light and moderately heavy nuclei. The calculations have demonstrated that for heavy nuclei the errors in the cross-sections associated with the distinction of N from Z does not exceed as a rule 50%.

Here

$$S_{\pm} = \frac{\mu_{\pm}}{E_0}\,\delta\left(\boldsymbol{\Omega}_0\boldsymbol{\Omega} - \sqrt{\frac{E}{E_0}}\right) e^{-\mu\Lambda(\mathbf{r},-\boldsymbol{\Omega}_0)},$$
$$\mu = \tilde{\mu}\rho,\ \mu_+ = \mu/\pi,\quad \mu_- = \mu/\pi(1+\gamma) \tag{68}$$

(i.e., knowing Φ_-, we can find Φ_+ by setting $\gamma = 0$), while the quantity $\Lambda\,(\mathbf{r},\boldsymbol{\Omega})$ is defined in Section A. In derivation of these KEs only the contribution of primary nucleons has been separated from the functions $\Phi_{\pm}$, i.e., their solution includes both cascade and quasifree nucleons. Hence, in order to calculate the cascade component of the cross-section the contribution of the latter (calculated separately under the same assumptions in which the solution itself was obtained) must be subtracted, whereas, to calculate the total distribution (Equation 1), the semiclassical expression (Equation 2), or the quantum-mechanical one (Equation 27) must be added to the result obtained.

In the domain of low energies under consideration, the dependence of the distribution functions of cascade nucleons on the direction $\boldsymbol{\Omega}$ of the nucleon momentum is significantly weaker than that at the values of the energy close to the initial one. Hence, we can seek the solution of Equation 66 in the so-called P_1-approximation, i.e., in the form of a linear function of $\boldsymbol{\Omega}$ (see Case and Zweifel[13]):

$$\Phi_-(\mathbf{r},E,\boldsymbol{\Omega}) = \frac{1}{4\pi}\,[\Phi_0(\mathbf{r},E) + 3\boldsymbol{\Omega}\boldsymbol{\Phi}_1(\mathbf{r},E)]. \tag{69}$$

For the functions Φ_0 and $\boldsymbol{\Phi}_1$, we can obtain the system of equations from which the function $\boldsymbol{\Phi}_1$ can be excluded by means of the standard procedure of the P_1-approximation. Then, using the Mellin transformation in order to separate the energy variable, for the function

$$H(\mathbf{r},\eta,\gamma) = \int_0^{E_0} dE\left(\frac{E}{E_0}\right)^{\eta-1} \Phi_0(\mathbf{r},E),$$

$$\Phi_0(\mathbf{r},E) = \int d\boldsymbol{\Omega}\,\Phi_-(\mathbf{r},E,\boldsymbol{\Omega}) \tag{70}$$

we get the following equation[2]

$$\Delta H - e^2 H = S_0 e^{-\mu\Lambda(\mathbf{r},-\boldsymbol{\Omega}_0)} \tag{71}$$

$$e^2 = \frac{3\mu^2}{\eta(2\eta+1)}\left(\frac{2}{1+\gamma} - \eta\right)\left(\frac{3-\gamma}{1+\gamma} - 2\eta\right), \tag{72}$$

$$S_0 = \frac{6\mu^2}{\eta(2\eta + 1)(1 + \gamma)}\left(\frac{3 - \gamma}{1 + \gamma} - 4\eta\right), \tag{73}$$

$$\Lambda(\mathbf{r}, -\boldsymbol{\Omega}_0) \equiv \Lambda(r,\tilde{\varkappa}) = r\tilde{\varkappa} + [R^2 - r^2(1 - \tilde{\varkappa}^2)]^{1/2}, \ \tilde{\varkappa} = \boldsymbol{\omega}\boldsymbol{\Omega}_0, \boldsymbol{\omega} = \frac{\mathbf{r}}{r} \tag{74}$$

A continuous single-valued solution of this equation which we need can be obtained, if we prescribe properly the value of the function H at the surface of a nucleus, i.e., the quantity $H(\mathbf{R},\eta,\gamma)$. Since the boundary condition (Equation 67) determines the fluxes of nucleons at the surface of a nucleus as functions of two sets of angular variables, namely, $\boldsymbol{\Omega}$ and $\boldsymbol{\omega}$, and $H(R\boldsymbol{\omega},\eta,\gamma)$ depends only on one of them, we must average Equation 67 over one of the sets of angles, proceeding from physical formulation of the problem, in order to obtain the proper boundary condition for Equation 71. Namely, taking into account the fact that double differential cross-sections for production of cascade nucleons are determined by the expression 73a, Chapter 1, we can formulate the boundary condition of the absence of the flux into the nucleus at an arbitrary angle from outside (an analogue of Equation 67) in the following natural way*:

$$\int_{\omega\Omega<0} d\boldsymbol{\omega}(\boldsymbol{\omega}\boldsymbol{\Omega})\, \Phi_{\pm}(R\boldsymbol{\omega},E,\boldsymbol{\Omega}) = \int_{\omega\Omega<0} d\boldsymbol{\omega}(\boldsymbol{\omega}\boldsymbol{\Omega})\, \Phi_{\pm}(R\boldsymbol{\omega},\eta,\boldsymbol{\Omega}) = 0. \tag{75}$$

Then for function H at the surface of a nucleus we get the following expression:

$$H(R\omega,\eta,\gamma) = \sum_{l=0}^{\infty} \frac{2l + 1}{4\pi} H_l(R,\eta,\gamma)\, p_l(\omega\Omega_0)\ , \tag{76}$$

$$H_l(R,\eta,\gamma) = 2\pi \frac{A_l I_{l+1/2}(eR) - \int_0^R dr r^{3/2} I_{l+1/2}(er) L_l(r)}{B_l I_{l+1/2}(eR) + eR\, I_{l-1/2}(eR)}\ , \tag{77}$$

$$A_l = \frac{12a}{(1 + \gamma)(2\eta + 1)}\left[\frac{(l + 1)f_{l+1} + l f_{l-1}}{(l + 1)p_{1,l+1} + l p_{1,l-1}}\right], \tag{78}$$

$$B_l = l\frac{p_{1,l-1}}{p_{2,l}} - 2_l - 1 - \frac{a}{(2\eta + 1)}\left(\frac{3 - \gamma}{1 + \gamma} - 2\eta\right)\frac{p_{1,l}}{p_{2,l}}\ , \tag{79}$$

* It should be noted that this condition differs from the Marshak condition[73]

$$\int_{\omega\Omega<0} d\boldsymbol{\Omega}(\boldsymbol{\omega}\boldsymbol{\Omega})\, \Phi_{\pm}\, (R\boldsymbol{\omega},E,\boldsymbol{\Omega}) = 0$$

adopted in the "macroscopic" neutron physics. The latter corresponds to another physical formulation of the problem, for instance, the absence of the flux into the nucleus, averaged over the angle, at any point of its surface.

$$L_l(r) = \frac{S_0}{\sqrt{R}} \int_{-1}^{1} d\tilde{\varkappa}\, P_l(\tilde{\varkappa})\, e^{-\mu\Lambda(r,\tilde{\varkappa})}, \quad p_{\sigma,l} = \int_0^1 d\tilde{\varkappa} P_l(\tilde{\varkappa})\tilde{\varkappa}^{\sigma}, \tag{80}$$

$$f_l = p_{1,l}\left[(-1)^l p_{0,l} + \int_0^1 d\tilde{\varkappa} P_l(\tilde{\varkappa})\, e^{2a\tilde{\varkappa}}\right], \quad a = \mu R \tag{81}$$

where $I_\nu(x)$ is the modified Bessel function of the first kind, and $Pl(x)$ the Legendre polynomial. Finally, carrying out the inverse Mellin transformation and using the formulas 38, 51, 65, and 76-81, we obtain the following expression for the double differential cross-sections[2]:

$$\frac{d^2\sigma_{\alpha_0\alpha}}{d\epsilon d\Omega} = \frac{R^2}{E_0}\sum_{l=0}^{\infty}\frac{2l+1}{(4\pi)^2 i} p_{1,l}P_l(\Omega\Omega_0)\int_{\sigma-i\infty}^{\sigma+i\infty} d\eta e^{\eta u} \times$$
$$[H_l(R,\eta,0) + \alpha_0\alpha\, H_l(R,\eta,\gamma)], \tag{82}$$

$$u = \ln(E_0/E) \tag{83}$$

It follows from Equations 82 and 83 that the energy distribution of secondary nucleons has the form

$$\frac{d\sigma_{\alpha_0\alpha}}{d\epsilon} = \frac{R^2}{E_0}\frac{1}{8\pi i}\int_{\sigma-i\infty}^{\sigma+i\infty} d\eta e^{\eta u}[H_0(R,\eta,0) + \alpha_0\alpha H_0(R,\eta,\gamma)], \tag{84}$$

where in accordance with Equations 73 and 77-81

$$H_0(R,\eta,\gamma) = 8\left\{\left[\frac{\bar{\sigma}^{in}}{R^2(1+\gamma)} + \frac{\pi(2\eta+1)}{6\mu\sqrt{R}}\int_0^R dr r L_0(r)\frac{\sinh(er)}{\sinh(eR)}\right] \times\right.$$
$$\left.\left[\frac{3-\gamma}{1+\gamma} - 2\eta + \frac{2}{3}\frac{(2\eta+1)}{a}[1 - eR\,\mathrm{ctnh}(eR)]\right]^{-1}\right\}. \tag{85}$$

Here $\bar{\sigma}^{in}$ is the average cross-section of inelastic interaction of a nucleon with a nucleus determined by the formula 5 in which a_0 must be replaced by a. For $u \gg 1$ ($\epsilon \ll \epsilon_0$), the expression 84 can be represented in the form

$$\frac{d\sigma_{\alpha_0\alpha}}{d\epsilon} = \frac{\bar{\sigma}^{in}}{E_0}[Q(0,eR)e^{\eta(o,a)u} + \alpha_0\alpha Q(\gamma,eR)e^{\eta(\gamma,a)u}]. \tag{86}$$

TABLE 1
The Values of the Parameters Q and η (γ,a) for ^{27}Al and ^{64}Cu Nuclei

Nucleus	Q(o,eR)	Q(2,eR)	η(o,a)	η(2,a)
^{27}Al	0.914	0.217	0.77	0.30
^{64}Cu	0.958	0.190	0.93	0.36

Here

$$Q(\gamma,eR) = \frac{R^2}{4\bar{\sigma}^{in}} \lim_{\eta\to\eta(\gamma,a)} \{H_0(R,\eta,\gamma)[\eta - \eta(\gamma,a)]\}, \tag{87}$$

η (γ,a) is the single pole of H_0 on the positive part of the real axis of the η-plane, $\eta(0,a) < 3/2$ and

$$\frac{1}{2}\frac{3-\gamma}{1+\gamma} < \eta\ (\gamma,a) < \frac{2}{1+\gamma}$$

for $\gamma \approx 1.5$-2.5 (which corresponds the actual situation)*. For ^{27}Al and ^{64}Cu nuclei the values of the parameters Q and $\eta(\gamma,a)$ at $r_0 = 1.3$ fm and $\mu = 0.3$ fm^{-1} are listed in Table 1. For relatively small u, the integral 84 can be represented in the form of a power series[2]:

$$\frac{d\sigma_{\alpha_0\alpha}}{d\epsilon} = \frac{2\pi R^2}{E_0} \sum_{n=0}^{\infty} \frac{1}{n!} \left[b_n(0) + \frac{\alpha_0\alpha}{1+\gamma} b_n(\gamma) \right] u^n, \tag{88}$$

$$b_n(\gamma) = \frac{1+\gamma}{8\pi} \frac{1}{n!} \frac{d^n}{d\left(\frac{1}{\eta}\right)^n} [\eta H_0(R,\eta,\gamma)]_{\eta\to\infty}. \tag{89}$$

The term with $l = 1$ in the sum 82 can be evaluated thus and is equal to

$$\frac{d^2\sigma_{\alpha_0\alpha}}{d\epsilon d\Omega} = \frac{1}{4\pi}\frac{d\sigma_{\alpha_0\alpha}}{d\epsilon} + \frac{R^2(\Omega\Omega_0)}{4E_0} \sum_{n=0}^{\infty} \frac{1}{n!} \left[a_n(0) + \frac{\alpha_0\alpha}{1+\gamma} a_n(\gamma) \right] u^n, \tag{90}$$

$$a_n(\gamma) = \frac{1+\gamma}{2\pi} \frac{1}{n!} \frac{d^n}{d\left(\frac{1}{\eta}\right)^n} [\eta H_1(R,\eta,\gamma)]_{\eta\to\infty}. \tag{91}$$

* Here and in what follows we set $\gamma = 2$.

Numerical calculations have demonstrated that the contribution from subsequent terms of the expansion 82 in l hardly affects the value of the cross-section. For this reason, it will not be taken into account. The expressions 82, 84, 88, and 90 contain the contribution from quasifree nucleons. It can easily be shown that the summation over n in the expressions 88 and 90 begins from unity, if this contribution is subtracted from them.

Finally, for the differential cross-sections for production of cascade nucleons in the P_1 - approximation we obtain

$$\frac{d\sigma^{(c)}_{\alpha_0\alpha}}{d\epsilon} = \frac{2\pi R^2}{E_0} \sum_{n=1}^{\infty} \frac{1}{n!} \left[b_n(0) + \frac{\alpha_0\alpha}{1+\gamma} b_n(\gamma) \right] u^n, \tag{92}$$

$$\frac{d^2\sigma^{(c)}_{\alpha_0\alpha}}{d\epsilon d\Omega} = \frac{1}{4\pi} \frac{d\sigma^{(c)}_{\alpha_0\alpha}}{d\epsilon} + \frac{R^2(\Omega\Omega_0)}{4E_0} \sum_{n=1}^{\infty} \frac{1}{n!} \left[a_n(0) + \frac{\alpha_0\alpha}{1+\gamma} a_n(\gamma) \right] u^n, \tag{93}$$

where the quantities $b_n(\gamma)$ and $a_n(\gamma)$ are determined by the formulas 89 and 91. To calculate the total distribution (Equation 1) we must add the expression 2 or 27 (or one of the expressions integrated over the angle, if we are interested in the energy distribution) to the result obtained.

E. NUCLEONIC CASCADE AT LOW ENERGIES

In this section, we shall consider the solution of the system of KEs 56, Chapter 1, for the functions Φ_α describing the transport of the primary, quasifree, and cascade nucleons for the energy of the primary nucleon of about several tens of MeV. On the basis of this solution we shall find inclusive cross-sections for production of secondary nucleons in this energy range. In addition to this, we shall discuss briefly pre-equilibrium models which are widely used for description of NRs at low energies.

1. Cross-Section for Production of Quasifree and Cascade Nucleons at Low Energies

As the energy of both incident and outgoing nucleons decrease, the system of semiclassical KEs 56, Chapter 1, which we use for the description of the nuclear cascade can become incorrect because of an increasing role of quantum-mechanical effects affecting, above all, the behavior of wave functions of these nucleons in the effective nuclear (and for protons in the Coulomb potential as well) potential field V_α. Moreover, in this energy range, the assumption that an NR is a succession of independent binary collisions with vacuum cross-sections is less justified than at higher energies. However, it is not inconceivable[14] that the INC-model (with due regard for the effect of the field V_α on the particle motion) supplemented with the evaporation model is the most effective method for the calculation of the cross-section of even an NR involving low-energy nucleons. Therefore, in order to elucidate the validity range of the outlined approach it is of interest to consider the intranuclear cascade within the framework of the INC-model (the system of KEs

56, Chapter 1) even in the domain of low energies. It is obvious that in so doing we must take into account the effects associated with the field V_α as well as the effects caused by the influence of the Fermi motion of the nuclear nucleons on the indicatrix K_q of the elastic scattering of excited nucleons.

Unfortunately, obtaining the solution of this system of KEs for excited nucleons with allowance for the effect of the potential V_α on their behavior is a rather complicated problem which to the best of our knowledge has not yet been investigated. The neglect of this effect is apparently far too crude an approximation for the description of the angular distributions of secondary nucleons (especially in the back hemisphere). On the other hand, one can hope that such an approximation may turn out to be satisfactory for the description of the energy distributions of secondary nucleons.

The cross-section for production of quasifree nucleons is described to a sufficiently good accuracy by the semiclassical expression 2. We shall use this expression to calculate the quasifree component of the cross-section in the domain of low energies under consideration as well. Since we are interested only in the energy spectra of secondary nucleons, rather than in the double differential cross-sections, i.e., in the quantities which are less sensitive to the details of quasifree scattering, we can hope that such an approximation will not result in too large errors. For the same reason we shall consider the solution of the system of KEs 56, Chapter 1, in the small-angle approximation (see Section C) directly for the function

$$\Phi_\alpha(\tilde{t},E) = \int d\Omega\, \Phi_\alpha(r(\tilde{t}),E,\Omega) \tag{94}$$

(where $\tilde{t}$ is defined by the formula 45). Then for $\Phi_\alpha(\tilde{t},E)$ we obtain the following system of KEs[15]

$$\left[\frac{d}{d\tilde{t}} + f(\alpha)\,\sigma_{11}^{eff} + f(-\alpha)\,\sigma_{1-1}^{eff}\right]\Phi_\alpha(\tilde{t},E) =$$

$$\int_E^{E_0} dE'\{\Phi_\alpha(\tilde{t},E')[2f(\alpha)\sigma_{11}^{eff} + f(-\alpha)\sigma_{1-1}^{eff}] + \tag{95}$$

$$\Phi_{-\alpha}(\tilde{t},E')\, f(\alpha)\sigma_{1-1}^{eff}\}\, \tilde{K}_q(E' \to E) + \delta_{\alpha\alpha_0}\,\delta(E - E_0)\,\delta(\tilde{t})$$

with the "boundary" condition

$$\Phi_\alpha(\tilde{t},E\Big/_{\tilde{t} = -0}^{= 0} \tag{96}$$

The quantities $\sigma_{11(1\text{-}1)}^{eff}$ and $f(\alpha)$ are defined in sEction A, and the function $\tilde{K}_q(E' \to E)$ is connected with the function $\tilde{K}_q(E',\Omega' \to E,\Omega)$ through the relation

$$\widetilde{K}_q(E' \to E) = \int d\boldsymbol{\Omega}\widetilde{K}_q(E',\boldsymbol{\Omega}' \to E,\boldsymbol{\Omega}). \tag{97}$$

Furthermore, choosing* $\widetilde{K}_q(E' \to E)$ in the form[6]

$$\widetilde{K}_q(E' \to E) = (E' - E_F)^{-1}, \tag{98}$$

using the Mellin transformation with respect to E and confining ourselves to the terms proportional to β^0 and β^1 (as well as in Section C) in the expansion of the function $\Phi_\alpha(\widetilde{t},E)$ in series in the small parameter $\beta = (N\text{-}Z)/A$ after some simple, but cumbersome calculations, we obtain the solution of the system of KEs 95 in the form[15]

$$\begin{aligned}\Phi_\alpha(\widetilde{t},E) = {} & \delta_{\alpha\alpha_0}\,\delta(E - E_0)\Theta(\widetilde{t})\exp\Big\{-\Big[f(\alpha)\sigma^{el}_{11}(E_0) + \\ & f(-\alpha)\sigma^{el}_{1-1}(E_0)\Big]\,\widetilde{y}\left(\frac{E_F}{E_0}\right)\widetilde{t}\Big\} + \delta_{\alpha\alpha_0}\Big\{\frac{f(\alpha)}{A}\,\widetilde{L}_1(\widetilde{t},E,0) + \\ & \frac{f(-\alpha)}{A}\,\widetilde{L}_1(\widetilde{t},E,\gamma) + \alpha\beta\Delta[\widetilde{L}_1(\widetilde{t},E,0) - \widetilde{L}_1(\widetilde{t},E,\gamma) - \widetilde{L}_2(\widetilde{t},E,0) + \\ & \widetilde{L}_2(\widetilde{t},E,\gamma)]\Big\} + \delta_{-\alpha\alpha_0}\frac{f(\alpha)}{A}\,[\widetilde{L}_1(\widetilde{t},E,0) - \widetilde{L}_1(\widetilde{t},E,\gamma)].\end{aligned} \tag{99}$$

Here

$$\widetilde{L}_1(\widetilde{t},E,\gamma) = \frac{\Theta(\widetilde{t})e^{-\widetilde{\mu}\widetilde{t}}}{(E_0 - E_F)\widetilde{u}}\sqrt{\tau(E,\gamma)\widetilde{t}}\;I_1\left(\sqrt{4\tau(E,\gamma)\widetilde{t}}\right), \tag{100}$$

$$\widetilde{L}_2(\widetilde{t},E,\gamma) = \frac{\Theta(\widetilde{t})e^{-\widetilde{\mu}\widetilde{t}}}{(E_0 - E_F)2\widetilde{u}^2}\,\tau(E,\gamma)\widetilde{t}\;I_2\left(\sqrt{4\tau(E,\gamma)\widetilde{t}}\right); \tag{101}$$

$$\tau(E,\gamma) = 2\widetilde{\mu}\widetilde{u}/(1 + \gamma), \quad \widetilde{u} = \ln\frac{E_0 - E_F}{E - E_F}, \quad \Delta = 1 - 1/\gamma \tag{102}$$

($I_n(x)$ is the modified Bessel function of the first kind and the quantities $\widetilde{\mu}$ and γ are determined by the formula 42). It should be noted that the formula 99 at $E_F = 0$ coincides with the integrated over the angle ϑ expression (Equation 52) for the function $\Phi_\alpha(\widetilde{t},E,\vartheta)$, which was obtained by another method.

* Numerical calculations show that such a dependence allows us to describe the mean energy of a nucleon which experiences a single act of scattering in a nucleus to within 10% and the energy distribution of nucleons which experience two acts of scattering in the energy range under consideration qualitatively.

Using the formulas in Equation 73a, Chapter 1, and 99-102, we readily obtain the following expressions for the differential cross-section $d\sigma_{\alpha_0\alpha}/d\epsilon$ for the production of secondary nucleons of a given type α and for their average multiplicity $\langle N_{\alpha_0\alpha}\ (\epsilon_\alpha)\rangle$ with the energy larger than a certain value ϵ_α[15]:

$$\frac{d\sigma_{\alpha_0\alpha}}{d\epsilon} = \delta_{\alpha\alpha_0}\left\{\frac{f(\alpha)}{A}\,\widetilde{L}_1(\epsilon,0) + \frac{f(-\alpha)}{A}\,\widetilde{L}_1(\epsilon,\gamma) + \propto\beta\Delta\right.$$
$$\left.[\widetilde{L}_1(\epsilon,0) - \widetilde{L}_1(\epsilon,\gamma) - \widetilde{L}_2(\epsilon,0) + \widetilde{L}_2(\epsilon,\gamma)]\right\} + \tag{103}$$
$$\sigma_{-\alpha\alpha_0}\frac{f(\alpha)}{A}\,[\widetilde{L}_1(\epsilon,0) - \widetilde{L}_1(\epsilon,\gamma)],$$

$$\langle N_{\alpha_0\alpha}(\epsilon_\alpha)\rangle \equiv \frac{1}{\sigma^{in}}\int_{\epsilon_\alpha}^{\epsilon_0} d\epsilon\,\frac{d\sigma_{\alpha_0\alpha}}{d\epsilon} = \frac{\delta_{\alpha\alpha_0}}{\sigma^{in}}\left\{\frac{f(\alpha)}{A}\,N_1(\epsilon_\alpha,0) + \right.$$
$$\frac{f(-\alpha)}{A}\,N_1(\epsilon_\alpha,\gamma) + \alpha\beta\Delta[N_1(\epsilon_\alpha,0) - N_1(\epsilon_\alpha,\gamma) - N_2(\epsilon_\alpha,0) + \tag{104}$$
$$\left. N_2(\epsilon_\alpha,\gamma)]\right\} + \frac{\delta_{-\alpha\alpha_0}}{\sigma^{in}}\frac{f(\alpha)}{A}\,[N_1(\epsilon_\alpha,0) - N_1(\epsilon_\alpha,\gamma)];$$

where

$$N_{1(2)}(\epsilon_\alpha,\gamma) = \int_{\epsilon_\alpha}^{\epsilon_0} d\epsilon\,\widetilde{L}_{1(2)}(\epsilon,\gamma), \tag{105}$$

$$\widetilde{L}_1(\epsilon,\gamma) \equiv 2\pi\int_0^\infty b_\perp\,db_\perp\,\widetilde{L}_1(\widetilde{t}(b_\perp),\epsilon - V_N,\gamma) =$$
$$\frac{2\pi}{(E_0 - E_F)\widetilde{u}}\int_0^\infty b_\perp\,db_\perp e^{-\widetilde{\mu}\,\widetilde{t}(b_\perp)}\sqrt{\tau(\epsilon - V_N,\gamma)\,\widetilde{t}(b_\perp)}\ \times \tag{106}$$
$$I_1\left(\sqrt{4\tau(\epsilon - V_N,\gamma)\,\widetilde{t}(b_\perp)}\right),$$

$$\widetilde{L}_2(\epsilon,\gamma) \equiv 2\pi\int_0^\infty b_\perp\,db_\perp\,\widetilde{L}_2(\widetilde{t}(b_\perp),\epsilon - V_N,\gamma) =$$

$$\frac{\pi}{(E_0 - E_F)\tilde{u}^2} \int_0^\infty b_\perp \, db_\perp e^{-\tilde{\mu}\tilde{t}(b_\perp)} \, \tau(\epsilon - V_N, \gamma) \, \tilde{t}(b_\perp) \times \tag{107}$$
$$I_2\left(\sqrt{4\tau(\epsilon - V_N, \gamma)\tilde{t}(b_\perp)}\right)$$

and the function $\tilde{t}(b_\perp)$ is determined by the formula 62.

In accordance with Equation 99 for the cross-section σ^{in} of the inelastic interaction between a nucleon of the type α_0 and a nucleus, we get

$$\sigma^{in} = 2\pi \int_0^\infty b_\perp \, db_\perp \left[1 - \exp\left\{-[f(\alpha_0)\, \sigma_{11}^{el}(E_0) + f(-\alpha_0)\, \sigma_{1-1}^{el}(E_0)]\, \tilde{y}\left(\frac{E_F}{E_0}\right) \tilde{t}(b_\perp)\right\}\right]. \tag{108}$$

For a nucleus of a radius R with a sharp boundary and N = Z, the expression 104 for $\langle N_{\alpha_0\alpha}(\epsilon_\alpha)\rangle$ is reduced in view of Equations 5 and 108, to a more simple form[15]:

$$\langle N_{\alpha_0\alpha}(\epsilon_\alpha)\rangle = \frac{1}{(2a)^2\xi_0}[\bar{N}_1(\epsilon_\alpha, 0) + \alpha_0\alpha\bar{N}_1(\epsilon_\alpha, \gamma)], \tag{109}$$

where

$$\bar{N}_1(\epsilon_\alpha, \gamma) = \sum_{n=0}^{\infty} \left(\frac{2}{1+\gamma}\right)^{n+1} (n+2)\left[1 - e^{-2a} \sum_{m=0}^{n+2} \frac{(2a)^m}{m!}\right] \times \left[1 - e^{-\tilde{u}_\alpha} \sum_{m=0}^{n} \frac{(\tilde{u}_\alpha)^m}{m!}\right]; \tag{110}$$

$$\begin{aligned} a &= \tilde{\mu}\rho R = 3\tilde{\mu}/4\pi R^2], \\ \tilde{u}_\alpha &= ln[(\epsilon_0 - V_N - E_F)/(\epsilon_\alpha - V_N - E_F)], \\ \xi_0 &= 1 - [1 - (1 + 2a_0)e^{-2a_0}]\,(2a_0^2)^{-1}, \\ a_0 &= \frac{3A}{8\pi R^2}\left[\sigma_{11}^{el}(E_0) + \sigma_{1-1}^{el}(E_0)\right]\tilde{y}\left(\frac{E_F}{E_0}\right). \end{aligned} \tag{111}$$

It follows from Equation 109 that the expression for the total number of the knocked-out nucleons $\langle N_{\alpha_0}\rangle = \sum_\alpha \langle N_{\alpha_0\alpha}\rangle$ with the energy larger than $\tilde{\epsilon}$ has the following simple form:

$$\langle N_{\alpha_0}\rangle = \overline{N}_1\,(\widetilde{\epsilon},0)/(2a^2\xi_0). \tag{112}$$

It should be noted that in the formulas 103 and 104 the contribution from quasifree nucleons was calculated within the framework of the same approximations that were used in the calculation of the contribution from cascade nucleons. This can turn out to be too crude an approximation for the calculation of the quantities in question in the domain of low energies of primary nucleons ($\epsilon_0 \lesssim 100$ MeV). Hence, at low-energies, this contribution must be subtracted and an appropriate "exact" expression following from Equation 2 is to be used instead of it. It can be easily seen that the subtraction of this contribution is reduced to the subtraction of the first terms of the expansion of $I_1(I_2)$ in series in $\sqrt{4\tau(E,\gamma)\,\widetilde{t}}$ from $I_1(I_2)$ in 100, 101, i.e., to the substitution of

$$\begin{aligned}
\widetilde{L}_1(\widetilde{t},E,\gamma) &= \frac{\Theta(\widetilde{t})e^{-\widetilde{\mu}\widetilde{t}}}{(E_0 - E_F)\widetilde{u}}\sqrt{\tau(E,\gamma)\widetilde{t}}\ \times \\
&\left[I_1\left(\sqrt{4\tau(E,\gamma)\widetilde{t}}\right) - \sqrt{\tau(E,\gamma)\widetilde{t}}\right], \\
\widetilde{L}_2(\widetilde{t},E,\gamma) &= \frac{\Theta(\widetilde{t})e^{-\widetilde{\mu}\widetilde{t}}}{(E_0 - E_F)2\widetilde{u}^2}\,\tau(E,\gamma)\,\widetilde{t}\ \times \\
&\left[I_2\left(\sqrt{4\tau(E,\gamma)\widetilde{t}}\right) - \frac{\tau(E,\gamma)\widetilde{t}}{2}\right]
\end{aligned} \tag{113}$$

for $\widetilde{L}_1$ and $\widetilde{L}_2$ in Equations 100 and 101.

In this case, Equations 103 and 104 describe the differential cross-section for the production of cascade nucleons of the type α and their average multiplicity $\langle N_{(c)\alpha 0\alpha}\ (\epsilon_\alpha)\rangle$. The expression 103 (with regard to Equation 113) will be used below in the calculation of the cascade component of the cross-section (Equation 1) in the domain of the energy of primary nucleons corresponding to the values of about several tens of MeV. To calculate the energy distributions and average multiplicities of secondary nucleons in the domain $\epsilon_0 \gtrsim 100$ MeV, we shall use the expressions 100-109.

2. Pre-Equilibrium Models of NRs at Low Energies

The so-called pre-equilibrium models are often used for description of NRs at the energies $\epsilon_0 \lesssim 100$MeV (see the reviews[16,17]). The pre-equilibrium Harp-Miller-Berne model,[18] in which the establishment of statistical equilibrium in a highly-excited nucleus was considered, is one of the closest to the INC-model in its formulation. The relaxation of a nucleon Fermi gas through subsequent binary collisions was described by the system of coupled KEs for the occupation numbers of single-particle nuclear states contained in an arbitrary energy bin of a width ΔE, the entire energy space of single-particle levels being divided into such bins. By its physical meaning, this system of KEs is intimately related to the system of KEs

49, Chapter 1, for the occupation numbers of single-particle nuclear states in the phase space, which is applied to the description of inclusive NRs. For this reason, it will not be considered here. Moreover, this model has not gained wide acceptance, because its use encounters considerable computational difficulties.

The exciton model whose basis has been laid in Griffin[19] is most extensively used.[16,17] In this model, a state of a nucleus is characterized by the exciton number n, that is, the total number of excited particles p and holes h, $n = p + h$, and by excitation energy $E^* = \epsilon_0 + B_N$. All states with equal number of excitons are considered as identical. Starting from an initial nonequilibrium state, an excited nucleus evolves towards the equilibrium redistributing the initial excitation energy over an ever-increasing number of excitons, owing to a residual two-body interaction. A two-body nature of residual interactions imposes the selection rules upon allowed transitions, namely $\Delta n = 0$ or ± 2. At the initial stage of the reaction, an excited system evolves predominantly towards the states of increasing complexity, passing subsequently through the states with $n = 3,5,7$, etc. As the equilibrium is approached, transitions with $\Delta n = 0$ and $\Delta n = -2$ become more and more important. In the state of statistical equilibrium which is characterized by an equilibrium number of excitons n_{eq}, all three types of transitions are equiprobable. This stage of the process is described within the framework of the evaporation model (see Chapter 3). In the course of the evolution of the system, among possible configurations with a fixed number of excitons there exist such states in which at least one nucleon is in a single-particle state of a continuous spectrum, i.e., it can be emitted by nucleus*. An outlined process of nuclear relaxation is described by the KE (or the master equation) for the probability P(n,t) to find n excitons in a nucleus at the instant of time t[17]

$$\frac{dP(n,t)}{dt} = \lambda_+(n-2,E^*)\,P(n-2,t) + \lambda_-(n+2,E^*)\,P(n+2,t) - \left[\lambda_+(n,E^*) + \lambda_-(n,E^*) + \sum_\alpha \Gamma_\alpha(n,E^*)\right] P(n,t) \tag{114}$$

with the initial condition

$$P(n,0) = \delta_{nn_0}. \tag{115}$$

In Equation 114, $\lambda_\pm$ are the probabilities of transitions with $\Delta n = \pm 2$ per a unit time, Γ_α is the probability of the emission of an α-type particle (n,p,d,t, ^{3}He, ^{4}He, etc). in a continuous spectrum per a unit time, and n_0 the initial number of excitons.

* In a modified exciton model, namely the hybrid-model, it is assumed that among all n-exciton states the main contribution to the emission of a particle with the energy ϵ comes from such states that have one particle with the energy ϵ in the domain of a continuous spectrum. Exit in other states is realized as a result of collisions of just this particle, whereas other collisions are not taken into consideration. With allowance for the geometry of the reaction the hybrid-model takes into account the effect of the diffuseness of a nuclear density and that of the potential on the emission of nucleons.

(The value of n_0 is a free parameter of the model, and it is assumed that $n_0 = 3$ for the NA-reaction).

In the first order of the perturbation theory with respect to a small residual two-body interaction, for the transition probability $\lambda_{n\to n+\Delta n}$ (n,E*) we get

$$\lambda_{n\to n+\Delta n}(n,E^*) \equiv \lambda_{+,-,0}(n,E^*) = (2\pi/\hbar)\langle|\hat{M}|^2\rangle\, \omega_f^{(+,-,0)}(n,E^*) \quad (116)$$

$$\Delta n = 0, \pm 2$$

where $\langle|\hat{M}|^2\rangle$ is the value of the squared matrix element averaged over allowed transitions and $\omega_f^{(+,-,0)}$ (n,E*) the density of final states which are really accessible in this transition. For the case of an equidistant single-particle spectrum with the density g, we get[17,20]

$$\omega_f^{(+)}(p,h,E^*) = \frac{g}{2}\frac{(gE^*)^2}{(p+h+1)},$$

$$\omega_f^{(-)}(p,h,E^*) = \frac{g}{2}[ph\,(p+h-2)], \quad (117)$$

$$\omega_f^{(0)}(p,h,E^*) = \frac{g^2E^*}{2(p+h)}[p(p-1)+4ph+h(h-1)].$$

Incorporation of the Pauli exclusion principle which reduces the number of accessible final states leads to more complicated expressions for these quantities[17,20]. If n is small, $\omega_f^{(+)} >> \omega_f^{(-)}$ and transitions with $\Delta n = +2$ predominate. It is clear that the equilibrium is attained when $\lambda_+ = \lambda_-$. It follows from this condition, and Equations 116 and 117 that for a typical case $gE^* >> 1$ the equilibrium number n_{eq} of excitons is determined by relation $n_{eq} \simeq \sqrt{2gE^*}$. Thus, the equidistant model allows one to calculate the density of nuclear states. As for $\langle|\hat{M}|^2\rangle$, the situation is less definite. At present, it is impossible to calculate $\langle|\hat{M}|^2\rangle$ exactly. Therefore, while analyzing experimental data on the basis of the exciton model, we are forced to consider $\langle|\hat{M}|^2\rangle$ as a free parameter or estimate it proceeding from the probability of collision of nucleons in nuclear matter.[17,20]

The partial width of emission of a pre-equilibrium particle can be written in the form[17]

$$\Gamma_\alpha(n,E^*) = \int_{V_{c,\alpha}}^{E^*-B_\alpha} \frac{(2s_\alpha+1)}{\pi^2\hbar^3}\mu_\alpha\epsilon\sigma^\alpha_{in\vartheta}(\epsilon)\gamma_\alpha R_\alpha(p) \times \frac{\omega(p_\alpha,0,E^*-E_f^*)}{g}\frac{\omega(p-p_\alpha,h,E_f^*)}{\omega(p,h,E^*)}d\epsilon\,. \quad (118)$$

Here ϵ, s_α,μ_α,B_α,$V_{c,\alpha}$ and σ^α_{inv} are, respectively, the energy, the spin, the reduced mass, the binding energy, the Coulomb barrier, and the cross-section of the inverse reaction for an emitted particle, and $\omega(p,h,E^*)$ and $\omega(p\text{-}p_\alpha,h,E^*_f)$ the densities of quasiparticle states of the decaying and the residual (with the excitation energy $E^*_f = E^*\text{-}\epsilon\text{-}B_\alpha$) nucleus. In the case of an equidistant scheme of single-particle levels with the density g, the quantity $\omega(p,h,E^*)$ has the form[17,20]

$$\omega(p,h,E^*) = \frac{g(gE^*)^{p+h-1}}{p!\ h!\ (p + h - 1)!}. \tag{119}$$

The factor $\omega(p_\alpha,0,E^*\text{-}E^*_f)/g$ is the number of states of an emitted complex particle. The factor $R_\alpha(p)$ takes into account the fact that a combination p_α of nucleons chosen from the total number p of excited particles has an isotopic composition corresponding to an emitted complex particle of the type α.

The factor γ_α describes the probability of a formation of a complex particle α form p_α excited particles of the required isotopic composition. If we identify γ_α with the overlap integral of wave functions of independent nucleons and a complex particle and assume that the wave functions are constant in appropriate volumes, then[20]

$$\gamma_\alpha \simeq p_\alpha^3 \left(\frac{p_\alpha}{A}\right)^{p_\alpha - 1}. \tag{120}$$

In the case of nucleon emission, all these three factors are equal to unity.

Unfortunately, we are deprived of the possibility of discussing in detail other pre-equilibrium models, including the ones based on the use of quantum KEs for open finite Fermi systems. The exciton model is chosen here not only because it is extensively used for the analysis of NRs, but also because there exists its Monte Carlo realization. This makes it compatible with the Monte Carlo description of the INC and the evaporation cascade and allows us to use it for the study of the energy dissipation in various NRs in subsequent chapters.

II. SOLUTION OF THE SYSTEM OF KES OF THE INC-MODEL BY MEANS OF THE MONTE CARLO TECHNIQUE

Analytic methods used for solving KEs play a significant role in the substantiation of the INC-model and in the study of the dependence of characteristics of reactions on the details and parameters of the model. Since the derivation of an analytic solution is a rather challenging mathematical problem, a considerable progress in the development of these methods has been made only recently. On the other hand, it becomes possible to find an analytic solution of the system of KEs at the cost of introducing a number of simplifying assumptions which cannot be always justified.

With the help of numerical methods of solving KEs we can consider a wide range of characteristics (both inclusive and exclusive ones) of various NRs without resorting to serious simplifications. It is well known from the transport theory[21] that the Monte Carlo technique (a method of statistical simulation) is one of the methods used to obtain numerical solution of KEs.

By a statistical simulation we mean a process, when instead of real physical quantities having certain statistical properties, random variables are considered which have the same probability distributions as the physical quantities corresponding to them. Real physical quantities are approached as a result of multiple repeated choice of random variables, i.e., their Monte Carlo random sampling.

A mathematical nature of this method is adequate to a statistical nature of such a complicated and diverse phenomenon as INC. For the first time, this method was applied to the description of the NA-interaction in Goldberger's paper.[22] During 40 years which have elapsed, a number of scientists studied the Monte Carlo technique as applied to the analysis of the INCs. The model has been considerably refined, extended to cover the domain of high energies (up to approximately 10^3 GeV), and generalized to the case of NRs initiated by photons, pions, antinucleons, and nuclei. Since the Monte Carlo realization of the INC-model has been already described in detail in reviews and monographs,[1,6,23] we shall confine ourselves here to a succinct presentation of its underlying principles.

A. STANDARD MONTE CARLO INC-MODEL

It has been mentioned above that the macroapproximation outlined in Section IIG of Chapter 1 forms the basis of the standard INC model. The codes realizing this model actually consist in solving Equation 43, Chapter 1, through calculating the terms of the von Neumann series (series in collisions) by means of the Monte Carlo technique.

1. General Scheme of the Monte Carlo Simulation of INCs

Figure 3 shows the general scheme of the calculation which realizes the basic principles of the INC-model. It corresponds to a simulation of the "fate" of an incident particle colliding with a nucleus. In this block-diagram, rectangles denote separate subprograms (or operators) performing certain logically closed tasks. Logical operators which control various ramifications of the code are depicted as ovals.

Block 1 takes into account a change in the projectile momentum under the action of the nuclear potential. In block 2, the momentum and the isospin of an intranuclear nucleon (the so-called partner) which interacts with the projectile are sampled. Then, the mean free path L of the particle in nuclear matter is determined from the total cross-section $\sigma^{tot}(E')$ of an elementary interaction (E' is the kinetic energy of the particle in the reference frame co-moving with the partner) calculated beforehand and the interaction point is subjected to random selection.

In block 3 it is verified whether this point lies inside the nucleus. If this is not the case, the particle is considered as passing through the nucleus without undergoing any collision. If the interaction point is inside the nucleus, then in block 4 a type of the interaction (elastic, charge exchange, production of one or several pions,

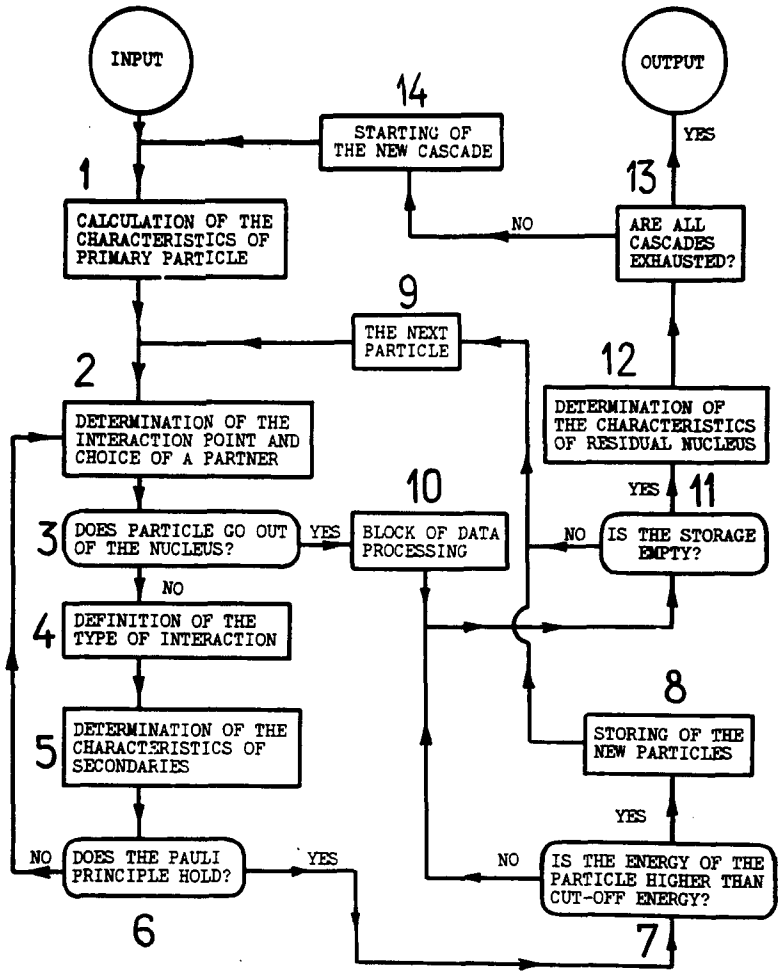

FIGURE 3. This is a general scheme of the calculation of the INC.

etc.) is determined from the partial cross-sections $\sigma_i(E')$. In accordance with the chosen type of interaction, characteristics of all secondary particles (their type, multiplicity, and kinematic characteristics as well) are determined in block 5. Block 6 verifies whether the constraints imposed by the Pauli exclusion principle are satisfied or not. If among secondary particles there is a nucleon with the energy lower than the Fermi energy E_F, then this interaction is considered as prohibited, and the trajectory of the particle is traced further from the forbidden point. In block 7, energies of particles are compared with the so-called cut-off energy E_{cutoff}. Particles with the energy $E > E_{cutoff}$ participate in the development of the INC. Their characteristics are stored in block 8, and then for each of them the cascade calculation is repeated by going over from block 9 to block 2. It is assumed that

a particle with $E \leq E_{cutoff}$ is absorbed by the nucleus. It is not considered in the subsequent analysis and contributes only to the characteristics of an R-nucleus.

The calculation is carried out until all secondary particles are absorbed or leave the nucleus. Blocks 8,9, and 11 are responsible for this. If the "history" of the projectile is traced completely (i.e., if the memory is empty), then the characteristics of an R-nucleus, namely, the numbers of protons (Z), neutrons (N), and excitons (n) in it (See Section IE2), its excitation energy E*, angular momentum I, and momentum $\mathbf{p}_r$, are determined in block 12. Then the "history" of another projectile is simulated (blocks 13 and 14) and so on, until the required statistics are collected. The resultant information on the NR is accumulated in block 10.

Various cascade calculations carried out by numerous groups in the domain of intermediate energies[24-28] (and see earlier studies cited[23]) are fit in the general scheme depicted in Figure 3. The existing versions of the INC-model differ in the form of specific blocks which are dictated by a choice of the model of a nucleus and by the diversity of elementary processes taken into consideration in a given calculation. Let us consider these blocks in greater detail using the version developed in *JINR*(Dubna)[23] as an example.

2. Model of a Target Nucleus

A T-nucleus is treated as a mixture of degenerate Fermi gases of neutrons and of protons in the spherical potential well V_α (r) (see Section IIC, Chapter 1). According to Equation 17, Chapter 1, a corresponding distribution of intranuclear nucleons over the magnitude of the momentum p has the form

$$W(p) = \begin{cases} 3p^2/p_{F,\alpha}^3 \ , & p \leq p_{F,\alpha} \\ 0 \ , & p > p_{F,\alpha} \end{cases} \tag{121}$$

where the momentum $p_{F,\alpha}$ is connected with the density of nucleons of the type α ($\alpha = 1$ for protons and $\alpha = -1$ for neutrons) through Equation 18, Chapter 1.

The case of a diffuse boundary of a nucleus is usually considered. In addition to this, it is assumed that the same function describes the distribution of intranuclear nucleons $\rho_\alpha(r)$ and the charge distribution obtained in the experiments on the electron scattering,[29] namely

$$\rho_N(r) \equiv \rho_p(r) + \rho_n(r) = \rho_0\left\{1 + \exp\left(\frac{r - c}{a}\right)\right\}^{-1}, \tag{122}$$

where $c = 1.07\ A^{1/3}$ fm and $a = 0.545$ fm. The nucleus is divided by several concentric spheres into separate zones with a constant nucleon density in each zone. The partitioning into seven zones approximates the initial distribution $\rho_N(r)$ to a good accuracy. In principle, one can deal without dividing the nucleus into zones as was done in Reference 30, where $p_{F,\alpha}$ was assumed to be a smooth function of $\rho_N(r)$.

The use of such a crude model of a nucleus is justified by the fact that characteristics of an inelastic interaction between a high-energy particle and a nucleus are hardly sensitive to the nuclear structure (this refers, above all, to deep inelastic channels of this interaction). However, in a number of cases, the use of a more realistic model of a nucleus is desirable. For instance, in calculations of INCs in light T-nuclei, Fraenkel et al.[26] used the shell model.

3. Characteristics of an Incident Particle Inside a T-Nucleus

The value of the impact parameter b and that of the asimuthal angle φ which determine the point at which the particle (falling onto a disc of a radius R) enters a nucleus are sampled with the help of two random numbers β_1 and β_2 uniformly distributed in the segment [0,1]:

$$b = R\sqrt{\beta_1}, \quad \varphi = 2\pi\beta_2. \tag{123}$$

Here R is the radius of the last zone of a nucleus*.

The potential $V_\alpha(r)$ acting on nucleons is defined by the relation (see also Section IA)

$$V_\alpha(r) = -E_{F,\alpha}(r) - B_{N,\alpha}, \tag{124}$$

where $E_{F,\alpha}(r) = p^2_{F,\alpha}(r)/2m_N$ is the Fermi energy of a nucleon of the type α at the point r, and $B_{N,\alpha}$ the energy required for separation of the last nucleon (the nucleon with the minimum binding energy) averaged over the domain of adjacent nuclei. Usually it is assumed that $B_{N,\alpha} = B_N = 7$ MeV. The potential V_α is often considered as a parameter whose value is found from the condition of the best fit to experimental data. Problems concerned with choice of the magnitude of the potential for other particles will be discussed in other chapters.

A jump in the potential at the boundary of a nucleus (or its zones) leads to a refraction and reflection of particles. Obviously, this effect is most pronounced for particles of comparatively low energies. Taking into account the conservation of squared four-momentum $\hat{p}^2 = p^{02} - \mathbf{p}^2$ ($cp^0 = E + mc^2$ is the total energy of the particle and m its mass) and assuming that V_α is time component of the four-vector, we obtain the expression for the radial component of the momentum inside the nucleus in the form

$$p_R'^2 = (p^{0\prime})^2 - (p^0)^2 + p_R^2 = V_\alpha^2/c^2 - 2V_\alpha\, p^0/c + p_R^2 \tag{125}$$

and the relation $\sin\Theta = \varkappa_R \sin\Theta'$ between the angle of incidence Θ and angle of refraction Θ' ($\varkappa_R = \sqrt{(E + V_\alpha)/E}$ is the index of refraction). The total internal reflection takes place for angles $\Theta > \Theta_{cr}$ ($\cos\Theta_{cr} = \sqrt{V_\alpha(2cp^0 - V_\alpha)}/cp$). In a more realistic case of a smooth potential, the effects associated with refraction are less pronounced. Therefore, they are disregarded in a number of calculations.

* We disregard the effect of Coulomb field which is justified in the case of high-energy projectiles.

4. Search of a Partner and an Interaction Point

For a particle moving in a uniform medium with a density ρ_N, the probability of undergoing a collision in the segment $[l, l+dl]$ of its way is given by the expression

$$W(l)\,dl = e^{-l/L}dl/L, \tag{126}$$

where $L = 1/\rho_N\sigma^{tot}$ is the mean free path of the particle. The distance run by the particle until it undergoes the act of interaction is determined by one random number β:

$$l = -L\ln\beta. \tag{127}$$

The cross-section σ^{tot} of the interaction between a particle and an intranuclear nucleon depends on a relative velocity of colliding particles, i.e., on the Fermi motion of the partner. To take into account this effect the kinetic energy of the partner and the direction of its motion are sampled in accordance with Equation 121, the procedure involving three random numbers

$$E = E_F\beta_1^{2/3},\ \cos\vartheta = 1 - 2\beta_2,\ \varphi = 2\pi\beta_3. \tag{128}$$

Then one finds the kinetic energy E' of the particle in the reference frame co-moving with the partner and the mean free path L which corresponds to this energy and which is averaged over the type of the partner

$$L = \frac{1}{\rho_N}\left[\sigma_p^{tot}(E')\frac{Z}{A} + \sigma_n^{tot}(E')\frac{A-Z}{A}\right]^{-1}. \tag{129}$$

A relative magnitude of terms occurring in this expression determines the probability of the interaction of the particle with an intranuclear neutron and a proton, i.e., the type of the partner. To take into account the dependence of ρ_N on **r** one must use the relation

$$\ln\beta = -\int\frac{dl}{L(\mathbf{r},E')},\quad L(\mathbf{r},E') = 1/\rho_N(\mathbf{r})\,\sigma^{tot}(E'). \tag{130}$$

where the integral is taken along the trajectory of the particle, instead of Equation 127.

5. Calculation of an Elementary Interaction

Once the interaction point **r** and the momentum **p** and the isospin of the partner have been determined, the type of an elementary process is sampled. To this end it is necessary to know partial cross-sections σ_i of all its channels over the entire energy range under consideration.

The majority of the versions of INC-model were confined to a consideration of two types of cascade particles, namely, nucleons and pions. The version presented in References 1 and 23 is most universal. The version analyzes the NN- and πN-collisions in the energy range $\lesssim$ 20 GeV and takes into consideration the following elementary subprocesses:

$$\mathrm{NN} \rightarrow \mathrm{NN}, \quad \mathrm{NN} \rightarrow \pi\mathrm{NN}, \quad \mathrm{NN} \rightarrow \mathrm{i}\pi\mathrm{NN} \quad (\mathrm{i} \geq 2), \tag{131a}$$

$$\pi\mathrm{N} \rightarrow \pi\mathrm{N}, \quad \pi\mathrm{NN} \rightarrow \mathrm{NN}, \quad \pi\mathrm{N} \rightarrow \pi\pi\mathrm{N}, \quad \pi\mathrm{N} \rightarrow \mathrm{i}\pi\mathrm{N}\ (\mathrm{i} \geq 3). \tag{131b}$$

(in the πN $\rightarrow$ πN channel, elastic scattering and charge exchange reactions are separated). The cross-sections of all these subprocesses are presently well known.[31] Therefore, tables with empirical values of the total and partial cross-sections of pp-, pn-, and $\pi^{\pm}$N-interactions for separate characteristic values of the energy are put into the memory of a computer (intermediate values are found by means of interpolation). All other cross-sections (for the nn-, $\pi^{\pm}$n-, π^{0}p- and other interactions) are found from the isotopic invariance. Once the cross-sections of elastic scattering σ^{el} (E′), charge exchange σ_{ex}(E′), production of one pion σ_{π}(E′), and multiple production of pions $\sigma_{i\pi}$(E′) have been calculated, the type i of the elementary subprocess is sampled with the help of a random number β. To this end it is necessary to determine the interval $\left[\sum_{j=1}^{i-1} \xi_j, \sum_{j=1}^{i} \xi_j\right]$ ($\xi_j = \sigma_j(E')|/\sigma^{tot}(E')$) in the segment [0,1] within which the random number β falls.

It is well known that a pion can be absorbed by a nucleus with a noticeable probability. In view of the energy-momentum conservation law it cannot be absorbed by one free nucleon. At least two nucleons must be involved in this process. To describe a two-nucleon absorption of a pion πNN $\rightarrow$ NN we can use the quasideuteron model[32] in which the cross-section of absorption by a nucleus is connected with the cross-section of absorption by a deuteron through the relation

$$\sigma_A(\epsilon_0) = f(A,Z,\epsilon_0)\ \sigma_d\ (\epsilon_0). \tag{132}$$

Here the function f takes into account the difference between the absorption by a np-pair in a deuteron and a nucleus, e.g., for pions $f(A,Z,\epsilon_0) = 4Z$.[32] Since the pion absorption is one of possible reaction channels, it effectively contributes the total cross-section σ^{tot} and affects the mean free path of a pion inside a nucleus. This fact is taken into consideration not only in the sampling of the type of interaction, but also in that of the interaction point. Another specific feature of this subprocess is that, in this case, the second partner is sampled and that an effect of the total momentum of a nucleon pair $\mathbf{p}_{ass} = \mathbf{p}_1 + \mathbf{p}_2$ on the pion absorption is taken into account.

In addition to the reactions in Equation 131, this version[23] of the INC-model includes the subprocesses realizing principal mechanisms of absorption of intermediate-energy photons by nuclei, namely, an absorption by a quasideuteron pair

$$\gamma + (\mathrm{np}) \rightarrow \mathrm{np} \tag{133a}$$

and absorption through the pion production

$$\gamma \mathrm{N} \rightarrow \pi \mathrm{N}, \quad \gamma \mathrm{N} \rightarrow \pi\pi \mathrm{N} \tag{133b}$$

as well. A two-nucleon absorption of a photon is described by the quasideuteron model.[33] In this case, the function f in Equation 132 for photons is given by $f(A,Z,\epsilon_0) = 10Z(1 - Z/A)$.[34] Incorporation of the subprocesses of Equation 133 allows one to use the INC-model for analysis of photonuclear reactions in the energy range 50 MeV $< E_\gamma <$ 1,2 GeV.[34,35]

Once the type of an elementary process has been determined, kinematic characteristics of all secondaries produced in it are found. To this end this version[1,23] of the INC-model employs an approach based on the use of inclusive experimental distributions (angular, momentum, etc.) which are subjected to sampling by means of the Monte Carlo technique. This allows one to find exclusive characteristics of an individual act of elementary interaction. Corresponding integral distributions

$$W_\vartheta(\cos\vartheta) = \int_0^{\cos\vartheta} w_\vartheta(2z - 1)dz\left(\int_0^1 w_\vartheta(2z - 1)dz\right)^{-1}, \tag{134}$$

$$W_p(p) = \int_0^p w_p(zp_{max})\, dz\left(\int_0^1 w_p(zp_{max})dz\right)^{-1}. \tag{135}$$

which are smoother functions of the angle and momentum* are used in it instead of differential distributions $w_\vartheta(\cos\vartheta)$ and $w_p(p)$. In the Monte Carlo sampling, the value of the angle and that of the momentum are determined as inverse functions $\cos\vartheta = W_\vartheta^{-1}(\beta)$ and $p = W_p^{-1}(\beta)$ of the random number β for each particle. Taking account of the energy-momentum conservation law gives automatically the correct values of the average multiplicity of secondaries. The use of a sample with additional conditions according to experimental distributions (e.g., to distribution over the transverse momentum) allows one to improve the accuracy of such a procedure. A further simplification of calculations can be achieved, if polynomial approximations of $W_\vartheta^{-1}(\beta)$ and $W_p^{-1}(\beta)$ are used. A search for such approximations involves a rather cumbersome numerical analysis of a large body of experimental data. However, once it has been carried out, the approximations obtained turn out to be quite effective for the simulation of the cascade. Details for the calculations and tables containing polynomial coefficients of the approximations of the functions $W_\vartheta^{-1}(\beta)$ and $W_p^{-1}(\beta)$ for the sampling of characteristics of secondaries produced

* In binary processes, the characteristics of secondaries are completely determined, if the value of the angle ϑ is preset. In this case, it is sufficient to use one distribution $W_\vartheta(\cos\vartheta)$.

in πN- and NN-collisions for energies $E \leqslant 20$ GeV are given in Reference 1 and for γN-collisions in the energy range $E_\gamma \leqslant 1.2$ GeV in the paper.[35] Empirical approximations for πN- and NN-collisions in the domain of high energies ($E \leqslant 10^3$ GeV) were obtained in Reference 36.

In the energy range $E \lesssim 3$ GeV, elementary processes with production of one or two pions play a decisive role. In a number of papers,[24,30] an elementary interaction is described by the isobar model (i.e., in the assumption that a pion is created through the production of the isobar Δ (1232) and its subsequent decay into a pion and a nucleon) in this energy range. Since this resonance is rather narrow, it lives long enough in the nucleus to interact with a nucleon before its decay. Therefore, a number of versions of the INC-model includes the Δ-isobar along with pions and nucleons in the cascade. In this case, the elementary processes $\Delta N \rightarrow \Delta N$ and $\Delta N \rightarrow NN$ are incorporated in the cascade. A two-nucleon absorption of a pion is visualized as a two-stage process: first the isobar is formed in the reaction $\pi N \rightarrow \Delta$, then it is scattered by an intranuclear nucleon $\Delta N \rightarrow NN$.

It should be noted that the use of the isobar model is justified in a relatively narrow energy range in the vicinity of the (3,3)-resonance. In addition to this, the cross-sections of the interaction between the Δ-isobar and nucleons, as well as the depth of the potential well for the Δ-isobar, are not known. Usually these quantities are considered as parameters of the model and assumed to be equal to the nucleon values. On the other hand, the use of empirical approximations for πN- and NN-interactions takes into account effects of production of a Δ-isobar in the corresponding energy range and does not call for the introduction of additional parameters. The calculation of the cascade with allowance for a two-nucleon absorption $\pi NN \rightarrow NN$ and the corresponding calculation taking account of the Δ-isobar production differ from one another only slightly.[30]

As the energy increases in the range $E > 1$ GeV, the cross-sections for production of heavier baryonic resonances (Δ,N*) and mesons (K,ρ,η,ω, ...) in NN- and πN-collisions become larger. To include these new objects in the cascade we need models which describe their production in an elementary act. With this end in view one can make use of various modifications of the statistical model of multiple production of particles,[37] of the model of quark-gluon strings, and of some other models.[38,39]

Without going into details of a simulation of an elementary act, we would like to note that the relations of relativistic kinematics are used, as a rule, in the calculation of the INC.

6. Cut-Off Energy

It has been already mentioned in Section V of Chapter 1 that a low-energy particle with a large value of the de Broglie wavelength cannot be considered in a nucleus as a classical particle and its interaction with a nucleus as collisions with individual nucleons. Therefore, it is assumed in the model that it can be done, if the energy E of the particle is larger than a certain value called the cutoff energy $E_{cut\text{-}off}$. The magnitude of $E_{cut\text{-}off}$ is the parameter of the model. Usually it exceeds the energy necessary for escape of a particle from a nuclear potential well by several

MeV. It is assumed sometimes that E_{cutoff} depends on the orbital momentum of a particle.[1] Particles with $E < E_{cutoff}$ are assumed to be absorbed by a nucleus and their further evolution is described by the models of subsequent stages of an NR. It is important to emphasize,[1] however, that even spectra of slow particles emitted in a reaction depend only slightly on E_{cutoff}, if these subsequent stages are taken into consideration.

7. Characteristics of an R-Nucleus

After the completion of a cascade, the Fermi-sea contains a certain number h of holes equal to the number of collisions experienced by cascade particles in nuclear matter and a certain number of excited nucleons p equal to a number of slow cascade nucleons absorbed by a nucleus. The excitation energy E* of an R-nucleus is equal to the sum of energies E_i^h, E_i^p of quasiparticles measured from the Fermi energy:

$$E^* = \sum_{i=1}^{h} E_i^h + \sum_{i=1}^{p} E_i^p. \tag{136}$$

The numbers, "e,s", of nucleons A and of protons Z, the momentum $\mathbf{p}_r$, and the angular momentum $\mathbf{I}$ of an R-nucleus are determined by the relations:

$$\begin{aligned} A &= A_t + q_0 - \sum_{i=1}^{N_c} q_i^c, \quad Z = Z_t + e_0 - \sum_{i=}^{N_c} e_i^c, \\ \mathbf{P}_r &= \mathbf{p}_0 - \sum_{i=1}^{N_c} \mathbf{p}_i^c, \qquad \mathbf{I} = \mathbf{I}_0 = \sum_{i=1}^{N_c} \mathbf{l}_i^c, \end{aligned} \tag{137}$$

where A_t and Z_t are the numbers of nucleons and protons in a T-nucleus; q_0, e_0, $\mathbf{p}_0$, and $\mathbf{I}_0$, respectively, the baryon number, the charge, the momentum, and the angular momentum which a projectile brings in a nucleus; $q_i^c, e_i^c, \mathbf{p}_i^c$, and l_i^c, respectively, the baryon number, the charge, the momentum, and the angular momentum brought away by the i-th cascade particle; and N_c is the number of cascade particles (see also Section IV in Chapter 1).

A nucleus formed after the completion of a cascade is usually identified with a thermalized R-nucleus. However, a system of Fermi-particles formed can be, in principle, nonequilibrium (i.e., its number of quasiparticles n = p + h can be smaller than the equilibrium value n_{eq}, see Section I.E.2). Such a system can emit pre-equilibrium particles during the attainment of the equilibrium. As a result, the excitation energy and the nucleonic composition of an initial and a thermalized R-nucleus will be different. To take this effect into account the process of equilibration in an R-nucleus whose particle-hole configuration is determined by the INC-model is described within the framework of the master equations of the exciton model (see Section IE2). These master equations are solved by the Monte Carlo method. Such a combined model was called the cascade-exciton model.[20]

The computational code of the outlined version of the standard INC-model is given in Reference 40.

B. TRAWLING EFFECT IN THE INC

It has already been mentioned that the standard version of the INC-model is based on the macroapproximation (see Section II.G. of Chapter 1) which is valid if the number N_c of cascade nucleons is small as compared to the number A_t of nucleons in a T-nucleus ($N_c << A_t$) so that the properties of a T-nucleus remain unchanged during the development of the cascade. For πA- and NA-interactions, this condition can be violated at the energies higher than 3-5 GeV[41] (see also Section V, Chapter 1), when a multiple production of pions comes to dominate in an elementary act. In this process, there can arise even such a situation, when a larger number of nucleons can be knocked out of a nucleus than were contained in it. In fact, a rigorous solution of the equations of the INC-model (e.g., in the form of the von Neumann series in collisions in Equations 40 and 41, Chapter 1, in collisions) leads to another pattern of the process. Owing to the knockout of intranuclear nucleons by fast secondary particles (mainly by pions) at the first stage of the cascade, a subsequent low-energy component of cascade particles (mainly nucleons) passes through the domains of the nucleus with a lower density and leaves it most often without colliding with intranuclear nucleons.

A Monte Carlo version of the INC-model taking into account this effect of depletion of the nuclear density during the development of the cascade (the so-called trawling effect)* was proposed by Barashenkov et al[41] According to this version for each "history" of a collision between a projectile and a nucleus, positions of centers of nucleons are randomly selected by the Monte Carlo method with the help of the distribution $\rho_N(r)$ (Equation 122). In this procedure, a condition is imposed that the distance between their centers is not smaller than $2r_c$ (r_c = 0.4 fm is the radius of a nucleon core). It is assumed that during the time required for the completion of the cascade the positions of centers do not vary (approximation of frozen nucleons), whereas the intranuclear nucleons themselves obey the Fermi momentum distribution (Equation 121).

A fast particle (a primary one or a particle formed during the development of the cascade) can interact with any intranuclear nucleon situated inside a cylinder of a radius $r_{int} + \lambda\!\!\!^{-}$ (here r_{int} = 1.3 fm is the range of strong interaction and $\lambda\!\!\!^{-}$ the de Broglie wavelength of the particle) whose z'-axis is directed along the velocity vector **v** of the particle (see Figure 4). Such an approach is similar to that used for analysis of the collision term in the Liouville equation carried out in Section IIB of Chapter 1, the cylinder of Figure 4 playing the role of "macroscopically small" volume. Along the lines similar to those used for the derivation of Equation 35, Chapter 1, which represents the product of probabilities to avoid a collision of each pair of nucleons running a given distance, we can readily show that, in the present case, the particle will avoid a collision with one fixed nucleon situated on its way in the cylinder with the probability given by the expression[41]

$$q = \exp[-\sigma^{tot}/\pi(r_{int} + \lambda\!\!\!^{-})^2]. \tag{138}$$

* The abbreviation INCT-model will be used in what follows for the INC-model with trawling.

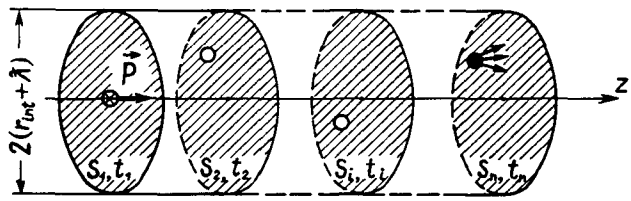

FIGURE 4. This shows the pattern of the motion of a cascade particle in a nucleus during the INC with trawling. The asterisk indicates the cascade particle, circles indicate intranuclear nucleons, and the circle with arrows indicates the intranuclear nucleon with which the particle has interacted.

Obviously, the particle under consideration will collide with the i-th nucleon (which the particle passes by) with the probability given by the expression

$$w_i = q^i (1 - q). \tag{139}$$

These relations are used in the code to determine which one of i nucleons has been involved in the act of the interaction to find thereby the point of the collision.

A peculiar feature of the INCT-model is that an intranuclear nucleon which has been involved in any act of the interaction is henceforward "excluded" from the composition of the nucleus. This results in a variation of the nuclear density during the development of the cascade.

The trawling effect calls for the analysis of a time development* of the INC. This can be done approximately by tracing, above all, the evolution of the fastest cascade particle.[41] Within the framework of the INCT-model the time coordinate was taken into account explicitly in Reference 42. In this case, for each particle produced in an elementary act, the interaction point is sampled and the corresponding instant of time $t_i = t + \Delta t_i$ is calculated. Here t is the instant of time at which an elementary interaction takes place, and $\Delta t_i = \sum_{j=1}^{n} \Delta s_j/\bar{v}_j$, where $\Delta s_j = s_{j+1} - s_j$ are the projections of the internucleon separations on the direction of motion of a cascade particle (see Figure 4), $\bar{v}_j$ is the mean velocity of the particle in the interval Δs_j, and summation is carried out over nucleons inside the cylinder of a radius $r_{int} + \lambda\!\!\!^{-}$. The calculation of the successive elementary act is carried out for the earliest act of interaction corresponding to the minimum t_i. It has been found in Reference 42 that the results of the calculations in which the development of the INC in time was taken into account approximately and exactly differ only slightly.

Thus, the following variations are to be introduced into the general scheme of the calculation of the INC (Figure 3) in order to take into consideration the trawling effect. Alongside with the calculation of characteristics of an incident particle, positions of centers of all nucleons of a T-nucleus are to be determined in block 1. In block 2, of all intranuclear nucleons, those are found with which a given cascade particle can interact, and a nucleon is determined which has already been

* The time coordinate was introduced explicitly in the standard INC-model in Reference 25.

involved in the act of interaction with the particle. In block 8, not only secondaries produced in a given act of interaction are put into the memory, but also an intranuclear nucleon which has been involved in a given act of interaction is excluded from the memory. Other blocks, including the one in which the elementary πN- or NN-interaction is sampled, remain unchanged. The code for calculation of the INC with allowance for the trawling effect is given in Reference 40.

It has been mentioned above that the INCT-model proposed in Reference 41 was later refined, namely, a time coordinate was introduced explicitly in the cascade[42] and a time variation of positions of intranuclear nucleons as a result of the Fermi motion was taken into consideration.[43] Finally, it was used as a basis for the cascade model of nucleus-nucleus interaction[44] in which the trawling effect plays a more prominent role.

The fact that an elementary interaction has a space structure (and is not a point interaction) was taken into consideration for the first time in the analysis of the trawling effect within the framework of the INC-model. To be more specific, the range r_{int} of the strong interaction was introduced. On the other hand, it is well known[45] that strong interaction is not instantaneous and has a finite time duration τ_{int}. According to the INC-model, the length $L_f \sim E\hbar/m^2c^3$ [45] of formation of secondary particles (so called hadronization length) corresponding to this time is significantly smaller than their mean free path L. However, at high energies ($E \gtrsim 10$ GeV) this condition is violated, and the hadronization length becomes not only comparable with L, but can even exceed the radius of the nucleus. In this case, secondary particles leave the nucleus practically without interacting with it. This calls for an appropriate modification of the INC-model.

Recently in a number of research centers, the Monte Carlo generators of hadron-nucleus and nucleus-nucleus collisions have been developed for this domain of high energies.[37-39,44] These computational codes are mostly concerned with a simulation of transitions of quarks and gluons to hadrons. These codes are based on the dual parton model, the model of quark-gluon strings, the parton phenomenology and the model of additive quarks.[37-39,44] Since analysis of nuclear processes at high energies ($E \gtrsim 10^2$ GeV) is beyond the scope of our book, here we confine ourselves to a mere mentioning of these models.

III. CONCLUSIONS

The system of KEs describing an INC can be solved using both analytic and numerical methods. It becomes possible to obtain an analytic solution for a nucleonic cascade (disregarding the meson production) at the expense of introducing certain approximations. For example, the cascade component of the inclusive cross-section that includes the contribution from nucleons of the second and higher cascade generations is determined by the solution of the system of KEs obtained within the framework of the small-angle approximation, which is justified for relatively high energies of secondary nucleons and in the P_1-approximation, which is correct at low energies. A reasonably accurate semiclassical expression (which can be considerably improved, if it is replaced by its more rigorous quantum-mechanical

analogue) is obtained for the quasifree component of the inclusive cross-section that is determined by a single nucleon scattering. In the domain of low initial energies $\epsilon_0 \lesssim 100$ MeV, where pre-equilibrium models are widely used, it is possible to obtain an analytic solution of the system of KEs which approximately takes into consideration the Fermi motion of intranuclear nucleons.

The Monte Carlo technique whose mathematical character is adequate to the statistical nature of the INC is an effective method for solving the system of KEs for the many-particle distribution function. The use of this method allows one to generalize the INC-model to a wide range of NRs initiated by nucleons, antinucleons, photons, various mesons, and heavy ions and to extend the INC-model to the domain of high energies ($\sim 10^3$ GeV). An advancement to the domain of high initial energies within the framework of the INC-model calls for incorporation of effects associated with the existence of space-time structure of strong interaction range (e.g., the incorporation of the trawling effect at $\epsilon_0 \sim 5$ GeV and the effect of a finite length of hadron production for $\epsilon_0 \gtrsim 10$ GeV, i.e., it becomes necessary to take into consideration the transition of quarks and gluons to hadrons). The Monte Carlo INC-model supplemented with the Monte Carlo statistical model of decay of an R-nucleus allows one to obtain a complete exclusive description of the interaction between an intermediate-energy particle and a T-nucleus. Monte Carlo methods of analysis of decay of highly-excited nuclei will be described in the next chapter.

REFERENCES

1. **Barashenkov, V. S. and Toneev, V. D.,** *Interaction of High Energy Particles and Nuclei with Atomic Nuclei* [in Russian], Atomizdat, Moscow, 1972.
2. **Kazarnovsky, M. V. and Paryev, E. Ya.,** Analytic calculation of an intranuclear cascade by means of kinetic equations, *Sov. J. Nucl. Phys.*, 33, 345, 1981.
3. **Kalashnikov, N. P., Remizovich, V. S., and Ryazanov, M. I.,** *Collisions of Fast Charged Particles in Solids* [in Russian], Atomizdat, Moscow, 1980.
4. **Kazarnovsky, M. V. and Paryev, E. Ya.,** Polarization effects in inclusive nucleon-nucleus reactions at medium energies, *Sov. J. Nucl. Phys.*, 49, 605, 1989.
5. **Fernbach, S., Serber, R., and Taylor, T.,** The scattering of high energy neutrons by nuclei, *Phys. Rev.*, 75, 1352, 1949.
6. **Kikuchi, K. and Kawai, M.,** *Nuclear matter and nuclear reactions*, North-Holland, Amsterdam, 1968.
7. **Hayakawa, S., Kawai, M., and Kikuchi, K.,** Nuclear reactions at moderate energies and Fermi gas model, *Progr. Theor. Phys.*, 13, 415, 1955.
8. **Lock, W. O. and Measday, D. F.,** *Intermediate Energy Nuclear Physics*, Methuen & Coltd, London, 1970.
9. **Jacob, G. and Maris, Th. A. J.,** Quasi-free scattering and nuclear structure, *Rev. Mod. Phys.*, 38, 121, 1966; also, 45, 6, 1973.
10. **Bunakov, V. E. and Matvejev, G. V.,** The model used for solution of quantum kinetic equations describing nuclear reactions with nucleons, *Izv. Akad. Nauk SSSR, Ser. Fiz.*, 47, 2115, 1983.

11. **Daskalov, G. M., Kazarnovsky, M. V., and Paryev, E. Ya.,** The role of quantum effects in the intranuclear cascade model, *Sov. J. Nucl. Phys.*, 52, 41, 1990.
12. **Akhiezer, A. I., Sitenko, A. G., and Tartakovsky, V. K.,** *Nuclear Electrodynamics* [in Russian], Naukova Dumka, Kiev, 1989.
13. **Case, K. M. and Zweifel, P. F.,** *Linear Transport Theory,* Addison-Wesley, Reading, MA, 1967.
14. **Bunakov, V. E.,** Master equations in the nuclear reaction theory, *Part. Nucl.*, 11, 1285, 1980.
15. **Daskalov, G. M., Kazarnovsky, M. V., and Paryev, E. Ya.,** Analytical calculation of an spectra and multiplicities of secondary nucleons in the intermediate energy nucleon-nucleus interactions, Preprint INR P-0528, Moscow, 1987.
16. **Blann, M.,** Preequilibrium decay, *Annu. Rev. Nucl. Sci.*, 25, 123, 1975.
17. **Seidel, K., Seeliger, D., Reif, R., and Toneev, V. D.,** Precompound decay in the nuclear reactions, *Part. Nucl.*, 7, 499, 1976.
18. **Harp, G. D., Miller, J. M., and Berne, B. J.,** Attainment of statistical equilibrium in excited nuclei, *Phys. Rev.*, 165, 1166, 1968.
19. **Griffin, J. J.,** Statistical model of intermediate structure, *Phys. Rev. Lett.*, 17, 478, 1966.
20. **Gudima, K. K., Mashnik, S. G., and Toneev, V. D.,** Cascade-exciton model of nuclear reactions, *Nucl. Phys. A*, 401, 329, 1983.
21. **Spanier, J. and Gelbard, E. M.,** *Monte Carlo principles and neutron transport problems,* Addison-Wesley, Reading, MA, 1968.
22. **Goldberger, M.,** The interaction of high energy neutrons and heavy nuclei, *Phys. Rev.*, 74, 1269, 1948.
23. **Barashenkov, V. S., Iljinov, A. S., Sobolevsky, N. M., and Toneev, V. D.,** Interactions of particles and nuclei of high and superhigh energies with nuclei, *Usp. (Sov. Phys.)*, 16, 31, 1973.
24. **Harp, G. D.,** Extension of the isobar model for intranuclear cascades to 1 GeV, *Phys. Rev. C*, 10, 2387, 1974.
25. **Bertini, H. W., Culkowski, A. H., Hermann, O. W., Gove, N. B., and Guthrie, M. P.,** High energy ($E \leqslant 1000$ GeV) intranuclear cascade model for nucleons and pions incident on nuclei and comparisons with experimental data, *Phys. Rev. C*, 17, 1382, 1978.
26. **Fraenkel, Z., Piasetzky, E., and Kalbermann, G.,** Intranuclear cascade calculation of pion-nucleus reactions in the resonance region, *Phys. Rev. C*, 26, 1618, 1982.
27. **Cugnon, J.,** Proton-nucleus interaction at high energy, *Nucl. Phys. A*, 462, 751, 1987.
28. **Tang, H. H. K., Srinivasan, G. R., and Azziz, N.,** Cascade statistical model for nucleon-induced reactions on light nuclei in the energy range 50 MeV- 1 GeV, *Phys. Rev. C*, 42, 1598, 1990.
29. **De Jager, C. W., De Vries, H., and De Vries, C.,** Nuclear charge- and magnetization-density-distribution parameters from elastic electron scattering, *At. Data Nucl. Data Tables*, 14, 479, 1974.
30. **Amelin, N. S.,** A model of intranuclear cascade allowing for resonances, JINR Communication P2-80-661, Dubna, 1980.
31. **Flaminio, V., Moorhead, W. G., Morrison, D. R. O., and Rivoire, N.,** Compilation of cross-sections I: π^+ and π^- induced reactions, CERN-HERA 83-01, 1983; Compilation of cross-sections III: p and $\bar{p}$ induced reactions, *CERN-HERA* 84-01, 1984.
32. **Brueckner, K. A., Serber, R., and Watson, K. M.,** The interaction of π-mesons with nuclear matter, *Phys. Rev.*, 84, 258, 1951.
33. **Levinger, J. S.,** The high energy nuclear photoeffect, *Phys. Rev.*, 84, 43, 1951.
34. **Gudima, K. K., Iljinov, A. S., and Toneev, V. D.,** A cascade model for photonuclear reactions, *JINR Communication* P2-4661, Dubna, 1969.
35. **Barashenkov, V. S., Gereghi, F. G., Iljinov, A. S., et al.,** A cascade-evaporation model for photonuclear reactions, *Nucl. Phys. A*, 231, 462, 1974.
36. **Barashenkov, V. S. and Slavin, N. V.,** Phenomenological approximation of inelastic π-N and N-N interactions at high energies, *Acta Phys. Pol. B*, 12, 951, 959, 1981.
37. **Hänssgen, K.,** Hadronic event generation for hadron cascade calculations and detector simulation-part IV: the application of the intranuclear cascade model to reactions of pions, nucleons, kaons, and their antiparticles with nuclei below 6 GeV/c, *Nucl. Sci. Eng.*, 95, 135, 1987.

38. **Amelin, N. S.,** COLLI — Monte-Carlo generator of soft hadronic, hadron-nucleus and nucleus-nucleus collisions at high energies, *JINR Communication* P2-86-837, Dubna, 1986.
39. **Andersson, B., Gustafson, G., Ingelman, G., and Sjöstrand, T.,** Parton fragmentation and string dynamics, *Phys. Rep.*, 97, 31, 1983.
40. **Iljinov, A. S.,** Code for the calculation of intranuclear cascades, *JINR Communication* B1-4-5477, B1-4-5478, Dubna, 1970.
41. **Barashenkov, V. S., Iljinov, A. S., and Toneev, V. D.,** Further development of the intranuclear cascade model, *Yad. Fiz.*, 13, 743, 1971.
42. **Barashenkov, V. S., Kostenko, B. F., and Zadorogny, A. M.,** Time-dependent intranuclear cascade model, *Nucl. Phys. A*, 338, 413, 1980.
43. **Sano, H., Nagae, T., Tokushiku, K., et al.,** Quasifree production of ρ^0 and f_2^0 mesons in π^+-nucleus reactions, in *Proc. 17th INS Int. Symp. on Nucl. Phys. at Intermediate Energy.* Fukuda, T., Nagae, T., Eds. World Scientific, 165, 1989.
44. **Toneev, V. D. and Gudima, K. K.,** Particle emission in light and heavy ion reactions, *Nucl. Phys. A*, 400, 173c, 1983.
45. **Nikolaev, N. N.,** Quark interactions in collisions of high energy leptons, photons and hadrons with atomic nuclei, *Usp. Fiz. Nauk*, 134, 369, 1981.

Chapter 3

DECAY AND PROPERTIES OF HIGHLY-EXCITED NUCLEI

A formation of a highly-excited nucleus with a large (as compared to the time during which the INC proceeds) lifetime after the completion of the INC (and pre-equilibrium emission) is an important result of investigations of the energy dissipation in a deep inelastic interaction carried out in Chapters 1 and 2 within the framework of a kinetic approach. It has been demonstrated that internal degrees of freedom of this nucleus have had time to come into equilibrium before the nucleus decays. This implies that decay of such a nucleus does not depend on the way of its formation. Therefore, this intermediate nucleus is a separate object of investigation, which has universal nature.

An equilibrium statistical model based on the concept that a compound nucleus (C-nucleus) does exist is used, as a rule, in such investigations. This concept, proposed by N. Bohr as far back as 50 years ago,[1] was extensively used in analysis of various nuclear processes and developed by a large number of authors. A detailed account of the model can be found in numerous monographs and reviews.[2-5] Here we shall succinctly discuss the semiclassical formulation of the equilibrium statistical model which is used, as a rule, for description of decay of highly-excited nuclei with large values of the angular momentum I and in which the effects associated with large values of the excitation energy E^* and of I have clear physical interpretation.

I. DECAY OF A C-NUCLEUS WITH ZERO ANGULAR MOMENTUM

A. BASIC TENETS OF STATISTICAL MODEL OF DECAY OF A C-NUCLEUS

Let us first illustrate basic tenets of statistical model by a simple example of the case in which we can disregard the effect of angular momentum (this version of the model is used, as a rule, for analysis of decay of a C-nucleus formed in hadron-nucleus interactions[2]).

Large values of the excitation energy of C-nuclei introduce their specific features into the substantiation of the model. In this case, nuclear levels have large widths Γ and overlap. Generally speaking, interference of levels violates the basic assumption of the model that the decay of a C-nucleus is independent of its formation. However, the study of the decay of a C-nucleus is always associated with an uncertainty of the energy which is in the same order of magnitude as the width Γ of the level. In actual experiments, the existence of the energy spread of the beam of impinging particles results in averaging over even a wider energy range $\Delta E^* > \Gamma$. Therefore, taking into account a stochastic nature of a C-nucleus, we can assume[2,3] that phases corresponding to various excited states are distributed randomly. Then interference terms cancel each other on averaging over ΔE^*. In this case, the cross-section σ $(i \rightarrow j)$ of the reaction proceeding from the entrance channel i to the exit

channel j through an intermediate C-nucleus with the excitation energy E* is determined by the well known relation[2,3]

$$\sigma\ (i \rightarrow j) = \sigma_{CN}\ (i,E^*)\ \frac{P_j(E^*)}{P_{tot}(E^*)}\ , \tag{1}$$

where σ_{CN} (i,E*) is the cross-section for the formation of a C-nucleus in the entrance channel i, P_j the probability per unit time of the decay of the C-nucleus in the j channel, $P_{tot} = \sum_j P_j$ the total probability of the decay of the C-nucleus, and $\Gamma \equiv \hbar\ P_{tot.}$

Using further the principles of detailed balance, we can obtain the expression for the probability per unit time of decay of a C-nucleus which is accompanied by the emission of a given particle j with the energy lying in the interval from ϵ_j to $\epsilon_j + d\epsilon_j$[2,3] in the form

$$P_j(\epsilon_j)\ d\epsilon_j = \frac{(2s_j + 1)}{\pi^2\hbar^3}\ \mu_j \epsilon_j \sigma_{inv}(\epsilon_j)\ \frac{\rho_j(E^* - B_j - \epsilon_j)}{\rho_{CN}(E^*)}\ d\epsilon_j\ . \tag{2}$$

Hence for the energy spectrum we obtain

$$\sigma_j(\epsilon_j) = \sigma_{CN}(i)\ \frac{(2s_j + 1)\mu_j\epsilon_j\sigma_{inv}(\epsilon_j)\rho_j(E^* - \epsilon_j - B_j)}{\sum_j (2s_j + 1)\mu_j \int_0^\infty \epsilon_j\sigma_{inv}(\epsilon_j)\rho_j(E^* - \epsilon_j - B_j)\ d\epsilon_j} \tag{3}$$

(Expressions describing the pre-equilibrium emission of particles have the similar form (see Section IE.2, Chapter 2)). Here s_j, μ_j and B_j are the spin, the reduced mass, and the binding energy of the particle, respectively, ρ_{CN} and ρ_j the level density of the C-nucleus and R-nucleus, and σ_{inv} is the cross-section of the inverse reaction.

Equations 1-3 contain all characteristics features of decay of a C-nucleus. It follows that emission of particles from an equilibrium nuclear system is characterized completely by the constants of motion of the system and its dimensions and shape. The density of nuclear levels and the cross-section of the inverse reaction are basic quantities in the statistical description of the decay. Universal nature of the principle of detailed balance and of concept of the phase space used in the derivation of the expressions in Equations 2 and 3 ensures a reliable theoretical basis for the equilibrium statistical model. Therefore, it is extensively used to obtain quantitative information on the properties of excited nuclei, such as level density, lifetime, Coulomb barriers for emitted particles, etc.[5]

The cross-section σ_{inv} for the absorption of a particle by an excited nucleus cannot be measured in experiments directly. Therefore, in the statistical model, it is usually calculated with the help of the optical model. It should be noted that it is essential to take into account the effect of barrier penetrability in the statistical model, since the energies ϵ_j of emitted particles are small. Usually the results of

calculations of the inverse cross-section carried out within the framework of the optical model are approximated with the help of the following simple expression:[6]

$$\sigma_{inv}(\epsilon_j) = \begin{cases} \sigma_g c_1(1 + c_2/\epsilon_j) & \text{for } j = n, \\ \sigma_g(1 + c_3)(1 + c_4\, V_{c,j}/\epsilon_j) & \text{for } j = p,d,t,\ ^3He,\alpha, \end{cases} \tag{4}$$

where $\sigma_g = \pi r_0^2(A_{fj}^{1/3} + A_j^{1/3})^2$ is the geometrical cross-section, A_{fj} and A_j are atomic numbers of an R-nucleus and an emitted particle respectively, $V_{c,j}$ is the Coulomb barrier for the emitted particle, and c_j are the parameters (their values are given in Reference 6). For large values of E*, the dimensions, the shape, and the potential barrier penetrability of an excited nucleus can differ significantly from the corresponding characteristics of the nucleus in the ground state. The appearance of the inverse cross-section in the Equations 2 and 3 offers a possibility (at least in principle) of using the statistical model for the study of these global (so-called "macroscopic") properties of highly-excited nuclei (these questions will be considered below).

B. LEVEL DENSITY OF HIGHLY EXCITED NUCLEI

Density of nuclear levels is an important characteristic lying in the basis of the statistical model of decay of a C-nucleus. It is studied experimentally in a narrow interval of the excitation energy $E^* \lesssim 20$ MeV.[4,5] Hence, for a successful development and utilization of a statistical approach we must have reliable theoretical methods for the calculation of the level density in domain of high values of E*. Recently, considerable progress has been made in the development of theoretical formalism capable of calculating the level density on the basis of current realistic models of a nucleus.[4]

For high values of the excitation energy, single-particle degrees of freedom of a nucleus must dominate, since the number of collective modes is small compared to the total number of degrees of freedom of its constituent particles.[5] A sharp increase in the density of nuclear levels with increasing E*, which is observed in experiments, is the result of the additivity (or of quasiadditivity) of energies of single-particle fermionic states, i.e., a given value of the excitation energy can be realized in a great number of ways of its distribution over these states. It is hence clear that a calculation of the density of nuclear levels is, to a large extent, a combinatorial problem.

A combinatorial method based on the direct count of all possible states of a highly-excited nucleus is the most accurate method of calculation of ρ.[7] However, because of a sharp increase in the level density with increasing excitation energy E*, and a considerable increase in the volume of calculations associated with it, this method is limited to relatively low $E^* \lesssim 10$ MeV. In the domain of high excitation energies, another method has received wide acceptance. It uses methods of statistical mechanics to obtain the solution of the combinatorial problem. The

density of states of a system which consists of A particles and which has the energy $\mathscr{E}$ can be defined[4,5] as

$$\rho(\mathscr{E},A) = \sum_j \delta(A - A_j)\, \delta(\mathscr{E} - \mathscr{E}_j) , \tag{5a}$$

where $\mathscr{E}_j$ is the energy of the j-th nucleus containing A_j nucleons. Using the integral representation of the delta function, we can rewrite this relation in the form

$$\rho(\mathscr{E},A) = (2\pi i)^{-2} \int_{\gamma_1 - i\infty}^{\gamma_1 + i\infty} d\beta \int_{\gamma_2 - i\infty}^{\gamma_2 + i\infty} d\alpha \exp(\beta\mathscr{E} - \alpha A)\, Q(\alpha,\beta) . \tag{5b}$$

Here $Q(\alpha,\beta) \equiv \exp\,[-\beta\Omega(\alpha,\beta)]$ is the partition function of the grand canonical ensemble characterized by the thermodynamical temperature $t = \beta^{-1}$ (such a notation will hopefully not lead to a confusion, because the time variable is not used explicitly in this chapter), and the chemical potential $\lambda = \alpha t$, and Ω the thermodynamical potential of the system.* Evaluating the integrals (Equation 5) by the method of the steepest descent, we obtain

$$\rho(\mathscr{E},A) = (2\pi)^{-1}\mathscr{D}^{-1/2}(\alpha_0,\beta_0) \exp[S(\alpha_0,\beta_0)] , \tag{6}$$

where the determinant $\mathscr{D}$ has the form

$$\mathscr{D} = \begin{vmatrix} \dfrac{\partial^2\Omega}{\partial\alpha^2} & \dfrac{\partial^2\Omega}{\partial\alpha\,\partial\beta} \\ \dfrac{\partial^2\Omega}{\partial\alpha\,\partial\beta} & \dfrac{\partial^2\Omega}{\partial\beta^2} \end{vmatrix}_{\substack{\alpha=\alpha_0 \\ \beta=\beta_0}} ,$$

and the entropy $S(\alpha_0,\beta_0)$ is defined as the value of the logarithm of the integrand of Equation 5. The determinant $\mathscr{D}$ and the entropy S are evaluated at the values of the variables α and β equal to α_0 and β_0, respectively. The latter are to be determined from the solution of the system of equations for the saddle point:

$$\frac{\partial S}{\partial\alpha} = 0, \qquad \frac{\partial S}{\partial\beta} = 0 . \tag{7}$$

Equations 5-7 can be readily generalized to the case of an arbitrary number of constants of motion.[4]

The thermodynamic potential for the system consisting of A noninteracting fermions has the form[4]

* It has been shown in Reference 5 that the expressions in Equations 5-7 can be obtained without resorting to thermodynamical concepts. However, the concept of the grand canonical ensemble is often used in practice, since it allows one to give a lucid physical interpretation of quantities appearing in these equations.

$$-\beta\Omega = \sum_i \ln[1 + \exp(\alpha - \beta E_i)] \ . \tag{8}$$

Its entropy is given by

$$S = \sum_i [\bar{n}_i \ln \bar{n}_i + (1 - \bar{n}_i) \ln (1 - \bar{n}_i)] \ , \tag{9}$$

where

$$\bar{n}_i = [1 + \exp (\beta E_i - \alpha)]^{-1} \ , \tag{10}$$

and E_i and $\bar{n}_i$ are the energies and the average occupation numbers of single-particle states, respectively. Substituting Equation 9 in Equation 7, we get

$$A = \sum_i \bar{n}_i, \qquad \mathscr{E} = \sum_i \bar{n}_i E_i \ . \tag{11}$$

Solving the system of Equations 11, we find the parameters α_0 and β_0 and evaluate the entropy S (Equation 9), the excitation energy

$$E^* = \sum_i \bar{n}_i E_i - \sum_{i=1}^{F} E_i \tag{12}$$

and the level density ρ (Equation 6). (The index F in Equation 12 implies that the summation is carried out up to the Fermi surface).

There exist various means for solving the system of Equation 11. In recent years, a numerical method[2,4] based on the use of the discrete single-particle spectrum, which can be borrowed, e.g., from the calculations carried out in accordance with the shell model of a nucleus, has been developed and extensively used. This method takes into account the structure of the single-particle spectrum of a heated nucleus in a natural way. This allows one to study the effect of the shells on statistical properties of excited nuclei*. Moreover, within the framework of the method we can also take into account residual interactions of the correlation type as well. The generalization of Equations 6-12 to this case is considered in detail by Ignatyuk.[4] However, a numerical method of solution does not allow one to obtain simple analytic expressions for statistical characteristic of nuclei. This motivates the necessity of developing approximate methods for solving the system of Equation 11. As a first step towards the analytic solution, let us assume that instead of the discrete spectrum E_i we can introduce the density of single-particle states g(E) which is a smooth function of the energy E. Then we can replace the summation in Equation 8 by integration and obtain the following system of equations instead of those in Equation 11:

* This question will be considered in detail below.

$$A = \int \frac{g(E)\,dE}{1 + \exp(\beta E - \alpha)} \quad , \qquad \mathscr{E} = \int \frac{E\,g(E)\,dE}{1 + \exp(\beta E - \alpha)} \, . \tag{13}$$

It can be solved numerically with the density of single-particle states calculated within the framework of one or another model of a nucleus.

The following approximate (within the terms proportional to $g'''(\lambda)$ and to higher derivatives of g with respect to λ) expressions have been obtained in Reference 8:

$$A \simeq \lambda g(\lambda) - \frac{\lambda^2}{2} g'(\lambda) + \frac{\lambda^3}{6} g''(\lambda) + \frac{\pi^2}{6} g'(\lambda) t^2 \, , \tag{14}$$

$$\mathscr{E} \simeq \frac{\lambda^2}{2} g(\lambda) - \frac{\lambda^3}{6} g'(\lambda) + \frac{\lambda^4}{24} g''(\lambda) + \frac{\pi^2}{6} g(\lambda) t^2 + \tag{15}$$

$$\frac{\pi^2}{6} g'(\lambda) \lambda t^2 + \frac{7\pi^4}{120} g''(\lambda) t^2 \, ,$$

$$S \simeq \frac{\pi^2}{3} g(\lambda) t \left(1 + \frac{7\pi^2}{30} \frac{g''(\lambda)}{g(\lambda)} t^2\right) . \tag{16}$$

They are valid in the domain

$$t << \lambda \approx E_F \tag{17}$$

where $E_F \approx$ 30-40 MeV is the Fermi energy. It follows from Equations 14-17 and the condition of the conservation of the number of particles that the equation relating the excitation energy, the entropy, and the temperature to each other can be written as[9]

$$E^* = at^2 (1 + bt^2 + \ldots) \, , \tag{18}$$

$$S = 2at \left(1 + \frac{2}{3} bt^2 + \ldots\right) , \tag{19}$$

$$a = \frac{\pi^2}{6} g_0, \; b = \frac{7\pi^2}{20} \frac{g_0''}{g_0} - \frac{\pi^2}{4} \left(\frac{g_0'}{g_0}\right)^2 , \tag{20}$$

where $g_0 \equiv g(E_F)$ is the density of single-particle states in the vicinity of their Fermi energy. Even more simple expressions are used, as a rule, to describe the properties of highly-excited nuclei:

$$E^* = at^2 \, , \tag{21}$$

$$S = 2at \,. \tag{22}$$

They are obtained from Equations 14-16 in the special case of the equidistant scheme of single-particle levels ($g(E) = \text{const}$), and also for a strongly degenerate Fermi-gas whose single-particle states are excited in a narrow region near the Fermi energy. Such an approximation is valid for not very high values of the excitation energy E^* of a nucleus or, to be more specific, for $E^* << E_F A^{1/3}$.[5] For a Fermi gas with a constant density we have that $g_0 \approx 3A/2E_F$, and hence the parameter of the level density is given by $a = \pi^2 A/4E_F \approx A/15\ \text{MeV}^{-1}$. The allowance for a smoothness of the potential at the periphery of a nucleus yields[5] the value of parameter a approximately equal to $A/10\ \text{MeV}^{-1}$. To determine the other parameter b which characterizes the level density it is necessary to know the behavior of the spectrum E_i of single-particle states of a nucleus over a wide energy range. Corresponding experimental data for large values of E_i are lacking.

Calculations[5,9] of the energy dependence of the density of single-particle states carried out within the framework of various models of a nucleus give the following results: $g(E) \sim E^{1/2}$ for a rectangular potential well with infinitely high walls, $g(E) \sim E$ (near the Fermi surface) for the Woods-Saxon potential and $g(E) \sim E^2$ for the harmonic oscillator potential. Using these results as a starting point, Botvina et al.[9] have calculated the equations of state (Equations 18 and 9), which have been obtained by means of the numerical solution of the system of Equation 13 with various functions g(E). As a result, it turned out that the parameter of the level density can assume the value $b \approx -(2.5 \pm 1.5)\ 10^{-3}\ \text{MeV}^{-2}$ (the error reflects the fact that the value of the density g(E) is not known at large E to a sufficient accuracy). Eliminating t from Equations 18 and 19, we get

$$S(E^*) \approx 2a^{3/4}|b|^{-1/4}\,[q - (q^2 - E^*)^{1/2}] - \frac{4}{3}\,a^{1/4}|b|^{1/4} \times [q - (q^2 - E^*)^{1/2}]^{3/2} \,. \tag{23}$$

Here the value of $q^2 = a/(4|b|)$ is sufficiently large, namely, $q^2 \approx 10 \cdot A$ MeV. The expression of Equation 23 is valid over the entire energy range $E^* < q^2$, in which the C-nucleus may exist (see below). For small values of the excitation energy $E^* << q^2$ it is reduced to the expression for strongly degenerate Fermi gas

$$S(E^*) = 2\sqrt{aE^*} \,. \tag{24}$$

A well known formula for the level density of a nucleus consisting of A nucleons corresponds to this expression, which has been obtained from the solution of the system of Equations 11

$$\rho(E^*,A) = \frac{1}{\sqrt{48}}\,\frac{1}{E^*}\,\exp(2\sqrt{aE^*}) \,. \tag{25a}$$

The expression for the Fermi gas consisting of two types of particles, namely, Z protons and N neutrons, has the form

$$\rho(E^*,Z,N) = \frac{\sqrt{\pi}}{24\ a^{1/4}E^{*5/4}} \exp(2\sqrt{aE^*}) \ . \tag{25b}$$

It is worth noting that it would be more proper to calculate thermodynamic characteristics of highly-excited nuclei within the framework of the theory of finite Fermi systems[10] rather than with the help of the shell model. As a matter of fact, after the separation of a mean field, residual interactions between nucleons are still strong, and hence the nucleus should be considered as a gas of strongly interacting particles or a Fermi liquid. However, even in this case, while calculating thermodynamic characteristics we can make use of the Fermi-gas relations, bearing in mind that they must be applied to the description of quasiparticles in a Fermi system.[4,10] It turned out that the entropy and the temperature of a Fermi liquid are connected through the relation of Equation 19 as well. It follows from the results of numerical calculations[11] carried out within the framework of the theory of finite Fermi systems that in the temperature range $t \lesssim 8$ MeV the value of the parameter $b \approx -(2 \div 3)\ 10^{-3}\ \mathrm{MeV}^{-2}$ is close to the Fermi-gas value.

To describe the decay of highly-excited nuclei we can use the simple formula in Equation 24 instead of the expression of Equation 23 to a good accuracy, even at sufficiently high temperatures $t \approx 5$ MeV. This is a corollary of two facts: the coefficient b is small, and a highly excited nucleus emits a large number of particles in the process of decay, thus reducing its energy E^*. The latter diminishes noticeably the contribution of initial steps of de-excitation during which the temperature of nucleus is still high to total characteristics of a reaction.

C. EFFECT OF A HIGH EXCITATION OF A NUCLEUS ON ITS STRUCTURE

There exist two principal types of "thermal" effects. The first of them is caused by the fact that the nuclear shells are washed out, since single-particle states become populated over a more and more wide energy interval around the Fermi energy E_F, as the temperature t for the nucleus increases (see the Equation 10). The second one affects macroscopic, liquid-drop properties of a nucleus. Their variation with temperature is similar to the variation of properties of a classical liquid drop whose temperature increases.

1. Disappearance of Shell Effects at High Values of the Excitation Energy

Since shell effects are caused by the existence of fluctuations of distances between single-particle levels of a nucleus,[12] they affect, above all, its level density ρ. Indeed, experimental values of the parameter a of the level density obtained from the analysis of data on neutron resonances at $E^* \approx B_n$, deviate strongly from a smooth functional dependence (Equation 20) in the vicinity of magic nuclei (see Figure 1). A numerical method of solution of Equations 9-12 which uses realistic

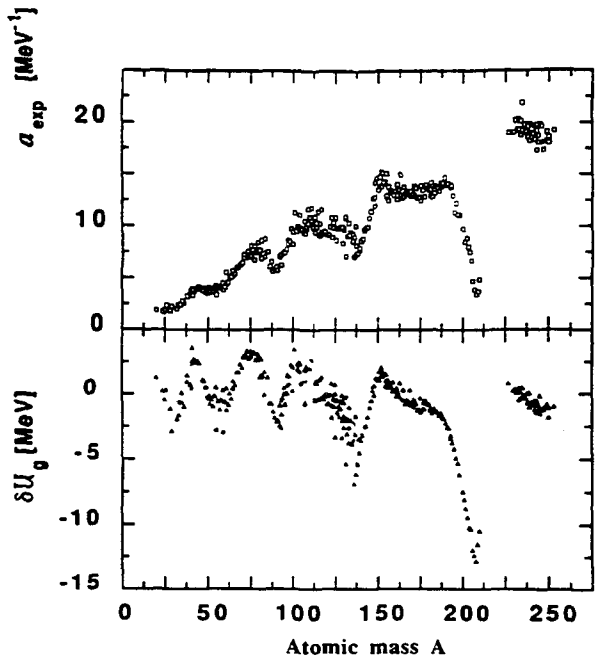

FIGURE 1. These are experimental values of the level density parameter a_{exp} and the empirical ground state shell corection δU_g as functions of the atomic mass A. The values [13] of a_{exp} extracted with collective effects are shown. The values of the shell correction are determined on the basis of Myers-Swiatecki liquid-drop parameters.[15]

schemes of single-particle levels allows one to consider the influence exerted by shell effects on the level density and other statistical properties of nuclei in a consistent way. A number of important conclusions have been drawn with the help of this approach:[4]

1. Shell effects turn out to be most pronounced for small values of E*. Even at E* ≈ 50-100 MeV the squared entropy $S^2 = 4\,a(E^*)\,E^*$ coincides with the Fermi-gas value $S^2 = 4\tilde{a}\,E^*_{LD}$ in which the excitation energy is measured from the energy of the ground state $E^*_{LD} = E^* + \delta U$ of the liquid-drop model (δU is the shell correction in the formula for the nuclear mass), rather than from the energy of the actual ground state.
2. The parameter a of the level density depends on E* and approaches its Fermi-gas value $\tilde{a}$ only at relatively high values of the temperature t≈1.5 - 2 MeV. Its energy dependence can be represented in the form[4]

$$a(E^*) = \tilde{a}\,[1 + f(E^*)\,\delta U/E^*]\,, \tag{26}$$

where

$$f(E^*) \simeq 1 - \exp(-eE^*) \tag{27}$$

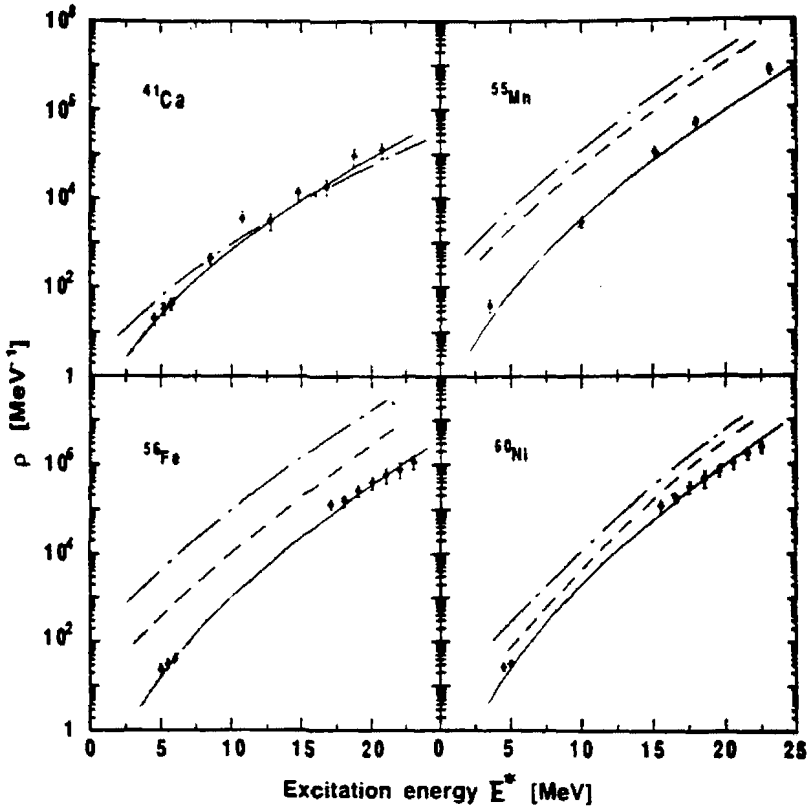

FIGURE 2. This shows energy dependence of the level densities of nuclides ^{41}Ca, ^{55}Mn, ^{56}Fe and ^{60}Ni. Points are the experimental data.[13] The solid curves correspond to the calculation carried out in accordance with phenomenological systematics (Equations 26-31). The dashed and the dash-dotted curves show the results of the calculations carried out in accordance with the shell model without and with allowance for pairing, respectively.

(e is a constant).

3. In the case of the Woods-Saxon potential, the asymptotic (with respect to E*) Fermi-gas value of the parameter ã of the level density is ã = (0.105±0.005)A MeV^{-1}.

Thus, all conclusions above are indicative of the fact that for sufficiently high values of the excitation energy E* shell effects disappear, and a nucleus behaves as a Fermi gas.

However, in spite of a considerable progress made in attempts to take into account shell effects in heated nuclei, a consistent numerical approach cannot yet pretend to be a method which enables one to carry out exact calculation of the level density because of the above-mentioned uncertainty in the structure of the single-particle spectrum and disregard of a contribution from collective states (see Figure 2). In addition to this, the numerical method is too complicated to be easily incorporated in statistical calculations of NRs. Therefore, to determine the parameters

appearing in Equations 26 and 27 a technique is used[4] according to which theoretical results are to be related to experimental data concerned with the level density. In this method, the analytic form (Equation 25) of the level density forms the basis, whereas the effect of residual interactions is taken into account by substituting the effective value $E^* - \delta$ for E^*, where $\delta = 12\,\chi/\sqrt{A}$ is the pairing energy measured in MeV ($\chi = 0,1$ or 2 for odd-odd, odd or even-even nuclei, respectively). The functional dependence of $\tilde{a}$ on A is prescribed in the form[4]

$$\tilde{a} = cA + dA^{2/3} \tag{28}$$

where c and d are constants. Here the presence of the term proportional to the surface area of a nucleus is caused by the existence of the gradient of the nucleon density distribution in the nucleus. The coefficient d is connected with the surface area of a nucleus through the relation $d = \text{const}\cdot b_S$, where b_S is the ratio of the surface area of the nucleus to the surface area of a sphere of the same volume. For the ground state of the nucleus, $b_S \approx 1$. The contribution of a rotational and a vibrational motion to the observed level density is taken into account in the approximation of their adiabatic separation[4,14]

$$\rho_{tot}(E^*) = k_{rot}\cdot k_{vib}\cdot \rho(E^*)\ . \tag{29}$$

A collective enhancement of the level density is especially large for deformed nuclei. The coefficient of rotation enhancement of the level density is determined by the expression

$$k_{rot} = \begin{cases} 1 & \text{for spherical nuclei} \\ \theta_\perp t/\hbar^2 & \text{for deformed nuclei} \end{cases} \tag{30a}$$

where t is the temperature of a nucleus and $\theta_\perp$ is the perpendicular component of the moment of inertia of a nucleus. A liquid-drop estimate of the coefficient of vibrational enhancement gives the following result:[4]

$$k_{vib} \approx \exp(0.0555A^{2/3}t^{4/3}) \tag{30b}$$

Here and in what follows the temperature t is measured in MeV. For deformed nuclei the rotational enhancement of the level density $k_{rot} \approx 10 - 100$ is significantly larger than the vibrational enhancement $k_{vib} \approx 3$ at the energy $E^* \approx B_n$.

An empirical set of parameters* obtained in Reference 13 from the analysis of 512 experimental values of ρ by the method of least squares namely, the values

$$c = 0.090\text{MeV}^{-1},\quad d = -4.00\cdot 10^{-2}\text{MeV}^{-1},\quad e = 7.0\cdot 10^{-2}\text{MeV}^{-1} \tag{31}$$

* This set of parameters was obtained with an "empirical" shell correction determined by the relation $\delta U(A,Z,\alpha) = M_{exp}(A,Z) - M_{LD}(A,Z,\alpha_0)$, where the liquid-drop component $M_{LD}(A,Z,\alpha_0)$ in the mass formula for the equilibrium nuclear deformation α_0 was borrowed from Reference 15.

allows one to calculate the level density to a accuracy better than within a factor of three at $E^* \approx$ 10-20MeV(see Figure 2). Such a high degree of an accuracy ensures the reliability of extrapolation of the level density to the domain of high energies. The empirical value of $\tilde{a} \approx 0.1\text{MeV}^{-1}$ for medium-weight and heavy nuclei is close the asymptotic value obtained in the shell model.[4,5]

The phenomenon of the thermal washing out of shell effects is of universal nature and manifests itself not only in the level density, but also in other properties of nuclei. This statement can be illustrated, in particular, by the example of the shell correction δU to the energy. Its expression for the ground state[12]

$$\delta U = \sum_{i=1}^{F} E_i - \int_0^{\lambda} EG(E)\, dE \tag{32}$$

can be generalized to the case of finite temperatures in the following way:[16]

$$\delta U = \sum_i E_i \bar{n}_i - \int_0^{\infty} EG(E)\, n(E)\, dE\ . \tag{33}$$

Here G(E) is the smoothing function in the method of the shell correction.[12] The shell correction to the energy is contained in the first term of Equations 32 and 33 and is separated in its pure form by the subtraction of a smooth component represented by the integral. Thus, as the excitation energy E^* increases, a larger and larger number of single-particle states becomes populated. As a result, the shell effect contained in the first term of Equations 32 and 33 is washed out, and the quantity δU decreases.

Analytic expressions for shell corrections to the total energy $\delta\mathscr{E}$, to the entropy δS and to the free energy δF^* for simple single-particle spectra are given in Reference 5 and the results of numerical calculations for realistic single-particle spectra in Diebel et al[17]. It has been found that the values of shell corrections tend to zero as an exponential function with increasing temperature and practically vanish at $t \approx$ 1.5-2 MeV. As a result, equilibrium deformations of nuclei and the surface of the potential energy in the nuclear fission tend to their smooth "liquid-drop" values, as the temperature t increases. This leads to the disappearance of the two-humped structure of the fission barriers, to a change in the moments of inertia of nuclei in the fission saddle point, to an increase in the probability of fission, etc.[5,18]

Although the theory predicts a wide range of nuclear phenomena, in which shell effects manifest themselves at intermediate values of the excitation energy, experimental data concerned with them are rather scarce. Therefore, to make up the deficiency of data, specific corollaries of destruction of shell effects in various NRs will be considered in subsequent sections.

* The free energy F defined by the relation $F = E - tS$ plays the role of the generalized potential energy in the case when the temperature of a system is finite.

2. Changes in Macroscopic Properties of a Nucleus Caused by an Increase in its Excitation Energy

A large value of the excitation energy of a nucleus can affect its macroscopic properties, such as the distribution of nuclear density, the magnitude of its radius, properties of the surface layer, etc. First attempts to estimate macroscopic thermal effects were made as far back as 40 years ago with the help of the most simple (liquid-drop, as a rule) models of a nucleus.[2] These pioneering works were naturally qualitative in character. It has been demonstrated in particular that, as the temperature increases, a nucleus must expand, and hence, the Coulomb barrier for emission of charged particles must decrease. However, it is the surface layer of a nucleus that must be influenced most dramatically by its heating, i.e., a considerable increase in diffuseness, a decrease in the surface energy and in the fission barrier height were to be expected. On the other hand, it became clear from these first estimates that macroscopic thermal effects can be manifested at high temperatures that once seemed unattainable. Therefore, investigations of thermal effects in nuclei have been postponed for the time being.

The recent advent of accelerators providing intensive beams of hadrons and heavy ions of intermediate energies offered new possibilities for production of highly-excited nuclei. This rekindled interest in the study of macroscopic thermal effects. As a result, a number of theoretical investigations have been carried out at a more refined, modern level. Temperature dependence of global properties of nuclei has been analyzed on the basis of two approaches, within the framework of the Thomas-Fermi model and by the Hartree-Fock method, which have been generalized to the case of finite temperatures.[16] Both approaches give qualitatively the same results, but the Hartree-Fock method better describes the surface properties of nuclei most sensitive to thermal effects. For this reason we shall set forth succinctly the basic idea used in the generalization of this method to the case of nonzero temperatures.

Macroscopic thermal properties of nuclei can be studied on the same basis as the temperature dependence of shell effects. The standard Hartree-Fock equation[16]

$$-(\hbar^2/2m_N)\,\nabla^2\varphi_i(x) + \int d^3x' U(x,x')\,\varphi_i(x') = E_i\varphi_i(x)\,, \tag{34}$$

in which the kernel $U(x,x')$ is given by the expression

$$U(x,x') = \delta(x - x')\int d^3x'' V(x,x'')\,\rho(x,x'') - V(x,x')\,\rho(x,x')\,, \tag{35}$$

is generalized to the case $t \neq 0$ by introducing the occupation factors (Equation 10) into the single-particle density matrix (see Section IVB, Introduction).

$$\rho(x,x') = \sum_{i=1}^{\infty} \varphi_i(x)\,\varphi_i^*(x')\,n_i\,. \tag{36}$$

The occupation factors n_i and the single-particle states φ_i are to be found from the general condition of equilibrium of quantum statistical mechanics, i.e., via minimization of the Gibbs potential

$$G = F - \lambda A = \mathscr{E} - tS - \lambda A \ . \tag{37}$$

The single-particle states and the energies found by the Hartree-Fock method generalized in such a way depend on the temperature of a nucleus.

Equations 34-37 take into account the effect of the excitation energy on the properties of a nucleus in a self-consistent way. A change in the nuclear density caused by the excitation of highly-lying states affects the states of other nucleons through the self-consistent field. Thus, the result of the calculation takes into account both the washing out of nuclear shells and the variation of macroscopic properties of a nucleus with increasing temperature.

The Hartree-Fock calculation[16] of the binding energy and of the distribution of the nuclear density in the temperature interval $0 \leqslant t \leqslant 6$ MeV was carried out with the Skyrme NN-potential whose parameters were chosen in such a way as to ensure the best description of properties of the ground state of nuclei over the entire periodic table of elements. The distributions of the nuclear density $\rho_N(r)$ thus obtained demonstrate that the thermal expansion is small:

$$R_{1/2}(t) \approx R_{1/2}(0)\cdot(1 + 4\cdot 10^{-4}t^2) \ . \tag{38}$$

Such a small variation of the radius $R_{1/2}$ of the half-density of a nucleus reflects the strong incompressibility of nuclear matter. A conclusion which is important for the investigation of shell effects (see the preceding section) can be drawn from this result, i.e., the parameters of the mean field and the scheme of single-particle levels remain practically constant upon heating of a nucleus in the temperature range $0 \leqslant t \leqslant 6$ MeV.[16] On the other hand, the temperature variation of the "tail" of the distribution of the nuclear density $\rho_N(r)$ is far more pronounced than that of its radius $R_{1/2}$. This leads to a considerable increase in the thickness Δ of the diffuse layer of a nucleus:

$$\Delta(t) \approx \Delta(0)\cdot(1 + 9\cdot 10^{-3}t^2) \ . \tag{39}$$

Mosel[16] has also determined the temperature dependences of the volume ($\mathscr{E}_V$), the surface ($\mathscr{E}_S$), and the Coulomb ($\mathscr{E}_c$) components of the liquid-drop energy of a nucleus, which correspond to the terms with a definite dependence on the number of nucleons A and protons Z in the mass formula. They are described by the following relations

$$\mathscr{E}_v(t) \approx \mathscr{E}_v(0)\cdot(1 - 3\cdot 10^{-3}t^2) \ , \tag{40a}$$

$$\mathscr{E}_s(t) \approx \mathscr{E}_s(0)\cdot(1 + 8\cdot 10^{-3}t^2) \ , \tag{40b}$$

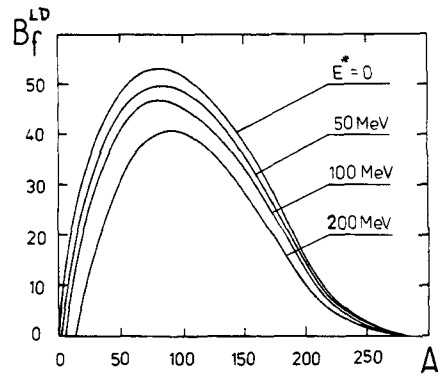

FIGURE 3. This graphs the height B_f^{LD} (in MeV) of the fission barriers of nuclei along the β-stability line for various values of their excitation energy E*. The curves correspond to the calculation of Reference 19 carried out with the standard parameters of the liquid-drop model.[15]

$$\mathscr{E}_c(t) \approx \mathscr{E}_c(0)\cdot(1 + 1\cdot 10^{-3}t) \ . \tag{40c}$$

The surface tension is an important characteristic of a nucleus, since it stabilizes the nucleus with respect to fission. This quantity can be found from the solution of equations for the free energy F. The temperature dependence of the surface term of the free energy has the form[16]

$$F_s(t) \approx F_s(0)\cdot(1 - 6\cdot 10^{-3}t^2) \ , \tag{41}$$

It follows that the surface tension γ_s of a nucleus decreases with increasing temperature:

$$\gamma_s(t) \approx \gamma_s(0)\cdot(1 - 7\cdot 10^{-3}t^2) \ . \tag{42}$$

This leads to a thermal decrease in the height B_f^{LD} of the liquid-drop barrier for the fission of a nucleus. If we substitute the found temperature dependence of the liquid-drop energies in the standard model of a liquid drop [15], we can calculate the barrier height for the fission of a heated nucleus. The results of the calculations [19] are shown in Figure 3. It is seen that the decrease in the height of the fission barrier is especially large for medium-weight nuclei with A ≈80-100, namely, at E* = 200MeV the quantity B_f^{LD} can decrease by 10-15 MeV. This gives rise to a considerable increase in the probability of fission of such nuclei.

A reduction of the Coulomb barrier $V_{c,j}$ (Equation 4) for emission of charged particles from a highly-excited nucleus is another corollary of macroscopic thermal effects. This reduction of $V_{c,j}$ in combination with an increase in the radius $R_{1/2}$ because of thermal expansion of a nucleus changes the inverse cross-section σ_{inv}

(Equation 4) and hence the probability of emission and the energy spectrum of charged particles. These effects might be discovered in experiments. However, thermal expansion of a nucleus is so small that it cannot noticeably affect either the value of the geometrical cross-section σ_g (see Equation 4), or $V_{c,j}$. The decrease in the Coulomb barrier $V_{c,j}$ is caused mainly by the fact that owing to an increase in the diffuseness of a nucleus, the range of the nuclear interaction spreads over larger distances. In order to estimate this effect we must calculate the convolution of the effective NN-interaction V_{12} with the density $\rho_j(r)$ of a cold evaporated particle and that $\rho_{A^*}(r)$ of a hot nucleus:[16,20]

$$V_{c,j}(\mathbf{r},t) = \int \rho_j(\mathbf{r}_1)V_{12}(\mathbf{r} - \mathbf{r}_1 + \mathbf{r}_2)\, \rho_{A^*}(\mathbf{r}_2)\, d\mathbf{r}_1 d\mathbf{r}_2 \,. \tag{43}$$

Here **r** is the radius-vector drawn from the center of the nucleus to the center of the particle. The calculations[16,20] have demonstrated that an increase in $V_{c,j}$ is small and does not exceed 10% even at high temperature $t \approx 5$ MeV. Thus, in the first approximation, it is reasonably safe to suggest that the quantity σ_{inv} is described by the result of optical calculations for the cross-section of the interaction between a particle and a "cold" nucleus.

An uncertainty of these theoretical estimates of thermal effects is rather large. For example, calculations carried out within the framework of the Thomas-Fermi method[20] yield a more pronounced temperature dependence of macroscopic properties of a nucleus than those obtained in the Hartree-Fock method. A more correct description of nuclear properties by the Hartree-Fock method[21,22] has also led to a conclusion that the role of thermal effects is far more important. In addition, an increase in the values of the coefficients occurring in the relations of Equations 38-42 by a factor of 2-3 was also obtained within the framework of this method. Equations forming the basis of the Hartree-Fock method represent an approximate form of more rigorous equations of the theory of finite Fermi systems.[10] Calculations of thermodynamic properties of nuclei[11,23] carried out within this framework have demonstrated that in the temperature range $t < 8$MeV both approaches give similar results for thermal expansion and for a decrease in the surface tension of nuclei. As the temperature t increases further, the influence of thermal effects becomes more pronounced than is predicted by the expressions in Equations 38-42. In particular, the coefficient γ_S decreases linearly with increasing t until it turns to zero at a certain value $t_{lim} \approx 17$ MeV.[23] This leads to a number of interesting physical consequences in what is concerned with the behavior of a hot nuclear system. They will be considered at greater length in Section V. For the time being, it should be noted that an existing uncertainty of theoretical predictions makes the quest for observable characteristics of NRs, which are sensitive to thermal effects on the one hand, and which be studied in experiments on the other hand, very urgent. A subsequent analysis of NRs will use the Mosel's[16] results to estimate the minimum scale of the manifestation of thermal effects.

II. DECAY OF A C-NUCLEUS WITH HIGH ANGULAR MOMENTUM

A. BASIC RELATIONS OF SEMICLASSICAL MODEL

Properties and decay of C-nuclei with high values of angular momentum are characterized by a number of peculiar features which are manifested in various properties of NRs. The independence between decay and formation of a C-nucleus is violated above all. To be more specific, the decay of a C-nucleus depends on the value of the angular momentum, i.e., on the entrance channel. Therefore, the basic relation (Equation 1) of the statistical model is to be used for a given value of the angular momentum of a C-nucleus. Equations 2 and 3 will assume another form as well. To obtain it we shall make use of a semiclassical approach.[24]

In cases when a C-nucleus has a high value $I \gg 1$ of the angular momentum, we can disregard the spins of particles and consider angular momenta of an initial $\mathbf{I}$ and a final $\mathbf{I}_j$ nucleus, as well as the orbital momentum of an emitted particle as classical vectors*. The use of the principle of detailed balance allows one to obtain[24] the following expression for the probability per unit of time of emission of the j-th particle with the orbital momentum l in the direction $\mathbf{n}$ from a C-nucleus with the angular momentum $\mathbf{I}$

$$P_I(l,\mathbf{n},\epsilon_j)\, d^3l = \frac{\rho_j(E_j^*,\mathbf{I}_j)}{\rho_{CN}(E^*,\mathbf{I})}\,(2s_j + 1)\,\frac{\mu_j\epsilon_j}{\pi^2\hbar^3}\, d\sigma_l^{inv}(\mathbf{n},\epsilon_j)\,. \tag{44}$$

Here the cross-section for the capture of a particle with the orbital momentum $-l$ entering a nucleus in the direction $-\mathbf{n}$ is determined by the relation

$$d\sigma_l^{inv}(\mathbf{n},\epsilon_j) = \lambda\!\!\!^{-2}_j T_j(l)\,\delta(\mathbf{n},l)\, d^3l\,, \tag{45}$$

where delta function takes into account the fact that the orbital momentum l is perpendicular to the direction $\mathbf{n}$ of motion of the particle, $\lambda\!\!\!^{-}$ is the de Broglie wavelength, and T_j the transmission coefficient for a given j-particle.

Upon introducing the corresponding thermodynamical potential into the partition function Q (Equation 5) we can obtain the dependence of the level density on the angular momentum of a nucleus.[4,5] Then, within the framework of the Fermi-gas model we get[5,24]

$$\rho(E^*,I) = \frac{1}{\sqrt{\pi}}\,\frac{\sqrt{6}}{48}\left(\frac{\hbar^2}{\Theta_{rb}}\right)^{3/2}(2I + 1)(E^* - E_R)^{-7/4} \times \exp\left[2\sqrt{a(E^* - E_R)}\right], \tag{46}$$

where $E_R = \hbar^2 I(I+1)/2\Theta_{rb}$ is the rotational energy and Θ_{rb} the rigid body moment of inertia of a nucleus. Equation 46 implies that a nucleus can be considered as a

rotator with the rotational energy E_R, which is inaccessible to internal thermal excitation, i.e., $\rho(E^*,I) = \rho(E_{th},O)$, where $E_{th} = E^* - E_R$ is the thermal excitation energy. The following expression obtained in the approximation of low angular momenta when $E_R << E^*$, is often used in statistical calculations:[5,24]

$$\rho(E^*,I) \approx \frac{2I+1}{2\sqrt{2\pi}\,J^3}\,\rho(E^*)\exp(-I^2/2J^2)\,. \tag{47}$$

Here $J^2 = \Theta t/\hbar^2$ is the parameter which characterizes the spin dependence of the level density. Proceeding from the scheme of single-particle levels E_i, we can calculate this parameter with the help of the relation[4]

$$J^2 = \sum l_i\,\bar{n}_i\,(1-\bar{n}_i) \tag{48}$$

where l_i are the projections of the momenta of nucleons in single particle states. It follows from the calculations carried out within the framework of the shell model that the value of the moment of inertia of a nucleus is affected by shell effects. Even at relatively low values of E* and I their influence disappears, and the moment of inertia assumes the rigid-body value Θ_{rb}.

Substituting the level density of Equation 47 in Equation 44, and taking into account the angular momentum conservation law, we obtain the differential cross-section for particle emission integrated over the angular momentum of C-nuclei formed:[24]

$$\sigma(\mathbf{n},\epsilon_j) \sim \int I T_i(I)\,dI \int l T_j(l) S(I,l)\,W_{Il}(\vartheta,\epsilon_j)\,dl \tag{49}$$

Here T_j is the transmission coefficient for the I-th partial wave in the entrance channel,

$$W_{Il}(\vartheta,\epsilon_j) = \frac{1}{4\pi}\,\frac{\sum_{k=0}^{\infty}(-1)^k(4k+1)\left[\frac{(2k)!}{(2^k k!)^2}\right]^2 j_{2k}(iIl/J_j^2)\,P_{2k}(\cos\vartheta)}{j_0(iIl/J_j^2)}\,, \tag{50}$$

ϑ is the angle between the direction of motion of an outgoing particle and the beam, $j_{2k}(x) = \sqrt{\pi/2x}\,J_{2k+1/2}(x)$ the spherical Bessel function, $J_o(x) = x^{-1}\sin x$, $P_{2k}(\cos\vartheta)$ is the Legendre polynomial $S(I,l) = \Gamma_I^{-1}\exp[I^2/2J_{CN}^2 - (I^2+l^2)/2J_j^2]$ and Γ_I is the total decay width of a C-nucleus having the angular momentum I.

The extent to which the orbital momentum l is affected by the angular momentum **I** of a C-nucleus depends on the value of the parameter Il/J_j^2. In the case of complete absence of coupling between the vectors **I** and l, i.e., when $J_j \to \infty$, we

* Here and in what follows angular momenta are measured in the units of $\hbar$. The spins s_j of particles are taken into account only in the corresponding statistical factors.

obtain the isotropic angular distribution $W_{lI} \rightarrow 1/4\pi$ and the standard expression (Equation 3) for the energy spectrum of particles. In the weak-coupling limit $Il/J_j^2 << 1$, orbital angular momenta of emitted particles are hardly oriented with respect to the direction of the vector **I**. As $x \rightarrow 0$, the spherical Bessel functions $j_n(x)$ occurring in Equation 50 tend to the value $i^n x^n/(2n+1)!!$, and the angular distribution assumes the form[24]

$$\sigma(\mathbf{n},\epsilon_j) \approx \sigma(\epsilon_j)\,\frac{1}{4\pi}\left[1 + \frac{\bar{I}^2\bar{l}^2}{12J_j^4}\,P_2(\cos\vartheta)\right], \tag{51}$$

where

$$\bar{I}^2 = \int I\,T_i(I)\,I^2\,dI \Big/ \int I\,T_i(I)\,dI\,,$$

and

$$\bar{l}^2 = \int l\,T_j(l)\,l^2 dl \Big/ \int l\,T_j(l)\,dl\,.$$

Another limiting case is the strong-coupling limit $Il/J_j^2 >> 1$, when the orbital momentum l is completely oriented along the vector of the angular momentum **I** as a result of constraints imposed by angular momentum conservation law on the magnitude of $\mathbf{I}_j$. Then the spherical Bessel functions $j_n(ix)$ tend to the limit $i^n e^x/2x$ as $x \rightarrow \infty$, and the angular distribution is determined by the relation[24]

$$\sigma(\mathbf{n},\epsilon_j) \approx \frac{\sigma(\epsilon_j)}{2\pi^2 \sin\vartheta}\,. \tag{52}$$

Thus, if the value of the angular momentum of a C-nucleus is high, then the energy of an emitted particle depends on the angle of emission, and the angular distribution of particles is anisotropic.

B. THE EFFECT OF A HIGH VALUE OF THE ANGULAR MOMENTUM ON THE PROPERTIES OF A NUCLEUS

As well as a high-energy excitation, a high value of the angular momentum affects both micro- and macroscopic properties of a nucleus. For example, as I increases, the centrifugal and the Coriolis force come to play a more prominent role, and as a result the system undergoes a transition from a superfluid state to a normal one, shell effects can be manifested in some other way, deformation of a nucleus increases, its moment of inertia varies, etc. The range of these phenomena is rather wide and diverse.[3,5] Here we shall succinctly consider basic effects which are essential for the description of decay of highly-excited nuclei formed in NRs with intermediate-energy particles.

Effects caused by the rotation of a nucleus are manifested with maximum clarity in its fission properties. The most important of them, i.e., the fission barrier height B_f, was studied in detail as a function of the angular momentum within the framework of the liquid-drop model.[25] It has been demonstrated that as the rotation is intensified, a nucleus becomes more and more deformed, until the critical value I_{cr} is achieved for which the fission barrier preventing the disintegration of a nucleus disappears (for medium-weight nuclei, $I_{cr} \approx 100$). A decrease in B_f with increasing I can be described to good accuracy by the relation

$$B_f(I) \approx B_f(0) - (E_R - E_{RS}) , \tag{53}$$

where E_{RS} is the rotational energy of a nucleus at the fission saddle point. Since the moment of inertia of a nucleus at the saddle point Θ_S is always larger than that of a nucleus with equilibrium deformation Θ (and hence $E_R > E_{RS}$), then the fission barrier decreases with increasing angular momentum for any type of nuclei.

Residual nuclei with moderate values ($I \sim 10$) of the angular momentum are produced, as a rule, in NRs with intermediate-energy particles (see Chapter 5). To describe their decay it is sufficient to take into account only the dependence (Equation 53) of the fission barrier on the angular momentum. Other effects (e.g., an abrupt enhancement of the emission of fragments from superdeformed strongly rotating nuclei[26]) manifest themselves at the value of I close to the critical one I_{cr}. They are characteristic of reactions with heavy ions and can be neglected here. In any case, since even not so high values ($I \sim 30$) of the angular momentum affect the properties of nuclei significantly stronger than sufficiently high excitation energy ($E^* \sim 100$ MeV), it is desirable, while analyzing thermal effects, to select such processes in which weakly rotating nuclei are produced.

III. GENERAL PATTERN OF DECAY OF A HIGHLY EXCITED NUCLEUS AND METHODS USED IN CALCULATION OF THE EVAPORATION CASCADE

A highly-excited C-nucleus can decay in various exit channels j: it can emit a γ-quantum, a nucleon, or a light nucleus, or undergo fission. A competition between these channels is determined by the partial decay widths Γ_j, which can be easily obtained by integration of Equations 2 or 44 over all variables characterizing an emitted particle.

In the case $I = 0$ for the partial width Γ_j of the emission of nucleons (n,p), lightest nuclei (d, t, ^{3}He, α) and heavier fragments we get

$$\Gamma_j = \sum_{i=0}^{k} \int_0^{E^* - B_j - E_j^i} \frac{2s_j^i + 1}{\pi^2 \hbar^3} \mu_j \sigma_{inv}(\epsilon_j) \frac{\rho_j(E^* - B_j - E_j^i - \epsilon_j)}{\rho_{CN}(E^*)} \epsilon_j d\epsilon_j . \tag{54}$$

Here the summation is carried out over all excited states of the emitted fragment E^i ($i = 0,1,\ldots,k$) stable with respect to the emission of a nucleon. (This summation

is naturally absent in calculations of the partial widths of the emission of nucleons and those lightest nuclei which do not have excited states.) To calculate the cross-section of the inverse reaction we can use the approximation of Equation 4 for nucleons and lightest nuclei and the approximation

$$\sigma_{inv}(\epsilon_j) = \begin{cases} (1 - V_{c,j}/\epsilon_j) \text{ for } \epsilon_j \geq V_{c,j} + 1 \text{ MeV} \\ (V_{c,j} + 1)^{-1} \exp[c_5(\epsilon_j - V_{c,j} - 1)] \text{ for } \epsilon_j < V_{c,j} + 1 \text{ MeV} \end{cases} \tag{55}$$

with the values of the parameters r_0 and c_5 borrowed from Botvina et al[27] for heavier fragments. Under the assumption that dipole E1-transitions play a decisive role in the emission of γ-quanta from a highly-excited nuclei, we obtain the following expression for the partial width of this process:[13]

$$\Gamma_\gamma = (\pi\hbar c)^{-2} \int_0^{E^*} \sigma_{\gamma A}(\epsilon_\gamma) \frac{\rho_\gamma(E^* - \epsilon_\gamma)}{\rho_{CN}(E^*)} \epsilon_\gamma^2 \, d\epsilon_\gamma \, . \tag{56}$$

Here $\sigma\gamma_A$ is the cross-section of the photoabsorption by a nucleus given by the expression

$$\sigma_{\gamma A}(\epsilon_\gamma) = \frac{\sigma_0 \epsilon_\gamma^2 \Gamma_R^2}{(\epsilon_\gamma^2 - E_{GR}^2)^2 + \Gamma_R^2 \epsilon_\gamma^2} \tag{57}$$

where $\sigma_0 = 2.5$ A mb, $\Gamma_R = 0.3 \cdot E_{GR}$, $E_{GR} = 40.3 \cdot A^{-1/5}$MeV are the empirical parameters of the giant dipole resonance.[13] For the fission width the well known expression[28]

$$\Gamma_f = \frac{1}{2\pi \rho_{CN}(E^*)} \int_0^{E^* - B_f} \rho_s(E^* - B_f - \epsilon) \, d\epsilon \tag{58}$$

is used as a rule. Here B_f is the fission barrier height and ρ_S the level density in the fission saddle point. In the simplest case $I = 0$, it is possible to obtain analytic expressions for the partial widths only if the influence of shell effects is disregarded and the level density if represented by the Fermi-gas expression (Equation 25) without the pre-exponential factor. Even with such approximations it seems impossible to integrate Equation 44 for $I \neq 0$. However, if the angular momentum of a C-nucleus is not too high ($I < I_{cr}$), we can obtain[29] approximate analytic expressions for partial widths Γ_j which take into account both the disappearance of shell effects and the influence of rotation. The partial width of the emission of a particle is determined by the relation[29]

$$\Gamma_j \approx \frac{(2s_j + 1)\, \mu_j K_j}{\pi^2 \hbar^2} \sigma_g \frac{\rho_j(E_{th} - B_j)}{\rho_{CN}(E_{th})} t_j \times$$

$$\left[(B_j - E_{th} - t_j - c_j + V_j') \exp\left(\frac{B_j - E_{th}}{t_j}\right) + t_j \exp(-V_j'/t_j) + c_j\right], \tag{59}$$

where $K_j = c_1$, $c_j = c_2$ and $V_j' = 0$ for a neutron, $k_j = 1 + c_3$, $c_j = 0$ and $V_j' = c_4 V_{c,j}$ for a proton and light nucleus and c_1, c_2, c_3 and c_4 are the coefficients in Equation 4 for the cross-section of the inverse reaction. The fission width with allowance for a decrease in the fission barrier of a rotating nucleus (Equation 53) has the form[29]

$$\Gamma_f \approx \frac{t_f}{2\pi} \frac{\rho_s(E_{th}^s - B_f)}{\rho_{CN}(E_{th})} \left(1 - \exp\frac{B_f - E_{th}^s}{t_f}\right), \tag{60}$$

where ρ_S and $E_{th}^S = E^* - E_{RS}$ are the level density and the thermal energy of a nucleus in the saddle point. The temperature of an R-nucleus is calculated according to the following formula

$$t = \left(\frac{d \ln\rho}{dE^*}\right)^{-1} = \sqrt{\frac{E'}{a(E')}} \times \left\{1 + \frac{\delta U}{E'} \frac{\tilde{a}}{a(E')} [(1 + eE') \exp(-eE') - 1]\right\}^{-1}, \tag{61}$$

where $E' = E^* - E_R - B_j$.

A competition between different channels of decay of a highly-excited nucleus appears rather complicated even at zero angular momentum. It depends, to a great extent, on individual characteristics of a specific nucleus, such as the value of the binding energy B_j and that of the Coulomb barrier $V_{c,j}$ for particles, fission barriers, etc. On the other hand, a number of general regularities of the process can be noted:

- the probability of a given decay channel $w_j = \Gamma_j/\Gamma_{tot}$($\Gamma_{tot}$ is the total decay width) increases rapidly with E^* for $E^* - (B_j + V_{c,j}) > 0$
- the emission of γ-quanta competes noticeably with other processes for $E^* \lesssim B_j + V_{c,j}$
- for high excitations more rare decay channels become comparatively more probable, since in this case the values of B_j and $V_{c,j}$ do not diminish the density of accessible levels of an R-nucleus to such a great extent

The pattern of decay becomes even more complicated for high values of the angular momentum. The effect of the angular momentum on the partial decay widths has been studied by a number of authors.[3] Therefore, we shall succinctly consider here only general corollaries of this effect.

First, a heated rotating C-nucleus emits mainly neutrons. A neutron takes away a large portion of the excitation energy $\overline{\Delta E}^* \approx B_n + 2t$, but only a small part of

the angular momentum $l \approx$ 1-2.[30] Therefore, on emitting subsequently several neutrons, the nucleus releases the most part of its excitation energy, but retains its angular momentum almost completely. The emission of an α-particle increases dramatically in the domain $E_{th} \approx B_n$, since it can remove a large orbital momentum 1, and in addition to this, $B_\alpha < 0$ for a number of nuclei. And finally, if emission of particles is forbidden by the energy conservation law (for $E_{th} < B_n$),emission of γ -quanta begins to play a decisive role. First, the nucleus emits several statistical dipole γ-quanta, then, changing its angular momentum only slightly, it turns out to be in the domain $E_{th} \lesssim 1.5$ MeV, where the emission of quadrupole γ -quanta is predominant. Quadrupole γ-transitions remove the whole remaining angular momentum of the nucleus.

It is clear that an analytic description of such a complicated process as a subsequent emission of a great number of different particles from a highly-excited rotating nucleus involves enormous difficulties. The Monte Carlo technique whose mathematical nature is adequate to a stochastic character of the de-excitation process turns out to be rather effective for the description of the evaporation cascade.[30] In this method, the sampling of the type and characteristics of a particle emitted from a C-nucleus with given values of E* and I is carried out according to the densities of conditional probabilities which are obtained by an appropriate integration of Equation 44. First, the channel of decay of a C-nucleus (n, p, d, t, ^{3}He, α, γ, f) is determined from the decay probabilities $w_j = \Gamma_j/\Gamma_{tot}$. Then, for a chosen type of decay, the sampling of the energy ϵ_j, of the orbital momentum l and of the angle ϑ between the vectors **I** and $\boldsymbol{l}$ is carried out with the help of the three-dimensional probability density

$$w(\epsilon_j, P, \cos\vartheta) \sim l \exp 2\{a[E^* - \epsilon_j - \hbar^2(I^2 + l^2)/2\theta + \hbar^2 I l \cos\vartheta/\theta]\}^{1/2} . \quad (62)$$

This probability density is obtained,[30] if the level density in the form Equation 46 is substituted in Equation 44 and the transmission coefficients are used in the form given by the sharp cut-off approximation:

$$T_j(l) = \begin{cases} 1 \text{ if } l < l_{max} = \dfrac{R}{\hbar}\sqrt{2\mu_j(\epsilon_j - V_{c,j})} \\ \\ 0 \text{ if } l \geq l_{max} \end{cases} \quad (63)$$

Then, characteristics of an R-nucleus $\mathbf{I}_j = \mathbf{I}\text{-}\boldsymbol{l}$, $U_j = E^*\text{-}\epsilon_j\text{-}B_j$ are calculated and the process of the particle emission is repeated until the excitation of a nucleus is removed completely. As many evaporation cascades are simulated with the help of a computer, as is necessary to obtain the desired statistical accuracy of calculations.

This method[30,31] includes a widely known Monte Carlo calculation of the evaporation cascade for a nucleus with zero angular momentum[2,6] as a specific case. Presently, such a method of calculation of de-excitation of a nucleus with high angular momentum is also developed by other authors.[32,33] Unlike the other methods

of calculation,[26,34,35] it takes into account exactly (in each evaporation chain, rather than in the average) the laws of the conservation of the angular momentum, the energy, the momentum, the charge, and the mass number. This allows one to correctly take into account the role of fluctuations in the evaporation cascade and to calculate a wide set of characteristics of the process (distributions over the angles, the energy, the orbital momentum, and the number of particles of various types, the isotope yield, fission probability, etc.).

IV. ANALYSIS OF DATA CONCERNED WITH THE PROPERTIES AND DECAY OF EXCITED C-NUCLEI

Two facets which are intimately related to one another can be segregated in the study of deep inelastic hadron-nucleus processes: 1) the study of the mechanism of the deep inelastic interaction and of dissipation of energy supplied to a nucleus, and (2) the study of decay and properties of excited nuclei produced as a result of this interaction. Since there are considerable gaps in the comprehension of both of this facets, it is expedient to isolate and to independently investigate in detail its second facet to obtain a reliable solution to the problem on the whole. Preparatory to analyzing reactions with intermediate-energy particles, it seems reasonable to fix the parameters of the evaporation model on the basis of data concerned with statistical properties of nuclei and with decay of C-nuclei produced in reactions with particles and heavy ions of low energies.

A. STATISTICAL PROPERTIES OF C-NUCLEI PRODUCED IN REACTIONS WITH LOW-ENERGY PARTICLES

It has been already mentioned that a large body of information on the nuclear level density ρ (E*) has been accumulated in experiments with low-energy particles. Data on spacings between neutron resonances which correspond to the nuclear excitation energy $E^* = B_n$ form a considerable part of this information. Its other part consists of data obtained from analysis of low-lying bound states (low excitations $E^* < B_n$), whereas at higher energies ($B_n < E^* \lesssim 20$MeV) these are the data on the level spacing obtained in reactions (γ,n), (p,γ), (p,p′), (p,α), (α,γ), (α,n), (d,p), (^{3}He,d), (^{3}He,α), etc., and data obtained from the measurements of the Ericson fluctuations.[13] On the basis of this information a phenomenological approximation of the nuclear levels density (Equations 25-31) has been constructed which describes experimental data in the excitation energy range $B_n \lesssim E^* \lesssim 20$ MeV to a high accuracy (see Figures 1 and 2). The data on the level density are indicative of the fact that shell effects exert strong influence on this nuclear characteristic for the excitation energies lying in this range. Therefore, thermal destruction of shells in nuclei is the principal physical phenomenon that must be taken into account in the evaporation model. In particular, this is concerned with the approximations of ρ (E*).

Data on the radiation width Γ_γ and on the lifetime τ_{cN} of a C-nucleus[13] form another class of data on statistical properties of nuclei in this range of excitations

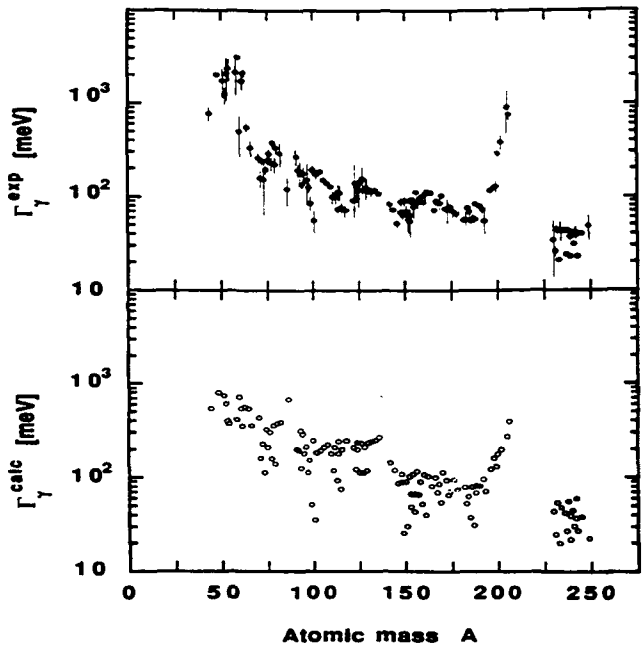

FIGURE 4. The dependence of the neutron resonance radiative width Γ_γ on A is represented here. Full circles correspond to experimental data[13] and the open circles to the calculation of Reference 13.

($E^* \lesssim 20$ MeV). The lifetime is connected with the magnitude of the total decay width $\Gamma_{tot} = \sum_j \Gamma_j$ through the relation

$$\tau_{CN} = \hbar / \Gamma_{tot} \,. \tag{64}$$

The total and the partial width of decay of a C-nucleus are determined by the ratio of the level density of a C-nucleus to that of an R-nucleus (see Equation 56), rather than by the level density itself. It follows from the analysis of Reference 13 that relations of the equilibrium statistical model which use phenomenological approximation of the nuclear level density describe satisfactorily this class of data as well (see Figure 4).

In addition to this, a large amount of data exists on the cross-section for fission of heavy nuclei ($A \gtrsim 170$) induced by low-energy particles.[36] Since emission of a neutron and fission are principal channels of decay of heavy C-nuclei, the energy dependence of the ratio Γ_f/Γ_n of partial widths can be extracted from these data. Analyzing this ratio with the help of Equations 54-61 we can study the density of levels of a nucleus in the fission saddle point. At this point, the nucleus has the largest possible deformation, and collective effects influence dramatically the level density. Moreover, an analysis of the energy dependence of the ratio Γ_f/Γ_n allows

one to investigate the influence exerted by shell effects on the nuclear level density over a wider energy range $E^* \lesssim 80$ MeV.

It is of interest from this viewpoint to investigate the fissility of nuclei in two domains of nuclide chart, i.e., that of preactinides and actinides. Nuclei in the vicinity of lead have maximum deformation at the saddle point (they are dumbbell-shaped). A large shell correction in the ground state affects dramatically the level density in the neutron channel and leads to a high fission barrier. As a result the fissility of preactinides is sensitive both to collective and shell effects in nuclei whose deformation is equilibrium. Actinides have double-humped structure of the fission barrier because of a strong irregular dependence of a shell correction on the deformation. For most heavy transuranium nuclei the fission barrier height B_f is almost completely determined by the shell component. Therefore, the fissility of actinides is sensitive to shell effects at the fission barrier, and the energy dependence of the fissility to the rate of damping of shell effects with the excitation energy.

Let us first consider the fissility of preactinide nuclei. Since the parameters of level density of a nucleus in the neutron channel are obtained from the data on ρ, the ratio Γ_f/Γ_n depends, above all, on two parameters: on the fission barrier height B_f and on the parameter of the level density of a nucleus at the saddle point, i.e., on the ratio a_f/a_n. The fission barrier height B_f is connected with its liquid-drop component B_f^{LD} and with shell corrections to the mass of a nucleus in the ground state δU_g and the saddle point δU_S through the relation

$$B_f = B_f^{LD} - \delta U_g + \delta U_{sp} . \tag{65}$$

For preactinides, the shell component of the potential energy of a nucleus is small ($\delta U_S \approx 0$), because the nucleus has the largest possible deformation at the saddle point, and its configuration is close to that of the scission point. Owing to the manifestation of the shell structure in the ground state of a nucleus (nuclei in the vicinity of lead have the shell correction $\delta U_g \approx -10$ MeV), the fission barrier B_f increases as the closed shell ($N = 126$) is approached from below, and becomes as large as 20 MeV.

A noticeable distinction between the deformation (and the shape) of a nucleus in the ground state and those of a nucleus in the saddle point must lead to an asymptotic value of the level density parameter which is larger at the saddle point than in the ground state, i.e., $\tilde{a}_f/\tilde{a}_n > 1$ (see Equation 38 and recall that $b_S \approx 2^{1/3}$ for the saddle point of preactinides[36]).

A pronounced dependence of the fission probability on the excitation energy (see Figure 5) is a specific feature of preactinides. Owing to this fact the fission barrier height B_f is to be found at the point where an abrupt fall in Γ_f/Γ_n is observed, which is caused by a decrease in the probability of penetrating the fission barrier for the values of energy close to B_f. Therefore, the values of B_f determined from the data on Γ_f/Γ_n depend weakly on the model description of the level density in the neutron and the fission channel. Thus, the fission barrier B_f is extracted first from the description of the experimental ratio Γ_f/Γ_n in the domain of lowest energies

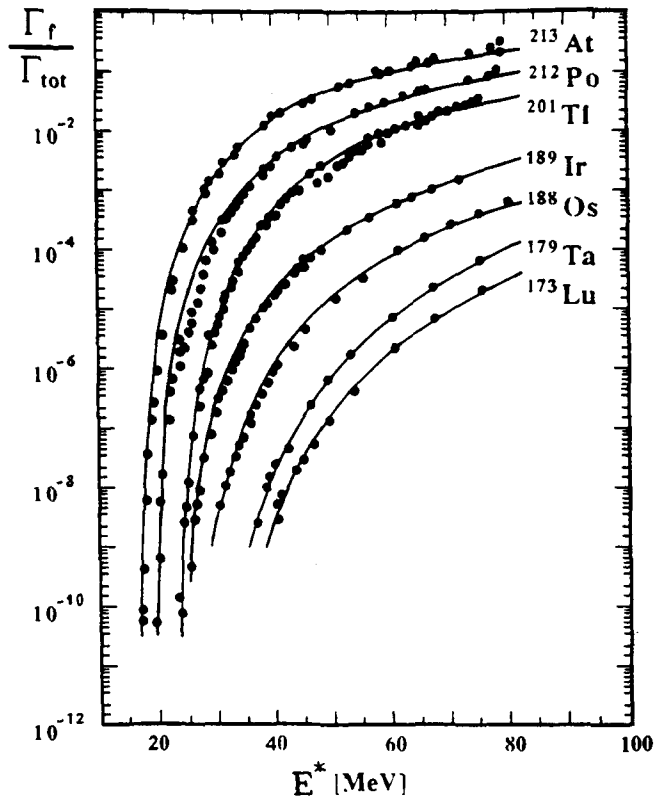

FIGURE 5. This graphs the dependence of the fissility Γ_f/Γ_{tot} of different C-nuclei on the excitation energy. The points correspond to experimental data,[36] and the curves to the calculation of Reference 13.

E^*, then the parameter $\tilde{a}_f/\tilde{a}_n$ is determined from the description of experimental points at higher energies. It has been shown[13] that liquid-drop barriers B_f^{LD} extracted from empirical barriers B_f with the help of the expression in Equation 65 agree well with the results of calculations of Myers and Swiatecki[15] carried out in accordance with the liquid-drop model. For preactinides empirical values of the ratio $\tilde{a}_f/\tilde{a}_n \approx 1.05 \div 1.10$ fall within the limits of uncertainties of various theoretical estimates (see Figure 6). One should use these values of the ratio $\tilde{a}_f/\tilde{a}_n$ with caution, since the contribution from pre-equilibrium effects and from the "second chance fission" after the emission of a neutron in the domain of high values of E^* can reduce the value of $\tilde{a}_f/\tilde{a}_n$ approximately by $0.02 \div 0.04$.[13]

In contrast to the case of preactinides, shell effects play a crucial role at the fission barrier for actinide nuclei. The shell correction at the fission barrier is comparable to its liquid drop component. Moreover, the shell correction to the nuclear energy is a nonmonotonic function of the deformation. This leads to a

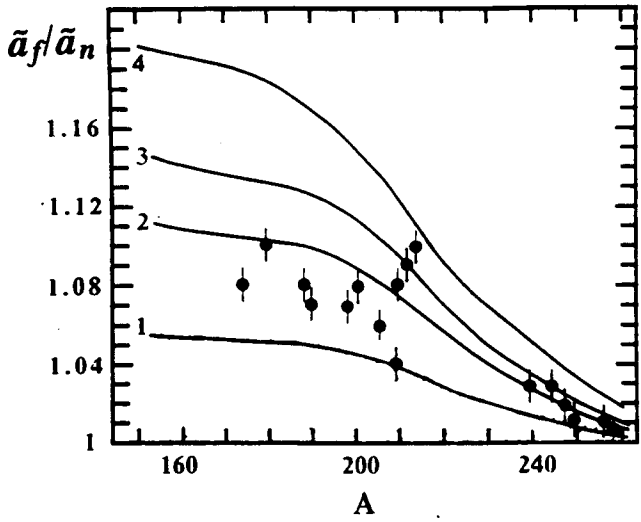

FIGURE 6. Here is the dependence of the $\tilde{a}_f/\tilde{a}_n$ ratio on A. The curves 1-4 represent the results of various theoretical estimates.[13] The points represent the results of the analysis of experimental fissilities of nuclei.[13]

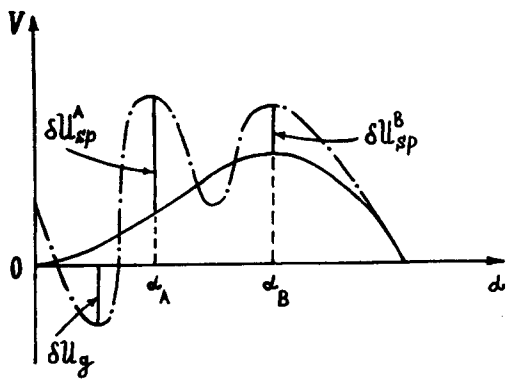

FIGURE 7. This is a schematic graph of a two-humped fission barrier. The solid curve shows the dependence of the liquid-drop potential energy $\tilde{V}$ of a nucleus on its deformation α. The dash-dotted curve shows the same dependence for the potential energy V with allowance for shell effects. Two saddle points are denoted by the letters A and B. The shell corrections δU^A_{sp} and δU^B_{sp} at these saddle points and the shell correction δU_g in the ground state are also shown.

double-humped shape of the fission barrier (see Figure 7). In this case, the heights B_f^A and B_f^B of the double-humped fission barrier are given by the expression

$$B_f^i = \tilde{V}(\alpha_i) - \delta U_g + \delta U^i_{sp} . \tag{66}$$

where δU^i_{sp} is the shell correction for the i-th peak of the potential energy of a nucleus measured from the liquid-drop potential energy $\tilde{V}(\alpha_i)$ for a corresponding deformation*. The parameters of the double-humped barrier of fission of actinide nuclei were measured in experiments with low-energy particles.[37] Taking experimental values of B^A_f, B^B_f and δU_g and the values of $\tilde{V}(\alpha_i)$ calculated in accordance with the liquid-drop model,[15] we can find the "empirical" values of the shell corrections δU^A_{sp} and δU^B_{sp} with the help of Equation 66.

In the case of a double-humped barrier, the fission width is determined by the expression[38]

$$\Gamma_f = \frac{\Gamma_A \Gamma_B}{\Gamma_A + \Gamma_B} \tag{67}$$

where Γ_A and Γ_B are the fission widths for the corresponding saddle points. Each of these widths is calculated in accordance with the formula of Equation 60 with its own shell correction. Rotational enhancement coefficient k^A_{rot} and k^B_{rot} are calculated differently than in preactinides. Since heavy nuclei have a small deformation at the saddle point and axially symmetrical form at the hump A, the coefficient k^A_{rot} is calculated in accordance with the formula in Equation 30a. At the hump B, the nucleus loses its mirror symmetry and as a result the coefficient k^B_{rot} has the value which is twice as large as that given by Equation 30a, namely $k^B_{rot} = 2\Theta_\perp t$.[36]

In the domain of actinides, the ratio $\Gamma_n/\Gamma_{tot} \approx \Gamma_n/\Gamma_f$ (since $\Gamma_f \gg \Gamma_n$) is extracted from experimental cross-sections. Data on the cross-sections of the (HI,xn)-reactions are used to this end as a rule. Figure 8 shows experimental data on Γ_n/Γ_f and their comparison to the calculation of Reference 29. In the calculation of Γ_f, empirical values of the fission barriers B^A_f and B^B_f and of shell corrections δU^A_{sp} and δU^B_{sp} were used, whereas the parameter $\tilde{a}_f/\tilde{a}_n$ was determined from the condition of the best fit to experimental data. The values of $\tilde{a}_f/\tilde{a}_n$ thus obtained are shown in Figure 6. Figure 8 shows the results of the calculation of Γ_n/Γ_f without regard for shell effects. The fissility of transuranium nuclei is very sensitive to shell effects as well. It is seen from Figure 8 that shell effects are destroyed rapidly, as the excitation energy increases, and disappear at the energies $E^* \gtrsim 30$ MeV. In the domain of low energies ($E^* \lesssim 20$ MeV), shell effects hamper the fission of a heavy nucleus. This phenomenon is of special importance in the domain of superheavy nuclei whose increased stability is determined completely by shell effects.[12]

Recently, investigations of emission of heavy clusters from C-nuclei attracted particular interest. To analyze experimental data obtained[39] the evaporation model was widely used.[40,41] Without going into details of various versions of this model, we would like to notice that the evaporation model, using the approximation in Equation 55 for the cross-section of the inverse reaction, describes the data on the

* Deformations of transuranium nuclei $\alpha_A = 0.3$ and $\alpha_B = 0.6$ depend only slightly on their nucleonic composition.

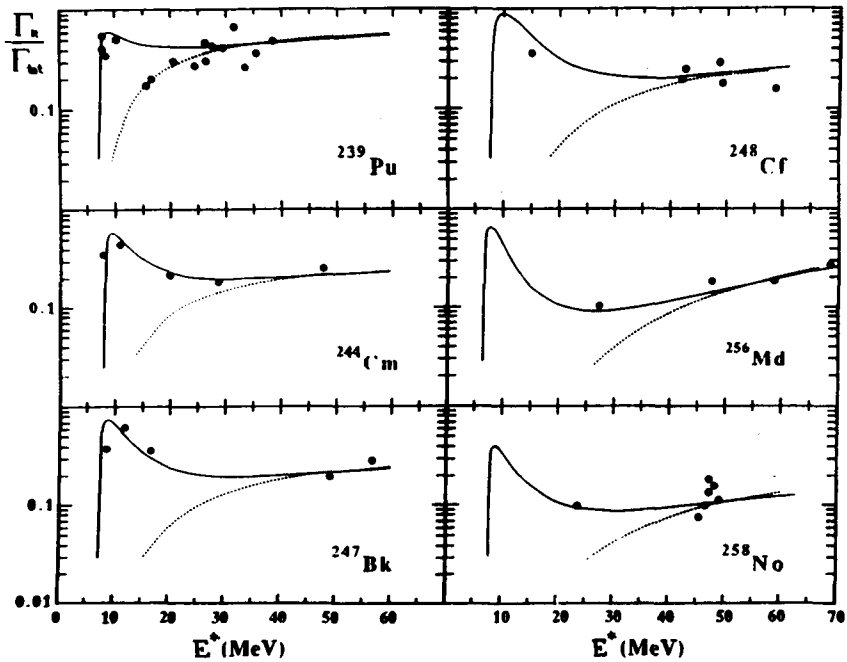

FIGURE 8. These graphs represent the energy dependence of the neutron emission probability Γ_n/Γ_{tot} for transuranium nuclei. The experimental points are borrowed from Reference 29. The solid curves represent the results of calculations[13] with shell effects, and the dashed curves correspond to calculations[13] without shell effects.

cross-section of production of various fragments and on their energy spectra to a good accuracy (see Figure 9).

B. DECAY OF C-NUCLEI PRODUCED IN HEAVY-ION-INDUCED REACTIONS

A considerable progress made in investigations of highly excited nuclei was due to the use of beams of heavy ions. A large probability of a complete fusion of two nuclei leading to a formation of a C-nucleus with a high angular momentum ($I \lesssim 100$) is the most spectacular and appealing feature of a NR with heavy ions of low energies ($\lesssim$ 10 MeV/nucleon). A large body of data on the decay of excited nuclei with the energy $E^* \lesssim 150$ MeV has been obtained in experiments aimed at the investigation of reactions in which a complete fusion of nuclei takes place. These data can be analyzed with the help of a semiclassical statistical model[30,31] as applied to the description of the decay of a C-nucleus with high angular momentum I. The calculation of the cross-section σ_{CN} for formation of a C-nucleus which is necessary for this analysis was carried out with the help of the optical approach:

$$\sigma_{CN} = \pi \lambda\!\!\!^{-}{}_i^2 \sum_{I=0}^{\infty} (2I + 1)\, T_i(I)\, P^I_{fus} \simeq \pi \lambda\!\!\!^{-}{}_i^2 \sum_{I=0}^{I_{CN}} (2I + 1)\, P^I_{fus}\,. \qquad (68)$$

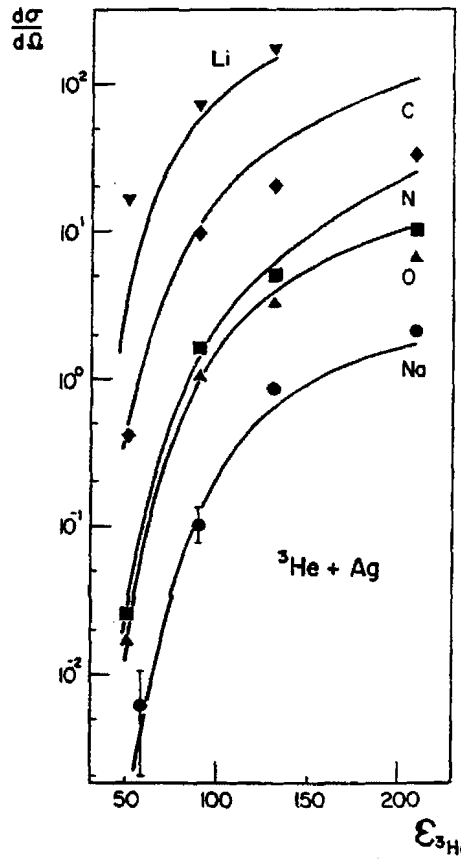

FIGURE 9. The cross-section for emission of heavy clusters at backward angles (Θ = 120° - 160°) as a function of kinetic energy of ^{3}He in the l.s. are graphed here. The data[39] and the curves show the results of the calculations carried out in accordance with the evaporation model.

Here $\lambda\!\!\!^{-}_i$ is the de Broglie wavelength of an ion, I_{CN} the limiting angular momentum for the production of a C-nucleus and $T_i(I)$ and P^I_{fus} are the transmission coefficient and the fussion probability for the I-th partial wave respectively. The optical potential, describing the nucleus-nucleus interaction was used in the form

$$V_I(r) = V_c(r) + V_R(r) + V_n(r) . \tag{69}$$

where r is the distance between the centers of nuclei, and V_c, V_R and V_n are the Coulomb, the centrifugal, and the nuclear part of the potential, respectively. (Empirical values of the parameters of the potential $V_I(r)$ are given in Reference 31). The value of the limiting angular momentum I_{CN} was found with the help of an empirical systematics[31] of the probability of complete fusion of nuclei given by the relation $P_{fus} = \sigma_{CN}/\sigma_R$, where σ_R is the total inelastic cross-section. A systematic analysis of a wide range of data on the decay of C-nuclei produced in reactions

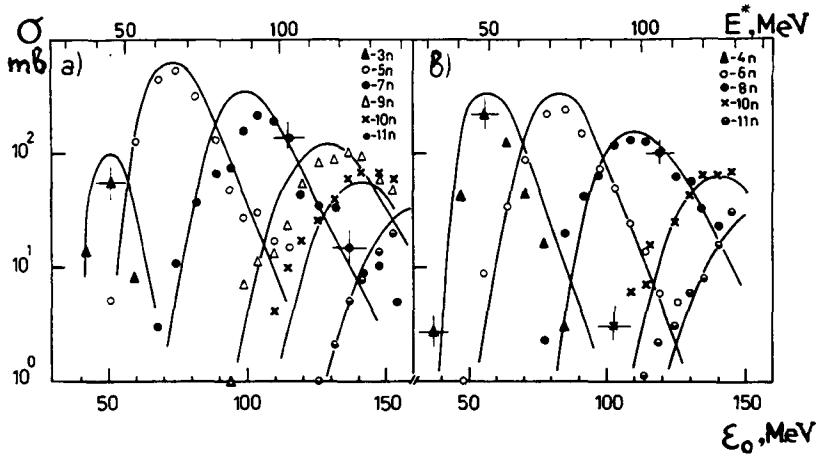

FIGURE 10. These lines trace the excitation functions for the reactions a) ^{130}Te(^{12}C,xn) $^{142-x}$Ce and b) ^{130}Te(^{13}C,xn) $^{143-x}$Ce. The curves correspond to the calculation and the points to experimental data.[31]

with heavy ions of energies up to 10MeV/nucleon has been carried out[31] on the basis of the evaporation model. Both inclusive characteristics of particles emitted from C-nuclei (such as their average multiplicities, mean values of the angular momentum taken away by a particle, the energy, and the angular distributions) and cross-sections for various reactions (fission, radiative capture, and (HI, xnyp)-reactions considered as functions of the primary energy were studied in detail. Figures 10-12 illustrate a typical accuracy of the description of experimental data within the framework of the evaporation model. An analysis[31] has demonstrated that the equilibrium statistical model of decay of a C-nucleus based upon the pattern of a subsequent emission of particles and γ-quanta, and the fission as well, can describe a large body of experimental data at least up to the values of the excitation energy E* approximately equal to 150 MeV. Shell effects are manifested in the characteristics of decay of a C-nucleus only in the range of comparatively low excitations $E^* \lesssim 30$ MeV($t < 1.5$ MeV). In the case of higher excitations, owing to a thermal damping of shell effects and averaging over the steps of the evaporation cascade, one can describe the decay with the help of simple statistical relations obtained within the framework of the Fermi-gas model.

V. EXPLOSIVE DECAY OF HOT NUCLEI

A concept of a C-nucleus lying behind the equilibrium statistical model considered in this chapter assumes that the condition $\tau_{CN} \gg \tau_{eq}$, where τ_{CN} is the lifetime of a C-nucleus and τ_{eq} the time during which a thremodynamical equilibrium is established in it, is satisfied. An analysis[42] of the process of nuclear thermalization proceeding through binary NN-collisions gives the values of $\tau_{eq} \sim 10^{-22} \div 10^{-21}$s. Such a fast equilibration with respect to internal degrees of freedom is confirmed in experiments with deep inelastic transfer reactions.[43] Within the framework of

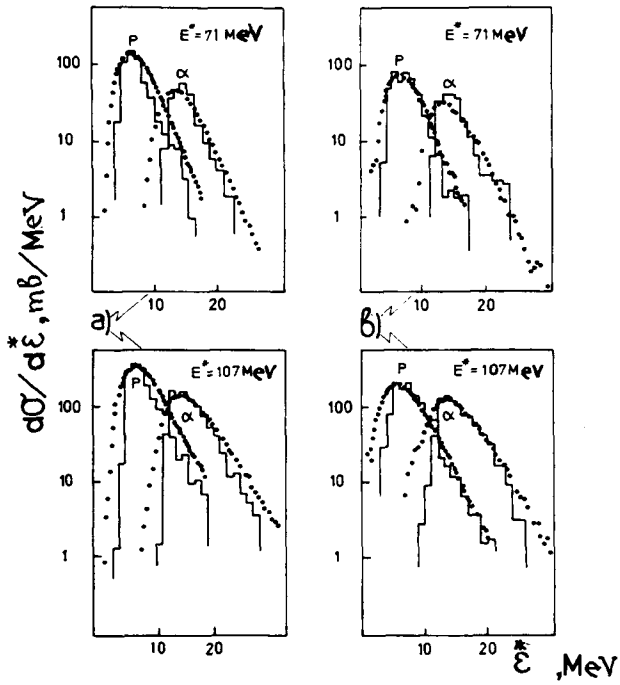

FIGURE 11. Here are the spectra of protons and α-particles emitted from ^{117}Te C-nucleus formed in the reactions a) ^{14}N + ^{103}Rh, and b) ^{40}Ar + ^{77}Se, with E* = 71 and 107 MeV. The histograms correspond to the calculation and the points to experimental data.[31]

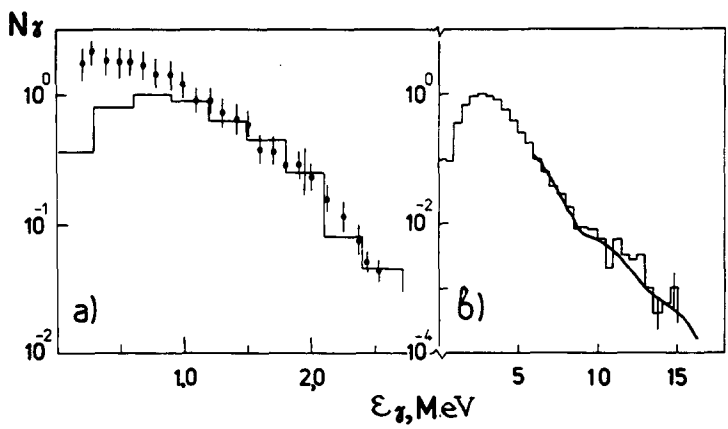

FIGURE 12. Here is the spectrum of γ-quanta (in relative units) emitted from C-nuclei formed in the reactions a) ^{22}Ne + Cu, and b) ^{34}S + ^{130}Te with E* = 74 and 61 MeV, respectively. The points and the curve correspond to experimental data.[31] The rest of the notation is the same as in Figure 11.

statistical model, the value of τ_{CN} is usually calculated with the help of the relation in Equation 64. This leads to the values which turn out to be too small ($\tau_{CN} \sim 10^{-20}$ - 10^{-21}s) even for the energies $E^* > 100$ MeV. This casts some doubt of the validity of the equilibrium statistical model. It has been shown,[44] however, that in the case of a strong overlap of levels such an estimate is not corrrect and significantly underestimates the value of τ_{CN}. Experimental data obtained[45] with the help of the crystal-blocking technique seem to be indicative of relatively large values of the lifetime of a C-nucleus in the domain $E^* \sim 100$MeV. On the other hand, the issue on the lifetime of a hot C-nucleus remains presently open both from the theoretical and the experimental viewpoint. This does not allow us to determine the validity range of the concept of a C-nucleus on the basis of considerations concerned with the analysis of the duration of various time intervals.

Limits in which a C-nucleus may exist are readily obtained from energy considerations. It is evident that if a thermal energy of nuclear nucleons is larger than their total binding energy $\mathscr{E}_b$, nuclear forces cannot confine nucleons together, and the nucleus undergoes an "instantaneous" breakup (explosion) into nucleons and fragments. Using Equation 18 and the condition $E^* = \mathscr{E}_b$, we obtain that this phenomenon takes place at the limiting temperature $t_{lim} \approx 10$ MeV. The condition $t < B_n \approx 7$ MeV bounding the region in which it is not yet unreasonable to consider the evaporation of particles gives a close value of t_{lim}.

A. FERMI BREAKUP OF LIGHT NUCLEI

For light nuclei ($A \sim 10$-20) an explosive mechanism of decay can manifest itself at a relatively low-value of the excitation energy ($E^* \sim 100$ MeV). The statistical Fermi model[46] is used to describe the breakup of a light nucleus. For the first time it was applied to the case of a multiple production of hadrons in NN- and πN-collisions. (References to early papers concerned with Fermi breakup of light nuclei are in Barashenkov and Toneev.[2]) An assumption about an explosive breakup of a nucleus directly into a final state forms the physical basis of this model. The final state (breakup channel) represents a set of particles (nucleons and fragments) in the phase space. Their momenta satisfy the energy-momentum conservation law, and the total charge and the mass number are equal to the charge Z and the mass number A of a disintegrating nucleus, respectively. It is believed that decay of a nucleus takes place in a certain breakup volume. After that, nuclear interaction between the particles ceases to act and they diverge in the resultant Coulomb field created by all particles.

It is assumed that a statistical equilibrium is established in a nucleus with the excitation energy E^*, and that the probability of each channel is in direct proportion to its phase volume:

$$W = \frac{S}{G}\left[\frac{V_f}{(2\pi\hbar)^3}\right]^{n-1} \int d^3\mathbf{p}_1 \ldots d^3\mathbf{p}_n\, \delta\left(\sum_{1\le i\le n} \mathbf{p}_i\right) \delta\left(\sum_{1\le i\le n} \frac{p_i^2}{2m_i} - E_{kin}\right). \tag{70}$$

Here n is the number of particles produced in the decay of the nucleus, $m_i (i = 1,\ldots,n)$ the mass of the i-th particle, $S = \prod_{1 \le i \le n} (2s_i + 1)$ the spin factor (s_i is the spin of the i-th particle), $G = \prod_{1 \le j \le l} n_j!$ the factor taking into account the fact that some of the particles may be identical (n_j is the number of particles of a given type j, and l the number of different types), $\mathbf{p}_i$ the momentum of the i-th particle, V_f the volume accessible to a free motion of particles at the instant of breakup, and E_{kin} the kinetic energy of particles at the instant of breakup. The assumption that the phase space plays the dominant role is justified for the case, when the value of the excitation energy is high and the nucleus breaks up into a large number of particles. Carrying out the integration in Equation 70, we obtain

$$W = \frac{S}{G}\left[\frac{V_f}{(2\pi\hbar)^3}\right]^{n-1}\left(\frac{\prod_{1 \le i \le n} m_i}{\sum_{1 \le i \le n} m_i}\right)^{3/2} \frac{(2\pi)^{3(n-1)/2}}{\Gamma\left(\frac{3}{2}(n-1)\right)} E_{kin}^{3n/2 - 5/2}, \tag{71}$$

where Γ (x) is the gamma function. The energy E_{kin} is found from the energy balance equation and is given by

$$E_{kin} = E^* - \left(\sum_{1 \le i \le n} m_i c^2 - M_A c^2\right) - B_c, \tag{72}$$

where M_A is the mass of a nucleus, B_c the energy of the Coulomb interaction of particles of a given channel which are situated in the breakup volume. The energy B_c can be found in the Wigner-Seitz approximation which gives

$$B_c = \frac{3}{5}\frac{e^2}{r_0}\left(1 + \frac{V_f}{V_0}\right)^{-1/3}\left(\frac{Z^2}{A^{1/3}} - \sum_{1 \le i \le n} \frac{Z_i^2}{A_i^{1/3}}\right), \tag{73}$$

where A_i and Z_i are the mass number and the charge of the i-th particle of a given channel, respectively. The free volume V_f is the parameter of the model and has the same order of magnitude as the volume of a nucleus $V_0 = 4/3\ \pi r_0^3 A$.

Usually the Fermi breakup is simulated by means of the Monte Carlo technique.[2,47-49] The procedure of calculations is organized to include the possibility that fragments of the nuclear decay can be produced both in the ground state and in excited states (with the energies E_i). All states of fragments which are stable with respect to emission of nucleons are considered permissible. Experimental values of masses and spins of particles constituting a channel are used to calculate the probability of the decay channel. Fragments in the i-th excited state with the energy E_i are treated as separate particles with the spin equal to the spin of this state and the mass $m_i = m_g + E_i$ (where m_g is the mass of the ground state of this

fragment). Formation of unstable fragments of the type ^{5}He, ^{5}Li, ^{8}Be, ^{9}B, etc., whose lifetimes $\tau \gtrsim 10^{-18}$s are significantly larger than the breakup time are also taken into consideration.

It is assumed in the model that after the breakup of the nucleus into particles, the latter undergo an isotropic divergence in the c.m.s. The kinetic energy of all particles at an infinity is the sum of their energies at the instant of the breakup and an additional Coulomb repulsion: $T_{kin} = E_{kin} + B_c$. Kinetic energies of separate particles are determined under the assumption that the total kinetic energy T_{kin} is distributed uniformly over the entire phase volume of the breakup channel. The energy of each particle is found by means of a random sampling over the distribution given by the integrand of Equation 70 with allowance for the conservation laws. The secondary decay of unstable fragments after the divergence of all particles in accordance with the channels $^5\text{He} \rightarrow \alpha + n$, $^5\text{Li} \rightarrow \alpha + p$, $^8\text{Be} \rightarrow \alpha + \alpha$, $^9\text{B} \rightarrow p + \alpha + \alpha$, etc., is also taken into account in Botvina et al.[49]

Here we present the results of the investigation of basic regularities of decay of an excited light nucleus obtained with the help of the Fermi breakup model. A breakup into a definite number of particles begins from a certain threshold energy necessary to detach at least one particle from a nucleus. The threshold energy can be found from the Fermi condition $E_{kin} \geqslant 0$, where E_{kin} is defined by the balance Equation 72. As the excitation energy increases, new breakup channels open and the breakup into a larger number of particles becomes more probable. The dependence of the probability of formation of a definite fragment on the excitation energy has a threshold character and changes dramatically with increasing E*, being sometimes nonmonotonic (see Figure 13). This is because the fragments can be produced in different channels which dominate at different energies. If excited states of fragments are taken into account correctly in the decay of a nucleus, then the probability of production of heavy fragments with $A \geqslant 10$ increases significantly.

To explicity demonstrate the effect of separate channels on the yield of fragments, we present the probabilities of some decay modes for a ^{15}N nucleus in which the fragments ^{11}B (modes: 1 - $^{15}\text{N} \rightarrow \alpha + {}^{11}\text{B}$; 2 - $^{15}\text{N} \rightarrow d + d + {}^{11}\text{B}$; 3 - $^{15}\text{N} \rightarrow p + p + n + n + {}^{11}\text{B}$) and ^{6}Li (modes: 4 - $^{15}\text{N} \rightarrow {}^9\text{Be} + {}^6\text{Li}$; 5 - $^{15}\text{N} \rightarrow d + {}^7\text{Li} + {}^6\text{Li}$; 6 - $^{15}\text{N} \rightarrow p + n + {}^7\text{Li} + {}^6\text{Li}$) are produced. Each of such modes includes all decay channels resulting in formation of these fragments both in the ground state and in excited states. Many-body channels dominate at higher excitations. The existence of the second peak for the mode $^{15}\text{N} \rightarrow \alpha + {}^{11}\text{B}$ at $E^* \approx 25$ MeV is of interest. This peak is associated with the fact that for these values of the excitation energy the formation of the fragment ^{11}B in excited states becomes possible, and new more probable channels open. This is illustrated by the insert of Figure 13 which shows the probability of channels with formation of ^{11}B in the ground state (curve 1a) and in excited states with the energies 2.13 MeV, 4.45 MeV and 5.02 MeV (1b) and 6.47 MeV, 6.79 MeV, 7.29 MeV and 8.56 MeV (1c) in the decay mode under consideration.

To describe the de-excitation of a light nucleus, we can use the evaporation model at least in the domain of low E*. It should be recalled, however, that a

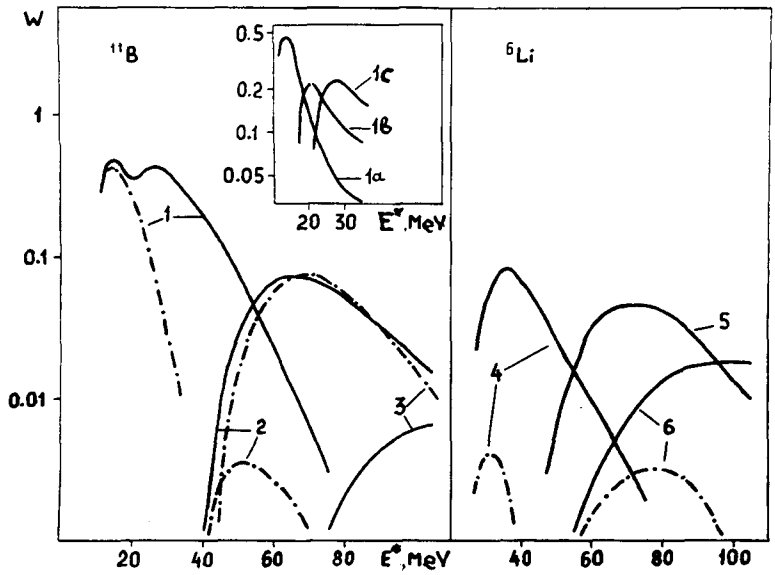

FIGURE 13. This shows the probability of certain decay modes of a ^{15}N-nucleus with production of ^{11}B (on the left) and ^{6}Li (on the right) as functions of the excitation energy E*. The solid curves correspond to the calcualtions carried out in accordance with the Fermi breakup model, and the dash-dotted curves are calculated by means of the evaporation model. Figures by the curves indicate the number of the corresponding decay mode (see text).

number of assumptions of this model (e.g., an assumption that there exists a large number of excited levels described by the level density considered as a smooth function of the energy E*) can loose its validity. Therefore, we must bear in mind that we obtain here only qualitative characteristics of the evaporation process and use them for comparison with the Fermi breakup aimed at elucidation of distinctions between these mechanisms of decay.

Comparison of the probabilities of various decay modes calculated with the help of the evaporation and the Fermi breakup model is shown in Figure 13. A larger value of the probability of the decay channel $^{15}N \rightarrow \alpha + {}^{11}B$ at low excitations obtained in the evaporation model is due to the fact that it is most favorable from the viewpoint of the energy considerations. In all other cases evaporation decay through emission of fragments is strongly suppressed. Large fragments are produced only in small amounts, if any, in this process and in combination with a certain number of nucleons. Therefore, multiple production of fragments in the decay process signalizes the presence of the mechanism responsible for an explosive breakup of a nucleus. The heavier the correlating fragments, the more certain this conclusion is. For example, during evaporation the probability of the channel with formation of ^{6}Li nuclei is small, the modes 4 and 6 are strongly suppressed, and the mode 5 is practically absent (see Figure 13).

B. MULTIFRAGMENT BREAKUP OF MEDIUM-WEIGHT NUCLEI

Explosive breakup of medium-weight nuclei consisting of a sufficiently large number of nucleons ($A \sim 100$) is of particular interest. As a matter of fact, investigations of thermodynamical stability of hot nuclear matter carried out by various techniques (Thomas-Fermi approximation, Hartree-Fock formalism, etc.) have demonstrated that its equation of state has the Van der Waals form characteristic of systems undergoing the liquid-gas phase transition.[16] For mean density of nucleons $\rho_N < \rho_0 \approx 0.15\ \mathrm{fm}^{-3}$ and at temperature lower than the critical temperature $t < t_c \approx 15$ - 20 MeV, a uniform distribution of matter is thermodynamically unfavorable, and it must split into a liquid (dense) and a gaseous (rarified) phase. This phase transition is a consequence of the fact that NN-interaction is attractive at large and repulsive at small distances, and it is the balance between the attractive and repulsive forces that determines the equilibrium state of cold nuclear matter at the value of the density equal to ρ_0. If the mean nucleon density if smaller than ρ_0, the situation is dominated by attractive forces. This leads to an increase in density fluctuations and a clusterization of matter.

It should be emphasized that these predictions are valid for a hypothetical nuclear system of an infinite size in which the Coulomb interaction is not considered. In real nuclear systems containing about a hundred nucleons, effects associated with a finite number of particles can noticeably distort the pattern of the phase transition. Moreover, the surface and Coulomb energy must be taken into account in the realistic nuclear calculations. At sufficiently low densities $\rho_0 < \rho_0/2$ and temperatures $t < t_c$, surface tension and Coulomb interaction result in a disintegration of the liquid phase into a multitude of drops of different sizes. These drops of nuclear liquid are nothing else but ordinary excited nuclei (nuclear fragments). Thus, the multiple formation of nuclear fragments with a broad mass spectrum, called multifragmentation, can serve a specific signal for a liquid-gas type phase transition. It should be noted that the term "multifragmentation" is more appropriate than the term "liquid-gas type phase transition" for small nucler systems.

In the last few years, a large variety of models have been proposed to describe nuclear multifragmentation.[50,51] Currently existing models can be conventionally divided into five groups: probability models (combinatorics, minimum information principle, percolation theory), macroscopic models (phase separation, Fisher's condensation theory, critical exponents), microscopic models (Hartree-Fock theory, molecular dynamics), kinetic models (BUU-equation, Boltzmann-Langevin equation, unstable modes, fluctuation), and statistical models. Deprived of the possibility of even a brief description of all these models, we shall dwell at length on the statistical model of multifragmentation whose basic principles have been formulated.[52] This model deserves particular attention, since it generalizes the concept of a C-nucleus and liquid-drop description, which form the basis of the evaporation model, to the case of highly-excited nuclei. After a subsequent development of the model,[53-56] it turned out that the model gives the most realistic description of the decay of hot nuclei formed in specific nuclear processes and is most convenient for an analysis of experimental data.

1. Statistical Model of Multifragmentation

Suppose a hot nucleus has certain fixed values of the excitation energy (E_0^*), the number of nucleons (A_0), and protons (Z_0). For large values of the excitation energy $E_0^* \sim \mathscr{E}_b$, the surface tension is small,[23] and the balance between the forces of Coulomb repulsion and surface tension is disturbed in a hot nuclear system. As a result, nuclear matter will expand. The order of magnitude of the expansion time of the system till its breakup can be estimated with the help of expression

$$\tau_{ex} \sim R/v_s \ , \tag{74}$$

where $v_s = \sqrt{K/9m_N}$ is the velocity of sound in nuclear matter ($K \approx 230$ MeV is the compressibility of the nucleus and m_N the nucleon mass).

The velocity of sound in the phase separation region may be considerably smaller than its normal value, and hence the expansion must proceed rather slowly. An intensive exchange of mass, charge, and energy takes place between various parts of the system during expansion. Hence, it can be assumed that partial or complete thermodynamical equilibrium is established by the instant of breakup. The instant of breakup corresponds to the situation when the mean separation of drops ($d \approx (1 \div 2)$fm) becomes equal to the range of nuclear forces r_{int} in order of magnitude, and strong interaction does not play any significant role. After this, separate drops move apart, turning into prefragments (primary fragments). According to estimates,[52] the average nucleon density ρ_{br} at which the breakup occurs is about $\rho_0/2 \div \rho_0/3$. Subsequently, the primary fragments fly apart under the action of long-range Coulomb interaction and undergo de-excitation through evaporation of particles or secondary Fermi breakup. The masses of primary fragments determine which of these two possibilities is realized.

According to the general principles of statistical mechanics, the probability of breakup in the f channel is in direct proportion to its statistical weight

$$W_f \sim \exp[S_f(E_0^*, A_0, Z_0)] \ , \tag{75}$$

where S_f is the entropy of the f channel, i.e., the entropy of the system in the state corresponding to the f decay channel. In the simplest case, the channels are characterized merely by a set of multiplicities N_{AZ} of fragments having a mass A and a charge Z. Obviosuly the following constraints are imposed on N_{AZ} by the baryon number and the charge conservation laws:

$$\sum_{A,Z} N_{AZ} \cdot A = A_0 \quad , \qquad \sum_{A,Z} N_{AZ} \cdot Z = Z_0 \ . \tag{76}$$

It is assumed further that thermodynamic equilibrium is established in every channel, i.e., equiprobable distribution of energy among internal and external degrees of freedom of the fragments takes place. This allows us to introduce the concept of the channel temperature t_f and to make use of thermodynamical relations. The temperature t_f is determined by the energy balance equation

$$E_0^* = F_f - t_f \frac{\partial F_f}{\partial t_f} \tag{77}$$

where F_f is the free energy in the f channel. The entropy S_f is connected with F_f through the relation

$$S_f = -\frac{\partial F_f}{\partial t_f} . \tag{78}$$

Calculation of the free energy is based on the use of the liquid-drop description of individual fragments generalized to the case of finite temperatures. It is also assumed that the fragments obey the Boltzmann statistics, since the number of identical products (except lightest ones) in the breakup of a finite nuclear system does not exceed one, as a rule. The contribution of the Coulomb interaction of fragments is calculated in the Wigner-Seitz approximation in Equation 73. Separating the mean Coulomb energy, we can write the free energy of the system of fragments in the form

$$F_f = \sum_{A,Z} N_{AZ} F_{AZ} + \frac{3}{5} \frac{Z_0^2 e^2}{r_0 A_0^{1/3} (1 + \varkappa_c)^{1/3}} . \tag{79}$$

Here, F_{AZ} is the free energy of an individual fragment. It is represented as the sum of the volume (F^v_{AZ}), surface (F^s_{AZ}), symmetry (F^{sym}_{AZ}), Coulomb (F^c_{AZ}), and translational (F^t_{AZ}) terms:

$$F_{AZ} = F^v_{AZ} + F^s_{AZ} + F^{sym}_{AZ} + F^c_{AZ} + F^t_{AZ} , \tag{80}$$

$$F^v_{AZ} = [-W_0 - t_f^2 / \tilde{\epsilon}_0 (A)] \cdot A , \tag{80a}$$

$$F^s_{AZ} = \beta_0 [(t_c^2 - t_f^2)/(t_c^2 + t_f^2)]^{5/4} \cdot A^{2/3} \equiv \beta(t) \cdot A^{2/3} , \tag{80b}$$

$$F^{sym}_{AZ} = \gamma (A - 2Z)^2 / A , \tag{80c}$$

$$F^c_{AZ} = \frac{3}{5} \frac{Z^2 e^2}{r_0 A^{1/3}} [1 - (1 + \varkappa_c)^{-1/3}] , \tag{80d}$$

$$F^t_{AZ} = - t_f \ln(g_{AZ} V_f / \lambda_t^3) + t_f \ln(N_{AZ}!) / N_{AZ} . \tag{80e}$$

Here $W_0 = 16$ MeV, $\beta_0 = 18$ MeV and $\gamma = 25$ MeV are the coefficients in the Bethe-Weizsacker formula at $t = 0$, g_{AZ} is the spin factor ($g_{AZ} = 2s + 1 = 2$ for nucleons and $g_{AZ} = 1$ for other fragments which are the Boltzmann particles), $\lambda_t = (2\pi\hbar^2/m_N t)^{1/2}$ the thermal wavelength, $r_0 = 1.17$ fm, $t_c = 18$ MeV the critical temperature of the liquid-gas phase transition, and $\tilde{\epsilon}_0(A)$ the inverse level density

of the fragment with the mass A. Its dependence on A is taken in the form $\tilde{\epsilon}_0(A) = \tilde{\epsilon}_0 [1 + 3/(A - 1)]$, which takes into account approximately the decrease in the number of excited states in light nuclei. In this model, $\tilde{\epsilon}_0$ is considered as a parameter whose value depends on the fraction of energy transferred to internal degrees of freedom of fragments. The Fermi-gas value of this parameter $\tilde{\epsilon}_0 = 4\pi^{-2} E_F \approx 16$ MeV corresponds to the complete statistical equilibrium between the internal and external (translational) degrees of freedom. The free volume V_f accessible to translational motion of fragments is parametrized in the form

$$V_f = V_0 = \varkappa \frac{4}{3} \pi r_0^3 A_0 , \tag{81}$$

where V_0 is the initial volume of a hot nuclues. Thus, it is assumed that by the instant of the breakup, the system expands to the volume $(1 + \varkappa) \cdot V_0$. The parameter $\varkappa \sim 1$ depends on the fragmentation channel. Its dependence on the multiplicity M of fragments in which the system breaks up is taken in the form[53,54]

$$\varkappa = \left[1 + \frac{d}{r_0 A_0^{1/3}} (M^{1/3} - 1) \right]^3 - 1 \tag{82}$$

($\varkappa = 0$ for $M = 1$). The use of one and the same parameters for the description of both translational and Coulomb energies[53,54] is a rather crude approximation. Therefore, in calculating the Coulomb energy from Equations 79 and 80 we introduce an additional parameter $\varkappa_c$ which differs from $\varkappa$. The value of $\varkappa_c$ can be determined from the intensity of the fission peak in the mass distribution of the breakup products of sufficiently heavy nuclei, such as Au and U. In the case of two touching fragments, $\varkappa_c = 2$.

Thus, by calculating the free energy E_f from Equation 89, we can find the temperature t_f from the balance Equation 77, and then the entropy S_f from Equation 78. After this, we calculate the probability W_f of the breakup channel f with the help of Equation 75. If the probabilities of all possible breakup channels are known, we can calculate different inclusive and exclusive characteristics containing information on the basic properties of the breakup of a hot nucleus.[53-55] The Monte Carlo method[53-55] turns out to be convenient for solution of this problem. Formulations of a statistical model of multifragmentation based upon microcanonical, canonical, and macrocanonical ensembles were used. At high values of the excitation energy, all three versions of the statistical model give similar results concerning the basic properties of the nuclear breakup process. Here, we shall describe in detail the microcanonical formulation of the statistical model of multifragmentation.

2. Basic Properties of Multifragmentation

A statistical model of multifragmentation allows us to describe the evaporation and the multifragmentation decay within the framework of a unified approach and to study the evolution of the decay mechanism with increasing excitation energy

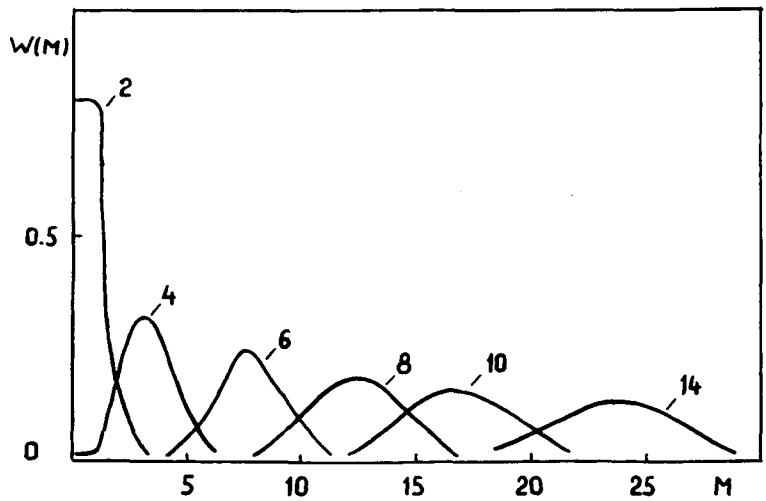

FIGURE 14. The microcanonical calculation of the probability W(M) of a system with $A_0 = 100$ and $Z_0 = 44$ undergoes a breakup into M fragments. The figures by the curves indicate the excitation energy in MeV/nucleon.

of the nucleus. The final state, containing only one fragment with $A = A_0$ and $Z = Z_0$, will be called the C-nucleus channel. The probability W(M) of the breakup of a nucleus into M fragments (including nucleons), the mean multiplicity of fragments $\langle M \rangle$, the mean temperture t at the instant of breakup, and the probability W_{comp} of the C-nucleus channel are shown in Figures 14-16 as functions of the excitation energy.

It can be seen that the probability of the C-nucleus channel dominates at low values of the excitation energy $E_0^* \lesssim$ 2-3 MeV/nucleon (later on, the C-nucleus decays through particle emission or fission). In the range of intermediate excitation energies ranging from the multifragmentation threshold $E_{thr}^* \approx$ 2-3 MeV/nucleon up to the energies $E_0^* \approx$ 4-5 MeV/nucleon, both mechanisms of decay coexist. In this range, the breakup into a small number (M = 2 - 4) of fragments plays the dominant role. Here (see Figures 17 and 18), a significant contribution comes from the "quasievaporation" (breakup into a large R-nucleus and one or two light clusters) and the "quasifission" (breakup into two fragments with comparable masses and one or two light clusters) channel. The characteristics of the products of these channels are similar to ordinary decay modes of a C-nucleus. In this case, the mass spectrum of breakup fragments for a medium-weight system with $A \approx 100$ has a characteristic U-shape (see Figure 17). The average number of fragments $\langle M \rangle$ increases monotonically with increasing excitation energy E_0^* and at sufficiently high energies $E_0^* \gtrsim 5$ MeV/nucleon channels corresponding to the breakup into a large number of small fragments turn out to be dominant, i.e., the principal role is played by the mechanism of multifragmentation. In this case, the mass spectrum of fragments $\langle N_A \rangle$ has the form of a power dependence and the peak corresponding

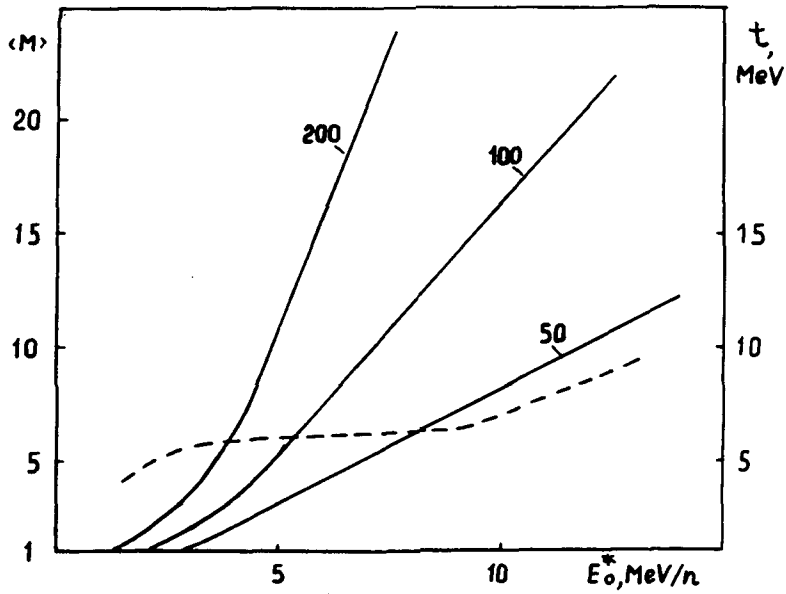

FIGURE 15. The microcanonical calculation are shown of the average multiplicity ⟨M⟩ of fragments (the solid curves, the left-hand scale) and the average temperature, t, (the dashed curve, the right-hand scale) vs. the excitation energy of the decaying system. The figures by the solid curves show the dimensions of the system: 50 corresponds to $A_0 = 50$ and $Z_0 = 24$, 100 to $A_0 = 100$ and $Z_0 = 44$, and 200 to $A_0 = 200$ and $Z_0 = 88$. The dashed curve shows the temperature for the system with $A_0 = 100$ and $Z_0 = 44$.

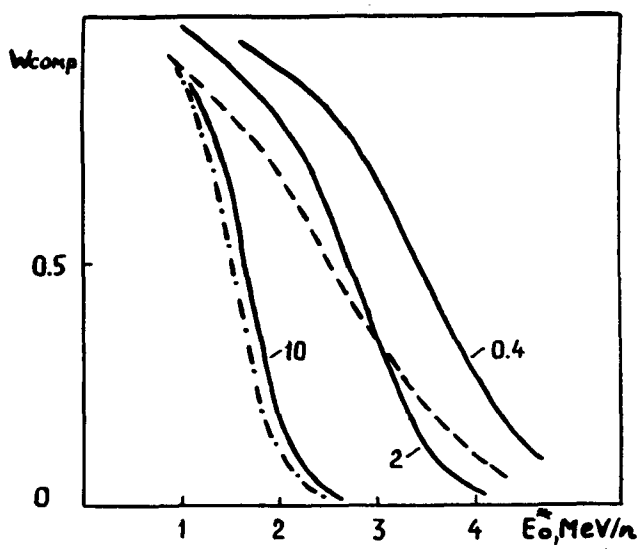

FIGURE 16. This graphs the probability W_{comp} of formation of a C-nucleus vs. the excitation energy in the decaying system with $A_0 = 100$ and $Z_0 = 44$. The solid curves show the results of the microcanonical calculation with the $\tilde{\epsilon}_0 = 16$ MeV and the parameter $\varkappa_c$ given in the figure. The dashed curve corresponds to the canonical calculation with $\tilde{\epsilon}_0 = 16$ MeV and $\varkappa_c = 2$ and the dash - dotted curve to the microcanonical calculation with $\tilde{\epsilon}_0 = 40$ MeV and $\varkappa_c = 2$.

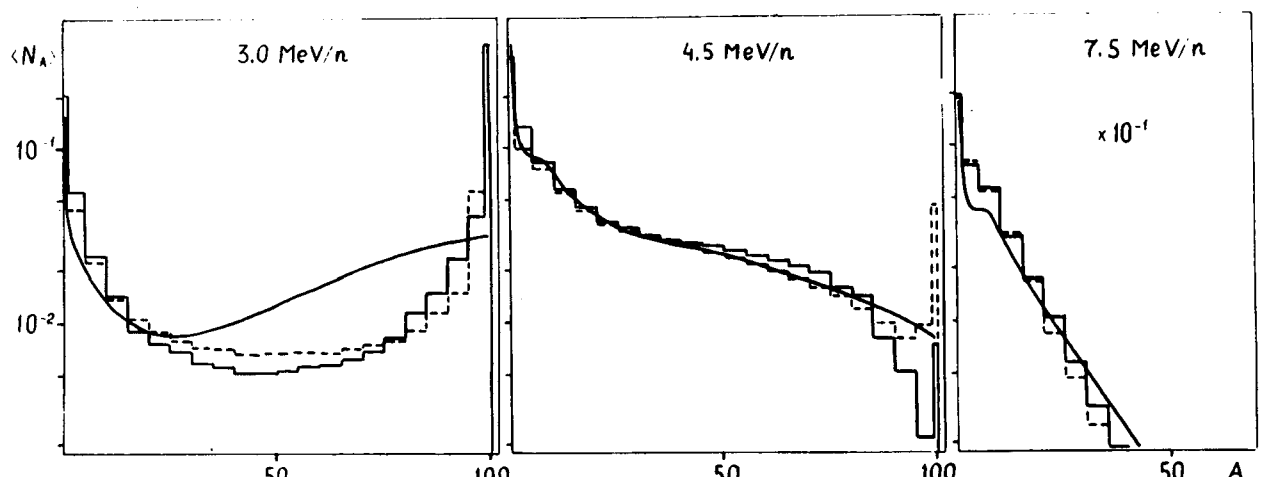

FIGURE 17. The average multiplicity $\langle N_A \rangle$ of fragments vs. their mass A for the system with $A_0 = 100$ and $Z_0 = 44$ is represented here. The excitation energies are shown in the figure. The solid curve presents the macrocanonical calculation. The solid histogram corresponds to the microcanonical calculation, and the dashed one to the canonical calculation.

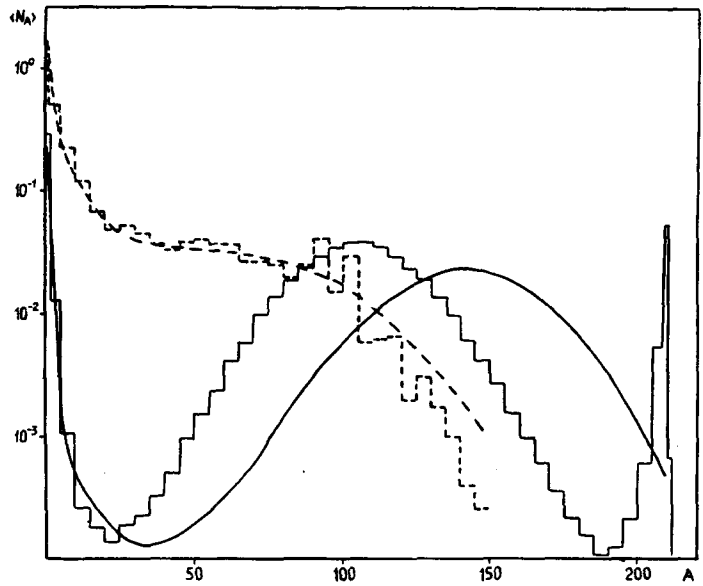

FIGURE 18. This is the inclusive mass distribution $\langle N_A \rangle$ of fragments produced as a result of disintegration of a system with $A_0 = 211$ and $Z_0 = 85$. Calculations were made with $\varkappa = 3$ and $\tilde{\epsilon}_0 = 16$ MeV. Solid lines correspond to $t = 3$ MeV, and dashed lines to $t = 5$ MeV. The rest of notation is the same as in Figure 17.

to "quasifission" of heavy nuclei disappears (see Figures 17 and 18).

Such a form of the spectrum is realized over a wide range of excitation energies up to the limiting value of about 10 MeV/nucleon at which the nucleus disintegrates into nucleons and lightest fragments (d, t^3, He, α). It should be noted that the temperature t_f of the sytem remains practically constant, $t_f = t^* \approx 5 \div 6$ MeV, in this range of excitation energies. This so-called "cracking" temperature is considerably lower than the critical temperature $t_c \approx 18$ MeV for the liquid-gas phase transition in an infinite nuclear matter. The multifragmentation or "cracking" phase transition is just a manifestation of the liquid-gas phase transition in a finite nuclear system.

It can be seen from Figures 16 and 17 that the results obtained with the help of a canonical and a microcanonical description are in good agreement over the entire range of excitation energies under consideration. The macrocanonical approach gives a reasonable result only in the domain of sufficiently high excitation energies $E_0^* \gtrsim 5$ MeV/nucleon, when a hot nucleus decays into a large number of fragments.

3. Simulation of Multifragment Disintegration

These averaged inclusive characteristics of fragmentation contain information only on the most general features of the breakup process of a finite system. To analyze the experimental data one must be able to calculate the exclusive charac-

teristics of the breakup reactions as well. With this in view, a numerical Monte Carlo technique has been developed.[55] Its underlying principles are as follows.

At comparatively low temperatures $t \lesssim 5$ MeV, when the system disintegrates into a small number of fragments $M \lesssim 4$, the number of decay channels is still not enormous, and a correct microcanonical solution of the problem is possible. To isolate the case of low excitations a direct sorting of all the decay channels with $M \leqslant 4$ is carried out at first in this technique. Then using microcanonical statistical weights W_f for the selected breakup channels defined by Equation 75, one is to calculate the average multiplicity $\langle M \rangle$ of fragments. If it turns out to be very small, namely $\langle M \rangle \leqslant M_1$ ($M_1 \simeq 3.3$ for $A_0 \approx 100$ and $M_1 \approx 2.6$ for $A_0 \approx 200$), then the set of channels under consideration is believed to be suitable for a correct description of the breakup. Further, using the probability distribution for channels obtained, one is to make a random selection of a specific channel with given values of A and Z by means of the Monte Carlo method.

If the calculated value of $\langle M \rangle$ turns out to be close to four, this means that configurations with $M > 4$ play a significant role (the high temperature decay of the nucleus). In this case, the number of possible channels of multifragmentation turns out to be very large (for example, $2 \cdot 10^8$ for $A_0 = 100$), and their direct sampling becomes impossible even with the help of modern computers. In this case, a less accurate (but more effective) Monte Carlo technique is employed for the random selection of the disintegration channel. This technique is based on the macrocanonical approximation.

As has been demonstrated, the macrocanonical and the microcanonical approximation give similar results in the high excitation energy range. However, the virtue of the macrocanonical approach is the possibility of obtaining with its help[55] the following analytic expressions for the probability density to find a fragment with a given mass A and a given charge Z in the system:

$$\langle N_{AZ} \rangle = g_{AZ} \frac{V_f}{\lambda_t^3} A^{3/2} \exp\left(- \frac{F_{AZ}^{int} - \mu A - \nu Z}{t} \right) . \tag{83}$$

Here $F_{AZ}^{int} = F_{AZ} - F_{AZ}^{t}$ is internal free energy of the (A,Z) fragment, and μ and ν are the chemical potentials which guarantee the fulfilment of the conservation laws (Equation 76) at the level of average multiplicities. The probability density for the emergence of fragments with a given mass A in the system has the form:[55]

$$\begin{aligned} \langle N_A \rangle = g_A \frac{V_f}{\lambda_t^3} A^{3/2} \exp\Bigg\{ - \frac{1}{t} \Bigg[\left(- W_0 - \frac{t^2}{\epsilon_0} \right) A + \\ \gamma \left(1 - 2 \frac{\langle Z_A \rangle}{A} \right)^2 A + \beta(t) A^{2/3} + \frac{3}{5} \frac{e^2}{r_0} \times \\ [1 - (1 + \varkappa_c)^{-1/3}] \langle Z_A \rangle^2 \cdot A^{-1/3} - \mu A - \nu Z \langle A_A \rangle \Bigg] \Bigg\} . \end{aligned} \tag{84}$$

Here, $g_A = g_{AZ} = 1$, whereas the probability density for the emergence of a fragment having the charge Z and a given mass A is described by the Gaussian[55]

$$N_A(Z) \sim \exp\left[- \frac{(Z - \langle Z_A \rangle)^2}{2(\sigma_Z^A)^2} \right] \tag{85}$$

with the average charge

$$\langle Z_A \rangle = \frac{(4\gamma + \nu)A}{8\gamma + 2[1 - (1 + \varkappa^{-1/3}]A^{2/3}} \tag{86}$$

and the dispersion of the charge

$$\sigma_Z^A \simeq \sqrt{At/8\gamma} \, . \tag{87}$$

Therefore, the Monte Carlo simulation of the fragmentation channel is realized as follows:

1) using the distribution $\langle N_A \rangle$ given by Equation 84, we make a random selection of the mass number A of the fragment in the range $[1,A_0]$;
2) using the Gaussian distribution $N_A(Z)$ given by Equation 85 with the average charge (Equation 86) and dispersion (Equation 87), we randomly select the charge of the fragment in the range $[0,Z_0]$;
3) the procedure of selection of A and Z is repeated, until the contributions from the last fragment added to all the preceding fragments give the values A_0 and Z_0 for the total number of nucleons and the total charge, respectively. If the sum of nucleons and the charge of all fragments exceed the values A_0 and Z_0, then the procedure is repeated, starting from the first fragment.

These two methods based on the microcanonical and the macrocanonical approximation work well at low and high values of the excitation energy, respectively. In the intermediate region corresponding to the values of the excitation energy of about 4.5 MeV/nucleon both methods give similar results.[55,56]

The calculation of the energy spectrum of fragments calls for an extension of the model. In addition to the mass and the charge number, it is also necessary to know the momentum, excitation energy, and spatial position of each fragment at the instant of the breakup. This is because the long-range Coulomb interaction of the fragments, which persists at the stage of their divergence, changes their energies. The de-excitation of hot primary fragments leads to a change in the energy distribution of fragments as well. Analysis shows[55] that these processes weakly influence one another, and hence can be regarded as independent (de-excitation after divergence).

In accordance with the choice of translational energy in the form of Equation 80e, it is assumed that at the instant of the breakup the kinetic energy $\overset{*}{\epsilon}$ of the

fragments in the c.m.s. obeys the Boltzmann distribution characterized by the temperature t_f:

$$\frac{dN_{AZ}}{d\overset{*}{\epsilon}} \sim \sqrt{\overset{*}{\epsilon}} \cdot \exp\left(-\frac{\overset{*}{\epsilon}}{t_f}\right) . \tag{88}$$

Hence, before performing the random selection of the energy $\overset{*}{\epsilon}$ of fragments in macroncanonical calculations, we find the refined values of the channel temperature t_f by solving the microcanonical equation of the energy balance (Equation 77) (deviation from the "initial" macrocanonical temperature t is ± 1 MeV). The initial conditions for the divergence of the system of fragments are determined by random selection of their coordinates distributed with equal probabilities over the breakup volume and momenta (energies) distributed according to Equation 88. The divergence of fragments was assumed to be isotropic in the c.m.s. The fragments subjected to the random selection were required to satisfy the constraints imposed on the free volume of the system ($V_f = \varkappa V_0$), the total thermal energy ($E_{th} = 3/2\ M\ t_f$), and the total momentum which must be equal to zero. In accordance with the energy-balance equation (Equation 77), the temperature t_f also determines the average excitation energy of each fragment:

$$E^*_{AZ}(t_f) = \frac{t_f^2}{\tilde{\epsilon}_0} A + \left[\beta(t_f) - t_f \frac{d\beta(t_f)}{dt_f} - \beta_0\right] A^{2/3} . \tag{89}$$

(It is assumed that there is not internal excitation of clusters with $A < 4$, while $E^*_{42}(t_f) = 4t_f^2/\tilde{\epsilon}_0$ for α - particles.) Then Newton's equations of motion are solved for all fragments in the self-consistent time-dependent Coulomb field. The asymptotic energies of fragments determined as a result of this procedure differ from the initial values by the Coulomb repulsion energy.

Finally, the last stage of the de-excitation of hot fragments is analyzed. For fragments with the mass number $A \leqslant 16$, this process is simulated with the help of the Fermi breakup model already outlined. An evaporation model is used for heavier fragments. Calculation of de-excitation of fragments is carried out by means of the Monte Carlo technique as described above. Calculations take into account the change in the kinetic energy of fragments because of the emission of particles.

4. Difference in Characteristics of the Evaporation and the Multifragment Decay

Since R-nuclei formed in a real NR initiated by hadrons have a broad distribution over the excitation energy as a rule (see subsequent chapters), products of their decay by various mechanisms are observed. The main mechanisms among these are the evaporation cascade and multifragmentation. To reliably segregate the contribution from multifragmentation we must determine the characteristic of the decay of a highly-excited nucleus that is most sensitive to this mechanism. With this end

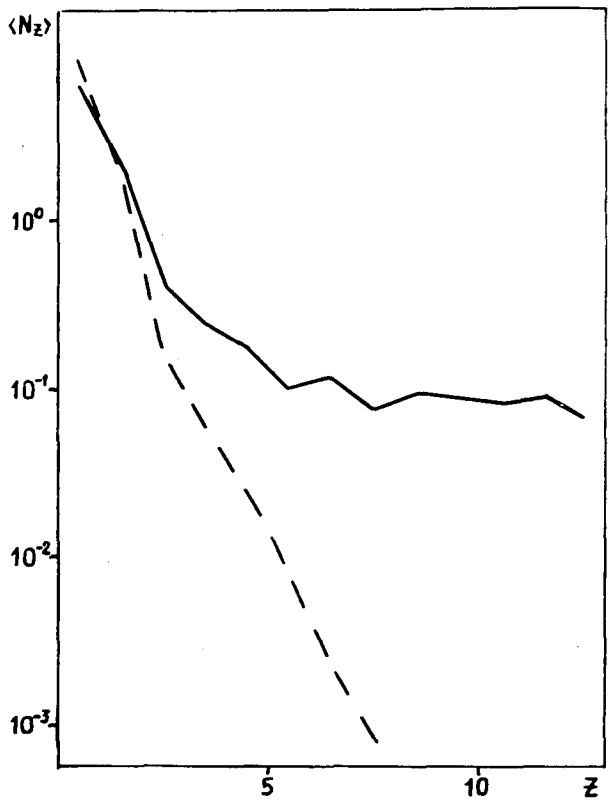

FIGURE 19. This represents the average multiplicity of fragments with the charge Z emitted by a disintegrating system with $A_0 = 100$, $Z_0 = 44$ and $E_0^* = 5$ MeV/nucleon. The solid and the dashed line correspond to the calculations for the multifragment breakup and for the evaporation cascade, respectively.

in view, let us compare the results of calculations of observable characteristics for the decay of a nucleus with fixed values of E_0^*, A_0, and Z_0 carried out by means of the methods described above.

Inclusive mass spectrum of fragments is often used for the study of multifragmentation.[50] It was mentioned that multifragmentation is characterized by a spectrum (close to a power-law dependence) which decreases slowly with increasing A, whereas evaporation gives a rapid exponential decrease of the spectrum. Another characteristic, the inclusive charge spectrum of fragments, is shown in Figure 19. It is seen that, starting from $Z \geqslant 3$, multifragmentation gives a considerably larger yield of heavy fragments and a much smoother decrease of the yield with increasing Z than evaporation. At the same time, other modifications[40,41] of the evaporation model can give a larger yield of heavy fragments in inclusive mass and charge distributions. Therefore, one should invoke other characteristics to obtain a more reliable segregation of decay mechanisms.

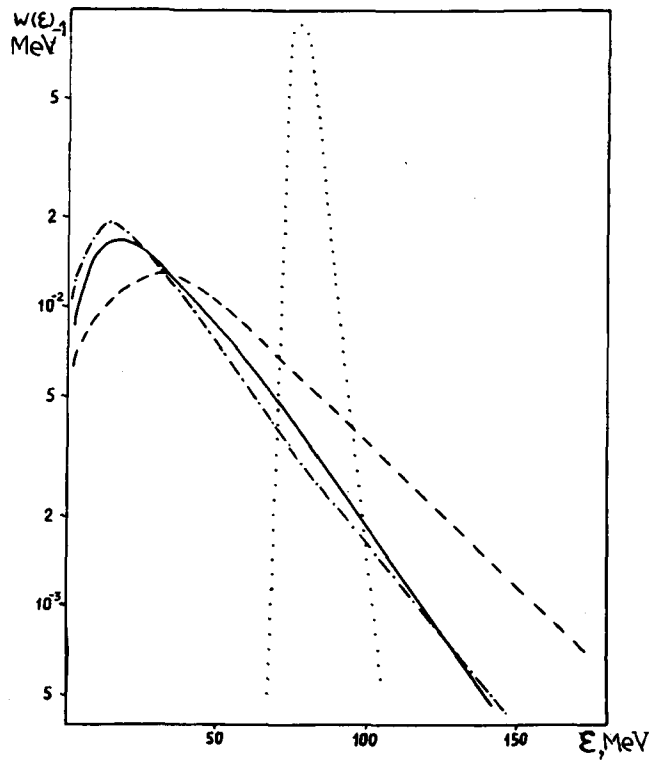

FIGURE 20. This graphs the energy distribution of fragments with A = 27 (which had a mass A ≈ 40 before the de-excitation) emitted as a result of disintegration of the system with A_0 = 211, Z_0 = 85, and E_0^* = 6 MeV/nucleon. The solid and the dashed line correspond to the calculations with $\tilde{\epsilon}_0$ = 16 MeV and with $\varkappa$ = 1 and 0.2, respectively. The dash-dotted line corresponds to the calculation with $\varkappa$ = 1 and $\tilde{\epsilon}_0 = \infty$("cold" multifragmentation). The dotted line shows the evaporation spectrum for fragments with A = 27. The area under the curves is normalized to unity.

One such characteristic is the energy spectrum of fragments. For decay through evaporation, the position of the peak of the spectrum is determined by the value of Coulomb barrier which is proportional to the charge Z of the fragment. Therefore, the peak of the spectrum is shifted noticeably towards higher values of energy as Z increases. In the case of multifragmentation, such a shift of the peak of the spectrum with increasing Z is very small, and the peak itself appears at an energy which is considerably lower than the value of the Coulomb barrier (see Figure 20). In addition to this, the multifragmentation spectrum decreases not so rapidly at low and high values of the energy, and is considerably broader than the evaporation spectrum. This can be explained by the fact that evaporation is a two-body process characterized by a definite Coulomb barrier. As a result, the energy spectrum has a well pronounced peak. In the multifragment breakup, the Coulomb barrier decreases, owing to the expansion of the system before its decay. Moreover, the barrier is broadened because of a combination of contributions from various many-

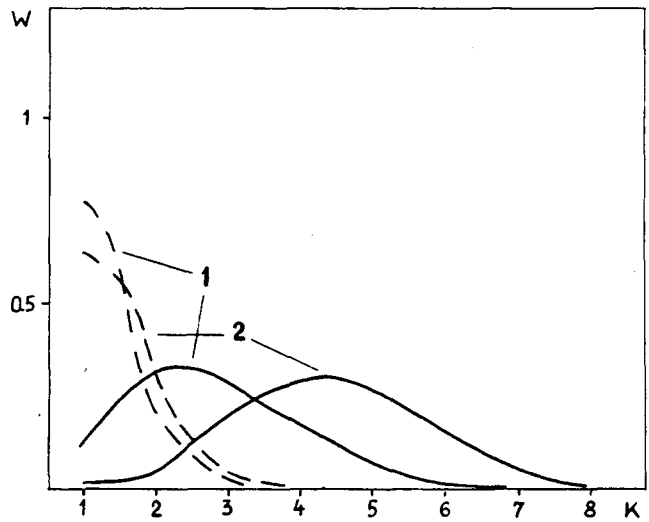

FIGURE 21. Here we have the probability of emission of a given number K of large fragments with $Z \geqslant 3$ in a single breakup event for the system with $A_0 = 100$, $Z_0 = 44$ and the excitation energy $E_0^* = 5$ MeV/nucleon (1) and $E_0^* = 10$ MeV/nucleon (2). The rest of the notation is the same as in Figure 19.

body final states containing the observable fragment. It should also be noted that the slope of the high energy "tail" of the spectrum changes as a result of redistribution of Coulomb energy between fragments at the stage of divergence. For example, the slope of the high-energy part of the spectrum of fragments emitted from a nucleus with the temperature $t = 6.1$ MeV corresponds to the Boltzmann distribution with the temperature $t \approx 20$ MeV (see Figure 20).

However, it is the correlations of yields of heavy ($Z \geqslant 3$) fragments rather than the inclusive characteristics that are of crucial importance for isolation and investigation of the mechanism of multifragmentation. The simplest of such correlations is the probabilitiy of multiple emission of several fragments in one event of the breakup of the nucleus. It is clear from Figure 21, showing the results of the calculation of this correlation, that selection of the breakup events with three or more heavy fragments is a reliable criterion for the isolation of multifragmentation. It should be noted that the breakup of a nucleus into several heavy fragments occurs in a comparatively narrow range of excitation energies. The probability of such an event becomes significant for $t \gtrsim t^*$ and vanishes at a temperature of about 15 MeV as a result of rapid decrease in the mass of the fragments formed. While choosing a specific nuclear process for experimental investigation of this phenomenon, one should take into consideration such an energy dependence of the probability of multiple production of heavy fragments.

Concluding the discussion of the statistical model of multifragmentation, we would like to note that in the case of very high excitations it is difficult to substantiate the basic assumption of statistical approach that an intermediate thermalized state

does exist. Characteristic time τ_{ex} of the collective expansion of the system till its breakup estimated with the help of Equation 74 is about 10^{-21}s. Evaluation of the formation time of fragments carried out by TDHF technique[57] and with the help of Vlasov's equation[58] gives the same order of magnitude for this quantity. Although the characteristic time of explosive decay exceeds several times both the characteristic time of the INC and the time during which the statistical equilibrium with respect to single-particle degrees of freedom of a nucleus is established, it is nevertheless only the comparison of the predictions of the model with experimental data that can provide more convincing arguments in favor of the validity of the assumption about the existence of the stage of preparation of a thermalized hot nucleus and the stage of its subsequent breakup. This issue will be considered in detail in Chapter 7.

VI. CONCLUSIONS

The use of statistical methods at high values of the excitation energy E* is motivated by two peculiar features inherent in this case: 1) it is theoretically impossible, in this energy range, to consider the properties of separate nuclear states, and 2) in the experimental study of nuclear structure, we can obtain only such information that is averaged over a large number of states. An equilibrium statistical model, based on the idea that a compound nucleus exists, uses universal physical concepts of the phase space and of detailed balance principle and is consequently a reliable tool for investigation of properties of highly-excited nuclei. In recent years, the main line in the development of this model was connected with the introduction of new physical effects caused by high values of the excitation energy E* and of angular momentum I of a nucleus into the basic quantities of the model, such as density of nuclear levels and cross-section of inverse reaction.

Since the number of collective modes is small as compared to the total number of degrees of freedom of particles constituting a nucleus, single-particle degrees of freedom must dominate at high excitation energies. To analyze the averaged microscopic properties of a nucleus, which are associated with them, a model considering the nucleus as a Fermi gas of quasiparticles is widely used. Even at the energies $E^* \approx$ 100-200 MeV a medium-weight nucleus with $A \approx 100$ represents a highly degenerate Fermi gas. In the energy range $E^* \lesssim 100$ MeV ($t < 2$ MeV), a washing out of nuclear shells with an increase in the excitation energy is the main thermal effect. As we go over to a nondegenerate Fermi gas, certain effects arise that manifest themselves in the Equations 18 and 19 and in the density of levels at the values of nuclear temperature lying in the range $t \gtrsim 4$ MeV.

When the excitation energy becomes comparable to the total binding energy of a nucleus ($E^* > 200$ MeV), thermal effects manifest themselves in the macroscopic liquid-drop properties of the nucleus as well. They exert the most strong influence on the properties of the nuclear surface. This is revealed in an increase in the surface diffuseness and decreae in the surface tension. The fission barrier and the probability of fission which is determined by it are also very sensitive to thermal effects.

The existence of the large nuclear angular momentum affects strongly microscopic and macroscopic properties of the nucleus, thus masking the manifestation of thermal effects. The main consequence of this influence is that the rotation enlarges the deformation of the nucleus. This leads to its fission in the end, when the angular momentum exceeds its critical value I_{cr}. In addition to this, a large deformation may result in a significant enhancement of the fragment emission from the nucleus.

Principal mechanism responsible for the decay of a highly-excited C-nucleus is a sequential emission of particles and γ-quanta, and nuclear fission. Intermediate nuclei which are formed in the evaporation cascade are distributed over the entire spectrum of the excitation energy from the initial value to the minimum possible one. Hence, in calculating the de-excitation of the nucleus one must take into account the whole range of both low-energy and high-energy phenomena. Moreover, a large angular momentum which imposes a constraint upon the accessible phase volume strongly affects the decay of the nucleus. As a result, angular dependence of emitted particles becomes anisotropic, and emission of γ-quanta and α-particles and fission are intensified. A method of calculation based on a statistical simulation of decay of a highly-excited rotating nucleus turned out to be rather effective for the description of this process. An analysis of experimental data carried out with the help of this method allows us not only to study thermal effects in nuclei, but also to determine the validity range of the equilibrium statistical model.

The evaporation mechanism of decay of a highly-excited nucleus is of decisive importance in the excitation energy range $E^* \lesssim$ 2-3 MeV/nucleon. At higher energies $E^* \gtrsim 5$ MeV/nucleon, when the excitation energy of a nucleus becomes close to its total binding energy, the mechanism of explosive breakup of a hot nucleus turns out to be dominant. (In the intermediate range of the excitation energy E^*, both mechanisms of disintegration coexist). Disintegration of a nucleus into a large number of fragments, i.e., multifragmentation, signalizes that the mechanism of explosive breakup is realized. An enormous number of open decay channels each containing a large number of fragments and nucleons is a specific feature of multifragmentation of a hot nucleus. In view of the complicated nature of this phenomenon, use of statistical approach for constructing a model of multifragmentation is quite natural. The developed statistical model of multifragmentation allows us to study basic regularities of this process, to calculate its exclusive characteristics, and to compare the multifragmentation and the evaporation mechanism on the basis of a unified theoretical approach. An analysis of correlations of the yield of heavy ($Z \geqslant 3$) fragments is of decisive importance for the isolation of contributions coming from these mechanisms.

The assumption that there exists an intermediate thermalized nuclear state forms the basis of the statistical approach. At very high excitation energies $E^* \sim 10$ MeV/nucleon, when the mechanism of the explosive breakup of a hot nuclear system plays the principal role, a consistent theoretical substantiation of this assumption does not exist nowadays. The same holds true for the assumption about the existence of the stage of preparation of such a system and its subsequent breakup. To prove

the validity of these assumptions it is necessary to carry out a systematic analysis of experimental data within the framework of statistical approach. Here the advancement from low excitation energies $E^* \approx$ 1-2 MeV/nucleon, where the assumption that the statistical equilibrium is established is sufficiently reliable, to higher energies $E^* \approx$ 5-10 MeV is desirable not only from the viewpoint of the study of decay and properties of highly-excited nuclei, but also for the development of thermodynamical approach in the study of properties of hot hadronic matter.

REFERENCES

1. **Bohr, N.**, Neutron capture and nuclear constitution, *Nature*, 137, 344, 1936.
2. **Barashenkov, V. S. and Toneev, V. D.**, *Interaction of High Energy Particles and Nuclei with Atomic Nuclei* [in Russian.], Atomizdat, Moscow, 1972.
3. **Bass, R.**, *Nuclear Reactions with Heavy Ions*, Springer, Berlin, 1980.
4. **Ignatyuk, A. V.**, *Statistical Properties of Excited Atomic Nuclei* [in Russian], Energoatomizdat, Moscow, 1983.
5. **Bohr, A. and Mottelson, B. R.**, *Nuclear Structure*, Vol. 1, Benjamin, New York, 1969; Vol. 2, Benjamin, New York, 1974.
6. **Dostrovsky, I., Fraenkel, Z., and Friedlander, G.**, Monte Carlo calculations of nuclear evaporation processes, III: applications to low energy reactions, *Phys. Rev.*, 116, 683, 1959.
7. **Vdovin, A. I., Voronov, V. V., Malov, L. A., Solov'ev, V. G., and Stoyanov, C.**, Semi-microscopic description of the nuclear state density, *Part. Nucl.*, 7, 952, 1976.
8. **Gilbert, A. and Cameron, A. G. W.**, A comoposite nuclear level density formula with shell corrections, *Can. J. Phys.*, 43, 1446, 1965.
9. **Botvina, A. S., Iljinov, A. S., Mebel, M. V., and Sobolevskii, N. M.**, Equation of state and density level of highly-excited nuclei in the model of independent particles [in Russian], *Preprint P-0316*, INR AN SSSR, Moscow, 1983.
10. **Migdal, A. B.**, *Theory of Finite Fermi Systems and Propeties of Atomic Nuclei* [in Russian], Nauka, Moscow, 1983.
11. **Bunatyan, G. G.**, On the statistical description of the properties of compound states, *Yad. Fiz.*, 29, 10, 1979.
12. **Brack, M., Damgaard, J., Jensen, A. S., Pauli, H. C., and Strutinsky, V. M.**, Funny hills: the shell correction approach to nuclear shell effects and its applications to the fission process, *Rev. Mod. Phys.*, 44, 320, 1972.
13. **Iljinov, A. S., Mebel, M. V., Bianchi, N., De Sanctis, E., et al**, Phenomenological statistical analysis of level densities, decay widths and lifetimes of excited nuclei, *Nucl. Phys. A*, 543, 517, 1992.
14. **Bjørnholm, S., Bohr, A., and Mottelson, B. R.**, Role of symmetry of the nuclear shape in rotational contributions to nuclear level densities, in *Proc. Symp. Phys. Chem. Fission*, Vol. 1, IAEA, Vienna, 1974, 367.
15. **Myers, W. D. and Swiatecki, W. J.**, Anomalies in nuclear masses, *Ark. Fysik*, 36, 343, 1967.
16. **Mosel, U.**, Fusion and fission of heavy nuclei, in *Heavy Ion Collisions*, Vol. 2, Bock, R., Ed., North-Holland, Amsterdam, 1980, 275.
17. **Diebel, M., Albrecht, K., and Hasse, R. W.**, Microscopic calculations of fission barriers and critical angular momenta for excited heavy nuclear systems, *Nucl. Phys. A*, 355, 66, 1981.

18. **Moretto, L. G.,** Fission probabilities in ligther nuclei, in *Proc. 3rd Symp. Phys. Chem. Fission,* Vol. 1, *IAEA*, Vienna, 1974, 329.
19. **Iljinov, A. S., Cherepanov, E. A., and Chigrinov, S. E.,** An analysis of nuclear fissility for intermediate-energy proton induced reactions, *Z. Phys. A,* 287, 37, 1978.
20. **Chen, X. S., Ngo, C., Tomassi, E., Barranco, M., Vinas, X., and Ngo, H.,** Real part of the nuclear interaction potential between α or p and excited heavy nuclei, *Nucl. Phys. A,* 401, 143, 1983.
21. **Pi, M., Vinas, X., and Barranco, M.,** Estimation of temperature effects on fission barriers, *Phys. Rev. C,* 26, 733, 1982.
22. **Campi, X. and Stringari, S.,** Temperature dependence of nuclear surface properties, *Z. Phys. A,* 309, 239, 1983.
23. **Ivanov, Yu. B.,** Surface tension in heated nuclei, *Yad. Fiz.,* 34, 45, 1981.
24. **Ericson, T.,** The statistical model and nuclear level densities, *Adv. Phys.,* 9, 425, 1960.
25. **Cohen, S., Plasil, F., and Swiatecki, W. J.,** Equilibrium configurations of rotating charged or gravitating liquid masses with surface tension, *Ann. Phys.,* 82, 557, 1974.
26. **Blann, M.,** Decay of deformed and superdeformed nuclei formed in heavy ion reactions, *Phys. Rev. C,* 21, 1770, 1980.
27. **Botvina, A. S., Iljinov, A. S., Mishustin, I. N., Bondorf, J. P., Donangelo, R., and Sneppen, K.,** Statistical simulation of the breakup of highly excited nuclei, *Nucl. Phys. A,* 475, 663, 1987.
28. **Bohr, N. and Wheeler, J. A.,** The mechanism of nuclear fission, *Phys. Rev.,* 56, 426, 1939.
29. **Cherepanov, E. A., Iljinov, A. S., and Mebel, M. V.,** The energy dependence of the neutron emission-to-fission ratio Γ_n/Γ_f for transuranium nuclei, *J. Phys. G:Nucl. Phys.,* 9, 1397, 1983.
30. **Iljinov, A. S. and Toneev, V. D.,** Calculation of subsequent particle emission from highly-excited nucleus with high angular momentum, *Yad. Fiz.,* 9, 48, 1969.
31. **Iljinov, A. S. and Cherepanov, E. A.,** Decay of highly-excited compound nuclei: statistical approach, *JINR Communications,* P7-84-68, Dubna, 1984.
32. **Hillman, M. and Eyal, Y.,** Fast detailed evaporation code for reactions of complex nuclei, in *Proc. Eur. Conf. Nucl. Phys. Heavy Ions,* Vol. 1, Caen, 1976, 109.
33. **Gomes del Campo, J., Stokstad, R. G., Biggerstaff, J. A., Dayras, R. A., Snell, A. H., and Stelson, P. H.,** Fusion and peripheral reactions of $^{12}C + ^{14}N$ at energies up to 13 MeV/A, *Phys. Rev. C,* 19, 2170, 1979.
34. **Grover, R. and Gilat, J.,** Deexcitation of highly excited nuclei, *Phys. Rev.,* 157, 862, 1967.
35. **Puhlhofer, F.,** On the interpretation of evaporation residue mass distributions in heavy ion induced fusion reactions, *Nucl. Phys. A,* 280, 267, 1977.
36. **Ignatyuk, A. V., Smirenkin, G. N., Itkis, M. G., Malgin, S. I., and Okolovich, V. N.,** Investigation of the fissility of the pre-actinide nuclei in charged-particle induced reactions, *Sov. J. Part. Nucl.,* 16, 307, 1985.
37. **Dahlinger, M., Vermeulen, D., and Schmidt, K.-H.,** Empirical saddle-point and ground-state masses as a probe of the droplet model, *Nucl. Phys. A,* 376, 94, 1982.
38. **Bjørholm, S. and Strutinsky, V. M.,** Intermediate states in fission, *Nucl. Phys. A,* 136, 1, 1969.
39. **McMahan, M. A., Moretto, L. G., Padgett, M. L., Wozniak, G. J., Sobotka, L. G., and Mustafa, M. G.,** Mass-asymmetric barriers from excitation functions for complex-fragment emission, *Phys. Rev. Lett.,* 54, 1995, 1985.
40. **Moretto, L. G.,** Statistical emission of large fragments: a general theoretical approach, *Nucl. Phys. A,* 247, 211, 1975.
41. **Friedman, W. A. and Lynch, W. G.,** Statistical formalism for particle emission, *Phys. Rev. C,* 28, 16, 1983.
42. **Weidenmüller, H. A.,** Transport theories of heavy ion reactions, in *Progress in Particle Nuclear Physics,* Vol. 3, Wilkinson, D., Ed., Pergamon Press, Oxford, 1980, 49.
43. **Volkov, V. V.,** *Nuclear Reactions of Deep Inelastic Transfer* [in Russian], Energoizdat, Moscow, 1982.

44. **Lyuboshits, V. L.,** Probability distribution of wave packet time delays for strong overlapping of resonance levels, *Yad. Fiz.*, 37, 292, 1983.
45. **Bugrov, V. N. and Karamyan, S. A.,** Duration of ^{238}U fission induced by ^{3}He ions, *Yad. Fiz.*, 34, 577, 1981.
46. **Fermi, E.,** High energy nuclear events, *Progr. Theor. Phys.*, 5, 570, 1950.
47. **Goxmen, A., Mathews, G. J., and Viola, V. E.,** Intranuclar cascade and Fermi breakup calculations of ^{1}H and ^{4}He-induced reactions on light target nuclei, *Phys. Rev. C*, 29, 1606, 1984.
48. **Subramanian, T. S., Romero, J. L., Brady, F. P., et al,** Double-differential inclusive hydrogen and helium spectra from neutron-induced reactions at 27.4, 39.7 and 60.7 MeV: oxygen and nitrogen, *Phys. Rev. C.*, 34, 1580, 1986.
49. **Botvina, A. S., Golubeva, Ye. S., and Iljinov, A. S.,** Statistical simulation of the break-up of light nuclei in hadron-nucleus reactions, Preprint *INR*, P-0657, Moscow, 1990.
50. **Hüfner, J.,** Heavy fragments produced in proton-nucleus and nucleus-nucleus collisions at relativistic energies, *Phys. Rep.*, 125, 129, 1985.
51. **Lynch, W. G.,** Nuclear fragmentation in proton- and heavy-ion-induced reactions, *Annu. Rev. Nucl. Part. Sci.*, 37, 493, 1987.
52. **Bondorf, J. P., Mishustin, I. N., and Pethick, C. I.,** Multifragmentation of heavy nuclei [in Russian] in *Proc. Int. Workshop Physics Heavy Ions, JINR*, D7-83-147, Dubna, 1983, 354.
53. **Bondorf, J. P., Donangelo, R., Mishustin, I. N., Pethick, C. I., Schulz, H., and Sneppen, K.,** Statistical multifragmentation of nuclei. (I) formulation of the model, *Nucl. Phys. A*, 443, 321, 1985.
54. **Bondorf, J. P., Donangelo, R., Mishustin, I. N., and Schulz, H.,** Statistical multifragmentation of nuclei. (II) application of the model to finite nuclei disassembly, *Nucl. Phys. A*, 444, 460, 1985.
55. **Botvina, A. S., Iljinov, A. S., Mishustin, I. N., Bondorf, J. P., Donangelo, R., and Sneppen, K.,** Statistical simulation of the breakup of highly excited nuclei, *Nucl. Phys. A*, 475, 663, 1987.
56. **Botvina, A. S., Iljinov, A. S., and Mishustin, I. N.,** Multifragment breakup of nuclei by intermediate-energy protons, *Nucl. Phys. A*, 507, 649, 1990.
57. **Strack, B. J.,** Fragmentation of hot quantum drops, *Phys. Rev. C*, 35, 691, 1987.
58. **Vinet, L., Gregoire, C., Schuck, P., Remaud, B., and Sebille, F.,** A study of the disintegration of highly excited nuclei with the Vlasov-Uehling-Uhlenbeck equation, *Nucl. Phys. A*, 468, 321, 1987.

Chapter 4

ANALYSIS OF THE INTERACTION OF NUCLEONS AND LIGHTEST NUCLEI WITH NUCLEI ON THE BASIS OF THE INC-MODEL

In this chapter, we shall consider the possibility of describing certain important characteristics of inelastic interaction of nucleons, having various energies, and lightest nuclei with nuclei on the basis of the INC-model. In our study, we shall make use of the analytic and the Monte Carlo approach outlined in Chapters 1 and 2. In addition, we shall generalize the description of this interaction to the case when the polarization effects in NN-collisions must be taken into account.

I. INCLUSIVE CROSS-SECTIONS FOR PRODUCTION OF SECONDARY NUCLEONS

Let us first consider the results of numerical calculations of the energy spectra, the average multiplicities and the double differential cross-sections for production of secondary nucleons and compare them with experimental data.

A. ENERGY SPECTRA AND AVERAGE MULTIPLICITIES OF SECONDARY NUCLEONS

Figures 1a and 1b show the energy spectra of protons for the reactions ^{27}Al(p,p′)X and ^{64}Cu(p,p′)X corresponding to the energy of incident protons equal to 400 MeV. These spectra have been calculated by various methods.[1-3] It is seen that, if an analytic approach is used, this characteristic is hardly affected by the approximate manner in which the angular dependence of the distribution function of excited nucleons is taken into account. The small-angle approximation (formulas 100–103 and 105–108, Chapter 2) and the P_1-approximation (formula 88, Chapter 2), which differ essentially from one another, lead to similar results. In the domain of energies close to the initial one, an agreement between the analytic and the Monte Carlo calculation is improved significantly, if the contribution from quasifree protons is taken into account correctly. This procedure does not exert any essential influence in the domain of lower energies. As we might expect, the expansion (86, Chapter 2) which represents the first term in the asymptotic expansion in $1/\ln(\epsilon_0/\epsilon)$ describes the proton spectra at low energies ϵ reasonably well.

To illustrate the applicability of the model at low primary energies we present the energy spectra of protons produced in the reaction ^{54}Fe(p,p′) X at $\epsilon_0 = 39$ and 62 MeV in Figure 2. The spectra shown in this figure have been calculated within the framework of various approximations and compared with experimental data. It is seen that the calculations carried out according to the formulas of Section IE1 of Chapter 2 agree satisfactorily with experimental data (except for maybe the domain of the lowest energies ϵ), if the contribution from quasifree protons is taken into account correctly. This agreement is not worse than that obtained with the help of other sufficiently accurate methods.

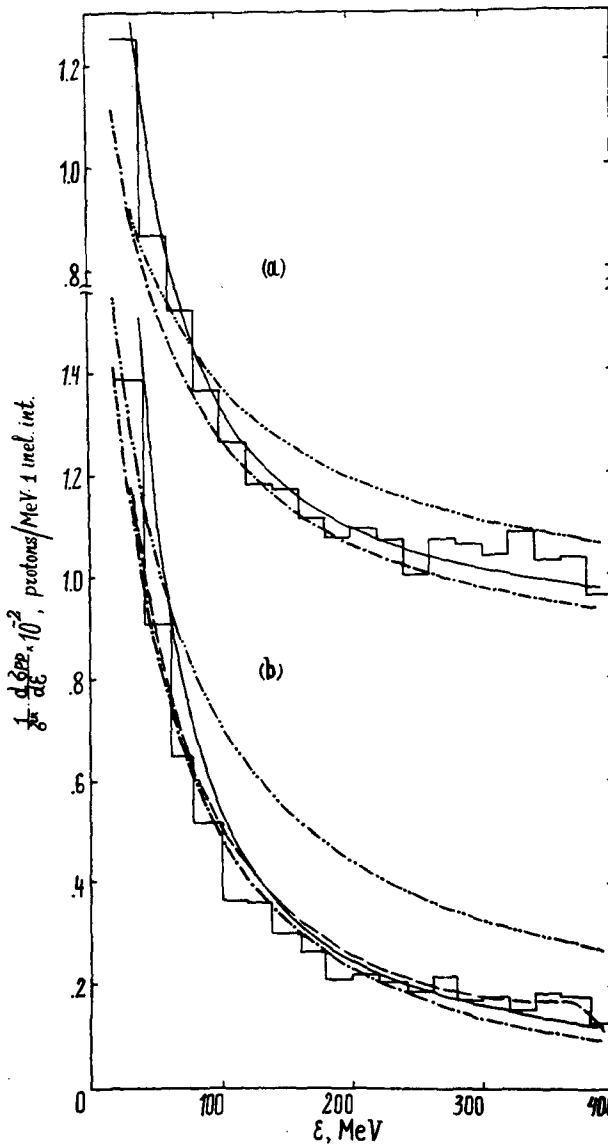

FIGURE 1. This shows the energy spectra of protons in the interaction of 400 MeV protons with ^{27}Al(a) and ^{64}Cu (b) nuclei. The histogram corresponds to the calculation by the Monte Carlo code for the INC with a three-zone nucleus (Section IIA2, Chapter 2), the dashed curve to the analytic calculation with a correct taking account of the contribution from quasifree protons (the calculation of spectra of cascade and quasifree protons was carried out in accordance with the formula 92, Chapter 2, for a nucleus of a radius $R = 1.3\ A^{1/3}$ fm with a uniform density and in the form of the integral of Equation 26, Chapter 2, over the angle for a three-zone nucleus, respectively), and the solid curve to the calculation in accordance with the formulas 100-103 and 105-108 in Chapter 2 with the Woods-Saxon distribution of nuclear density. The dash-dotted curve and the dashed curve with two dots show the results of the

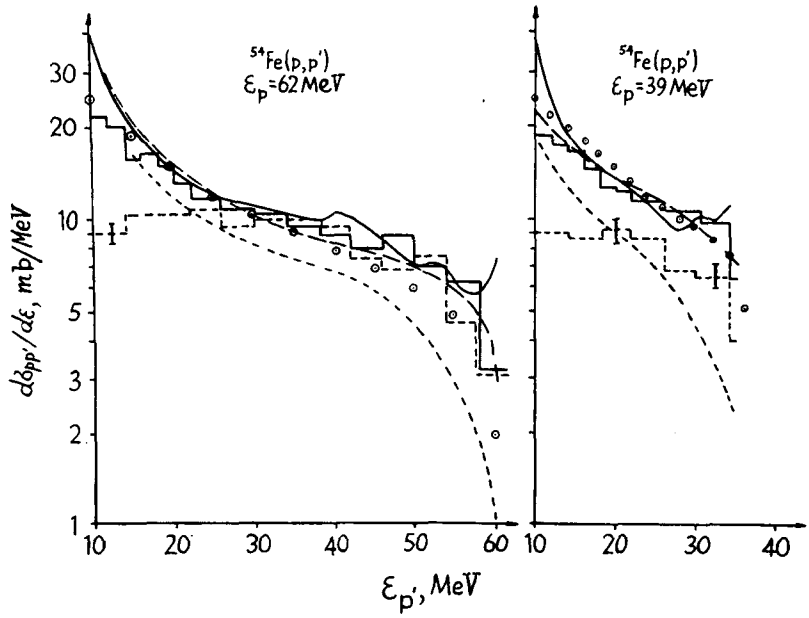

FIGURE 2. This shows the energy spectra of protons in the interaction of the 39 MeV and 62 MeV protons with ^{54}Fe nuclei. The solid line shows experimental data. The solid and the dashed histogram correspond to the Monte Carlo calculations in accordance with the codes ORNL and BNL, and the short and the long dash to the calculations carried out in accordance with the Harp-Miller-Berne model and the Blann[5] hybrid model with regard for the geometry of the reaction (see Section IE2, Chapter 2). The circles correspond to the calculations[6] carried out in accordance with the formulas 103, 105-107, and 113, Chapter 2 for cascade protons and to the calculation of the integral of Equation 26, Chapter 2, over the angle for quasifree protons for the three-zone model of a nucleus in the local Fermi gas approximation.

Since the problems associated with the effect of the structure of nuclear surface and of the momentum distribution of intranuclear nucleons in its vicinity on the properties of secondary nucleons are of great importance,[7] we have also calculated the spectra of secondary protons within the framework of the model of a uniform nucleus and the model of three-zone nucleus with an enhanced Fermi energy in the external zone* for the cases under consideration. These calculations are in worse agreement with experimental data for ϵ close to ϵ_0. However, in the NRs under consideration, this part of the spectrum of secondary protons is formed owing largely

FIGURE 1 (continued). calculations carried out in accordance with the formulas 86 and 88, Chapter 2, for a uniform nucleus of a radius R = 1.3 $A^{1/3}$ fm, respectively. In analytic calculations, we used the values E_F = 28.5 MeV and B_N = 8 MeV and calculated effective cross-sections $\sigma^{eff}_{11(1-1)}$ according to the formula 25, Chapter 2, in which the cross-sections $\sigma^{el}_{11(1-1)}$ were borrowed from Reference 4.

* The effect of the momentum distribution of intranuclear nucleons on double differential cross sections for production of secondary protons will be considered in the next section.

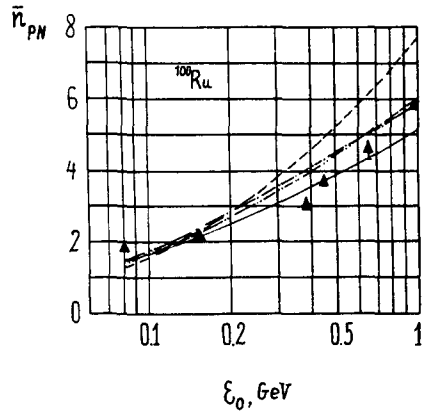

FIGURE 3. This shows the dependence $\bar{n}_{pN} = \langle N_{pp}\rangle + \langle N_{pn}\rangle$ in the p+^{100}Ru reaction on ϵ_0. The full triangles correspond to the Monte Carlo calculation.[3,4] The curves show the results of the calculations[2] carried out according to the formulas 104-108 in Chapter 2 with $B_N = 8$ MeV and $\epsilon_p = \epsilon_n = 10$ MeV: the dashed curve corresponds to $E_F = 20$ MeV, the dashed curve with two dots to $E_F = 28.5$ MeV, the solid curve to $E_F = 37$ MeV, and the Woods-Saxon density of intranuclear nucleons (Equation 122, Chapter 2); and the dash-dotted curve to $E_F = 28.5$ MeV and a uniform nucleus with $R = 1.3\ A^{1/3}$ fm.

to the excitation of the discrete nuclear levels,[8] and hence cannot be, in principle, described within the framework of the INC-model. Therefore, the results obtained do not allow one to argue that the model of a nucleus with a diffuse boundary, in which the local Fermi momentum decreases with the density slower than $\rho^{1/3}(\mathbf{r})$, is less realistic than the model of the local Fermi gas.

Figure 3 shows the dependence of the average multiplicity of fast secondary nucleons $\bar{n}_{pN} \equiv \langle N_{pp}\rangle + \langle N_{pn}\rangle$ on ϵ_0 for the interaction of protons with ^{100}Ru nuclei. It is seen that analytic calculations which are correct for $\epsilon_0 \lesssim 1$ GeV agree satisfactorily with the Monte Carlo calculations practically over the entire range of ϵ_0 defined by the above inequality. For a fixed value of ϵ_0, the quantity $\bar{n}_{pN}$ depends only slightly on the properties of the nuclear surface as well. A decrease in E_F leads to an increase in $\bar{n}_{pN}$. This is explained by the weakening of the effect of the Pauli exclusion principle on the interaction of excited intranuclear nucleons with unexcited ones. Calculations[2] have demonstrated that $\bar{n}_{pN}$ depends only slightly on the moderate variations in the dimensions of a T-nucleus and its values of N and Z as well, and that it is determined mainly by the mass number A and the boundary energy $\epsilon_{p(n)}$.

B. DOUBLE DIFFERENTIAL CROSS-SECTIONS FOR PRODUCTION OF SECONDARY PROTONS

The results of the calculations of double differential cross-sections for production of secondary protons in the pA-interaction at intermediate energies carried out by various methods and their comparison with experimental data are presented in Figures 4-7. Figure 4 shows the double differential cross-sections for production

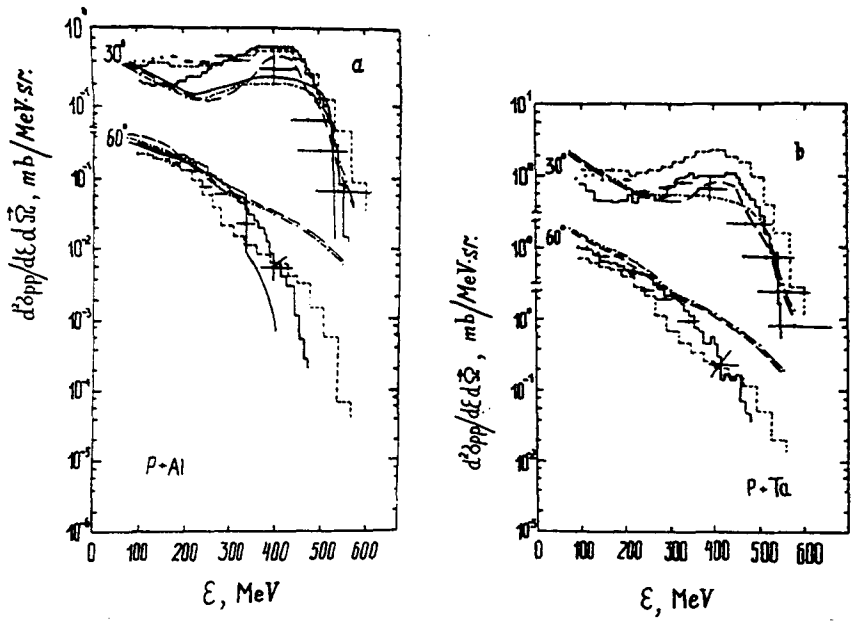

FIGURE 4. This shows the double differential cross-sections for production of protons at various angles (which are indicated by figures near the corresponding curves) in the interaction of 600 MeV protons with ^{27}Al(a) and ^{181}Ta(b) nuclei: the points (the errors are indicated) correspond to experimental data,[9] the solid and the dashed histogram to the calculation by the Monte Carlo method,[9,10] and by the model of single scattering[11] (which takes into account the contribution of the high-momentum component in the momentum distribution of intranuclear nucleons), and the solid, the dashed, and the dash-dotted line to analytic calculations in which

1) for the data shown by the dashed and the dash-dotted curves the contribution of cascade protons is calculated in the P_1-approximation (according to Equation 93, Chapter 2) and that of quasifree protons according to the three-zone and the uniform model of a nucleus according to the formulas 26, and 14, 21, Chapter 2, respectively
2) for the data shown by the solid curve the contribution of cascade protons is calculated in the small-angle approximation (according to Equations 58-62, Chapter 2) and that of quasifree protons according to the model of a nucleus with a uniform density.

In analytic calculations, the contribution of cascade protons in the small-angle and in the P_1-approximation was evaluated for a uniform nucleus with $R = 1.3\ A^{1/3}$fm.

of secondary protons at various angles for the interaction of protons of the energy $\epsilon_0 = 600$ MeV with the ^{27}Al and ^{181}Ta nuclei. It follows from this figure that semiclassical formulas describe experimental data reasonably well. As we might expect, the small-angle approximation is more accurate in the domain of high energies than the P_1-approximation (the use of the latter leads to the isotropization of a highly anisotropic angular distribution of fast secondary protons). The value of the maximum at high ϵ, which corresponds to the single collision, depends strongly on the structure of the nuclear surface and turns out to be approximately

the same in the analytic and the Monte Carlo calculations with the same distribution of intranuclear nucleons over coordinates and momenta. This is confirmed by the detailed analysis carried out in Reference 1. It is seen from Figures 4 and 5 that both the analytic and the Monte Carlo calculations, which consider the nucleus as a local Fermi gas with a diffuse boundary, deviate from experimental data in the vicinity of the peak by a factor of about two.[1,13] Calculations with the momentum distribution of intranuclear nucleons which do not depend on the coordinate agree better with experimental data. This apparently reflects the fact that the momentum distribution of intranuclear nucleons decreases with the density slower than in the model of the local Fermi gas. As ϵ_0 decreases, the peak in the spectra of secondary nucleons at small angles ϑ, which corresponds to a quasifree scattering, becomes less pronounced (see Figures 5 and 6).

However, the double differential distributions of secondary protons calculated according both to semiclassical formulas and to the cascade-exciton model (see Section IIA7 in Chapter 2) at $\vartheta = 20°$ are underestimated, as compared to experimental data, by a factor of two on the average. As ϑ increases, the agreement between the calculations and experimental data is improved. It follows from Figure 7 that the principal reason for this discrepancy at small angles is the disregard of quantum-mechanical effects, primarily, in the calculation of the quasifree component of the cross-section. At the angles $\vartheta \leqslant 40°$ energy spectra of protons produced as a result of bombardment of ^{12}C nuclei by protons with the energy 200 MeV are described to a good accuracy, if the quasifree component of the cross-section is calculated in the DWIA-approximation (see Section IB in Chapter 2). It is also seen from this figure that, for $\vartheta > 40°$, calculations taking into account the contribution of quasifree protons both by semiclassical and by quantum-mechanical methods agree satisfactorily with experimental data and that the quasifree scattering is the dominating mechanism in the formation of the inclusive spectra of secondary protons in the forward hemisphere. Since the fraction of the cascade nucleons in the products of the NA-reaction decreases with decreasing ϵ_0, one can hope that the quantum-mechanical description of the first NN-collision in the nucleus is to improve the agreement between the calculations and experimental data in the domain of small angles even for $\epsilon_0 < 200$ MeV.

It should be emphasized that the double differential cross-sections of secondary protons at the angles $\vartheta \gtrsim 90°$ calculated according to formulas 14, 58, and 93 in Chapter 2 agree at best only qualitatively with experimental data in the domain of ϵ_0 under consideration. The error of the calculation of the hard part of these distributions is significantly larger than that in the case of the calculation by the Monte Carlo technique and can be as large as one-two orders of magnitude. The calculation in which the contribution of cascade protons is evaluated in the P_1-approximation overestimates the high-energy part of cross-sections, whereas the calculation in the small-angle approximation with allowance for this contribution underestimates it. This is associated both with the approximations used in solving the system of KEs (Equation 56, Chapter 1) and with the fact that these equations do not take into account the mechanism of absorption of intermediate pions by two-nucleon asso-

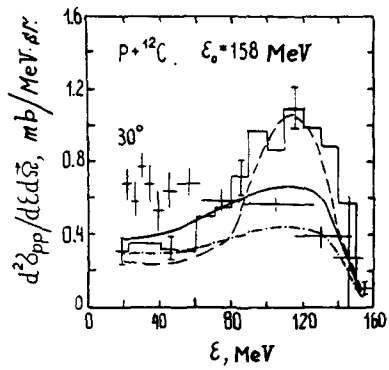

FIGURE 5. This graphs the double differential cross-section for production of protons at an angle of 30° in the interaction of 158 MeV protons with ^{12}C-nuclei. The crosses correspond to experimental data,[12] and the histogram to the Monte Carlo calculation within the framework of the INC-model according to Bertini's code.[12] The solid, the dashed, and the dash-dotted line show the results of the calculation in the P_1-approximation with allowance for the contribution from quasifree protons evaluated within the framework of the local and nonlocal Fermi gas model. The dashed line corresponds to the three-zone model of a nucleus, the dash-dotted one to the uniform nucleus, and the solid line to the three-zone model of a nucleus with the momentum distribution of intranuclear nucleons, which is independent of the coordinate and corresponds to the nucleon density in the center of a nucleus.

ciations incorporated into the Monte Carlo calculation. The latter mechanism becomes dominating as the angle of divergence of nucleons and their energy increase.[15]

Finally, it should be noted that phenomenon of nuclear scaling has been discovered, see, for example, Reference 18, in inclusive reactions induced by intermediate-energy particles (such as p,n, etc.). To be more specific, it turned out that invariant inclusive cross-sections for production of various fast secondaries (p,n,d,t,π,K,$\bar{p}$, etc.) at backward angles to the beam can be represented in the simple universal nearly exponential form (which does not depend on the type of the secondary particle) and extend up to sufficiently high energies. Such a characteristic behavior of the energy spectra of secondaries at backward angles depends only slightly on the mass number A of a T-nucleus and on the initial energy of a primary particle over a wide range of energies from several hundreds of MeV to about hundred GeV. A number of models have been proposed to account for such a peculiar behavior of the energy spectra of secondaries at backward angles.

According to the mechanism of production of these particles considered in these models, they can be divided by convention into two groups: 1) models in which it is assumed that particles are produced in the single act of a quasifree scattering of a primary particle on individual intranuclear nucleons or nucleon clusters, and 2) models based on multiple interactions of primary and intermediate particles and resonances with intranuclear nucleons, such as the INC-model, the coalescence model, as well as the models which consider the formation of excited intermediate subsystems (clusters, fluctuons, fireballs, and moving sources) with their subsequent decay. The models of the first group call for the existence of a considerable

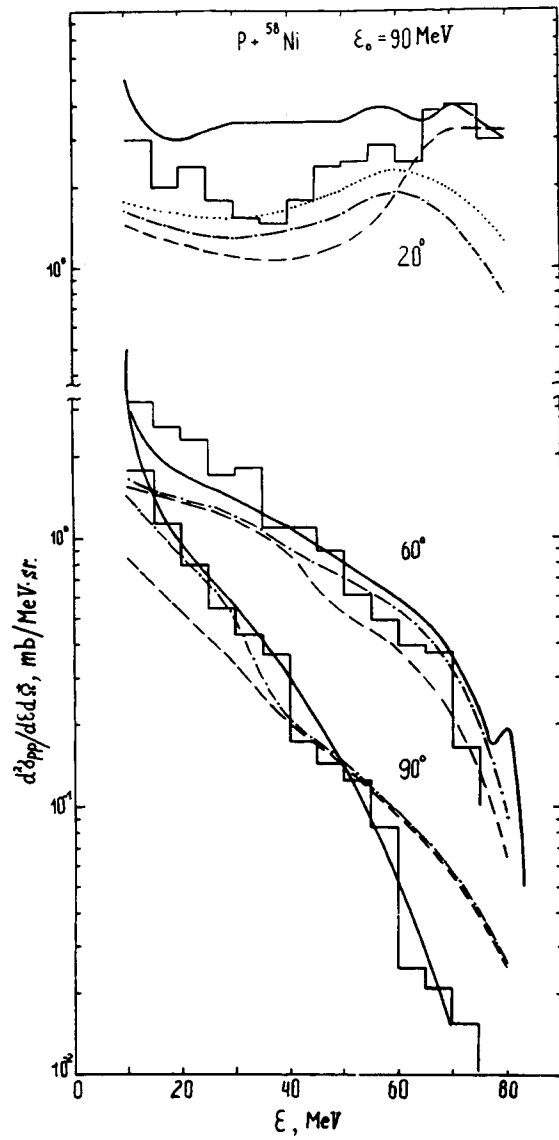

FIGURE 6. This graphs the double differential cross-sections for production of protons at the angles of 20, 60 and 90° in the interaction of 90 MeV protons with ^{58}Ni nuclei. The solid line corresponds to experimental data[14] and the histogram to the calculation within the framework of the cascade-exciton model.[15] The dashed, the dash-dotted, and the dotted line show the results of analytic calculations. The dashed and the dash-dotted line correspond to the same models as in Figure 4, and the dotted one to the calculation in the small-angle approximation with allowance for the contribution from quasifree protons evaluated according to the model of a uniform nucleus.

high-momentum component in the momentum distribution of intranuclear nucleons. Both types of the models describe, as a rule, the observed pecularities of the energy spectra. This plagues the comprehension of the mechanism of production of fast secondary particles at backward angles so far and calls for further its experimental and theoretical study.

On the whole, the results obtained demonstrate that the analytic and the numerical method developed in Chapters 1 and 2 to find the solution of KEs of the INC-model allow one to calculate to a sufficient accuracy inclusive cross-sections of NRs initiated by intermedite-energy nucleons, and to study the effects of parameters and details of the employed model of a nucleus on the results of the calculation of these cross-sections as well. Agreement of various versions of calculations with one another and with experimental data counts in favor of the hypothesis that, at the energies $\epsilon_0 \gtrsim 50$ MeV, the NA-interaction is really determined by the cascade of quasifree collisions with individual intranuclear nucleons, and thus confirms the basic assumptions of the INC-model. Taking account of quantum-mechanical effects in the calculation of a quasifree component of the cross-section allows one to significantly improve the description (especially at small angles) of double differential cross-sections for production of secondary protons in the interaction of intermediate-energy protons with nuclei on the basis of the INC-model.

II. POLARIZATION EFFECTS IN INCLUSIVE NUCLEON-NUCLEUS REACTIONS AT INTERMEDIATE ENERGIES

A large number of facets of inelastic NA-interaction at intermediate energies were explained on the basis of the INC-model[4] (see also the preceding section and Chapters 5-7). However, the polarization effects in NN-collisions in a nucleus have not been considered yet in this analysis. Obviously, taking account of these effects[19] offers radically new possibilities for the application of the INC-model to the study of NA-reactions in the domain of continuous spectrum of the reaction products. The performance of such experiments has begun recently. The analyzing power A_y in the reaction A(**p**,p′)X on a number of T-nuclei at the energy ϵ_0 = 200-800 MeV[20-26] and the polarization $\mathcal{P}$ of secondary protons in the interaction of protons of the energy 640 MeV and 1 GeV with various nuclei[27] have been measured. Theoretical analysis of these data,[20,23] which does not take into account the effects of multiple rescattering of nucleons in a nucleus, has demonstrated that it is important to take them into consideration. In this section, we shall describe a method[19] of calculation of inclusive cross-sections and polarization observables of NA-reactions at intermediate energies. This method takes these effects into account within the framework of the INC-model and is the generalization of the approach developed in Chapters 1 and 2 for the calculation of NA-reactions on the basis of the solution of the corresponding system of KEs to the case when it is necessary to take into consideration the spin dependence of the NN-interaction.

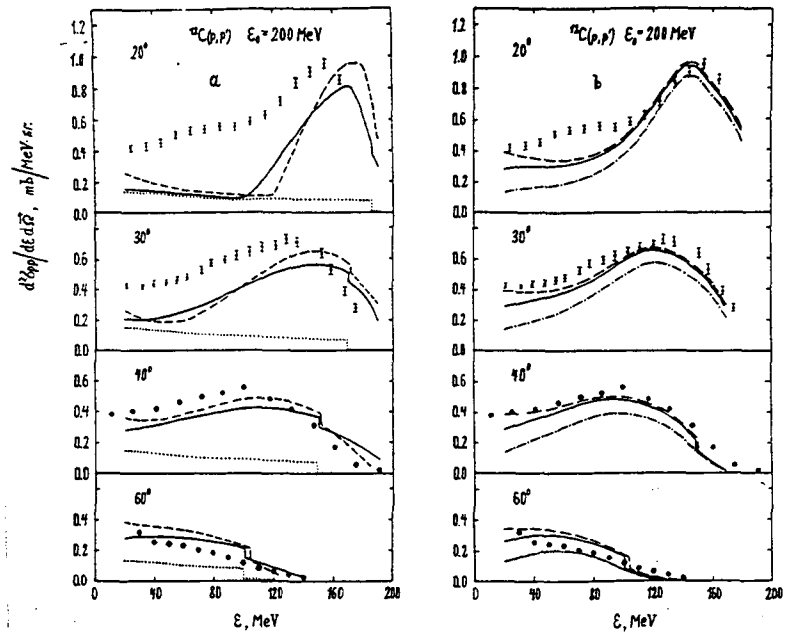

FIGURE 7. These graphs track the double differential cross-sections for production of protons in the $^{12}C(p,p')X$ reaction for ϵ_0 = 200 MeV at the angles of 20, 30, 40, and 60°. Experimental data are borrowed from Reference 16. The curves correspond to the calculations[17] with B_N = 8 MeV and γ = 2. The calculations are carried out (a) according to Equations 58-62, Chapter 2: the solid and the dashed curve show the results of the calculations with $\rho(r) = \rho_0(1 + ar^2)e^{-br^2}$, a/b = (A − 4)/6 and b = 0.363 fm^{-2} at E_F = 28.5, and 20 MeV, respectively, and the dotted curve corresponds to the same case as the solid one in which the contribution of quasifree protons to the cross-section is subtracted (b) according to Equations 27-35, Chapter 2, describing the quasifree component of the cross-section within the framework of the DWIA method. The values $U_1(\epsilon) = -60$ MeV + 0.2ϵ, $U_2(\epsilon) = -3.3$ MeV − 0.1ϵ, $\tilde{b}_0$ = 2.51 fm, $E_{101/2} = -34.0$ MeV, $E_{113/2} = -14.7$ MeV, $\tilde{\alpha}^2$ = 0.37 fm^{-2} and $d\sigma^{el}_{11(1-1)}/d\overset{*}{\Omega} = \sigma^{el}_{11(1-1)}/4\pi$ correspond to the dash-dotted curve. The specification of solid and dashed curves is the same as in Figure 7a, with the difference that the quasifree component is depicted as the dash-dotted curve.

A. INCLUSIVE POLARIZATION CHARACTERISTICS OF NA-REACTIONS

It has been shown in Chapters 1 and 2 that, if the polarization effects are not taken into account, then within the framework of the INC-model all observable inclusive characteristics of NA-reactions can be expressed in terms of linear functionals of the single-particle phase density $\Psi_\alpha(\mathbf{r},\mathbf{p},t)$ (Equation 48, Chapter 1) which have the form of Equation 73a, Chapter 1. The generalization of such an approach aimed at taking account of these effects has been proposed.[19] Instead of Ψ_α an eight-component function $\Psi^\nu_\alpha(\mathbf{r},\mathbf{p},t)$ (ν = 0,1,2,3 and $\alpha = \pm 1$) has been introduced. Its properties are as follows: 1) the component Ψ^0_α coincides with Ψ_α, i.e.,

it represents the average (over the ensemble) number of protons ($\alpha = 1$) or neutrons ($\alpha = -1$) in a unit phase volume with the center at the point $(\mathbf{r},\mathbf{p})$, where $\mathbf{r}$ is the radius vector and $\mathbf{p}$, the momentum at the instant of time t, and 2) for $\nu \neq 0$, the component Ψ^{ν}_{α} satisfies the relation $\Psi^{\nu}_{\alpha} = \zeta^{\nu}_{\alpha}\Psi^{0}_{\alpha}$, where ζ^{ν}_{α} is the ν-th component of the polarization vector ζ_{α} of α-type nucleons with the momentum $\mathbf{p}$ ($|\mathbf{p}| > p_{F\alpha,(r)}$) at the point $\mathbf{r}$ at the instant of time t. Similarly to Equation 73a, Chapter 1, all observable inclusive characteristics of NRs corresponding to the case when the polarization effects are taken into account[19] can be expressed in terms of the functional of Ψ^{ν}_{α}

$$\frac{d^2\sigma^{\nu}_{\alpha_0\alpha,\zeta\alpha_0}}{d\epsilon d\boldsymbol{\Omega}} = R^2 \int\limits_{\omega\Omega)>0} d\boldsymbol{\omega}(\boldsymbol{\omega}\boldsymbol{\Omega})\, \Phi^{\nu}_{\alpha}(R\boldsymbol{\omega},\epsilon,\boldsymbol{\Omega}),\ \nu = 0,1,2,3; \tag{1}$$

$$\Phi^{\nu}_{\alpha}(\mathbf{r},E,\boldsymbol{\Omega}) = R^2 v \frac{d\mathbf{p}}{dEd\boldsymbol{\Omega}} \int\limits_{(\omega_0\Omega_0)<0} d\boldsymbol{\omega}_0 |\boldsymbol{\omega}_0\boldsymbol{\Omega}_0| \int\limits_0^{\tau_{cas}} dt\ \Psi^{\nu}_{\alpha}(\mathbf{r},\mathbf{p},t,\mathbf{R}_0,\zeta_{\alpha_0}) \tag{2}$$

Here $\boldsymbol{\omega}_0 = \mathbf{R}_0/R_0$, $\boldsymbol{\omega} = \mathbf{R}/R$ and τ_{cas} is the time during which the cascade stage of the reaction is completed (see Section IA, Chapter 1). To emphasize the dependence of the function Ψ^{ν}_{α} on $\mathbf{R}_0$ and ζ_{α_0} these vectors are written down explicitly as the arguments of this function.

The double differential cross-section for production of the secondary α-type nucleons moving with the energy ϵ in the direction of the unit vector $\boldsymbol{\Omega}$ by the α_0-type nucleons falling onto a nucleus with the energy ϵ_0 in the direction $\boldsymbol{\Omega}_0$ is $d^2\sigma^{0}_{\alpha_0\alpha,\zeta_{\alpha_0}}/d\,\epsilon\, d\,\boldsymbol{\Omega}$. The analyzing power $A_{y,\alpha}$, the polarization vector $\zeta_{\alpha,\zeta_{\alpha_0}}$, and the polarization $\mathcal{P}_{y,\alpha}$ of secondary nucleons have the form[19]

$$A_{y,\alpha} = \left(\frac{d^2\sigma^{0}_{\alpha_0\alpha,\zeta\alpha_0=\uparrow}}{d\epsilon d\boldsymbol{\Omega}} - \frac{d^2\sigma^{0}_{\alpha_0\alpha,\zeta\alpha_0=\downarrow}}{d\epsilon d\boldsymbol{\Omega}}\right) \Big/ \left(\frac{d^2\sigma_{\alpha_0\alpha,\zeta\alpha_0=\uparrow}}{d\epsilon d\boldsymbol{\Omega}} + \frac{d^2\sigma^{0}_{\alpha_0\alpha,\zeta\alpha_0=\downarrow}}{d\epsilon d\boldsymbol{\Omega}}\right)^2 \tag{3}$$

$$\zeta^{\nu}_{\alpha,\zeta\alpha_0} = \frac{d^2\sigma^{\nu}_{\alpha_0\alpha,\zeta\alpha_0}}{d\epsilon d\boldsymbol{\Omega}} \Big/ \frac{d^2\sigma^{0}_{\alpha_0\alpha,\zeta\alpha_0}}{d\epsilon d\boldsymbol{\Omega}} \qquad \nu = 1,\ 2 \tag{4}$$

$$P_{y,\alpha} = \zeta_{\alpha,\zeta\alpha_0=\ 0} \cdot n_r, \qquad n_r = \alpha\alpha_0\, [\boldsymbol{\Omega}_0\boldsymbol{\Omega}]/|[\boldsymbol{\Omega}_0\boldsymbol{\Omega}]| \tag{5}$$

where the symbol $\zeta_{\alpha_0} = \uparrow$ ($\zeta_{\alpha_0} = \downarrow$) denotes that the polarization vector ζ_{α_0} of incident nucleons is parallel (antiparallel) to the normal to the reaction plane (to the vector $\mathbf{n}_r$), the absolute value of the vector ζ_{α_0} being equal to unity.

B. THE SYSTEM OF KES FOR THE FUNCTIONS Φ^{ν}_{α} AND ITS SOLUTION FOR QUASIFREE NUCLEONS

For the sake of simplicity, we shall disregard the meson production in NN-collisions, consider a nucleus as a degenerate unpolarized local Fermi gas of

nucleons, and confine ourselves to the macroapproximation (see Chapter 1). Moreover, we shall neglect the deviation of the nucleon trajectories from the straight line between the collisions which is caused by the action of the effective potential V_α. Then, similarly to Equations 56, Chapter 1, and 39, Chapter 2, we readily find that the functions Φ^ν_α satisfy the system of stationary KEs:[19]

$$[\boldsymbol{\Omega}\nabla + \mu_\alpha(\mathbf{r},E)]\,\Phi^\nu_\alpha(\mathbf{r},E\boldsymbol{\Omega}) = \int d\boldsymbol{\Omega}' \int_E^{E_0} dE' \sum_{\alpha',\nu'}$$
$$K^{\nu'\to\nu}_{\alpha'\to\alpha}(\mathbf{r};,E',\boldsymbol{\Omega}' \to E,\boldsymbol{\Omega}) \times$$
$$\Phi^{\nu'}_{\alpha'}(\mathbf{r},E',\boldsymbol{\Omega}') + \zeta^\nu_{\alpha_0}\delta_{\alpha\alpha_0}\delta(E - E_0)\,\delta(\boldsymbol{\Omega} - \boldsymbol{\Omega}_0)\,\delta(z - z_0)\,, \tag{6}$$

which has the desired single-valued solution if the boundary condition in the form

$$\Phi^\nu_\alpha(\mathbf{R},E,\boldsymbol{\Omega}) = 0 \text{ for } \boldsymbol{\Omega}\mathbf{R} < 0 \tag{7}$$

is satisfied. Here $\zeta^\nu_{\alpha_0}$ is the ν-th component of the polarization vector $\boldsymbol{\zeta}_{\alpha_0}$ ($\zeta^0_{\alpha_0} = 1$) of a primary nucleon of the type α_0,

$$\begin{aligned} K^{\nu'\to\nu}_{\alpha'\to\alpha}(\ldots) = \Big[& 2\langle\alpha,E',\boldsymbol{\Omega}' \to \alpha,E,\boldsymbol{\Omega}\,\big|\,\Pi^{\nu'\to\nu}_{\alpha\alpha\to\alpha}\rangle_\alpha + \\ & \langle\alpha,E',\boldsymbol{\Omega}' \to \alpha,E,\boldsymbol{\Omega}\,\big|\,\Pi^{\nu'\to\nu}_{\alpha-\alpha\to\alpha}\rangle_{-\alpha}\Big]\,\delta_{\alpha'\alpha} + \\ & \langle-\alpha,E',\boldsymbol{\Omega}' \to \alpha,E,\boldsymbol{\Omega}\,\big|\,\Pi^{\nu'\to\nu}_{-\alpha\alpha\to\alpha}\rangle_\alpha(1 - \delta_{\alpha'\alpha}); \end{aligned} \tag{8}$$

$$\begin{aligned} & \Pi^{0\to0}_{\alpha\gamma(-\alpha\alpha)\to\alpha} = 1,\ \Pi^{\nu\to0}_{\alpha\gamma\to\alpha} = \Pi^{0\to\nu}_{\alpha\gamma\to\alpha} = \zeta^{(0)}_{\alpha\gamma}(s,\overset{*}{\vartheta})n^\nu\,, \\ & \Pi^{\nu\to0}_{-\alpha\alpha\to\alpha} = \Pi^{0\to\nu}_{-\alpha\alpha\to\alpha} = -\,\zeta^{(0)}_{-\alpha\alpha}(s,\overset{*}{\widetilde{\vartheta}})n^\nu,\quad \overset{*}{\widetilde{\vartheta}} = \pi - \overset{*}{\vartheta}\,; \end{aligned} \tag{9}$$

$$\begin{aligned} \Pi^{\nu'\to\nu}_{\alpha\gamma\to\alpha} \equiv D^{\alpha\gamma}_{\nu'\nu} = D^{\alpha\gamma}_{nn}\,n^{\nu'}n^\nu + D^{\alpha\gamma}_{mm}\,m^{\nu'}m^\nu + D^{\alpha\gamma}_{ll}\,l^{\nu'}l^\nu + \\ D^{\alpha\gamma}_{lm}(m^{\nu'}l^\nu - l^{\nu'}m^\nu)\,, \end{aligned} \tag{10}$$

$$\begin{aligned} \Pi^{\nu'\to\nu}_{-\alpha\alpha\to\alpha} \equiv K^{-\alpha\alpha}_{\nu'\nu} = K^{-\alpha\alpha}_{nn}n^{\nu'}n^\nu + K^{-\alpha\alpha}_{mm}l^{\nu'}l^\nu + K^{-\alpha\alpha}_{ll}m^{\nu'}m^\nu - \\ K^{-\alpha\alpha}_{lm}(m^{\nu'}l^\nu - l^{\nu'}m^\nu)\,; \end{aligned} \tag{11}$$

$\gamma = \alpha,\ -\alpha$ and the symbol $<\beta',E',\boldsymbol{\Omega}' \to \beta,E,\boldsymbol{\Omega}|\Pi>_\alpha$ (Π is an arbitrary function) has the following meaning

$$\begin{aligned} \langle\beta',E',\boldsymbol{\Omega}' \to \beta,E,\boldsymbol{\Omega}\,\big|\,\Pi\,\rangle_\alpha = \frac{2}{(2\pi\hbar)^3}\frac{1}{v'}\frac{d\mathbf{p}}{dEd\boldsymbol{\Omega}}\int d\mathbf{p}''d\mathbf{p}''' \\ \Theta(p_{F,\alpha} - p'') \times \\ \Theta(p''' - p_{F,\alpha'})\ w_{\beta'\alpha}(\mathbf{p}',\mathbf{p}'' \to \mathbf{p},\mathbf{p}''')\,\Pi\,, \end{aligned} \tag{12}$$

where $\beta' + \alpha = \beta + \alpha'$, the quantities $w_{\beta'\alpha}$ and μ_α are determined by formulas 14 and 58, Chapter 1, respectively, $D^{\alpha\gamma}_{\nu'\nu}$ and $K^{-\alpha\alpha}_{\nu'\nu}$ are the depolarization tensor and the tensor of transfer of polarization in NN-collisions[28] which depend on the energy $\sqrt{s}$ and the scattering angle $\overset{*}{\vartheta}$ in the c.m.s., and $\zeta^{(0)}_{\beta'\alpha}$ is the polarization arising upon the elastic scattering of unpolarized nucleons of the type β' and α. Moreover, it was assumed that the amplitudes of the pp- and the nn-scattering are described by the matrix M_1 and the amplitude of the np-scattering by the matrix $(M_0 + M_1)/2$. The matrix M_T (where $T = 0, 1$ is the isotopic spin of the NN-system) was taken in the following commonly accepted form:[19,28]

$$M_T(\overset{*}{\mathbf{k}},\overset{*}{\mathbf{k}}') = a_T + b_T(\boldsymbol{\sigma}_1,\mathbf{n})(\boldsymbol{\sigma}_2\mathbf{n}) + c_T(\boldsymbol{\sigma}_1\mathbf{n} + \boldsymbol{\sigma}_2\mathbf{n}) + e_T(\boldsymbol{\sigma}_1\mathbf{m}) \times$$
$$(\boldsymbol{\sigma}_2\mathbf{m}) + f_T(\boldsymbol{\sigma}_1 l)(\boldsymbol{\sigma}_2 l)\ \mathbf{n} = [\overset{*}{\mathbf{k}},\overset{*}{\mathbf{k}}']/|[\overset{*}{\mathbf{k}},\overset{*}{\mathbf{k}}']|,\ \mathbf{m} = (\overset{*}{\mathbf{k}} - \overset{*}{\mathbf{k}}')/|\overset{*}{\mathbf{k}} - \overset{*}{\mathbf{k}}'|, \quad (13)$$
$$l = (\overset{*}{\mathbf{k}} + \overset{*}{\mathbf{k}}')/|\overset{*}{\mathbf{k}} + \overset{*}{\mathbf{k}}'|.$$

Here $\boldsymbol{\sigma}_1$ and $\boldsymbol{\sigma}_2$ are the Pauli matrices, $\overset{*}{\mathbf{k}}$ and $\overset{*}{\mathbf{k}}'$ the unit vectors in the direction of the initial and the final momentum in the c.m.s. The quantities n^ν, m^ν, and l^ν in Equations 10 and 11 are the ν-th components of the vectors $\mathbf{n}$, $\mathbf{m}$, and l, respectively.

The solution of the system of KEs 6 for Φ^ν_α, as well as has been done for the function Φ_α satisfying the system 56, Chapter 1, can be represented in the form of the von Neumann series (see Section F, Chapter 1). The first term of this series is the single-particle phase density of primary nucleons, the second one is the same for nucleons of the first generation (quasifree nucleons), whereas other terms describe cascade nucleons. Hence, similarly to Equation 1, Chapter 2, we can represent the functional 1 in the form

$$d^2\sigma^{\nu}_{\alpha_0\alpha,\zeta_{\alpha_0}}/d\epsilon d\boldsymbol{\Omega} = d^2\sigma^{\nu,(q)}_{\alpha_0\alpha,\zeta_{\alpha_0}}/d\epsilon d\boldsymbol{\Omega} + d^2\sigma^{\nu,(c)}_{\alpha_0\alpha,\zeta_{\alpha_0}}/d\epsilon d\boldsymbol{\Omega}\,. \quad (14)$$

As in Section IA of Chapter 2 the distribution of quasifree nucleons will be calculated to the highest possible accuracy, while that of cascade nucleons will be calculated within the framework of more crude approximations. We can show (see, for example, Reference 29) that the cross-section for production of quasifree nucleons has the form[19]

$$\frac{d^2\sigma^{\nu,(q)}_{\alpha_0\alpha,\zeta_{\alpha_0}}}{d\epsilon d\boldsymbol{\Omega}} = \int d\mathbf{r}\ \varphi_{\alpha_0}\,[\Lambda(\mathbf{r}, -\boldsymbol{\Omega}_0),\ E_0(\mathbf{r});\mathbf{r},\boldsymbol{\Omega}_0]\,\cdot$$
$$\varphi_\alpha[\Lambda(\mathbf{r},\boldsymbol{\Omega}),E(\mathbf{R});\mathbf{R},\boldsymbol{\Omega}] \sum_{\nu'} K^{\nu'\to\nu}_{\alpha_0\to\alpha}\,(\mathbf{r};E_0,\boldsymbol{\Omega}_0 \to E,\boldsymbol{\Omega})\ \zeta^{\nu'}_{\alpha_0}\,, \quad (15)$$

which is similar to the expression 2, Chapter 2 obtained for the case when the polarization effects in NN-collisions are disregarded. The function φ_α is determined

by the formula 3, Chapter 2. Substituting the expression 15 in 3 and 5 we easily find that within the framework of the outlined approach the following relation is valid for quasifree scattering:*

$$A^{(q)}_{y,\alpha} = \mathcal{P}^{(q)}_{y,\alpha} = \sum_{\nu=1}^{3} \frac{d^2\sigma^{\nu,(q)}_{\alpha_0\alpha,\zeta_{\alpha_0}=0}}{d\epsilon d\boldsymbol{\Omega}} n^{\nu}_{r} \Big/ \frac{d^2\sigma^{0,(q)}_{\alpha_0\alpha,\zeta_{\alpha_0}=0}}{d\epsilon d\boldsymbol{\Omega}} . \tag{16}$$

To obtain approximate estimates of the numerator and the denominator of Equation 16, which are necessary for the analysis of experimental data on the analyzing power in the reaction A(**p**,p′)X, we shall use the model of a uniform nucleus of a radius R and disregard the difference between the Fermi momentum $p_{F,1}$ of protons and that of neutrons $p_{F,-1}$. Then making use of Equations 8-12 and 14, and taking into account the fact that for small angles of scattering the quantity $\boldsymbol{\Omega}$ can be replaced by $\boldsymbol{\Omega}_0$ in the function $\varphi_1[\Lambda(\mathbf{r},\boldsymbol{\Omega}),E(\mathbf{R});\mathbf{R},\boldsymbol{\Omega}]$, we get

$$\sum_{\nu=1}^{3} \frac{d^2\sigma^{\nu,(q)}_{11,\zeta_1=0}}{d\epsilon d\boldsymbol{\Omega}} n^{\nu}_{r} = I^{(q)}_0 \, [2ZJ_{11}(E_0\boldsymbol{\Omega}_0 \to E,\boldsymbol{\Omega}) + NJ_{1-1}(E_0,\boldsymbol{\Omega}_0 \to E,\boldsymbol{\Omega})], \tag{17}$$

$$J_{\alpha\gamma}(E_0,\boldsymbol{\Omega}_0 \to E,\boldsymbol{\Omega}) = \frac{3}{4\pi p_F^3 v_0} \int d\mathbf{p}'' d\mathbf{p}''' \, \Theta(p_F - p'') \, \Theta(p''' - p_F) \times w_{\alpha\gamma}(\mathbf{p}_0,\mathbf{p}'' \to \mathbf{p},\mathbf{p}''') \, \zeta^{(0)}_{\alpha\gamma}(s,\overset{*}{\vartheta}(\mathbf{n}_r\mathbf{n}) \frac{d\mathbf{p}}{dEd\boldsymbol{\Omega}} \tag{18}$$

Here the quantity $I^{(q)}_0$ is determined by Equation 22, Chapter 2; $\alpha = 1$, $\gamma = \pm 1$ and $p_F = p_{F,1} = p_{F,-1}$.

The cross-section $d^2\sigma^{0,(q)}_{11,\zeta_1=0}/d\epsilon\, d\boldsymbol{\Omega}$ appearing in the denominator of Equation 16 is determined by the expression in 14, Chapter 2, with $I^{(q)}(\vartheta = 0°) = I^{(q)}_0$.

C. SOLUTION OF THE SYSTEM OF EQUATIONS FOR CASCADE NUCLEONS

Describing the transport of cascade nucleons, we shall confine ourself, for the sake of simplicity, to the case N=Z and disregard the anisotropy of elastic NN-scattering in the c.m.s. We shall also neglect the Fermi motion of intranuclear nucleons in NN-collisions and relativistic effects. Then, it can be shown[19] that

* For elastic scattering, the equality $A_y = \mathcal{P}_y$ follows from the invariance of scattering with respect to the inversion of time. However, the experiments have demonstrated that, even in the case of inelastic scattering with the excitation of discrete levels, A_y and $\mathcal{P}_y$ are most often approximately equal to one another.[30] In a recent paper,[31] it has been found that this relation is satisfied to within experimental errors in the case of an inclusive quasifree scattering of protons with the energy 290 and 420 MeV on ^{12}C nuclei over the entire domain of a quasifree peak as well.

$$K^{\nu'\to\nu}_{\alpha'\to\alpha}(\mathbf{r};E',\boldsymbol{\Omega}'\to E,\boldsymbol{\Omega}) = \frac{A}{2}\rho(\mathbf{r})\frac{\tilde{y}(E_F/E')}{2\pi E'}\delta\left(\boldsymbol{\Omega}'\boldsymbol{\Omega} - \sqrt{\frac{E}{E'}}\right)\times$$
$$\left\{\delta_{\alpha'\alpha}\left[2\sigma^{el}_{\alpha\alpha}(E')\,\Pi^{\nu'\to\nu}_{\alpha\alpha\to\alpha}(E',\overset{*}{\vartheta}) + \sigma^{el}_{\alpha-\alpha}(E')\,\Pi^{\nu'\to\nu}_{\alpha-\alpha\to\alpha}(E',\overset{*}{\vartheta})\right] + \right. \tag{19}$$
$$\left.(1-\delta_{\alpha'\alpha})\,\sigma^{el}_{-\alpha\alpha}(E')\,\Pi^{\nu'\to\nu}_{-\alpha\alpha\to\alpha}(E',\overset{*}{\vartheta})\right\},$$

where $\rho(\mathbf{r})$ is the density of intranuclear nucleons normalized to unity, and the function $\tilde{y}$ is determined by the formula 12, Chapter 2. Moreover, we confine ourselves to the case of E close to E_0. Then we can obviously neglect the dependence of the quantities $\mu_\alpha, \sigma^{el}_{\alpha\gamma}$, $\Pi^{\nu'\to\nu}_{\ldots}$ and $\tilde{y}$ on the energy and seek the solution of Equation 6 in the small-angle approximation (see Section IC, Chapter 2) in which the following relations take place:

$$\mathbf{n} \simeq [\boldsymbol{\Omega}_0(\boldsymbol{\vartheta} - \boldsymbol{\vartheta}')]/|\boldsymbol{\vartheta} - \boldsymbol{\vartheta}'|,\ \mathbf{m} \simeq -(\boldsymbol{\vartheta} - \boldsymbol{\vartheta}')/|\boldsymbol{\vartheta} - \boldsymbol{\vartheta}'|\,,$$
$$\mathbf{l} \simeq \boldsymbol{\Omega}_0;\ \boldsymbol{\Omega}\,\nabla\,\Phi^\nu_\alpha \simeq d\Phi^\nu_\alpha/dz\,. \tag{20}$$

Introducing a new variable $\tilde{t}$ (see Equation 45, Chapter 2) instead of z and making use of the Mellin transformation with respect to E, and the Fourier transformation with respect to $\boldsymbol{\vartheta}$ (see Equation 46, Chapter 2) for the functions

$$\Phi^\nu_\pm = \Phi^\nu_{\alpha_0} \pm \Phi^\nu_{-\alpha_0} \tag{21}$$

we get[19]

$$\Phi^\nu_\pm(\tilde{t},E,\boldsymbol{\vartheta}) = \frac{1}{4\pi^2 iE_0}\int_{\sigma-i\infty}^{\sigma+i\infty} d\eta\,\exp\left(\eta\ln\frac{E_0}{E}\right)\int_0^\infty \xi d\xi\,\Xi^\nu(\xi,\tilde{t},\eta,\boldsymbol{\vartheta})\,. \tag{22}$$

$$\Xi^0 = e^{\omega_\pm}\,[J_0(\xi\vartheta)c(\varphi_\pm, + \varkappa_{1,\pm}) + \zeta^y_{\alpha_0}J_1(\xi\vartheta)F^{(1)}_\pm(\xi)S(\varphi_\pm)]\,, \tag{23}$$

$$\Xi^x = \frac{1}{2}\zeta^x_{\alpha_0}\,[e^{\nu_\pm}c(\lambda_\pm, - \varkappa_{2,\pm})I_- + e^{\omega_\pm}c(\varphi_\pm, - \varkappa_{1,\pm})I_+] +$$
$$\zeta^z_{\alpha_0}e^{\nu_\pm}H^{(1)}_\pm(\xi)S(\lambda_\pm)J_1(\xi\vartheta)\,, \tag{24}$$

$$\Xi^y = \frac{1}{2}\zeta^y_{\alpha_0}\,[e^{\nu_\pm}c(\lambda_\pm, - \varkappa_{2,\pm})I_+ + e^{\omega_\pm}c(\varphi_\pm, - \varkappa_{1,\pm})I_-] +$$
$$e^{\omega_\pm}F^{(1)}_\pm(\xi)S(\varphi_\pm)J_1(\xi\vartheta)\,, \tag{25}$$

$$\Xi^z = e^{\nu_\pm}\,[\zeta^z_{\alpha_0}c(\lambda_\pm, + \varkappa_{2,\pm})J_0(\xi\vartheta) - \zeta^x_{\alpha_0}H^{(1)}_\pm(\xi)S(\lambda_\pm)J_1(\xi\vartheta)]\,;$$

$$S(a) = \frac{1}{a}\sinh(a\tilde{t}),\ c(a, \pm\varkappa) = \cosh(a\tilde{t}) \pm \frac{\varkappa}{a}\sinh(a\tilde{t})\ ;$$

$$\varkappa_{1,\pm} = \frac{1}{2}[K^{0\to 0}_{\pm}(\xi) - \gamma_{1,\pm}],\ \varkappa_{2,\pm} = \frac{1}{2}[L^{(0)}_{\pm}(\xi) - \gamma_{\pm}]\ ,$$

$$\omega_{\pm} = \frac{1}{2}[K^{0\to 0}_{\pm}(\xi) + \gamma_{1,\pm}]\tilde{t} - \mu_0\tilde{t},\ \nu_{\pm} = \frac{1}{2}[L^{(0)}_{\pm}(\xi) + \gamma_{\pm}]\tilde{t} - \mu_0\tilde{t}\ ; \tag{26}$$

$$\varphi_{\pm} = (\varkappa^2_{1,\pm} - [F^{(1)}_{\pm}(\xi)]^2)^{1/2},\ \lambda_{\pm} = (\varkappa^2_{2,\pm} + [H^{(1)}_{\pm}(\xi)]^2)^{1/2}\ ,$$

$$I_{\pm} = J_0(\xi\vartheta) \pm J_2(\xi\vartheta),\ \vartheta = |\boldsymbol{\vartheta}|\ ;$$

$$\mu_0 = \frac{A}{2}\left[\sigma^{el}_{11}(E_0) + \sigma^{el}_{1-1}(E_0)\right]\tilde{y}\left(\frac{E_F}{E_0}\right),\ A = N + Z\ ; \tag{27}$$

$$K^{0\to 0}_{\pm}(\xi) = (\tilde{\omega}_{\pm}/\eta)e^{-\xi^2/4\eta}\ ,$$

$$\tilde{\omega}_{\pm} = \frac{A}{2}\left[2\sigma^{el}_{11}(E_0) + \sigma^{el}_{1-1}(E_0) \pm \sigma^{el}_{1-1}(E_0)\right]\tilde{y}\left(\frac{E_F}{E_0}\right)\ ; \tag{28}$$

$$\gamma_{\pm} = \frac{1}{2}\left[M^{(0)}_{\pm}(\xi) - M^{(2)}_{\pm}(\xi) + N^{(0)}_{\pm}(\xi) + N^{(2)}_{\pm}(\xi)\right],$$

$$\gamma_{1,\pm} = \frac{1}{2}\left[N^{(0)}_{\pm}(\xi) - N^{(2)}_{\pm}(\xi) + M^{(0)}_{\pm}(\xi) + M^{(2)}_{\pm}(\xi)\right], \tag{29}$$

$$\begin{pmatrix} F^{(k)}_{\pm}(\xi) \\ N^{(k)}_{\pm}(\xi) \\ M^{(k)}_{\pm}(\xi) \\ L^{(k)}_{\pm}(\xi) \\ H^{(k)}_{\pm}(\xi) \end{pmatrix} = A\tilde{y}\left(\frac{E_F}{E_0}\right)\int_0^{\infty}\vartheta d\vartheta J_k(\xi\vartheta)e^{-\eta\vartheta^2}\left[2\sigma^{el}_{11}(E_0)\begin{pmatrix} \zeta^{(0)}_{11}(E_0,\overset{*}{\vartheta}) \\ D^{11}_{nn}(E_0,\overset{*}{\vartheta}) \\ D^{11}_{mm}(E_0,\overset{*}{\vartheta}) \\ D^{11}_{ll}(E_0,\overset{*}{\vartheta}) \\ D^{11}_{lm}(E_0,\overset{*}{\vartheta}) \end{pmatrix} + \right.$$

$$\left.\sigma^{el}_{1-1}(E_0)\begin{pmatrix} \zeta^{(0)}_{1-1}(E_0,\overset{*}{\vartheta}) \mp \zeta^{(0)}_{1-1}(E_0,\overset{*}{\tilde{\vartheta}}) \\ D^{1-1}_{nn}(E_0,\overset{*}{\vartheta}) \pm K^{1-1}_{nn}(E_0,\overset{*}{\tilde{\vartheta}}) \\ D^{1-1}_{mm}(E_0,\overset{*}{\vartheta}) \pm K^{1-1}_{ll}(E_0,\overset{*}{\tilde{\vartheta}}) \\ D^{1-1}_{ll}(E_0,\overset{*}{\vartheta}) \pm K^{1-1}_{mm}(E_0,\overset{*}{\tilde{\vartheta}}) \\ D^{1-1}_{lm}(E_0,\overset{*}{\vartheta}) \mp K^{1-1}_{lm}(E_0,\overset{*}{\tilde{\vartheta}}) \end{pmatrix}\right] \tag{30}$$

Here $\tilde{t} > 0$, $J_k(x)$ is the Bessel function of the first kind, $\Phi^{x,y,z}_{\pm}$ and $\zeta^{x,y,z}_{\alpha_0}$ are the projections of corresponding vectors on the coordinate axes x,y, and z directed along the vectors $\boldsymbol{\vartheta}$, $[\boldsymbol{\Omega}_0\boldsymbol{\vartheta}]$ and $\boldsymbol{\Omega}_0$.

In the particular case of the interaction of unpolarized nucleons ($\zeta_{\alpha_0} = 0$) with a nucleus, we have

$$\Phi^{x}_{\pm} = \Phi^{z}_{\pm} = 0,\ \Phi^{y}_{\pm}(\tilde{t},E,\vartheta) = \frac{1}{4\pi^2 iE_0}\int_{\sigma-i\infty}^{\sigma+i\infty} d\eta e^{\eta \ln E_0/E} \times$$
$$\int_0^{\infty} \xi d\xi J_1(\xi\vartheta)\, F^{(1)}_{\pm}(\xi) S(\varphi_{\pm}) e^{\omega_{\pm}} . \tag{31}$$

Finally, according to Equation 21 we get

$$\Phi^{\nu}_{\alpha_0,-\alpha_0}(\tilde{t},E,\vartheta) = \frac{1}{2}[\Phi^{\nu}_{+}(\tilde{t},E,\vartheta) \pm \Phi^{\nu}_{-}(\tilde{t},E,\vartheta)] . \tag{32}$$

Equations 1, 3-5, and 22-32 determine the cross-sections and any polarization characteristics of inclusive NA-reactions, if the parameters of the NN-interaction are known. However, even without carrying out specific calculations, we can arrive at the following conclusions:

1) even in the case of the interaction of unpolarized nucleons with nuclei, the double differential distribution of secondary nucleons differs from that obtained without regard for polarization effects in NN-collisions (see Equations 1, 23, and 32), namely, their angular distribution is "washed out" to a greater extent;
2) the analyzing power $A_{y,\alpha}$ is equal to the polarization $\mathcal{P}_{y,\alpha}$ of secondary nucleons in the case of the interaction of unpolarized nucleons with nuclei with allowance for their rescattering in a nucleus.

Specific calculations carried out in accordance with the formulas obtained are very cumbersome. Here we shall confine ourselves to a mere presentation of results of these calculations for analyzing power and their comparison with experimental data. These results and methods used for their derivation are described in detail in Reference 19. The same paper contains some other results, in particular, an account of a method which allows one to take into consideration approximately the deflection of proton trajectories by the nuclear and the Coulomb field.

D. ANALYZING POWER IN THE REACTION A(p,p')X

Figure 8 shows an example of comparison of experimental data[22] with the analyzing power $A_{y,1}$ in the reaction A(**p**,p')X calculated[19] at ϵ_0 = 200 MeV as a function of the angle ϑ of divergence of secondary protons with the energy ϵ_q corresponding to the peak of the quasifree scattering at a given angle (a), and with the energy which is smaller than ϵ_q by 15 MeV (b). The curve 1 corresponds to the contribution from quasifree protons in (a) and to the contribution from cascade protons* in (b). The curves 2 and 3 depict the results of the calculations which

* The parameters of the NN-interaction are borrowed from References 32-36.

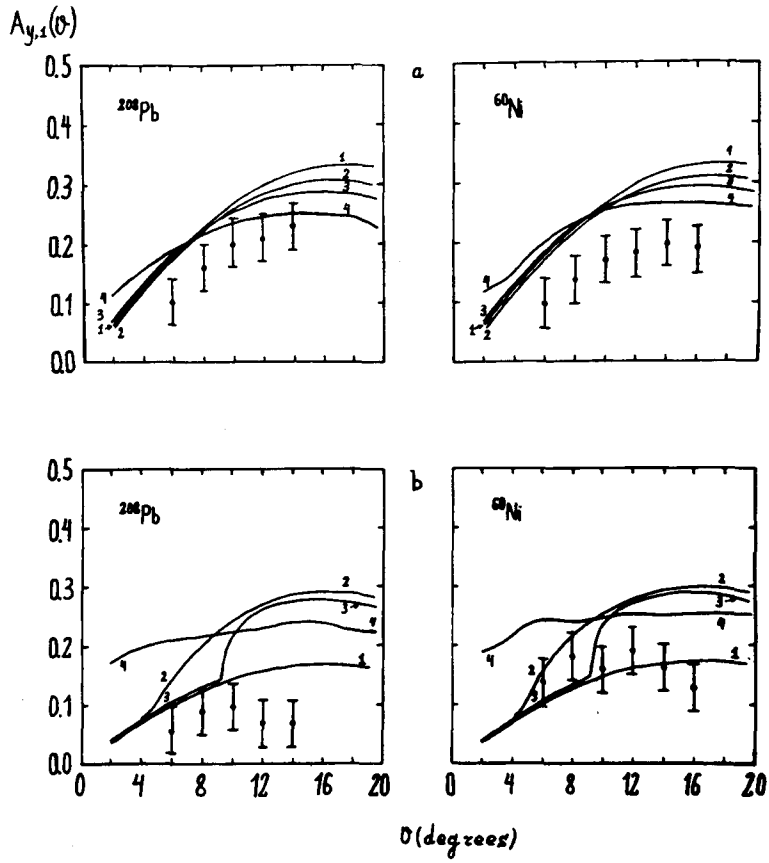

FIGURE 8. The analyzing power $A_{y,1}$ for the interaction of 200 MeV protons with ^{60}Ni and ^{208}Pb nuclei as a function of the angle of divergence of secondary protons: (a) with the energy ϵ_q corresponding to the position of the peak of quasifree scattering at a given angle, and (b) with the energy of secondary protons ϵ_q − 15 MeV. Experimental data are borrowed from Reference 22. The curves correspond to various versions of the calculation of Reference 19.

take into account the Fermi motion in a quasifree pN-collision in a nucleus and which are carried out for B_N = 8 MeV. The former corresponds to the Woods-Saxon nuclear density (Equation 122, Chapter 2), whereas the latter corresponds to the uniform one with R = $1.3A^{1/3}$fm and E_F = 28.5 MeV. The curve 4 shows the results of the calculations carried out under the same assumptions as those used in the calculations depicted by the curve 3 but with allowance for the deflection of proton trajectories by the nuclear and the Coulomb field.

The following is seen from the figure:

1) a qualitative agreement between the calculations[19] and experimental data is observed

2) taking account of the deflection of the proton trajectories by the nuclear and the Coulomb field somewhat improves an agreement with experimental data in the domain of larger angles, but this agreement deteriorates at small angles
3) although the main contribution to the energy spectrum at the point of a maximum at a given angle comes from quasifree protons, the quantity $A_{y,1}$ depends only slightly on the structure of the nuclear surface and on the momentum distribution of intranuclear nucleons.

The discrepancy between the calculations[19] and experimental data can be caused by the following imperfections of the theory:

1) the quantum-mechanical effects which must affect, above all, the quasifree scattering (see Section IB) are disregarded
2) the Fermi motion of intranuclear nucleons is disregarded in the calculation of the cascade component of the cross-section
3) the polarization characteristics of the NN-interaction (especially the ones concerned with the pn-interaction) used in the calculations are inaccurate. Moreover, this interaction in a nucleus can differ from the free one.

To elucidate the latter effect and to clarify the mechanism of the excitation of a continuum in the reactions under consideration as well, it is necessary to carry out a more detailed theoretical analysis and to refine upon experimental methods aimed at more precise measurements.

III. PRODUCTION OF PARTICLES IN PROTON-NUCLEUS COLLISIONS

Production of particles (pions, kaons, hyperons, antinucleons, etc.) is one of the principal subjects of investigations in the intermediate-energy nuclear physics which is inherent in this energy range. Its study began immediately after the invention of accelerators enabling one to obtain protons with the energy sufficient for production of a pion, which is the lightest among the above-listed particles. (The mass m_π of a pion is approximately equal to 140 MeV and the threshold ϵ_{thr} of its production in NN-collisions in the l.s. to 290 MeV). A large body of experimental information on inclusive cross-sections for production of various particles in pA-interactions over a wide range of initial energies has been accumulated since then. Such information was of particular importance for construction of meson facilities, i.e., the high-current proton accelerators with the energy $\epsilon_0 \simeq$ 500-1000 MeV, and for the development of the projects of a new generation of such accelerators with the energy $\epsilon_0 \simeq 50$ GeV, i.e., kaon facilities. To analyze these data a wide range of models has been invoked, including the INC-model considered in preceding chapters. Being deprived of the possibility of presenting the entire set of data on the production of particles in pA-interactions, we shall discuss the production of pions in the energy range $\epsilon_0 < 1$ GeV and of K^+- mesons and antiprotons at $\epsilon_0 \gtrsim 1$ GeV within the framework of the INC-model.

A. PRODUCTION OF PIONS IN PROTON-NUCLEUS INTERACTIONS

1. System of KEs for Intranuclear Nucleonic-Mesonic Cascade

Earlier, while considering various inclusive characteristics of NA-reactions on the basis of the analytic solution of the systems of KEs 56, Chapter 1, and 6 obtained within the framework of the INC-model, we neglected, for the sake of simplicity, the meson production in NN-interactions. This allowed us to find rather simple analytic expressions for these characteristics. However, the production of pions on nuclei is observed[37] with a significant probability for the energies of primary protons $\epsilon_0 \gtrsim 200$ MeV. To describe these processes the system of KEs 56, Chapter 1, must be generalized to the case with allowance for the meson production in NN-collisions. This can be easily done by representing* it in the form[6]

$$[\boldsymbol{\Omega}\nabla + \mu_\alpha(\mathbf{r},E)]\,\Phi_\alpha(\mathbf{r},E,\boldsymbol{\Omega}) = \sum_{\alpha'} \int d\boldsymbol{\Omega}' \int dE'\, \Phi_{\alpha'}(\mathbf{r},E',\boldsymbol{\Omega}') \times K_{\alpha'\to\alpha}(\mathbf{r};E',\boldsymbol{\Omega}' \to E,\boldsymbol{\Omega}) + S_\alpha(\mathbf{r},E,\boldsymbol{\Omega}) , \tag{33}$$

$$[\boldsymbol{\Omega}\nabla + \varkappa_j(\mathbf{r},E)]\,\Pi_j(\mathbf{r},E,\boldsymbol{\Omega}) = \sum_{j'} \int d\boldsymbol{\Omega}' \int dE'\, \Pi_{j'}(\mathbf{r},E',\boldsymbol{\Omega}') \times A_{j'\to j}(\mathbf{r};E',\boldsymbol{\Omega}' \to E,\boldsymbol{\Omega}) + Q_j(\mathbf{r},E,\boldsymbol{\Omega}) ; \tag{34}$$

$$S_\alpha(\mathbf{r},E,\boldsymbol{\Omega}) = \int d\boldsymbol{\Omega}' \int dE' \left\{ \sum_{\alpha'} \Phi_{\alpha'}(\mathbf{r},E',\boldsymbol{\Omega}') K^{in}_{\alpha'\to\alpha}(\mathbf{r};E',\boldsymbol{\Omega}' \to E,\boldsymbol{\Omega}) + \sum_{j'} \Pi_{j'}(\mathbf{r},E',\boldsymbol{\Omega}')\, A^{in}_{j'\to\alpha}(\mathbf{r};E',\boldsymbol{\Omega}' \to E,\boldsymbol{\Omega}) \right\} + \delta_{\alpha\alpha_0}\delta(E - E_0)\,\delta(\boldsymbol{\Omega} - \boldsymbol{\Omega}_0)\,\delta(z - z_0) , \tag{35}$$

$$Q_j(\mathbf{r},E,\boldsymbol{\Omega}) = \int d\boldsymbol{\Omega}' \int dE' \sum_{\alpha'} \Phi_{\alpha'}(\mathbf{r},E',\boldsymbol{\Omega}') K^{in}_{\alpha'\to j}(\mathbf{r};E',\boldsymbol{\Omega}' \to E,\boldsymbol{\Omega}) , \tag{36}$$

$$\Phi_\alpha(\mathbf{R},E,\boldsymbol{\Omega}) = \Pi_j(\mathbf{R},E,\boldsymbol{\Omega}) = 0 \quad \text{for} \quad \boldsymbol{\Omega}\mathbf{R} < 0 . \tag{37}$$

Here $\Phi_\alpha(\mathbf{r},E,\boldsymbol{\Omega})$ and $\Pi_j(\mathbf{r},E,\boldsymbol{\Omega})$ are respectively the flux density of α-nucleons (α = p and n) and of j-pions (j = π^+, π^0 and π^-) at the point $\mathbf{r}$ moving with kinetic energy E in the direction of the unit vector $\boldsymbol{\Omega}$; $K_{\alpha'\to\alpha}$ and $K^{in}_{\alpha'\to\alpha}$ $(\mathbf{r};E',\boldsymbol{\Omega}' \to E,\boldsymbol{\Omega})$ the macroscopic (i.e., multiplied by the nuclear density; in particular, $K_{\alpha'\to\alpha}$ is determined by the formula 6, Chapter 2) double differential cross-sections (averaged over the Fermi motion of intranuclear nucleons) for production of α-nucleons at the point $\mathbf{r}$, which move with the energy E in the direction of the vector $\boldsymbol{\Omega}$ and which are created as a result of elastic and inelastic** collisions, respectively, of

* Carrying out this procedure, we neglect, for the sake of simplicity, the deflection of the particle trajectories under the action of the effective potential.

** That is collisions which are accompanied by the production of pions.

α'-nucleons moving with the energy E′ in the direction of the vector $\boldsymbol{\Omega}'$ with unexcited intranuclear nucleons; $A_{j'\to j}$ and $A^{in}_{j'\to\alpha}$ $(\mathbf{r};E',\boldsymbol{\Omega}' \to E, \boldsymbol{\Omega})$ the similar cross-sections for production of j-pions and α-nucleons created as a result of the interaction of j′-pions with unexcited intranuclear nucleons; $K^{in}_{\alpha'\to j}$ $(\mathbf{r};E',\boldsymbol{\Omega}' \to E,\boldsymbol{\Omega})$ is the same for production of j-pions owing to the interaction of cascade α'-nucleons with intranuclear nucleons, and

$$\varkappa_{\pi^+,\pi^0,\pi^-}(\mathbf{r},E) = \rho_p(\mathbf{r})\sigma_{\pi^+,\pi^0,\pi^-}(E) + \rho_n(\mathbf{r})\sigma_{\pi^-,\pi^0,\pi^+}(E) + \rho_N(\mathbf{r})\sigma_{\pi,a}(E) , \tag{38}$$

where σ_π is the total cross-section of the πp-interaction averaged over the Fermi motion of intranuclear nucleons and $\sigma_{\pi,a}$ the cross-section for the absorption of pions per one nucleon. The quantity $\mu_\alpha(\mathbf{r},E)$ is determined by the formula 11 in Chapter 2 in which the total cross-sections $\sigma^{el}_{\alpha\alpha'}$ of the elastic $\alpha\alpha'$-scattering must be replaced by the total cross-sections $\sigma^{tot}_{\alpha\alpha'}$ of the $\alpha\alpha'$-interaction. As we might expect, the system of KEs 56, Chapter 1, of a purely nucleonic cascade is obtained, if the meson production is disregarded (i.e., if we set all $K^{in}\ldots = 0$).

It should be noted that production of pions in NA-collisions has been considered[38-40] on the basis of more simple KEs.

2. General Scheme of Solution of the System of KEs for Intranuclear Nucleonic-Mesonic Cascade

Suppose that we know the Green functions G_{xx_1} $(\mathbf{r},E,\boldsymbol{\Omega};\mathbf{r}_1,E_1,\boldsymbol{\Omega}_1)$ of the system of Equations 33-37 (here we have introduced the notation $x = \alpha$, j; $x_1 = \alpha_1$, j_1). Then this system of equations can be represented in the form[6]

$$\Phi_\alpha(\mathbf{r},E,\boldsymbol{\Omega}) = \sum_{\alpha 1}\int d\mathbf{r}_1 dE_1 d\boldsymbol{\Omega}_1\, G_{\alpha\alpha_1}(\mathbf{r},E,\boldsymbol{\Omega};\mathbf{r}_1,E_1,\boldsymbol{\Omega}_1) \times S_{\alpha_1}(\mathbf{r}_1,E_1,\boldsymbol{\Omega}_1) ,$$

$$\Pi_j(\mathbf{r},E,\boldsymbol{\Omega}) = \sum_{j1}\int d\mathbf{r}_1 dE_1 d\boldsymbol{\Omega}_1\, G_{jj_1}(\mathbf{r},E,\boldsymbol{\Omega};\mathbf{r}_1,E_1,\boldsymbol{\Omega}_1) \times Q_{j_1}(\mathbf{r}_1,E_1,\boldsymbol{\Omega}_1) , \tag{39}$$

where the "sources" S_{α_1} and Q_{j_1} are determined by the expressions 35 and 36, (a similar procedure was used in Section IIE, Chapter 1 in order to go over from the integrodifferential equation to the purely integral one). It is convenient to seek the solution of this system of equations in the form of an expansion in the number of inelastic NN-collisions

$$\Phi_\alpha = \sum_{k=0}^{\infty}\Phi_{\alpha,k},\ \Pi_j = \sum_{k=0}^{\infty}\Pi_{j,k} , \tag{40}$$

where the functions $\Phi_{\alpha,k}$ and $\Pi_{j,k}$ are defined by the integrals 39 in which S_{α_1} and Q_{j_1} must be replaced by $S_{\alpha_1,k}$ and $Q_{j_1,k}$, given by the following expressions:

$$S_{\alpha_1,0} = \delta_{\alpha_1\alpha_0}\,\delta(E - E_0)\,\delta(\boldsymbol{\Omega} - \boldsymbol{\Omega}_0)\,\delta(z - z_0),\ Q_{j_1,0} = 0 \tag{41}$$

and for $k \neq 0$

$$\begin{aligned} S_{\alpha_1,k}(\mathbf{r},E,\boldsymbol{\Omega}) &= \int d\boldsymbol{\Omega}' \int dE' \Big\{ \sum_{\alpha'} \Phi_{\alpha',k-1}(\mathbf{r},E',\boldsymbol{\Omega}') \times \\ &K^{in}_{\alpha'\to\alpha_1}(\mathbf{r};E',\boldsymbol{\Omega}' \to E,\boldsymbol{\Omega}) + \sum_{j'} \Pi_{j',k}(\mathbf{r},E',\boldsymbol{\Omega}') \times \\ &A^{in}_{j'\to\alpha_1}(\mathbf{r};E',\boldsymbol{\Omega}' \to E,\boldsymbol{\Omega}) \Big\}, \\ Q_{j_1,k}(\mathbf{r},E,\boldsymbol{\Omega}) &= \int d\boldsymbol{\Omega}' \int dE' \sum_{\alpha'} \Phi_{\alpha',k-1}(\mathbf{r},E',\boldsymbol{\Omega}') \times \\ &K^{in}_{\alpha'\to j_1}(\mathbf{r};E',\boldsymbol{\Omega}' \to E,\boldsymbol{\Omega}) \,. \end{aligned} \tag{42}$$

Thus, the problem is reduced to a simple iteration procedure which converges rapidly in the energy range ($\epsilon_0 < 1$ GeV) under consideration, since any inelastic collision of nucleons is accompanied by a considerable loss of energy ($\geqslant 140$ MeV), and the cross-section of inelastic processes decreases rapidly with decreasing nucleon energy. In the case of reactions initiated by nucleons with the energy $\lesssim 0.8$ GeV, it is sufficient to take into account only the terms with $k = 0$ and 1^6 in the sums 40. For instance, it follows from equations 39 and 42 that the function Π_j necessary for the calculation of inclusive cross-sections for production of pions has the form

$$\begin{aligned} \Pi_j(\mathbf{r},E,\boldsymbol{\Omega}) \equiv \Pi_{j,1}(\mathbf{r},E,\boldsymbol{\Omega}) &= \sum_{j_1} \int d\mathbf{r}_1 dE_1 d\boldsymbol{\Omega}_1\, G_{jj_1}(\mathbf{r},E,\boldsymbol{\Omega};\mathbf{r}_1,E_1,\boldsymbol{\Omega}_1) \times \\ &\int d\boldsymbol{\Omega}' \int dE' \sum_{\alpha'} \Phi_{\alpha',0}(\mathbf{r}_1,E',\boldsymbol{\Omega}') \times K^{in}_{\alpha'\to j_1}(\mathbf{r}_1;E',\boldsymbol{\Omega}' \to E_1,\boldsymbol{\Omega}_1) \,. \end{aligned} \tag{43}$$

Let us find the quantities appearing in this expression.

The Green functions for pions — For the energies of primary nucleons under considerations, pions in a nucleus are largely produced with the energy lying in the vicinity of the (3,3)-resonance. Such pions do not undergo practically inelastic (with the production of one more pion) scattering on intranuclear nucleons. Their elastic scattering on a nucleon is strongly anisotropic (it is forward and backward peaked) and is accompanied by a small loss of energy. Therefore, in the first approximation, we can neglect the scattering of pions on nucleons and assume that in such acts of scattering the direction of their motion and their energy do not undergo any change.* The same takes place in the charge exchange reactions involving pions. Hence, the meson Green functions G_{jj_1} can be approximately represented in the form[6]

* The same assumptions about the πN-interaction were used in References 38-40. It has been shown,[41] however, that taking account of this interaction in a more correct way only slightly affects the value of cross-sections for production of pions by intermediate-energy nucleons on nuclei.

$$G_{jj_1}(\mathbf{r},E,\boldsymbol{\Omega};\mathbf{r}_1,E_1,\boldsymbol{\Omega}_1) = G_{jj_1}(\tilde{t}_1)\Theta(\tilde{t}_1)\,\delta(\mathbf{x}_\perp)\times$$
$$\delta(E-E_1)\,\delta(\boldsymbol{\Omega}-\boldsymbol{\Omega}_1);\ \mathbf{x} = \mathbf{r}-\mathbf{r}_1 = x_{\parallel}\boldsymbol{\Omega}_1 + \mathbf{x}_\perp \tag{44}$$
$$\tilde{t}_1 = \int_0^{x_{\parallel}} \rho(\mathbf{r}_1 + x'\boldsymbol{\Omega}_1)\,dx',\ \Theta(\tilde{t}_1) = \frac{\tilde{t}_1 + |\tilde{t}_1|}{2|\tilde{t}_1|},$$

where $G_{jj_1}(\tilde{t}_1)$ are certain simple functions of the variable $\tilde{t}_1$. The following of them are necessary to calculate $\Pi_{\pi^+}(\mathbf{r},E,\boldsymbol{\Omega})$:

$$G_{++}(\tilde{t}_1) = G_1 + G_2 + G_3,$$
$$G_{+0}(\tilde{t}_1) = G_1 - \frac{Z}{N}\times\left(1+\sqrt{\frac{N}{Z}}\right)G_2 - \frac{Z}{N}\left(1-\sqrt{\frac{N}{Z}}\right)G_3,$$
$$G_{+-}(\tilde{t}_1) = G_1 + \left(\frac{Z}{N}\right)^{3/2}(G_2 - G_3)$$
$$G_1 = \exp\left[-A\sigma_{\pi,a}(E)\tilde{t}_1\right]\Big/\left[1+\frac{N}{Z}+\left(\frac{N}{Z}\right)^2\right],$$
$$G_2 = \exp\left\{-A\left[\sigma_{\pi,a}(E)+\sigma_{ex}(E)\left(1+\sqrt{NZ}/A\right)\right]\tilde{t}_1\right\}\Big/\left\{2\left[1+\frac{Z}{N}+\sqrt{\frac{Z}{N}}\right]\right\}, \tag{45}$$
$$G_3 = \exp\left\{-A\left[\sigma_{\pi,a}(E)+\sigma_{ex}(E)\left(1-\sqrt{NZ}/A\right)\right]\tilde{t}_1\right\}\Big/\left\{2\left[1+\frac{Z}{N}-\sqrt{\frac{Z}{N}}\right]\right\}.$$

Here $\sigma_{ex}(E)$ is the cross-section for the pion charge exchange reactions averaged over the Fermi motion of intranuclear nucleons

Functions $K^{in}_{\alpha'\to j_1}(\mathbf{r};E',\boldsymbol{\Omega}'\to E,\boldsymbol{\Omega})$ — In the range of nucleon energies under consideration, the production of one pion through the (3,3)-resonance is the principal process of pion production in NN-collisions. For this process[6,38,39]

$$K^{in}_{\alpha'\to j_1}(\mathbf{r};E',\boldsymbol{\Omega}'\to E,\boldsymbol{\Omega}) = \frac{6}{5}\rho(\mathbf{r})\alpha'_{j_1}d^2\sigma_{pp\to\pi^+}(E',\boldsymbol{\Omega}'\to E\boldsymbol{\Omega})/dE\,d\boldsymbol{\Omega}; \tag{46}$$

$$p_+ = \frac{10Z+N}{12},\quad p_0 = \frac{Z+2N}{6},\quad p_- = \frac{N}{12};$$
$$n_+ = \frac{Z}{12},\quad n_0 = \frac{N+2Z}{6},\quad n_- = \frac{10N+Z}{12}. \tag{47}$$

Here $d^2\sigma_{pp\to\pi^+}/dEd\Omega$ is the double differential cross-section for production of one π^+-meson in an inelastic pp-collision averaged over the Fermi motion of intranuclear nucleons.

Distribution functions of nucleons undergoing elastic scattering — Since the cross-section $d^2\sigma_{pp\to\pi^+}/dEd\Omega$ for production of pions decreases rapidly with decreasing nucleon energy,[42] the functions $\Phi_{\alpha',0}$ taken at the energies E′ close to E_0 give the main contribution to the integral 43. To calculate $\Phi_{\alpha',0}$ in this range of E′ we can neglect, in the first approximation, the deflection of nucleons from the initial direction (given by the vector Ω_0) as a result of elastic scattering and the Fermi motion of intranuclear nucleons. Then, for N = Z, the solution of the system of KEs (Equation 33) for these functions with allowance for the anisotropy of the NN-scattering in c.m.s. has the form[6]

$$\Phi_{\alpha',0}(r,E,\Omega) = \delta(\Omega - \Omega_0)\{\delta_{\alpha'\alpha 0}\,\Theta(\tilde{t})e^{-\mu^{tot}\tilde{t}}\delta(E - E_0) + \Phi_{\alpha',0}(\tilde{t},E)\}\,, \tag{48}$$

$$\Phi_{\alpha',0}(\tilde{t},E) = \frac{1}{2}\,[\Phi(\tilde{t},E,a_1,b_1) + \alpha_0\alpha'\Phi(\tilde{t},E,a_2,b_2)]\,. \tag{49}$$

$$\Phi(\tilde{t},E,a_{1,2},b_{1,2}) = \Theta(\tilde{t})e^{-\mu^{tot}\tilde{t}}\sum_{n=1}^{\infty}\frac{(A\tilde{t})^n}{n!}\,C^{(n)}(E,a_{1,2},b_{1,2})\,, \tag{50}$$

$$C^{(n)}(E,a_{1,2},b_{1,2}) = \int_E^{E_0} K(E_1 \to E)\,dE_1 \ldots \int_{E_{n-1}}^{E_0} K(E_n \to E_{n-1})\,\delta(E_n - E_0)\,dE_n\,, \tag{51}$$

$$\mu^{tot} = \frac{A}{2}\left[\sigma^{tot}_{11}(E_0) + \sigma^{tot}_{1-1}(E_0)\right], \tag{52}$$

where $\tilde{t}$ is determined by the relation 45, Chapter 2. It is convenient to use the following approximations (which describe satisfactorily experimental data on elastic NN-collisions) for the functions $K(E' \to E)$:

$$\begin{aligned} &K(E' \to E) = \frac{1}{E'}\left\{a_{1,2} + b_{1,2}(E')\left[\left(2\frac{E}{E'} - 1\right)^2 - \frac{1}{3}\right]\right\}, \\ &a_1 = \sigma^{el}_{11}(E_0) + \sigma^{el}_{1-1}(E_0),\ a_2 = \sigma^{el}_{11}(E_0)\,, \\ &b_1(E') = 2\pi[6.48 + B(E')],\ b_2(E') = 2\pi B(E')\,, \\ &B(E') = 10.15\left[1 - \left(\frac{500}{E'}\right)^4\right]\Theta(E' - 520)\,\Theta(900 - E')\,. \end{aligned} \tag{53}$$

Here E′ is measured in MeV, and B in mb/sr. Substituting the expressions 43-48 in the formula 73a, Chapter 1, we obtain the following expression for the cross-section of production of j-type pions in the interaction of protons with nuclei[6]

$$\frac{d^2\sigma_j}{d\epsilon d\boldsymbol{\Omega}} = \frac{6}{5}\sum_{j_1}\int d\mathbf{r}\rho(\mathbf{r})\, G_{jj_1}(\tilde{t}_1)\left\{p_{j_1}e^{-\mu^{tot}\tilde{t}} \times \right.$$
$$\frac{d^2\sigma_{pp\to\pi^+}(E_0,\boldsymbol{\Omega}_0 \to \epsilon - V_\pi,\boldsymbol{\Omega})}{d\epsilon d\boldsymbol{\Omega}} + \int dE'[p_{j_1}\Phi_{1,0}(\tilde{t},E') + \tag{54}$$
$$\left. n_{j_1}\Phi_{-1,0}(\tilde{t},E')]\frac{d^2\sigma_{pp\to\pi^+}(E',\boldsymbol{\Omega}_0 \to \epsilon - V_\pi,\boldsymbol{\Omega})}{d\epsilon d\boldsymbol{\Omega}}\right\};$$
$$\tilde{t} = \int_0^{\Lambda(\mathbf{r},-\boldsymbol{\Omega}_0)} \rho(\mathbf{r} - x'\boldsymbol{\Omega}_0)dx',\ \tilde{t}_1 = \int_0^{\Lambda(\mathbf{r},\boldsymbol{\Omega})} \rho(\mathbf{r} + x'\boldsymbol{\Omega})dx'.$$

Here V_π is the effective nuclear potential for pions and $\Lambda(\mathbf{r},\boldsymbol{\Omega})$, the distance from the point $\mathbf{r}$ to the boundary of a nucleus measured along the vector $\boldsymbol{\Omega}$.

3. Inclusive Cross-sections for Pion Production—Comparison with Experimental Data

Let us analyze experimental data on inclusive cross-sections for production of pions by protons on nuclei within the framework of the INC-model. Consider, first, the domain of initial energies in the vicinity (and below) the threshold for pion production in NN-collisions.

It has been already mentioned that, in the vicinity of the threshold, pions can be produced mainly in the first collision of an incident proton with an intranuclear nucleon. In this case, along with the standard subprocess

$$p + N \to N + N + \pi, \tag{55a}$$

which is taken into account in various versions of the INC-model, there exists a subprocess

$$p + N \to d + \pi, \tag{55b}$$

which plays a significant role in the vicinity of the threshold.[43] As the energy ϵ_0 decreases, the relative contribution of the deuteron channel (Subprocess 55b) to the pion production increases. This is a corollary of the different energy dependence of the cross-sections of the channels 55a and 55b in the vicinity of the threshold,[43] namely, $\sigma(pN \to d\pi) \sim \sqrt{\epsilon_0^2 - \epsilon_{thr}^2}$, whereas $\sigma(pN \to NN\pi) \sim (\epsilon_0 - \epsilon_{thr})^2$. Later on, a direct experimental indication to the contribution of the channel 55b has been obtained.[44] To be more specific, the analyzing power of the reaction $A(\mathbf{p},\pi^+)A'$ on light nuclei turned out to be similar to the analyzing power of the elementary

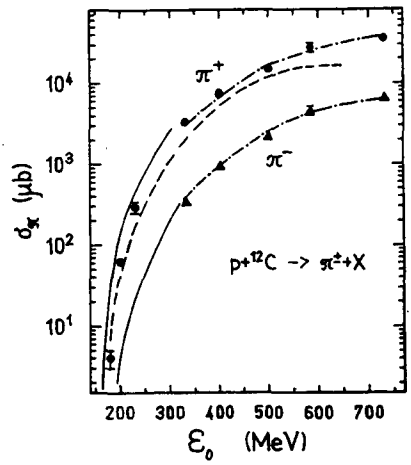

FIGURE 9. This indicates the total cross-section σ_π for production π^+ and π^--mesons on ^{12}C-nuclei as a function of the proton energy ϵ_0. The solid, the dashed, and the dash-dotted curve show σ_π calculated according to the INC-model with the use of weight functions,[43] to the BUU-equation[45] and to the INC-model with direct simulation,[46,47] respectively. The points show experimental[45] data for π^+(●) and π^-(▲).

reaction pp $\rightarrow$ dπ^+ in the vicinity of the threshold.

A specific feature of the near-threshold domain ($\epsilon_0 \lesssim 350$ MeV) is that here the cross-section of the pion production is a small fraction ($\lesssim 10^{-2}$) of the total cross-section of the reaction. In view of this fact, a method of direct Monte Carlo simulation of the INC which is used most often turns out to be rather ineffective in this domain. Therefore, a method of weight functions has been used[43] to calculate inclusive cross-sections for subthreshold pion production. Unlike the method of direct simulation, in any act of inelastic pA-interaction, only those events are considered in this method which are accompanied by the production of a pion in the first collision of an incident proton with an intranuclear nucleon of the momentum $\mathbf{p}_t$. Angular and energy characteristics of secondary nucleons and a pion produced are sampled in the same way as in the method of direct simulation, and the effect of the Pauli exclusion principle on the secondary nucleons is taken into account (see Section IIA, Chapter 2). A pion leaving a nucleus is remembered with the weight $w_\pi = \sigma^\pi_{NN}(\mathbf{p}_0,\mathbf{p}_t)/\sigma^{tot}_{NN}$, where σ^π_{NN} and σ^{tot}_{NN} are the cross-section for the pion production and the total cross-section for the NN-interaction, respectively.

Figure 9 shows the results of the INC-model calculations[43] of the energy dependence of total cross-section of pion production by protons on the ^{12}C nucleus for $\epsilon_0 \leqslant 350$ MeV. Using the method of weight functions, one can also calculate the cross-section of pion production down to the energies close to threshold value $\epsilon_0 \approx 150$ MeV for production on a nucleus. It is seen that these results slightly overestimate experimental data, whereas the results of the calculation[45] on the basis of numerical solution of the BUU-equation (in which the probability of production

of various particles on a nucleus is represented as a sum of probabilities of their production in all possible NN-collisions) considered in Chapter 1 by means of the test particle method, underestimate them. Both methods of calculation are indicative of the fact that it is not necessary to invoke the high-momentum component of the distribution of intranuclear nucleons for the description of the subthreshold production of pions, but it is sufficient to use the ordinary Fermi gas distribution. Owing to the Fermi motion of intranuclear nucleons, the production of pions at the energies ϵ_0, which are significantly smaller than the threshold value for pion production in the free NN-interaction, becomes possible. Figure 10 illustrates a high efficiency of the method of weight functions for the calculation not only of the total cross-section σ_π, but also of the double differential pion cross-sections. The INC-model describes satisfactorily experimental energy spectra of both π^+- and π^--mesons. It should be noted that, in this case, the cross-section for production of π^--mesons is smaller than that for production of π^+-mesons almost by an order of magnitude (see also Figure 9).

The domain of the energies higher than the threshold value (400 MeV $< \epsilon_0 <$ 1000 MeV) in which the cross-section of the pion production becomes comparatively large and varies only slightly with the energy ϵ_0 (see Figure 9) is studied in greater detail both theoretically and in experiments than the domain of subthreshold energies. Here the production of a pion in the NN-collision proceeds mainly through the formation and subsequent decay of the $\Delta(1232)$-isobar. In accordance with the hypothesis of isotopic invariance, one can show that the ratio $\sigma_{\pi^+}/\sigma_{\pi^-}$ of the cross-sections for production of π^+- and π^--mesons in pN-collisions is equal[38] to 11 (see also the relations 47 at N = Z). This is reflected partially in the data presented in Figures 9 and 10.

However, in the case of heavy nuclei, this ratio is significantly smaller and approximately equal to two.[38] This reflects the increasing role of the charge exchange between the pions and nucleons of these nuclei. Various modifications of the INC-model,[46,47,52] which take into account the process of formation and subsequent decay of the $\Delta(1232)$-isobar, are capable of describing the data on the production of pions by protons on nuclei to a reasonable accuracy (see Figure 9). Figure 11 shows the comparison of the results of the Monte Carlo (see Section IIA, Chapter 2) and the analytic[6] (according to the formula 54) calculation of the double differential distributions of π^+-mesons produced in the interaction of 585 MeV protons with the ^{64}Cu nuclei at an angle of 22.5° with experimental data.[53] It is seen that, on the whole, the double differential distributions of the produced pions which have been calculated by various methods agree satisfactorily with one another. The existing discrepancies can be explained by different descriptions of the elementary subprocess NN $\rightarrow$ NNπ and by the simplifications made in solving the system of KEs 33–37. Experimental data are in rather good agreement with the results of both calculations.

Figure 12 demonstrates the variation of the pion spectrum (at an angle of 90°) with increasing initial energy ϵ_0. It is seen, that as the energy ϵ_0 changes from 400 to 730 MeV, the cross-section at the maximum of the spectrum remains practically constant, but the spectrum itself becomes considerably more hard. On the whole,

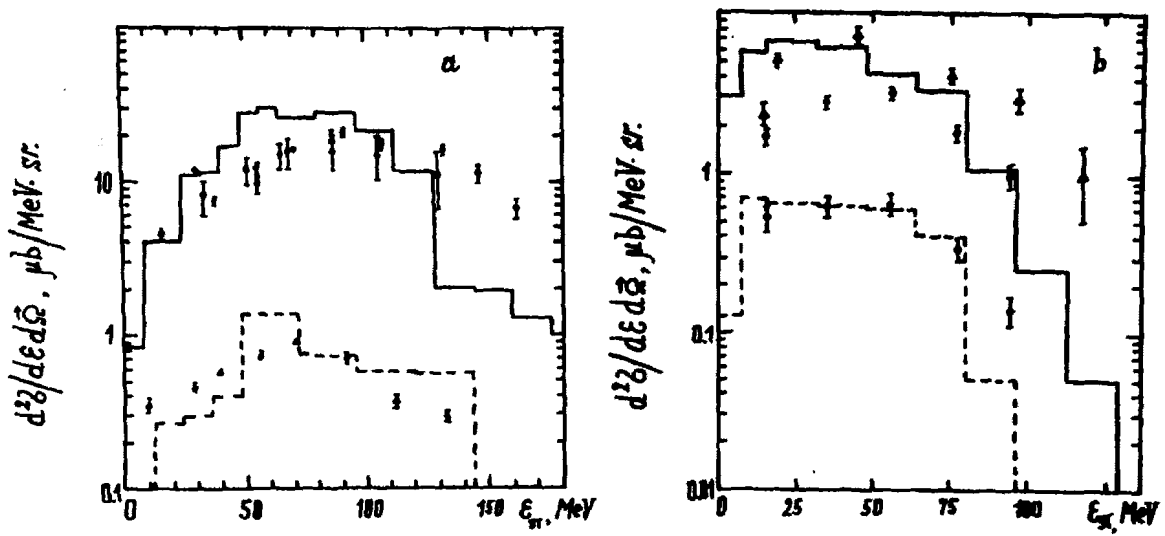

FIGURE 10. This charts the energy spectrum of π-mesons emitted at the angles of 0° (a) and 90° (b) as a result of the interaction of 350 MeV protons with ^{12}C-nuclei. The solid and the dashed histogram correspond to the calculation[43] for π^+- and π^--mesons, respectively. The points show experimental data borrowed from References 48-51.

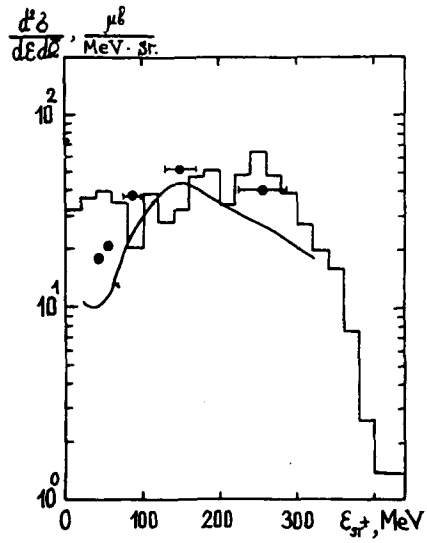

FIGURE 11. Here is the energy spectrum of π^+-mesons produced at an angle of 22.5° by 585 MeV protons on ^{64}Cu nuclei. The histogram and the curve show the results of the Monte Carlo calculation and that of the analytic calculation according to Equation 54 (for a uniform nucleus with R = 1.3 $A^{1/3}$ fm, μ^{tot} = 217.6 fm^2, $|V_N|$ = 36.85 MeV and V_π = 0; the cross-section of the charge exchange and that of pion absorption were borrowed from References 39 and 40, and the cross-section for production of π^+-mesons in pp-collisions from Reference 42). The points correspond to experimental data of Reference 53.

the calculation carried out within the framework of the INC-model and the analytic calculation[38] describe experimental[53-55] spectra to a good accuracy. However, in the domain of low pion energies ϵ_{π^+}, the spectrum calculated in accordance with the INC-model exceeds the experimental one. The experiment[53] has demonstrated that, in the domain of small ϵ_π, the spectrum of π^+-mesons differs significantly from that of π^--mesons, especially in the case of heavy T-nuclei. This is indicative of an importance of the role played by Coulomb interaction between a charged pion and a nucleus which is usually taken into account rather crudely in the INC-model. The INC-model encounters a number of serious problems in the description of the passage of pions produced through nuclear matter. This all calls for an introduction of the corresponding improvements into the INC-model. We shall consider these issues in Chapter 5, using the π A-interaction as an example in which these problems can be studied in a purer form.

B. PRODUCTION OF K$^+$-MESONS IN PROTON-NUCLEUS INTERACTIONS

In this section, we shall consider the production of K$^+$-mesons in pA-collisions at various energies. Interest in this problem has quickened in recent years in connection with projects of creating a new generation of high-current proton accelerators (kaon facilities) and of carrying out experiments on them. However, we shall first

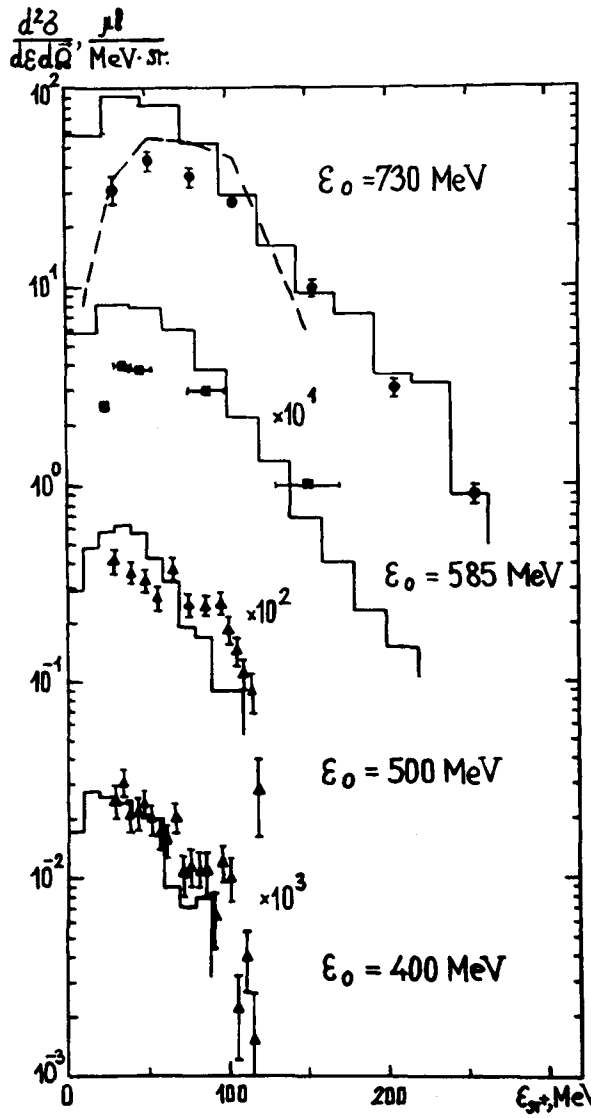

FIGURE 12. This represents the energy spectra of π^+-mesons produced at an angle of 90° by protons of various energies on ^{64}Cu nuclei. The histogram corresponds to the Monte Carlo calculation within the framework of the INC-model according to the code of Reference 3 and the dashed curve to the analytic calculation of Reference 38 for pions produced in collisions of a primary proton with intranuclear nucleons. The points show experimental data borrowed from References 53-55.

consider the problem of production of K^+-mesons in pp-collision, since it is an important elementary process in the INC-model which leads to the production of kaons in pA-collisions. This is caused by the fact that, unlike the case of pion production in NN-interaction which is studied and described in detail in the domain

of intermediate energies we are concerned with, the data on the production of K^+-mesons are rather scarce, even in pp-collisions.

1. Inclusive Cross-Sections for Production of K^+-Mesons in pp-Collisions

The total cross-section $\sigma_{pp\to K^+X}$ for production of K^+-mesons in pp-collisions was measured only for relatively low energies $\epsilon_0 \leqslant 7$ GeV of an incident proton. These measurements are not sufficiently reliable for $\epsilon_0 > 3$ GeV.[56-59]

The partial cross-sections for production of K^+-mesons in pp-collisions were measured for the reactions[56,60]

$$p + p \begin{array}{l} \nearrow N + \Lambda^0 + K^+ + n\pi, \\ \searrow N + \Sigma + K^+ + n\pi, \end{array} \qquad n = 0,1,2 \tag{56}$$

in the energy range $\epsilon_0 \leqslant 7$ GeV as well.

To correctly take into account the behavior of $\sigma_{pp\to K^+X}$ both in the vicinity of the threshold and at high energies, the following approximation has been proposed:[59]

$$\sigma_{pp\to K^+X}(s) = \sigma_1 F_1\left(\frac{s}{s_{min}}\right) + \sigma_2 F_2\left(\frac{s}{s_{min}}\right), \tag{57}$$

$$\begin{aligned} F_1(x) &= (1 + 1/\sqrt{x})\ln(x) - 4(1 - 1/\sqrt{x}), \\ F_2(x) &= 1 - (1/\sqrt{x})[1 + \ln(\sqrt{x})]. \end{aligned} \tag{58}$$

Here $\sigma_1 = (2.8 \pm 0.8)$mb, $\sigma_2 = (9.7 \pm 1.5)$mb, and $\sqrt{s_{min}} = m_p + m_{\Lambda^0} + m_K = 2.548$ GeV (m_p, m_{Λ^0} and m_K are the rest masses of a proton, Λ^0 -hyperon and K^+-meson, respectively, and s is the squared invariant energy). This approximation is characteristic of the multiperipheral models of the Regge type and has a correct behavior in the vicinity of the threshold ($\sigma_{pp\to K^+X}(s) \sim (s-s_{min})^2$ for $s \to s_{min}$). It has been shown[59] that all experimental data on the partial cross-sections of the reactions 56 are approximated to a satisfactory accuracy by simple expressions of the type

$$\sigma_{pp\to NYK^+n\pi}(\epsilon_0) = \frac{A_{NYn\pi}(\epsilon_0 - \epsilon_{NYn\pi})^2}{1 + B_{NYn\pi}(\epsilon_0 - \epsilon_{NYn\pi})^2}\ \mu b, \tag{59}$$

where the constants A,B, and ϵ are given in Table 1.

The invariant inclusive cross-section for production of K^+-mesons in pp-collisions at $\epsilon_0 \leq 3$ GeV takes into account principally three- and four-particle reactions of the type 56 at n = 0 and 1.[59,61] In the vicinity of the threshold, their matrix elements depend only slightly on the momenta of outgoing particles and, in the first approximation, are the functions only of s. Therefore, we can assume that

TABLE 1
Parameters in the Approximation of Partial Cross Sections for Production of K^+-Mesons in pp-Collisions

Reaction	$A_{NY\pi\pi}$	$B_{NY\pi\pi}$	$\epsilon_{NY\pi\pi}$
$p + p \to p + \Lambda^0 + K^+$	122,943	2,015	1,58
$p + p \to N + \Sigma + K^+$	104,026	1,006	1,78
$p + p \to N + \Lambda^0 + K^+ + \pi$	20,941	0,077	1,98
$p + p \to N + \Sigma + K^+ + \pi$	16,493	0,192	2,20
$p + p \to N + \Lambda^0 + K^+ + 2\pi$	2,385	0,001	2,39
$p + p \to N + \Sigma + K^+ + 2\pi$	4,893	0	2,60

the double differential distributions of outgoing kaons are simply proportional to the corresponding phase volumes for the NY- and the NYπ-systems. Then we can obtain the following expressions[59] for the invariant cross-sections for production of K^+-mesons in these reactions

$$p_K^0 \frac{d\sigma_{pp\to NYK^+}}{d\mathbf{p}_K} = \frac{\pi}{4} \frac{\sigma_{pp\to NYK^+}(\epsilon_0)}{I^{(3)}} \frac{\lambda(s_{YN},m_Y^2,m_N^2)}{s_{YN}} , \tag{60}$$

$$I^{(3)} = \left(\frac{\pi}{2}\right)^2 \int\limits_{(m_Y+m_N)^2}^{(\sqrt{s}-m_K)^2} \frac{\lambda(s_{YN},m_Y^2,m_N^2)}{S_{YN}} \frac{\lambda(s,s_{YN},m_K^2)}{s} ds_{YN} , \tag{61}$$

$$\lambda(x,y,z) = \sqrt{[x - (\sqrt{y} + \sqrt{z})^2][x - (\sqrt{y} - \sqrt{z})^2]} , \tag{62}$$

$$s_{YN} = s + m_K^2 - 2(p_p^0 + m_p)p_K^0 + 2p_0p_K \cos(\vartheta) \geqslant (m_Y + m_N)^2 ; \tag{63}$$

$$p_K^0 \frac{d\sigma_{pp\to NYK^+\pi}}{d\mathbf{p}_K} = \frac{1}{2}\left(\frac{\pi}{2}\right)^2 \frac{\sigma_{pp\to NYK^+\pi}(\epsilon_0)}{I^{(4)}} \int\limits_{(m_Y+m_N)^2}^{(\sqrt{s_{YN\pi}-m_\pi})^2} \times \frac{\lambda(s_{YN},m_N^2,m_Y^2)}{s_{YN}} \frac{\lambda(s_{YN\pi},s_{YN},m_\pi^2)}{s_{YN\pi}} ds_{YN} , \tag{64}$$

$$I^{(4)} = \left(\frac{\pi}{2}\right)^3 \int\limits_{(m_Y+m_N)^2}^{(\sqrt{s-m_\pi-m_K})^2} \frac{\lambda(s_{YN},m_N^2,m_Y^2)}{s_{YN}} \times \int\limits_{(\sqrt{s_{YN}+m_\pi})^2}^{s(\sqrt{s-m_K})^2} \frac{\lambda(s_{YN\pi},s_{YN},m_\pi^2)}{s_{YN\pi}} \cdot \frac{\lambda(s,s_{YN\pi},m_K^2)}{s} ds_{YN\pi} , \tag{65}$$

$$s_{YN\pi} = s + m_K^2 - 2(p_p^0 + m_p)\, p_K^0 + 2p_0p_K \cos(\vartheta) \geqslant (m_N + m_Y + m_\pi)^2 . \tag{66}$$

Here p_p^0, p_K^0 and $\mathbf{p}_0$, $\mathbf{p}_K$ are the total energies and momenta of the primary proton and kaon, respectively, in the l.s., $\cos(\vartheta) = \mathbf{p}_0\mathbf{p}_K/p_0\, p_k$ and m_N, m_Y and m_π are the rest masses of a nucleon, Y -hyperon ($\Sigma^{0,\pm}$ or Λ^0) and a pion, respectively. It is seen from Figure 13 that the results of calculations[59] of these cross-sections at $\epsilon_0 = 2.54$, 2.88, and 3.03 GeV at various angles in the l.s. carried out in accordance with the formulas 60-66 agree with experimental data[61] reasonably well. Taking account of the contribution from the reactions with production of one pion improves this agreement significantly at $\epsilon_0 = 2.88$ and 3.03 GeV.

An expression for $p_K^0\, d\sigma_{pp\to K^+X}/d\mathbf{p}_K$ has been proposed[59] in the form which is reduced to Equation 60 for $s \to s_{min}$ and has the scaling nature for $s \to \infty$ (i.e., it is the function of three variables s, $p_\perp$, and x_R[62]):

$$p_K^0 \frac{d\sigma_{pp\to K+X}}{d\mathbf{p}_K} = f(s,p_\perp,x_R) , \tag{67}$$

$$x_R = \overset{*}{p}{}_K^0/(\overset{*}{p}{}_K^0)_{max} = \frac{2(p_p^0 + m_p)\, p_K^0 - 2p_0p_K \cos(\vartheta)}{s - (m_p + m_{\Lambda_0})^2 + m_K^2} . \tag{68}$$

Here $p_\perp$ is the transverse momentum of the K^+-meson, $\overset{*}{p}{}_K^0$ and $(\overset{*}{p}{}_K^0)_{max}$ are its total energy in c.m.s. and its maximum possible value, and the function f is chosen in the form

$$f(s,p_\perp,x_R) = B(s)(1 - x_R)^{n(s)} \exp[b - \sqrt{b^2 + c^2(s)\, p_\perp^2}] , \tag{69}$$

$$B(s) = \left[200 + 2600 \frac{7{,}66\, x^{2.9}}{1 + 6{,}66\, x^{2.9}}\right] \frac{\text{GeV} \cdot \mu\text{b}}{(\text{GeV}/c)^3\text{sr}} ;$$

$$n(s) = 0.5 + 2.25\, x,\ b^2 = 3,\ c^2(s) = 21x^2; \tag{70}$$

$$x = w_1/(0{,}075 + w_1),\ w_1 = (\sqrt{s/s_{min}} - 1)^2 .$$

Comparison of the results of the calculations[59] of double differential cross-sections for production of K^+-mesons in pp-collisions which were carried out according to these formulas with experimental data for 2.54 GeV $\leq \epsilon_0 \leq$ 1500 GeV has demonstrated (see, e.g., Figure 14) that a reasonably good agreement of the calculations with experimental data is observed over a wide range of energies of incident protons for $p_\perp \lesssim 1.5$ GeV/c. This allows one to hope that the expressions 67-70 are applicable practically for all energies.

2. Production of K^+-Mesons in Proton-Nucleus Collisions at Various Energies

Knowing the cross-section for production of kaons in NN-collisions, we can calculate this cross-section in NA-collisions within the framework of the INC-model

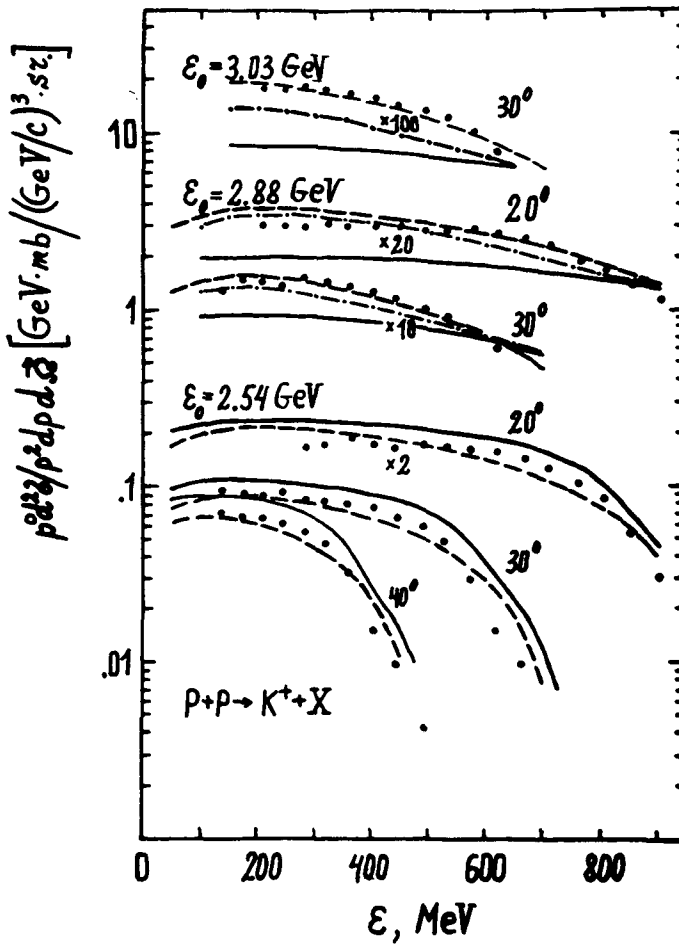

FIGURE 13. This represents the dependence of the inclusive invariant cross-sections for the production of K^+-mesons on their kinetic energy ϵ in the pp-collisions at different primary-proton energies ϵ_0 and at different angles (indicated by the numbers near the curves) in the l.s. The experimental data are taken from Reference 61. The curves are the calculation[59] by Equations 60-70: the solid curves correspond to the calculation using the model of the phase volume with the inclusion of three-particle channels (n = 0), the dash-dotted curves to the same with the inclusion of four-particle channels as well (n = 0 and 1), and the dashed curves to the calculation by Equations 67-70.

(and vice versa, experimental information on pA-collisions can be used to refine upon the models of kaon production in pp-collisions). If we confine ourselves to the domain of intermediate energies, the necessity does not even arise of modifying the system of KEs 33-37 describing the nucleon-pion cascade, since the cross-sections for the processes of production of strange particles are relatively small in this domain of energies, and taking account of these processes affects only slightly the distribution functions of nucleons and pions. Therefore, the system of KEs describing intranuclear cascade with allowance for kaon production includes, in

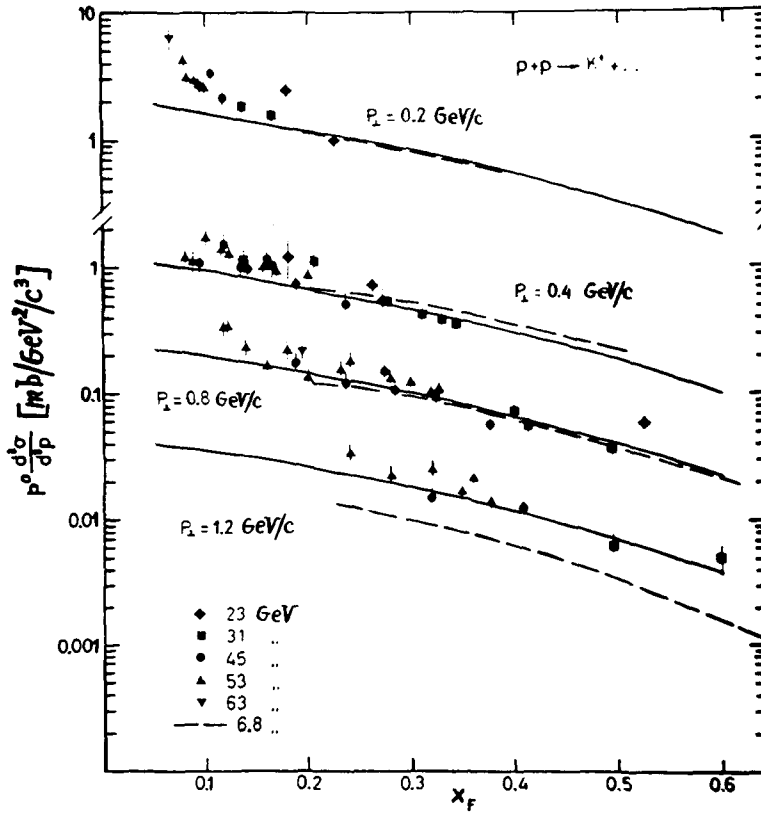

FIGURE 14. Here are inclusive invariant cross-sections for the production of K^+-mesons in the pp-interactions at different collision energies $\sqrt{s}$ (indicated by the numbers in the figure) as functions of $x_F = 2\overset{*}{p}_\pi/\sqrt{s}$ ($\overset{*}{p}_\pi$ is the longitudinal momentum of a K^+-meson in the c.m.s.) at fixed values of their transverse momentum $p_\perp$. The experimental data are taken from Reference 63. The solid curves are the calculations[59] by Equations 67-70 at $\sqrt{s}$ = 53 GeV.

addition to Equations 33-37, only the system of KEs which describes the transport of kaons in a nucleus and which is similar to Equation 34 for pions. The convolutions of the distribution functions of nucleons and pions with inclusive double differential distributions of kaons produced in the corresponding collisions (the quantities similar to the functions $K^{in}_{\alpha'\to j}$ defined by Equation 46) are the "sources" (analogous to the quantities Q_j defined by Equation 36) in the latter system of KEs.

Since this system of equations is rather cumbersome, we shall not write it down, especially as it is possible to obtain an approximate estimate of double differential cross-sections for production of K^+-mesons in pA-collisions for not very heavy nuclei without solving this system of equations. The matter is that kaons produced in the first inelastic pN-interaction in a nucleus represent a noticeable fraction of

kaons formed in such collisions. The inclusive cross-section of such a process can be written approximately in the form[59]*

$$p_k^0 \frac{d\sigma_{pA\to K+X}}{d\mathbf{p}_K} = I_V \int d\mathbf{p}_t\, g(\mathbf{p}_t) \left[p_K^0 \frac{d\sigma_{pp\to K+X}(\sqrt{s})}{d\mathbf{p}_K} \right], \tag{71}$$

$$I_V = A \int \rho(\mathbf{r})d\mathbf{r} \exp\left[-\mu(p_0) \int_{-\infty}^{0} \rho(\mathbf{r} + x'\boldsymbol{\Omega}_0)\, dx' - \mu(p_K) \int_0^{\infty} \rho(\mathbf{r} + x'\boldsymbol{\Omega})\, dx' \right]; \tag{72}$$

$$\begin{aligned} \mu(p_0) &= \sigma_{pp}^{in}(p_0)Z + \sigma_{pn}^{in}(p_0)N, \\ \mu(p_K) &= \sigma_{K^+p}^{tot}(p_K)Z + \sigma_{K^+n}^{tot}(p_K)N\,. \end{aligned} \tag{73}$$

Here $g(\mathbf{p}_t)$ is the momentum distribution of nucleons in a T-nucleus normalized to unity, σ_{pp}^{in} (σ_{pn}^{in}) the free cross-section of an inelastic pp(pn)-interaction, $\sigma_{K^+p}^{tot}$ ($\sigma_{K^+n}^{tot}$) the total free cross-section of K^+p (K^+n)-interaction, $\boldsymbol{\Omega}_0 = \mathbf{p}_0/p_0$ and $\boldsymbol{\Omega} = \mathbf{p}_K/p_K$. It is assumed in the latter expressions that the cross-sections for production of a K^+-meson in a pp- and a pn-collision are equal to one another.[64]

In the case when $\mu(p_0)$ and $\mu(p_K)$ are close to one another, $\boldsymbol{\Omega}$ is close to $\boldsymbol{\Omega}_0$, and the nuclear density is represented by a Gaussian ($\rho(\mathbf{r}) = (b_0/\pi)^{3/2} \exp(-b_0 r^2)$), we obtain approximately[59]

$$I_V = A(1 - e^{-x_G})/x_G, \quad x_G = [\mu(p_0) + \mu(p_K)]\, b_0/2\pi\,. \tag{74}$$

In the case of a nucleus of a radius R with a uniform density, the integral 72 is calculated exactly and given by the expression

$$I_V = AI^{(q)}(0°)\,. \tag{75}$$

Here the quantity $I^{(q)}(0°)$ is determined by Equation 18, Chapter 2, in which one must set

$$a_1 = 3\mu(p_K)/2\pi R^2, \quad a_2 = 3\mu(p_0)/2\pi R^2\,. \tag{76}$$

Since the nucleus reveals an increased transparency for fast secondary particles because of a finite time of their formation (see Chapters 1 and 2), it is of interest

* The formula 54 for inclusive cross-section for production of pions on a nucleus assumes a similar form, if we neglect the possibility of the charge exchange reactions involving pions and intranuclear nucleons.

to consider the integral 72 in the limiting case $\sigma^{tot}_{K^+p(K^+n)} = 0$. In this case, we readily obtain[59]

$$I_V = \frac{\pi A}{\mu(p_0)} \int_0^{\infty} db_\perp^2 \left\{ 1 - \exp\left[-\mu(p_0) \int_{-\infty}^{+\infty} \rho\left(\sqrt{b_\perp^2 + t^2}\right) dt \right] \right\} . \quad (77)$$

In particular, for the Gaussian nuclear density we get

$$I_V = \frac{A}{\tilde{x}_G} \int_0^1 \frac{dt}{t} (1 - e^{-\tilde{x}_G t}), \quad \tilde{x}_G = \mu(p_0) b_0 / \pi , \quad (78)$$

whereas for a nucleus with a uniform density we must set $a_1 = 0$ in Equation 75.

The results of the calculations[59] of double differential cross-sections for production of K^+-mesons by protons on Be nuclei carried out in accordance with the formulas 67-74 and 78 are compared with experimental data[65,66] in Figures 15 and 16. Figure 15 corresponds to protons with the momenta 18.8 GeV/c (the dashed curve) and 23.1 GeV/c (the solid curve) at the angles 0 and 5.7° and Figure 16 to $p_0 = 400$ GeV/c for K^+-mesons with $p_\perp = 0$ and 0.5 GeV/c, respectively, for $\sigma^{tot}_{K^+p(K^+n)} \neq 0$ (the solid curve) and $\sigma^{tot}_{K^+p(K^+n)} = 0$ (the dashed curve). It is seen that, on the whole, the calculations agree with experimental data reasonably well, although there is a slight discrepancy in the softest part of the spectra. This discrepancy is apparently associated with the rescattering of kaons in nuclear matter (which is disregarded in the derivation of the expression 71).

Rigorously speaking, the calculation of production of kaons on heavy nuclei calls for taking account of a number of additional factors. They include, in particular, rescattering of a nucleon in nucleus before the act of production of a kaon and a rescattering of a kaon. However, it follows[67,68] that experimental data on the cross-section for production of kaons on heavy nuclei (at least for $\epsilon_0 = 24$-400 GeV and $p_\perp \lesssim 0.5$ GeV/c) are approximately described by the dependence similar to Equation 71, where

$$I_V(A) = \left(\frac{A}{A_{Be}}\right)^{\alpha(x_F)} I_V(Be),$$
$$\alpha(x_F) = 0.82 - 0.63\, x_F + \frac{x_F}{|x_F|} 0.26\, x_F^2, \quad x_F = \frac{\overset{*}{p}_{\parallel}}{(\overset{*}{p}_{\parallel})_{max}} . \quad (79)$$

This is clearly illustrated in Figure 17 which also shows the results of the Monte Carlo calculation[69] and is carried out within the framework of the model of independent quark-gluon strings.[70] In this model, the system of relativistic KEs of the type 56, Chapter 1, describing the hadron-nucleus interaction in which strings are

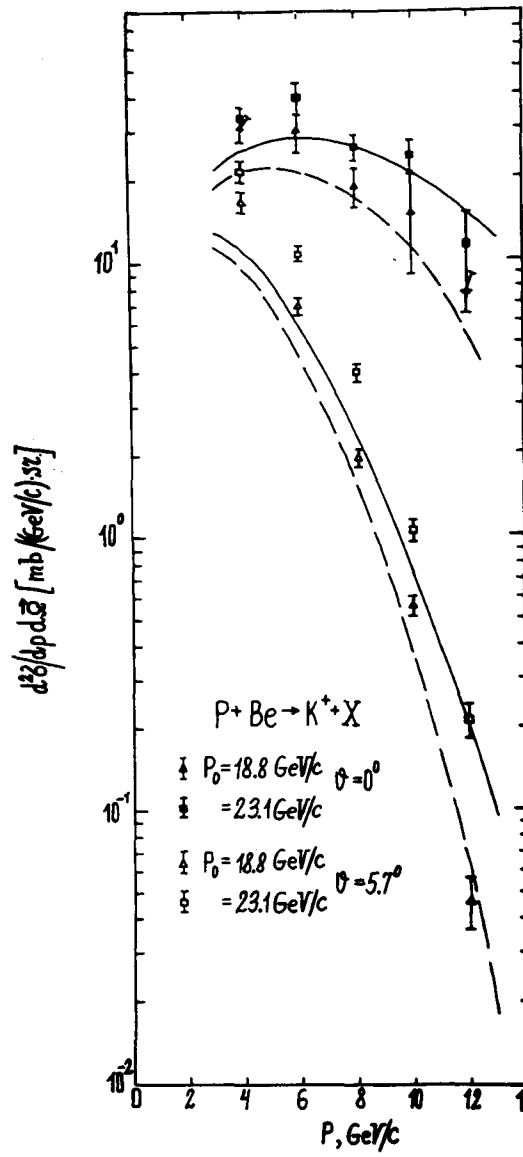

FIGURE 15. This graphs the double differential cross-sections for production of K^+-mesons at angles of 0 and 5.7° in the interaction of protons of momenta 18.8 GeV/*c* and 23.1 GeV/*c* with Be nuclei as functions of the K^+-meson momentum.

produced, is solved by the Monte Carlo technique with allowance for a finite time of hadron production. It is seen from this figure that the calculations agree well with experimental data.

Thus, the INC-model and, in particular the closed analytic formulas for inclusive cross-sections of production of K^+-mesons in pA-collisions, which were considered above, describe satisfactorily experimental data over a wide range of energies of

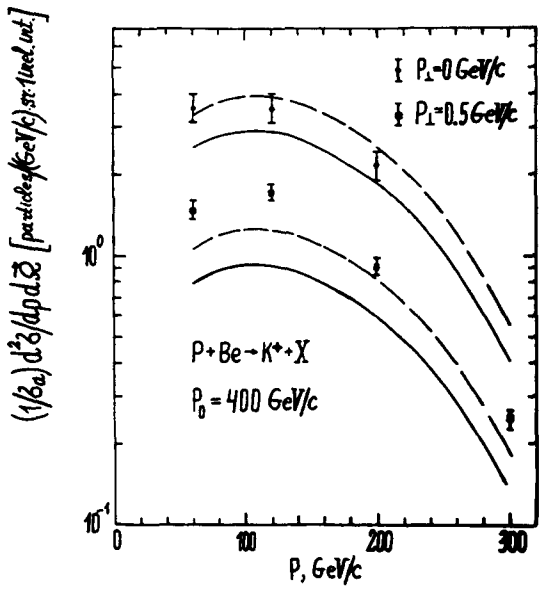

FIGURE 16. This presents the double differential cross-sections for production of K^+-mesons per proton interacting with Be nuclei for p_o = 400 GeV/c and at $p_\perp$ = 0 and 0.5 GeV/c as functions of the K^+-meson momentum.

primary protons. Therefore, it can be believed that predictions about cross-sections obtained with their help are sufficiently reliable. As an example of such a prediction, Figure 18 shows invariant cross-sections for production of K^+-mesons at zero angle by protons with the energy 30 and 3000 GeV on nuclei of Be and Pb as functions of the kaon momentum p_K. It is seen that, in this domain of energies ϵ_0, the yield of kaons with $p_K < 10$ GeV/c varies only slightly with ϵ_0. In experiments scheduled on kaon facilities, this domain of kaon momenta seems most interesting. This justifies the choice of the energy $\epsilon_0 \lesssim 50$ GeV as an optimum energy of a primary beam of protons of kaon facilities under the condition of a high intensity of this beam.

Finally, let us discuss briefly first results on the subthreshold production of K^+-mesons in pA-interactions which have appeared in the recent years.

In Reference 64 the total cross-sections for production of K^+-mesons in pA-collisions in the range of proton energies 800-1000 MeV were measured for different T-nuclei. Theoretical analysis based both on the INC-model[64] and on a simple analytic model[71] of kaon production in two channels of the reactions: $pN \to K^+ \Lambda^0 N$ and $pN \to \pi NN$, $\pi N \to K^+ \Lambda^0$ shows that the mechanism associated with the production of kaons by intermediate pions allows one to account for the observed values of the cross-sections and does not call for taking account of the high-momentum component in the distribution function of intranuclear nucleons. A similar conclusion can be drawn from the analysis of the production of pions and antiprotons (see next section) and of the subthreshold production of η-mesons (see

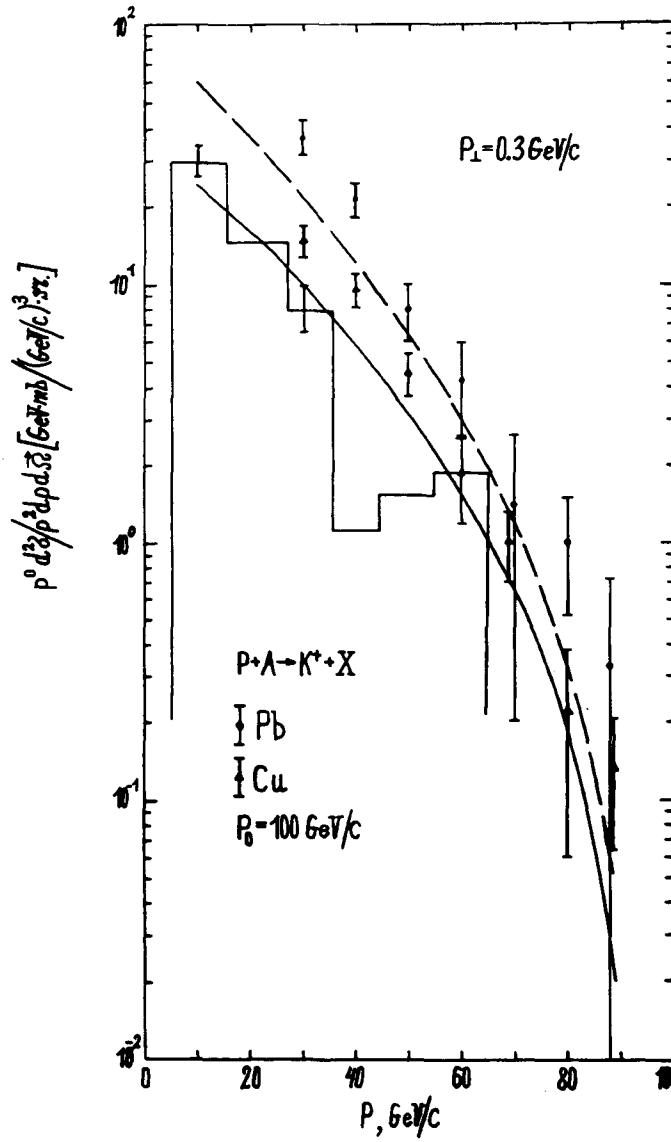

FIGURE 17. This graphs the dependence of the inclusive invariant cross-sections for production of K^+-mesons in collisions of protons with p_0 = 100 GeV/*c* with Cu and Pb nuclei on their momentum at $p_\perp$ = 0.3 GeV/*c*. The experimental data are taken from Reference 67. The solid and the dashed curves are the calculation[59] by Equations 67-74, and 79, respectively, for Cu and Pb nuclei. The histogram corresponds to the calculation[69] by the Monte Carlo method within the framework of the independent quark-gluon strings model[70] for Cu nuclei.

Chapter 6). To achieve a better comprehension of the phenomenon of the sub-threshold kaon production in pA-interactions, it is obviously necessary to obtain more detailed experimental data, in particular, double differential cross-sections for their production in these interactions.

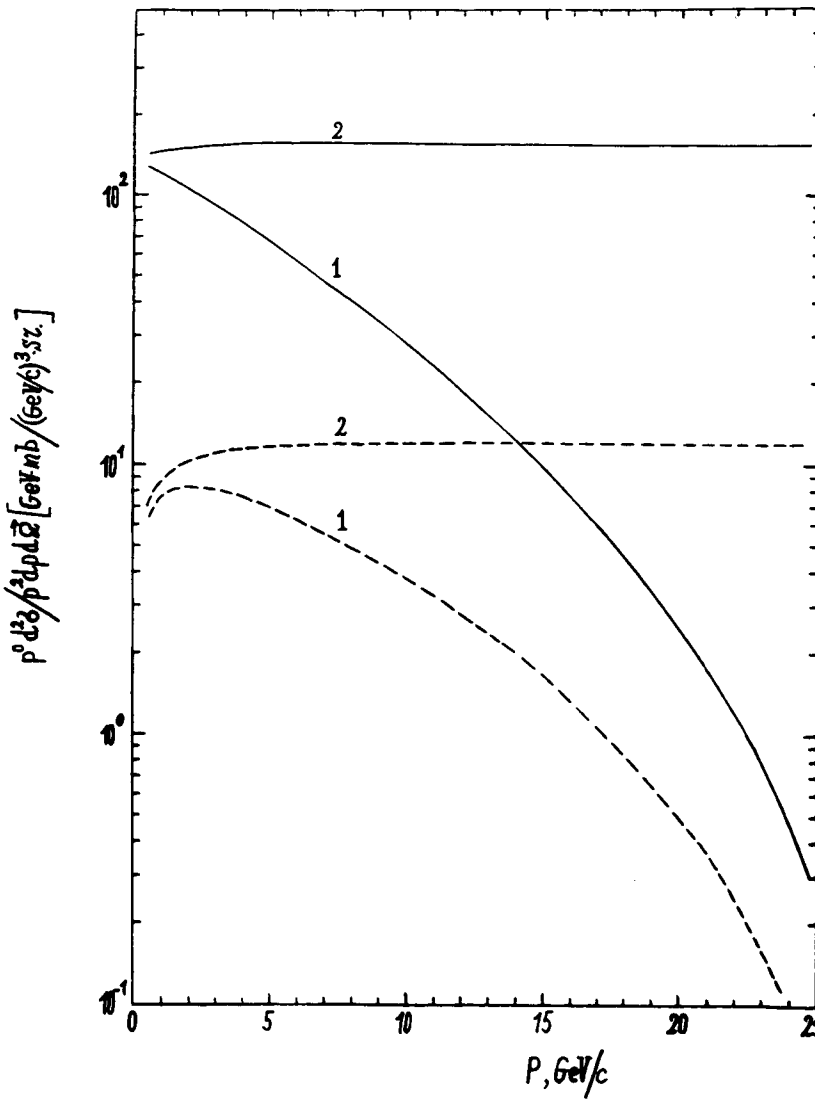

FIGURE 18. This figure traces the inclusive invariant cross-sections for production of K^+-mesons at a zero angle by 30 GeV(1) and 3000 GeV(2) protons on Be (the dashed curves) and Pb (the solid curves) nuclei as functions of the kaon momentum. The data shown in this figure were calculated[59] by Equations 67-74 and 79.

C. PRODUCTION OF ANTIPROTONS IN PROTON-NUCLEUS INTERACTIONS

Let us now consider production of antiprotons in pA-collisions at the energies of primary protons of about several GeV, i.e., below threshold or near it* (recall

* In this energy range, as well as in the cases of the near-threshold production of particles considered above, only the contribution of the first inelastic collision of an incident proton with an intranuclear nucleon is significant, and it is not necessary to solve the system of cascade KEs.

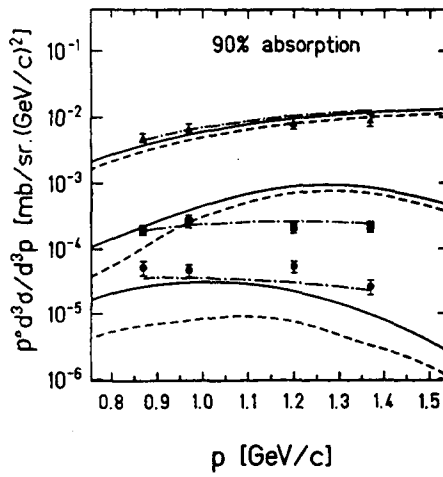

FIGURE 19. This graphs the invariant cross-section for antiproton production in the reaction p + ^{63}Cu at $\vartheta = 0°$ as a function of the antiproton momentum in the l.s. The experimental data[73,76] correspond to bombarding energies of 4.0 GeV (circles), 4.55 GeV (squares), and 6.1 GeV (triangles). The dash-dotted curve corresponds to a calculation[73] with allowance for the antiproton production in direct pN-collisions with the use of momentum distribution 82 of intranuclear nucleons. The dashed and the solid curve show the results of a calculation[77] on the basis of the BUU-equation with allowance for the antiproton production in NN- and BB-collisions (B = N, Δ(1232) and N*(1440)), respectively.

that the threshold energy ϵ_{thr} of their production in free NN-collisions in the l.s. is approximately equal to 5.6 GeV). The study of the subthreshold production of particles which is accompanied by a large transfer of momentum is of importance for the gain of information on the intranuclear structure for small relative internucleon distances or on the high-momentum component in the momentum distribution of intranuclear nucleons.[72,73] It is obvious that the heavier the particles produced, the larger the intranuclear momenta, and hence the smaller internucleon distances play a significant role in their production. It has been already mentioned that such experiments were carried out with the production of both pions and kaons. However, in view of the above discussion, the subthreshold production of antiprotons is of paramount importance. There is a number of data[74-76] on this process nowadays. Among them, data[76] on the production of antiprotons by protons on the Cu nucleus in the interval of initial energies 2.88-6.1 GeV are most complete. They are partially presented in Figure 19. The same figure shows (the dash-dotted curve) the results of the calculation[73] of the cross-section for the production of antiprotons in direct pN-collisions carried out in accordance with the following formula (compare it with the expression 71 for the cross-section of the production of K^+-mesons in pA-collisions):

$$p^0_{\bar{p}} \frac{d\sigma_{pA\to\bar{p}X}}{d\mathbf{p}_{\bar{p}}} = \int d\mathbf{p}_t g(\mathbf{p}_t) \left[p^0_{\bar{p}} \frac{d\sigma_{pN\to\bar{p}ppN}(\sqrt{s})}{d\mathbf{p}_{\bar{p}}} \right] . \tag{80}$$

The invariant cross-section $p_{\bar{p}}^0\, d\sigma_{pN\to\bar{p}ppN}/d\mathbf{p}_{\bar{p}}$ for production of antiprotons in an elementary reaction

$$p + N \to \bar{p} + p + p + N \tag{81}$$

was calculated within the framework of the model of four-particle relativistic phase volume under the assumption that its matrix element (a free parameter) is constant. The momentum distribution $g(\mathbf{p}_t)$ of intranuclear nucleons takes into account the contribution from the high-momentum component and is chosen in the form (compare with Equation 17, Chapter 1 and Equation 36, Chapter 2)

$$g(\mathbf{p}_t) = \frac{1}{(2\pi)^{3/2}(1+\delta)}\left[\frac{e^{-p_t^2/2\sigma_{1,t}^2}}{\sigma_{1,t}^3} + \delta\,\frac{e^{-p_t^2/2\sigma_{2,t}^2}}{\sigma_{2,t}^3}\right], \tag{82}$$

where $\sigma_{1,t} = 0.115$ GeV/c, $\sigma_{2,t} = 0.230$ GeV/c and the parameter δ which determines the contribution of the high-momentum component is chosen to be 0.06 for the ^{12}C nucleus and proportional to $A^{1/3}$ for other T-nuclei (0.102 for ^{63}Cu). The values of $\sigma_{1,t}$ and $\sigma_{2,t}$, δ have been found from independent experiments. It is seen that the results of the calculation agree well with experimental data over a wide range of initial energies*. However, a similar approach to the description of the antiproton production in the reactions $^{28}Si + {}^{28}Si$ and $^{12}C + {}^{63}Cu$ at the energies 1.65, 2.0, and 3.65 GeV/nucleon with the matrix element obtained from the condition of the best fit to the data on the reaction $p + {}^{63}Cu \to \bar{p} + X$ gives the calculated values of the cross-sections which are smaller than experimental values by several orders of magnitude. Therefore, these experimental data on the production of antiprotons were analyzed within the framework of a different approach.[77] It was assumed in this paper that antiprotons are produced in an elementary reaction of the type

$$B + B \to \bar{p} + p + N + N\,, \tag{83}$$

where $B \equiv N$, and $\Delta(1232)$ and $N^*(1440)$ are the resonances. The evolution of the single-particle phase functions of pions and baryons (B) in the course of the reaction was determined by means of a numerical solution of the corresponding BUU-equations under the assumption that the nuclear potential for Δ and N^* is the same as for nucleons and equal to zero for pions. It was assumed as well as in the calculation of Reference 73 that the invariant inclusive cross-section for production of antiprotons in the reaction 83 is proportional to the relativistic phase volume for the pNN-system and normalized to the total cross-section $\sigma_{pp\to\bar{p}X}$ of the inclusive process $p + p \to \bar{p} + X$, which is approximated by the expression of the form

$$\sigma_{pp\to\bar{p}X}(\sqrt{s}) = 0.01\,(\sqrt{s} - 3.7532\ \text{GeV})^{1.846}\,\text{mb}\,. \tag{84}$$

* It should be noted that data[64] on the subthreshold production of K^+-mesons in pCu-collisions are described to a good accuracy within the framework of the same approach.

The cross-section for production of antiprotons on a nucleus is found by summing the cross-sections of their production in all possible individual BB-collisions.

Absorption of antiprotons formed in nuclear matter is approximately estimated from the data on the cross-section of the $\bar{p}p$-annihilation and set to be equal to 90% in the calculations for the reaction $p + {}^{63}Cu$. Figure 19 shows the results of these calculations without and with allowance for the production of resonances. The dashed curve of this figure corresponds to the former case and the solid curve to the latter one. It is seen that for the energy 6.1 GeV the calculation (which does not take into account the high-momentum component in $g(\mathbf{p}_t)$) describes the experimental data to a reasonably good accuracy as well, the relative contribution of nucleon resonances to the cross-section being increased with decreasing initial energy. The results of the calculation[77] of the cross-section for production of antiprotons in the reaction ${}^{28}Si + {}^{28}Si$ at the energy 2.1 GeV/nucleon without allowance for their absorption in nuclear matter agree with experimental data only by order of magnitude. It should also be noted that the results of the calculation[77] turn out to be extremely sensitive to the form used to extrapolate the elementary cross-section 84 in the vicinity of the threshold energy.

Finally, notice that an analysis[72] of these data on the subthreshold production of antiprotons on the ${}^{63}Cu$ nucleus carried out on the basis of the expressions of the types of 71 and 82 under the assumption that they are produced both in direct processes of the type $pN \rightarrow \bar{p}ppN$ and in the interaction of intermediate pions with intranuclear nucleons (such as $pN \rightarrow \pi X$ and $\pi N \rightarrow \bar{p}pN$) is indicative of the fact that the fraction of the high-momentum component in the momentum distribution of intranuclear nucleons is several times smaller than that necessary for the explanation of spectra of nucleons diverging at large angles. Thus, the results of the analysis[72,77] apparently count in favor of the fact that a large contribution of the high-momentum component to the momentum distribution of intranuclear nucleons is not necessary for the description of the subthreshold production of antiprotons in pA-interactions as well.

Nonlocal processes (multiple interactions of particles and resonances formed in first acts of the interaction with other intranuclear nucleons) are an important source of their production. It is most likely that a large fraction of this component only imitates these processes. To verify further this conclusion and to achieve a better comprehension of the phenomenon of subthreshold production of antiprotons in pA-collisions, it is necessary

1) to measure the cross-sections for production of antiprotons in the elementary processes $pN \rightarrow \bar{p}ppN$ and $\pi N \rightarrow \bar{p}pN$ in the near-threshold domain (since their relative contribution essentially depends on the values of the cross-sections in this energy range)
2) to obtain new experimental data on the subthreshold production of antiprotons in these collisions (in particular, on the A-dependence* of the cross-sections for their production)

* Such experiments are now in progress.[75]

3) to carry out a more thorough analysis of the interaction of antiprotons produced with nuclear matter.

It is expedient to study the latter problem in a more pure form using the $\bar{p}A$-interaction as an example. This interaction will be considered in detail in Chapter 6.

IV. TRAWLING EFFECT

A. MANIFESTATION OF THE TRAWLING EFFECT IN pA-INTERACTION

For the proton energies $\epsilon_0 \lesssim 1$ GeV, the INC-model agrees well with experimental data, and its various versions agree with one another[78] and with analytic calculations based on KEs. However, in the energy range $\epsilon_0 > 3$-5 GeV, the INC-model reveals noticeable discrepancies with experimental data which increase rapidly with increasing ϵ_0.[13] These discrepancies are manifested, above all, in the characteristics of the low-energy secondaries.

Let us consider data obtained in photoemulsion experiments as an example. In these experiments, secondary particles are classified according to the value of the ionization produced by them. The following particles are distinguished in this classification:

- s (shower)-particles ($\pi^{\pm}$-mesons with the energy $\epsilon_\pi > 80$ MeV and protons with the energy $\epsilon_p > 500$ MeV);
- g(grey)-particles ($\pi^{\pm}$-mesons with $15 \leq \epsilon_\pi \leq 80$ MeV and protons with $30 \leq \epsilon_p \leq 500$ MeV);
- b (black)-particles ($\pi^{\pm}$-mesons with $\epsilon_\pi < 15$ MeV, protons with $\epsilon_p < 30$ MeV and lightest nuclei d,t,α etc.);
- h (heavy)-particles which comprise both, g- and b- particles.

In addition to methodological meaning, such a classification also has a physical meaning. The s-particles provide information on collisions of fast particles with intranuclear nucleons and, above all, on pions produced. The g-particles are mainly the recoil protons. Their number characterizes the total number of collisions which take place inside a nucleus. The b-particles are associated with the process of de-excitation of an R-nucleus and contain information on its characteristics.

Figure 20 shows the energy dependence of the average numbers of s-, g-, and h-particles produced in the interaction of protons with nuclei of photoemulsion and the results of the calculations carried out within the framework of the standard INC-model. It is seen that the theoretical values of the average multiplicities $\bar{n}_g$ and $\bar{n}^h$ in the pA-reaction agree well with experimental data for $\epsilon_0 \lesssim 1$ GeV, but do not show the "saturation" at $\epsilon_0 \gtrsim 3$-5 GeV observed in experiments. On the other hand, the calculated values of $\bar{n}_s$ remain close to experimental ones up to the energies $\epsilon_0 \simeq 20$ GeV. Barashenkov et al.[89] have related such a change in the energy dependence of $\bar{n}_g$ and $\bar{n}^h$ to the manifestation of the nuclear trawling effect (see Section IIB, Chapter 2). A high energy component of the INC knocks nucleons out of a nucleus, and as a result, a low-energy component of cascade particles

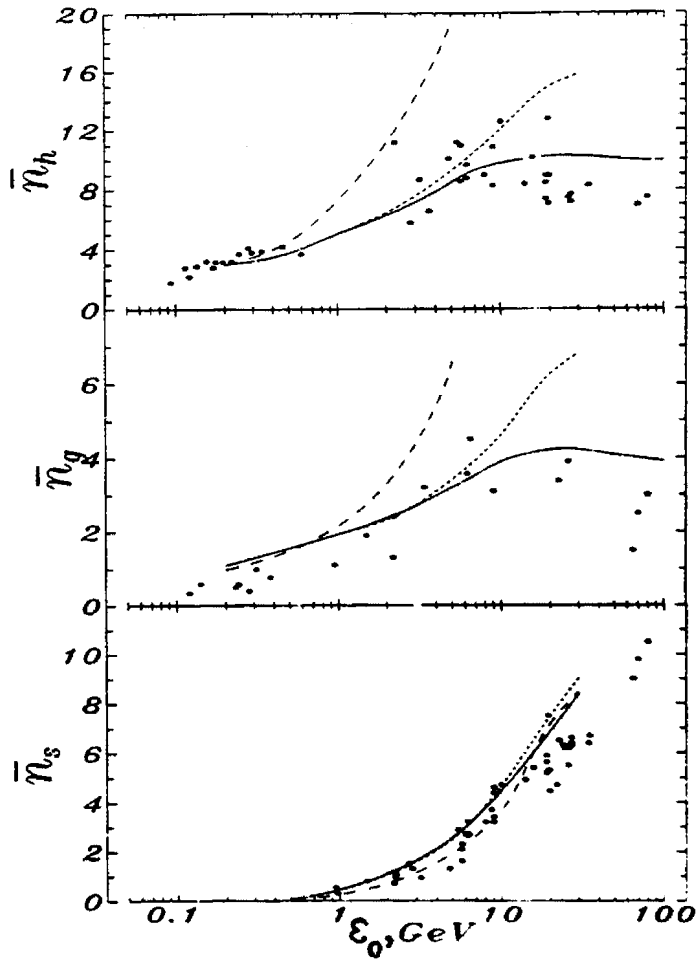

FIGURE 20. This is the energy dependence of the average multiplicity of g-, h-, and s-particles emitted in the interaction of protons with nuclei of photoemulsion. The points show experimental data.[4,79] The dashed, the dotted, and the solid curve show the results of the calculations[79,80] carried out within the framework of the INC-model and the INCT-model without and with regard for the process in which intranuclear nucleons leave the nucleus, respectively. The calculations are carried out under the condition that $n_b > 1$.

encounters nuclear matter of lower density on its way. Hence, the number of collisions of cascade particles with intranuclear nucleons decreases (i.e., the number of g-particles decreases) and the excitation energy of an R-nucleus decreases, too (i.e., the number of the evaporating b-particles decreases). Indeed, the INCT-model constructed in Reference 82 reproduces correctly the saturation of the energy dependence of $\bar{n}_g$ and $\bar{n}_h$ in the domain of high energies $\epsilon_0 \gtrsim 5$ GeV(see Figure 20).

The standard INC-model differs from the INCT-model in two main aspects. First, the INC-model considers nuclear matter as a continuous uniform medium, whereas the INCT-model treats it as a discrete medium consisting of a set of

scattering nucleon centers (see Chapter 2). Hence, these models reveal maximum distinction from one another in the description of the transport of those cascade particles in nuclear matter which have an anomalously large cross-section of the interaction with a nucleon, e.g., of pions with the energy in the vicinity of the (3,3)-resonance. In the INC-model, a number of collisions experienced by such particles in a nucleus is considerably larger than that in the INCT-model.

Secondly, unlike the INC-model, the INCT model takes into account the effect of trawling of a nucleus by fast particles. To elucidate the influence exerted by different description of pion transport in a nucleus and by the trawling effect on the observed characteristics of NRs, Golubeva et al.[80] have carried out calculations within the framework of the INCT-model which take into account the fact that nucleon centers may come out of a play in the development of the INC, and calculations without allowance for such a process, i.e., when an intranuclear nucleon remains on its place after a collision with a cascade particle. It is seen from Figure 20 that the trawling effect is manifested in full measure in the energy range $\epsilon_0 \gtrsim 5$ GeV and that the saturation of $\bar{n}_g$ and $\bar{n}_h$ is a corollary of this effect. Moreover, owing to a weaker absorption of pions in a nucleus, there is an additional decrease in the number of collisions of cascade particles with nucleons in the INCT-model. As a result, the number of nucleons knocked out of a nucleus and the excitation energy of an R-nucleus decrease as well, and this effect turns out to be principal in the energy range 1 GeV $\lesssim \epsilon_0 \lesssim$ 5 GeV.

It has been shown[13,82] that the effects in question are even more pronounced in the correlations of particles emitted in a reaction, and above all, in the dependences of the average numbers of g-particles and h-particles on the number of s-particles (i.e., in the functions $\bar{n}_g(n_s)$ and $\bar{n}_h(n_s)$). The correlation $\bar{n}_g(n_s)$ (and the correlation $\bar{n}_p$ $(n_{\pi^\pm})$ similar to it) reflects the relationship between a pion and a nucleon component of the INC and is, thus, an instrument for the study of the energy dissipation in a deep inelastic interaction.

Before proceeding to the analysis of experimental data, we shall consider several simplified cases which, although being limiting cases, can serve as useful milestones in the discussion of the behavior of the correlation $\bar{n}_p$ (n_π) (or $\bar{n}_g(n_s)$).

Let pions be produced only in the first collision between an incident particle and an intranuclear nucleon, whereas the secondary processes of the production of pions by cascade particles can be disregarded. Then, there can exist two limiting situations in what is concerned with the absorption of pions by a nucleus.

In the case of weak absorption of a pion by a nucleus, pions escape from a nucleus upon undergoing one-two acts of rescattering on nucleons (an elastic one or one accompanied by the charge exchange), whereas a two nucleon absorption (i.e., true absorption) does not play any significant role. Then, more pions have escaped from a nucleus, more acts of rescattering have taken place, and a larger number of nucleons have been knocked out of them. As a result, the average number of knocked-out nucleons $(\bar{n}_g)$ increases with the number of emitted pions (n_s).

In the case of strong absorption of pions by a nucleus, pions undergo a sufficiently large number of collisions with nucleons, with a two-nucleon absorption playing a significant role. (Such a situation can take place for pions with the energy

in the vicinity of the (3,3)-resonance because of both the large cross-section of their interaction with nucleons and the existence of a peak in the cross-section of the reaction $\pi + NN \rightarrow NN$, which occurs just at this energy.) Then, the smaller fraction of pions created by the initial particle has escaped from a nucleus (i.e., the larger fraction of them has been absorbed in a nucleus), the larger number of nucleons has been emitted in an NR. As a result, the average number $(\overline{n}_g)$ of emitted nucleons decreases with increasing number of outgoing pions (n_s).

Let now pions be produced with high efficiency in collisions of both initial particles and cascade ones with intranuclear nucleons. Later on, they escape from a nucleus after several acts of rescattering on nucleons. Then, more pions have been produced, more such collisions have taken place, and more nucleons have been knocked out in such collisions. The average number of nucleons $(\overline{n}_g)$ increases with increasing number (n_s) of pions in this case as well.

A specific NR is, to be sure, a more complicated case than examples outlined above. However, for certain initial energies, there can rise conditions close to these idealized cases. Be that as it may, the calculations carried out within the framework of the INC-model take into account peculiar features of a specific NR. Let us compare the results of such calculations with experimental data.

For proton energies $\epsilon_0 < 5\text{-}7$ GeV, a not very large number of pions is produced in a collision of an incident particle with an intranuclear nucleon, and their energies turn out to be close to the energy of the (3,3)-resonance. Since average energies of secondary particles produced in this collision (the more so, in subsequent ones) is significantly smaller than the initial energy, the contribution from the cascade particles to the multiple pion production is small, and such reactions are close to the first idealized case. In this range of energies ϵ_0, the main difference between the INC-model and the INCT-model is caused by the distinction in the description of pion transport in a nucleus. The calculations carried out within the framework of the INC-model are close to the case of a strong pion absorption and give a decreasing form of the dependence for the correlation $\overline{n}_g(n_s)$. The calculations carried out in accordance with the INCT-model are closer to the case of weak pion absorption and give an increasing form of the dependence for the correlation $\overline{n}_g(n_s)$ at $\epsilon_0 = 6.2$ GeV (see Figure 21). As the energy ϵ_0 decreases, the energy of pions produced approaches the energy of the (3,3)-resonance. Such pions are more strongly absorbed by nuclei. This leads to a change in the slope of the correlation $\overline{n}_g(n_s)$ calculated within the framework of the INCT-model, and this correlation becomes a slowly decreasing function of its argument at $\epsilon_0 = 3.7$ GeV (see Figure 21). Experimental data[83,84] agree with the calculation carried out in accordance with the INCT-model and contradict the calculation carried out within the framework of the INC-model. This is indicative of the overestimation of an absorption of pions by a nucleus in the latter model.

For high initial energies $\epsilon_0 > 10$ GeV, collisions of cascade particles of the second and the third generation give a considerable contribution to the pion production. Such reactions are closer to the second idealized case. The majority of pions produced under these conditions has the energy which is considerably higher than the energy of the (3,3)-resonance. Here the cross-sections of πN-collisions do

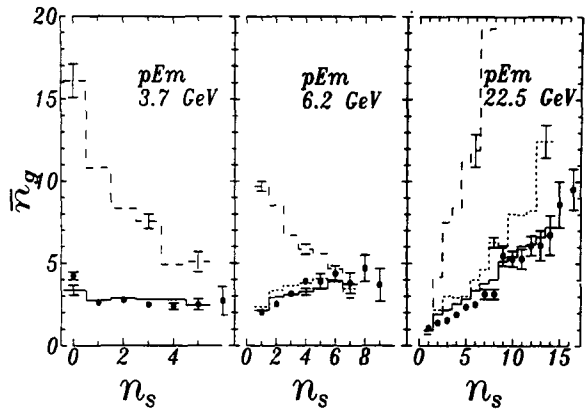

FIGURE 21. This traces the correlation between the average multiplicity of g-particles and the number of s-particles in stars formed by protons of various energies (whose values are indicated in the figure) in the photoemulsion. The points correspond to experimental data[83,84] and the histograms to the calculation. The rest of notation is the same as in Figure 20.

not differ significantly from NN-cross-sections, while the cross-section of a two-nucleon absorption is small. In this energy range, the principal distinction between the INC-model and the INCT-model is associated with the trawling effect. In the INC-model, relatively high-energy pions escape form a nucleus, but undergo a larger number of the acts of rescattering than in the INCT-model, since in the latter model low-energy pions pass through the domain of rarified nuclear matter. As a result both the INC- and the INCT-model give an increasing type of behavior of the correlation $\bar{n}_g(n_s)$, but the number of protons knocked out in events of multiple pion production is significantly larger in the INC-model than in the experiment. The INCT-model, in which pions are absorbed by a nucleus considerably weaker, agree well with experimental data.[84] This is indicative of the fact that, for high energies ϵ_0, absorption of secondary pions by a nucleus is relatively weak as well.

The correlation $\bar{n}_h(n_s)$ reveals the same type of behavior as the correlation $\bar{n}_g(n_s)$ (see Figure 22). However, the effects discussed above affect the correlation $\bar{n}_h(n_s)$ more strongly because of their influence both on the g- and the b-particles which enter into the composition of the h-particles. Thus, a good agreement between this correlation and the results obtained within the framework of the INCT-model and a qualitative discrepancy between it and the calculations carried out in accordance with the INC-model serve as an additional and even more convincing argument in favor of the INCT-model (see Figure 22).

The calculations[13,82] carried out in accordance with the INCT-model have demonstrated that the value of the initial energy ϵ_0 at which the multiplicities $\bar{n}_g(\epsilon_0)$ and $\bar{n}_h(\epsilon_0)$ reach the plateau depends on the mass number A of a T-nucleus, namely, the saturation is manifested at higher ϵ_0 for nuclei with larger values of A. In particular, for light nuclei of the ^{12}C type, the saturation takes place even at $\epsilon_0 \approx$ 0.5-1 GeV.[13,82]

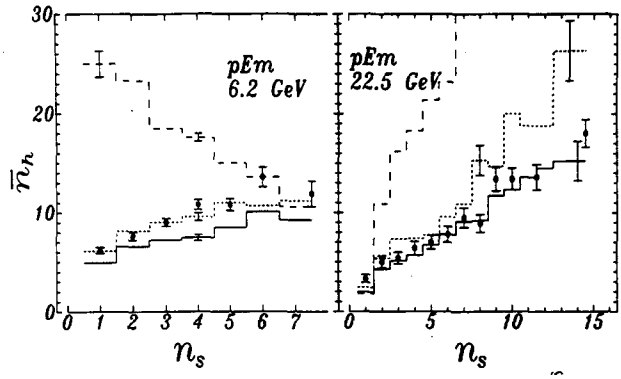

FIGURE 22. The correlation between the average multiplicity of h-particles and the number of s-particles in stars produced by protons of various energies in the photoemulsion. The points show the experimental data of Reference 84. The rest of notation is the same as in Figure 21.

It has been already noted that the trawling effect leads to the saturation of the number of recoil nucleons and of the value of the excitation energy of an R-nucleus. As a result, this effect is manifested in other observable characteristics of NRs as well. For example, the excitation functions for production of fragments reach the plateau at the energy $\epsilon_0 \sim$ 3-5 GeV, and a decrease in the cross-section for the fission of heavy T-nuclei is slowed down (see Chapter 7). Moreover, the saturation of the average number of nucleons lost by T-nuclei is also observed as the initial energy reaches this value. This is confirmed by the analysis[85] of data on the cross-sections for the isotope production in the interaction of protons with medium-weight nuclei.

In the domain of high energies $\epsilon_0 > 20$ GeV, the principal role is played by other effects which lead to an increase in the transparency of a nucleus with respect to products formed in a primary elementary act. This is, above all, the effect of a finite length of hadron formation (see Chapter 2). As a consequence, the result of hadron-nucleus interaction at high energies becomes similar to that of hadron-nucleon interaction. Thus, the energy $\epsilon_0 \approx$ 3-5 GeV is the optimum energy of hadrons from the viewpoint of production of highly-excited nuclei. This conclusion is also confirmed by the results of experiment reported in Reference 86.

B. EFFECT OF RESONANCE PRODUCTION

In addition to the trawling effect, there is one more effect which, in principle, might lead to similar results at the energies $\epsilon_0 \approx$ 3-20 GeV. It consists in the production of mesonic and baryonic resonances which become intensive in this energy range. For the resonances of the width $\Gamma \sim$ 100-200 MeV, the lifetime in its rest system is about $(0.7\text{-}0.3)10^{-23}$s. If we take into account the relativistic retardation of time and the effect of Pauli exclusion principle, which suppresses the decay of low energy isobars in a nucleus, this time turns out to be long enough for resonance to interact with an intranuclear nucleon before it decays. From the

kinematic viewpoint it is equivalent to the case when intranuclear nucleon interacts simultaneously with several particles which stuck together. In this case, the effective number of collisions inside the nucleus must decrease. This entails a decrease in the excitation energy of a nucleus and in a number of nucleons knocked out of a nucleus.

The authors of Reference 81 have estimated the influence exerted by the effect of the resonance production on those characteristics of low-energy secondary particles in which considerable deviations from the results of calculations carried out in accordance with the standard INC-model are observed. The choice of assumptions made in this paper on the formation and further "history" of resonances in a nucleus was motivated by the desire to obtain the maximum contribution from this effect on the one hand, and by the necessity to remain within a realistic physical situation on the other hand. The value of the potential acting on the resonance inside a nucleus and that of the cross-section of its interaction with a nucleon were set to be equal to pion values for mesonic resonances and to nucleon values for baryonic resonances. It was assumed that resonances undergo decay only after the escape from a nucleus. It was also assumed that one or two resonances* are produced with probability equal to unity in each πN- and NN-collision, which can result in formation of one or several pions: NN $\rightarrow$ N*N, NN $\rightarrow$ $N_1^*N_2^*$, πN $\rightarrow$ N*, πN $\rightarrow$ N*ρ, πN $\rightarrow$ N*$\rho\pi$, NN $\rightarrow$ $N_1^*N_2^*\pi$, etc. For such an exaggerated estimate of the resonance production in an elementary act, the role of reactions in which they "survive" (N_1^*N $\rightarrow$ N_2^*N) and in which they are multiplied (N*N $\rightarrow$ $N_1^*N_2^*$, ρN $\rightarrow$ N*ρ, etc.) increases dramatically. The reaction in which a baryonic resonance disappears (N*N $\rightarrow$ NN) was also taken into account.

In spite of the fact that assumptions listed above favor strongly the effect of the resonance production, the calculations carried out according to the INC-model with resonances give only a slight decrease in the average number of slow secondary particles and in the number of collisions experienced by cascade particles inside a nucleus (at $\epsilon_0 \approx 30$ GeV this number decreases only by a factor of two, whereas in the calculations carried out according to the INCT-model it decreases by a factor of ten). The calculation carried out with resonances do not describe the correlation $\overline{n}_g(n_s)$[81] as well. The small value of the resonance effects** can be qualitatively explained on the basis of the following simple considerations. The larger number of cascade particles is "united" in the resonances, the more considerable decrease in the average multiplicity of secondary particles is observed. However, taking into account a rapid decrease in the average energy of particles in subsequent generations of the cascade shower, we can easily see that up to the energy $\epsilon_0 \sim 20$ GeV only particles of the first and the second generation take part in production of resonances. Their fraction in the total number of particles is relatively small.

* For the sake of simplicity we denote the baryonic resonance by the symbol N* and the mesonic resonance by ρ.

** It should be kept in mind that here we are dealing only with principal characteristics of the pA-reaction. For separate channels of this reaction, we can, for certain, indicate the quantities which essentially depend on the effect of the resonance production. However, this problem is not considered here.

Thus, the observed discrepancy between the results of calculations carried out in accordance with the INC-model and experimental data for the pA-reaction in the energy range $\epsilon_0 > 3$-5 GeV is mainly caused by a nonlinear effect of a local decrease in the nuclear density, rather than by the contribution of resonances. Let us now consider the variation of the manifestation of this effect with increasing number of nucleons interacting with a T-nucleus.

C. MANIFESTATION OF THE TRAWLING EFFECT IN REACTIONS INITIATED BY LIGHTEST NUCLEI (d, t, AND α)

First attempts[87,88] to generalize the INC-model to the case of inelastic interactions of lightest nuclei with nuclei were based on the assumption that the interaction of two nuclei can be reduced to a set of independent cascades initiated by nucleons of an incident nucleus inside a T-nucleus. It is clear that the assumption on the independence of these cascades can be justified only in the energy range $\epsilon_0 < 1$GeV/nucleon, when the number of cascade particles is small. For higher initial energies, cascades generated by different nucleons of an incident nucleus turn out to be effectively coupled with one another owing to the trawling effect.

The INCT-model for inelastic interactions of lightest nuclei with nuclei has been constructed. It has been assumed in this model[89,90] that, in the rest system of an incident nucleus, momentum distributions of its nucleons have the form

$$W_d(p) \sim p^2/(p^2 + m_N\tilde{\epsilon})^2, \tag{85a}$$

$$W_{t,^3He,\alpha}(p) \sim p^2\exp(-p^2/\tilde{p}^2) \tag{85b}$$

where $\tilde{\epsilon} = 2.23 \cdot 10^{-3}$ GeV and $\tilde{p} = 0.1$ GeV/c for nuclei of t and ^{3}He and $\tilde{p} = 0.16$ GeV/c for α-particles. These distributions describe approximately the squared modulus of the corresponding wave functions in the momentum representation. It is also assumed that a deuteron is represented as a dumb-bell with a shoulder $l = 2R_d$ ($R_d = 2.16$ fm). The nucleons are situated at the vertices of a triangle in the nuclei of t and ^{3}He and at the vertices of a tetrahedron in the α-particles. The coordinates of the vertices are found from the data on the nucleon density distribution in these nuclei. In the calculations the orientation of these polygons in space was assumed to be equiprobable. Each of the nucleons of an incident nucleus can initiate a cascade inside a T-nucleus or leave it freely with the energy and momentum defined by the distribution (Equation 85) and by the velocity of a primary nucleus. To calculate intranuclear cascades initiated by nucleons, we made use of the INCT-model described in Chapter 2. This allowed us to take into account the coupling between the cascades.

Such a simple model describes the experimental data on inelastic interactions of intermediate-energy deuterons and α-particles with nuclei to a good accuracy (a systematic comparison of the model with experimental data is given in References 13,90,91). Without dwelling at length on the detailed quantitative comparison of

the conclusions drawn with the help of the INCT-model with experimental data for various characteristics of NRs, we shall consider here only the principal qualitative corollaries of the manifestation of the trawling effect in the energy dependence of average multiplicities of secondary particles. Figure 23 shows the results of the calculations of this dependence for the interaction of d, t, and α nuclei with photoemulsion. These calculations were carried out with the same values of parameters of the INCT-model as in the case of incident protons. It is seen from the comparison of Figure 20 and Figure 23 that saturation of the average multiplicities $\bar{n}_g$ and $\bar{n}_h$ of low-energy secondaries takes place at lower energies as the number of nucleons interacting with a T-nucleus increases. For instance, in the case of the dA- and the αA-reaction, the trawling effect must be taken into account even at $\epsilon_0 \approx 1$ GeV/nucleon (see Figure 23). Needless to say that as we go over to reactions with intermediate-energy heavy ions, there arise specific effects (the development of the INC in each of the interacting nuclei, the manifestation of collective effects, etc.). However, any model of deep inelastic nucleus-nucleus interaction must take into account the trawling effect.

V. CONCLUSIONS

Analysis of various experimental inclusive characteristics (energy spectra, average multiplicities, and double differential distributions of secondary nucleons) of NA-reactions in the domain of intermediate energies based on the analytic and the numerical method of solution of KEs which were considered in Chapter 2 has demonstrated that these methods allow one to satisfactorily calculate these characteristics and to effectively study the influence exerted by the variation of parameters of the nuclear model used on the results of the calculations of these characteristics. An agreement of different methods of calculations with one another and with experimental data is indicative of the fact that for the energies $\epsilon_0 \gtrsim 50$ MeV, deep inelastic interaction of an incident nucleon with a nucleus is genuinely characterized by a cascade of quasifree collisions with individual intranuclear nucleons, and thus confirms the validity of the basic assumptions of the INC-model. Taking account of quantum-mechanical effects in the calculation of the quasifree component of the cross-section allows one to considerably improve the description of double differential cross-sections for production of secondary protons at small angles in pA-interactions at intermediate energies within the framework of the INC-model. The generalization of the approach, developed in Chapter 2 to calculate the NA-reactions on the basis of the solution of the corresponding system of KEs, to the case which calls for taking account of the spin dependence of the NN-interaction allows one to find analytic expression for polarization observables of these reactions in the domain of a continuum. The comparison of the calculated analyzing power A_y in the A(**p**,p′)X reaction at the energy $\epsilon_0 = 200$ MeV with experimental data confirms the validity of the basic assumptions of the INC-model as well.

To describe the pion production in NA-interactions, a system of KEs for intranuclear nucleonic-mesonic cascade has been formulated. This system of equations takes into account the meson production in NN-collisions, and on the basis of its

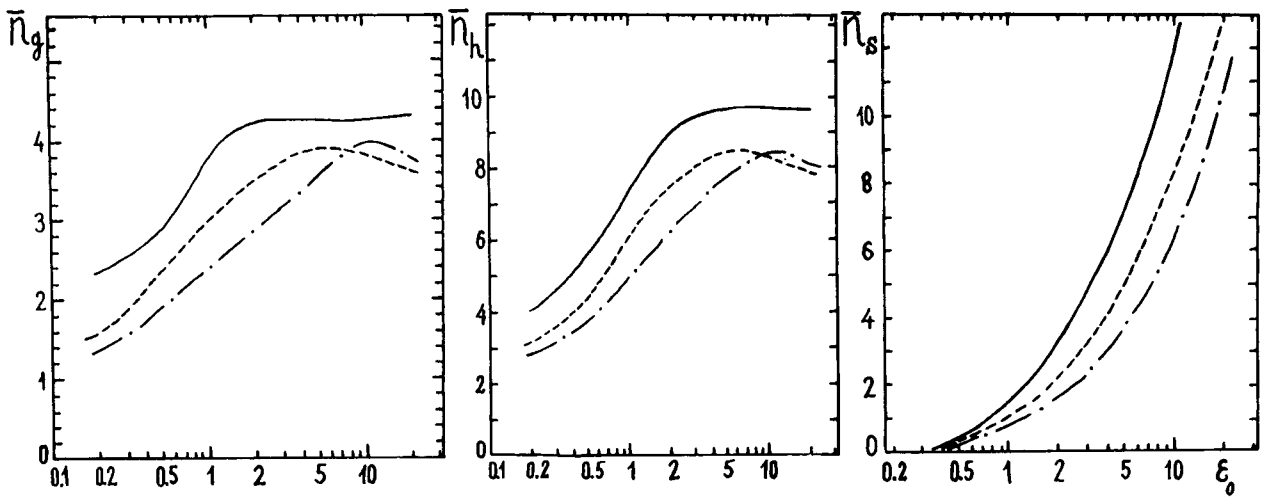

FIGURE 23. These are the average multiplicities of g-, h-, and s-particles emitted in the interaction of deuterons (the dash-dotted curve), tritons (the dashed curve), and α-particles (the solid curve) with nuclei of the photoemulsion as functions of the initial energy ϵ_0(GeV/nucleon). The curves show the results of calculations[89,90] carried out under the condition $n_h > 1$.

solution at the energies $\epsilon_0 < 1$ GeV analytic expressions for inclusive cross-sections of pion production have been found. An analysis of experimental data on inclusive cross-sections for production of pions by protons on nuclei at $\epsilon_0 < 1$GeV carried out with the help of these expressions, of the Monte Carlo calculations, and of the calculations using the numerical solution of the BUU-equation, has demonstrated that the INC-model describes satisfactorily these data both above the threshold of pion production in NN-collisions, and in the vicinity of the threshold and below it. Near the threshold, a subprocess $pN \rightarrow d\pi$ plays a significant role, along with the standard subprocess $pN \rightarrow \pi NN$. To describe the subthreshold pion production we are not to invoke the high-momentum component of the nucleon distribution. The use of the ordinary Fermi gas distribution turns out to be quite sufficient.

The analysis of production of K^+-mesons by protons of various energies on light nuclei carried out with the help of simple approximations of the cross-sections for their production in pp-collisions within the framework of the INC-model allows one to obtain closed analytic formulas for inclusive cross-sections of production of kaons on these nuclei at small angles. The use of a phenomenological dependence of these cross-sections on A leads to similar formulas for heavy nuclei which describe satisfactorily experimental data over a wide range of the energy of primary protons. Results of an analysis of the subthreshold production of K^+-mesons and of antiprotons in pA-interactions count in favor of the fact that a large value of the high-momentum component of the nucleon momentum distribution is not necessary for the description of these processes as well. Nonlocal processes (such as multiple interactions of particles and resonances formed at the initial stage of the reaction with other intranuclear nucleons) can serve as an important source of production of kaons and antiprotons.

The effect of trawling of a nucleus by fast cascade particles comes to manifest itself at the nucleon energies $\epsilon_0 \gtrsim 5$ GeV. As a result of this effect, the average number of nucleons knocked out of a T-nucleus and the average excitation energy of an R-nucleus remain practically constant as the energy ϵ_0 increases. The correlation between the numbers of low energy nucleons and pions emitted in the reaction is most sensitive to the manifestation of the trawling effect. This correlation reflects the coupling between the nucleonic and the pionic component of the INC and is, thus, an effective means for the study of the energy dissipation in a deep inelastic interaction. Although for the energies $\epsilon_0 \gtrsim 5$ GeV mesonic and baryonic resonances are produced in an elementary interaction of a primary particle with intranuclear nucleons (this also leads to a decrease in the number of collisions experienced by cascade particles inside a nucleus), the "saturation" of the average number of nucleons knocked out of a T-nucleus and that of the average excitation energy of an R-nucleus are predominantly caused by the trawling effect, rather than the effect of the resonance production. The manifestations of the trawling effect are enhanced as the number of nucleons interacting with a nucleus increases. For instance, in the case of the interaction of α-particles with nuclei, this effect must be taken into account at the energy $\epsilon_0 \approx 1$ GeV/nucleon. It is even more important in a deep inelastic interaction of intermediate-energy heavy ions with nuclei.

REFERENCES

1. **Kazarnovsky, M. V. and Paryev, E. Ya.**, Analytic calculation of an intranuclear cascade by means of kinetic equations, *Sov. J. Nucl. Phys.*, 33, 345, 1981.
2. **Daskalov, G. M., Kazarnovsky, M. V., and Paryev, E. Ya.**, Analytic calculation of spectra and multiplicities of secondary nucleons in the intermediate-energy nucleon-nucleus interactions, Preprint *INR* P-0528, Moscow, 1987.
3. **Iljinov, A. S.**, Code for calculation of intranuclear cascade in the energy range $\lesssim$ 5 GeV, *JINR* Communication B1-4-5478, Dubna, 1970.
4. **Barashenkov, V. S. and Toneev, V. D.**, *Interaction of High Energy Particles and Nuclei with Atomic Nuclei* [in Russian], Atomizdat, Moscow, 1972.
5. **Blann, M.**, Pre-equilibrium models for nuclear reactions, *UR-NSRL*- 92, C00-3494-13, Lectures of the Romanian Summer School in Nuclear Physics, Predeal, Romania, September 4-13, 1974.
6. **Kazarnovsky, M. V. and Paryev, E. Ya.**, Unified optical + cascade model of nuclear reactions at intermediate energies, *Izv. Akad. Nauk Kaz. SSR, Ser. Fiz.-Mat.*, N4, 28, 1983.
7. **Bunakov, V. E. and Matvejev, G. A.**, Taking account of surface effects in the method of intranuclear cascade, *Izv. Akad. Nauk SSR, Ser. Fiz.*, 45, 2047, 1981.
8. **Bertrand, F. E. and Peelle, R. W.**, Complete hydrogen and helium particle spectra from 30- to 60-MeV proton bombardment of nuclei with A = 12 to 209 and comparison with the intranuclear cascade model, *Phys. Rev. C*, 8, 1045, 1973.
9. **Cordell, K. R., Thornton, S. T., Dennis, L. C., Doering, R. R., Parks, R. L., and Schweizer, T. C.**, Proton-inclusive cross sections from 600 MeV proton-nucleus reactions, *Nucl. Phys. A*, 352, 485, 1981.
10. **Stevenson, J. D.**, Classical many-body calculation of relativistic nuclear collisions, *Phys. Rev. Lett.*, 41, 1702, 1978.
11. **Hatch, R. L. and Koonin, S. E.**, High momentum nucleons from relativistic nuclear collisions, *Phys. Lett. B*, 81, 1, 1979.
12. **Peelle, R. W., Love, T. A., Hill, N. W., and Santoro, R. T.**, Differential cross sections for the production of protons in the reactions of $\sim$160 MeV protons on nuclei, *Phys. Rev.*, 167, 981, 1968.
13. **Barashenkov, V. S., Iljinov, A. S., Sobolevsky, N. M., and Toneev, V. D.**, Interaction of particles and nuclei of high and superhigh energies with nuclei, *Usp. (Sov. Phys.)* 16, 31, 1973.
14. **Wu, J. R., Chang, C. C., and Holmgren, H. D.**, Charged-particle spectra: 90 MeV protons on ^{27}Al, ^{58}Ni, ^{90}Zr and ^{209}Bi, *Phys. Rev. C*, 19, 698, 1979.
15. **Gudima, K. K., Mashnik, S. G., and Toneev, V. D.**, Cascade-exciton model of nuclear reactions, *Nucl. Phys. A*, 401, 329, 1983.
16. **Förtsch, S. V., Cowley, A. A., Pilcher, J. V., Whittal, D. M., Lawrie, J. J., Van Staden, J. C., and Friedland, E.**, Continuum yields from ^{12}C(p,p′) at incident proton energies of 90 and 200 MeV, *Nucl. Phys. A*, 485, 258, 1988.
17. **Daskalov, G. M., Kazarnovsky, M. V., and Paryev, E. Ya.**, The role of quantum effects in the intranuclear cascade model, *Sov. J. Nucl. Phys.*, 52, 41, 1990.
18. **Franz, J., Koncz, P., Rössle, E., et al.**, Neutron-induced production of protons, deuterons and tritons on copper and bismuth, *Nucl. Phys. A*, 510, 774, 1990; **Boyarinov, S. V., Gerzon, S. A., Evseev, I. I., et al.**, Cumulative kaon production by 10-GeV protons, *Yadernaya Fiz.*, 50, 1605, 1989.
19. **Kazarnovsky, M. V. and Paryev, E. Ya.**, Polarization effects in the inclusive nucleon-nucleus reactions at medium energies, *Sov. J. Nucl. Phys.*, 49, 605, 1989.
20. **Roy, G., Greeniaus, L. G., Moss, G. A., et al.**, Inclusive scattering of protons on helium, nickel and tantalum at 500 MeV, *Phys. Rev. C*, 23, 1671, 1981.
21. **Källne, J., Stetz, A. W., and Woloshyn, R. M.**, Analyzing power of inclusive nuclear reactions, *Phys. Lett. B*, 74, 170, 1978.
22. **Lisantti, J., Tinsley, J. R., Drake, D. M., et al.**, Analyzing power for the inelastic continuum with 200 MeV protons, *Phys. Lett. B*, 147, 23, 1984.

23. **Moalem, A., Frekers, D., Gurvitz, S. A., et al.**, Inclusive analyzing power and scattering mechanisms in proton-nucleus scattering at backward angles, *Phys. Lett. B*, 183, 269, 1987.
24. **Frankel, S., Frati, W., Gazzaly, M., Hoffmann, G. W., Van Dyck, O., and Woloshyn, R. M.**, Analyzing power in inclusive proton-nucleus cross sections, *Phys. Rev. Lett.*, 41, 148, 1978.
25. **Brody, H., Frankel, S., Frati, W., and Van Dyck, O. B.**, Elastic and inclusive analyzing power of deuterium for 0.8 GeV protons, *Phys. Rev. C*, 24, 2157, 1981.
26. **Moss, J. M., Carey, T. A., McClelland, J. B., DiGiacomo, N. J., Seestrom-Morris, S. J., Bertsch, G. F., Scholten, O., Adams, G. S., Gazzaly, M., Hintz, N., and Nanda, S.**, Excitation of the giant-resonance continuum with intermediate-energy protons, *Phys. Rev. Lett.*, 48, 789, 1982.
27. **Belostotsky, S. L., Dotsenko, Yu. V., Erö, J., et al.**, Polarization in inclusive scattering of protons from nuclei at 1 GeV, *Phys. Lett. B*, 124, 469, 1983. **Zulkarneev, R. Ya., Kutuev, P. Kh., and Murtazaev, Kh.**, Angular and momentum dependence of polarization of protons emitted in pC collisions at 640 MeV, *Yad. Fiz.*, 32, 889, 1980.
28. **Schumacher, C. R. and Bethe, H. A.**, Usefulness of polarized targets and the polarization transfer tensor in reconstruction of the nucleon-nucleon scattering matrix, *Phys. Rev.*, 121, 1534, 1961.
29. **Kalashnikov, N. P., Remizovich, V. S., and Ryazanov, M. I.**, *Collisions of fast charged particles in solids*, Atomizdat, Moscow, 1980.
30. **Zhu, X., Wong, S. S. M., and Mobed, N.**, Difference between P and A_y in forward angle inelastic proton-nucleus scattering at intermediate energies, *Phys. Lett. B*, 174, 142, 1986.
31. **Chan, C., Drake, T. E., Abegg, R., Frekers, D., Häusser, O., Hicks, K., Hutcheon, D. A., Lee, L., Miller, C. A., Schubank, R., and Yen, S.**, A complete measurement of spin-observables for intermediate-energy inclusive quasielastic polarized proton scattering from ^{12}C, *Nucl. Phys. A*, 510, 713, 1990.
32. **Cheng, D., Macdonald, B., Helland, J. A., and Ogden, P. M.**, Nucleon-nucleon polarization between 300 and 700 MeV, *Phys. Rev.*, 163, 1470, 1967.
33. **Landolt, H., Börnstein, R.**, *Elastische und Ladungsaustausch-Streuung von Elementarteilchen*, Springer-Verlag, Berlin, B.9, 1980.
34. **Clough, A. S., Gibson, D. R., Axen, D., et al.**, Neutron-proton elastic scattering between 200 and 500 MeV.I. Experimental details and measurements of the D_t and P parameters, *Phys. Rev. C*, 21, 988, 1980. **Sowinski, J., Byrd, R. C., Jacobs, W. W., Vigdor, S. E., Whiddon, C., Wissink, S. W., Knutson, L. D., and Jolivette, P. L.**, A measurement of the spin correlation parameter $C_{NN}(\vartheta)$ in n-p scattering at 181 MeV, *Phys. Lett. B*, 199, 341, 1987.
35. **Besset, D., Do, Q. H., Favier, B., Greeniaus, L. G., Hess, R., Lechanoine, C., Rapin, D., Werren, D. W., and Weddigen, Ch.**, Measurement of the spin-dependent parameters D, R, A, and P for small-angle p-p elastic scattering between 300 and 600 MeV, *Phys. Rev. D*, 21, 580, 1980.
36. **Axen, D., Dubois, R., Keeler, R., et al.**, Neutron-proton elastic scattering between 200 and 500 MeV. II measurement of R_t and A_t, *Phys. Rev. C*, 21, 998, 1980.
37. **Bimbot, L., Bellini, V., Bolore, M., Charlot, X., Guet, C., Hisleur, J. M., Jourdain, J. C., Julien, J., Kristiansson, P., Lanzano, G., Million, B., Oskarsson, A., Palmeri, A., Pappalardo, G. S., Poitou, J., Reide, F., and Willis, N.**, Inclusive $(p,\pi^{\pm})$ reactions at 201 and 180 MeV, *Nucl. Phys. A*, 440, 636, 1985. **Marrs, R. E. and Pollock, R. E.**, Inclusive (p,π^{+}) cross sections near threshold, *Phys. Rev. C*, 20, 2446, 1979. **Gavron, A. and Yariv, Y.**, Cascade calculation of subthreshold π^{o} production, *Phys. Rev. C*, 41, 2442, 1990.
38. **Sternheim, M. M. and Silbar, R. R.**, Model for production of π^{+} and π^{-} by protons from nuclei, *Phys. Rev. D*, 6, 3117, 1972.
39. **Silbar, R. R. and Sternheim, M. M.**, Nuclear effects in the production of π^{+} and π^{-} by protons on nuclei, *Phys. Rev. C*, 8, 492, 1973.
40. **Sparrow, D. A., Sternheim, M. M., and Silbar, R. R.**, Semiclassical model for pion production by neutrons on nuclei, *Phys. Rev. C.*, 10, 2215, 1974.

41. **Yang, Kuo-Ho, Holstein, B. R., Sternheim, M. M., and Sparrow, D. A.,** Multiple-scattering and nucleon-recoil effects in pion production by nucleons on nuclei, *Phys. Rev. C,* 14, 1083, 1976.
42. **Beder, D. S. and Bendix, P.,** Calculations of π^+ production in nuclei, *Nucl. Phys. B,* 26, 597, 1971.
43. **Iljinov, A. S., Kazarnovsky, M. V., and Nazaruk, V. I.,** Cross section for pion production on nuclei by protons with the energy 250 MeV [in Russian], in *Program of Experimental Investigations on the Meson Facility of INR AN SSSR,* Moscow, 1979, 23.
44. **Cao, Z.-J., Ward, T. E., Bent, R. D., Brown, J. D., Korkmaz, E., Nann, H., and Throwe, T. G.,** ^{7}Li(p,π^+) ^{8}Li and ^{7}Li(p,π^-)^{8}B reactions at 200 MeV, *Phys. Rev. C,* 35, 825, 1987.
45. **Cassing, W., Metag, V., Mosel, U., and Niita, K.,** Production of energetic particles in heavy-ion collisions, *Phys. Rep.,* 188, 363, 1990.
46. **Yariv, Y. and Fraenkel, Z.,** Intranuclear cascade calculation of high-energy heavy-ion interactions, *Phys. Rev. C,* 20, 2227, 1979.
47. **Yariv, Y. and Fraenkel, Z.,** Intranuclear cascade calculation of high-energy heavy-ion collisions: effect of interactions between cascade particles, *Phys. Rev. C,* 24, 488, 1981.
48. **Dudziak, W. F.,** Production of charged pions in the p ^{12}C-interactions at 350 MeV, preprint *UCRL*-2501, 1954.
49. **Passman, S., Block, M. M., and Havens, W. W.,** Excitation function for charged π-meson production in hydrogen and carbon by 345 to 380 MeV protons, *Phys. Rev.,* 88, 1247, 1952.
50. **Richmann, C., Weissbluth, M., and Wilcox, H. A.,** Production cross sections for π^+ and π^--mesons by 340 MeV protons on carbon and lead at 90° to the beam, *Phys. Rev.,* 85, 161, 1952.
51. **Merritt, J. and Hamlin, D. A.** Production of π^+-mesons at 0° by 335 MeV protons on deuterium and complex nuclei, *Phys. Rev.,* 99, 1523, 1955.
52. **Harp, G. D.,** Extension of the isobar model for intranuclear cascades to 1 GeV, *Phys. Rev. C.,* 10, 2387, 1974.
53. **Crawford, J. F., Daum, M., Eaton, G. H., et al.,** Measurement of cross sections and asymmetry parameters for the production of charged pions from various nuclei by 585-MeV protons, *Phys. Rev. C,* 22, 1184, 1980.
54. **Cochran, D. R. F., Dean, P. N., Gram, P. A. M., et al.,** Production of charged pions by 730-MeV protons from hydrogen and selected nuclei, *Phys. Rev. D,* 6, 3085, 1972.
55. **Krasnov, V. A., Kurepin, A. B., Reshetin, A. I., Oganesjan, K. O., and Pasyuk, E. A.,** Analysis of pion spectra in production by 240-500 MeV protons on nuclei, *Phys. Lett. B,* 108, 11, 1982.
56. **Flaminio, V., Graf, I. F., Hansen, J. D., Moorhead, W. G., and Morrison, D. R. O.,** Compilation of cross-sections: P and $\bar{p}$ induced reactions. *CERN-HERA* 79-03, 1979.
57. **Zwermann, W.,** Kaon production in relativistic heavy-ion collisions: the role of the elementary cross section, *Mod. Phys. Lett. A,* 3, 251, 1988.
58. **Barz, H. W. and Iwe, H.,** Cascade-model studies of pion and strange-particle production in C on Ta reactions at E/A = 3.36 GeV, *Nucl. Phys. A,* 453, 728, 1986.
59. **Efremov, S. V., Kazarnovsky, M. V., and Paryev, E. Ya.,** K^+ production in the pp and pA interactions at various energies, *Yad. Fiz.,* 55, 521, 1992; *Z. Phys. A,* 344, 181, 1992.
60. **Firebaugh, M., Ascoli, G., Goldwasser, E. L., Sard, R. D., and Wray, J.,** *Strange-particle* production in 8-BeV/c proton-proton interactions, *Phys. Rev.,* 172, 1354, 1968.
61. **Hogan, W. J., Piroue, P. A., and Smith, A. J. S.,** K^+-meson production in p-p collisions at 2.5-3.0 GeV, *Phys. Rev.,* 166, 1472, 1968.
62. **Taylor, F. E., Carey, D. C., Johnson, J. R., Kammerud, R., Ritchie, D. J., Roberts, A., Sauer, J. R., Shafer, R., Theriot, D., and Walker, J. K.,** Analysis of radial scaling in single-particle inclusive reactions, *Phys. Rev. D.,* 14, 1217, 1976.
63. **Capiluppi, P., Giacomelli, G., Rossi, A. M., Vannini, G., Bertin, A., Bussiere, A., and Ellis, R. J.,** Charged particle production in proton-proton inclusive reactions at very high energies, *Nucl. Phys. B,* 79, 189, 1974.

64. **Koptyev, V. P., Mikirtyhyants, S. M., Nesterov, M. M., Tarasov, N. A., Shcherbakov, G. V., Abrosimov, N. K., Volchenkov, V. A., Gridnyev, A. B., Yeliseyev, V. A., Ivanov, E. M., Kruglov, S. P., Malov, Yu. A., and Ryabov, G. A.,** Subthreshold production of K^+-mesons in proton-nuclear interactions, *Eksp. Teor. Fiz.*, 94, 1, 1988.
65. **Dekkers, D., Geibel, J. A., Mermod, R., Weber, G., Willitts, T. R., Winter, K., Jordan, B., Vivargent, M., King, N. M., and Wilson, E. J. N.,** Experimental study of particle production at small angles in nucleon-nucleon collisions at 19 and 23 GeV/c, *Phys. Rev.*, 137, B962, 1965.
66. **Atherton, H. W., Bovet, C., Doble, N., Von Holtey, G., Piemontese, L., Placci, A., Placidi, M., Plane, D. E., Reinharz, M., and Rossa, E.,** Precise measurements of particle production by 400 GeV/c protons on beryllium targets, *CERN Report, CERN* 80-07, 1980.
67. **Barton, D. S., Brandenburg, G. W., Busza, W., et al.,** Experimental study of the A dependence of inclusive hadron fragmentation, *Phys. Rev. D*, 27, 2580, 1983.
68. **Geist, W. M.,** Atomic mass dependence in soft and hard pA collisions, *Nucl. Phys. A*, 525, 149c, 1991.
69. **Gudima, K. K., Laptev, V. D., Smirnova, O. N., and Sobolevsky, N. M.,** Double differential cross sections for kaon production in proton-nucleus interactions at the energies 7.5, 45 and 3000 GeV [in Russian], Preprint *INR* Moscow, 740/91, 1991.
70. **Amelin, N. S., Gudima, K. K.,and Toneev, V. D.,** Ultrarelativistic nucleus-nucleus collisions within a dynamical model of independent quark-gluon strings, *Yad. Fiz.*, 51, 1730, 1990.
71. **Cassing, W., Batko, G., Mosel, U., Niita, K., Schult, O., and Wolf, Gy.,** Subthreshold K^+-production in proton-nucleus reactions, *Phys. Lett. B*, 238, 25, 1990.
72. **Kopeliovich, V. B.,** Antinucleon and heavy quark subthreshold production as a method of studying intranuclear structure, *Yad. Fiz.*, 42, 854, 1985.
73. **Shor, A., Perez-Mendez, V., and Ganezer, K.,** Internal nuclear momentum and subthreshold anti proton production in p-nucleus and nucleus-nucleus collisions, *Nucl. Phys. A*, 514, 717, 1990.
74. **Chamberlain, O., Segre, E., Wiegand, C., and Ypsilantis, T.,** Observation of antiprotons, *Phys. Rev.*, 100, 947, 1955. **Piroue, P. A., and Smith, A. J. S.,** Particle production by 2.9-BeV protons incident on beryllium and platinum, *Phys. Rev.*, 148, 1315, 1966.
75. **Lepikhin, Yu. B., Smirnitskii, V. A., and Sheinkman, V. A.,** Subthreshold and nearthreshold antiproton production at the energies 3.7-9.2 GeV [in Russian], in *Nucleon-Nucleon and Hadron-Nucleus Interactions at Intermediate Energies, Proc. Symp.*, Leningrad, 1986, 299.
76. **Dorfan, D. E., Eades, J., Lederman, L. M., Lee, W., Ting, C. C., Piroue, P., Smith, S., Brown, J. L., Kadyk, J. A., and Trilling, G. H.,** Production of antiprotons via nuclear motion, *Phys. Rev. Let.*, 14, 995, 1965.
77. **Batko, G., Cassing, W., Mosel, U., Niita, K., and Wolf, Gy.,** Antiproton production in p-nucleus and nucleus-nucleus collisions, *Phys. Lett. B.*, 256, 331, 1991.
78. **Barashenkov, V. S., Bertini, H. W., Chen, K., et al.,** Medium energy intranuclear cascade calculations: a comparative study, *Nucl. Phys. A*, 187, 531, 1972.
79. **Barashenkov, V. S., Kostenko, B. F., and Zadorogny, A. M.,** Time-dependent intranuclear cascade model, *Nucl. Phys. A.*, 338, 413, 1980.
80. **Golubeva, E. S., Iljinov, A. S., and Pshenichnov, I. A.,** Correlation between numbers of secondary pions and nucleons in nuclear reactions involving intermediate-energy particles, Preprint *INR* 284, Moscow, 1993.
81. **Iljinov, A. S. and Toneev, V. D.,** Effect of the resonance production on the nuclear reaction mechanism, *Acta Phys. Pol. B*, 4, 225, 1973.
82. **Barashenkov, V. S., Iljinov, A. S., and Toneev, V. D.,** Further development of the intranuclear cascade model, *Yad. Fiz.*, 13, 743, 1971.
83. **Bubnov, V. I., Gaitinov, A. Sh., Eremenko, L. E., et al.,** Nuclear interactions of 4.5 GeV/c protons in emulsion and the cascade-evaporation model, *Z. Phys. A*, 302, 133, 1981.
84. **Winzeler, H.,** Proton-nucleus collisions in the multi-GeV region, *Nucl. Phys.*, 69, 661, 1965.
85. **Rudstam, G.,** Systematics of spallation yields, *Z. für Naturforsch.*, 21a, 1027, 1966.

86. **Nakai, K., Shibata, T.-A., En'yo, H., et al.,** Stopping and energy deposition of GeV particles in target nuclei, *Phys. Lett. B,* 121, 373, 1983.
87. **Barashenkov, V. S., Gudima, K. K., and Toneev, V. D.,** Mechanism of interaction of fast deuterons with nuclei, *Yad. Fiz.,* 9, 528, 1969.
88. **Gabriel, T. A., Santoro, R. T., and Alsmiller, R. G.,** An approximate high-energy alpha-particle nucleus collision model, *Nucl. Sci. Eng.,* 44, 104, 1971.
89. **Barashenkov, V. S., Iljinov, A. S., and Toneev, V. D.,** Interaction of relativistic deuterium and tritium nuclei with photoemulsion ones, *Acta Phys. Pol. B,* 4, 219, 1973.
90. **Barashenkov, V. S., Gudima, K. K., Gereghi, F. G., Iljinov, A. S., and Toneev, V. D.,** Inelastic interactions of high energy helium ions with atomic nuclei, *Yad. Fiz.,* 17, 434, 1973.
91. **Barashenkov, V. S., Musulmanbekov, J. J., and Gereghi, F. G.,** Cascade model of inelastic interactions of α-particles with nuclei, *Z. Phys. A,* 296, 371, 1980.

Chapter 5

INELASTIC PION-NUCLEUS INTERACTION

Pions play an important role in inelastic interaction of nucleons (see Chapter 4) and other particles with nuclei at the energies higher than the threshold of pion production. Moreover, the specific nature of a pion offers unique possibilities for investigations of nuclear structure and mechanisms of NRs. For example, a slow pion, being absorbed by a nucleus, is capable of transferring a large amount of energy to the nucleus. Unlike a nucleon, it also contributes the rest mass $m_\pi \simeq$ 140 MeV to the nucleus in addition to its kinetic energy. Therefore, the study of a "pure" case, i.e., the pion-nucleus interactions, is of great importance for the development of the theory of NRs. The absorption of slow pions is of special interest, since decay of highly-excited nuclei in the energy range $E^* \lesssim m_\pi$ is studied in sufficient detail in reactions with heavy ions. It has been demonstrated in Chapter 3 that an equilibrium statistical model of de-excitation of such nuclei is sufficiently reliable. This creates favorable conditions for investigation of the mechanism of absorption of pions by nuclei and of the dissipation of energy released in this process.

I. ABSORPTION OF STOPPED π^--MESONS BY NUCLEI

Absorption of stopped π^--mesons by atomic nuclei plays a peculiar role in modern physics, because it involves an interplay of various problems of mesoatomic physics, meson-nucleus interaction, NRs, and nuclear structure. Investigation of this interesting phenomenon began as far back as 40 years ago, as soon as pion beams were obtained. Since then a large body of experimental information has accumulated and a lot of theoretical work has enabled one to understand basic regularities of this process.[1-6] However, most of both theoretical and experimental investigations have been devoted to studying absorption of pions by light nuclei. More complex, but not less important reactions involving medium-weight and heavy nuclei have not been studied in such detail.

Considerable progress has been made in experimental investigations of the absorption of stopped pions by nuclei after putting meson facilities into operation. Considerable new data have been obtained for medium-weight and heavy targets. This has inspired a renewed interest in the theoretical study of this phenomenon, and a number of models[7-14] close to one another in spirit have been proposed to analyze new data on the absorption of stopped π^--mesons by complex nuclei. A succinct account and comparison of these models will be given in the next section.

A. OPTICAL + CASCADE MODEL OF PION ABSORPTION FROM MESOATOMIC STATES BY NUCLEI

1. General Pattern of the Process

An absorption of a slow π^--meson by a nucleus is generally a rather complicated process which proceeds in several stages:[7]

1) capture of a pion by the Coulomb field of a nucleus and formation of a pionic atom
2) de-excitation of the π-atom through emission of Auger-electrons and X-rays (atomic electromagnetic cascade)
3) capture of the pion from a mesoatomic orbit by a pair (or a larger number) of intranuclear nucleons
4) rescattering of fast nucleons produced in a primary act of pion absorption in the nucleus (intranuclear nucleonic cascade)
5) attainment of a thermodynamic equilibrium in an R-nucleus and decay of a highly-excited C-nucleus (evaporation cascade)

A proposed approach[7] is based on the synthesis of the optical and the cascade model of NRs. In this approach, the initial stages (1 and 2) of the process in which quantum-mechanical effects play a prominent role are described within the framework of the optical model (with the help of the known optical potential). A wide range of experimental data on pionic atoms and on scattering of pions by nuclei can be described with the help of pion-nucleus potential which is obtained theoretically from fundamental properties of πN-interaction. The derivation and the properties of the πA-potential are described in detail in References 4 and 6. The primary act of absorption — (stage 3), in which a pion disappears and a sufficiently large amount of energy ($\approx m_\pi$) released is transferred to nucleons formed in this act—serves as a natural boundary between initial stages of the process and the successive stage of the reaction. Emergence of fast nucleons diverging at large angles with respect to one another destroys quantum-mechanical interference effects. This allows us to describe stage (4) during which the energy released in the primary act of absorption is transferred to internal degrees of freedom of a T-nucleus, within the framework of semiclassical approximation. Dissipation of the energy proceeds through a rescattering of nucleons, produced as a result of absorption, in nuclear matter. Since the kinetic energy of these nucleons is not high ($\lesssim$ 100 MeV), the standard INC-model outlined in Chapter 2 is used to describe this stage of the reaction. Finally, the last, evaporation stage (5), is described with the help of statistical model of decay of highly-excited nuclei outlined in Chapter 3.

Thus, the underlying principle of the approach is that the initial conditions for the KE describing the deep inelastic process initiated by the products of pion absorption are determined with the help of the optical model. Let us now turn our attention to a more detailed analysis of these initial conditions.

2. Radial Dependence of the Probability of Absorption of a Pion by a Nucleus

Spatial dimensions of a source of initial particles which are preset by the radial dependence of the probability $P_{abs}(r)$ of pion absorption are among the most important characteristics of the process. To find this value it is necessary to carry out a consecutive quantitative analysis of the stages of formation and de-excitation of an π-atom. To this end Ericsons' standard optical πA-potential consisting of a local

and a nonlocal term (the latter also takes into account absorption) is often used[15] in the form

$$2\mu V_{opt}(\mathbf{r}) = \beta(r) - \nabla\alpha(r)\nabla , \tag{1}$$

where

$$\beta(r) = 4\pi[k_1 b_0 \rho'(r) + k_1 b_1 \rho''(r) + k_2 B_0 \rho'^2(r)] , \tag{1a}$$

$$\alpha(r) = \alpha_0(r)/[1 - \xi\alpha_0(r)/3] , \tag{1b}$$

$$\alpha_0(r) = 4\pi[k_1^{-1} c_0 \rho'(r) + k_1^{-1} c_1 \rho''(r) + k_2^{-1} C_0 \rho'^2(r)] . \tag{1c}$$

Here $\rho'(r) = \rho_p(r) + \rho_n(r)$ and $\rho''(r) = \rho_n(r) - \rho_p(r)$ are expressed in terms of the distributions of protons ρ_p and of neutrons ρ_n in a nucleus; $k_1 = 1 + m_\pi/m_N$ and $k_2 = 1 + m_\pi/2m_N$; m_π is the pion mass, m_N the nucleon mass, μ the reduced mass of the π-atom, ξ the correlation parameter of the potential, b_0, b_1, c_0, and c_1 are the single-nucleon parameters of the potential, and B_0 and C_0 the two-nucleon parameters of the potential. In calculations, we used the values of the potential parameters[17] from the analysis of the energy shifts and level widths of 59 pionic atoms over the entire periodic systems of elements. Parameters of the distribution of nuclear density were borrowed from Reference 18. It was also assumed that $\rho_p(r)/Z = \rho_n(r)/N$.

The energy states of a pion were determined through the solution of the Klein-Gordon equation

$$(-\nabla^2 + \mu^2 + 2\mu V_{opt})\psi = (E + V_c)^2\psi \tag{2}$$

with the potential of Equation 1. Here the Coulomb potential V_c takes into account the vacuum polarization in the lowest order of the perturbation theory. It follows from the expression for the divergence of the flux density j_μ

$$\partial_\mu j_\mu = -2\,\mathrm{Im}\,(\psi^* V_{opt}\psi)$$

corresponding to Equation 2 that the radial distribution of the probability of pion absorption has the form[17]

$$\begin{aligned} P_{abs}(r) &= \int r^2 d\Omega\{2\beta_I|\psi|^2 + 2\alpha_I|\nabla\psi|^2 - \nabla(\psi^*\alpha_I\nabla\psi + \psi\alpha_I\nabla\psi^*)\}, \\ \beta_I(r) &\equiv |\mathrm{Im}\,\beta(r)|, \quad \alpha_I(r) \equiv |\mathrm{Im}\,\alpha(r)| . \end{aligned} \tag{3}$$

Probability distributions $p_{nl}(r)$ for pion absorption from each (n,l)-state of a mesoatom were found[16] from a numerical solution of Equations 2 and 3. Then they were summed up with allowance for corresponding probabilities W_{nl}^{abs} of absorption

from each mesoatomic state in order to determine the desired total probability of pion absorption

$$P_{abs}(r) = \sum_{n,l} W_{nl}^{abs}\, p_{nl}(r) \,. \tag{4}$$

The absorption probabilities

$$W_{nl}^{abs} = \omega_{nl}\, \Gamma_{nl}(abs)/\Gamma_{nl}(tot) \tag{5}$$

were calculated according to the code of an atomic cascade which takes into consideration electric dipole Auger-transitions, radiation transitions, and nuclear absorption as well.[19] Here ω_{nl} is the population of the state, $\Gamma_{nl}(tot) = \Gamma_{nl}(abs) + \Gamma_{nl}(\gamma) + \Gamma_{nl}(a) + \Gamma_{\pi}$ the total level width equal to the sum of four terms, namely, the partial widths of absorption Γ (abs), of emission of photons Γ (γ) and of Auger-electrons Γ (a), and the decay width of a pion $\Gamma_{\pi} = \hbar/\tau_{\pi}$. The electromagnetic widths $\Gamma(\gamma)$ and Γ (a) are calculated by the standard method through corresponding dipole matrix elements and wave functions of a hydrogen-like atom,[4-6] whereas the nuclear widths are evaluated in accordance with the formula

$$\Gamma_{nl}(abs) \sim \int \mathrm{Im}\, V_{opt} |\psi_{nl}(r)|^2 r^2 dr \,. \tag{6}$$

To calculate the atomic cascade it is necessary to preset an initial distribution of pions captured by the Coulomb field of a nucleus over the quantum numbers n and l. For present purposes, it is sufficient to confine oneself to a simple statistical distribution[4-6]

$$c_{nl} \sim \delta_{nn_0}\, (2l + 1) \cdot \exp(\chi l) \tag{7}$$

(where $n_0 = \sqrt{m_{\pi}/m_e} = 17$ and $\chi \approx 0.2$), since fine details of the interaction between a pion and the electronic shell of an atom at the initial stage of the transition of the pion from a continuous spectrum to a discrete one, which are not taken into account in the calculations, cannot significantly affect the form of the function $P_{abs}(r)$.

The results of the calculation[16] of the atomic cascade are indicative of the fact that the capture of a pion from an orbit of a mesoatom takes place in the surface layer of a nucleus (see Figure 1). The distribution $P_{abs}(r)$ can be approximated[7] by the expression

$$P_{abs}(r) \sim \exp\left[-\frac{1}{2} \left(\frac{r - R_m}{D} \right)^2 \right] . \tag{8}$$

The values of the parameters of the Gaussian distribution are listed in Table 1. The same table shows the results of the calculations with the Kisslinger potential,[20]

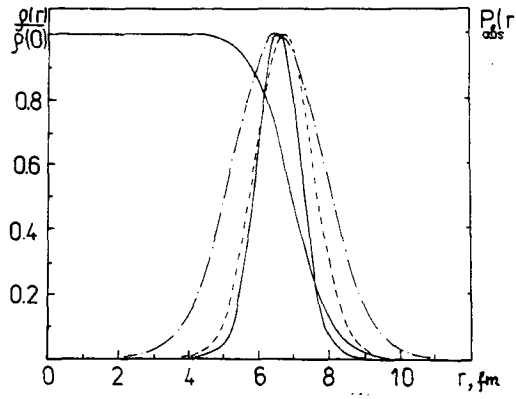

FIGURE 1. This describes radial distribution of nuclear density $\rho(r)/\rho(0)$ and that of absorption probability $P_{abs}(r)$ (relative units) for a ^{238}U nucleus. The solid, the dashed, and the dash-dotted curve correspond to the calculation[16] of $P_{abs}(r)$ in accordance with the formula in Equation 8 with D = 0.62, 0.83, and 1.3 fm, respectively.

TABLE 1
Parameters of the Gaussian Describing the Distribution of Pion-Nuclear Absorption P_{abs} (r)

Nucleus	R_m(fm)	D(fm)	$\rho_N(R_m)/\rho_N(0)$	$R_{1/2}$(fm)	Δ(fm)
^{31}P	3.10	0.623	0.618	3.508	2.3
^{40}Ca	3.37	0.645	0.647	3.6903	2.3
^{59}Co	4.01	0.627	0.618	4.2601	2.3
^{65}Cu*	3.99	0.694	0.587	4.2	2.59
^{75}As	4.39	0.619	0.622	4.6470	2.3
^{127}I	5.29	0.615	0.645	5.6045	2.3
^{181}Ta	5.99	0.615	0.664	6.3439	2.3
^{181}Ta**	6.10	0.775	0.616	6.4	2.81
^{197}Au	6.17	0.619	0.666	6.5334	2.3
^{209}Bi	6.29	0.617	0.674	6.6688	2.3
^{238}U	6.60	0.613	0.671	6.4754	2.3
^{238}U***	6.76	0.836	0.603	6.4754	2.3

* Calculations borrowed from Orth et al.[10]
** Calculations carried out with the help of the Kisslinger πA-potential.
***The parameter Δ is the thickness of the diffuse layer of a nucleus.

whose parameters were obtained by forcing the results to fit the data on π- atoms, and the results[10] of the calculation of P_{abs}. It follows from Table 1 that the position $R_m = R_{1/2} + \Delta R$ of the peak of the Gaussian can be identified to a sufficiently high degree of reliability, since the theoretical value of the parameter ΔR which determines its shift with respect to the half-density radius $R_{1/2}$ depends only slightly on the form of the potential V_{opt} and is close to zero. The value of the dispersion D^2 can depend on the parameters of both V_{opt} and the distribution $\rho_N(r)$ of nuclear density.

3. Mechanism for Absorption of a Pion by a Nucleus

The number and energies (momenta) of nucleons produced in an elementary act of absorption also appear in the initial conditions of the KE which describes the transfer of products of pion absorption in nuclear matter. Since the energy-momentum conservation law forbids the absorption of a pion by a free nucleon, this process is suppressed strongly in the case of absorption by an intranuclear nucleon as well. It follows from experimental data[3] that the probability of a single-nucleon absorption is very small ($\sim 10^{-3} - 10^{-4}$) even in the case of ^{6}Li and decreases with increasing A. Therefore, it will be disregarded in our calculations.

A pion is absorbed predominantly by nuclear substructures, namely by multi-nucleon associations. Analysis of experimental data shows[1-3] that a pion is absorbed mainly by the simplest association consisting of two nucleons:

$$\pi^- + (\mathrm{np}) \rightarrow \mathrm{n} + \mathrm{n} , \tag{9a}$$

$$\pi^- + (\mathrm{pp}) \rightarrow \mathrm{n} + \mathrm{p} . \tag{9b}$$

Such a quasideuteron mechanism was proposed for the first time by Brueckner et al.[21] In the simplest case when we neglect the spin effects, the charge state of two nucleons is determined by the number of pairs of a given type. Then the probability of absorption by a np-pair is given by the expression

$$w_{np} = \frac{NZ}{NZ + Z(Z - 1)/2} . \tag{10}$$

It follows from Equation 10 that, in this case, a pion is absorbed more often by np-pairs than by pp-pairs:

$$\eta = w_{np}/w_{pp} = 2N/(Z - 1) > 2 . \tag{11}$$

It should be noted that taking account of isospin effects can change significantly the value of η. Various theoretical estimates of this quantity fall within the limits $0 < \eta < 10$ (see the analysis of the isospin effect on the value of η carried out in References 10 and 11). Presently, experimental data also do not allow one to reliably fix the value of η, since the characteristics of reaction which are used for determination of η_{exp} are strongly influenced by the effects of the final state interaction. Therefore, the values of η_{exp} are very uncertain and can vary from one to 18.[3,10,11,22] In this connection, the quantity η should be considered as a parameter of the model whose value is determined from the comparison with experimental data. The simple combinatorial estimate (Equation 11) is usually taken as a starting point in the procedure of forcing the theory to fit the data.

Once a pion has been absorbed by a pair of nucleons, its mass m_π is converted into kinetic energy of nucleons each of which has the energy $E_N = m_\pi/2$ in the c.m.s., if the pion and the quasideuteron were at rest before absorption. In the

c.m.s., nucleons diverge in opposite directions isotropically. In the l.s., the energy of particles have a certain spread about the value $m_\pi/2$ because of nonzero values of momenta of intranuclear nucleons. The smear over the momenta of nucleon pairs in a nucleus was taken into account in the calculations in the following way: the momentum of the pair was taken as a sum of momenta of two intranuclear nucleons which were determined from the corresponding Fermi distribution (Equation 121, Chapter 2).

In principle, not only two, but also a larger number of nucleons (e.g., multinucleon associations ^{3}He, ^{4}He, ^{4}Li, etc.) can absorb a pion. It follows from the analysis of experimental data[2,14,22] that the probability of a multinucleon absorption in light nuclei can be about 5-25%. In the domain of medium-weight and heavy nuclei, the role of such an absorption mechanism is not practically studied. The α-particle mechanism* of absorption proposed for the first time in Reference 23 was considered alongside the two-nucleon one in Reference 7. In this case, the following reactions proceed on the ^{4}He nucleus with the relative probabilities W determined in the experiment[22]

$$\pi^- + (^4\mathrm{He}) \rightarrow t + n, \quad W_2 = (19.4 \pm 1.8)\% , \tag{12a}$$

$$\pi^- + (^4\mathrm{He}) \rightarrow d + 2n, \; W_3 = (58 \pm 7)\% , \tag{12b}$$

$$\pi^- + (^4\mathrm{He}) \rightarrow p + 3n, \; W_4 = (26 \pm 6)\% . \tag{12c}$$

It is incorrect to apply these probabilities directly for the calculation of the α - particle absorption in nuclear matter, if for no other reason than the contribution to the absorption of a pion by a free ^{4}He nucleus coming from the two-nucleon mechanism. Proceeding from these consideration and pursuing the aim of evaluating the maximum effect, we can make an assumption that only the channel (Equation 12c) with four particles in the final state (with W_4 = 100%) is realized after the absorption. From the viewpoint of kinematics, the reaction is the limiting one with respect to the reaction (Equation 9), since the pion mass is converted here into kinetic energy of four nucleons rather than into that of two nucleons. Nucleon momenta in the channel (Equation 12c) were calculated in accordance with the Fermi statistical model (see Section VA, Chapter 3), and their angular distribution was assumed to be isotropic in the c.m.s. Each act of decay of an α-particle must satisfy the energy-momentum conservation law and the Pauli exclusion principle, i.e., the energy of each nucleon must be higher than the Fermi energy.

4. Method of Calculation

Two (four in the case of α- particle absorption) "parallel" intranuclear cascades, initiated by the products of pion absorption were described with the help of the

* For the sake of simplicity the term "α-particle" is used in what follows to denote the set of four nucleons.

INC-model (see Section II, Chapter 2), and the decay of highly-excited C-nuclei with the help of the evaporation model (see Section I, Chapter 3). No additional parameters were introduced, since all parameters of these models were determined independently from analysis of reactions with nucleons and heavy ions. All stages of the absorption were calculated by the Monte Carlo technique, as it was described in Sections IA2 and IA3 in this chapter. The use of a KE with a many-particle distribution function in the INC-model is crucial for the description of exclusive characteristics of deep inelastic processes with many-particle initial conditions (see Section A1 and 2). The spallation of a nuclei caused by the absorption of a slow pion is just the process of such a type.

The optical + cascade model (OC-model) which consistently takes into consideration all stages of nuclear absorption of pions was proposed for the first time in Reference 7. Some years later a similar model was considered.[10] An analytic version of the OC-model aimed at description of characteristics of fast secondary particles with no regard for the evaporation stage of the process has been developed.[11]

Alongside the OC-model, an approach based on the use of the exciton model (master equation of the form of Equation 114, Chapter 2) for description of the dissipation of energy released as a result pion absorption was developed.[8,12-14] The main difficulty of exciton models is associated with the determination of the initial quasiparticle configuration of the excited nuclear system described by the master-equation. It is assumed in the case under consideration[8] that after the pion absorption, each of two independent nucleonic cascades is characterized by the initial configuration 1p-1h with the total energy of quasiparticles $m_\pi/2$. The principal drawback of the exciton approach is that it does not take into account the surface nature of the absorption of a pion by a nucleus (stages 1 and 2 of the process). This flaw can be remedied to some extent by assuming that a fraction of primary nucleons leaves the nucleus freely without entering into any interaction.[14] The fraction of such "direct" nucleons is a parameter determined from the comparison with experimental data. As a result, the role of the exciton model[8] is reduced to the description of the last (5) stage, whereas, the initial conditions for the master Equation 114, Chapter 2 are prescribed by the "direct" (4) stage, of the process. Thus, the evolution of the exciton approach leads to its convergence with the optical + cascade approach. Hence, the OC-model is a more consistent model of absorption of the stopped π-mesons by nuclei, and it offers greater possibilities than the exciton one. In the next section, it will be used for the analysis of experimental data.

B. ANALYSIS OF EXPERIMENTAL DATA

1. Energy Spectra of Particles

Emission of neutrons is the most probable type of decay of a highly-excited nucleus formed as a result of pion absorption. By now, numerous experiments concerned with the measurement of energy spectra of neutrons[3] have been carried out. Spectra of neutrons corresponding to the case when π-mesons are absorbed by ^{59}Co and ^{197}Au nuclei are shown in Figure 2 as an example. The spectrum has

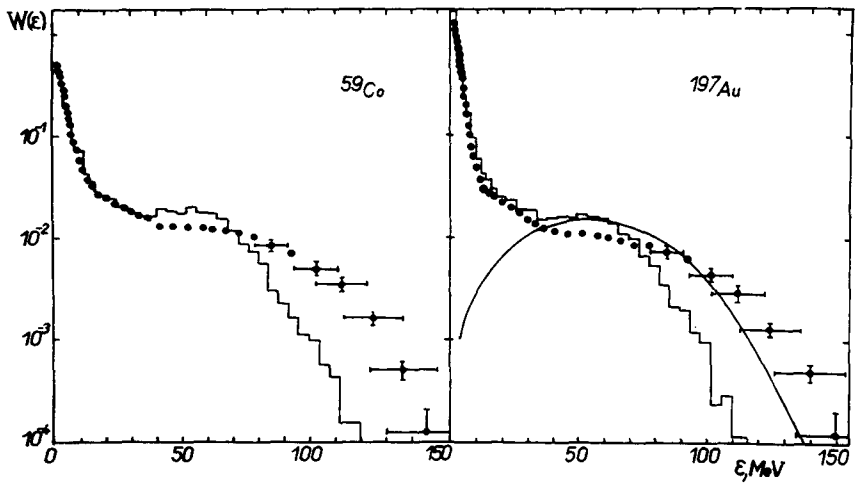

FIGURE 2. Here are energy spectra for neutrons (in neutrons/π^-·MeV) emitted upon the absorption of slow negative pions by ^{59}Co and ^{197}Au nuclei. Points correspond to experimental data,[24] histograms to the present OC-model calculation,[3,7] and the solid curve shows the results of the calculations borrowed from Reference 9.

a peculiar feature associated with the existence of the cascade (4) and the evaporation (5) stage of the absorption process. Two components are clearly manifested in the spectrum, the evaporation and the "direct" neutrons. Neutrons emitted by excited C-nuclei constitute the evaporation part of the spectrum, whereas a high-energy part of the spectrum is formed mainly from fast cascade particles escaping from the surface layer of the nucleus practically without collisions with intranuclear nucleons.

Because of the surface character of absorption, a high-energy part of spectrum depends only slightly on the atomic number of a target. For example, the average multiplicity of fast neutrons is equal to 1.38 and 1.32 neutrons per an absorbed pion for nuclei of ^{59}Co and ^{197}Au, respectively.[24] An increase in the total multiplicity from 4.04 neutrons for a nucleus of ^{59}Co to 6.31 neutrons for a nucleus of ^{197}Au[24] is indicative of the fact that the multiplicity of the evaporation neutrons depends on the mass number A_t of a target. To a large extent, this is a consequence of an increase in the excitation energy of a C-nucleus.

The theory describes the evaporation part of the spectrum to a good accuracy. On the other hand, the direct component turns out to be significantly softer than in experiments. Although the peak of this part of the spectrum is situated at the energy $m_\pi/2 - B_n \simeq 60$ MeV, its smearing in the domain of high energies is far from being sufficient. This is apparently indicative of the fact that the model does not describe correctly the high-momentum component of the distribution of intranuclear nucleons. The local density approximation (see Section IIA2, Chapter 2) used in the model gives small values of momenta of intranuclear nucleons situated at the periphery of the nucleus. As a result, the smearing of the neutron spectrum

turns out to be small. This conclusion can be confirmed by a simplified calculation[9] of the fast component of the neutron spectrum. Taking the momentum distribution of intranuclear nucleons in the form

$$f(p) \sim \exp(-p^2/\tilde{p}^2) , \tag{13}$$

where the parameter $\tilde{p}$ satisfies the inequality $13 \leq \tilde{p}^2/2m_N \leq 20$ MeV, one can obtain[9] the expression

$$dN/d\epsilon_n \sim \sqrt{\epsilon_n}\,(E_0 - \epsilon_n)\exp\left[-(m_N/\tilde{p}^2)(\sqrt{\epsilon_n} - \sqrt{E_0 - \epsilon_n})^2\right] , \tag{14}$$

for the neutron spectrum which ensures a better agreement with experimental data in the domain of high energies (see Figure 2). Here $E_0 = m_\pi - B_\pi + M(A,Z) - M(A,Z\text{-}1) - B_{2N}$, B_π is the binding energy of a pion in the mesoatom, B_{2N} the binding energy of two nucleons in the nucleus (A,Z-1), and M the mass of the corresponding nucleus. A discrepancy in the domain of high energy ($\epsilon_n > 100$ MeV) can be also explained by the contribution from the single-nucleon or the α-particle (Equation 12a) mechanism of absorption.

Energy spectra of charged particles are shown in Figure 3. All that was said above about the neutron spectra remains valid for the proton spectra except that for heavy nuclei the evaporation component of the proton spectrum manifests itself only slightly because it is suppressed by the Coulomb barrier. The direct component of the proton spectrum is formed as a result of the reaction in Equation 9b. Therefore, it would be possible, in principle, to extract the value of the parameter η from the comparison of calculated and experimental spectra at the energies $\epsilon_n > 30$ MeV. Unfortunately, the errors which are present in the measurement of the magnitudes of the energy spectra (these values obtained by different experimental groups can differ several times from one another[3]) do not yet allow one to determine η to a sufficient accuracy.

On the whole, the calculations have demonstrated[3,7] that inclusive spectra of emitted particles are hardly sensitive to the changes in the parameters of the model. Figures 2 and 3 show the results of the calculations with parameters D = 1.3 fm, $\Delta R = 0$ and with the combinatorial value of η (Equation 11). In what follows, this version of the calculation will be cited as a basic one. Taking account of the emission of pre-equilibrium particles at stage 4 leads to a very slight rise in the inclusive spectra in the energy range $\epsilon_N = 20 - 40$ MeV and does not practically affect this characteristic of the process.[7] The channel (Equation 12C) of the α-particle mechanism gives softer spectra of nucleons, but it seems impossible to isolate the contribution of this mechanism from the inclusive nucleon spectrum at the level $\lesssim 25\%$[7] (see Figure 4).

Analysis of spectra of complex charged particles is of particular interest, since it is usually assumed that such particles can be produced as a result of absorption of a pion by an association more complex than a two nucleon one. However, it is

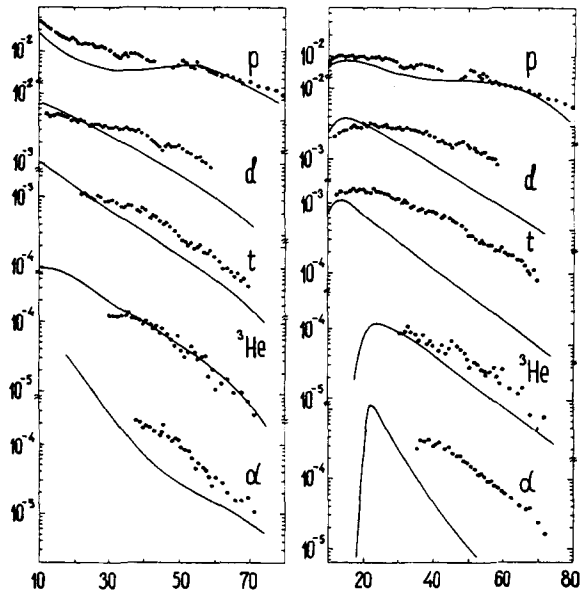

FIGURE 3. These are energy spectra of protons, deuterons, nuclei of tritium, and ^{3}He, and α-particles emitted upon absorption of stopped π^--mesons by ^{59}Co (on the left) and ^{197}Au (on the right) nuclei. The curves correspond to the calculations of References 3 and 7, and the points correspond to experimental data.[25] The number of particles per MeV per a stopped π^- is plotted along the vertical axis and the energy measured in MeV along the abscissa.

necessary to evaluate the contribution of other possible mechanisms to the production of such particles prior to investigating this issue in the case of complex nuclei. Among them the simplest mechanism is the evaporation one. Calculations[3] have demonstrated that it is impossible, in this case, to describe either the shape or the magnitude of the spectra depicted in Figure 3. It has been demonstrated[3] that pre-equilibrium processes give an important contribution to the spectra of complex charged particles. Figure 3 shows the results of calculations[3] taking into account pre-equilibrium emission. It is seen that the contribution of pre-equilibrium particles to the spectra is rather large. On the other hand, calculated curves lie lower than experimental points in the domain of high energies. Both the mechanism of direct emission after the capture of a pion by multinucleon associations, which was outlined above, and the mechanism of emission of complex particles at the stage of the INC, can remove the discrepancy in this domain. The process of the pickup of an intranuclear nucleon by a fast nucleon as well as knockout of clusters by cascade nucleons can be classified as the mechanisms of the latter type.

More definite conclusions on the role of the multinucleon pion absorption can be drawn from the analysis of data for light T-nuclei. It has been demonstrated[26] that in this case the pre-equilibrium emission affects only slightly the yields of complex particles. This is because the number of excitons after the completion of the cascade and the density of the exciton states in a light R-nucleus are both small.

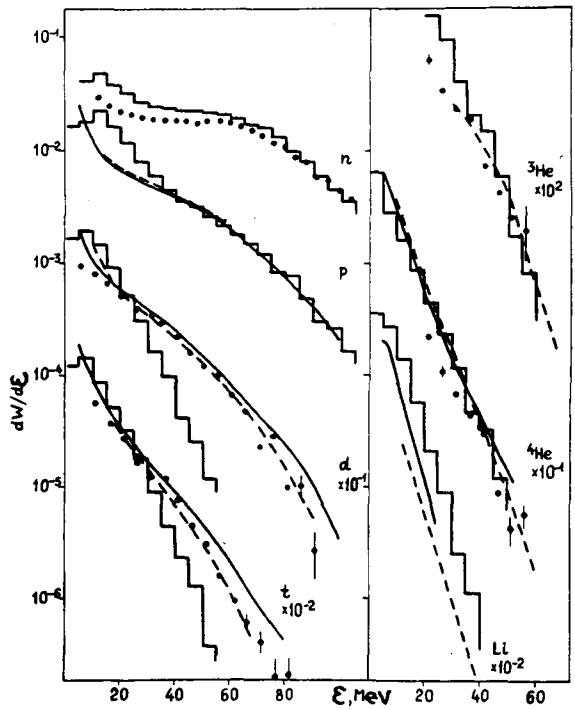

FIGURE 4. Energy spectra of nucleons and fragments (in the number of particles per MeV per π^-) produced upon the absorption of stopped π^- mesons by ^{12}C nucleus are graphed here. Registered particles are indicated in the figure. Histograms correspond to the calculation of Reference 26. Experimental data are shown by solid curves,[27] dashed curves,[28] points for neutrons,[22] and points for charged particles.[29]

The Fermi breakup (see Section VA, Chapter 3) is the principal mechanism responsible for the decay of an excited light R-nucleus. Figure 4 shows the results of the calculations[26] of the absorption of stopped π^--mesons by light nuclei. These calculations take into account the mechanism of the Fermi breakup.* The spectra of heavier fragments (^{3}He, ^{4}He, Li,...) are described by the theory to a good accuracy. This is indicative of the realization of the complete breakup of a T-nucleus in the reaction under investigation. A large yield of light fragments (d,t) with high energies can be explained by the contribution coming from the channels of multinucleon pion absorption, such as in Equations 12a and 12b, $\pi^- + (^3\text{He}) \rightarrow n + d$, etc.

Thus, the extraction of the contribution coming from the absorption of a pion by multinucleon associations from inclusive spectra of complex charged particles involves difficulties, since it is necessary to isolate it against the background of

* Calculations were carried out with $\eta = 7 \pm 2$. This value ensures the best description of the inclusive spectrum of neutrons and protons (see Figure 4).

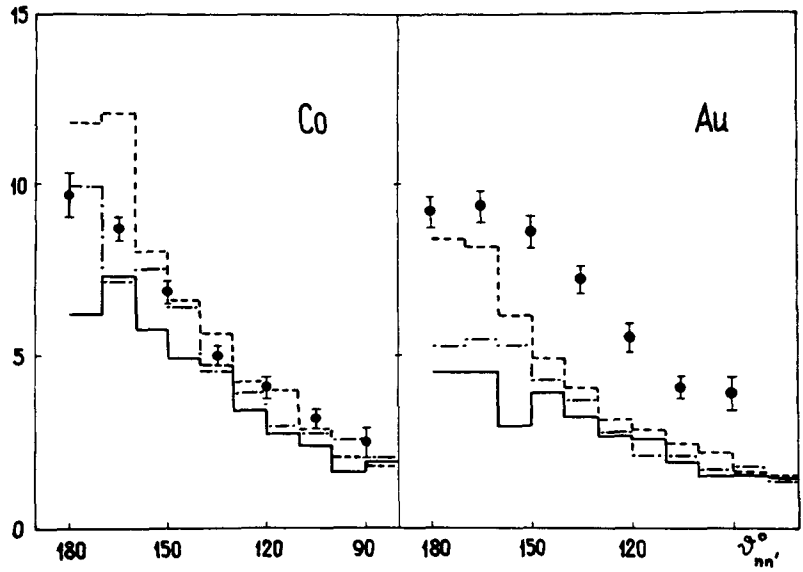

FIGURE 5. This charts angular correlation of two fast ($\epsilon \geqslant$ 20MeV) neutrons upon absorption of π^--mesons by ^{59}Co and ^{197}Au nuclei (in the number of particles per MeV·π^-·sr^2). The solid, the dash-dotted, and the dashed histogram depict the results of the calculation[16] with D = 0.62, 0.83 and 1.3 fm, respectively. Experimental data[24] are shown by the points.

other emission mechanisms. However, the solution of this problem is alleviated by the fact that the background mechanisms of emission of complex charged particles (such as evaporation, pre-equilibrium emission, and the pickup and knockout processes) are present in the pA-interaction at the energy $\epsilon_0 = m_\pi/2$ as well. Therefore, a simultaneous analysis of inclusive spectra of complex charged particles emitted in the π^-A-absorption and in the pA-interaction within the framework of the same model allows us to determine, in principle, the fraction of charged particles emitted after the absorption of a pion by a multinucleon association to a better accuracy.

2. Correlations Between Emitted Particles

Measurements of the energy and the angular distribution of various particles in coincidence give a more detailed information on the mechanism of pion absorption. Angular correlations of two neutrons or of a neutron and a proton have a pronounced peak at an angle of 180°, which is broadened as we go over to heavier nuclei (see Figure 5). Such a pattern corresponds to a two-nucleon pion absorption and is described by the model to a reasonable accuracy.

It has been mentioned that data obtained on light nuclei are of special interest for the study of the mechanism of pion absorption. Angular correlations of nucleons and fragments produced as a result of absorption of a π^--meson by a ^{12}C nucleus are shown in Figure 6. The experiment and the calculation are in qualitative agreement with one another except for the n-d and n-t correlations. The existence of a

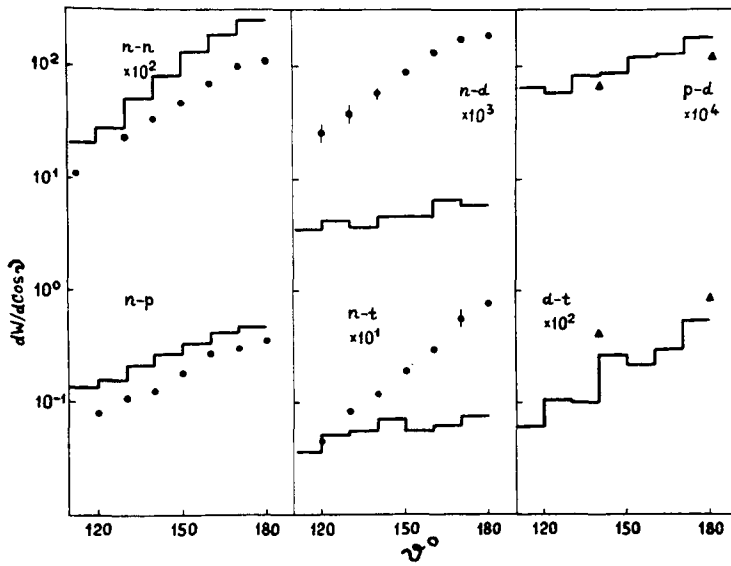

FIGURE 6. Here are angular correlations of nucleons and light fragments (in the number of particles per π^-) produced in the reaction of absorption of stopped π^--mesons by a ^{12}C nucleus. Particles registered in the correlations are indicated in the figure. Histograms depict the results of the calculations of Reference 26. Experimental data are shown by points[22] and triangles.[28]

pronounced peak at 180° in the latter correlations is indicative of the contribution coming from the three- and the four-nucleon absorption of a pion.

In addition to angular correlations, other more complex correlations have also been investigated. For instance, kinematically complete measurements[30] of the absorption of pions by lightest nuclei, such as ^3He and ^4He, (measurement of triple coincidences) have demonstrated that, in this case, the contribution of the multinucleon mechanism of absorption is about 25% of a two-nucleon one. Reviewing recent studies of this problem,[31,32] one can state that while the contribution of the multinucleon absorption decreases for complex nuclei, it nevertheless represents a noticeable part (about 10-15%) of the two-nucleon one.

In conclusion, one more correlation characteristic, namely the probabilities of separate multibody channels of a reaction, may be also touched upon. Experimental values[33] of these probabilities are listed in Table 2. The data presented in the table are described satisfactorily by the OC-model with a subsequent Fermi breakup of a light nucleus.[26] This shows that the development of this approach by taking account, above all, of the multinucleon pion absorption is very promising. From the viewpoint of the study of details of the primary act of pion absorption (stage 3), an analysis of characteristics of high-energy particles emitted from light nuclei is of particular interest. The entire set of these characteristics including the properties of R-nuclei can be determined with the help of OC-model as well. Here we shall pay special attention not to the analysis of the spectra of emitted particles, but to the discussion of the issue as to what information on the mechanism of the absorption

TABLE 2
Probabilities of Different Channels of Decay of ^{12}C and ^{16}O Nuclei upon Absorption of Stopped π^--Mesons

Nucleus	Decay channel	Experiment	Calculations	Decay channel	Experiment	Calculations
	np ^{10}Be	$3.1\ 10^{-2} - 1.7\ 10^{-1}$	$1.4\ 10^{-2}$	np ^{4}He ^{6}He	$2.7\ 10^{-3} - 2.5\ 10^{-2}$	$9.5\ 10^{-3}$
^{12}C	nd ^{9}Be	$3.6\ 10^{-2} - 1.6\ 10^{-1}$	$6.4\ 10^{-3}$	nd d ^{7}Li	$3.7\ 10^{-4} - 1.2\ 10^{-2}$	$4.7\ 10^{-3}$
	n ^{4}He ^{7}Li	$1.5\ 10^{-1} - 2.4\ 10^{-1}$	$9.5\ 10^{-3}$	ndt ^{6}Li	$4.6\ 10^{-4} - 2.1\ 10^{-2}$	$4.8\ 10^{-3}$
	n ^{3}He ^{8}Li	$2.2\ 10^{-4}$	$4.9\ 10^{-3}$	nd ^{3}He ^{6}He	$1\ 10^{-3} - 2.3\ 10^{-2}$	$1.1\ 10^{-3}$
	npt ^{7}Li	$1.8\ 10^{-3} - 2.2\ 10^{-2}$	$3.2\ 10^{-2}$	nt ^{4}He ^{4}He	$2.5\ 10^{-3} - 1.6\ 10^{-2}$	$5.4\ 10^{-3}$
	np ^{14}C	$6.2\ 10^{-3} - 1.2\ 10^{-1}$	$6.8\ 10^{-3}$	np ^{7}Li ^{7}Li	$0.9\ 10^{-4} - 6.5\ 10^{-3}$	$7.2\ 10^{-3}$
	nd ^{13}C	$1.4\ 10^{-3} - 1.3\ 10^{-1}$	$5.4\ 10^{-3}$	ndd ^{11}B	$3.7\ 10^{-4} - 6\ 10^{-3}$	$3.4\ 10^{-3}$
^{16}O	nt ^{12}C	$2.8\ 10^{-3} - 1.2\ 10^{-1}$	$2.8\ 10^{-3}$	ndt ^{10}B	$0.9\ 10^{-4} - 9.4\ 10^{-3}$	$2.2\ 10^{-3}$
	n ^{3}He ^{12}B	$1.9\ 10^{-3} - 1.4\ 10^{-2}$	$2.1\ 10^{-3}$	nd ^{3}He ^{10}Be	$1.8\ 10^{-4} - 1.1\ 10^{-2}$	$1.7\ 10^{-3}$
	n ^{4}He ^{11}B	$6.7\ 10^{-3} - 2.1\ 10^{-2}$	$1.7\ 10^{-2}$	nd ^{4}He ^{9}Be	$4.6\ 10^{-4} - 1.3\ 10^{-2}$	$1.9\ 10^{-3}$
	n ^{6}Li ^{9}Be	$1.4\ 10^{-3} - 1.7\ 10^{-2}$	$3\ 10^{-3}$	nd ^{6}He ^{7}Be	$4.6\ 10^{-4} - 9.4\ 10^{-3}$	$5\ 10^{-4}$
	npt ^{11}B	$1.8\ 10^{-4} - 1.1\ 10^{-2}$	$2.4\ 10^{-2}$	nd ^{6}Li ^{7}Li	$3.7\ 10^{-4} - 9.3\ 10^{-3}$	$2.3\ 10^{-3}$
	np ^{4}He ^{10}Be	$5.5\ 10^{-4} - 1.2\ 10^{-2}$	$2.2\ 10^{-2}$	nt ^{3}He ^{9}Be	$0 - 9.2\ 10^{-3}$	$5\ 10^{-4}$

Experimental values (with the upper and the lower boundary) are borrowed from Reference 33. Calculations were carried out in Reference 26 in accordance with the OC-model with allowance for the subsequent Fermi breakup.

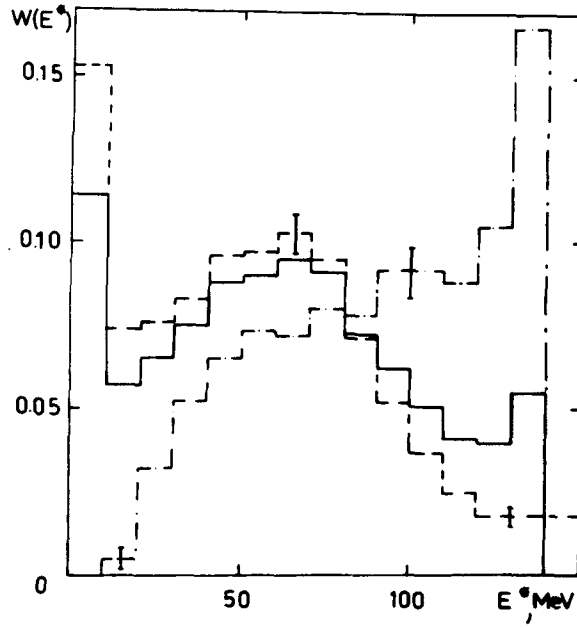

FIGURE 7. This is the distribution of C-nuclei are produced upon the absorption of π^--mesons by a ^{208}Pb nucleus over the excitation energy E*. The dashed line corresponds to the calculation according to the quasideuteron mechanism of absorption and the dash-dotted line to the calculation according to the α-particle mechanism of absorption. The solid histogram describes the situation in which a pion is absorbed by an α-particle in 25% of cases and by a quasideuteron in 75% of cases. The area under the histograms is normalized to unity.

of a pion by a nucleus can be extracted from characteristics of R-nuclei. The possibility of such a formulation of the problem is associated with the fact that the intermediate C-nucleus loses a memory about its formation only with respect to its internal single-particle degrees of freedom, whereas its excitation energy, momentum, and angular momentum preserve this memory about the interaction mechanism at the initial stages of de-excitation.

3. Excitation Energy of R-Nuclei and Isotope Yield

Since the energy of cascade nucleons varies in sufficiently wide limits (see Figures 2 and 3), the distribution of R-nuclei over the excitation energy is wide as well. In accordance with the INC-model the excitation energy of a nucleus is the sum of the energy of "particles" and "holes" measured from the Fermi energy (see Equation 17, Chapter 1 and Equation 124, Chapter 2). Hence, for our specific case of pion absorption we can obtain

$$E^* = m_\pi - \sum_i (\epsilon_i + B_N) , \tag{15}$$

where the summation is carried out over all cascade nucleons. Figure 7 shows the distribution of R-nuclei over the excitation energy before the evaporation stage as

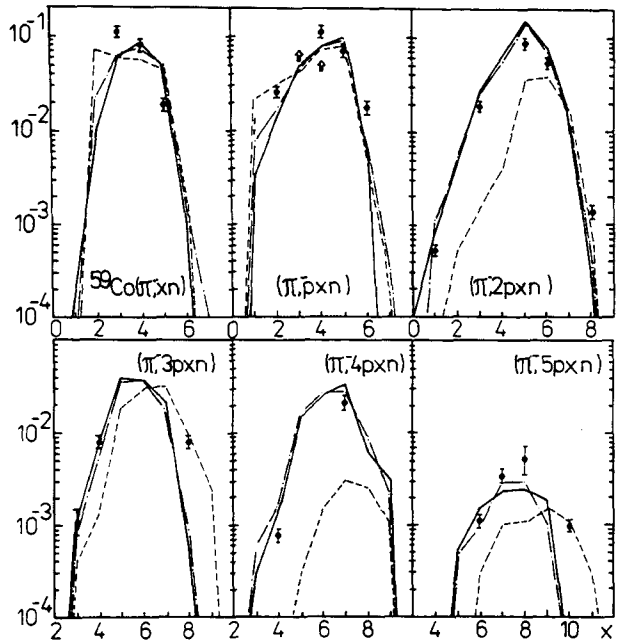

FIGURE 8. The isotope yield (in nuclei/π^-) upon the absorption of a π^--meson by a ^{59}Co nucleus is shown here. Experimental data[35] are shown by the points. The rest of the notation is the same as in Figure 5.

an example. For a heavy nucleus of Pb the excitation energy varies from several MeV to approximately 140 MeV. This corresponds to the absorption of all cascade nucleons and conversion of the entire pion mass to the excitation energy of the nucleus. As we go over to lighter nuclei, the distribution over E* is narrowed, and its peak is shifted towards the domain of smaller values of E*. The mean excitation energy $\bar{E}^*$ increases slowly with increasing mass number A_t of a target and achieves the value $\bar{E}^* \simeq m_\pi/2$ in the domain of heavy nuclei.[3]

As many as 15-17 nucleons can escape from a C-nucleus when the excitation energy E* is close to its maximum value $E^* \simeq m_\pi$. Indeed, a strong spallation of a nucleus after the π^--capture has been discovered as far back as 1954.[34] Since the distribution over E* is broad, the curve of the isotope yield is broad as well.

Figure 8 shows the comparison of the experimental yields of the reaction (π^-,xnyp) with calculations carried out for a two-nucleon mechanism of absorption. In the case of light and medium-weight targets, emission of charged particles gives a large contribution to the production of the final isotope (see Table 3). For heavy nuclei, a high Coulomb barrier hampers the emission of charged particles at last stages of the process, and the reaction (π^-, xn) dominates over all other reactions. The yield of (π^-,pxn) is smaller than the yield of (π^-,xn) in the domain of heavy nuclei, but it is the same order of magnitude, since the Coulomb barrier does not exert any noticeable influence on the escape of a fast proton produced by the pion absorption on the pp-pair. The information on the value of the parameter η can be

TABLE 3
Experimental and Theoretical Yields (%) of Different Channels of Reactions upon Absorption of Stopped π^--Mesons by ^{59}Co, ^{127}I and ^{197}Au Nuclei*

	^{59}Co		^{127}I		^{197}Au	
Reaction	**1**	**2**	**1**	**2**	**1**	**2**
(π^-,xn)	24 ± 3	23.2	58	51.0	74 ± 8	69.0
(π^-,pxn)	32 ± 3	25.4	22	30.6	20 ± 7	23.6
(π^-,2pxn)	24 ± 3	30.9	11	16.8	—	—
(π^-,3pxn)	12 ± 4	9.8	3	1.0	—	—
(π^-,4pxn)	6 ± 2	9.3	0.7	0.53	—	—
(π^-,5pxn)	1.5 ± 0.2	0.96	0.12	0.03	—	—
(π^-,6pxn)	—	—	0.03	—	—	—

* 1-experiment[34,35], 2-calculations.[3]

extracted, in principle, from the comparison of the yields of the xn- and pxn-reactions on heavy nuclei. However, one should take into account the influence exerted by the final state interaction effects on the experimental characteristic under investigation. The yield of reactions in which a small number of nucleons ($\Delta A \leqslant$ 4-5) leaves a T-nucleus is sensitive to the value of the parameter D, namely, their yield increases with increasing D.

The calculated yield of the reaction (π^-,xn) on heavy nuclei turns out to be sensitive to the contribution of the α-particle mechanism of pion absorption for $x > 12$, since, in this case, the conversion of m_π to E* occurs more effectively (see Figure 7). As a result, the quasideuteron and the α-particle mechanism of absorption give different positions of peaks in the distribution over the multiplicity of neutrons emitted from heavy nuclei (see Figure 9).

4. Angular Momentum of R-Nuclei and Excitation of High-Spin Isomeric States

The first observation[34] of the excitation of high-spin isomers as a result of absorption of stopped pions by nuclei remained unnoticed. Interest in this phenomenon was awakened when it was demonstrated[36] that the spin of the excited metastable states of a C-nucleus can be high ($\sim$ 10-20$\hbar$). How such a high angular momentum of a C-nucleus can arise, if the orbital momentum l_π of a pion on the orbit of the mesoatom from which the absorption takes place is small (see Table 4) seemed at the first glance something of a mystery. Therefore, during a short period of time, a large number of experiments devoted to the study of the excitation of high-spin isomers were carried out.[3]

This phenomenon was accounted for in Reference 7. An interpretation along similar lines of reasoning was given in References 10, 37, and 38. Proceeding from the expression in Equation 137, Chapter 2 for the angular momentum I_f of the final nucleus* formed as a result of absorption of the stopped π^-, we get

* The last link in the chain of nuclear transformation, namely the nucleus which can emit only γ-quanta, will be called the final nucleus.

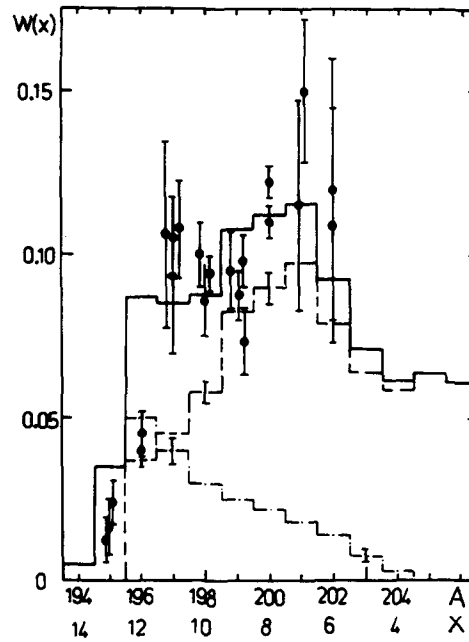

FIGURE 9. The distribution over the number x of neutrons emitted in the $^{208}Pb\ (\pi^-,xn)\ ^{208-x}Tl$ reaction is indicated here. Experimental data[36] are shown by the points. The rest of the notation is the same as in Figure 7.

TABLE 4
Relative Portion (in %) of Pion Absorption from a Given *l* State of a Mesoatom[15]

l Nucleus	0	1	2	3	4
^{31}P	3.32	87.93	8.747	—	—
^{40}Ca	1.79	69.98	28.23	—	—
^{59}Co	—	33.89	64.69	0.36	—
^{75}As	—	16.90	80.55	1.67	—
^{181}Ta	—	1.73	18.61	74.98	4.01
^{197}Au	—	1.67	12.54	77.13	7.96
^{209}Bi	—	1.63	9.70	75.95	12.0
^{238}U	—	1.60	5.73	66.34	25.45

$$\mathbf{I}_f = l_\pi + s_A - \sum_i l_c^i - \sum_i l_{ev}^i \tag{16}$$

where l_π is the orbital momentum of a pion in the mesoatomic state from which the pion has been absorbed (see Table 4), s_A the spin of a T-nucleus, and $\sum_i l_c^i$ and $\sum_i l_{ev}^i$ are the total momenta brought away by the cascade and the evap-

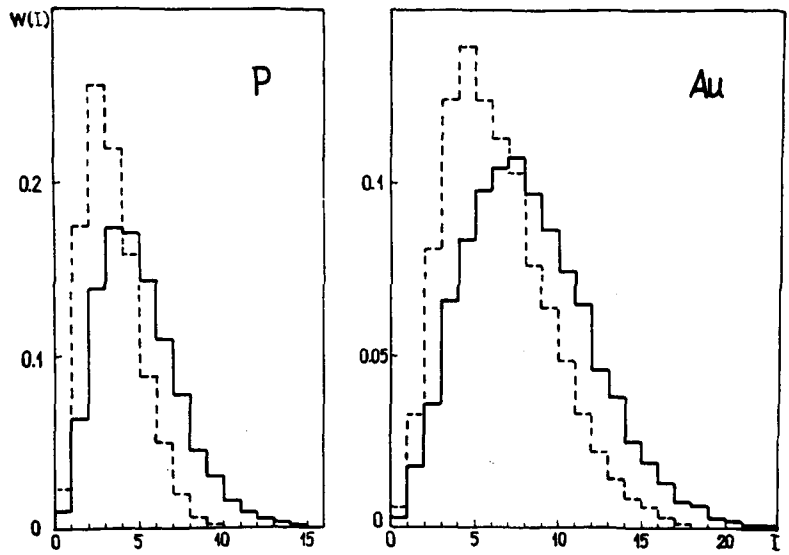

FIGURE 10. These chart the angular momentum distribution of final nuclei produced upon the absorption of π^--mesons by ^{31}P and ^{197}Au nuclei. The solid and the dashed histogram correspond to the calculation[16] with and without regard for evaporating particles, respectively. The area under the histograms is normalized to unity.

orated particles, respectively. The main contribution to $\mathbf{I}_f$ comes from the third term of Equation 16 which implies that a R-nucleus acquires a high angular momentum when a fast cascade nucleon escapes from the surface layer of the nucleus. Within the framework of the INC-model, angular momenta of high-energy nucleons are calculated with the help of the classical expression $\mathbf{l}_c^i = [\mathbf{r}_i\ \mathbf{p}_c^i]$. While calculating $\mathbf{I}_f$ we can approximately consider the vectors $\mathbf{l}_\pi$, $\mathbf{s}_A$, and $\mathbf{l}_{cv}^i$ as classical too, since $\left|\sum_i \mathbf{l}_c^i\right| >> 1$, and use the semiclassical method of calculation of de-excitation of a rotating nucleus outlined in Section II of Chapter 3 in order to determine their contribution. The mean angular momentum brought away by cascade nucleons increases with the mass number of a T-nucleus in accordance with expression $\bar{I}_f \simeq 0{,}92\ A_t^{1/3}$. This expression reflects the surface nature of absorption of a stopped π-meson by a nucleus.[3] Since the initial angular momentum $\mathbf{l}_\pi + \mathbf{s}_A$ is an irregular function of A_t, corresponding irregular deviations will be superimposed on this smooth dependence of the mean angular momentum of C-nuclei produced after the completion of the cascade stage of the process.

Figure 10 shows the distribution of final nuclei over the values of the angular momentum. It is seen that taking account of angular momenta of evaporated particles makes this distribution broader. Moreover, with allowance for all contributions in Equation 16, angular momenta of final nuclei can be as high as $I_f \approx 20$. Such high values of angular momenta of final nuclei are comparable with the values obtained in reactions with heavy ions. However, the source of the angular momentum is different, namely, in the HI-reactions the angular momentum is brought in a nucleus

by an impinging particle, whereas in the π^--absorption a nucleus acquires its additional angular momentum as a result of emission of fast nucleons from its surface layer.

It follows that the excitation of high-spin states is observed not only in the absorption of π-mesons by nuclei, but also in other deep inelastic processes with intermediate-energy particles. The integral angular momentum distribution of C-nuclei is a characteristic which is not sensitive enough to provide information on the mechanism of absorption of different particles by nuclei. This has been demonstrated[39] through the comparison of two similar reactions, the absorption of stopped pions and that of γ-quanta with the energy $\epsilon_0 = m_\pi$. It is well known that the mechanism responsible for the absorption of γ-quanta of such an energy is quasideuteron mechanism as well (see Section II of Chapter 2), but unlike the case of pions the absorption of γ-quanta occurs equiprobably over the entire volume of a nucleus. Calculations[39] have demonstrated that the distributions of C-nuclei over I obtained for these reactions are similar. Moreover, both calculations and experiments[10] have demonstrated that not only the distribution over I, but also isomeric ratios ξ_m for the excitation of separate high-spin states in one more similar process (the pA-reaction with $\epsilon_0 = m_\pi/2$) differ only slightly from the corresponding values for the π-absorption.

To study the mechanism of the absorption of a particle by a nucleus the authors of References 7 and 39 have proposed to use a more subtle characteristic than the integral distribution of nuclei over I_f, namely, the dependence of the mean angular momentum $\bar{I}_f$ on the number x of emitted particles. It can easily be shown[7] that the values of x are not equally effective in populating high-spin nuclear states. Let us find out what angular momentum a C-nucleus will have in the reaction (π^-,xn) before the commencement of the evaporation stage. The case of the maximum value of x, when all cascade nucleons are absorbed by a nucleus and only the evaporation neutrons will leave it isotropically later on, corresponds to low values of I (see Equation 16). Another limiting case $x = 2$, when two neutrons leave a nucleus in opposite directions after the absorption of π^- on the np-pair, gives a low value of I as well. It is evident that the maximum angular momentum is realized, when, after the absorption in the surface layer, one fast neutron leaves the nucleus without collisions, whereas another one is absorbed in the nucleus. In this case about 5-6 evaporation (on the average) neutrons leave the C-nucleus which has the excitation energy $E^* \simeq m_\pi/2$. Thus, in case of the surface absorption, the function $\bar{I}(x)$ has a peak at $x = 6$-7 (see Figure 11). In the case of the volume absorption of γ-quanta, the dependence of $\bar{I}$ on x has another form (see Figure 11).

Usually it is isomeric ratios ξ_m rather than the angular momenta of R-nuclei that are measured in experiments.[3] However, if we choose isomers with a sufficiently high value of the spin, then the dependence $\xi_m(x)$ is expected to have the same form as $\bar{I}(x)$.* The dependence of the probability of the excitation of high-

* The differences in the contributions to I_f coming from other terms in Equation 16 are to be reduced to a minimum. In particular, even-even isotopes of the same chemical element ($s_A = 0$ and the same values of ℓ_π) should be taken as targets.

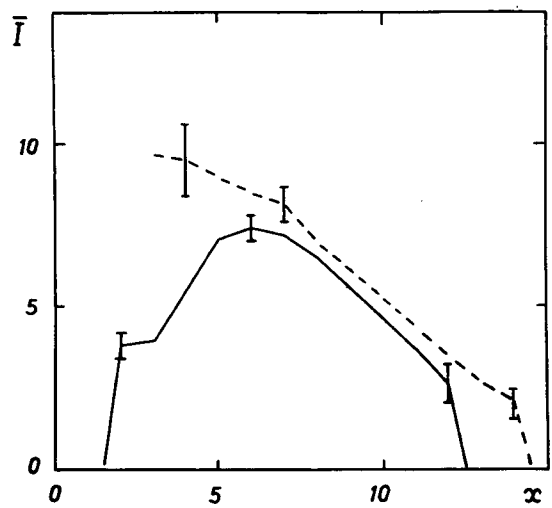

FIGURE 11. This shows the average angular momentum of C-nuclei as a function of a number x of neutrons emitted in the ^{208}Pb (π^-,xn) (the solid curve) and the ^{208}Pb (γ,xn) (the dashed curve) reaction.

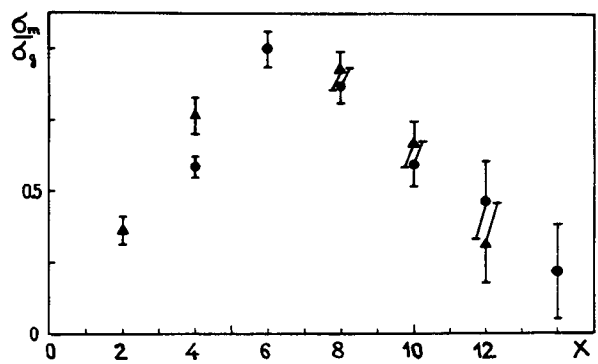

FIGURE 12. This illustrates the dependence of the isomeric ratio σ_m/σ_g (in relative units) on the number x of emitted neutrons for the reactions ^{112,114,116,118,120,122}Sn(π^-,xn) ^{108m}In(●) and ^{112,114,116,118,120,122}Sn(π^-,xn) ^{110m}In(▲). Experimental data[40] are shown by the points.

spin isomers ^{108m}In(7^+) and ^{110m}In(7^+) on the number of emitted neutrons in the reaction of absorption of π^--mesons by nuclei of ^{112}Sn, ^{114}Sn, ^{118}Sn, ^{120}Sn, ^{122}Sn, and ^{124}Sn has been measured. [40] The dependence of the isomeric ratio on the number of emitted neutrons behaves in the same manner as predicted by the theory (see Figure 12).

The conclusion[7,10,37,38] that fast nucleons emitted from the surface layer of a nucleus at the stage of the INC serve as a main source of a high angular momentum of a final nucleus seems correct. On the other hand, other mechanism of nuclear "twisting" are also possible. A fluctuation mechanism in which a nucleus acquires a high angular momentum as a result of random summation of the momenta $\vec{l}_{ev}$

brought away by evaporation particles has been considered.[16] It is evident that the role of this mechanism becomes more prominent as the number x of emitted particles increases. The excitation of the state with the spin equal to $16\hbar$ in the reaction $^{181}Ta(\pi^-,14n)$ which was discovered by Beetz et al.[41] is indicative of the existence of the fluctuation mechanism of nuclear twisting. Naturally, the probability of such a process is very small ($\sim 10^{-3}$ per an absorbed pion).

The discussion and calculations given were based on the two-nucleon mechanism of pion absorption. However, the calculations have demonstrated[7] that a nucleus can acquire a high value of the angular momentum upon the α-particle absorption as well. The channel (Equation 12a) in which the kinetic energy of a tritium nucleus is approximately equal to 35 MeV and that of a neutron to $\simeq$ 105 MeV is of particular interest from the viewpoint of the study of the excitation of high-spin states. Escape of a neutron of such a high energy from the surface layer of a nucleus and an absorption of a relatively slow tritium in the nucleus result in the emergence of angular momentum I which must be higher than that in the case of the quasideuteron absorption by a factor of 1.25. In this case, a C-nucleus is formed with the excitation energy $E^* \simeq$ 30-40 MeV. As a result, the dependence of the mean angular momentum on the number of emitted particles has a peak at $x = 4$ rather than at $x = 7$ as is the case for the quasideuteron absorption.

Thus, the method which uses the excitation of high-spin states as a tool for the study of the mechanism of absorption of slow π^--mesons by atomic nuclei has not yet exhausted its possibilities, and its further development seems to be expedient. As for other nuclear reactions initiated by intermediate-energy particles, a systematic study of angular momenta of final nuclei (isomeric ratios) is practically absent for them.

5. Momentum of an R-Nucleus

It follows that the study of such a characteristic of an R-nucleus as its angular momentum can give valuable information on the mechanism of absorption of a pion by a nucleus. The momentum of an R-nucleus is its another important characteristic. For light nuclei from which the products of absorption escape without any interaction with intranuclear nucleons, the measurement of the recoil momentum allows one to determine the momentum of a multinucleon association absorbing a pion. Here for a simple reaction $(\pi^-,2n)$, the momentum of a nucleus can be extracted from the analysis of a kinematically complete experiment.[3] For the case of absorption of a pion on complex nuclei, a large contribution of secondary processes makes the situation more complicated. To be more specific, the momentum of an R-nucleus depends now on various characteristics of the process, e.g., on the number of emitted nucleons ΔA. The Doppler effect is used as a rule for such nuclei to measure the recoil momentum.[3]

Within the framework of the model under consideration the momentum of an R-nucleus upon the π^--absorption is determined by the simple relation[7] (see Equation 74, Chapter 1, and Equation 137, Chapter 2)

$$\mathbf{p}_r = \sum_i \mathbf{p}_c^i - \sum_i \mathbf{p}_{ev}^i \tag{17}$$

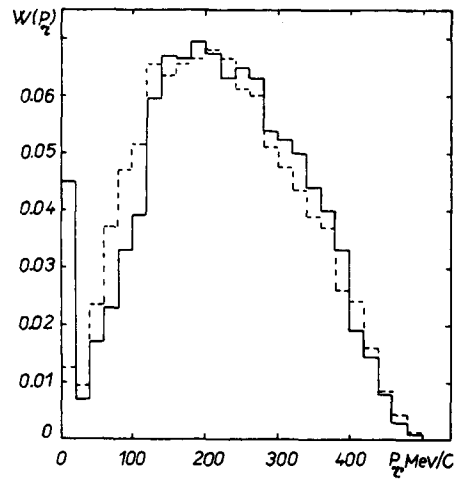

FIGURE 13. This reflects the momentum distribution of C-nuclei formed upon the absorption of π^--mesons by ^{31}P (the dashed histogram) and ^{208}Pb (the solid histogram) nuclei. The area under the histograms is normalized to unity.

where $\mathbf{p}_c^i$ and $\mathbf{p}_{ev}^i$ are the momenta of the cascade and the evaporated particles, respectively. Calculations[3] have demonstrated that the average momentum $\bar{p}_r$ acquied by a C-nucleus after the completion of the cascade stage of the process does not depend practically on the mass number of a target and is approximately equal to 220 MeV/c. Unlike the angular momentum, the distribution of C-nuclei over the magnitudes of momentum also depends only slightly on the type of a target (see Figure 13).

Figure 14 shows the comparison of experimental data with the calculated dependence of the average momentum $\bar{p}_r$ of a nucleus on the number of nucleons ΔA brought away from a T-nucleus once it has absorbed a pion. For small value of ΔA ($\Delta A \leqslant 4$), the momentum $\bar{p}_r$ increases with increasing ΔA and then depends only slightly on ΔA. For a strong spallation of a nucleus (large values of ΔA), the contribution of evaporated particles to the momentum of an R-nucleus becomes comparable with the contribution of fast particles (see Figure 14). At $\Delta A = 4$, experimental points fall above the calculated curve. This may be due to an inadequate determination of the shape of the momentum distribution of an R-nucleus on which experimental values depend. (It should be recalled that the maximum momentum of a nucleon with $\epsilon_N = m_\pi$ after the pion absorption is equal to 510 MeV/c. This value is considerably smaller than the "experimental value" $\bar{p}_r \approx 600$ MeV/c for $\Delta A = 4$).

Here we have considered the results of first experiments concerned with the measurements of the momentum $\mathbf{p}_r$ of an R-nucleus. This work calls for a further development in respect of both elaboration of experimental technique and the application of these methods to the measurement of other characteristics of NRs. For instance, measuring the average momentum of a nucleus for metastable states with various values of the spin with the help of the Doppler effect, we can determine the dependence of p_r on the angular momentum I of the nucleus.

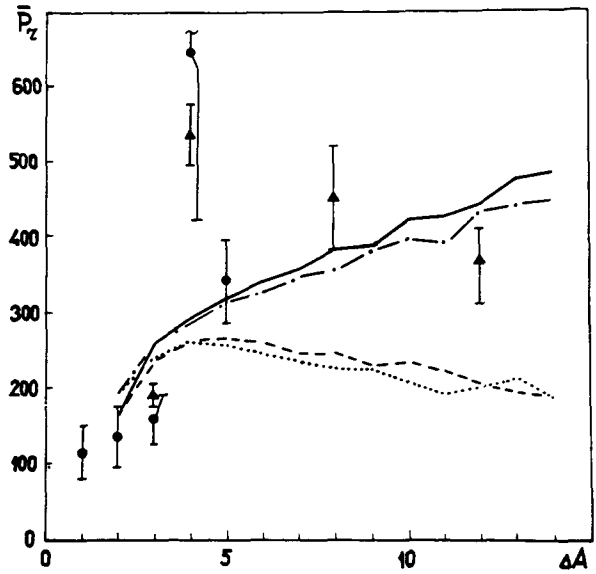

FIGURE 14. The dependence of the average momentum of a final nucleus (in MeV/c) on ΔA is graphed here. The solid and the dashed curve correspond to the calculation for a ^{40}Ca nucleus with and without regard for the contribution of evaporating particles, respectively. The dash-dotted and the dotted curve correspond to the calculations for a ^{31}P nucleus with and without the contribution of evaporating particles. The experimental data[42,43] are shown by full circles (●) for ^{31}P and by full triangles (▲) for ^{40}Ca.

The excitation of C-nuclei can be removed not only through emission of particles, but also through fission (see Chapter 3). The absorption of stopped π^--mesons can result not only in the fission of highly fissionable nuclei with the mass $A > 230$, but also in the fission of slightly fissionable nuclei with $150 \leqslant A < 230$. This is because the excitation energy of a nucleus can be as high as 140 MeV. The data on the nuclear fission initiated by stopped pions will be considered in Chapter 7.

II. INELASTIC PION-NUCLEUS INTERACTIONS AT THE ENERGIES LOWER THAN 300 MEV

When in the early 1970s meson facilities were put into operation, a systematic and precise experimental study of the interaction between pions of the energy $\epsilon_\pi \leqslant 300$ MeV and nuclei began. New data obtained during last two decades placed stringent demands on the quality of theoretical models.This generated a need for a substantial improvement of existing theoretical approaches and for the development of new ones.

Usually the attention of a theory was concentrated on the analysis of experimental data concerned with the processes in which a pion transfers a small amount of energy ($\leqslant B_N$) to a nucleus. Along these lines of pion-nucleus physics sufficiently

rigorous quantum-mechanical methods have been developed which are based on the use of the formal theory of NRs[6] (see Sections III and IV of the Introduction). In the energy range $\epsilon_\pi \leqslant 300$MeV the calculations of cross-sections for elastic scattering and scattering with the excitation of a fixed final state of a nucleus, as well as the calculations of such global characteristics as the total cross-section of the interaction σ^{tot} and the cross-sections of the reaction σ_R, of the absorption σ_{abs}, and of the charge exchange σ_{ex}, are carried out, as a rule, in DWIA-approximation, or with the help of various modifications of this method (see Section III of the Introduction). Within the framework of such an approach considerable progress has been made. In particular, rather detailed information on the potential of the πA-interaction has been extracted.

On the other hand, the work carried out on meson facilities provided a large body of experimental information on deep inelastic πA-reactions which are accompanied by a transfer of large amounts of energy to a nucleus and by an escape of a large number of particles from it. Up to the early 1970s the INC-model was the only model of such reactions.[44] New data obtained in the energy range $\epsilon_\pi \leqslant 300$ MeV are of great importance for the development of methods of calculation of deep inelastic πA-interaction, since it is easy to verify[45] that the validity conditions ($L \gg r_{int}$, $L \gg \lambda\!\!\!^{-}$) of the INC-model (see Sections I and V, Chapter 1) are not satisfied in this domain. In this connection, there appeared a number of papers[45-50] aimed at the introduction of quantum corrections and corrections describing the influence of the medium into calculations of the deep inelastic πA-reaction for $\epsilon_\pi < 300$ MeV carried out in accordance with the INC-model. We shall consider further the solution of this problem within the framework of the OC-model,[50] which is based on the use of the optical πA-potential.

A. OPTICAL + CASCADE MODEL FOR INELASTIC πA-INTERACTION

Pion absorption in flight on nuclei is a more complicated case than absorption at rest considered in Section I. First, there is no spherical symmetry in this problem. Second, a pion can now not only undergo absorption on a pair of nucleons (Equation 9), but also be scattered elastically by an intranuclear nucleon

$$\pi + N \rightarrow \pi' + N' , \tag{18a}$$

or enter into a charge-exchange reaction with it

$$\pi^{\pm} + N \rightarrow \pi^0 + N', \quad \pi^0 + N \rightarrow \pi^{\pm} + N' \tag{18b}$$

Finally, not only secondary nucleons formed in the process of thermalization of an R-nucleus, but also pions which left the nucleus upon being produced as a result of elementary reactions in Equations 18a and 18b are of interest. It is clear that the function P_{abs} which prescribes the initial conditions of the nucleonic INC in the OC-model has a rather complicated form, because the radial and energy characteristics of the source of nucleons for elementary processes in Equations 9, 18a,

and 18b differ from one another. Therefore, the function P^{ν}_{abs} was calculated in an implicit form by means of the Monte Carlo technique (ν = el, ex, abs). To this end one can take a generalized optical πA-potential of the second order[51] which enables one to analyze not only the data on π-atoms ($\epsilon_\pi \approx 0$), but also the data on the scattering of pions by nuclei for $\epsilon_\pi < 300$ MeV*:

$$2\omega V_{opt}(p,r) = \beta(p,r) - \nabla\alpha(p,r)\nabla - \nabla^2 q(p,r) ,$$

where

$$\beta(p,r) = 2\omega V_c(r) - 4\pi[b(r) - k_2 B_0 \rho_N^2(r)] ,$$
$$\alpha(p,r) = -\alpha_0 / \left(1 + \frac{\xi}{3}\frac{A-1}{A}\alpha_0\right), \alpha_0 = 4\pi\left[c(r) + \frac{C_0}{k_2}\rho_N^2(r)\right] , \tag{19}$$
$$b(r) = k_1[b_0\rho_N(r) - e_\pi b_1 \delta\rho_N(r)], \; c(r) = [c_0\rho_N(r) - e_\pi c_1 \delta\rho_N(r)]/k_1 ,$$
$$q(p,r) = 2\pi\left[(k_1 - 1)\, c(r) + \frac{k_2 - 1}{k_2} C_0 \rho_N^2(r)\right], \; \delta\rho_N(r) = \frac{N - Z}{A}\rho_N(r).$$

Here ω and p are the total energy and the momentum of a pion in the c.m.s. of the pion-nucleus system, $k_1 = (1 + A\omega/M)/(1 + \omega/M)$, and $k_2 = (1 + A\omega/2M)/(1 + \omega/M)$ the kinematic factors, e_π is the charge of a pion and M the mass of a nucleus. The value of the correlation parameter $\xi = 1$ was used in the calculation. The values of the single-nucleon parameters b_0, b_1, c_0, and c_1 were borrowed from Reference 51. Their imaginary parts were multiplied by the Pauli blocking factor 1-f (see Section IIC in Chapter 1 and Reference 52 as well). The same values as in Reference 51 were used for the two-nucleon parameters B_0 and C_0.

1. Mean Free Path of a Pion in Nuclear Matter

The mean free path L of a pion is defined as a distance at which $|\psi(r)|^2$ decreases by a factor of *e*. The wave function $\psi(r)$ of a pion is determined from the Klein-Gordon equation

$$(\nabla^2 + p^2 - 2\omega V_{opt})\, \psi(r) = 0 \tag{20}$$

with the potential (Equation 19) in the eikonal approximation.** Such a procedure was used in References 47,54, and 55. According to Reference 54

$$L^{-1} \approx 2\,\mathrm{Im}\left\{p^2 + \frac{1}{1+\gamma}\left(\frac{\nabla^2\gamma}{2} + \beta - \nabla^2 q + p^2\gamma\right) + \left[\frac{\nabla\gamma}{2(1+\gamma)}\right]^2\right\}^{-1/2}, \; \gamma = \alpha + q . \tag{21}$$

* In the limiting case $\epsilon_\pi \to 0$ this potential is reduced to the potential (Equation 1) which we have already used.

** It has been demonstrated[53] that the eikonal approximation is sufficiently accurate for pions whose energies lie in the range under consideration.

Let $f_{\pi N}(f_{\pi d})$ be the set of all single-nucleon (two-nucleon) parameters of potential and F the set of all other parameters. Then the expression for partial mean free paths can be written in the form[54,55]

$$L^{-1}(F;f_{\pi N},f_{\pi d}) = L_{sc}^{-1}(F;f_{\pi N},0) + L_{abs}^{-1}(F;0,f_{\pi d}) + L_{cor}^{-1}(F;f_{\pi N},f_{\pi d}) . \quad (22)$$

Here $L_{sc}(L_{abs})$ is the mean free path with respect to the channel of quasielastic scattering (two-nucleon absorption), if the channel of two-nucleon absorption (quasielastic scattering) is closed. Such an isolation of partial mean free paths is meaningful only in the case of weak coupling between the channels, which is manifested in the appearance of the term L_{cor}^{-1} in Equation 22. Indeed, the calculations have demonstrated[54] that the coupling between the channel of two-nucleon absorption and that of quasielastic scattering (i.e., the term L_{cor}) can be disregarded in the case of interaction of pions with the energy in the vicinity of the (3,3)-resonance with nuclei (this interaction has a surface character[45,46]). This means that events corresponding to the escape in these channels are statistically independent.

In the standard INC-model (see Chapter 2), the vacuum cross-section (with the allowance for the Pauli blocking factor 1-f) is used to calculate the partial length L_{sc}:

$$L_{sc}^{-1} = \rho_N(r)\, \sigma_{\pi N}(p)\, (1 - f) . \quad (23a)$$

The partial length L_{abs} is defined by the phenomenological expression

$$L_{abs}^{-1} = \rho_N(r)\, G\sigma_{\pi d}(p)\, Z/A \quad (23b)$$

which follows from the formula in Equation 132, Chapter 2, of the quasideuteron model. Here G = 4 is an empirical constant, and $\sigma_{\pi N}$ and $\sigma_{\pi d}$ are the experimental cross-sections of the πN-scattering and the reaction $\pi d \rightarrow NN$, respectively. It should be noted that the parametrization (Equation 23b) reflects poorly the radial dependence, since the mean free path is more likely to be inversely proportional to the squared density (or more precisely to the two-nucleon density). It is seen from Figure 15 that the low-density approximation is satisfactory only in the case of high-energy pions and the interaction at the periphery of a nucleus. In the interior of a nucleus and at low energies of pions, the mean free paths calculated with the help of Equations 22 and 23 differ significantly.

There is no term responsible for the charge exchange in the optical potential (Equation 19). Therefore, we shall make use of the relation

$$L_{ex}^{-1} = \rho_N(r)\, \sigma_{ex}(p)\, (1 - f) , \quad (24)$$

where σ_{ex} is the experimental cross-section of the charge exchange between a pion and a free nucleon, to determine the corresponding partial mean free path. Then instead of Equation 22 we finally get

$$L^{-1} \simeq L_{sc}^{-1} + L_{abs}^{-1} + L_{ex}^{-1} . \quad (25)$$

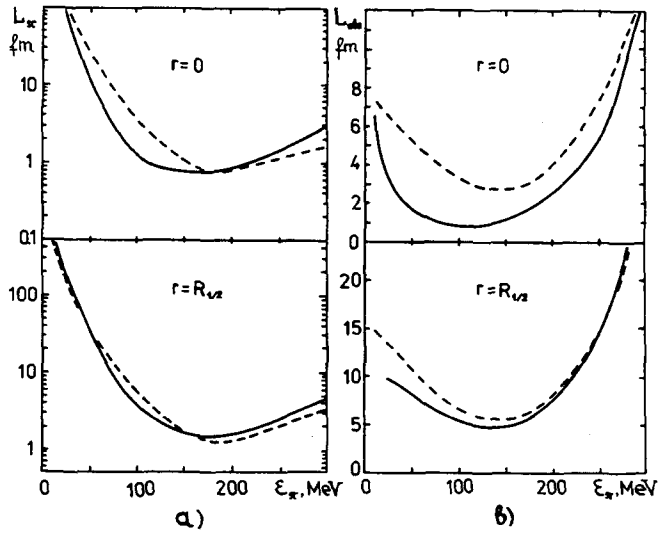

FIGURE 15. These curves represent the dependence $L_{sc}(a)$ and $L_{abs}(b)$ on the enregy of π^+-mesons at the center ($r = 0$) and in the diffuse layer ($r = R_{1/2}$) of a Cu nucleus. The solid and the dashed curve correspond to the calculations[50] carried out in accordance with Equations 22 and 23, respectively.

2. Potential Energy of a Pion in a Nucleus

To determine the potential energy V_π (p,r) of a pion in the field of a nucleus as a whole we shall find the optical potential (Equation 19) in the classical approximation and isolate its real part. As a result we get[54] the following expression:

$$V_\pi(p,r) = V_n(p,r) + V_c(r) + \widetilde{V}(p,r) ,$$

where (26)

$$V_n(p,r) \approx \frac{1}{2\omega} \mathrm{Re}\left\{\frac{p^2\gamma(p,r) - 4\pi[b(p,r) + k_2B_0(p)\rho_N^2(r)]}{1 + \gamma(p,r)}\right\} ,$$

$$\widetilde{V}(p,r) = V_c(r)\,\mathrm{Re}\left[\frac{1}{1 + \gamma(p,r)} - 1\right] .$$

The presence of the term $\widetilde{V}(p,r)$ describes the coupling between the Coulomb term V_c and the strong interaction part V_n which depends on the velocity. For the energies $\epsilon_\pi \gtrsim 50$ MeV, where the semiclassical approximation used by us is valid, the contribution of the term $\widetilde{V}(p,r)$ to $V_\pi(p,r)$ is negligibly small. The potential energy V_n depends strongly on the pion energy and on the radius r. The potential can be either attractive ($V_n < 0$) or repulsive ($V_n > 0$) (see Figure 16), depending on the values of these quantities. Therefore, the values $V_n = -25$ MeV or $V_n = -(E_F + B_N)$ used as a rule in the INC-model (see Section II, Chapter 2) are unjustified. As can be seen from Figure 16, it would be better to use the value of the potential

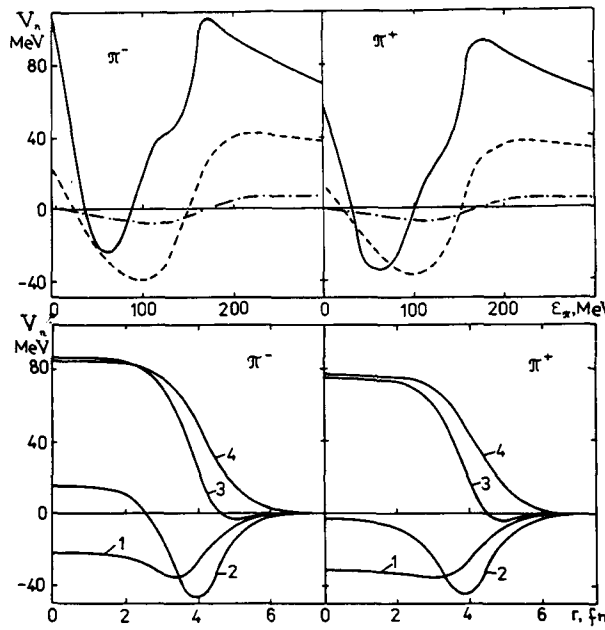

FIGURE 16. The upper figures show the energy, while the lower ones show the radial dependence $V_n(p,r)$ of $\pi^\pm$-mesons in a Cu nucleus.[50] In the upper figures, the solid curves correspond to r = 0, the dashed curves to r = $R_{1/2}$, and the dash-dotted curves to r = 5.5 fm. In the lower figures, the curves 1 correspond to ϵ_π = 50 MeV, the curves 2 to ϵ_π = 100 MeV, the curves 3 to ϵ_π = 160 MeV, and the curves 4 to ϵ_π = 250 MeV.

$V_n \approx 0$ to describe peripheral πA-reactions within the framework of the standard INC-model.

3. General Scheme of the Calculation

The mean free paths (Equation 25) and the pion potential (Equation 26) calculated within the framework of the optical model are incorporated in the algorithm of the calculation of the INC which was outlined in Section II, Chapter 2. Basic features which distinguish this method of the calculation from the standard INC-model are as follows. First, the mean free path (L(p,r) take into account the Pauli exclusion principle on their own. Second, the radius-independent Fermi momentum $p_F \sim \rho_0^{1/3}$ is used here, since the local density approximation $p_F(r) \sim \rho_N^{1/3}(r)$ for the momentum distribution of intranculear nucleons is not sufficiently correct[46,48] (see also Chapter 4). There arise certain difficulties in this approach associated with the fact that the mean free paths and the potential energy are expressed in terms of the vacuum momentum of a pion which is defined before the commencement of nuclear reaction. After the completion of the first elementary act we know the pion momentum $\bar{p}'$ in the nucleus. Given the value of $\bar{p}'$ we are to determine the pion momentum p′ (outside the nucleus) in terms of which new values of the mean free path and of the potential energy are expressed. To this end we can deem that the

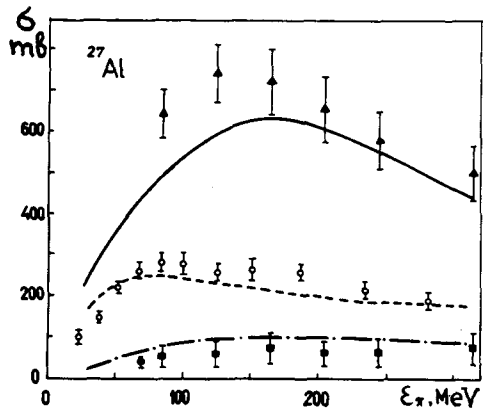

FIGURE 17. This traces the energy dependence of the cross-sections of the interaction of π^+-mesons with ^{27}Al nuclei. The curves correspond to the calculation[50] and the points to experimental data: σ_R is depicted by the triangles[56] and the solid curve, σ_{abs} by the circles and the dashed curve, and σ_{ex} by the squares[58] and the dash-dotted curve.

potential energy of a pion after the scattering is approximately equal to that before the scattering, i.e., $V_\pi(p,r) \approx V_\pi(p',r)$.

It should be noted that such an OC-model allows us to phenomenologically take into account a number of effects which are not present in the standard INC-model,[44] namely the dependence of the potential on the radius, the coupling between the channel of quasielastic scattering and that of absorption, the coupling between the electromagnetic interaction, and the part of the strong interaction which depends on the velocity, the Lorentz-Lorenz effect, etc.

B. COMPARISON WITH EXPERIMENTAL DATA

Let us analyze in the framework of the OC-model those experimental data on inelastic πA-reactions which we believe to be most representative. Figure 17 shows the reaction cross-section σ_R and cross-sections of absorption σ_{abs} and of charge exchange σ_{ex} as functions of the pion energy. It is well known that the INC-model is not intended for the description of such characteristics of a reaction. It is seen from Figure 17 that it is possible to obtain a reasonably good (approximately the same as in the standard quantum-mechanical approaches, e.g., in the DWIA) description of the experiment within the framework of the OC-model. Figures 18-20 show typical angular distributions and inclusive spectra of secondary particles. It is seen that the calculations agree reasonably well with experimental data.

This approach has many points in its favor. One of them is that it contains information on all particles (including R-nuclei) involved in reactions. This allows one to calculate, in principle, various correlations corresponding to accomplishment of experiments of various degrees of complexity in which certain characteristics of NRs are measured in coincidence. Figure 21 shows the distribution over the angle of divergence of two nucleons as an example. The peak at the large value of the angle is indicative of the contribution from a two-nucleon absorption of pions.

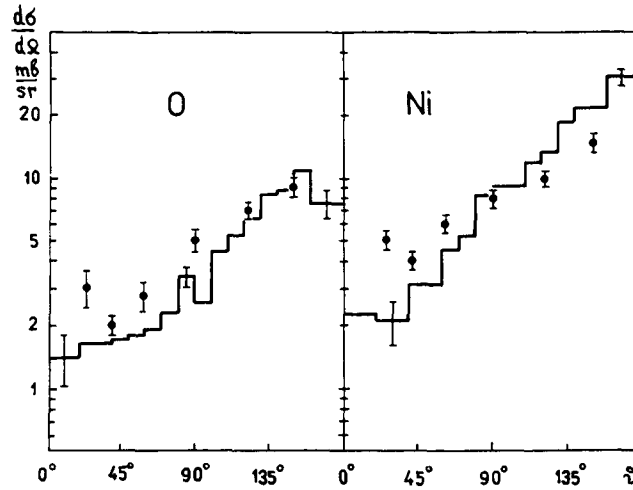

FIGURE 18. Here are angular distributions of π^0-mesons upon the charge exchange of π^+-mesons with $\epsilon_{\pi^+} = 100$ MeV on ^{16}O and ^{58}Ni nuclei. Histograms correspond to the calculation of Reference 50 and the points to experimental data.[59]

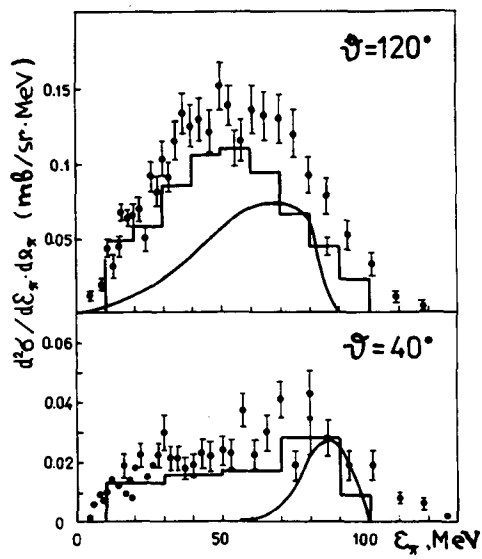

FIGURE 19. These represent the double differential distributions of π^0-mesons produced at the angles of 40° and 120° (in the l.s.) in the $^{16}O(\pi^+, \pi^0)X$ reaction at $\epsilon_{\pi^+} = 100$ MeV. The curves correspond to the calculation of Reference 46 and the points to experimental data.[59] The rest of the notation is the same as in Figure 18.

It has already been mentioned in the previous section that characteristics of R-nuclei formed are of great interest for the study of deep inelastic πA-interactions. The measurements of only one of them, that is the isotope yield, are presently available. It can be seen from Figure 22 that these data are indicative of a strong

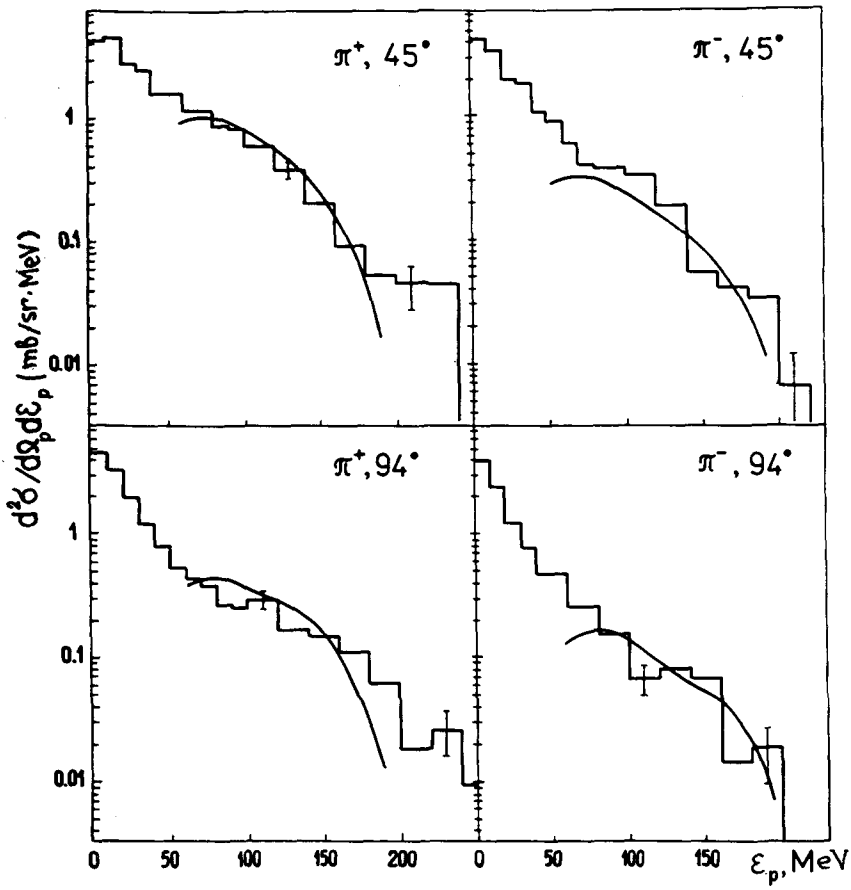

FIGURE 20. These illustrate the double differential distributions of protons produced at the angles of 45° and 94° (in the l.s.) in the interaction of π-mesons of the energy 220 MeV with ^{62}Ni nuclei. The curves correspond to experimental data.[60] The rest of the notation is the same as in Figure 18.

spallation of a T-nucleus. Usually the spallation reaction accompanies the reaction of nuclear fission, but hitherto there are no systematic measurements even for the total cross-section σ_f of fission for this inelastic channel, which is the main channel in the domain of heavy nuclei.

Concluding this section we shall compare the OC-model with other methods of calculation of deep inelastic πA-reactions. Calculations[50] carried out in accordance with the standard INC-model have demonstrated that this model gives a worse agreement with experimental data under consideration. This is especially the case for the charge-exchange reaction whose calculated cross-sections exceed the experimental ones several times. Taking the value $V_\pi \approx 0$ for the potential well of a pion, we can achieve a better agreement with experimental data in what is concerned with other characteristics. This is because the interaction of pions of energies $\epsilon_\pi < 300$ MeV is mainly concentrated in the diffuse layer of a nucleus,[45,46] where the low-density approximation works better and the potential of the strong

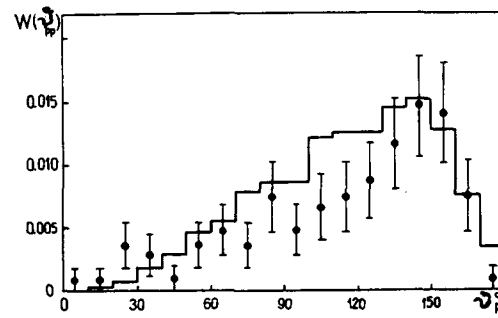

FIGURE 21. This is the distribution over the angle ϑ_{pp} of divergence of two protons emitted upon the absorption of π^+-mesons with the energy 45 MeV in the photoemulsion (measured in number of pp-pairs in the interval $\Delta\vartheta_{pp} = 10°$ per one act of absorption). The points correspond to experimental data.[61] The rest of the notation is the same as in Figure 18.

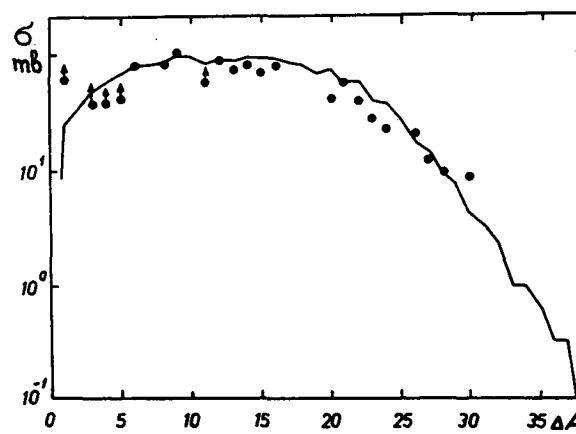

FIGURE 22. This describes the cross-sections for production of isotopes in the interaction of π^+-mesons of the energy 300 MeV with ^{197}Au nuclei. The points correspond to experimental data.[62] The calculated[50] cross-sections are connected by straight lines in order to provide a more apt presentation.

interaction is small (see Figures 15 and 16). For the same reason a fair agreement with experimental data is obtained for certain characteristics* in the approach[46] using the classical Boltzmann equation. The deeper a pion penetrates into a nucleus, the more dramatically the validity conditions of such classical approaches are violated. Therefore, to compare different approaches and to determine their validity ranges, it is of interest to invoke the reaction of production of pions by protons on nuclei in addition to the analysis of the charge-exchange reactions, since the former may reveal higher sensitivity to the potential of the strong interaction. To the best of our knowledge this has not been done yet.

Another way to overcome the difficulties of the classical approach is to incorporate the Δ-isobar[45,47,48] in the development of the INC. To some extent it is an

* Separate channels of the reaction are described rather poorly within the framework of this approach (see Figure 19).

advancement towards the creation of the dynamical theory of πA-scattering. In particular, such an approach takes into account the dynamics of a two-nucleon pion absorption through the reactions $\pi N \rightarrow \Delta$ and $\Delta N \rightarrow NN$. It has been already mentioned in Section II, Chapter 2, however, that such a way is associated with the introduction of unknown parameters which describe the interaction of the Δ-isobar with nuclear matter. In Reference 47 the OC-model was generalized to cover the case when both pions and Δ-isobars are involved in the development of the INC.

The mutual drawback of the models under consideration is that they are phenomenological. The problem of their substantiation is of current interest. An attempt[49] has been made to solve this problem. A self-consistent generalized semiclassical Boltzmann equation for single-particle Green functions in the Wigner representation has been obtained. It served as a basis for the formulation of a semiclassical OC-model which represents a numerical solution of the generalized Boltzmann equation by means of the Monte Carlo technique. However, the problem of creating a consistent semiclassical model of deep inelastic πA-interaction is not yet solved completely. On the other hand, the comparison with experimental data has demonstrated that the phenomenological OC-model outlined in this chapter describes reasonably well deep inelastic πA-interaction for energies $\epsilon_\pi < 300$ MeV. In the domain of higher energies, only incomplete and rather inaccurate experimental data are known for this interaction. Therefore, we shall give only a brief summary of the investigations performed in this domain.

On the whole, the standard INC-model describes satisfactorily the data[44] in the energy range $0.3 \lesssim \epsilon_\pi$ 3 GeV. However, for $\epsilon_\pi \gtrsim 3$ GeV it reveals deviations from the observed characteristics of low-energy secondary particles which have the same nature as for pA-reactions (see Chapter 4). The INCT-model eliminates this discrepancies. This allows one to extend the validity range of the model up to the energies $\epsilon_\pi \sim 50$ GeV. The INCT-model reproduces the "saturation" in the energy dependence of the average multiplicity of low energy g- and h-particles emitted in the interaction of pions with nuclei of photoemulsion which was observed in experiments at $\epsilon_\pi > 3$-5 CeV. It also predicts a similar form of the energy dependence of the average numbers of collisions of cascade particles inside the nucleus, and of the average number of nucleons knocked out of the nucleus and of the excitation energy of an R-nucleus. All these phenomena are caused by the trawling effect (see Chapter 4). Calculations carried out in accordance with the INCT-model agree well with the experimental correlation $\bar{n}_h$ (n_s) and $\bar{n}_p$ (n_π) (see Figure 23) which are most sensitive to this effect (see Chapter 4). Thus, the developed modifications of the INC-model can serve as a sufficiently accurate and reliable tool for description of deep inelastic πA-interaction over a wide range of the energy of incident particles. This provides reason enough to apply them in Chapter 6 to analysis of even more complicated process of annihilation of antinucleons on nuclei.

III. CONCLUSIONS

In what is concerned with the production of highly-excited nuclei, a pion differs from a nucleon in that once it has been absorbed by a nucleus it brings in not only

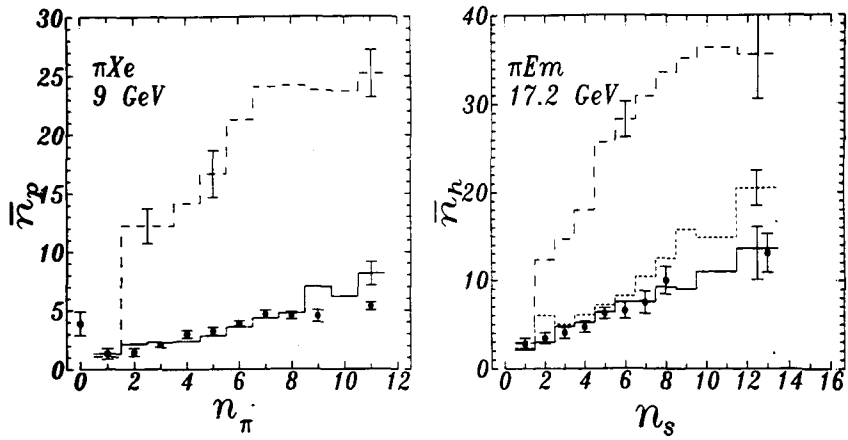

FIGURE 23. These depict the dependence of the average multiplicity $\bar{n}_p$ of protons on the mulitplicity n_π of pions produced in the interaction of π^--mesons of the energy 9 GeV with Xe nuclei (the left-hand figure), and the dependence of the average multiplicity $\bar{n}_h$ of h-particles on the multiplicity of s-particles produced in the interaction of π^--mesons of the energy 17.2 GeV with nuclei of photoemulsion (the right-hand figure). The points correspond to experimental data.[63,64] The dashed curve shows the results of the calculation carried out in accordance with the standard INC-model. The solid and the dotted histogram correspond to the calculations carried out in accordance with the INCT-model with and without regard of the processes in which intranuclear nucleons leave a T-nucleus.

its kinetic energy, but also its rest mass. In this connection, the case of pion absorption from mesoatomic states, when a rather large amount of the energy released is combined with small values of a momentum and angular momentum transferred, is of particular interest. Another peculiar feature of the absorption of a slow pion is that the distributions over the characteristics of C-nuclei formed are narrower than those obtained in the reactions with other intermediate-energy particles. Moreover, in this process C-nuclei are formed with the excitation energy $E^* \lesssim m_\pi$. They possess the properties which are studied in detail, and their decay is reliably described by the equilibrium statistical model. This favors the study of the mechanism of the deep inelastic πA-interaction at $\epsilon_\pi = 0$.

In this chapter, we have considered the OC-model of the nuclear absorption of pions from mesoatomic states. This is a complicated process proceeding in several stages. The initial stage of formation and de-excitation of a π-atom in which quantum effects play a significant role is described with the help of the optical model. The primary act of absorption of a pion by a multinucleon association, in which a sufficiently large amount of energy ($\approx m_\pi$) released is transferred to several nucleons, serves as a natural boundary between the initial and the final stages of the reaction. The next stage of the dissipation of energy released in the primary act of absorption proceeds through the rescattering of nucleons produced in the act of absorption in nuclear matter. This stage is analyzed within the framework of the INC-model.

Within the framework of the OC-model we have carried out a systematic analysis of a wide range of modern experimental data on the absorption of slow π^--mesons

by complex nuclei. These data include the energy spectra and correlations of emitted particles, the isotope yield, the probability of fission, and the angular momenta and the momenta of R-nuclei and are indicative of the fact that two-nucleon mechanism is the principal mechanism of the nuclear π-absorption. Calculations for the α-particle mechanism of absorption of a pion by a complex nuclei were also carried out. This allows one to study the sensitivity of various characteristics of a deep inelastic πA-reaction to its contribution. At the present time, it is difficult to exactly determine the probability of the absorption of a pion by associations heavier than two-nucleon ones because of the strong influence exerted by various secondary effects on observable quantities, since these effects manifest themselves at final stages of the process and mask the contribution from the primary act of absorption. We can only assert that it is smaller than 20%.

To gain a more penetrating insight into the mechanism of the nuclear π-absorption, one must invoke the data on the characteristics of R-nuclei. A C-nucleus formed in a deep inelastic interaction loses the memory of its creation only with respect to internal single-particle degrees of freedom, whereas its excitation energy, momentum and angular momentum retain information on initial stages of the reaction. The sensitivity of characteristics of R-nuclei to the details of the π-absorption was investigated with the help of the OC-model, and it was demonstrated that such a method of study of the mechanism of πA-interaction is rather fruitful. For example, the results of calculations and the experimental data on the de-excitation of π-atoms are indicative of the fact that the pion absorption takes place in the diffuse layer of a nucleus. The excitation of high-spin metastable states is the most vivid corollary of the surface absorption. This phenomenon can be explained in a natural way within the framework of the OC-model: an R-nucleus acquires a high angular momentum as a result of emission of a sufficiently energetic nucleon ($\epsilon_N \sim m_\pi/2$) from the surface layer of a nucleus. To study the mechanism of absorption of pions and other intermediate-energy particles by nuclei, we can use the dependence of the average total angular momentum (or the isomeric ratio for the excitation of a high-spin state) of a nucleus on the number of emitted nucleons. The formation of highly-excited C-nuclei with $E^* \approx m_\pi$ results in a strong spallation of a heavy nucleus with $A \approx 200$ when as many as 15-17 nucleons are brought away from the nucleus and in the fission of both heavy and medium-weight nuclei with $A \sim 100$.

Absorption of pions from mesoatomic states is the first example of a deep inelastic process studied in detail in meson facilities. Recently, the interest in such studies has shifted towards the domain of higher energies. As a result, more and more experimental information on an inelastic πA-interaction is being accumulated in the energy range $\epsilon_\pi < 300$ MeV. New data are of importance for the development of methods of analysis of deep inelastic NRs, since the validity conditions of the classical INC-model are not satisfied in this energy range. Therefore, the OC-model was generalized to the case of an inelastic interaction of fast pions with complex nuclei as well. In this approach, principal quantities used by the INC-model to describe the pion transfer in nuclear matter (the mean free path L_π and the depth of the potential well V_π of a pion) are calculated in the semiclassical approximation

with the use of the known optical πA-potential. Comparison with the available data, which are presently scarce, however, has demonstrated that the OC-model can serve as a sufficiently reliable tool for the study of a deep inelastic πA-interaction not only "at rest," but also "in flight". The OC-model can be rather easily generalized to the case of inelastic interactions of nuclei with other particles whose optical potential is known (K^-,$\bar{p}$, etc.)

The range of higher energies of pions is not studied in sufficient detail. The classical INC-model describes satisfactorily the available data in the energy range $0.3 < \epsilon_\pi < 3$ GeV. At higher energies (3 GeV $< \epsilon_\pi <$ 30 GeV) one must invoke the trawling effect and use the INCT-model to account for the basic regularities of a deep inelastic πA-interaction.

REFERENCES

1. **Hüfner, J.**, Pions interacts with nuclei, *Phys. Rep. C*, 21, 1, 1975.
2. **Kopaleishvili, T. I.**, Absorption of π-mesons and nuclear structure [in Russian], *Part. Nucl.*, 2, 440, 1971.
3. **Butsev, V. S., Iljinov, A. S., and Chigrinov, S. E.**, Absorption of negative pions by atomic nuclei at rest, *Part. Nucl.* 11, 900, 1980.
4. **Balashov, V. V., Korenman, G. Ya., and Eramjyan, R. A.**, *Absorption of mesons by atomic nuclei* [in Russian], Atomizdat, Moscow, 1978.
5. **Kim, Y. N.**, *Mesic Atoms and Nuclear Structure*, North-Holland, Amsterdam, 1971.
6. **Ericson, T. and Weise, W.**, *Pions and Nuclei*, Clarendon Press, Oxford, 1988.
7. **Iljinov, A. S., Nazaruk, V. I., and Chigrinov, S. E.**, Spallation and fission of nuclei as a result of the capture of stopped negative pions, *Nucl. Phys. A*, 268, 513, 1976.
8. **Gadioli, E. and Gadioli Erba, E.**, Pre-equilibrium model description of nuclear de-excitation following the π^- absorption at rest, *Nucl. Phys. A*, 256, 414, 1976.
9. **Mukhopadhyay, N. C., Haderman, J., and Junker, K.**, Theory of nuclear fission by stopped pions, *Nucl. Phys. A*, 319, 448, 1979.
10. **Orth, C. J., Daniels, W. R., Dropesky, B. J., et al.**, Stopped-pion interactions with Cu and Ta, *Phys. Rev. C*, 21, 2524, 1980.
11. **Chiang, H. C. and Hüfner, J.**, Nucleons after pion absorption, *Nucl. Phys. A*, 352, 442, 1981.
12. **Chatterjee, A. and Gupta, S. K.**, Exciton model description of energy spectra following pion absorption in ^{40}Ca, *Z. Phys. A*, 307, 269, 1982.
13. **Blann, M.**, Precompound analyses of spectra and yields following nuclear capture of stopped π^-, *Phys. Rev. C*, 28, 1648, 1983.
14. **Machner, H.**, Study of particle emission following π^--absorption at rest, *Nucl. Phys. A*, 395, 457, 1983.
15. **Ericson, M. and Ericson, T. E. O.**, Optical properties of low-energy pions in nuclei, *Ann. Phys.*, 36, 323, 1966.
16. **Iljinov, A. S., Leon, M., Seki, R., and Chigrinov, S. E.**, Nuclear absorption of π^--mesons from mesoatomic states, *Report INR* P-0188. Moscow, 1981.
17. **Seki, R.**, How much information of π-nucleus optical potential can π^--mesonic atom data provide?, *in Meson-Nuclear Pysics-1979*. Hungerford, E. V., Ed., *AIP*, New York, 1979, 616.

18. **Engfer, R., Schneuwly, H., Vuilleumier, J. L., et al.,** Charge-distributions parameters, isotope shifts, isomer shifts, and magnetic constants from muonic atoms, *At. Data Nucl. Data Tables,* 14, 509, 1974.
19. **Leon, M., and Seki, R.,** Atomic capture of negative mesons, *Nucl. Phys. A,* 282, 445, 1977.
20. **Kisslinger, L. S.,** Scattering of mesons by light nuclei, *Phys. Rev.,* 98, 761, 1955.
21. **Brueckner, K. A., Serber, R., and Watson, K. M.,** The interaction of π-mesons with nuclear matter, *Phys. Rev.,* 84, 258, 1951.
22. **Heusi, P., Isaak, H.-P., Pruys, H. S., et al.,** Coincident emission of neutrons and charged particles after π^--absorption in ^{6}Li, ^{7}Li, ^{12}C, ^{59}Co and ^{197}Au, *Nucl. Phys. A,* 407, 429, 1983.
23. **Shapiro, I. S. and Kolybasov, V. M.,** On the mechanism of π^--meson capture by light nuclei, *Eksp. Teor. Fiz.,* 44, 270, 1963.
24. **Hartman, R., Isaak, H.-P., Engfer, R., et al.,** Spectroscopy of single and correlated neutrons following pion absorption in ^{12}C, ^{59}Co and ^{197}Au, *Nucl. Phys. A,* 308, 345, 1978.
25. **Pruys, H. S., Engfer, R., Hartman, R., et al.,** Charge particle emission following the absorption of stopped π^- in ^{12}C, ^{59}Co and ^{197}Au, *Nucl. Phys. A,* 352, 388, 1981.
26. **Botvina, A. S., Golubeva, Ye. S., and Iljinov, A. S.,** Statistical simulation of breakup of light nuclei in hadron-nucleus reactions [in Russian], Preprint *INR* P-0657. Moscow, 1990.
27. **Mechtersheimer, G., Büche, G., Klein, U., Kluge, W., Matthäy, H., Münchmeyer, D., and Moline, A.,** Energy spectra of charged particles emitted following the absorption of stopped negative pions in ^{12}C nuclei, *Nucl. Phys. A,* 324, 379, 1979.
28. **Sennhauser, U., Dey, W., Pfeiffer, H.-J., et al.,** Spectroscopy of two coincident charged particles emitted following bound pion absorption in ^{12}C, ^{59}Co and ^{197}Au, *Nucl. Phys. A,* 386, 447, 1982.
29. **Gornov, M. G., Gurov, Yu. B., Ilyin, A. L., et al.,** Emission of composite particles in absorption of stopped negative pions by Be, C, Si, Cu, and Ge nuclei, *Yad. Fiz.,* 47, 1193, 1988.
30. **Backenstoss, G., Brodbeck, D., Izycki, M., et al.,** New pion-absorption modes observed from triple coincidences in ^{4}He, *Phys. Rev. Lett.,* 61, 923, 1988.
31. **Salcedo, L. L., Oset, E., Strottman, D., and Hernandez, E.,** Experimental test of three-body pion absorption, *Phys. Lett. B,* 208, 339, 1988.
32. **Papandreou, Z., Lolos, G. J., Huber, G. M., et al.,** Composite particle emission following negative pion absorption on ^{12}C at T_{π^-} = 165 MeV, *Phys. Rev. C,* 41, R1139, 1990.
33. **Batusov, Yu. A., Kostanashvili, N. I., Tret'yak, V. I., and Chernev, Kh. M.,** Investigation of slow π^--meson capture by C, N, O nuclei in emulsion with three charged particles production, *JINR* Preprint P1-88-417, Dubna, 1988.
34. **Winsberg, L.,** Interaction of negative pions with iodine, *Phys. Rev.,* 95, 198, 1954.
35. **Pruys, H. S., Engfer, R., Hartmann, R., et al.,** Absorption of stopped π^- in ^{59}Co, ^{75}As, ^{197}Au and ^{209}Bi investigated by in-beam and activation gamma-ray spectroscopy, *Nucl. Phys. A,* 316, 365, 1979.
36. **Butsev, V. S., Vandlik, Ya., Vylov, Ts., et al.,** Multiplicity distribution of neutrons in pion capture by lead nuclei, *Yad. Fiz.,* 23, 17, 1976.
37. **Locher, M. P. and Myhrer, F.,** A remark on pion capture in heavy nuclei, *Helv. Phys. Acta,* 49, 123, 1976.
38. **Gershtein, S. S.,** On the probability of excitation of high-spin states at capture of negative pions by nuclei, *Usp. Fiz. Nauk,* 124, 455, 1978.
39. **Iljinov, A. S. and Nazaruk, V. I.,** Excitations of high-spin metastable states as a method for the study of the mechanism of nuclear reaction [in Russian], in *Proceedings of the 1st All-Union Seminar on the Progam of Experimental Investigations on Meson Facility of INR AN SSSR,* Moscow, 1979, 146.
40. **Butsev, V. S., Gavrilov, Yu. K., Polikanov, S. M., et al.,** Correlation between angular momentum of a residual nucleus and multiplicity of neutrons in (π^-, xn) reaction, *Pis'ma v ZhETF,* 24, 117, 1976.
41. **Beetz, R., de Boer, E. W. N., Panman, J. K., et al.,** High spin states and neutron multiplicites after pion capture in ^{181}Ta and ^{209}Bi, *Z. Phys. A,* 286, 215, 1978.

42. **Engelhart, H. D., Lewis, C. W., and Ullrich, H.,** The absorption of π^- at rest on complex nuclei, *Nucl. Phys. A,* 258, 480, 1976.
43. **Stronach, C. E., Plendl, H. S., Funsten, H. O., Kossler, W. J., Lieb, B. J., and Lind, V. G.,** Interactions of stopped π^- and of fast π^- and π^+ near the delta(1232) resonance with calcium, *Nucl. Phys. A,* 308, 290, 1978.
44. **Barashenkov, V. S., Iljinov, A. S., Sobolevsky, N. M., and Toneev, V. D.,** Interaction of particles and nuclei of high and superhigh energies with nuclei, *Usp. Fiz. Nauk,* 109, 91, 1973.
45. **Ginocchio, J. N.,** Deep inelastic pion-induced nuclear reactions in the isobar model, *Phys. Rev. C,* 17, 195, 1978.
46. **Hüfner, J. and Thies, M.,** Pion-nucleus scattering and absorption as a solution of the Boltzmann equation, *Phys. Rev. C,* 20, 273, 1979.
47. **Ginocchio, J. N. and Johnson, M. B.,** Effect of the pion optical potential on deep inelastic pion-nuclear reactions, *Phys. Rev. C,* 21, 1056, 1980.
48. **Fraenkel, Z., Piasetzky, E., and Kalbermann, G.,** Intranuclear cascade calculation of pion-nucleus reactions in the resonance region, *Phys. Rev. C,* 26, 1618, 1982.
49. **Nesterov, M. M. and Tarasov, N. A.,** Role of coherent effects in inelastic interaction between fast particles and nuclei, *Eksp. Teor. Fiz.,* 86, 390, 1984.
50. **Iljinov, A. S., Nazaruk, V. I., and Chigrinov, S. E.,** Pion-nucleus reactions at energies below 300 MeV, *Yad. Fiz.,* 36, 646, 1982.
51. **Stricker, K., McManus, M., and Carr, J. A.,** Nuclear scattering of low energy pions, *Phys. Rev. C,* 19, 929, 1979.
52. **Landau, R. H. and McMillan, M.,** Pauli-principle effects in pion-nucleus scattering, *Phys. Rev. C,* 8, 2094, 1973.
53. **Zavarzina, V. P., Sergeev, V. A., and Stepanov, A. V.,** Cross sections of the interaction of pions with light nuclei in the energy range 100-400 MeV [in Russian], in *Proc. of the 2nd All-Union Seminar on the Program of Experimental Investigations on the Meson Facility of INR AN SSSR,* Moscow, 1982, 130.
54. **Nasaruk, V. I.,** On the possibility of unification of the elements of the optical and the cascade model of nuclear reactions, *Yad. Fiz.,* 34, 857, 1981.
55. **Hecking, P.,** Pion mean free path in nuclear matter, *Phys. Lett. B,* 103, 401, 1981.
56. **Navon, I., Ashery, D., Azuelos, G., Pfeifer, H. J., Walter, H. K., and Schlepütz, F. W.,** True absorption and scattering of π^+ on carbon in the (3,3) resonance region, *Phys. Rev. C,* 22, 717, 1980.
57. **Nakai, K., Kobayashi, T., Numao, T., et al,** Measurements of cross sections for pion absorption by nuclei, *Phys. Rev. Lett.,* 44, 1446, 1980.
58. **Bellotti, E., Bonetti, S., Cavalli, D., and Matteuzzi, C.,** The (π^+, πN) reactions on carbon at 1300 MeV: a bubble-chamber experiment, *Nuovo Cimento A,* 14, 567, 1973.
59. **Bowles, T. J., Geesaman, D. F., Holt, R. J., et al.,** Inclusive (π^+, π^0) reactions in nuclei, *Phys. Rev. C,* 23, 439, 1981.
60. **Jackson, H. E., Kaufman, S. B., Meyer-Schützmeister, L., et al.,** Energetic charged particle yields induced by pions on complex nuclei, *Phys. Rev. C,* 16, 730, 1977.
61. **Chakravartty, S. C. and Hebert, J.,** Inelastic interactions of pions with the complex nuclei of emulsions, *Phys. Rev. C,* 16, 1097, 1977.
62. **Kaufman, S. B., Steinberg, E. P., and Butler, G. W.,** Spallation of gold by 100-300 MeV pions, *Phys. Rev. C,* 20, 2293, 1979.
63. **Kohli, J. M.,** On the interactions of 17.2 GeV π^--mesons with emulsion nuclei, *Nucl. Phys. B,* 14, 500, 1969.
64. **Pavlyak, T., Peryt, V., and Radomanov, V. B.,** Correlation of secondary particles in π^- Xe-interaction, *Yad. Fiz.,* 54, 1613, 1992.

Chapter 6

ANNIHILATION OF ANTINUCLEONS ON NUCLEI

The ability to annihilate in nuclear matter is a peculiar property of antinucleons. This offers new possibilities for the study of NRs in comparison with reactions induced by nucleons or pions. In particular, a cardinal advancement to the most interesting domain of very high excitation energies $E^* \sim m_N$ comparable to the total binding energy of a nucleus can be achieved by generating the multipion-nucleus interaction (the $m\pi A$-interaction) in which several pions fly simultaneously into a nucleus, rather than by increasing the energy of an incident pion. A direct method of generation of the $m\pi A$-interaction by means of increasing the intensity of pion beams seems impossible not only with the help of modern accelerators, but also in the foreseeable future. Until now the interaction of multipion systems with nuclei was studied indirectly in the processes of multiple production of pions on nuclei by high-energy particles.[1] In this case, the motion of a source of pions in nuclear matter with a relativistic velocity puts the study of the space-time development of the process of multiple production in the forefront (see also Section IIB, Chapter 2).

In spite of progress during recent years, gaps which remain still in the understanding of the mechansim of hadron-nucleus interaction at high energies plagues the analysis of the $m\pi A$-interaction itself.[2] The problem of the generation of the $m\pi A$-interaction can be solved by another method, which is closer to the direct one: we can place a nonrelativistic source of pions in the immediate vicinity of the nuclear surface. To this end it was proposed[3] to use the process of absorption of an antiproton which is in the bound state in an orbit of a $\bar{p}$-atom by its nucleus. It is well known[4] that the absorption of an antiproton takes place in the "atmosphere" of a nucleus through the annihilation on a quasifree nucleon. In this case, the annihilation serves as a source of pions. A part of annihilating pions can fly simultaneously into the nucleus consisting of A-1 nucleons. In such a way, the $m\pi A$-interaction is generated.

I. MODELS OF ANTINUCLEON-NUCLEUS ANNIHILATION BASED ON THE MECHANISM OF THE INTRANUCLEAR CASCADE

A. OPTICAL + CASCADE MODEL FOR THE ABSORPTION OF ANTIPROTONS BY NUCLEI FROM A BOUND STATES OF A $\bar{p}$-ATOM

The absorption of a stopped antiproton by a nucleus is a complicated process[5] which proceeds through the same stages as the nuclear absorption of a stopped π^--meson (see Chapter 5). At the first stages, a highly-excited $\bar{p}$-atom is formed when an antiproton, which is decelerated in the medium, is captured by the Coulomb field of a nucleus. In the process of the de-excitation of the atom, the antiprotons, emitting Auger-electrons and X-rays, undergoes a transition to lower orbits, until

it is absorbed by the nucleus from one of them. Following the basic principles of the OC-model, we shall describe these stages within the framework of the optical model (i.e., using the optical $\bar{p}$A-potential).

The general scheme of the calculation[5] is completely similar to that outlined in Chapter 5. The differences are associated with the fact that the optical $\bar{p}$A-potential has a more simple form than the corresponding πA-potential:

$$V_{opt}(r) = -(4\pi^2\hbar^2/2\mu)[a_{\bar{p}p}\rho_p(r) + a_{\bar{p}n}\rho_n(r)] . \quad (1)$$

Here $a_{\bar{p}p}$ and $a_{\bar{p}n}$ are the $\bar{p}$p- and $\bar{p}$n-scattering lengths respectively and μ is the reduced mass of the $\bar{p}$N-system. In this case, the rate of the annihilation of an antiproton from the (n,l)-state of the atom on an intranuclear proton or neutron is described[4] by the expression

$$\Gamma^N_{nl} \sim \mathrm{Im}\, a_{\bar{p}N} \int \rho_\alpha(r)|\psi_{nl}(r)|^2 r^2 dr \quad (2)$$

where the index α specifies the quantities which refer to a proton or a neutron, i.e., $\alpha \equiv$ n, p. The radial distribution of the absorption probability is given by the expression

$$p_{nl}(r) \sim \rho_N(r)|\psi_{nl}(r)|^2 r^2 . \quad (3)$$

Solving the Schrödinger equation, which determines the energy states of an antiproton, with the potential (Equation 1), we can find the wave functions $\psi_{nl}(r)$, and hence the values of $p_{nl}(r)$ for each state of the $\bar{p}$-atom. The total absorption probability $P_{abs}(r)$, summed up with allowance for the absorption from each state of the $\bar{p}$-atom, is obtained from the calculation of the electromagnetic cascade, which is carried out in the same way as described in Chapter 5 with the initial value $n_0 = \sqrt{m_{\bar{p}}/m_e} = 43$.

Calculations[6] of the de-excitation of $\bar{p}$-atoms have demonstated that absorption of an antiproton occurs at the periphery of a nucleus (see Figure 1). As in the case of the π-absorption, the radial dependence of the total probability $P_{abs}(r)$ of the $\bar{p}$-absorption can be approximated by the Gaussian (Equation 8, Chapter 5). The peak of the Gaussian is situated at the value $R_m \simeq R_{1/2} + \Delta/2$. At this point, the density of nuclear matter is approximately equal to one tenth of its value at the center of a nucleus: $\rho_N(R_m) \simeq 0.1\ \rho_N(0)$ ($R_{1/2}$ is the radius at which the nuclear density is half its value at the center of anucleus and $\Delta = 2.3$ fm is the thickness of the diffuse layer of a nucleus). The value of the dispersion D^2 is approximately equal to 1.0 fm^2. Since there is no presently detailed information both on the optical $\bar{p}$A-potential and on the distribution of nucleons at far periphery of a nucleus, theoretical values[6] of the parameters of the Gaussian which depend on these factors cannot be considered reliable. It has been shown[7] that uncertainties in these factors can lead to a change in the value of the parameter R_m approximately by 10%, and in the value of the parameter D approximately by 20 to 30%. Therefore, the quantities R_m and

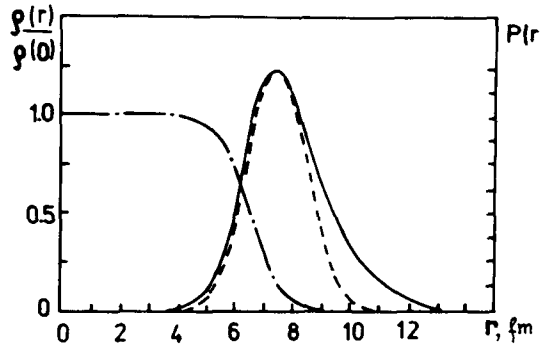

FIGURE 1. This traces the distribution of nuclear matter $\rho(r)/\rho(0)$ (the dash-dotted curve) and the probability distribution ($P_{abs}(r)$ for the antiproton absorption from states of a ^{208}Pb $\bar{p}$-atom (the solid curve corresponds to the calculation of Reference 6 and the dashed curve to the calculation carried out in accordance with Equation 8, Chapter 5, with R_m = 7.81 fm and D = 1.0 fm).

D were considered as parameters of the model whose value was varied to obtain a better agreement with experimental data.

Annihilation of an antiproton on a quasifree nucleon is the principal mechanism of the nuclear $\bar{p}$-capture, since the process takes place in the domain of small densities of nuclear matter, and hence, in the domain of large internucleon distances. In this case, we can deem that annihilation proceeds in the same manner as in vacuum. For small energies of antiprotons, the pion channel dominates in the annihiliation[8]

$$\bar{p}p \rightarrow k\pi^- + k\pi^+ + (n_\pi - 2k)\pi^0 , \tag{4a}$$

$$\bar{p}n \rightarrow k\pi^- + (k - 1)\pi^+ + (n_\pi - 2k + 1)\pi^0 . \tag{4b}$$

To carry out quantitative analysis of $m\pi A$-interaction it is necessary to know kinematic characteristics of all pions produced in a given act of annihilation. Therefore, the calculation of the reaction in Equation 4 was carried out by the Monte Carlo technique. The relations of the modified statistical Fermi model for the multiple production of particles formed a basis of such a calculation.[9] It was assumed that angular distribution of pions is isotropic in the c.m.s. In addition, a requirement was imposed that the energy-momentum conservation law was satisfied in each act of annihilation. The scheme of calculations and a thorough comparison with experimental data on $\bar{p}N$-annihilation are given in Reference 5. Here we shall show only principlal characteristics of the source of pions which will be useful for better understanding of properties of $m\pi A$-interaction. From two to eight pions are emitted in the act of annihilation.The distribution over the pion multiplicity n_π has a narrow peak at n_π = 5 (see Figure 2). The kinetic energy of pions emitted as a result of annihilation varies over a wide range from several MeV to the value $m_N - m_\pi$ (see Figure 3). Average values of the multiplicity and of the energy of pions emitted as a result of absorption are listed in Table 1.

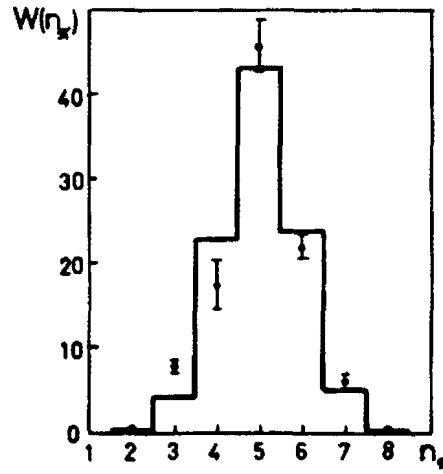

FIGURE 2. The probability (in percent) of production of a given number n_π of pions in the $\bar{p}p$-annihilation at rest is charted here. The histogram corresponds to the calculation of Reference 5 and the points to experimental data.[10]

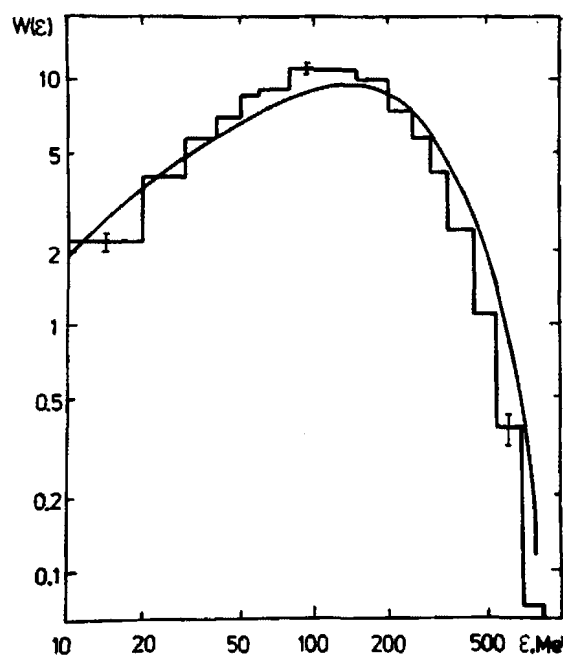

FIGURE 3. Here is the energy spectrum of charged pions (measured in the number of particles per MeV·10^3 $\bar{p}$) produced in the $\bar{p}p$-annihilation at rest. The curve corresponds to experimental data[11]. The rest of notation is the same as in Figure 2.

TABLE 1
Average Values of the Multiplicity, Momentum, and Kinetic Energy of Pions Produced as a Result of the $\bar{p}p$-Annihilation at Rest

Quantity	Experiment[10]	Calculations[5]
$\bar{n}_{\pi^\pm}$	3.05 ± 0.04	3.04
$\bar{n}_{\pi^0}$	1.96 ± 0.23	1.99
$\bar{n}_{\pi}$	5.01 ± 0.23	5.03
$\bar{p}_{\pi}$(GeV/c)	0.35	0.31
$\bar{E}_{\pi}$(GeV)	0.23	0.21

Charges of pions produced depend on whether the annihilation has taken place on a proton or a neutron. The ratio of the probability of annihilation on a neutron to that on a proton $\eta = w(\bar{p}n)/w(\bar{p}p)$ will be considered as another parameter of the model, since the value of η can be affected by the possible existence of the neutron halo,[12] by the presence of the bound states or resonances in the $\bar{p}N$ system,[13] and by some other phenomena. Here a simple estimate $\eta = N/Z$ was used.

To describe the $m\pi A$-interaction proper, a semiclassical approach was chosen in which the pattern of the process appears as follows: pions produced as a result of annihilation escape from point sources distributed over the space in accordance with Equation 8, Chapter 5, and move along their classical trajectories. Such a treatment is sufficiently reasonable, since the size of domain in which the annihilation takes place and the pion wavelength are small as compared with the internucleon spacing in the diffuse layer of a nucleus. Earlier a similar approach was used to advantage for the calculation of multiplicities[3] and inclusive spectra of pions and nucleons,[11] as well as for the calculations of the charge exchange of pions[14] produced after the capture of stopped antiprotons by nuclei.

Thus, the problem is reduced to the description of the interaction of several independent pions with one and the same nucleus consisting of A-1 nucleons. Interaction of each pion, produced as a result of the annihilation of antiprotons, with the nucleus was described with the help of the INC-model outlined in preceding chapters. It should be noted that the parameters of this model are determined from the analysis of data which are not concerned with $\bar{p}A$-reactions under consideration. The general scheme of the calculation of the nuclear absorption of a stopped antiproton, which was carried out by means of the Monte Carlo technique, is described in Reference 5. It has been already mentioned that this method reveals many important points in its favor when it is applied to the analysis of deep inelastic interactions which have multiparticle initial conditions and to the calculation of the characteristics of R-nuclei (it is just these characteristics that contain, in the main, the information on the $m\pi A$-interaction).

B. CASCADE MODEL OF DEEP INELASTIC INTERACTIONS OF INTERMEDIATE-ENERGY ANTINUCLEONS WITH NUCLEI

Let us describe the generalization[15] of the INC-model to the case of inelastic interactions of intermediate-energy antinucleons with nuclei. (Versions of the INC-

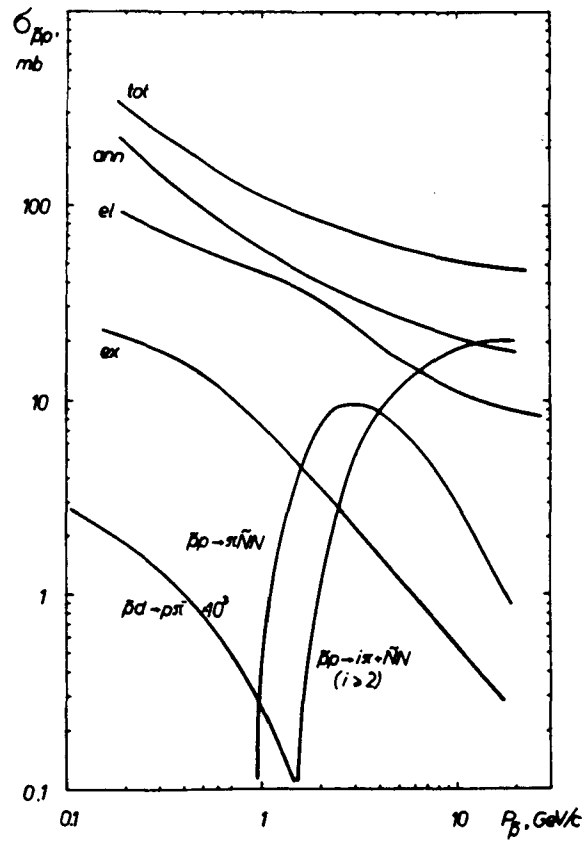

FIGURE 4. This represents the total and the partial cross-sections of the $\bar{p}p$-interaction vs. $\bar{p}$-momentum in l.s.

model for the $\bar{N}A$-reaction which are close in spirit to this one have been developed in References 16 and 17). We shall consider in greater detail those physical aspects of the model the introduction of which allows one to extend it to cover the case of the $\bar{N}A$-interaction.

It is usually assumed[15-17] that, in a nucleus, an antinucleon of intermediate energy interacts independently with each separate nucleon. Therefore, the central point of the model is the description of the elemementary $\bar{N}N$-interaction. In this version of the INC-model, it is carried out by using empirical approximations.[18] Figure 4 shows the energy dependence of the total cross-section σ^{tot} of $\bar{p}p$-interaction and that of the partial cross-sections of its various channels, which were introduced in the calculation of the INC. Empirical curves of Figure 4 were obtained from the analysis of experimental data.[19] It is seen from Figure 4 that for small initial momenta $p_{\bar{p}} < 1$ GeV/c, the following channels dominate in $\bar{p}p$-interaction:

$$\text{annihilation} \qquad \bar{p}p \rightarrow i\pi \quad (i \geqslant 2)\,, \tag{5a}$$

$$\text{elastic scattering} \qquad \bar{p}p \rightarrow \bar{p}p\,, \tag{5b}$$

$$\text{charge exchange} \quad \bar{p}p \rightarrow \bar{n}n \ . \tag{5c}$$

In the domain $p_{\bar{p}} > 1$ GeV/c, the channels of nonannihilation production of one or several pions

$$\bar{p}p \rightarrow \pi\bar{N}N \quad , \tag{5d}$$

$$\bar{p}p \rightarrow i\pi\bar{N}N \qquad (i \geqslant 2) \tag{5e}$$

open up. Usually the channels with production of kaons and other strange particles are disregarded.[15-17] The role of these particles is taken into account in Reference 20.

An antinucleon can be absorbed not only by a separate nucleon, but also by a correlated pair of nucleons:[21,22]

$$\bar{N} + NN \rightarrow N + \pi \ . \tag{6}$$

Within the framework of the quasideuteron model, the cross-section of the two-nucleon absorption on a nucleus is connected with the cross-section of the similar reaction on a deuteron[21] through the relation in Equation 132 in Chapter 2. An elementary cross-section of one of the channels of the two-nucleon absorption $\bar{p}d \rightarrow p\pi^-$ is given in Figure 4. It is indicative of the fact that the probability of the two-nucleon absorption is small as compared to that of the single-nucleon absorption.

The annihilation (Equation 5a) is the principal channel of the $\bar{N}N$-interaction (see Figure 4). To obtain data necessary for the analysis of the INC, kinematic characteristics of all pions produced in each act of the $\bar{N}N$-annihilation were calculated by means of the Monte Carlo technique on the basis of the relations of the modified statistical model.[9] It has been demonstrated[18] that the calculation describes experimental data on the inclusive (multiplicities and spectra) and the exclusive (topological cross-sections, correlations between the numbers of emitted particles) characteristics of pions produced in the $\bar{N}N$-annihilation to a good accuracy over the entire energy range.

The elastic scattering (Equation 5b) and the charge exchange (Equation 5c) are other important channels of the $\bar{N}N$-interaction. To obtain the complete description of the $\bar{N}N$-interaction, it is sufficient in this case to determine only the scattering angle. The presence of a pronounced peak at small angles in the angular distribution is a peculiar feature of the reactions of Equations 5b and 5c. For these reactions, the angular distribution in the c.m.s. can be described to a good approximation by the expression

$$f(\cos\vartheta) = \begin{cases} C_2 \exp(B_2 \cos\vartheta) & \text{for } \cos\vartheta < \cos\vartheta_0 \\ C_1 \exp(B_1 \cos\vartheta) & \text{for } \cos\vartheta \geqslant \cos\vartheta_0 \end{cases} \tag{7}$$

Empirical values of the parameters C_1, C_2, B_1, B_2, and $\cos \vartheta_0$ in this expression obtained by the method of least squares from the experimental cross-sections of the channels in Equations 5b and 5c and the technique of sampling of $\cos \vartheta$ by the method of inverse functions (see the expression of Equation 134, Chapter 2) are presented in Reference 18.

In the domain of momenta $p_{\bar{p}} > 1$ GeV/c, it is necessary to take into account the channels in Equations 5d and 5e of nonannihilation pion production as well. In the case of production of one pion, the following subchannels are possible:

$$\bar{p}p \rightarrow \bar{p}p\pi^0 + \bar{p}n\pi^+ + \bar{n}p\pi^- + \bar{n}n\pi^0 , \tag{8a}$$

$$\bar{p}n \rightarrow \bar{p}p\pi^- + \bar{p}n\pi^0 + \bar{n}n\pi^- . \tag{8b}$$

The channel in Equation 5e has a considerably larger number of subchannels. Unfortunately, the nonannihilation pion production received far less experimental study than the $\bar{N}N$-annihilation. Therefore, we make here an assumption that various subchannels of the reactions in Equations 5d and 5e are equiprobable. The available fragmentary experimental data[23,24] are indicative of the fact that kinematic characteristics of products of pion-creation reactions in the $\bar{p}p$ (the nonannihilation channel) and the pp-interactions are close one another for the same initial energies. Hence, to determine kinematic characteristics of the products of Equations 5d and 5e we can make use of the approximations of experimental data for the reactions $NN \rightarrow \pi NN$ and $NN \rightarrow i\pi NN$ (see Section IIA, Chapter 2).

To calculate the $\bar{N}A$-interaction it is necessary to know the characteristics of not only the $\bar{p}p$-interaction, but also those of the $\bar{p}n$, $\bar{n}p$, and $\bar{n}n$-interactions. Since the corresponding experimental data are either very scarce ($\bar{p}n$, $\bar{n}p$) or completely absent ($\bar{n}n$) it was assumed that all those interactions have identical characteristics (total and partial cross-sections, and spectral and angular characteristics of secondary particles).

Thus, from the viewpoint of the elementary interaction, an antinucleon differs from a nucleon in two respects: 1) the total cross-section of the $\bar{N}N$-interaction exceeds significantly the total cross section of the NN-intreaction at the same energy, and 2) there is a strong annihilation channel in the $\bar{N}N$-interaction. These distinctions call for the introduction of corresponding changes into the INC-model. Owing to the strong annihiliation, an antinucleon with the energy lower than 100 MeV is absorbed mainly on the periphery of a nucleus.[15-17] This conclusion follows both from the classical INC-model using $\sigma^{tot}_{\bar{N}N}$ and from the quantum-mechanical optical model of the $\bar{p}A$-interaction. Information on the optical $\bar{p}A$-potential was obtained from the analysis of data on $\bar{p}$-atoms,[4] on the cross-section σ_R of the inelastic $\bar{p}A$-interaction,[25] and on the elastic $\bar{p}A$-scattering.[26] According to experimental data both the imaginary $W \approx -200$ MeV and the real part $V \approx -100-200$ MeV of the optical potential are significnatly larger than the corresponding values of the pA-potential. Because of a stronger attraction between an antinucleon and a nucleus, the effect of refraction of the trajectory of an antinucleon becomes important. Therefore, the INC-model is extended to include the effects associated with the

refraction and reflection of antinucleons. To this end a nucleus is divided into seven zones (see Section IIA, Chapter 2). Since an antinucleon is strongly absorbed even in rarified nuclear matter, the last zone extends to the far periphery of a nucleus.

As a result of collisions with intranuclear nucleons, an antinucleon can lose such fraction of its initial energy that its kinetic energy is positive only within one or several central zones. Such a nucleon is assumed to undergo annihilation within one of these zones. The probability of the $\bar{N}N$-annihiliation in a given zone is in direct proportion to the ratio of the number of nucleons in this zone to the total number of nucleons in these zones. The annihilation point is sampled uniformly over the entire volume of this zone. Otherwise, the scheme of the calculation of the INC is the same as outlined in Chapter 2.

Since the annihilation channel of the multiple pion production is one of the main channels of the $\bar{N}N$-interaction, the trawling effect can be of importance in the $\bar{N}A$ reaction even for low initial energies, as opposed to the case of the NA-reaction. Therefore, the results of calculations carried out in accordance with the INCT-model will be given in the next section parallel with the results of the standard INC-model.

II. INCOHERENT MULTIPION-NUCLEUS INTERACTION

Let us consider the properties of the incoherent* $m\pi A$-interaction with the help of the outlined theoretical approach based on the assumption that annihilation pions interact with a nucleus independently of one another.

A. CHARACTERISTICS OF EMITTED PARTICLES

Because of the surface character of the $\bar{N}A$-absorption of antinucleons with the energy $\epsilon_{\bar{N}} \lesssim 200$ MeV by nuclei, a considerable part (about a half) of annihilation pions escapes from a nucleus. As a result the average number of emitted pions $\bar{n}_\pi$ decreases only slightly with increasing mass number A_t of a T-nucleus (see Figure 5) unlike the case of pA- and πA-reactions. Indeed, the energy of annihilation pions lies in the vicinity of the (3,3)-resonance (see Table 1), and so when these pions find themselves inside the nucleus with $r < R_{1/2}$, they are absorbed with the probability close to unity. Since the annihilation of stopped antiprotons occurs at the average radius $R_m \approx R_{1/2} + \Delta/2$ (see Section IA), the number of pions entering the nucleus is approximately determined by the solid angle $\Delta\Omega = 2\pi\,(1 - \cos\vartheta_{ann})$ (see Figure 6), and the dependence of the average multiplicity of outgoing pions on A is described by the simple relation[3]

$$\begin{aligned} &\bar{n}_\pi(A_t) = \bar{n}_\pi(\bar{p}N)\,[1 + (1 - R_{1/2}^2/R_m^2)^{1/2}]/2\,, \\ &R_{1/2}/R_m \approx A_t^{1/3}/(A_t^{1/3} + \Delta'), \quad \Delta' = \Delta/2r_0 \approx 1\,, \end{aligned} \tag{9}$$

where $\bar{n}_\pi(\bar{p}N)$ is the multiplicity of pions in the elementary act of annihilation averaged over the nucleonic composition. It is seen from Figure 5 that estimates

* The definition "incoherent" refers to annihilation pions.

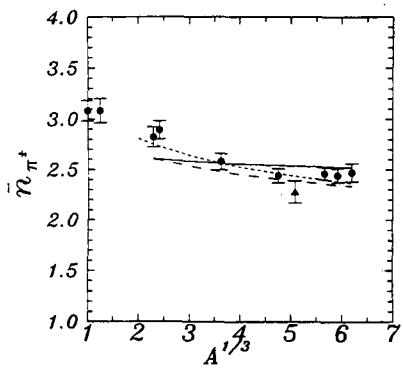

FIGURE 5. This shows the average number of charged pions produced upon the annihilation of stopped antiprotons on nuclei. The solid and the dashed line represent the INC calculations with and without allowance for the trawling effect, respectively. The dotted line presents the corresponding dependence on A found from Equation 9. The circles are experimental values[27] and the triangle is a value for Xe.[28]

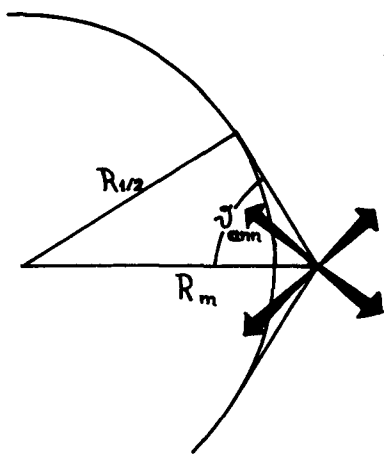

FIGURE 6. A simplified geometric pattern[3] estimates the average multiplicity of pions produced in the annihilation of a stopped antiproton on a nucleus. Arrows indicate annihilation pions.

carried out according to the simple Equation 9 agree rather well both with the results of the rigorous Monte Carlo calculations and with experimental data.

The distribution of the total charge of pions $Q = n_{\pi^+} - n_{\pi^-}$ was investigated in detail[12] to discover the neutron halo in nuclei. Since $Q = -1$ in the $\bar{p}n$-annihilation and $Q = 0$ in the $\bar{p}p$-annihilation, it is possible, in principle, to extract the value of the ratio of the probability for the absorption of antiprotons on a neutron to that on the proton from the measurement of Q on different nuclei. The distribution over Q is shown in Figure 7 for the absorption of antiprotons by nuclei in flight. The broadening of this distribution on nuclei and an excess of events with $Q < 0$

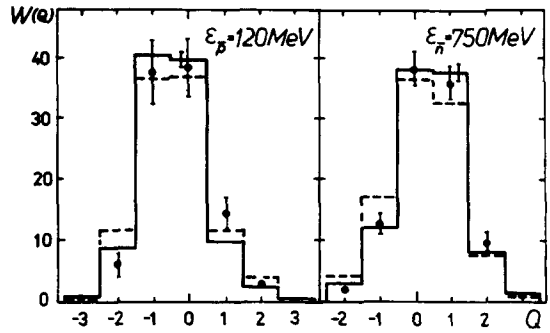

FIGURE 7. The probability (in percent) is charted for inelastic interactions of antinucleons with a C^{12} nucleus with a given charge Q carried away by pions. The dots are experimental values.[29,30] The rest of notation is the same as in Figure 5.

is caused, above all, by the charge exchange of the annihilation pions as they escape from the nucleus.[15] The contribution from the process $\pi N \rightarrow \pi\pi N$ becomes noticeable at the "tail" of the distribution W(Q). The authors of References 5 and 14 have arrived at the similar conclusions from the absorption of stopped antiprotons as well. Thus, to solve the problem of the neutron halo in nuclei, one has to carry out special, thorough analysis of all effects caused by the interaction of the annihilation pions with nuclei.

Owing to the surface absorption of antinucleons by nuclei, such pion characteristics of annihilation on nuclei as the distribution over their multiplicities, the average energy and the energy spectrum differ only slightly from the corresponding characteristics of the annihilation on a nucleon. The INCT-model describes the energy spectrum of pions to a better accuracy than the standard INC-model (see Figure 8). These versions differ from one another by the description of the transport of pions with the energy lying in the vicinity of the (3,3)-resonance. Such pions have an anomalously large cross-section of interaction with a nucleon (see Chapter 4). In the INC-model, the number of collisions of such pions with nucleons and the number of their two-nucleon absorptions in a nucleus are considerably larger than in the INCT-model. Hence, in the calculations carried out within the framework of the INCT-model, a larger part of pions with $\epsilon_\pi \approx 200$ MeV "survive" while escaping from the nucleus. As a result the "dip" at $\epsilon_\pi \approx 200$ MeV observed in the pion spectrum calculated with the help of the standard INC-model is washed out, and the low-energy part of the proton spectrum has a significantly smaller yield (see Figure 8).

Figure 9 shows the angular distribution of antineutrons produced in the charge exchange reaction of antiprotons on the ^{12}C nucleus. The distribution has a sharp peak at the angle $\vartheta = 0°$. This reflects the similar peculiarity of the elementary act (Equation 5c). A satisfactory agreement between experimental data and calculations both in the shape and magnitude of $d\sigma_{ex}/d\Omega$ is indicative of the fact that an incoherent charge exchange of antinucleons on separate quasifree nucleons of nuclear periphery is the principal mechanism of the $\bar{N}A$ charge exchange.

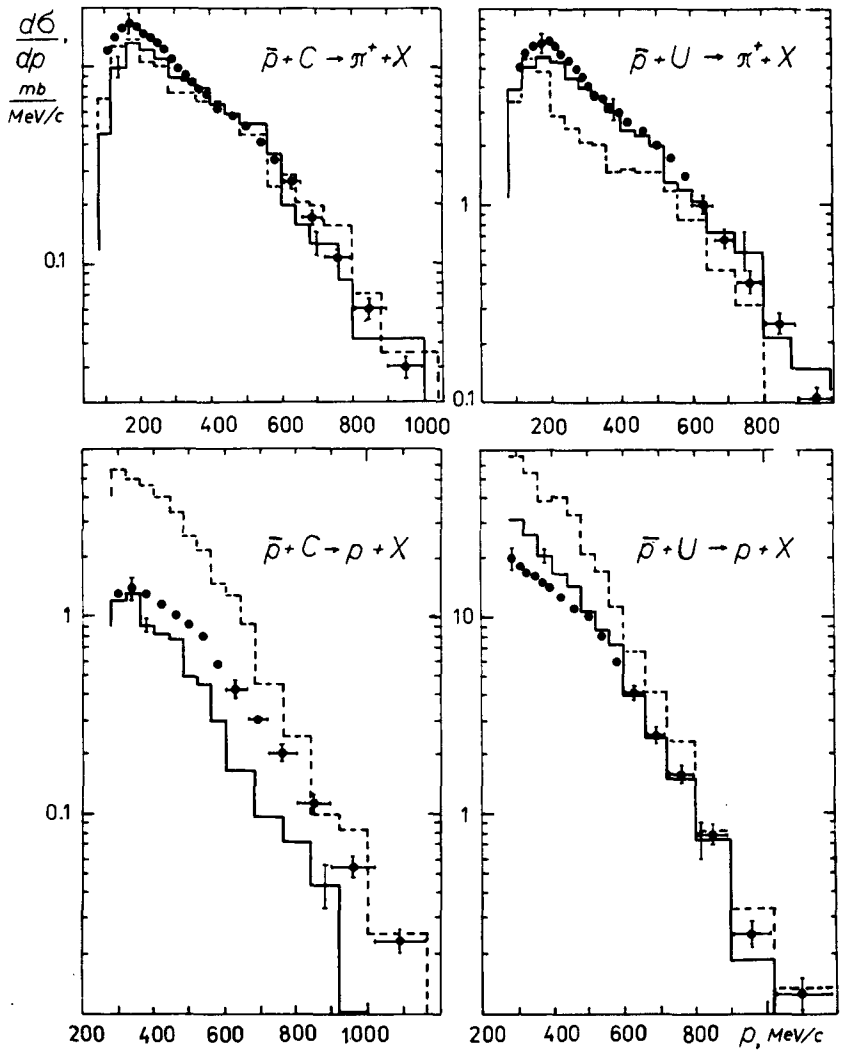

FIGURE 8. The momentum distribution is shown for π^+-mesons and protons produced in the annihilation of antiprotons with energy $\epsilon_{\bar{p}}$ = 180 MeV on ^{12}C and ^{238}U nuclei. The dots are experimental values.[31] The rest of notation is the same as in Figure 5.

In the $\bar{N}A$-annihilation, complex particles are emitted along with pions and nucleons. As in the nuclear absorption of pions (see Chapter 5), they can be produced as well at the stage of the establishment of the equilibrium in an R-nucleus and at the stage of evaporation from a C-nucleus. Moreover, as opposed to the case of pion absorption, another mechanism of production of complex particles, namely, coalescence of cascade nucleons,[33] can play an important role in the $\bar{N}A$-interaction. If a large number of nucleons is involved in the branched cascade, a part of them can unite in a complex particle. For instance, the np-pair can unite in a deuteron,

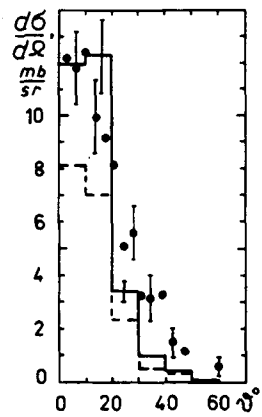

FIGURE 9. The angular distribution is charted here for antineutrons produced in the charge exchange of antiprotons with energy $\epsilon_{\bar{p}}$ = 170 MeV on a ^{12}C nucleus. The dots are experimental values.[32] The rest of notation is the same as in Figure 5.

2np and 2pn in a triton and ^3He, respectively, and 2n2p in an α-particle, if the difference between their momenta and the momentum of the cluster $\mathbf{p}_{cl} = (\Sigma \mathbf{p}_i)/A_{cl}$ satisfies the condition $|\mathbf{p}_i - \mathbf{p}_{cl}| \leq p_0$, where p_0 is the empirical parameter of the coalescence whose values are as follows:[34]

$$p_0 = \begin{cases} 90 \text{ MeV}/c \text{ for d}, \\ 108 \text{ meV}/c \text{ for t, } ^3\text{He}, \\ 115 \text{ MeV}/c \text{ for } \alpha \end{cases}$$

The energy spectra of complex particles are shown in Figure 10. The coalescence of cascade nucleons is the principal mechanism of deuteron production. The role of this mechanism decreases with increasing mass number of clusters, and the pre-equilibrium emission (coalescence of excitons) is the dominating mechanism for formation of t, ^3He, and α. The evaporation mechanism becomes important for production of α-particles. The competition between different mechanisms of emission of complex particles depends on the mass number A_t of a T-nucleus (see Figure 11). In particular, the Fermi breakup of an R-nucleus is the principal mechanism for the production of complex particles in the annihilation of antinucleons on light nuclei, as well as in the case of absorption of pions.

Figure 12 shows the distribution over the total number n_{ch} of charged particles produced in the interaction of antinucleons with a medium-weight nucleus ^{70}Ga of photoemulsion and with a heavy nucleus of ^{181}Ta. These data were obtained in experiments carried out with different energy thresholds for detection of charged particles. Similar criteria for selection of charged particles were used in calculations in order to carry out comparison with experimental data. It is seen from Figure 12 that the "tail" of the distribution $W(n_{ch})$ extends to the domain of large multiplicities n_{ch} = 10-20. This seems to be indicative of a strong spallation of an R-nucleus in

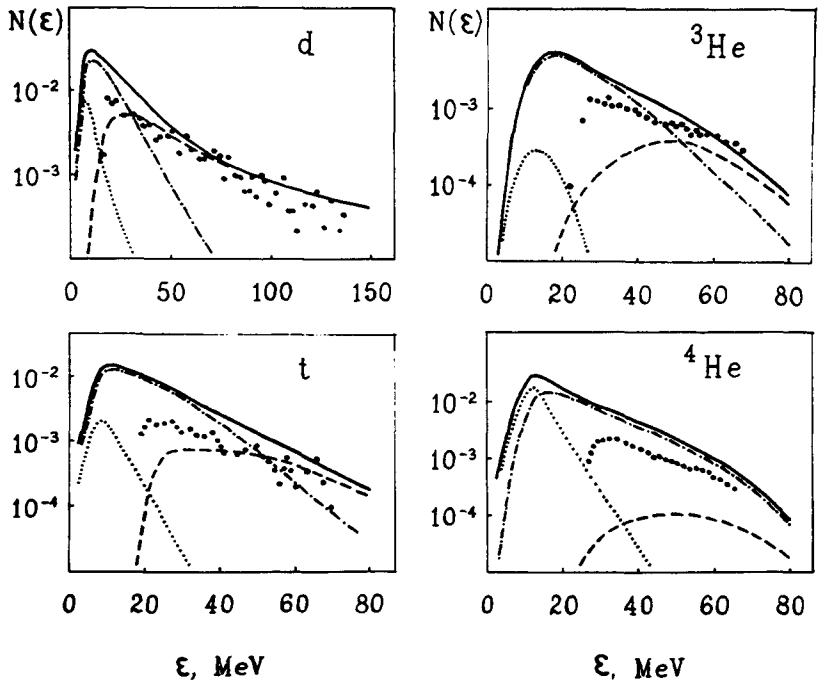

FIGURE 10. These graph the energy spectra $N(\epsilon)$ of d, t, ^{3}He, and ^{4}He produced in the reaction $\bar{p}$ (stopped) $+ {}^{98}$Mo. The results are given in absolute normalization per one absorbed antiproton. The points present experimental data.[35,36] The curves show the results of calculations corresponding to the contributions of various mechanisms: the dashed ones to the coalescence, the dash-dotted ones to the pre-equilibrium emission, the dotted ones to the evaporation, and the solid ones to the sum of all contributions.

the case, when annihilation of antinucleons takes place in the interior of a nucleus. The INCT-model describes the "tail" of the distribution $W(n_{ch})$ over the number of charged particles to a better accuracy than the INC-model.

The correlations between the numbers of emitted particles of different type can be more sensitive to the details of the mechanism of the $\bar{N}A$-interaction than inclusive characteristics (see Chapter 4). Figures 13 and 14 show those few correlations which have been studied in experiments. It is clear that at low energies the $\bar{N}A$-annihilation is close to the limiting case considered in Section IVA, Chapter 4, when pions are produced in the first elementary act and then absorbed strongly by a nucleus. Hence, the average number of h-particles (or protons) decreases with increasing number of s-particles (or pions) (see Figure 13). The calculations carried out within the framework of the INCT-model in which nucleon centers do not leave a T-nucleus after collisions with cascade particles have demonstrated that the trawling effect does not play any significant role at low energy $\epsilon_{\bar{N}}$. A larger number of emitted h-particles (or protons) in the INC-model, as compared to experimental data and to the INCT-model, is caused by a stronger absorption and rescattering of pions in this model, as has already been mentioned.

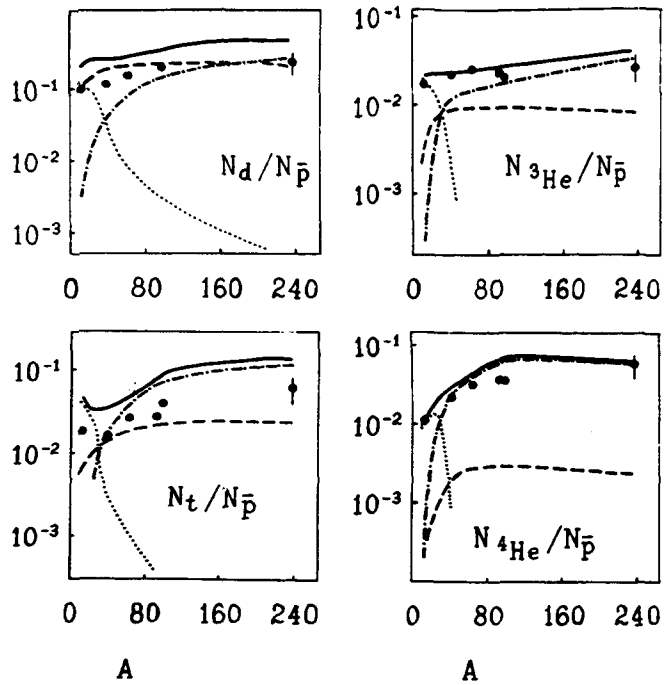

FIGURE 11. Here are the average yields of d, t, ^{3}He, and ^{4}He produced upon absorption of stopped antiprotons as functions of the mass number of a T-nucleus. The yields are given per one absorbed antiproton within the following energy ranges: 20 ÷ 120 MeV for d, 25 ÷ 60 MeV for t, and 36 ÷ 70 MeV for ^{3}He and ^{4}He. The rest of notation is the same as in Figure 10.

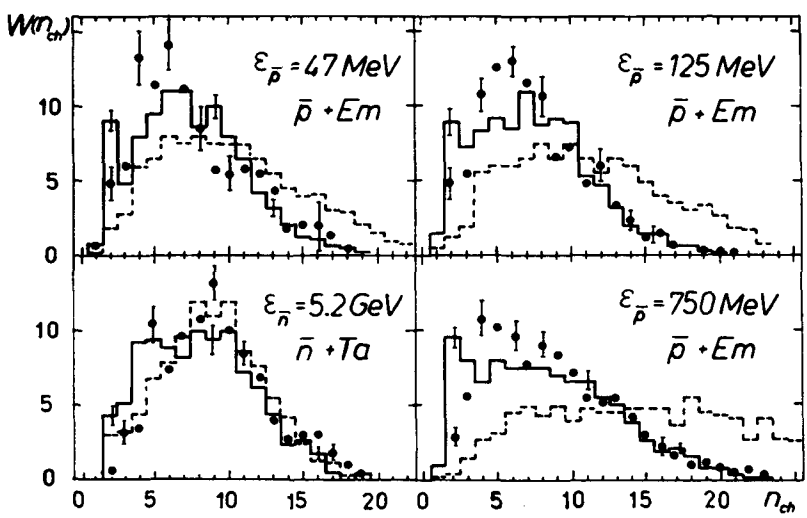

FIGURE 12. This shows the probability (in percent) of production of a given number n_{ch} of charged particles in the inelastic interaction of intermediate-energy antinucleons with medium-weight nuclei of a photoemulsion (Em) and ^{181}Ta. The dots are experimental values.[37,38] The rest of notation is the same as in Figure 5.

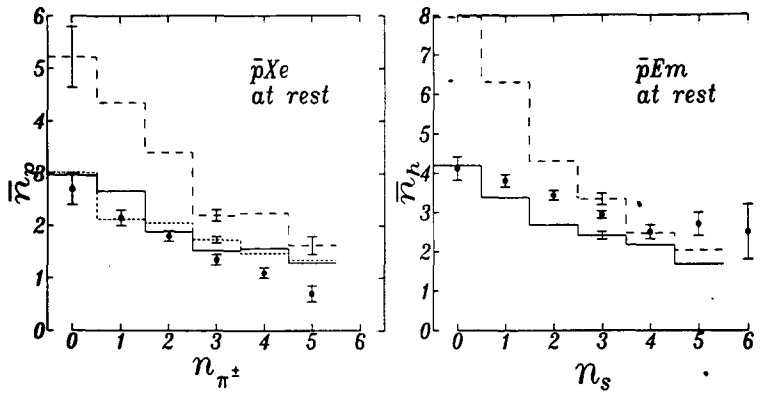

FIGURE 13. The average multiplicity $\bar{n}_p$ of protons is represented here as a function of the multiplicity of charged pions $n_{\pi^\pm}$ produced upon annihilation of stopped antiprotons on Xe nuclei (the left-hand figure) and the average multiplicity $\bar{n}_h$ of h-particles as a function of the multiplicity n_s of s-particles produced upon annihilation of stopped antiprotons on nuclei of photoemulsion (the right-hand figure). The points are experimental data.[39,40] The dashed histogram corresponds to the calculation carried out in accordance with INC-model. The solid and the dotted histogram correspond to the calculations carried out within the framework of the INCT-model with and without allowance for the escape of intranuclear nucleons from a T-nucleus, respectively.

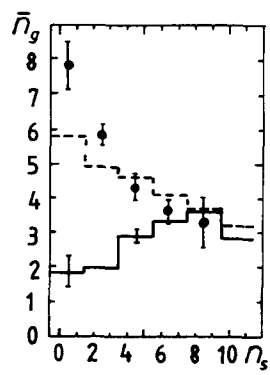

FIGURE 14. This contrasts the average number $\bar{n}_g$ of g-particles with the number n_s of s-particles emitted in the interaction of antineutrons of the energy $\epsilon_{\bar{n}}$ = 5.2 GeV with ^{181}Ta nuclei. The dots are experimental values.[38] The rest of notation is the same as in Figure 13.

In the $\bar{N}$A-interaction occurring at the energies $\epsilon_{\bar{N}} \gtrsim 5$ GeV, the annihilation pions are collimated forward and have the energy which is significantly higher than the energy of the (3,3)-resonance. In addition, the contribution of the nonannihilation pion production also becomes important. In this case, pions are created in collisions of both the primary and cascade particles with intranuclear nucleons, whereas the role of the two-nucleon absorption becomes insignificant. Thus, this process is closer to another limiting case considered in Section IVA, Chapter 4. It is realized in the pA- and the πA-reaction at the energies $\epsilon_0 \sim 10$ GeV. Hence, the correlation $\bar{n}_p$ (n_π) would have to be an increasing function (see Chapter 4). The trawling effect

must play a significant role and the INCT-model must agree with experimental data better than the INC-model, as is the case in the pA- and πA-reaction at high energies. However, contrary to the expectations, the opposite pattern is observed: the experimental correlation $\bar{n}_p$ ($n_{\pi^\pm}$) reveals a decreasing type of behavior, and the calculations carried out within the framework of the INC-model agree better with it (see Figure 14). The values of $\bar{n}_p$ calculated according to the INCT-model turn out to be several times smaller than experimental values for $n_{\pi^\pm}$ equal to zero or unity (see Figure 14). It seems as if there is an anomalously strong absorption of pions by a nucleus in the $\bar{N}$A-annihilation at high energies as compared to the pA- and the πA-reaction. Since the annihilation of a high-energy antinucleon takes place in saturated nuclear matter, this might be explained by the influence exerted by nuclear matter on the mechanism of the $\bar{N}$N-annihilation.[41] It is obvious that effects associated with this make themselves most conspicuous in the channels of the mesonless ($n_\pi = 0$) or the single-meson ($n_\pi = 1$) $\bar{N}$A-annihilation, which are absent in the $\bar{N}$N-annihilation in vacuum. However, it does not seem possible to arrive at more tenable conclusions until more precise experiments are carried out in which protons and $\pi^\pm$-mesons of different energies (including low energies) and π^0-mesons are detected, and which are aimed at the measurements of the correlation $\bar{n}_p(n_\pi)$.

B. CHARACTERISTICS OF R-NUCLEI

Let us now consider the characteristics of R-nuclei produced in the inelastic $\bar{N}$A-interaction. They contain basic information of the interaction of a multipion system produced in the $\bar{N}$N-annihilation with a nucleus. A highly-excited R-nucleus is formed effectively in such a mπA-interaction.[5] The initial energy $\epsilon_{\bar{N}} \sim 200 \div 1000$ MeV of antinucleons seems to be optimal for the production of hot thermalized nuclei. As a matter of fact, an antinucleon of such an energy penetrates deeper into a nucleus than a stopped antiproton, whereas annihilation pions have the energy lying in the vicinity of the (3,3)-resonance and the isotropic angular distribution of the same form as in the $\bar{p}$N-annihilation "at rest". Thus, a hot nucleus produced in the $\bar{N}$A-annihilation is uniformly heated, unlike the case of the high-energy πA- and pA-reactions in which secondary particles are strongly collimated forward. Another fact which favors the study of thermal effects is that an antinucleon of low energy brings in with it significantly smaller values of momentum and angular momentum than hadrons and especially smaller than a high-energy heavy ion (see Section II, Chapter 3).

The properties of the mπA-interaction were predicted in Reference 5. In particular, the contribution of processes with different number ν_π of pions involved in the interaction with a nucleus (i.e., the processes with the different multiplicity of the mπA-interaction) has been considered. To this end the history of each annihilation pion has been traced until its first act of interaction in nuclear matter. The probabilities of the mπA-interaction with different multiplicity ν_π are listed in Table 2 for the case of the annihilation of stopped $\bar{p}$ on nuclei of ^{70}Ga and ^{208}Pb. The distribution over the number of pions involved in the interaction is rather broad, namely, the probability that $\nu_\pi = 2,3$ and 4 are scores of percent, and the probability

TABLE 2
Probabilities (in percent) of mπA-Interactions with Various Multiplicity for the Absorption of Antiprotons by ^{70}Ga and ^{208}Pb Nuclei

Multiplicity ν_π	^{70}Ga	^{208}Pb
0	17.0	13.2
1	24.3	20.0
2	27.0	28.7
3	19.5	22.0
4	9.8	10.7
5	2.6	4.1
6	0.8	1.0
7	—	0.2
$\bar{\nu}_\pi$	1.91	2.15

that $\nu_\pi = 5$ and 6 are units of percent. As we go over to heavy nuclei, the probability of events with large ν_π increases. It is seen from Figures 15 and 16 that spallation of a T-nucleus ΔA, and the excitation energy E^*, the momentum p_r, and the angular momentum I of an R-nucleus increase with increasing ν_π. The following effects are indicative of the presence of the mπA-interaction (see Figure 16):

1) production of highly-excited nuclei with $2m_\pi \leqslant E^* \leqslant m_N$
2) strong spallation of a T-nucleus $\Delta A > 20$
3) large value of the momentum of an R-nucleus $p_r > 0.7$ GeV/c
4) production of rapidly rotating nuclei and population of high-spin isomers with $I > 20$.

The multiplicity of the mπA-interaction can be determined, in principle, in different coincidence experiments. For example, in the domain of light nuclei, one can simultaneously register the number of produced pairs of nucleons with the energy $\epsilon_N \sim m_\pi/2$ and the angle of divergence $\sim 180°$ in c.m.s. of each pair. These nucleons are produced after a two-nucleon absorption of annihilation pions. Another possible experiment is associated with a simultaneous measurement of properties of R-nuclei and characteristics of outgoing pions. This allows one to determine an effective missing mass and hence the number of pions which have entered the nucleus. However, only the simplest experiments which give information on the mπA-interaction averaged over ν_π have been carried out to the present day. Distributions (corresponding to such a situation) over characteristics of R-nuclei produced after the completion of the cascade are shown in Figure 17.

These R-nuclei have a broad distribution over the excitation energy which extends up to the values of E^* close to their total binding energy. During the cascade

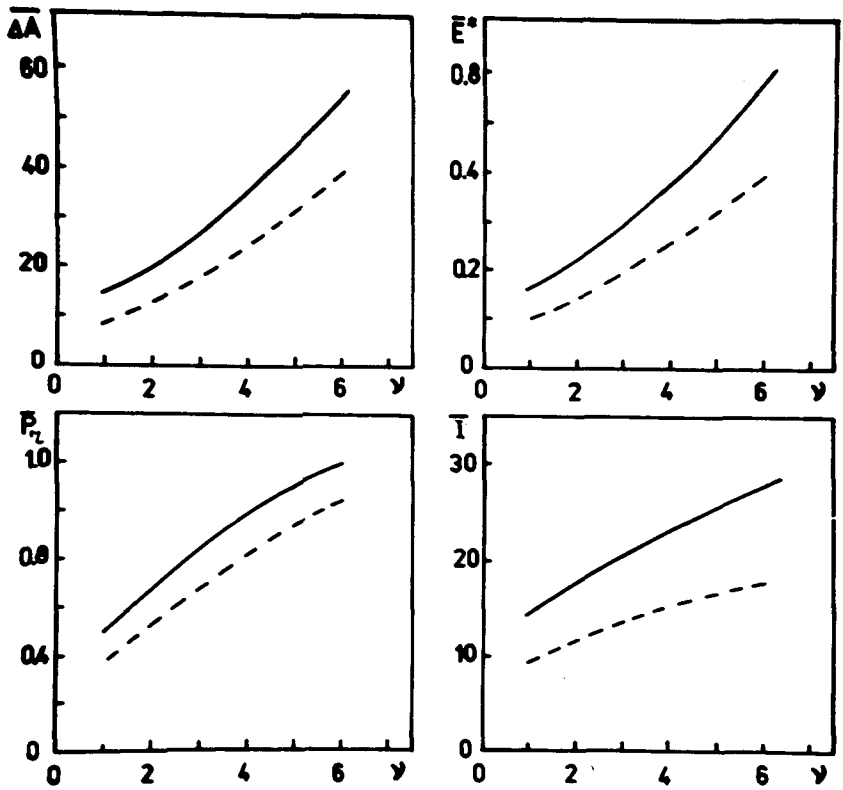

FIGURE 15. The average values $\overline{\Delta A}$, $\overline{E^*}$ (GeV), $\bar{p}_r$ (GeV/c) and $\bar{I}$ of C-nuclei as functions of the multiplicity ν_π of the mπA-interaction are presented here. The solid and dashed curves are the calculations of the absorption of stopped antiprotons by ^{208}Pb and ^{70}Ga nuclei, respectively.

stage of the $\bar{N}$A-interaction, a T-nucleus loses a great number of nucleons ΔA. After the completion of the cascade, the nucleus acquires large values of momentum p_r and angular momentum I. Large values of $p_r \sim 1$ GeV/c allow one to detect R-nuclei in experiments, whereas the large angular momentum I $\sim$ 30 offers the possibility of observing the population of high-spin isomeric states in the inelastic $\bar{N}$A-interaction in the same way as in the absorption of stopped π^--mesons (see Section IB, Chapter 5). Moreover, we can expect that isomers with significantly higher values of spin than in the πA-absorption are populated in the $\bar{p}$A-absorption. The number of collisions of cascade particles with intranuclear nucleons is smaller in the INCT-model than in the INC-model . As a result, in the INCT-model the yield of R-nuclei with very high values of the excitation energy E* and the momentum p_r decrease. The same holds true for the number ΔA of nucleons lost (see Figure 17).

In the subsequent decay, a hot R-nucleus loses again a large number of nucleons (the higher the excitation energy E*, the larger the number of nucleons lost). As

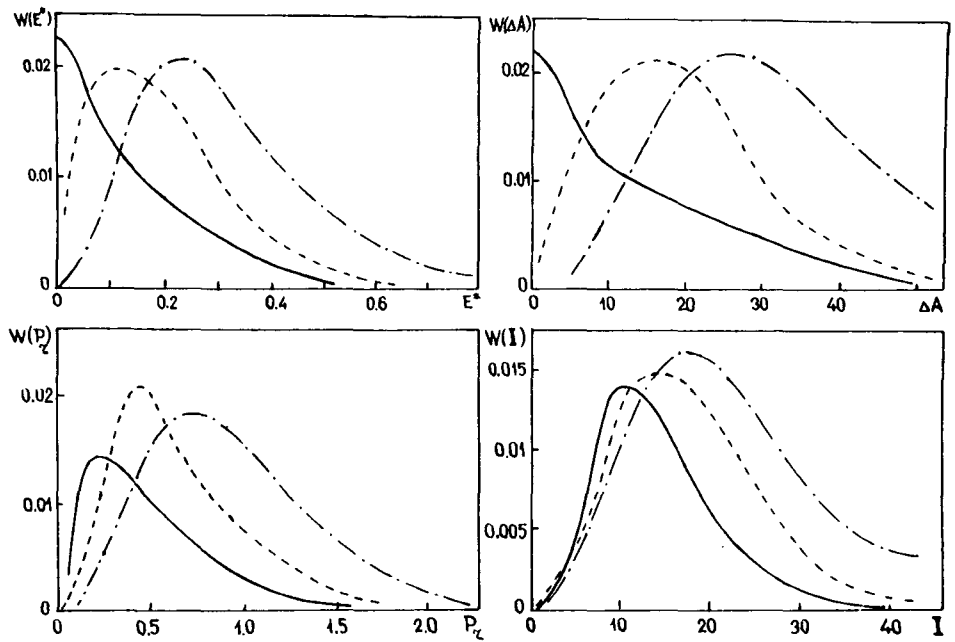

FIGURE 16. These graph the distribution (in relative units) of R-nuclei over E*(GeV), ΔA, p_r(GeV/c) and I for various multiplicity ν_π of the mπA-interaction. The curves show the results of the calculation[5] for absorption of stopped antiprotons by ^{208}Pb nuclei. The solid curve corresponds to $\nu_\pi = 1$, the dashed one to $\nu_\pi = 2$, and the dash-dotted one $\nu_\pi \geqslant 3$.

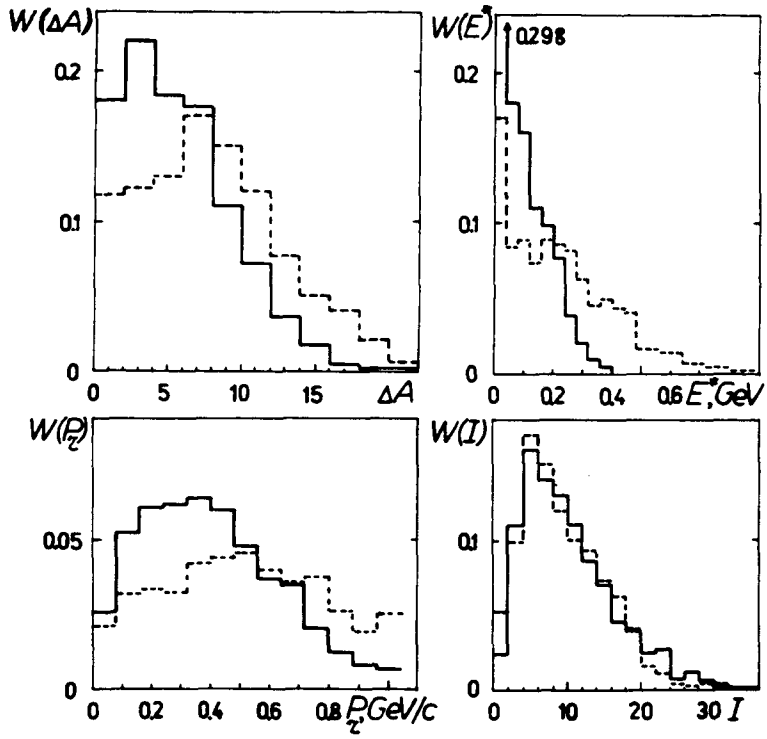

FIGURE 17. These correspond to the distribution of thermalized R-nuclei produced in the inelastic interaction of antiprotons of the energy $\epsilon_{\bar{p}}$ = 180 MeV with a ^{100}Ru nucleus over the number of nucleons ΔA carried away from a T-nucleus, excitation energy E*, momentum p_z, and angular momentum I. The histograms are normalized to a single event of nuclear absorption. The rest of notation is the same as in Figure 5.

a result, the $\bar{N}$A-interaction leads to a broad spectrum of nuclides remote both from the initial T-nucleus and from the β-stability line (see Figure 18).

Isotopes neighboring a T-nucleus (small ΔA and ΔZ) belong to a narrow domain in the yield of R-nuclei Y(Z,N). These nuclides are produced in weak INCs when all annihilation pions either leave the nucleus or knock out nucleons through elastic scattering (Equation 18a, Chapter 5) or charge exchange (Equation 18b, Chapter 5) in the elementary πN-interaction. In such cases, a weakly-excited C-nucleus, which emits one-two nucleons or only γ-quanta, is formed. There are two interesting groups in this domain.

First, nuclides with the charge number Z_t + 1 or Z_t + 2 exceeding the charge number Z_t of a T-nucleus can be produced with a rather large probability. These nuclides are formed in the process in which one or several annihilation pions undergo the charge exchange reaction on intranuclear nucleons independently of one another. Mainly the single, or less often the double, charge exchange takes place in the $\bar{N}$A-annihilation at rest.[42] The triple charge exchange of pions is also possible, but it occurs with a very small probability. The probability of the multiple charge exchange of pions increases with increasing excess of neutrons and atomic number A_t of a

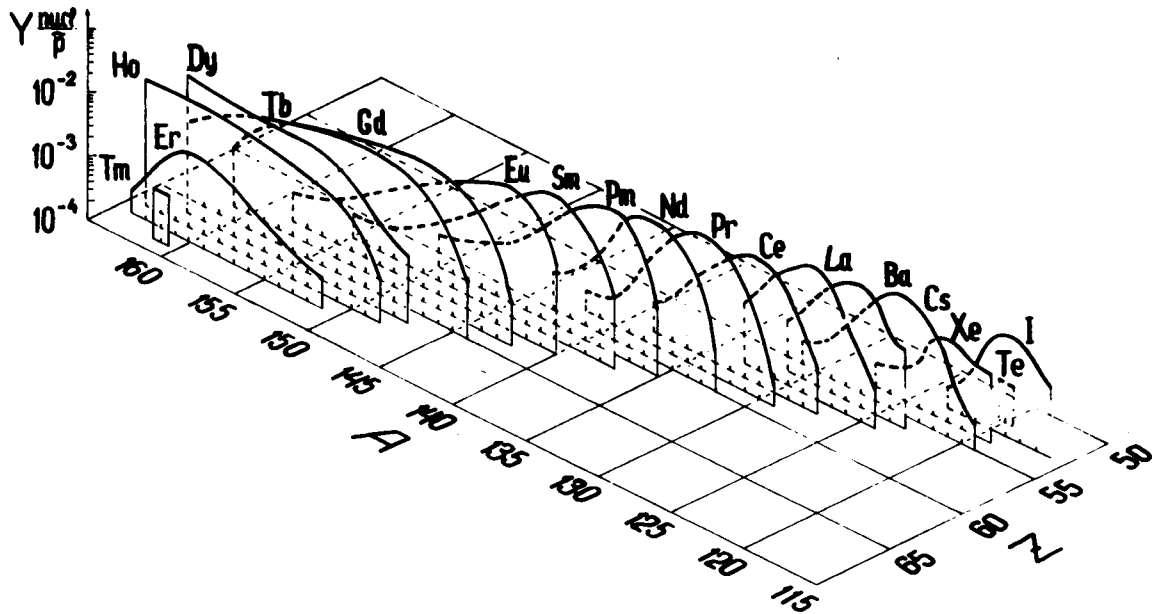

FIGURE 18. Here is the yield (per one antiproton) of nuclides with a given number of neutrons N and of protons Z in the absorption of stopped antiprotons by a ^{165}Ho nucleus. The curves represent the results of the INC-model calculations (without the trawling effect) which take into account subsequent evaporation from thermalized R-nuclei.

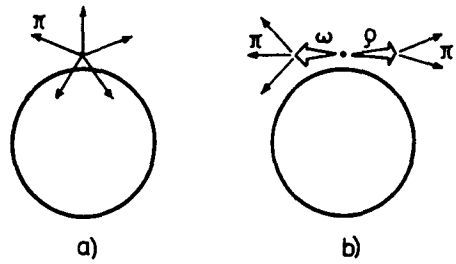

FIGURE 19. This represents the schematic pattern of antiproton annihilation on the nuclear surface. The diagrams show the difference between uncorrelated pion production and pion production through decay of heavy mesons, in which the probability that all pions leave the nucleus is higher.

T-nucleus. The charge exchange reaction, which involves pions and leads to the production of R-nuclei with $Z_t = Z_t + 1$, has been observed in experiments,[42] on the ^{165}Ho nucleus.

Second, it has been demonstrated[42] that certain nuclides with $\Delta A = 1$ have large yields. These nuclides are produced when all annihilation pions leave a T-nucleus and a C-nucleus acquires a low value of the excitation energy $E^* < B_n$. Such events correspond to the annihilation of an antiproton on a weakly-bound nucleon at a far periphery of a nucleus. The yield of nuclides with $\Delta A = 1$ can be caused not only by the presence of matter at a far periphery of a nucleus, but also by other specific effects, for instance, by the production of heavy mesons (ρ, η, ω, etc.) in the $\bar{p}$N-annihiliation which subsequently decay into pions. Figure 19 shows the difference between the noncorrelated emission of annihilation pions considered in this section and the correlated emission of pions through the production of heavy mesons. The noncorrelated emission leads, in some cases, to the interaction of a larger number of pions and a nucleus with a subsequent emission of a large number of nucleons, whereas the correlated emission of pions favors the formation of R-nuclei, which lose a small number of nucleons.

The INC-model describes reasonably well the experimental data which are concerned with not only the isotope yield but also with the nuclear fission in the $\bar{p}$A-annihilation.[15,43] This problem will be considered in greater detail in Chapter 7.

III. INTERACTION OF MESONIC RESONANCES WITH NUCLEI

It has already been mentioned that the model of incoherent mπA-interactions is based on the assumption that annihilation pions interact with a nucleus independently of one another. It is well known, however, that, in the $\bar{N}$N-annihilation, the mesonic resonances produced with a large probability decay later on to pions, kaons, and γ-quanta. At least one resonance is produced, as a rule, in each act of annihilation.[5] Let us estimate the role played by such resonances in the $\bar{N}$A-annihilation.

A. PRODUCTION OF MESONIC RESONANCES IN $\bar{N}N$-ANNIHILATION

To correctly take into consideration the effects associated with production of mesonic resonances we are to be able, above all, to calculate the exclusive characteristics of the $\bar{N}N$-annihilation in which these products are formed. A high multiplicity of particles produced and a large number of channels with neutral particles are specific features of the $\bar{N}N$-annihilation. Therefore, the experimental exclusive information is available only for a small fraction of annihilation channels. This does not allow one to construct any empirical approximations for a given elementary process. As a rule, one has to use some theoretical model of the $\bar{N}N$-annihilation, for instance, the statistical model with the SU(3)-symmetry[44] in which the $\bar{N}N$-annihilation is interpreted as a process with an intermediate stage. In this model, from two to six intermediate particles are permitted to be produced in the $\bar{N}N$-annihilation. These particles are π, η, ω, ρ, K, and K*. The probability of the channel of the $\bar{N}N$-annihilation in which n particles with the isotopic spins $I_1,\ldots,I_N$ and the hypercharges $Y_1,\ldots Y_n$ are produced has the form[44]

$$w_n(\sqrt{S};I_1,\ldots I_n;Y_1,\ldots Y_n) = V_n(\sqrt{S})\, s_n M_n(\sqrt{S}) \times \prod_{1\le i\le n} 2m_i \sum_{(p,q)} K^2_{(p,q)}(I,I_3,Y)\, U_n(p,q;I_1,\ldots I_n;Y,\ldots Y_n)\,. \tag{10}$$

Here $V_n(\sqrt{S}) = (2m_N V_0 \sqrt{S})^{n-1}$, $V_0 = 21.5\ \mathrm{GeV}^{-3}$ is the interaction volume, $\sqrt{S}$ the total energy, m_i and m_N are the masses of the i-th particle produced and of the nucleon, respectively, s_n is the spin factor, $K^2_{(p,q)}(I,I_3,Y)$ are the coefficients of the expansion of the initial state of the $\bar{N}N$-system ($I = 0, 1$; $I_3 = 0, +1$; $Y = 0$) in the irreducible representations (p,q) of the SU(3)-group, $U_n(p,q;I_1,\ldots I_n;Y_1,\ldots Y_n)$ is the isoscalar factor which includes the term taking into consideration the identity of particles and $M_n(\sqrt{S})$ is the Lorentz-invariant phase volume.

All possible channels of decay of intermediate particles were taken into account in the Monte Carlo method of the calculation of exclusive characteristics of the $\bar{N}N$-annihilation which was constructed[45] on the basis of this model. All available experimental data were used to verify this method. They include the multiplicities of the particles produced, inclusive spectra, topological cross-sections, and probabilities of channels with mesonic resonances. Table 3 and Figure 20 show the comparison of computational results with experimental data concerned with the multiplicities and spectra of heavy mesons. It is seen that the $\bar{N}N$-annihilation is the "factory" of mesonic resonances which produces ρ, η and ω mesons with high efficiency. However, the "beams" of mesonic resonances have poor energy resolution (see Figure 20), namely, there is a peak associated with the contribution of two-particle channels $\omega\rho$, $\eta\omega$, and $\eta\rho$ on a broad plateau in the spectra of η and ω.

The majority of mesonic resonances produced in the $\bar{N}N$-annihilation has such large decay widths that they undergo a decay inside the nucleus before they have a chance to interact with nucleons. However, ω and particularly η mesons have larger lifetimes. For instance, the decay width Γ_ρ of ρ-mesons is equal to 158 MeV and the corresponding lifetime τ_ρ is $4\cdot10^{-24}$s. These values for ω and η-mesons

TABLE 3
Average Values of the Multiplicity of Mesons Produced in the $\bar{p}p$-Annihilation at Rest

Meson multiplicity	Monte Carlo calculation	Experiment
$\bar{n}_\eta$	0.092	0.10 ± 0.09[46] 0.0698 ± 0.0079[47] 0.044 ± 0.004[48]*
$\bar{n}_\omega$	0.202	0.28 ± 0.16[46] 0.22 ± 0.01[48]*
$\bar{n}_{\rho^0}$	0.196	0.26 ± 0.01[48]*
$\bar{n}_{\rho^-}$	0.194	—
$\bar{n}_{\rho^+}$	0.194	—

* The data were obtained for the antiproton momentum 0.7 GeV/*c*.

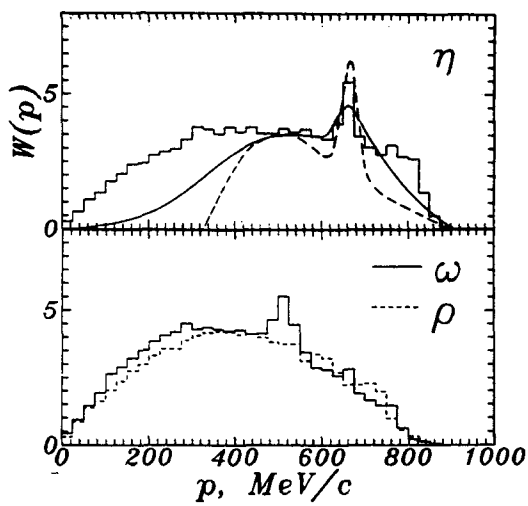

FIGURE 20. Here are the inclusive momentum spectra of η, ω, and ρ^0-mesons produced in the $\bar{p}p$-annihilation at rest. Histograms are the Monte Carlo calculation according to the statistical model with unitary symmetry (the histograms are normalized to 100%). Experimental data for η have been borrowed from Reference 49 (the dashed line and the detection threshold p_η = 342 MeV/c) and Reference 47 (the solid line).

are as follows: Γ_ω = 10.1 MeV, $\tau_\omega = 7{\cdot}10^{-23}$s, and Γ_η = 0.85 KeV, $\tau_\eta = 8{\cdot}20^{-19}$s. The decay mean free path of ω-mesons exceeds the internucleon spacing δ inside the nucleus, whereas for η-mesons it is even larger than nucleus itself. Thus, the INC-model must take into account not only the production of these mesons in an elementary process, but also their participation in the INC. This requires the knowledge of the cross-sections of the ηN and the ωN-interaction.

B. INTERACTION OF η- AND ω-MESONS WITH NUCLEONS

Although the interaction of η-mesons with a nucleon is studied in greater detail than that of ω-mesons, the experimental data on the cross-sections of the ηN-

reactions are fragmentary and contradictory. Later, we shall give the results of a theoretical estimate of these cross-sections obtained with the help of the coupled-channel isobar model for πN, ηN, and πNN-systems. It is assumed in this model that the reaction proceeds through the formation of intermediate states N*. The baryonic resonances $N^*(1440)P_{11}$, $N^*(1520)D_{13}$, and $N^*(1535)S_{11}$ were used as dynamical sources for the P-, D-, and S-wave interactions. In the energy range of annihilation η-mesons $\epsilon_\eta \leq 300$ MeV (see Figure 20), the contribution of the $N^*(1535)S_{11}$ is dominant.[50] The theoretical energy dependence of the total and the elastic cross-section is given in Figure 21. The cross-section of the reaction $\eta N \rightarrow \pi N$ has been found from experimental data[51] on the inverse reaction $\pi N \rightarrow \eta N$. The cross-section of the three-particle channel was estimated as a difference $\sigma(\eta N \rightarrow 2\pi N) = \sigma^{tot}_{\eta N} - \sigma^{el}_{\eta N} - \sigma(\eta N \rightarrow \pi N)$ with no regard to the $\eta N \rightarrow 3\pi N$ channel.

It has been noted[5] that in addition to the interaction of the η-meson with a separate nucleon, there can exist also the reactions of two-nucleon absorption $\eta + NN \rightarrow NN$ and $\eta + NN \rightarrow \pi NN$ in a nucleus. The calculations of a two-nucleon absorption of η-mesons (and of ω-mesons) in the nucleus can be carried out on the basis of the quasideuteron model (see Equation 132, Chapter 2). To follow this procedure it is necessary to know the energy dependence of the cross-sections of $\eta d \rightarrow NN$ and $\eta d \rightarrow \pi NN$ reactions. They were estimated by the diagram technique in the pole approximation.[52] It was assumed that an η-meson is absorbed through an elementary subprocess $\eta N \rightarrow N^*(1535) \rightarrow \pi N$. The partial cross-sections for the ηN- and the ηd-reaction are shown in Figure 21.

The situation with an ω-meson is even more uncertain. It is presently impossible to calculate the total and the elastic ωN-cross-section, because the baryonic resonances with the required values of masses and quantum numbers, which have decay channels with production of an ω-meson, are unknown. Therefore, it was assumed that the total and the elastic cross-section of the ωN-interaction have the same energy dependence as in the case of the ηN-interaction, whereas the ratio of the total cross-sections at low energies has the same value as in the domain of large energies, namely $\sigma^{tot}_{\omega N}/\sigma^{tot}_{\eta N} \approx 2$.[53] The cross-section for the reaction $\omega N \rightarrow \pi N$ was found from experimental data[51] on the inverse reaction $\pi N \rightarrow \omega N$. The ratio of the cross-section of the two-particle channel to that of the three-particle channel $\sigma(\omega N \rightarrow \pi N)/\sigma(\omega N \rightarrow 2\pi N) \approx 1.5$ was taken to have the same value as for the πN-interaction $\sigma(\pi N \rightarrow \pi N)/\sigma(\pi N \rightarrow 2\pi N)$ for the initial momentum of a pion corresponding to the same total energy $\sqrt{S}$ as in the ωN-reaction. The cross-sections of the $\omega d \rightarrow NN$ and the $\omega d \rightarrow \pi NN$ reaction can be roughly estimated with the use of experimental data[54] on the $\omega + {}^3He \rightleftarrows p + d$ process and the $\eta + {}^3He \rightleftarrows p + d$ process. Along these lines, it has been found[45] that the cross-sections of the ωd-reactions is smaller than the cross-sections of the corresponding ηd-reactions approximately by two orders of magnitude. Figure 21 shows the estimated energy dependence of the total and the partial cross-sections of the ωN and the ωd-interaction.

It should be noted that the estimates presented here give only a rough approximation to the values of the cross-sections of the ηN- and the ωN-interaction. Their uncertainty lies within a factor of two. Little is known about the nature of the

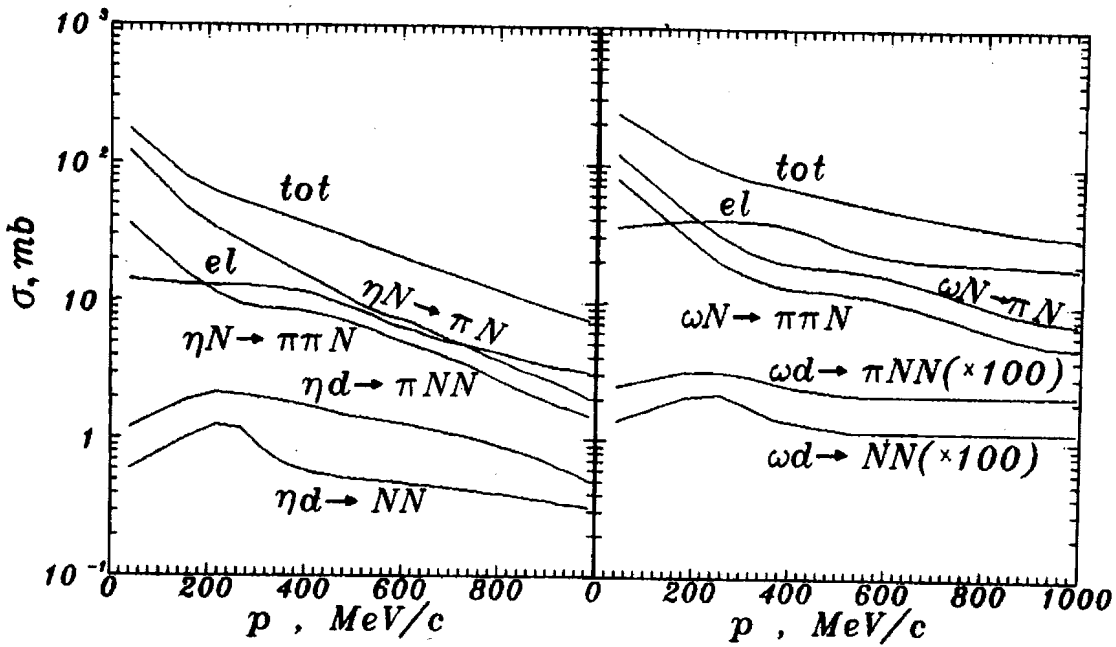

FIGURE 21. Here are total and partial cross-sections of ηN- and ωN-interactions.

interaction of η- and ω-mesons with nucleons and not all channels of these interactions can be reliably estimated. In such a situation, it seems more reasonable to solve the inverse problem, namely, to find the characteristics of the $\bar{N}A$-annihilation which are sensitive to the cross-sections of the ηN and the ωN-interaction and to extract information on these cross-sections from the comparison with experimental data.

C. INC-MODEL WITH MESONIC RESONANCES

To solve this problem a modified version of the INC-model* has been developed.[45] The introduction of the Monte Carlo procedure of the exclusive calculation of the production of mesonic resonances in the $\bar{N}N$-annihilation

$$\bar{N}N \rightarrow i\pi + j\rho + k\eta + l\omega \tag{11}$$

is one of the refinements of the theory. It is assumed in this procedure that the annihilation ρ-mesons undergo decay before they can interact with an intranuclear nucleon. The annihilation ω-mesons can enter into interaction with a nucleon or decay inside or outside the nucleus. The competition between the decay of an ω-meson and its interaction with an intranuclear nucleon was taken into account with the help of the corresponding expression for the mean free path:

$$L^{-1} = L_{dec}^{-1} + L_{int}^{-1} . \tag{12}$$

Here $L_{int} = (\rho_N \sigma_{\omega N}^{tot})^{-1}$, $L_{dec} = \beta(\hbar\Gamma_\omega\sqrt{1-\beta^2})^{-1}$, ρ_N is the nuclear density, and $\beta = v/c$ (v is the velocity of the particle). The lifetime of the annihilation η-meson is so large that it is considered as a stable particle inside the nucleus. The following modes of meson decay are taken into consideration in the model: $\rho \rightarrow 2\pi$, $\omega \rightarrow 3\pi$, $\omega \rightarrow 2\pi$ and $\omega \rightarrow \pi\gamma$.

In addition to the channels of elementary interaction in Equations 5, 6, and 11, and Equation 131, Chapter 2, the following reactions have been included in the calculation:

$$\eta N \rightarrow \eta N,\ \eta N \rightleftarrows \pi N,\ \eta N \rightarrow \pi\pi N,\ \eta + NN \rightarrow NN, \tag{13a}$$

$$\eta + NN \rightarrow \pi NN ,$$

$$\omega N \rightarrow \omega N,\ \omega N \rightleftarrows \pi N,\ \omega N \rightarrow \pi\pi N,\ \omega + NN \rightarrow NN, \tag{13b}$$

$$\omega + NN \rightarrow \pi NN .$$

The same function $f_{NN}(A,Z,\epsilon_0)$ in the relation of Equation 132, Chapter 2, as in the calculation of the two-nucleon absorption of pions, was used as a zeroth approximation for the description of the two-nucleon absorption of η- and ω-mesons.

* A simplified version of the INC-model aimed at the calculation of the average multiplicities of η and ω-mesons in the $\bar{N}A$-annihilation has been developed in Reference 55.

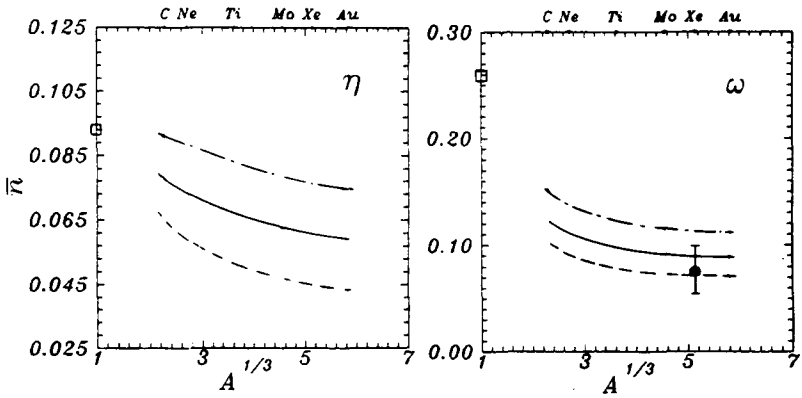

FIGURE 22. This shows mean multiplicities $\bar{n}$ of η and ω-mesons vs. the mass number of a T-nucleus. The solid line corresponds to the calculation with the cross-sections shown in Figure 21. The dashed line corresponds to the calculation with the cross-sections, which are larger by a factor of two. The dash-dotted line corresponds to the calculation with the cross-sections, which is smaller by a factor of two. The quad marks the yield of η- and ω- mesons in the $\bar{p}$ annihilation on a nucleon (averaged over p and n). The dot is an experimental value.[28]

The depths V_η and V_ω of the potential wells for η- and ω-mesons in a nucleus are free parameters of the model whose values are determined in such a way as to ensure the best description of experimental data.

D. PRODUCTION OF η- AND ω-MESONS IN $\bar{N}$A-ANNIHILATION

Since the effects of mesonic resonances have not yet been studied in experiments, let us estimate them from the comparison of the results of calculations carried out with and without allowance for these resonances. Among a large number of characteristics of the $\bar{p}$A-annihilation calculated,[45] we shall confine ourselves here only to those in which the effects under consideration manifest themselves most vividly. To study the sensitivity of these characteristics to the cross-sections of the ηN and the ωN-interaction, calculations[45] have been carried out both with cross-sections presented in Figure 21 and with those increased and decreased by a factor of two.

The average multiplicity and the energy spectrum of η- and ω-mesons are the characteristics of the $\bar{p}$A-annihilation associated directly with the production of mesonic resonances. The dependence of the average multiplicity on the mass number A_t of a T-nucleus is shown in Figure 22. The majority of heavy mesons produced in the $\bar{p}$A-annihilation leaves the nucleus. This is a corollary of the surface nature of the absorption of slow antiprotons by nuclei. As a result, this A-dependence is described by the same Equation 9 as in the case of emission of pions. Moreover, a considerable part of ω-mesons undergoes decay before they leave the nucleus. Therefore, a decrease in the multiplicity of ω-mesons produced in the $\bar{p}$A-annihilation relative to their multiplicity in the $\bar{p}$N-annihilation is larger than in the case of η-mesons. It is seen from Figure 22 that values of the average multiplicities of η- and ω-mesons are sensitive to the cross-sections of ηN- and ωN-interactions.

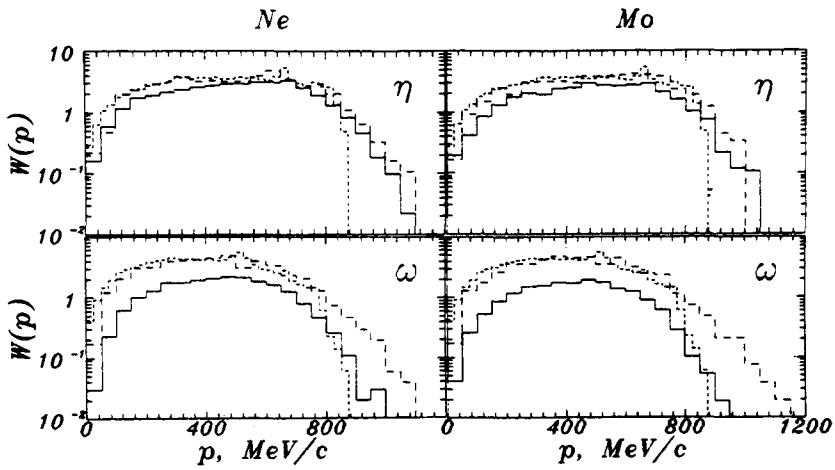

FIGURE 23. The momentum spectra W(p) of η and ω-mesons produced in antiproton annihilation on Ne and Mo nuclei are shown by the solid histograms. The dotted and the dashed histograms are the spectra of η and ω-mesons produced in antiproton annihilation on a nucleon at rest and on intranuclear nucleon, respectively. The second and the third histogram are normalized to 100%, the first histogram is normalized to $100\% \cdot \bar{n}(\bar{p}A)/\bar{n}(\bar{p}N)$.

Recent measurement[28] of the average multiplicity of ω-mesons for $\bar{p}$Xe annihilation is in accordance with the prediction of the INC-model[45] (see Figure 22).

The inclusive spectra of η- and ω-mesons serve as another source of information on their interaction with nuclei. Figure 23 shows both these spectra and the spectra of η- and ω-mesons produced in the $\bar{p}$N-annihilation in a vacuum and in a nucleus (i.e., with allowance for the Fermi-motion of nucleons). It is seen that owing to the Fermi motion the high-energy part of the spectrum of η- and ω-mesons is enhanced. Moreover, this motion smears the peak associated with two-body annihilation channels. The comparison of inclusive spectra in the $\bar{p}$N- and the $\bar{p}$A-annihilation demonstrates that a considerable part of the spectrum disappears as a result of the interaction with nuclei, especially in the case of ω-mesons.

Production of heavy mesons affects other characteristics of the $\bar{p}$A-annihilation as well. Decay of mesonic resonances to pions changes the shape of pion spectrum, namely, it increases the yield of most slow pions (especially with the energy lower than 5 MeV) and that of most energetic ones.[45] Since the fraction of neutral modes of decay of η- and ω-mesons is large, the yield of events with the zero number of charged particles and the zero number of protons and evaporation particles increases.[45] Moreover, inclusion of mesonic resonances in the calculation scheme leads to an increase in the yield of nuclei with $\Delta A = 1$ (approximately by a factor of two for heavy T-nuclei).[45] Calculations carried out in accordance with the standard INC-model and the INCT-model lead to the same conclusions about the influence exerted by the effects of production of mesonic resonances on the characteristics of the $\bar{p}$A-annihilation. However, these effects are more pronounced in the INCT-model. We present here the results of the calculations carried out within the frame-

work of the standard INC-model in order to demonstrate the lower bound for the effects of mesonic resonances.

Emission of a pair of high-energy nucleons which are the products of the two-nucleon absorption of η- and ω-mesons is a specific signal of the interactions of heavy mesons with nuclear matter.[5] If the two-nucleon absorption of an η-meson is described by the same two-nucleon constants as the case of a pion (see Section IIA4, Chapter 2), the detection of a pair of nucleons with the energies $\epsilon_p \geqslant 250$ MeV and the angle of divergence between 180° and 150° may allow one to isolate this process against the background of products of other reactions (see Figure 24). If in addition to the reaction $\eta + NN \rightarrow NN$ we take into consideration the competing channel $\eta + NN \rightarrow \pi NN$ as well, then the peak in the angular correlation will be shifted from $\vartheta_{NN} \simeq 180°$ to $\vartheta_{NN} \simeq 150°$. The contribution of the two-nucleon absorption of an ω-meson to this correlation is negligibly small, because the ωd-cross-section is small (see Figure 21). We can suppress the contribution from the two-nucleon absorption of η-mesons and enhance the relative fraction of the two-nucleon absorption of ω-mesons by lifting the threshold of the nucleon detection up to $\epsilon_p \geqslant 350$ MEV. The shape of the correlation of products of the two-nucleon absorption of an ω-meson is also given in Figure 24. This correlation is narrower than in the case of an η-meson and has the peak at $\vartheta_{NN} \approx 180°$. The magnitude of the effect is small and, in addition to this, is comparable to the background from other channels of the reaction. Therefore, the detection of this effect involves enormous difficulties.

It should be noted that the background conditions are significantly better at least in the case of the two-nucleon absorption of an η-meson than in traditional investigations of the two-nucleon absorption of a pion. Experimental study of this process can provide valuable information not only on the interaction of η and ω-mesons with nucleons, but also on the structure of a nucleus. It is well known[56] that the momentum $p_N \simeq c\sqrt{m_\pi m_N}$ of nucleons produced in the two-nucleon absorption of a pion determines the specific distance of this process according to the relation $r^{\pi}_{abs} = h/p_N \approx 0.6$ fm. The size $r^{K}_{abs} = 0.5$ fm of the interaction region corresponds to the two-nucleon absorption of kaons.[57] The specific distance for the η-absorption is $r^{\eta}_{abs} \approx 0.3$ fm, and for the ω-absorption $r^{\omega}_{abs} \approx 0.2$ fm. The channel (Equation 6) of the two-nucleon absorption of an antiproton has the close value of the distance: $r^{\bar{p}}_{abs} \sim h/m_N \approx 0.2$ fm. Thus, we can study the short-range correlations in nuclei with the help of the two-nucleon absorption of heavy mesons.

We can gain a crucial new insight into the problem in question if we go over to the distances smaller than those characteristic of the two-nucleon absorption of pions and kaons. The quantity f_{NN} appearing in Equation 132, Chapter 2, of the quasideuteron model takes into account corrections caused by the fact that the process takes place on one of the NN-pairs in a nucleus rather than on a free deuteron. These corrections are associated 1) with a larger number of NN-pairs involved in the reaction, and 2) with different values of the probability to find two nucleons in the deuteron $w_d(r_{abs}) \sim |\psi_d(r_{abs})|^2$ and in the nucleus $w_A(r_{abs}) \sim |\psi_{NN}(r_{abs})|^2$ at the specific distance determined by the momentum transferred to the products of absorption. At small distances $r_{abs} \sim 0.2$-0.3 fm, quark effects can play a

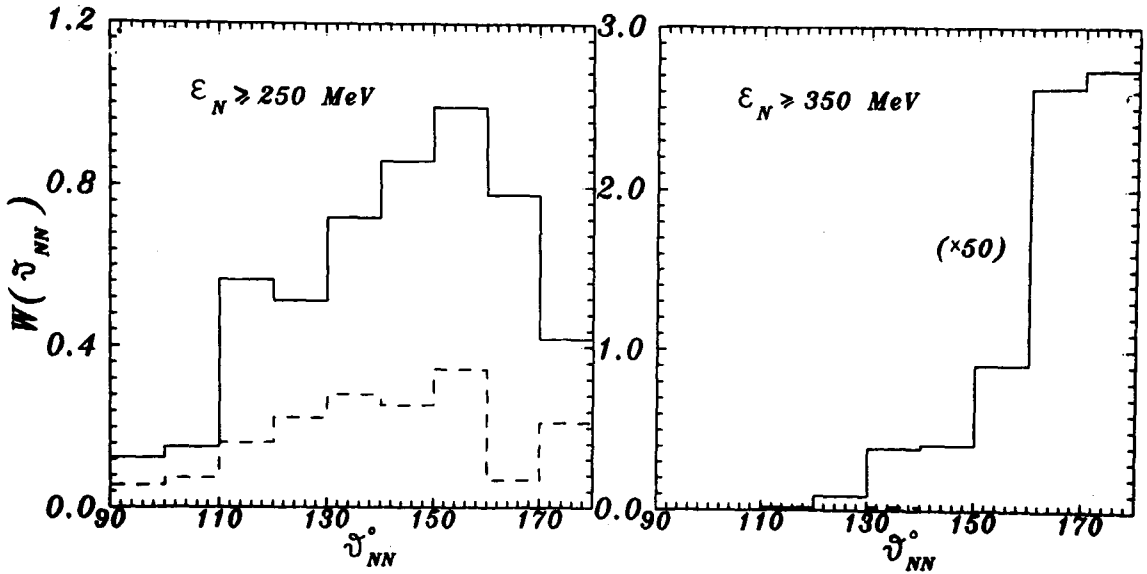

FIGURE 24. The left-hand figure shows angular correlations between two nucleons (measured in $N_{NN}/10^3\bar{p}\cdot sr$) produced upon two-nucleon absorption of η, and the right-hand figure shows the same correlations for two-nucleon absorption of ω-mesons in $\bar{p}C$-annihilation. The dashed line shows the contribution from background processes in the $\bar{p}C$-annihilation.

significant role in the wave functions ψ_d and ψ_{NN}.[58] It seems, hence, more correct to deem that a heavy meson is absorbed by a six-quark configuration rather than by two nucleons. This can lead to the suppression of the reaction of the two-nucleon absorption of η- and ω-mesons by nuclei and to the values of quasideuteron constants, which differ considerably from those characteristics of the case of the two-nucleon absorption of pions. It is possible that such a suppression has been discovered recently[59] where the first attempt has been made to observe the two-nucleon absorption of η and ω-mesons in the $\bar{p}$A-annihilation.

E. NEAR THRESHOLD PRODUCTION OF η- AND ω-MESONS BY PROTONS AND PIONS ON NUCLEI

Recently, interest was aroused in the study of production of heavy mesons on nuclei by different particles (protons, pions, photons, and heavy ions) near the threshold.[50,54,60-63] This allows one to investigate the same range of low energies of mesons ($\sim$ 10-100 MeV) as in the case of the $\bar{p}$A-annihilation considered in the previous section. Among heavy mesons, the η- and ω-mesons attracted maximum attention. This is associated not only with their long lifetime, but also with their microstructure. The η-meson belongs to the pseudoscalar meson octet and has the same values of the spin, parity, and C-parity as the π^0-meson, which is a member of the same octet. However, the η-meson has the value of the isotopic spin which differs from that of the π^0-meson and different quark composition, namely, in addition to the $\bar{u}u$ and the $\bar{d}d$ component, it contains the $\bar{s}s$ additive as well. The selective excitation of certain N* resonances (it has already been noted that in the vicinity of the threshold it is N*(1535)S_{11}-resonance) in the ηN-interaction is another appealing feature of η-mesons. This offers the possibility of studying the behavior of the N*(1535)-resonance in nuclear matter in addition to the study of the Δ(1232) dynamics in the πA-interaction. Finally, as opposed to the πN-interaction, the ηN-interaction is attractive and can be strong enough to form bound states of an η-meson in nuclei.[50] The ω-meson belongs to the nonet of vector mesons, the difference between ω-meson and another member of this nonet, the ρ^0-meson, being approximately the same as between the η- and the π^0- meson. However, the contribution of the $\bar{s}s$-component is small for an ω-meson.

First experiments concerned with the production of an η-mesons on nuclei by protons[61] and pions[60] near the threshold have already been carried out. To analyze these data we have included the procedure of the calculation of elementary processes of the η and the ω production on the intranuclear nucleons by pions and protons in the domain of the threshold energies in the INC-model with mesonic resonances outlined above.[64,65] We have taken into account the following elementary processes of production of η and ω mesons by protons:

$$pp \rightarrow pp\eta,\ pn \rightarrow pn\eta,\ pn \rightarrow d\eta\ , \tag{14}$$

$$pp \rightarrow pp\omega,\ pn \rightarrow pn\omega,\ pn \rightarrow d\omega\ , \tag{15}$$

and by pions

$$\pi^- p \rightarrow n\eta,\ \pi^+ n \rightarrow p\eta\ , \tag{16}$$

$$\pi^- p \rightarrow n\omega,\ \pi^+ n \rightarrow p\omega\ . \tag{17}$$

To calculate the cross-sections of the $pp \rightarrow pp\eta$ and the $pp \rightarrow pp\omega$ reaction and also the $\pi N \rightarrow \eta N$ and the $\pi N \rightarrow \omega N$ reaction (see Equations 16 and 17) we have used approximations of experimental data[51] obtained in Reference 65. To calculate the cross-sections of the $pn \rightarrow pn\eta$ reaction we have taken the results of the calculation[66] according to which, near the threshold, this cross-section exceeds the cross-section of the $pp \rightarrow pp\eta$ reaction by a factor of 3.5. It has already been noted that the results of calculations[52] were used to calculate the cross-section of the $pn \rightarrow d\eta$ reaction. The contribution of this subprocess is of paramount importance in the immediate vicinity of the threshold, because the subprocesses with two and three particles in the final state have different energy dependences of the cross section.* It has been noted that the cross-section of the $pn \rightarrow d\omega$ reaction is small, and the contribution of this subprocess is neglected in the analysis of production of ω-mesons on nuclei.

The momenta of products of the three-particle reactions of Equations 14 and 15 were calculated from the phase volume, and angular distributions of both three- and two-particle reactions (Equations 14-17) were assumed to be isotropic in the c.m.s. Since the cross-sections of production of η- and ω-mesons form a very small part of the total cross-section of the reaction, the calculations using the INC-model were carried out by the method of weight functions (as it was described in Chapter 4).

Figure 25 shows the results of the calculations[64,65] of the energy dependence of the cross-section for production of η-mesons on the ^{12}C nucleus carried out within the framework of the INC-model and their comparison with experimental data.[61] It is seen from this figure that the production of η-mesons on nuclei is noticeable for the initial energies ϵ_p of protons which are significantly smaller than the threshold of the η-production on a free nucleon. This fact is caused by the Fermi motion of intranuclear nucleons. In this energy range, the production cross-section σ_η increases dramatically with ϵ_p. It is interesting that the $NN \rightarrow NN\eta$ reaction is not the principal process here. The production of η-mesons by secondary pions $\pi N \rightarrow \eta N$ plays the leading role, whereas the contribution from the $pn \rightarrow d\eta$ subprocess is comparable with that from the $NN \rightarrow NN\eta$ reaction. Figure 26 shows the dependence of the cross-section σ_η on the mass number A of a T-nucleus. The variation of the value of the cross-section $\sigma_{\eta N}$ of the ηN-interaction changes not only the magnitude of the σ_η, but also the slope of the function σ_η (A) depicted at the logarithmic scale. The model describes first experimental data[61] on the production of η-mesons by protons on nuclei to a good accuracy, if the value of the cross-section $\sigma_{\eta N}$ used in the calculations is diminished by a factor of two in comparison with that depicted in Figure 21.

* Elementary processes of such a form must be taken into consideration in the mechanism of the INC in the case of other nuclear reactions as well, for instance, in the production of pions by protons on nuclei (see Section IIIA, Chapter 4).

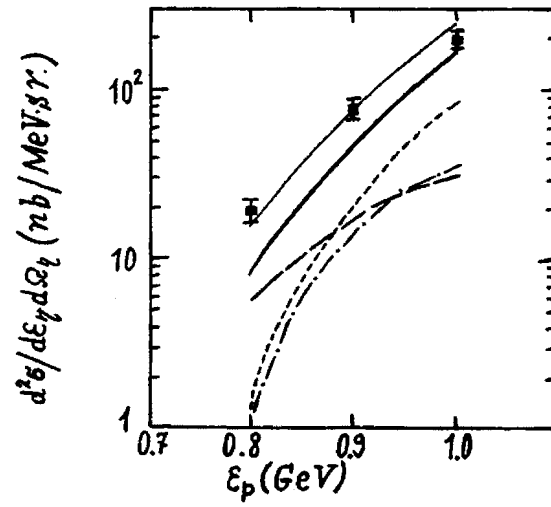

FIGURE 25. This illustrates the dependence of the double differential cross-section for η-production on a ^{12}C nucleus on the proton energy in the domain determined by the inequalities $30 \leqslant \epsilon_\eta \leqslant 100$ MeV (for the energy) and $0° \leqslant \vartheta_\eta \leqslant 40°$ (for the angle) in the l.s. The points are experimental data.[61] The curves are the results of the INC-model calculations.[64] The short and the long-dashed curve correspond to the production of η via NN → NNη and πN → ηN reaction, respectively. The dash-dotted curve shows the contribution from the pn → dη reaction. The ordinary cross-section $\sigma^{tot}_{\eta N}$ was used in these calculations. The heavy and the light solid curve represent the computational results for η-production via both NN → NNη, πN → ηN and pn → dη reactions with the "normal" cross section $\sigma_{\eta N}$ and $\sigma_{\eta N}/2$, respectively.

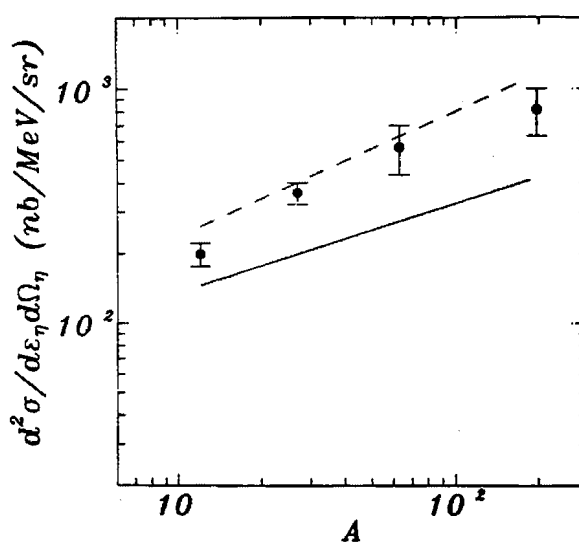

FIGURE 26. This shows the dependence of the double differential cross-section for η-production by 1 GeV protons on A in the domain determined by the inequalities $30 \leqslant \epsilon_\eta \leqslant 100$ MeV (for the energy) and $0° \leqslant \vartheta_\eta \leqslant 40°$ (for the angle) in the l.s. The points correspond to experimental data.[61] The solid and the dashed curve show the results of INC-model calculations[65] with the cross-section $\sigma_{\eta N}$ having the "normal" value and the value reduced by a factor of two, respectively.

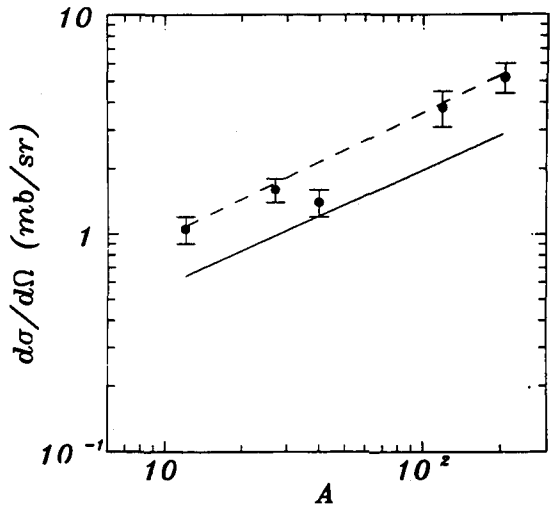

FIGURE 27. This illustrates the dependence of the cross-section for the η-production by 680 MeV/c pions on A for the values of the angles ϑ_η lying in the interval $0° \leq \vartheta_\eta \leq 15°$ in the l.s. The points correspond to experimental data.[60] The solid and the dashed curve show the results of INC-model calculations[65] with the cross-section $\sigma_{\eta N}$ having the "normal" value and the value reduced by a factor of two, respectively.

An analysis of proton data turns out to be more complicated, since the production of η-mesons by secondary pions plays a significant role in this case, and there are no reliable data on the cross-sections of the pn → pnη and the pn → dη subprocess nowadays. The production of η-mesons by pions on nuclei is a more simple and lucid case with a smaller number of subprocesses and a simple two-body kinematics. Figure 27 shows the A-dependence of the cross-section of production of η-mesons by pions. The calculation[65] carried out under the assumption that the cross-section $\sigma_{\eta N}$ is a half its predicted value[50] describes better the pion data[60] as well. The conclusion that the ηN-cross-section may be twofold smaller than the surmised value can cast doubt on the prediction[50] of the existence of bound states of η-mesons in nuclei. The calculations have demonstrated[65] that the energy spectrum of η-mesons produced is sensitive to the depth the potential well V_η. The best description of the experimental spectrum is obtained from the calculation with $V_\eta = -50$ MeV (see Figure 28).

Thus the INC-model with mesonic resonances describes to a good accuracy first experimental data on the production of η-mesons on nuclei by protons and pions. This gives reason enough to apply the model to prediction of basic characteristics of production of ω-mesons by protons and pions[65] on nuclei. There are no data for them up to now. One such characteristic, the energy dependence of the cross-section for production of ω-mesons by protons and pions on the ^{12}C-nucleus, is shown in Figure 29. The production of ω-mesons by secondary pions plays the principal role in energy range below the threshold. A sufficiently large value of

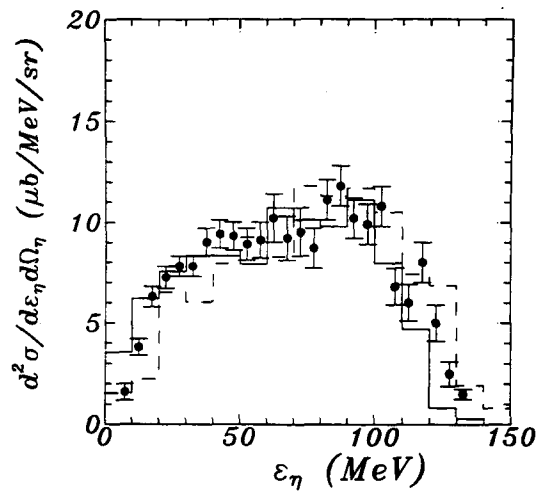

FIGURE 28. The energy spectrum is shown here for η-mesons produced by 680 MeV/*c* pions on ^{12}C nucleus for the values of the angle lying in the interval $0° \leq \vartheta_\eta \leq 15°$ in the l.s. The points correspond to experimental data.[60] The solid and the dashed curves show the results of INC-model calculations[65] with the potential well depth $V_\eta = -50$ MeV and $V_\eta = 0$, respectively (the calculation correspond to the $\sigma_{\eta N}$ reduced by a factor of two, as compared to its normal value).

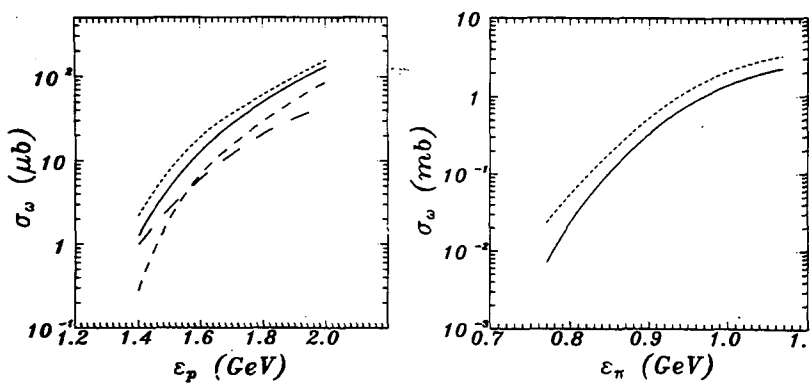

FIGURE 29. The energy dependence of the cross-section for the ω-production on a ^{12}C nucleus by protons is shown in the left-hand figure, and by pions in the right-hand figure. In the left-hand figure, the solid curve shows the total cross-section for the ω-production, the short-dashed and the long-dashed curves show the contribution of $NN \rightarrow NN\omega$ and $\pi N \rightarrow \omega N$ subprocess to this cross-section, respectively (the calculation with the "normal" value of the cross-section $\sigma_{\omega N}0$) and the dotted curve corresponds to the total cross-section for the ω-production calculated with the value of the cross-section $\sigma_{\omega N}$ reduced by a factor of two, as compared to its normal value. In the right-hand figure, the solid and the dotted curve show the results of INC-model calculations[65] with the cross-section $\sigma_{\omega N}$ having the "normal" value and the value reduced by a factor of two, respectively.

the production cross-section σ_ω($\sim$ 100μb for $\epsilon_p \approx$ 2 GeV and $\sim$ 1 mb for $\epsilon_\pi \approx$ 1 GeV) makes it quite possible to carry out experiments on modern accelerators having proton and pion beams of required energy.

Here we have only touched upon certain new possibilities concerned with the study of the mπA-interaction and with the elaboration of the OC-model, which are offered owing to the production of high-quality antiproton beams on the set-up LEAR in CERN. (In particular, we have omitted the application of this model to the study of nuclear aspects of the problem of registration of n-$\bar{n}$ oscillations in vacuum[7] and in nuclear matter[67] for reasons of space).

IV. CONCLUSIONS

An antiproton, being absorbed by a nucleus brings with it the energy ($\lesssim 2m_N$) which is significantly larger than the energy transferred to a nucleus by a pion. This offers broad possibilities for the study of highly-excited nuclei in a deep inelastic $\bar{p}$A-interaction. In the present chapter, we have considered the case of absorption of an antiproton by a nucleus from the states of the $\bar{p}$-atom. A small velocity of a pion source (the $\bar{p}$N-annihilation), a large number and isotropic emission of pions produced in the primary act of absorption, and the fact that their energy is close to the energy of the (3,3)-resonance especially favor the formation of thermalized hot nuclei and offer new possibilities for the study of the mπA-interaction. The generalization of the OC-model to the case of the annihilation of slow antinucleons on nuclei allows one to determine basic properties of the incoherent mπA-interaction, which leads, in particular, to the formation of highly-excited ($2m_\pi < E^* < m_N$) nuclei with large values of momentum ($p_r > 0.7$ GeV/c) and angular momentum ($I > 20$). Therefore, in deep inelastic $\bar{p}$A-reaction, we are to expect the population of high-spin isomers and strong spallation ($\Delta A \sim$ 50-100) of a T-nucleus. In addition to this, the manifestation of the explosive decay of hot ($E^* \sim m_N$) nuclei in the form of events of the complete breakup or multifragmentation of a T-nucleus is also a noticeable probability. This phenomenon will be discussed in detail in Chapter 7.

In the process of nuclear absorption of slow antiprotons, one can also study the interaction of heavy mesons (η, ω, etc.) produced in the $\bar{p}$N-annihilation with nuclei in the domain of low meson energy ($\sim$ 10-100 MeV). This kind of interaction is scantily studied. The investigation of this interaction complements the reactions of production of heavy mesons by protons and pions on nuclei in the vicinity of the threshold. Such a study is a natural extension of the physics of meson-nucleus interaction to new objects which have unique microstructure (the presence of the $\bar{s}$s-component in the η-meson) and which produce new elementary excitations of nuclear matter (the excitation of the N*(1535) baryonic resonance by the η-meson).

The INC-model turned out to be rather effective for the description of the annihilation of intermediate-energy antinucleons on nuclei as well. A wide range of experimental data can be described under the assumption that an antinucleon annihilates on an intranuclear nucleon, if we take into consideration the effects characteristic of the processes which involve a large number of particles (the co-

alescence of nucleons and so on). On the other hand, the effects associated with the influence of nuclear medium on the mechanism of the $\bar{N}N$-annihilation can manifest themselves in the channels of the mesonless or the one-meson annihilation when high energy antinucleons annihilate in saturated nuclear matter (the direct interaction of the annihilation fireball with nuclear matter in which the stage of meson production is bypassed, the multinucleon annihilation, etc.).

REFERENCES

1. **Beusch, W.**, Production of particles and resonances on nuclei, in *Proc. IVth Int. Conf. on High Energy Phys. and Nucl. Structure, Report JINR* D1-6439, Dubna, 1972, 39.
2. **Nikolaev, N. N.**, Quark interactions in collisions of high energy leptons, photons and hadrons with atomic nuclei, *Usp. Fiz. Nauk*, 134, 369, 1981.
3. **Iljinov, A. S.**, Method of investigation of multipion-nucleus interactions [in Russian], *Soviet Phys. - Lebedev Inst. Reports*, N 8, 7, 1980.
4. **Seki, R. and Wiegand, C. E.**, Kaonic and other exotic atoms, *Annu. Rev. Nucl. Sci.*, 25, 241, 1975.
5. **Iljinov, A. S., Nazaruk, V. I., and Chigrinov, S. E.**, Nuclear absorption of stopped antiprotons: Multipion-nucleus interactions, *Nucl. Phys. A*, 382, 378, 1982.
6. **Leon, M. and Seki, R.**, Determination of the neutron halo from antiproton absorption, *Phys. Lett. B*, 48, 173, 1974.
7. **Iljinov, A. S., Matushko, V. L., and Chigrinov, S. E.**, Annihilation of slow antineutrons on nuclei: detection of neutron-antineutron oscillations, *Yad. Fiz.*, 36, 878, 1982.
8. **Armenteros, R. and French, B.**, Antinucleon-nucleon interactions, in *High Energy Physics*, Vol. 4., Burhop, E. H. S., Ed., Academic Press, New York, 1969, 237.
9. **Orfanidis, S. J. and Rittenberg, V.**, Nucleon-antinucleon annihilation into pions, *Nucl. Phys. B*, 59, 570, 1979.
10. **Chesquiere, C.**, An inclusive view on $\bar{p}p \rightarrow n\pi$ at rest, in *Proc. Symp. on Antinucleon-nucleon Interactions*, Preprint *CERN* 74-18. Geneva, 1974, 436.
11. **Mes, H. and Hebert, J.**, Monte Carlo calculation of antiprotons annihilating (at rest) in nuclei, using the isobar model, *Can. J. Phys.*, 49, 441, 1971.
12. **Bugg, W. M., Condo, G. T., Hart, E. L., et al.**, Evidence for a neutron halo in heavy nuclei from antiproton absorption, *Phys. Rev. Lett.*, 31, 475, 1973.
13. **Wade, M. and Lind, V. G.**, Ratio of antiproton annihilations on neutrons and protons in carbon for low-energy and stopped antiprotons, *Phys. Rev. D*, 14, 1182, 1976.
14. **Gerace, W. J., Sternheim, M. M., and Walker, J. F.**, Influence of meson charge exchange on $\bar{p}$-absorption evidence for neutron halo, *Phys. Rev. Lett.*, 33, 508, 1974.
15. **Golubeva, E. S., Iljinov, A. S., Botvina, A. S., and Sobolevsky, N. M.**, Inelastic interactions of intermediate-energy antinucleons with nuclei, *Nucl. Phys.A.*, 483, 539, 1988.
16. **Clover, M. R., DeVries, R. M., DiGiacomo, N. J., and Yariv, Y.**, Low energy antiproton-nucleus interactions, *Phys. Rev. C*, 26, 2138, 1982.
17. **Cahay, M., Cugnon, J., and Vandermeulen, J.**, Low-energy antiproton annihilation in nuclei, *Nucl. Phys. A*, 393, 237, 1983.
18. **Golubeva, E. S., Iljinov, A. S., Matushko, G. K., and Sobolevsky, N. M.**, Inelastic interactions of intermediate-energy antinucleons with nuclei [in Russian], Preprint *INR* P-0444, Moscow, 1985.

19. **Flaminio, V., Moorhead, W. G., Morrison, D. R. O., and Rivoire, N.**, Compilation of cross-sections III: p and $\bar{p}$ induced reactions, Report *CERN-HERA* 84-01, Geneva, 1984.
20. **Cugnon, J., Deneye, P., and Vandermeulen, J.**, Strangeness production of antiproton annihilation on nuclei, *Phys. Rev. C*, 41, R 1339, 1990.
21. **Iljinov, A. S. and Matushko, V. L.**, Two-nucleon absorption of antiprotons by complex nuclei [in Russian], *Soviet Phys.-Lebedev Inst. Reports*, N7, 7, 1983.
22. **Cugnon, J. and Vandermeulen, J.**, Possibility of unusual antiproton annihilation on nuclei, *Phys Lett. B*, 146, 16, 1984.
23. **Bhowmik, B. and Singh, S.**, Pion production in 5-GeV/c peripheral antiproton-emulsion interactions, *Phys. Rev. D*, 9, 63, 1974.
24. **Ward, D. R., Simmons, A. J., Ansorge, R. E., et al.**, Exclusive annihilation processes in 8.8 GeV $\bar{p}p$ interactions and comparisons between $\bar{p}p$ non-annihilations and pp interactions, *Nucl. Phys. B*, 172, 302, 1980.
25. **Di Giacomo, N. J.**, Strong attraction in low-energy antiproton-nucleus scattering, *J. Phys. G: Nucl. Phys.*, 7, L169, 1981.
26. **Ingemarsson, A.**, Optical model calculations for intermediate energy antiproton scattering, *Nucl. Phys. A*, 454, 475, 1986.
27. **Minor, E. D., Armstrong, T. A., Bishop, R., Harris, V., Lewis, R. A., and Smith, G. A.**, Charged pion spectra and energy transfer following antiproton annihilation at rest in carbon and uranium, *Z. Phys. A*, 336, 461, 1990.
28. **Dolgolenko, A., Barmin, V. V., Barylov, V. G., et al.**, Strangeness production in $\bar{p}$Xe annihilation at low energy, *Yad. Fiz.*, 55, 1253, 1992.
29. **Agnew, L. E., Elioff, T., Fowler, W. B., et al.**, Antiproton interactions in hydrogen and carbon below 200 MeV, *Phys. Rev.*, 118, 1371, 1960.
30. **Besch, H.-J., Eisermann, H. W., Nöldeke, G., et al.**, An experimental study of the antineutron-light nucleus annihilation at 1.4 GeV/c, *Z. Phys. A.*, 292, 197, 1979.
31. **McGaughey, P. L., Bol, K. D., Clover, M. R., et al.**, Dynamics of low-energy antiproton annihilation in nuclei as inferred from inclusive proton and pion measurements, *Phys. Rev. Lett.*, 56, 2156, 1986.
32. **Nakamura, K., Fujii, T., Kageyama, T., et al.**, Reaction $\bar{p} + {}^{12}C \rightarrow \bar{n} + X$ at 590 MeV/c, *Phys. Rev. C*, 31, 1853, 1985.
33. **Butler, S. T. and Pearson, C. A.**, Deuterons from high-energy proton bombardment of matter, *Phys. Rev.*, 129, 836, 1963.
34. **Toneev, V. D. and Gudima, K. K.**, Particle emission in light and heavy ion reactions, *Nucl. Phys. A*, 400, 173c, 1983.
35. **Markiel, W., Daniel, H., von Egidy, T., et al**, Emission of helium ions after antiproton annihilation in nuclei, *Nucl. Phys. A*, 485, 445, 1988.
36. **Hofmann, P., Hartmann, F. J., Daniel, H., et al.**, Charged-particle spectra from antiproton annihilation at rest in A = 12-238 nuclei, *Nucl. Phys. A*, 512, 669, 1990.
37. **Batusov, Yu. A., Bunyatov, S. A., Falomkin, I. V., et al.**, Antiproton annihilation on Ag/Br nuclei, *Europhys. Lett.*, 2, 115, 1986.
38. **Andreev, V. F., Baranov, P. S., Levonyan, S. V., et al.**, Multiplicities and correlations of secondary charged particles in the interactions of antineutrons and antideuterons with a momentum of 6.1 GeV/c per nucleon with tantalum nuclei, *Nuovo Cimento A*, 103, 1163, 1989.
39. **Batusov, Yu. A., Bunyatov, S. A., Falomkin, I. N., et al.**, Experimental study of the annihilation of antiprotons at rest in nuclear photoemulsion and the optical-cascade approach, *JINR Communications* E1-90-486, Dubna, 1990.
40. **Matveev, V., Barmin, V. V., Barylov, V. G., et al.**, Pion and proton multiplicity correlations in $\bar{p}$Xe annihilations at low energy, *Yad. Fiz.*, 55, 1268, 1992.
41. **Rafelski, J.**, $\bar{p}$ Annihilation on heavy nuclei, *Phys Lett. B*, 91, 281, 1980.
42. **Moser, E. F., Daniel, H., von Egidy, T., et al.**, Residual nuclei after antiproton annihilation in Mo and Ho, *Z. Phys. A*, 333, 89, 1989.
43. **Golubeva, Ye. S., Iljinov, A. S., and Mebel, M. V.**, Fission of nuclei as a result of stopped antiproton capture, *Nuovo Cimento A*, 103, 781, 1990.

44. **Barashenkov, V. S. and Zinovjev, G. M.,** Unitary-symmetrical theory of multiple particle production, *Fortshr. Phys.*, 16, 719, 1968.
45. **Golubeva, Ye. S., Iljinov, A. S., Krippa, B. V., and Pschenichnov, I. A.,** Effects of mesonic resonance production in annihilation of stopped antiprotons on nuclei, *Nucl. Phys. A*, 537, 393, 1992.
46. **Levman, G., Singer, R., and Fields, T.,** Study of prompt e^+e^-, η°, and ω° production in low-energy $\bar{p}p$-annihilations, *Phys. Rev. D*, 21, 1, 1980.
47. **Chiba, M., Fujitani, T., Iwahori, J., et al.,** η and η' production in $\bar{p}p$- annihilation at rest, Preprint *KEK* 89-6, 1989.
48. **Hamatsu, R., Ganguli, S. N., Malhotra, P. K., et al.,** Inclusive production of non-strange mesons in $\bar{p}p$ annihilations, *Nucl. Phys. B*, 123, 189, 1977.
49. **Adiels, L., Backenstoss, G., Bergström, I., et al.,** Experimental study of the inclusive η-spectrum from $\bar{p}p$ annihilations at rest in liquid hydrogen, Preprint *CERN-EP* /88-142. Geneva, 1988.
50. **Liu, L. C.,** Physics with eta mesons, in *Proc. 3rd Int. Symp. on πN and NN Phys.*, Lopatin, I. V., Ed., Vol. 1, Leningrad Nucl. Phys. Inst., 1989, 299.
51. **Flaminio, V., Moorhead, W. G., Morrison, D. R. O., and Rivoire, N.,** Compilation of cross-sections I: π^+ and π^- induced reactions, Report *CERN-HERA* 83-01, Geneva, 1983.
52. **Laget, J. M., Wellers, F., and Lecolley, J. F.,** η-meson production in nucleon-nucleon collisions, *Phys. Lett. B*, 257, 254, 1991.
53. **Nakai, K.,** Quasifree hadron productions in 3.9 -GeV/c nuclear reactions, Preprint *KEK* 88-21, 1988.
54. **Plouin, F.,** Neutral meson production at SATURNE, in *Proc. 17th INS Int. Symp. on Nucl. Phys. at Intermediate Energy*, Fukuda, T., Nagae, T., Eds., World Scientific, Singapore, 1989, 251.
55. **Cugnon, J., Deneye, P., and Vandermeulen, J.,** The role of mesonic resonances in antiproton annihilation on nuclei, *Phys. Rev. C*, 40, 1822, 1989.
56. **Hüfner, J.,** Pions interact with nuclei, *Phys. Rep. C*, 21, 1, 1975.
57. **Wilkinson, D. H.,** The structure of the nuclear surface, in *Proc. Rutherford Jubelee Int. Conf.*, Birks, J. B., Ed., Academic Press, New York, 1961, 339.
58. **Kurovsky, V. V., Neudatchin, V. G., and Tchuvilsky, Yu. M.,** Total weight of "quark droplets" in atomic nuclei, *Yad. Fiz.*, 36, 87, 1982.
59. **Riedlberger, J., Amsler, C., Doser, M., et al.,** Antiproton annihilation at rest in nitrogen and deuterium gas, *Phys. Rev. C*, 40, 2717, 1989.
60. **Peng, J. C.,** Experiments on eta meson production, in *Proc. 3rd Int. Symp. on πN and NN Phys.*, Lopatin, I. V., Ed., Vol. 1, Leningrad Nucl. Phys. Inst., 1989, 315.
61. **Chiavassa, E., Dellacasa, G., De Marco, N., et al.,** Subthreshold inclusive η production in nuclei by 1 GeV protons, *Z. Phys. A*, 342, 107, 1992.
62. **Cassing, W., Batko, G., Vetter, T., and Wolf, G.,** η production in proton-nucleus reactions, *Z. Phys. A*, 340, 51, 1991.
63. **Bennhold, C. and Tanabe, H.,** Coherent and incoherent η-photproduction from nuclei, *Nucl. Phys. A*, 530, 625, 1991.
64. **Golubeva, Ye. S., Iljinov, A. S., Paryev, E. Ya., and Pshenichnov, I. A.,** Subthreshold η production on nuclei by protons, *Z. Phys. A*, 345, 223, 1993.
65. **Golubeva, Ye. S., Iljinov, A. S., and Pshenichnov, I. A.,** Near threshold η and ω production on nuclei by protons and pions, Preprint *INR* 774, Moscow, 1992, *Nucl. Phys. A*, to be published.
66. **Vetter, T., Engel, A., Biro, T., and Mosel, U.,** η production in nucleon-nucleon collisions, *Phys. Lett. B*, 263, 153, 1991.
67. **Iljinov, A. S., Mebel, M. V., and Chigrinov, S. E.,** Properties of nuclear radioactivity induced by nucleon instability, *Yad. Fiz.*, 37, 18, 1983.

Taylor & Francis
Taylor & Francis Group
http://taylorandfrancis.com

Chapter 7

FISSION AND MULTIFRAGMENTATION OF NUCLEI BY INTERMEDIATE-ENERGY PARTICLES

In preceding chapters, we have dealt with deep inelastic channels of the interaction between an intermediate-energy particle and a nucleus. Hadrons, lightest nuclei, and R-nuclei with the mass close to the mass of a T-nucleus are formed in these channels. Here we shall consider the processes in which one more or several nuclear fragments are formed along with such products of an NR. Such NRs are divided into two types according to masses of fragments. Two fragments each with the mass approximately equal to a half the mass of a T-nucleus are formed in the reaction of fission, whereas the products of the fragmentation are comparatively light fragments with $Z \geqslant 3$.

I. FISSION OF NUCLEI

The way in which an intermediate-energy particle excites collective modes of nuclear motion and, in particular fission, is one of the least understood aspects of the theory of NRs. Nuclear fission is one of the most interesting and peculiar phenomena of physics of NRs. However, a detailed discussion of the entire range of problems associated with the fission of nuclei by intermediate-energy particles lies far beyond the scope of the present work. Therefore, we shall restrict our consideration to a more narrow issue, namely, we shall try to find out as to which possibilities for the elucidation of the mechanism of deep inelastic interaction and of properties of highly-excited nuclei produced as a result of it are offered through the study of fission. Our inquiry will repose upon modern concepts of nuclear fission formed in the studies with low energy particles and heavy ions.

Fission offers unique possibilities for the development of such investigations. The point is that other channels of deep inelastic interaction (spectra of secondary particles) are contributed by both the fast stage of the INC and the slow evaporation stage. Fission is accompanied by the rearrangement of the entire nuclear structure and a cardinal change in the shape of a nucleus and is, therefore, relatively slow. The time τ_f of the nuclear fission must exceed the time τ_{SC} required for the passage from the saddle point to the scission point. Theoretical estimations[2] give $\tau_{SC} \approx 3 \cdot 10^{-21}$s, whereas the experimental value[3] for $E^* \approx 100$ MeV is $\tau_{SC} \approx 10^{-20}$s. The time $\tau_{rf} \approx 10^{-20}$s of the so-called fast fission[4] which is treated as fission with zero fission barrier can serve as another milestone for the estimate of the minimum fission time. Thus, C-nuclei undergo fission at the evaporation stage of an NR, and it can be used as a clear indication of the establishment of thermodynamical equilibrium in R-nuclei. Studying the process of fission in hadron-nucleus interaction, we can obtain, in principle, reliable information on characteristics of C-nuclei produced as a result of it. Experimental solution to this problem is facilitated by the fact that two heavy fragments of fission are produced in this process (the measurement of characteristics of fragments in coincidence with one another allows

one to determine the momentum of a C-nucleus and its mass and charge number as well).

A. PROBABILITY OF FISSION OF NUCLEI BY INTERMEDIATE-ENERGY PARTICLES

Let us consider the fission cross-section σ_f, which is the simplest integral characteristic of fission, and the probability W_f of fission (fissility) connected with it directly through the relation $W_f = \sigma_f/\sigma_R$. Within the framework of the two-stage pattern of the process which forms the basis of the INC-model, we obtain the following expression for the fission cross section:[5]

$$\sigma_f = \sum_{A_c} \sum_{Z_c} \sum_{I} \int \sigma_{CN}\,(A_c,Z_c,E^*,I)\; w_f(A_c,Z_c,E^*,I)\; dE^* \; . \qquad (1)$$

Here σ_{CN} is the cross-section for production of a C-nucleus which has A_c nucleons, Z_c protons, the excitation energy lying in the interval from E^* to $E^* + dE^*$ and angular momentum I, and w_f is the probability that this nucleus undergoes fission during a transition from an excited state to the ground state. The fissility of a C-nucleus is determined by the expression[5]

$$w_f = \sum_{k} P_k(E^*)\; w_k^f(A_c,Z_c,E^*,I) \; ; \qquad (2)$$

where P_k is the probability that a C-nucleus emits k particles as it passes to the ground state, and w_k^f is the probability that, in this process, the fission takes place in any link of the evaporation chain:

$$w_k^f = 1 - \prod_{i=1}^{k} [1 - \Gamma_f(A_i,Z_i,E_i^*,I_i)/\Gamma_{tot}(A_i,Z_i,E_i^*,I_i)] \; . \qquad (3)$$

A specific feature of fission of nuclei by intermediate-energy particles is that, unlike the case of fission by low-energy nucleons and heavy ions, C-nuclei have a broad distribution over the nucleon composition A_c,Z_c, over the excitation energy E^*, and over the angular momentum I. It should be noted that the higher the incident energy, the broader this distribution is (see preceding chapters). Since the fissility of a C-nucleus depends dramatically on these characteristics, its calculations must take into consideration the "smearing" of a C-nucleus over A_c,Z_c,E^* and I. A correct averaging of the fissility in Equations 1-3 can be carried out numerically by the Monte Carlo method.[5,6] In this technique, the fast stage of the process is described on the basis of the INC-model (see Chapters 1 and 2) and the slow one on the basis of the evaporation model (see Chapter 3).

Figure 1 shows the comparison of the results of such a calculation[6] with experimental data on the energy dependence of the cross-section for fission of nuclei by protons. This dependence has different form for heavy T-nuclei which reveal a

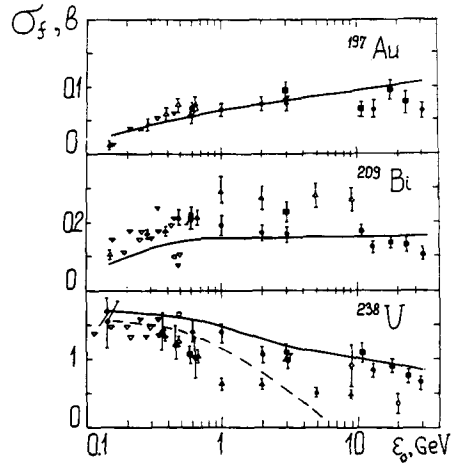

FIGURE 1. This graphs the energy dependence of the fission cross-sections for the nuclei of gold, bismuth, and uranium bombarded by protons of the energy ϵ_o. The solid and the dashed curves correspond to the calculations with and without trawling, respectively. The statistical error of the calculated results are about 7%. Marks, ■, ●, △, ○, ◆, ▽, ◇, and □ denote the experimental points.[6]

strong tendency to fission (^{238}U) and T-nuclei with low fissility (^{197}Au and ^{209}Bi), namely, σ_f decreases with increasing initial energy ϵ_p in the first case and increases in the second case. In the domain of not very high energies $\epsilon_p \lesssim 1$ GeV, the fissility of the ^{238}U remains approximately constant and close to unity, whereas the fissility of ^{197}Au and ^{209}Bi increases noticeably with ϵ_p. This is explained by the dependence of characteristics of the ensemble of C-nuclei on ϵ_p and by the distinction between the fission properties of preactinides and actinides. A small number of nucleons is knocked out of a T-nucleus for $\epsilon_p \sim 100$ MeV, and C-nuclei have the nucleonic composition and the fission properties which are almost the same as those of a T-nucleus. For preactinides, the ratio Γ_f/Γ_{tot} increases rapidly with the excitation energy E*, whereas for actinides it varies only slightly with increasing E* (see Section IVA, Chapter 3). Hence, the fissility of medium-weight nuclei increases rapidly with an increase in the initial energy ϵ_p leading to an increase in the excitation energy E* of C-nuclei. Under the same conditions the fissility of heavy (^{238}U) nuclei remains approximately constant. For $\epsilon_p \sim 1$ GeV, the spallation of a T-nucleus after the completion of INC becomes sufficiently strong. As a result, lighter C-nuclei are produced which have significantly larger fission barriers. The fissility of such nuclei is naturally smaller. Hence, an increase in the fission cross-section of medium weight nuclei (^{197}Au and ^{209}Bi) slows down, whereas the fission cross-section of heavy nuclei (^{238}U) comes to decrease faster with increasing ϵ_p.

Finally, for all T-nuclei, the fission cross-section becomes a slowly varying function of energy in the energy range $\epsilon_p \gtrsim 10$ GeV, since owing to the trawling effect (see Section IIB, Chapter 2, and Section IVA, Chapter 4), characteristics of the ensemble of C-nuclei hardly vary with primary energy. For example, for the interaction p + ^{238}U, the average excitation energy E* of C-nuclei is equal[6] to

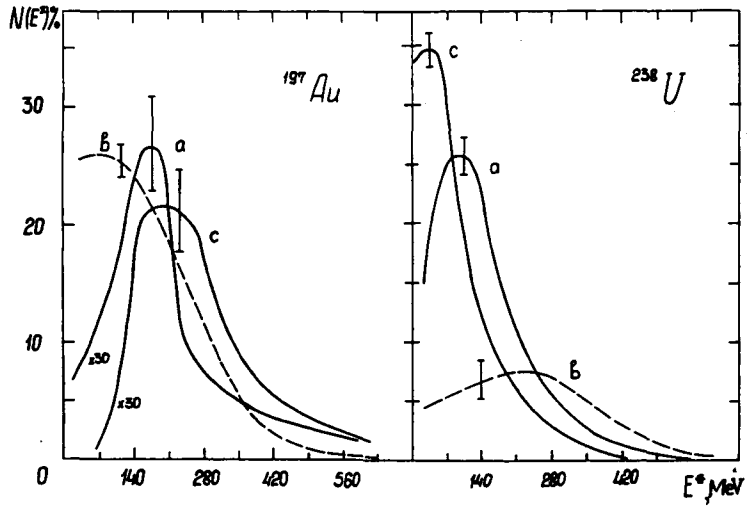

FIGURE 2. The excitation-energy distribution for R-nuclei generated in the 1 GeV proton bombardment of ^{197}Au and ^{238}U T-nuclei are shown as follows: (a) immediately after the INC for fission events, (b) immediately after the INC, but for events without fission, (c) just before fission.

365 ± 25 MeV and 376 ± 25 MeV for ϵ_p = 10 and 20 GeV, respectively. The calculation[6] carried out within the framework of the INCT-model describes the cross-section for nuclear fission in the domain of high energies to a good accuracy, whereas in the standard INC-model the spallation of a T-nucleus becomes so strong that the calculated fission cross-section σ_f decreases rapidly with ϵ_p (see Figure 1) and becomes smaller than the experimental value.

It should be noted that characteristics of C-nuclei which undergo fission differ from corresponding characteristics of those C-nuclei which avoid fission. Moreover, C-nuclei undergoing fission have different characteristics immediately after the completion of the INC and just before the fission. Figures 2 and 3 show the distributions of C-nuclei over the excitation energy and the mass number after the completion of the INC for C-nuclei undergoing fission ($W_c(E^*_{fc})$ and $W_c(A_{fc})$) and for C-nuclei which remove their excitation through emission of particles ($W_p(E^*_p)$ and $W_p(A_p)$). The same figures show the distributions for C-nuclei, which undergo fission, at the instant of time before fission ($W_f(E^*_f)$ and $W_f(A_f)$). The figures demonstrate that, before fission, a nucleus decreases, as a rule, its excitation energy, emitting particles. The smearing of nuclei over the nucleonic composition becomes even broader before fission than after the completion of the cascade (see Figure 3). Although T-nuclei which are heavier than gold have practically the same $\langle E^* \rangle$ of C-nuclei, the values of $\langle E^*_{fc} \rangle$ for different T-nuclei differ noticeably. For instance, at $\epsilon_p = 660$ MeV the calculation[6] gives $\langle E^*_{fc} \rangle$ = 203 ± 18 MeV for bismuth and $\langle E^*_{fc} \rangle$ = 138 ± 14 MeV for uranium, i.e., $\langle E^*_{fc} \rangle$ decreases as we go over to heavier T-nuclei. It is seen from Table 1 that for ^{238}U, experimental values of $\langle E^*_{fc} \rangle$ agree reasonably well with theoretical calculations.

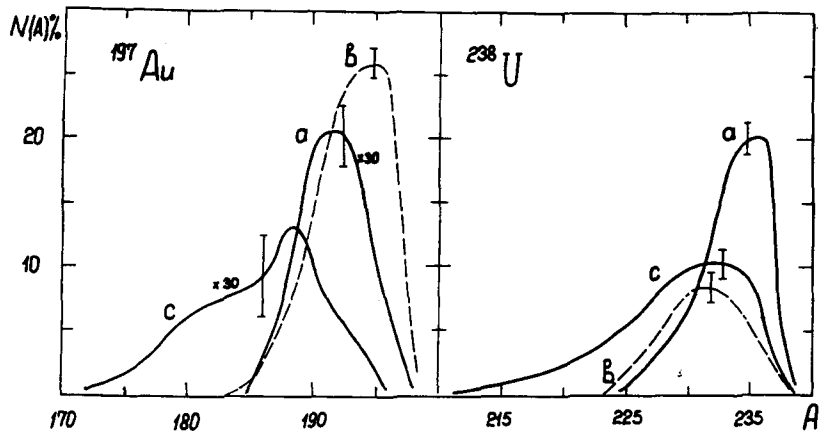

FIGURE 3. This is the distribution over the mass number of R-nuclei generated in the reactions $p+{}^{197}Au$ and $p+{}^{238}U$ at the energy $\epsilon_0 = 1$ GeV. Notation is the same as in Figure 2.

TABLE 1
Average Excitation Energy $\langle E^*_{fc} \rangle$ (Measured in MeV) of Nuclei Produced after the Completion of the INC p + ^{238}U

ϵ_p (MeV)	Experimental values	Theoretical values
140	80 ± 20^7	76 ± 7
350	140 ± 40^7	103 ± 10
460	135 ± 15^8	110 ± 11
	165 ± 45^7	
660	150^8	138 ± 14
	185 ± 60^7	

The isotope yield after evaporation from C-nuclei which avoid fission is directly connected with fissility, since it is determined (as well as W_f) by the competition between fission and evaporation. The probability that the fission takes place in no one of k links of the evaporation chain is given by the relation $w_k^{ev} = 1 - w_k^f$ (see Equation 3). This competition most strongly affects the yield of isotopes produced in the interaction of an incident particle with a heavy strongly fissile nucleus (e.g., ^{238}U). It is seen from Figure 4 that the cross-section for the production of neutron-deficient isotopes is reduced by several orders of magnitude, when fission is taken into account.

The yield of neutron-deficient isotopes from strongly fissile T-nuclei is very small, and the fissility W_f of weakly fissile T-nuclei with $A \sim 100$ is about $10^{-4} - 10^{-6}$. It is very difficult to calculate such small cross-sections by a direct Monte Carlo simulation. Here the method of weight functions is more effective. In this

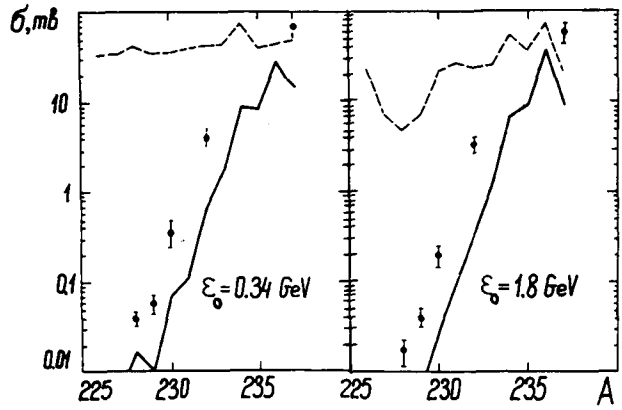

FIGURE 4. The yield of uranium isotopes in the reaction ^{238}U (p,pxn) $^{238-x}U$ at different energies ϵ_o of primary protons are shown. The solid and the dashed curves correspond to the calculations with and without regard for fission. Experimental points are taken from References 7 and 8.

technique, the probability that a C-nucleus undergoes fission (w_k^f) or avoids it (w_k^{ev}) in each evaporation chain after the completion of a given INC is calculated with the help of Equation 3. Then, while calculating the fissility W_f (the cross-section for production of a given isotope), one is to sum up all values of $w_k^f(w_k^{ev})$ and to average over all inelastic interactions (over the interactions in which a given isotope is produced).

Let us now consider the dependence of the probability of nuclear fission on A over a wide range of variation of A. Since such data were obtained with particles of not very high energies $\epsilon_p \leqslant 1$ GeV, their analysis[5] was carried out with the help of the standard INC-model. The parameters of the INC-model which describes the fast stage of the process were taken the same as in preceding chapters, whereas the data on the fissility of nuclei were reproduced by the variation of the parameters of the evaporation model which describes the slow stage of the process. Among them, the parameters of the level density of a nucleus with equilibrium deformation a_n and of a nucleus in the saddle point a_f are of paramount importance. Bearing in mind that, at high excitation energies $E^* > 30$ MeV, the shell effects in nuclei practically disappear (see Chapter 3), we have taken the asymptotic value $a_n \cong A/10$ MeV^{-1} for the parameter of the level density. The best agreement with experimental data has been achieved by varying the ratio a_f/a_n.

The height B_f of the fission barrier (see Chapter 3) is the principal factor that determines the fission width Γ_f and hence the fissility W_f. To calculate B_f, Myers and Swiatecki[11] have used the liquid drop model which reproduces the experimental values of preuranium nuclei to a sufficient accuracy, if the shell effect is taken into consideration (see Figure 5). This model also allows one to carry out extrapolation to the domain of nuclei for which such data are missing. The calculated values of B_f increase with decreasing mass number A, reach its maximum value $B_f^{max} \simeq 52$ MeV at $A \simeq 90$ and then decrease in the domain of light nuclei (see

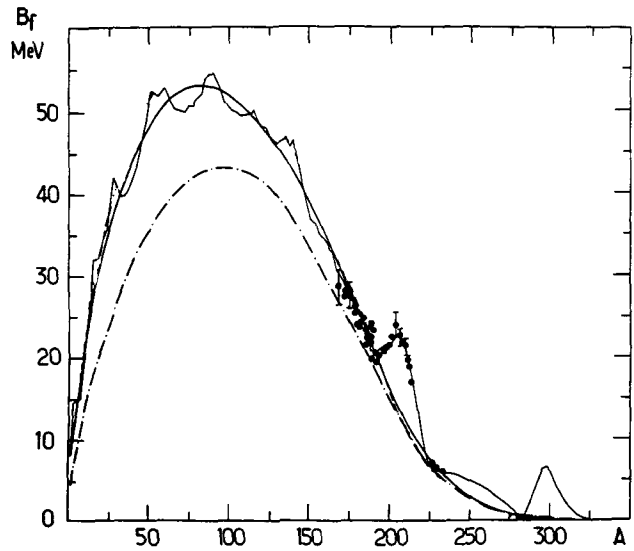

FIGURE 5. The height of fission barriers for nuclei along the β-stability line is shown here. Solid curves correspond to the calculation with parameters[11] with (the light curve) and without (the bold curve) regard for shell effects and the dash-dotted curve to the calculation with parameters taken from Reference 12. The points show experimental data.[6]

Figure 5). In accordance with such a behavior, the theoretical fissility W_f (as is seen from Figures 6 and 7) first decreases to a certain minimum value at A = 90, and then increases again in the domain of lighter nuclei.

Figures 6 and 7 show the experimental data on the fissility of nuclei by different particles as well. These data are divided into two groups. The first group comprises the reactions in which C-nuclei with not very high excitation energy (with the calculated $\langle E^* \rangle \sim 100$ MeV) are produced. They are the products of the interaction of protons of the energy 150-200 MeV and α-particles of the energy 167 MeV with nuclei and the products of nuclear absorption of stopped π^--mesons (Figure 5). The second group includes NRs initiated by protons with the energies 600-660 and 1000 MeV and γ-quanta with the energy 500-1000 MeV (Figure 6) in which the calculated values of $\langle E^* \rangle$ can be as large as 300 MeV. The calculations presented in Figures 6 and 7 are carried out for the following T-nuclei: ^{238}U, ^{235}U, ^{232}Th, ^{209}Bi, Pb, ^{197}Au, ^{184}W, ^{173}Yb, ^{159}Tb, ^{141}Pr, ^{122}Sb, ^{108}Ag, ^{96}Mo, ^{89}Y, ^{75}As, and ^{58}Ni. To make the figures more emphatic the values of W_f are connected by straight lines. The experimental fissility of heavy and medium-weight nuclei for which the height of the fission barrier is known can be described within the framework of the cascade-evaporation model, if for the ratio of the level density parameters a_f/a_n we shall take the value 1.05-1.10 which is close to the value obtained in experiments dealing with the fission of C-nuclei with $E^* \lesssim 100$ MeV produced in reactions with low-energy particles (see Section IVA, Chapter 3). For nuclei with

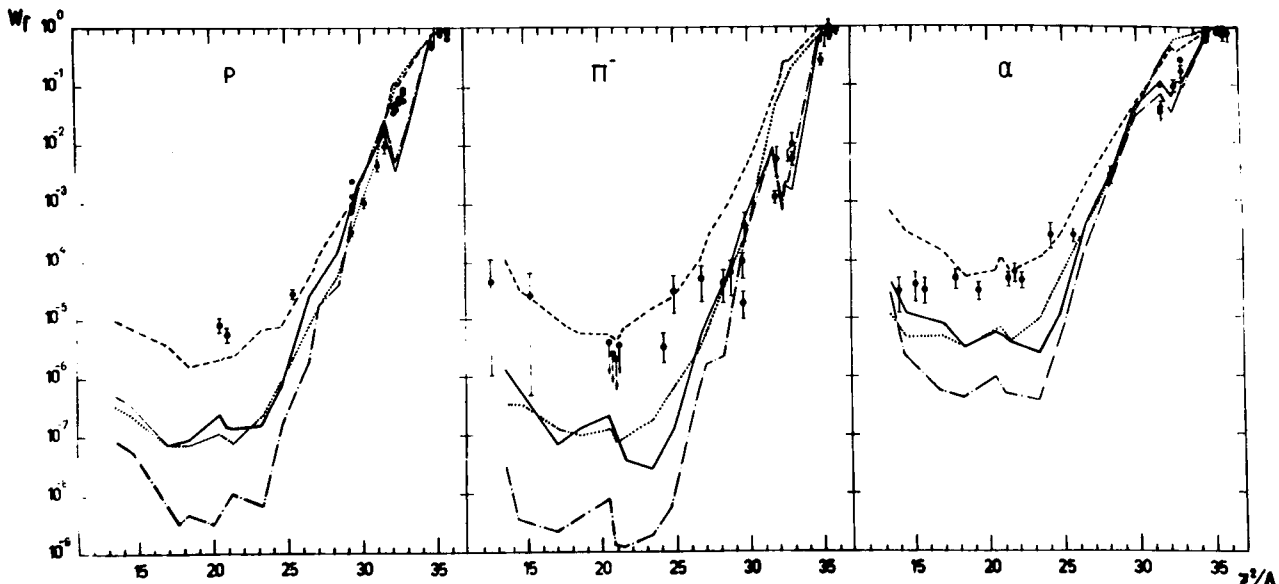

FIGURE 6. These portray the fissility W_f of nuclei by 150 MeV protons, stopped π^--mesons, and 167 MeV α-particles as a function of the quantity Z^2/A of a T-nucleus. The solid and the dotted curves correspond to the calculations[5] with and without regard for shell effects (a_f/a_n = 1.05 for protons, 1.10 for π^--mesons, and 1.08 for α-particles), and the dash-dotted curves to the calculation with allowance for pre-equilibrium particle emission (a_f/a_n = 1.17 for protons, 1.20 for π^--mesons, and 1.18 for α-particles). The fission barriers used in these calculations are obtained within the framework of the liquid-drop model.[11] The dashed curves correspond to the calculation with the same parameters as for the dotted curves, but with the fission barriers obtained with the help of the modified liquid-drop model.[12] The points show experimental data.[5]

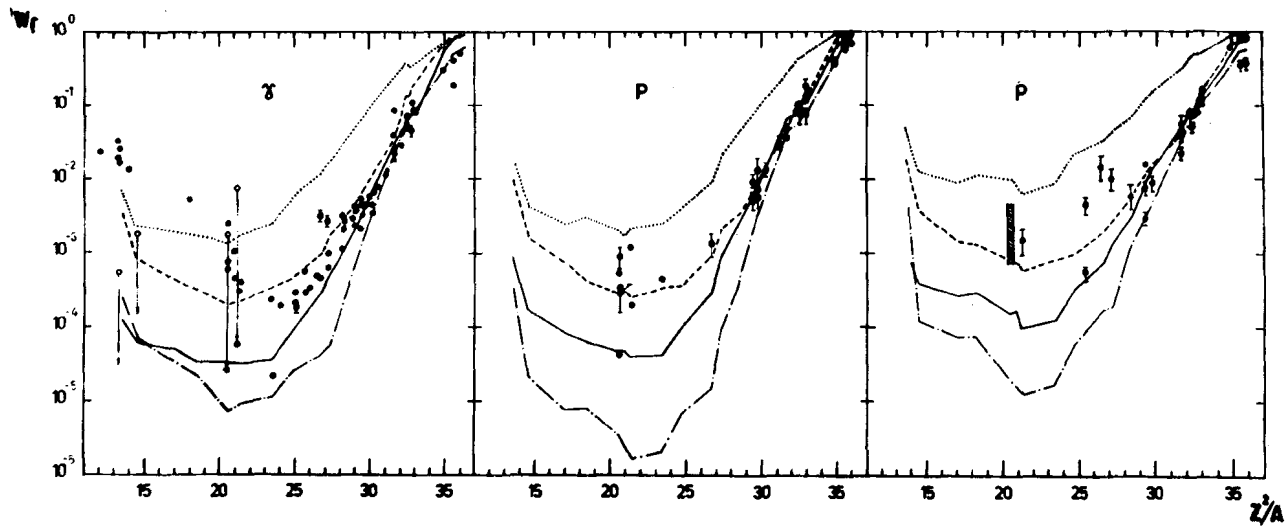

FIGURE 7. This presents the fissility W_f of nuclei by 600 MeV photons, 660 MeV protons, and 1000 MeV protons as a function of the quantity Z^2/A of a T-nucleus. The solid and the dotted curves correspond to the calculations[5] without and with regard for the dependence $B_f(E^*)$, respectively (a_f/a_n = 1.02 for γ-quanta, 1.01 for 660 MeV protons, and 1.00 for 1000 MeV protons) and the dash-dotted curves to the calculations with allowance for pre-equilibrium particle emission (a_f/a_n = 1.06 for γ-quanta, 1.05 for 660 MeV protons, and 1.04 for 1000 MeV protons). The fission barriers used in these calculations are obtained within the framework of the liquid-drop model.[11] The dashed curves correspond to the calculation with the same parameters as for solid curves, but with the fission barriers obtained with the help of the modified liquid-drop model.[12] All calculations depicted by different curves are carried out without regard for shell effects. The rest of notation is the same as in Figure 6.

$A \sim 100$, the calculated fissility turns out to be significantly smaller than experimental values (the reasons behind such a discrepancy will be discussed later).

Smearing of characteristics of C-nuclei leads to a significant broadening of the minimum in the dependence of W_f on Z^2/A. Obviously, this effect manifests itself most clearly in the case of high energies of incident particles, when a strong spallation of nuclei takes place during the fast stage of the process (see Figure 7). Hence, it is reasonable to begin the quest for an increase in the fissility of light nuclei predicted by the liquid drop model in reactions with particles of lower energies, where it is more pronounced. Even in this case, however, one is to expect a significant increase in W_f at rather small values of $Z^2/A \simeq 15$ (targets in the vicinity of Ni).

An increasing role of background processes at high initial energies makes it difficult to discover a rise in the fissility of medium-weight nuclei. As an example, we shall consider the data on the photofissility of nuclei in which an increase in W_f is observed for $Z^2/A < 22$ (see Figure 7). At first glance, these data contradict not only the calculations, but also experimental data for protons. However, a more rigorous selection of tracks of the fission fragments in solid state detectors aimed at excluding the contribution of fragmentation and recoil nuclei reduced the observed fissility of medium-weight nuclei approximately by a factor of 100 and eliminated this seeming contradiction (see Figure 7).

Let us now consider the effect of uncertainty in initial characteristics of C-nuclei introduced by the INC-model (largely because in this model the cascade is cut off by the parameter E_{cutoff}) on the fissility of nuclei. It has been mentioned above that there is an intermediate stage of the establishment of statistical equilibrium in a R-nucleus between the fast and the slow stage of the process. Emission of pre-equilibrium particles during this stage changes the excitation energy and the nucleonic composition of an initial C-nucleus.

A qualitative estimate for the magnitude of this effect can be obtained with the help of the exciton model for which the initial number of excitons is preset in the INC-model (see Section II, Chapter 2). Calculations[5] have demonstrated that pre-equilibrium emission can most dramatically affect the fissility of weakly fissile nuclei. The matter is that nuclei with $A \lesssim 150$ usually undergo fission at first steps of the evaporation cascade, when a C-nucleus still possesses a high excitation energy. Emission of a pre-equilibrium particle from an R-nucleus lowers considerably the excitation energy of a C-nucleus and, hence, reduces the probability of its fission. Calculations show that taking account of pre-equilibrium emission of particles can reduce the fissility by a factor of 10 to 100. To compensate for this decrease in W_f and to obtain an agreement with experimental data one has to take too large value of the ratio $a_f/a_n = 1.17$ for $\epsilon_p = 150$ MeV. However, even in this case, the results of the calculation are smaller than experimental values approximately by a factor of 10 to 100 in the domain of medium-weight nuclei (see Figure 6).

Thus, we can draw a conclusion from the comparison with experimental fissilities that the INC-model which assumes that emission of pre-equilibrium particles from R-nuclei can be neglected during the attainment of thermodynamical equilib-

rium in that it gives reasonable values for characteristics of C-nuclei. A quantitative estimate of the contribution coming from pre-equilibrium processes apparently calls for a more detailed analysis of the completion of the INC stage.

The study of the fissility of nuclei by intermediate-energy protons allows one to obtain information not only on the dissipation of energy, but also on the properties of highly-excited nuclei, in particular, on the manifestation of shell effects in them. Figure 6 shows the results of calculations of W_f carried out in two limiting cases: the shell effect is assumed either constant for any values of E* or completely absent. The "smearing" of C-nuclei over the nucleonic composition significantly weakens the influence exerted by these effects at high energies. They are most pronounced in the calculated fissilities of nuclei close to the double magic nucleus of ^{208}Pb for smaller initial energies. In this domain of nuclei, the calculations carried out within the framework of the liquid-drop model agree better with experimental data. This confirms the conclusion of Section IVA, Chapter 3, that the rapid damping of shell effects takes place as the nucleus is heated. On the other hand, a certain weakened influence of these effects on the fissility persists, since the distribution of C-nuclei over the excitation energy always contains small values of E* as well.

It has been noted in Chapter 3 that macroscopic "thermal" effects lead to the reduction of the height of the fission barrier at high values of the excitation energy (see Figure 3 in Chapter 3). Figure 7 shows the results of the calculations of the fissility which take into account the temperature dependence of the liquid-drop fission barrier. Taking account of a decrease in B_f with increasing E* leads to a rise in the fissility of nuclei with $A \simeq 100 \div 150$ which is especially noticeable for large incident energies. The comparison with experimental data is indicative of the fact that Equations 38-42, Chapter 3, seem to overestimate the role of thermal effects. However, we can draw more definite quantitative conclusions about the magnitude of thermal effects only on the basis of a more correct description of the thermalization of R-nuclei.

Finally, the study of the fissility of nuclei by intermediate-energy particles can provide information on the very process of fission, particularly on such an important characteristic of the process as B_f. For nuclei with $A \lesssim 100$, the quantities B_f are not studied in sufficient detail. On the other hand, the predictions of different versions of the liquid-drop model differ considerably from one another in this domain: in the standard model of Myers and Swiatecki[11] the maximum barrier B_f for the fission of nuclei along the β-stability line is equal to 53 MeV, in the liquid-drop model[13] $B_f^{max} \simeq 80$ MeV and in the modified model[12] taking into account the finite range of nuclear forces $B_f^{max} \simeq 43$ MeV (see Figure 5). It is seen from Figures 6 and 7 that fission barriers calculated on the basis of the modified liquid-drop model[12] eliminate the discrepancy between experimental and calculated fissilities of nuclei with $A \simeq 100$-150. Indications that the preference must be given precisely to this model were also obtained from the analysis of the cross-section for the fission of C-nuclei produced in reactions with heavy ions.[14]

Thus, the cascade-evaporation model gives a unified description of a large number of data on the fissility of nuclei by various intermediate-energy (p,π,γ, $\bar{p}$, and α) particles.[5,15] The assumption that a highly-excited thermalized R-nucleus

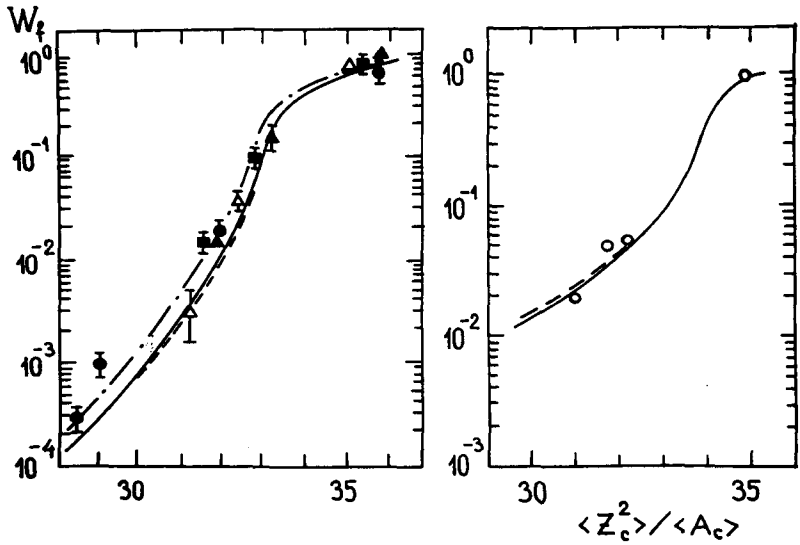

FIGURE 8. The values of fissility are shown for heavy nuclei excited by different probes, to be more specific by 200 MeV photons (■), 190 MeV protons (●), 80 MeVπ^+ (▲) and π^- (△)-mesons and stopped antiprotons (○).[16,17] The curves show the results of calculations carried out within the framework of the cascade-evaporation model. The left-hand figure corresponds to 200 MeV photons (the dash-dotted line), 190 MeV protons (the solid line), and 80 MeV π-mesons (the dashed line); and the right-hand figure to stopped antiprotons (the solid line), and 1.1 GeV photons (the dashed line).

whose decay does not depend on the manner of its production is formed in a deep inelastic interaction is one of the fundamental tenets of the model (see Chapters 1 and 2). It follows that the fission of nuclei in NRs initiated by different particles proceeds in the same way, if the ensembles of C-nuclei in different reactions do not differ from one another. To determine initial energies of different particles giving similar ensembles of C-nuclei the authors of Reference 16 have used the INC-model. The calculations have demonstrated that in the interactions of photons of the energy 200 MeV, protons of the energy 190 MeV, and pions of the energy 80 MeV with heavy nuclei, the distributions of C-nuclei over the excitation energy E*, the angular momentum I and over the losses of the mass ΔA and the charge ΔZ are close to one another.

Figure 8 shows the comparison of the calculated and experimental fissilities for these reactions. (The parameter $\langle Z_c^2 \rangle / \langle A_c \rangle$ averaged over the ensemble of C-nuclei is plotted on the axis of abscissae in order to take into account the fact that, for the same losses of mass ΔA and charge ΔZ, the mass A_c and the charges Z_c of C-nuclei produced in these reactions differ slightly from one another, because initial systems are different.) It is seen from Figure 8 that, for these NRs, the fissilities are approximately the same and do not depend on which probe was used to excite nuclei. (In Figure 8 the curve for the photofission lies slightly higher because of the fact that the average excitation energy $\langle E^* \rangle = 81$ MeV is somewhat

higher in this reaction than $\langle E^* \rangle = 70$ MeV for protons and pions.) In the domain of high-energy fission, similar ensembles of C-nuclei are formed in the interaction of photons of the energy 1.1 GeV and stopped antiprotons with heavy nuclei. The conclusion about the universal nature of fission of nuclei by different particles remains in force in this case as well (see Figure 8).

B. MASS-ENERGY DISTRIBUTION OF FISSION FRAGMENTS

In reactions with intermediate-energy particles, one can study the fission of nuclei for very high excitation energies. However, one has to encounter here a serious problem, namely, the distribution of C-nuclei over E^* becomes very broad, and it is very difficult to extract the actual dependence of the characteristics of the process on E^* from the observed fission properties, because the latter are the characteristics averaged over this distribution.

To determine the excitation energies of C-nuclei one has to obtain information not only on such an integral characteristic as the total cross-section σ_f of fission, but also on as complete a set of quantities as possible that characterizes both the fragments of fission and particles which accompany it. It is of course very difficult to carry out an exclusive experiment in which the fragments of fission and charged and neutral particles (neutrons and γ-quanta) are registered in each fission event, and up to now none of such experiments has been performed in the domain of intermediate energies. However, even simple experiments aimed at the measurement of correlations between the fragments of fission allow us to make an advancement towards the solution of the problem of determining E^*, since the characteristics of both fragments contain valuable information on C-nuclei. The matter is that the subsequent evolution of the fission fragments (the evaporation of nucleons from them) changes only slightly the values of the mass A_f, of the charge Z_f, and of the momentum $\mathbf{p}_f$, which they have acquired at the instance of fission, because these fragments are rather heavy ($A_f \approx 100$). Hence, knowing the masses A_{f1} and A_{f2}, and the charges Z_{f1} and Z_{f2}, we can find the values of the mass $A_{cN} \approx A_{f1} + A_{f2}$ and of the charge $Z_{cN} \approx Z_{f1} + Z_{f2}$ of a C-nucleus before the fission to a sufficient accuracy. Further, since the fragments diverge in opposite directions in the reference frame co-moving with a C-nucleus, the measurement of the momenta of fragments $\mathbf{p}_{f1}$ and $\mathbf{p}_{f2}$ allows us to determine the value of the momentum $\mathbf{p}_r = \mathbf{p}_{f1} + \mathbf{p}_{f2}$ of a C-nucleus before fission.*

To analyze the results of such experiments, we need models that provide a possibility of calculating not only the fission probability, but also the mass-energy distribution of fragments of fission of excited C-nuclei. Let us consider the models used for the calculations of properties of fragments formed as a result of fission of a C-nucleus consisting of A_0 nucleons, Z_0 protons, and having the excitation energy E_0^*.

* In what follows, we shall omit the subscripts c and f appearing in the notation of parameters characterizing, respectively, C-nucleus and fission fragment in order to avoid too cumbersome expressions.

1. Diffusion Model of Formation of Distribution of Fragments Produced as a Result of Fission of Highly Excited C-Nuclei

At high excitations $E_0^* \gtrsim 50$ MeV (at temperatures $t > 1.5$ MeV), the potential energy surface of a nucleus has the liquid drop-shape because of the disappearance of shell effects (see Section IC, Chapter 3). Therefore, the nucleus undergoes predominantly symmetric fission.[2] To describe the properties of fragments of fission of hot nuclei, a number of theoretical approaches have been developed. Up until the late 1970s, there existed two principal approaches, e.g., the statistical[19] and the dynamic[20] model (for the references to other papers, in which these models are considered, see Reference 21). Neither of these models is capable of explaining the dependence of the dispersions of the mass and the energy distribution of fragments on the fissility parameter Z_0^2/A of a nucleus and on its excitation energy E_0^* as well (see Reference 22). Considerable advances in the comprehension of the formation of mass-energy distributions have been made within the framework of a new approach[21] to the description of fission dynamics. This approach is based on the multi-dimensional Fokker-Planck equation (FPE). A physically similar formulation of this approach, called the diffusion model,[21,23] can also be realized[24,25] on the basis of the system of stochastic Langevin equations, which is equivalent to the multi-dimensional FPE. The diffusion model makes it possible to trace the dynamics of the nuclear motion from the saddle point to the scission point. It also allows us to take into the account the dissipative nature of this motion and thermal and quantum fluctuations of collective nuclear variables. This model allows one to describe a wide range of data on the properties of fission fragements. In particular, to solve the problem associated with an increase in the dispersion of the mass and the energy distribution with increasing excitation energy and mass of a C-nucleus. This model can serve as a reliable basis for predicting the properties of nuclear fission in the scantily investigated domain of excitations $E_0^* > 100$ MeV. Therefore, we shall choose the diffusion model[21] to describe the high energy fission.

In this model, the fission process is described by a small number of collective degrees of freedom interacting with the "heat bath" formed by all other single-particle degrees of freedom. Then, the dynamics of collective variables becomes similar to the dynamics of the Brownian motion, since the change in the energy of the collective subsystem in one act of the interaction with the single-particle subsystem is insignificant. Dynamic evolution of collective degrees of freedom is described by the FPE for the distribution function $f(\mathbf{q},\mathbf{p},\tau)$, where $\mathbf{q} = (q_1, \ldots, q_n)$ are collective coordinates, $\mathbf{p} = (p_1, \ldots, p_n)$ momenta conjugate to them, and n is the number of degrees of freedom. In the most general case, when the tensors of the inertion (m_{ij}), friction (γ_{ij}), and diffusion (D_{ij}) coefficients are symmetrical nondiagonal matrices and depend (as well as the potential energy V) on the coordinates, the FPE has the form

$$\frac{\partial f}{\partial \tau} = -\mu_{ij} p_j \frac{\partial f}{\partial q_i} + \left[\frac{\partial V}{\partial q_i} + \frac{1}{2}\frac{\partial \mu_{jk}}{\partial q_i} p_j p_k\right]\frac{\partial f}{\partial p_i} + \gamma_{ij}\mu_{jk}\frac{\partial}{\partial p_i}(p_k f) + D_{ij}\frac{\partial^2 f}{\partial p_i \partial p_j} \tag{4}$$

where $\|\mu_{ij}\| = \|m_{ij}\|^{-1}$ and summation over the repeated subscripts, running the values from 1 to n, is implied.

While considering the dynamic evolution of a nucleus on the basis of the FPE, it is important to choose an appropriate parametrization of the shape of the nucleus undergoing fission. It should be emphasized that the choice of parametrization predetermines the number of collective degrees of freedom. On the one hand, a large number of collective coordinates make it possible to obtain a better approximation of shapes that can be taken by a nucleus on its way to scission point. On the other hand, an introduction of any new collective coordinate entails a dramatic increase in the volume of calculations. A well-known parametrization $\{c, h, \alpha\}$[26] is the optimum one. In this parametrization, c is the parameter of elongation of a nucleus, the parameter h describes a change in the thickness of the neck of the nucleus for its given elongation, and the parameter α of the mass asymmetry defines the ratio of the volumes (masses) of fragments that are to be formed.

Since the effects of pair correlations of nucleons and shell effects disappear at high excitation energies, the liquid-drop model, with parameters of Myers and Swiatecki, is used to calculate the potential energy of deformation of a nucleus undergoing fission.[11] The main features of the potential energy surface in the liquid-drop model is the presence of three conditional extrema,[2] i.e., the set of points (c, h) at which $\partial V/\partial h = 0$:

a. Minima corresponding to unified shapes of the nucleus (their set forms the bottom of the fission valley),
b. Minima corresponding to two separate fragments (the bottom of the fragment valley), and
c. Maxima between these valleys (the crest between the valleys).

At a certain value of the parameter c, the crest between two valleys disappears. This implies that, for such an elongation of the nucleus, only the configuration with two separate fragments can be stable.

If the fission dynamics is studied by using the parametrization $\{c, h, \alpha\}$, the parameter c of nuclear elongation naturally plays the role of the fission coordinate. Instead of the coordinate c, the coordinate r, i.e., a half distance between the center of mass of fragments which are to be formed, is often chosen[21,26] as the fission coordinate. The dependence of the potential energy on coordinates is approximated by the formula

$$V(x, h, \alpha) = V(x, h, \alpha = 0) + C_\alpha(x, h)\frac{\alpha^2}{2}, \tag{5}$$

where x stands for the fission coordidnate (c or r) and $C_\alpha(x, h) = [\partial^2 V/\partial\alpha^2]_{\alpha=0}$ is the local rigidity relative to the coordinate α of the mass asymmetry.

The tensors of the inertion and friction coefficients of the FPE are calculated in the hydrodynamical approximation by the Werner-Wheeler[27] technique. The hydrodynamic approximation for the tensor γ_{ij} of the friction coefficients corre-

sponds to the assumption that nuclear viscosity is of a two-body nature which is inherent in ordinary liquids. Under this assumption all components of γ_{ij} are in direct proportion to the coefficient ν_0 of two-body nuclear viscosity. The value $\nu_0 = (1.5 \pm 0.5)\cdot 10^{-23}\mathrm{MeV\cdot s\cdot fm^{-3}}$ was obtained from the analysis of experimental data.[21] It corresponds to a relatively small nuclear viscosity. In this case, the time τ_{sc} of the descent from the saddle point to the scission point is about $5\cdot 10^{-21}$ s. It has been pointed out in Reference 28 that, in principle, conditions ensuring the validity of the description of nuclear viscosity by the two-body mechanism can be violated. Nevertheless, the two-body mechanism was widely used for analysis of experimental data to great advantage for a long time.[27] As for one-body mechanism of nuclear viscosity, it yields overestimated values.[27] As a result, nuclei turn out to be superviscous and $\tau_{sc} \sim 10^{-19} - 10^{-20}$ s.

The components D_{ij} of the diffusion tensor (except for the mass asymmetric component $D_{\alpha\alpha}$) are calulated according to Einstein's formula

$$D_{ij} = \gamma_{ij} t \,, \tag{6}$$

where t is the temperature of internal degrees of freedom of the nucleus. The component $D_{\alpha\alpha}$ is calculated with allowance for quantum fluctuations, i.e.,

$$D_{\alpha\alpha} = \gamma_{\alpha\alpha} t^*_\alpha \,, \tag{7}$$

where t^*_α is the corresponding effective temperature defined by the well-known expression

$$t^*_\alpha = \frac{\hbar\omega_\alpha}{2} \operatorname{cth}\left[\frac{\hbar\omega_\alpha}{2t}\right] , \; \omega_\alpha = \sqrt{C_\alpha / m_{\alpha\alpha}} \,. \tag{8}$$

The FPE is solved by the method of global moment approximation in which the distribution function $f(\mathbf{q},\mathbf{p},\tau)$ is sought in the form of the Gaussian distribution. In this case, we must solve the system of ordinary differential equations for average values of collective variables and their dispersions which determine completely the function $f(\mathbf{q},\mathbf{p},\tau)$ at any instant of time (a detailed account of this method is given in Reference 21).

Since the formation of many observable distributions of fission fragments takes place at the stage of descent of a nucleus undergoing fission from the saddle point to the scission point, the initial distribution function is chosen in accordance with the Bohr-Wheeler concept of transient state (see Section III, Chapter 3) in the statistically equilibrium form. It is assumed that the distribution of collective variables is formed from the saddle point to a certain configuration for which an "instantaneous" rupture of the neck of the nucleus occurs without any change in its elongation. Instantaneousness implies that rupture occurs during a time interval which is significantly smaller than the time of descent from the saddle point. The line that singles out the set of the scission configurations on the (x,h)-plane is called the "scission line". It should be noted that, at present, there is no unambiguous

criterion determining the set of the scission configurations through which nuclei disintegrate into fragments. Here, the scission line is chosen from the condition of balance between the forces of Coulomb repulsion and nuclear attractions of fragments which are to be formed (for details see Reference 21).

Calculation of any observable characteristic Ω of fission fragments, which is a function of collective variables $\zeta = (x,h,\alpha,p_x,p_h,p_\alpha)$, is carried out in the following way

$$<\overline{\Omega}> = N^{-1} \int_0^\infty d\tau \int d\zeta \cdot f(\zeta,\tau) \cdot \Omega(\zeta) \cdot \delta[\phi(x,h)] \ , \tag{9}$$

where $N = \int_0^\infty d\tau \int d\zeta \cdot f(\zeta,\tau) \cdot \delta[\phi(x,h)]$.

Here angular brackets imply averaging over the ensemble and the bar over the corresponding quantities averaging over time. Occurrence of delta-functions in the integrands implies that only nuclei having scission configurations are taken into account. Integration over time is also carried out because different nuclei can take scission configurations at different instants.

Expressions (9) for the calculation of the moments of observable characteristics of fission can be also generalized[21] to cover the case of the calculation of distributions $W(\mathbf{\Omega})$ of observed fragments themselves. In particular, the diffusion model[21] makes it possible to calculate the two-dimensional mass-energy distribution $W(E_k,A)$. In this case $\mathbf{\Omega} = \{E,A_k\}$ and the variables E_k and A are functions of collective variables $\zeta = (r, h, \alpha, p_r, p_h, p_\alpha)$:

$$\begin{cases} E_k = V_c(r,h,\alpha) + E_{ps}(r,h,p_r,p_h) \\ A = A(r,h,\alpha) \end{cases} \tag{10}$$

Here, V_c is the energy of Coulomb repulsion of fragments and E_{ps} is prescission kinetic energy (the energy of collective motion along the principal fission coordinate).

Although the two-dimensional mass-energy distribution $W(E_k,A)$ is the most complete and apt way of representation, one-dimensional energy and mass distributions of fission fragments, characterized by average values and dispersions, are usually considered in experiments and theoretical analysis. The energy distribution obtained as a result of averaging the distribution $W(E_k,A)$ over the masses of fragments has the form of a curve with one peak and is usually approximated by a Gaussian, characterized by the average value $\overline{E}_k$ and dispersion σ_E^2, both in experimental and theoretical works. At sufficiently high excitation energies, the mass distribution, which is obtained in a similar way by averaging the distribution $W(E_k,A)$ over E_k, is also approximated by a Gaussian with the average value $\overline{A} = A_0/2$ and dispersion σ_A^2.

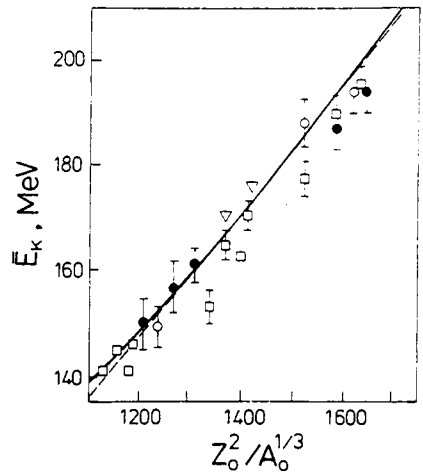

FIGURE 9. The average kinetic energy $\bar{E}_k$ of fragments of fission of C-nuclei as a function of the parameter $Z_0^2/A_0^{1/3}$: the solid line corresponds to the calculation carried out within the framework of the diffusion model[21] and the dashed line to the systematics of Reference 30. (For the information on experimental works, see Reference 21.)

Figures 9 through 11 show the first and second moments of the energy and the mass distributions, obtained by averaging the distribution $W(E_k,A)$ over A and E_k, respectively, as functions of the nucleonic composition and the excitation energy of a nucleus undergoing fission (or of the temperature t_{sd} of the nucleus in the saddle point, which corresponds to the internal excitation energy $E^*_{in} = E^* - B_f$). These characteristics are rather sensitive to the dynamics of descent of a nucleus undergoing fission from the saddle point to the scission point and to the shapes of scission configurations. In Figure 9, the data on the average kinetic energy $\bar{E}_k$ of fragments are compared with the results of calculations carried out within the framework of diffusion model.[21] These data are usually described by simple systematics[30] in which the dependence $\bar{E}_k$ on $(Z_0^2/A_0^{1/3})$ is linear. Although the calculation reveals a certain deviation from the linear dependence, it agrees well both with the experimental data and systematics of Reference 30.

Figures 10 and 11 show the dependence of the dispersions of the energy distribution σ_E^2 and the mass distribution σ_A^2 on the parameter Z_0^2/A_0 and on the temperature t_{sd}. A significant increase in σ_E^2 observed in experiments involving heavier nuclei is well described by the diffusion model. It should be noted that neither the static[19] nor dynamic model with zero viscosity[20] can yield even a qualitative description of the dependence of σ_E^2 on Z_0^2/A_0. The reasons behind a considerable increase in σ_E^2 with increasing parameter Z_0^2/A_0 are associated mainly with a change in the value of the dispersion σ_{vc}^2 of Coulomb energy as a result of the changeover from light to heavy fissile nuclei. A changeover to more elongated scission configurations and the preservation of "memory" of the system undergoing fission about its prehistory during the descent from the saddle point are the reasons for an increase in the dispersion of σ_A^2 with the increasing mass of a nucleus. The

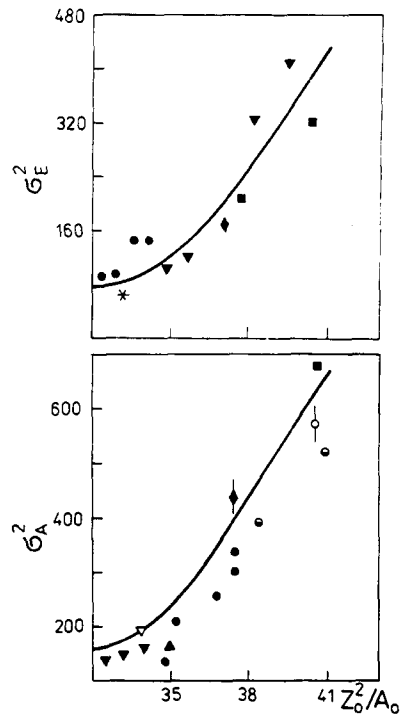

FIGURE 10. The dispersions of the averaged energy and the averaged mass distribution of fragments of fission of C-nuclei vs. the parameter Z_0^2/A_0: the solid line corresponds to the calculation carried out within the framework of the diffusion model[21] for t_{sd} = 1.5 MeV and experimental points correspond to the interval $1.5 \leq t_{sd} \leq 2.0$ MeV (information on experimental works can be found in the Reference 21).

dependence of σ_E^2 on the temperature t_{sd} also agrees reasonably well with experimental data (see Figure 11). For sufficiently large $t_{sc} \gtrsim 1.2$ MeV, the dependence of σ_E^2 on t_{sd} is close to the linear one, whereas deviations from it are observed for smaller values of t_{sd}. The dependence of σ_A^2 on t_{sd} behaves similarly (see Figure 11). The deviation from the linear dependence observed for temperatures $t_{sd} \leq 1.2$ MeV is a result of the quantum fluctuation of the mass-asymmetric mode. Their effect on the value of σ_A^2 becomes insignificant for $t_{sd} > 1.2$ MeV in comparison with the effect of thermal fluctuations of this mode (for a detailed discussion of these issues, see the Reference 21).

Correlation of parameters of the mass-energy distribution carries additional information on the dynamics of descent of a system undergoing fission and on the last stage that immediately precedes the scission of the nucleus into fragments. In particular, the dependence of the shape of the scission configuration on the ratio of masses of fragments is directly reflected in the correlation of these parameters. Figure 12 shows the comparison of correlations of $E_k(A)$ and $\sigma_E^2(A)$, calculated within the framework of the diffusion model, with the experimental date of Reference 31. In the first approximation, the dependence of $\bar{E}_k$ on A can be taken in the parabolic form:[31]

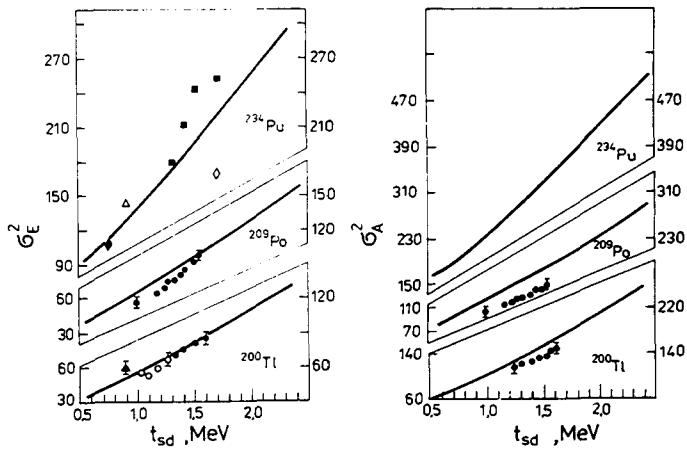

FIGURE 11. The dispersions of the averaged energy (on the left-hand side) and the averaged mass (on the right-hand side) distribution of fragments of fission of C-nuclei vs. the temperature of the nucleus at the saddle point. The notation is the same as in Figure 10.

$$\bar{E}_k(A) = \bar{E}_k(A_0/2)\cdot\left[1 - \epsilon\left(1 - \frac{2A}{A_0}\right)^2\right]. \tag{11}$$

On the whole, it reflects the dependence of the Coulomb repulsion energy and the distance between the centers of mass of fragments, which are to be formed, at the instant of scission on the mass of a fragment. The calculated dispersion $\sigma_E^2(A)$ is partically constant up to a certain value of the ratio A/A_0 of masses and decreases only slightly with a further increase in A. This correlation can be approximated by the expression

$$\sigma_E^2(A) = \begin{cases} \sigma_E^2(A_0/2) & \text{for } \gamma < \dfrac{A}{A_0} \le 0.5 \\ \sigma_E^2(A_0/2)\cdot\left[1 - \beta\left(1 - \dfrac{A}{\gamma A_0}\right)^2\right] & \text{for } \dfrac{A}{A_0} \le \gamma \end{cases} \tag{12}$$

The values of parameters β, γ and ϵ appearing in expressions 11 and 12 were found in Reference 32 by analyzing the results of the calculations carried out within the framework of the diffusion model in a broad interval of masses A_0, charges Z_0, and excitation energies E_0^*.

It is also possible to calculate the charge distribution of fragments by introducing the charge coordinate Δ, defined as a deviation of the charge of a fragment from the value that should be expected for the unvaried density of the charge distribution in the nucleus undergoing fission, into the FPE.[33] It is assumed in this method that dipole isovector vibrations play the principal role in the formation of this distribution

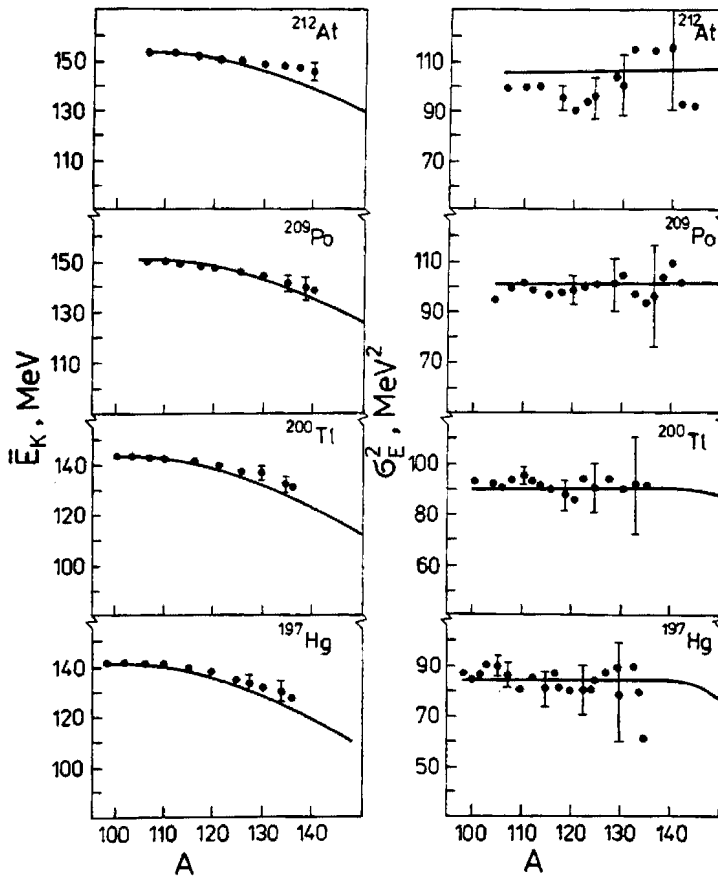

FIGURE 12. The moments of the mass-energy distribution of fragments of fission of C-nuclei calculated within the framework of the diffusion model[21] (solid lines) for the excitation energies corresponding to the experimental data of Reference 31 (points).

since they result in the most effective redistribution of charge between fragments and can be easily excited during the splitting of the nucleus. Then, the inertion parameter corresponding to the charge exchange between fragments is determined by the rigidity C_Δ relative to the charge variable and frequencies of dipole isovector vibrations, which are found in the hydrodynamic approximation. The charge distribution can be approximated to a good accuracy by a Gaussian with the average value $\bar{Z}_p$ and dispersion σ_z^2. The dispersion of the charge of a fragment is given by the relation[33]

$$\sigma_z^2 = t_\Delta^*/C_\Delta \,, \tag{13}$$

where t_Δ^* is the corresponding effective temperature.

It should be noted that parameters of the charge distribution, calculated according to the diffusion[21] and the statistical[19] model, coincide with each other to a

good accuracy. This is because the statistical equilibrium, with respect to the charge mode, has time to be established at any instant over almost the entire time interval of descent from the saddle point to the scission point, except for its last stage immediately preceding the rupture of the neck. Calculations[32] carried out within the framework of the diffusion model have shown that, in contrast to the dispersions σ_A^2 and σ_E^2, the charge dispersion σ_z^2 depends only slightly on the excitation energy E_0^*. The dependence of σ_z^2 on A is approximated to a good accuracy by the expression of the form 11 and the average value $\overline{Z}_p$ by the expression

$$\overline{Z}_p = \frac{A}{A_0} Z_0 + \Delta Z , \tag{14}$$

Theoretical values of parameters of the charge distribution of nuclei undergoing fission were obtained[32] for a broad interval of masses A_0, charges Z_0, and excitation energies E_0^*.

Fragments formed as a result of fission of a C-nucleus will also be excited. The total excitation energy U of both fragments at the instant of disintegration is determined by the difference between the total released energy $E_0^* + M_0 - M_1 - M_2$ and the potential energy, which is equal to the sum of energy of their Coulomb repulsion V_c and the deformation energies of fragments $D_1 + D_2$. Then, taking into account the fact that Coulomb energy of fragments is converted to their kinetic energy E_k we get

$$U = E_0^2 + M_0 - M_1 - M_2 - E_k - D_1 - D_2 . \tag{15}$$

Here M_0, M_1, and M_2 are the mass of the nucleus undergoing fission and the masses of the first and the second fragment, respectively. They can be calculated from the mass formulas of Reference 11 and the deformation energies D_1 and D_2 from the formulas of the liquid-drop model.

The value of the total excitation energy U of fragments determines the temperature of the nucleus as a whole at the instant immediately preceding the disintegration according to the relation $t = \sqrt{U/(a_1 + a_2)}$. After the disintegration, fragments have the same temperature t. Then, in view of the fact that the parameter a_i of the level density is proportional to the mass A_i of a fragment, the total excitation energy U is distributed between the fragments in direct proportion to their masses. Taking into account a subsequent increase in the excitation energy of a fragment by the value of its deformation energy, which is converted to the internal excitation energy, we finally get

$$U_i = U \frac{A_i}{A_0} + D_i . \tag{16}$$

In the case of high-energy fission, fragments derive large excitation energy which is sufficient not only for evaporating several nucleons or lightest nuclei, but also for their subsequent fission. It is necessary to take into account this effect in calculating the mass and the charge distribution of fission fragments.

2. Empirical Approximations of Fragment Distributions in the Case of Fission of C-Nuclei with Low Excitation

Let us now consider the case of fission of a nucleus having A_0 nucleons, Z_0 protons, and relatively low excitation energy $E_0^* \leq 50$ MeV (the corresponding temperature $t \leq 1.5$ MeV). In this range of energy E_0^*, the fission turns out to be a rather complicated process because it is strongly influenced by shell effects. In particular, there appear two (or even more) fission valleys on the potential energy surface as a result of these effects. This leads to the coexistence of the mode of symmetric fission and one or several modes of asymmetric fission (see Reference 31). Modern models predict and qualitatively explain the multimode nature of fission. Moreover, certain advances have also been made in the quantitative description of the mass-energy distribution of fragments of spontaneous fission and induced fission of nuclei with $E_0^* \leq B_n$ within the framework of these models. However, at present there are no theoretical models capable of taking consistently into account the manifestation of shell effects at larger excitation energies and their thermal damping in the mass-energy distribution of fission fragments. Therefore, we shall focus here on the empirical approximation of this distribution, obtained in Reference 32, on the basis of the analysis of experimental data for $E_0^* \leq 50$ MeV. Experimental data show (see, for example, Reference 1) that the mass distribution Y(A) consists of the symmetric and the asymmetric component:

$$Y(A) = (Y)_{sym}(A) + F \cdot Y_{asym}(A) , \tag{16}$$

Here $F(E_0^*, A_0, Z_0)$ is a function that determines the relative contribution of these fission modes. As follows from Reference 34, experimental data can be approximated to a rather good accuracy if one fission channel is taken into account in the symmetric mode

$$Y_{sym}(A) \sim \exp\left[-\frac{(A-A_s)^2}{2\sigma_{AS}^2}\right] \tag{17}$$

and two fission channels in the asymmetric mode

$$\begin{aligned} Y_{asym}(A) \sim \exp\left[-\frac{(A-A_2)^2}{2\sigma_{A2}^2}\right] + \exp\left[-\frac{\{A-(A_0-A_2)\}^2}{2\sigma_{A2}^2}\right] + \\ C_{as}\left\{\exp\left[-\frac{(A-A_1)^2}{2\sigma_{A1}^2}\right] + \exp\left[-\frac{\{A-(A_0-A_1)\}^2}{2\sigma_{A1}^2}\right]\right\} \end{aligned} \tag{18}$$

Here $A_s = A_0/2$, A_1, and A_2 are the average values of the corresponding Gaussians; σ_{AS}^2, σ_{A1}^2, and σ_{A2}^2 are their dispersions; and the quantity C_{as} prescribes the relation between the two modes of asymmetric fission. All nuclei undergoing asymmetric fission have approximately the same values of $A_1 \simeq 134$ and $A_2 \simeq 141$ (see References 32 and 34). This is indicative of the universal nature of the modes of asymmetric fission. It is worthy of note that theory[35] also confirms the conclusion

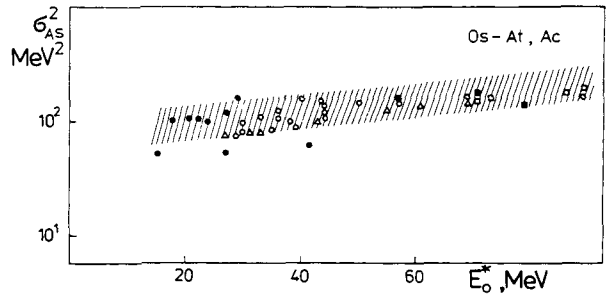

FIGURE 13. The dispersion σ^2_{AS} of the mass distribution of fragments of symmetric fission as a function of the excitation energy E^*_0 of a C-nucleus. Experimental data (see Reference 32) are labeled with different signs for the reactions induced by different particles: ● corresponds to p and d, △ to ^{3}He, ○ to α, ■ to ^{12}C, and □ to ^{16}O. The region of C-Nuclei undergoing fission is indicated in the figure. The cross-hatched region shows the energy dependence calculated by using the experimental data with regard for evaporation of particles before fission (see text).

of the existence of these universal modes. Moreover, an anlaysis[32] of experimental data shows that the quantity C_{as} has the value $C_{as} \simeq 1/2$, which remains approximately the same for all nuclei. This analysis[32] yields the following values for the dispersions of asymmetric fission

$$2\sigma_{A1} = \sigma_{A2} = \begin{cases} 5.6 & \text{for } A_0 \leq 235 \\ 5.6 + 0.096(A_0 - 235) & \text{for } A_0 > 235 \end{cases} \tag{19}$$

As for the symmetric mode of fission, the experimental data reveal no evidence for the dependence of the dispersion σ^2_{AS} on the mass of a nucleus undergoing fission. The energy dependence $\sigma^2_{AS}(E^*_0)$ is shown in Figure 13, where the values σ^2_{AS}, extracted in Reference 32 from the experiments on fission of various C-nuclei at various values of the excitation energy E^*_0, are also presented. It was taken into account in our analysis that evaporation particles, emitted from a C-nucleus before fission, take away a part of the initial excitation energy E^*_0. To estimate the influence exerted by this effect on the function $\sigma^2_{AS}(E^*_0)$, we have calculated the average excitation energy of a C-nucleus before fission, for reactions presented in Figure 13, with the help of the evaporation model (see Chapter 3). Taking account of this effect leads to a horizontal shift to the left of the points in Figure 13. Upon such a shift, the overwhelming majority of points fall within the cross-hatched region in this figure. Finally, the energy dependence of the dispersion of symmetric fission, corresponding to this cross-hatched region, is approximated by the expression

$$\sigma^2_{AS} = \exp\,(5.53 \cdot 10^{-3} E^*_0 + 2.1386) \tag{20}$$

(Here, and in what follows, the energy E^*_0, appearing in the empirical approximations, is given in MeV).

The function F appearing in expression 16 is found from the ratio F_{sa} of the altitudes of the symmetric and the asymmetric fission peaks in the mass distribution

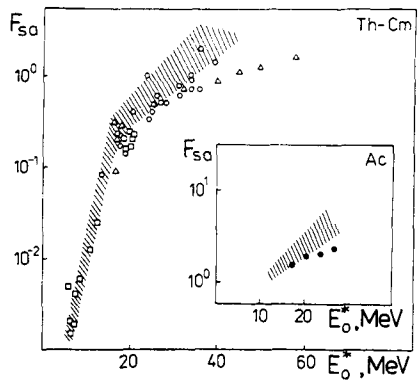

FIGURE 14. The ratio F_{sa} of the peak of symmetric fission to that of asymmetric fission in the mass distribution of fragments as a function of the excitation energy E_0^* of C-nuclei undergoing fission. The experimental data (see Reference 32) are labeled with different signs for reactions induced by different particles: □ corresponds to n, △ to p, ○ to α, and ● to p and d (insert). The rest of notation is the same as in Figure 13.

Y(A), which is measured in experiments. According to the charge of a nucleus undergoing fission, all data are divided into three groups: (A) $96 \geq Z_0 \geq 90$, (B) $Z_0 = 89$, and (C) $Z_0 \leq 88$, since the energy dependence of F_{sa} are quite different in these three groups. For instance, in Group A, asymmetric fission dominates at small E_0^*, whereas the probability of the symmetric mode increases rapidly with increasing E_0^*. In Group B, both modes are comparable for small E_0^*, whereas lighter nuclei of Group C undergo predominantly symmetric fission for all values of E_0^*

Figure 14 shows the energy dependence $F_{sa}(E_0^*)$ for nuclei from the Groups A and B. As in Figure 13, the region to which experimental points are shifted is shown by cross-hatching. These are obtained in reactions with different particles as a result of taking into account the evaporation of particles from a C-nucleus before fission. The following empirical approximation corresponds to this region:[32]

$$F_{sa} = \begin{cases} \exp(0.5385E_0^* - 9.9564) & \text{for } E_0^* \leq 16.25 \text{ MeV} \\ \exp(0.09197E_0^* - 2.7003) & \text{for } E_0^* > 16.25 \text{ MeV} \end{cases} \tag{21a}$$

$$F_{sa} = \exp(0.09197E_0^* - 1.0808) \quad \text{for } Z_0 = 89 \tag{21b}$$

Nuclei with $Z_0 = 86$ to 88 are of special interest because, in this intermediate region, the asymmetric fission mode is replaced by the symmetric one as the mass of the nucleus is reduced. This region was studied in Reference 31, though only for the energies close to the fission barrier $E_0^* \leq B_f + 10$ MeV. From the analysis of these data carried out under the assumption that the energy dependence of F_{sa} is the same as that for nuclei from the Group B, the authors of Reference 32 have constructed the following approximation

$$F_{sa} = \exp[0.3(227 - A_0)]*\exp\{0.09197[E_0^* - (B_f - 7.5)] - 1.0808\} \text{ for } Z_0 \leq 88 \tag{21c}$$

(For $A > 227$ and $E_0^* < B_f - 7.5$, the corresponding factors occurring in exponential functions vanish.)

In order to express the function F in terms of F_{sa}, it is sufficient to take into account the effect of the "tails" in the distribution of one of the fission modes on the value of the maximum yield in the other mode:

$$F = \frac{F_{sa} - I_{asym}}{I - F_{sa} \cdot I_{sym}}, \tag{22}$$

where $I_{asym} = Y_{asym}(A_s)$ and $I_{sym} = Y_{sym}((A_1 + A_2)/2)$ (see expressions 17 and 18). The latter relation suggests that the yield of the asymmetric mode is maximum at $A \simeq (A_1 + A_2)/2$.

The experimental data on the charge distribution of fragments are well approximated by a Gaussian with the dispersion $\sigma_z^2 \simeq 0.36$, which is dependent of the mass of a fragment, and the average value $\overline{Z}_p$ described by formula (14) with the parameter

$$\Delta Z = \begin{cases} -0.45 & \text{for } A \geq 134 \\ -0.45(A - A_0/2)/(134 - A_0/2) & \text{for } A_0 - 134 < A < 134 \\ 0.45 & \text{for } A \leq A_0 - 134 \end{cases} \tag{23}$$

To determine the dependence of the average kinetic energy $\overline{E}_k$ of fission fragments on the mass and the charge of a nucleus undergoing fission, the empirical systematics of Reference 30 are used (Figure 9):

$$\overline{E}_k = 0.1178\, Z_0^2/A_0^{1/3} + 5.8 \text{ MeV} \tag{24}$$

The distribution of this energy among fragments is different for the symmetric and the asymmetric fission modes.

In the symmetric fission, fragments of mass $A = A_s$ have maximum kinetic energy $\overline{E}_k^{max}$.[1,31,34] Figure 15 shows the experimental data for the ratio of the average kinetic energy of fission fragments to this maximum energy as a function of the mass of a larger fragment. They are approximated by the expression[32]

$$\epsilon(A) \equiv \frac{\overline{E}_k(A)}{\overline{E}_k^{max}} = \begin{cases} 1 - b[(A - A_m)/A_0]^2 & \text{for } A_s \leq A \leq A_m + 10 \\ 1 - b(10/A_0)^2 - 2(10/A_0) \cdot b \cdot (A - A_m - 10)/A_0 & \text{for } A > A_m + 10 \end{cases} \tag{25}$$

where $A_m = A_s$ and $b = 5.32$. It is also assumed that, for the symmetric mode, the root mean square deviation of kinetic energy from its average value is independent of A and takes the value $(\sigma_E^2)^{1/2} \simeq 8$ MeV.[1]

In the case of asymmetric fission, fragments with maximum kinetic energy are produced if fission takes place in such a way that the larger fragment has the mass $A = A_1 = 134$.[1,31,32] Figure 15 shows the experimental data for the ratio of the average kinetic energy to this maximum kinetic energy as a function of the mass

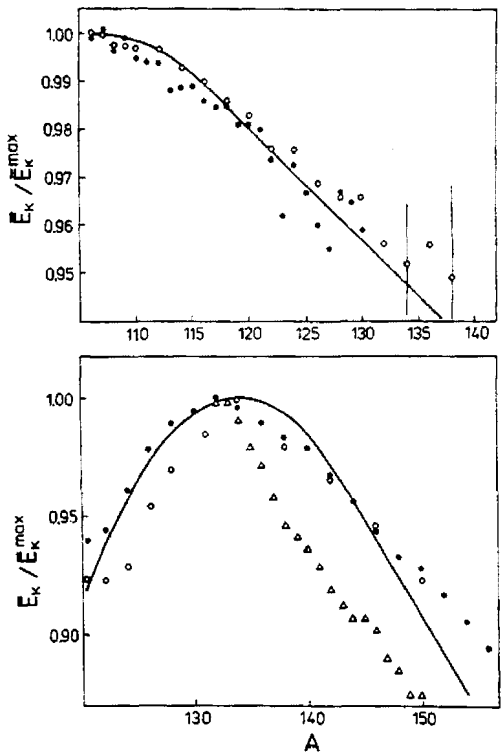

FIGURE 15. The ratio of the average values of kinetic energy of fragments to the maximum kinetic energy $\bar{E}_k/\bar{E}_k^{max}$ vs. the mass number A of the larger fragment for the symmetric (upper figure) and the asymmetric (lower figure) fission. The curves correspond to the calculation carried out according to the approximation (25). The experimental data (see Reference 32) are labeled with different signs for reactions induced by different particles: • corresponds to 53 MeV α + Bi, ○ to 45 MeV α + Bi (upper figure), • to 10 MeV p + ^{241}Am, ○ to 13 MeV p + ^{226}Ra, and △ to n + ^{235}U (lower figure).

of the larger fragment for this case as well. These data can also be approximated by expression 25 with the parameters $A_m = A_1$ and b = 23.5. For the root-mean-square deviation of kinetic energy in the asymmetric mode, we have $(\sigma_E^2)^{1/2} \simeq 10$ MeV.[1,31,32]

Thus, to determine kinetic energy of fission fragments, we must know the maximum kinetic energy $(\bar{E}_k^{max})_i$ separately for the symmetric (i = asym) and the asymmetric (i = asym) mode of fission. It is found from the average kinetic energy of fragments in a given mode $(\bar{E}_k)_i$ by scaling according to the relation

$$(\bar{E}_k^{max})_i = (\bar{E}_k)_i \left[\frac{\int \epsilon(A) Y_i(A) dA}{\int Y_i(A) dA} \right]^{-1} . \tag{26}$$

It follows from the analysis of data[32] that, in the asymmetric mode, the average kinetic energy of fragments is higher than that in the symmetric one by approximately 12.5 MeV. Therefore,

$$\begin{cases} (\bar{E}_k)_{sym} = \bar{E} - 12.5\ X_{asym}\ \text{MeV} & (27a) \\ (\bar{E}_k)_{asym} = \bar{E}_k + 12.5\ X_{sym}\ \text{MeV} & (27b) \end{cases}$$

where X_{asym} and X_{sym} are fractions of fission fragments formed in the symmetric and asymmetric modes, respectively. They can be found from the mass distributions $Y_{asym}(A)$ and $Y_{sym}(A)$ with the help of the relations

$$\begin{cases} X_{sym} = F\int Y_{sym}(A)dA / \int Y(A)dA \\ X_{asym} = \int Y_{asym}(A)da / \int Y(A)dA \end{cases}$$

For both the symmetric and the asymmetric mode of fission, the distribution over the kinetic energy of fragments of given mass A is described by a Gaussian with their own average values $\bar{E}_k(A)$ and dispersions σ_E^2 obtained by the method previously outlined.

3. Analysis of Experimental Data on the Formation of Fragments of Fission of Nuclei by Intermediate-Energy Particles

On the basis of the methods developed in Sections IB.1 and IB.2 for analysis of fission of C-nuclei, a modified cascade-evaporation model was proposed in Reference 32, which is capable of calculating the mass-energy distribution of fragments of fission of a nucleus by intermediate-energy particles. If fission takes place in one of the links of the evaporation chain of disintegration of a C-nucleus formed after the completion of the INC, then, in this model, the characteristics of fragments of fission of this C-nucleus are sampled by the Monte Carlo technique. The Monte Carlo calculation of characteristics of fission fragments is reduced to the following procedure:

a. The mass A_1 of the fission fragment (the mass of the conjugate fragment is given by the relation $A_z \equiv A_0 - A_1$) is sampled with the help of the mass distribution Y(A).*
b. The charge Z_1 of the fission fragment (the charge of the conjugate fragment is $Z_2 \equiv Z_0 - Z_1$) is determined by sampling with the help of the charge distribution $Y_A(Z)$* of fission fragments having the mass A.
c. The kinetic energy of fragments is sampled with the help of the distribution $Y_A(E_k)$* of kinetic energy of fragments with given mass A.
d. The excitation energies U_1 and U_2 of fragments are found with the help of expressions 15 and 16, and the evaporation cascade is calculated by the Monte Carlo technique for each of the fragments. In this procedure, the energy-momentum conservation law is taken into account correctly at all stages of the calculation. Variations of the momentum of an R-nucleus and of fission

* If the excitation energy E_0^* of a C-nucleus undergoing fission does not exceed 50 MeV, the parameters of the distribution are given by the empirical systematics (Section IB.1). In the opposite case $E_0^* >$ 50 MeV, they are calculated within the framework of the diffusion model (Section IB.2).

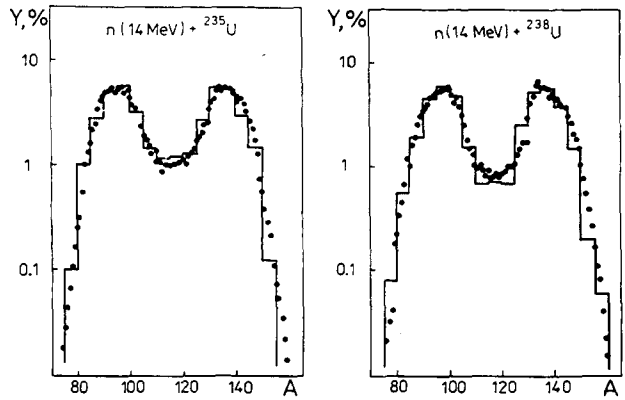

FIGURE 16. The mass distribution of fragments of fission of U nuclei. The initial particle is shown in the figure. The histogram corresponds to the calculation carried out within the framework of the evaporation model with an empirical approximation for the low-energy fission and the points correspond to the experimental data of Reference 36.

fragments after the evaporation of particles from them are taken into account as a result.

The developed Monte Carlo method of calculation contains information on particles of the fast stage, on evaporation particles before fission, on particles evaporating from fission fragments and on fission fragment themselves. Therefore, it enables one to calculate various correlations between these particles and fragments, and exclusive characteristics of the process. A modern formulation of the INC-model makes it possible to analyze data on fission of nuclei by various intermediate-energy particles. Let us compare the characteristics of fragments of nuclear fission, obtained through the calculations carried out within the framework of the cascade-evaporation model, with certain experimental data.

The inclusive mass distribution of fragments is one of the most important and principal characteristics of fission. It has been mentioned above that, owing to shell effects, fission of heavy nuclei with low excitation energy is asymmetric, and the mass distribution has the characteristic two-humped shape (Figure 16). Such a shape of the mass distribution can be used as a criterion for segregating the fraction of C-nuclei with low excitation energy from the entire ensemble of a R-nuclei formed in the interacton of intermediate-energy particles with a T-nucleus. The contribution of asymmetric fission decreases rapidly with increasing initial energy, and the inclusive mass distribution of fragments becomes practically symmetric at the initial energy of protons of about 200 MeV (Figure 17). The cascade-evaporation model describes correctly this changeover to the predominantly symmetric nuclear fission, which is caused by an increase in the fraction of C-nuclei having the excitation energy $E_0^* > 50$ MeV with increasing initial energy.

From the viewpoint of studying the high-energy fission, nuclear fission induced by antiprotons is of particular interest. Following we will analyze its characteristics

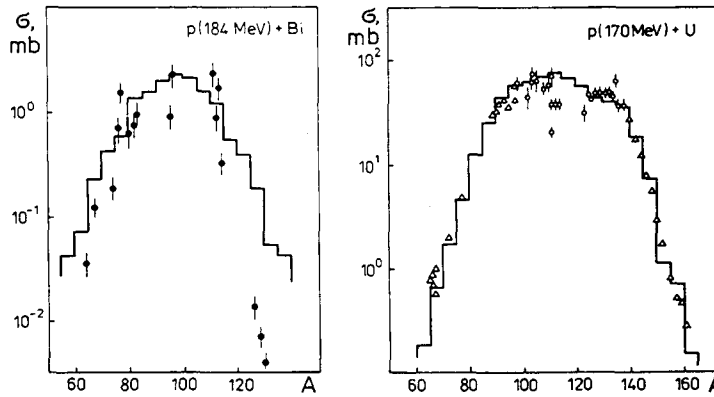

FIGURE 17. The mass distribution of fragments of fission of Bi and U nuclei by protons having the energy about 200 MeV. The histograms correspond to the calculation of Reference 32 carried out within the framework of the cascade-evaporation model and the points to the experimental data (different signs label data obtained by different groups, whose publications are cited in Reference 32).

in some detail. First, let us consider the distribution of two fission fragments over the total mass. The total mass $M_t = M_1 + M_2$ is connected with the loss of the total mass Δm through the relation $\Delta m = A_t - 1 - M_t$, where A_t is the mass of a T-nucleus and subtraction of unity takes into account the fact that annihilation reduces the mass number of the T-nucleus by unity.* In principle, the total loss of mass (or the total mass of fragments) is the measure of the excitation energy of a C-nucleus. Calculations of the $\bar{p}$A-annihilation carried out within the framework of the cascade-evaporation model (see Chapter 6) predict approximately linear dependence of the average excitation energy E_0^* on the total loss of mass (Figure 18). On the average, about 10 MeV of the excitation energy is spent on the mass loss $\Delta m = 1$. Therefore, the distribution over the total mass can be approximately interpreted as the distribution over the excitation energy of C-nuclei formed in the $\bar{p}$A-annihilation. Figure 19 shows the distribution over the total mass for U, Th, and Bi targets. This distribution is broad, which is indicative of the broad distribution of C-nuclei produced in the $\bar{p}$A-annihilation over the excitation energy E_0^*. In particular, events with the total loss of mass of about 70 to 80 (Figure 19) observed in this distribution are indicative of the formation of the C-nuclei with high excitation energies (up to 600 to 700 MeV). Experimental data and theoretical calculations agree reasonably well with each other. The discrepancy between them at maximum values of the total mass is caused by the experimental resolution with respect to the total mass, which was equal to 11 amu.

Figure 20 shows the inclusive mass distribution. As expected, it is symmetric in the $\bar{p}$A-fission. The width of this distribution increases with increasing mass of a target. This effect cannot be related to the temperature of the nucleus undergoing fission since C-nuclei produced in the annihilation of antiprotons on heavy nuclei have very close distributions over the excitation energy E_0^*.

* Here all quantities are measured in atomic mass units (amu).

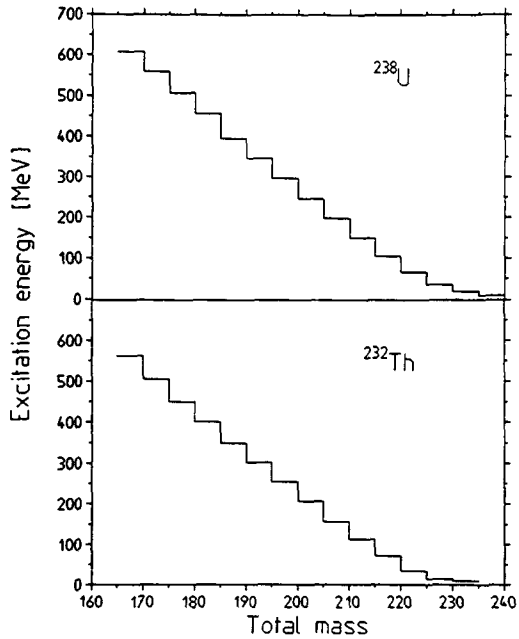

FIGURE 18. The average excitation energy E_0^* of a C-nucleus as a function of the total mass of fission fragments. The T-nucleus is shown in the figure. The histograms correspond to the calculation[37] carried out within the framework of the cascade-evaporation model.

The nature of this phenomenon becomes clear if we plot the mass distributions for various values of the mass loss Δm, which is equivalent to sorting of events according to the value of the excitation energy E_0^*. Figure 21 shows the mass distributions for various intervals of Δm for the U target. Two distributions for minimum values $\Delta m = 0 - 4$ and $\Delta m = 5 - 14$ contain considerable contribution from asymmetric fission and are, therefore, more broad than distributions for larger values of Δm. In view of the fact that the resolution with respect to the total mass is approximately equal to 11 amu, the experimental mass distribution for the bin $\Delta m = 0 - 4$ is, in fact, smeared over a considerably broader interval Δm. In the case of a good mass resolution, the changeover from the asymmetric to the symmetric fission would be even more sharp, which is seen from the calculation of the mass distribution for three bins $\Delta m = 0 - 4$, $0 - 6$, and $0 - 8$ (Figure 21). As we go over to the Th target, the contribution from the events of asymmetric fission decreases and disappears completely for the case of Bi target. Thus, a decrease in the width of the mass distribution with decreasing mass of the target is caused by reduction of the contribution from asymmetric fission.

The distribution of two fission fragments over the total kinetic energy is sensitive to the dynamics of descent of a nucleus undergoing fission from the saddle point to the scission point (see Section IB.1). The theoretical and the experimental distribution over the total kinetic energy are shown in Figure 22. The width of this distribution increases with increasing mass of a T-nucleus. This is a corollary of

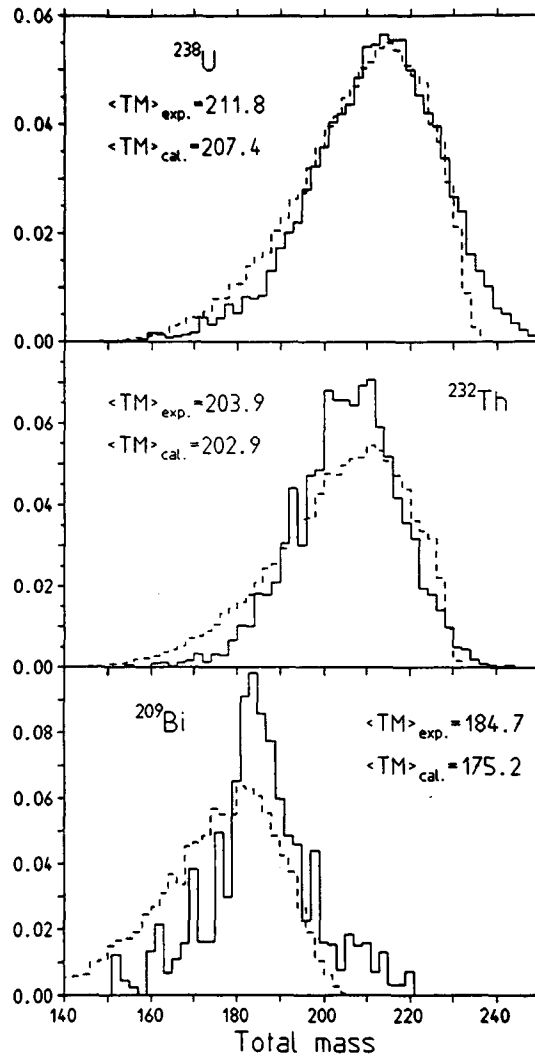

FIGURE 19. The distribution over the total mass for fission of heavy nuclei by antiprotons. The T-nucleus and the average value of the total mass are shown in the figure. The solid histogram shows the experimental results of Reference 37 and the dashed histogram corresponds to the calculation carried out within the framework of the cascade-evaporation model. The histograms are normalized to one fission event.

an increase in the dispersion σ_E^2 with the mass of a C-Nucleus, which is observed in experiments with low-energy particles and described by the diffusion model (see Section IB.1).

In addition to this, the diffusion model predicts an increase in the dispersion σ_E^2 with increasing temperature of a nucleus at the saddle point (with increasing E_0^*). To investigate this effect we will isolate distributions over the total kinetic

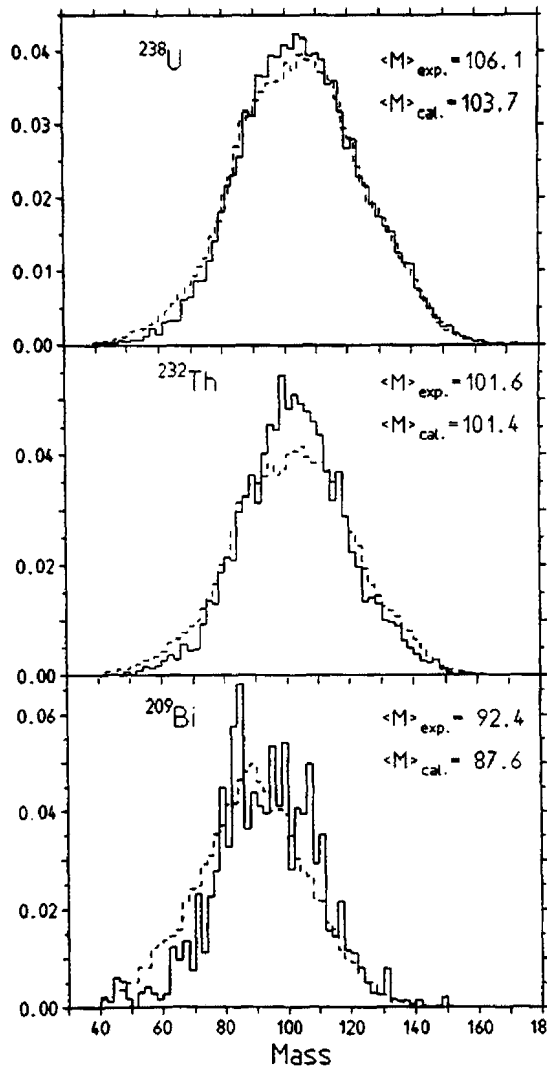

FIGURE 20. The mass distribution for fission of heavy nuclei by antiprotons. The notation is the same as in Figure 19.

energy corresponding to different intervals of the mass loss Δm. Figure 23 shows the distributions over the total kinetic energy for the same bins of the mass loss as those for which the mass distributions are plotted in Figure 21. The width of the distribution over the total kinetic energy increases with increasing mass loss Δm (excitation energy E_0^*) both in the theory and experiment. However, the calculated distribution becomes broader than the experimental one for large mass losses $\Delta m \geq 35$, and this deviation increases with increasing mass loss (excitation energy of a C-nucleus). The diffusion model apparently overestimates the dispersion σ_E^2 for

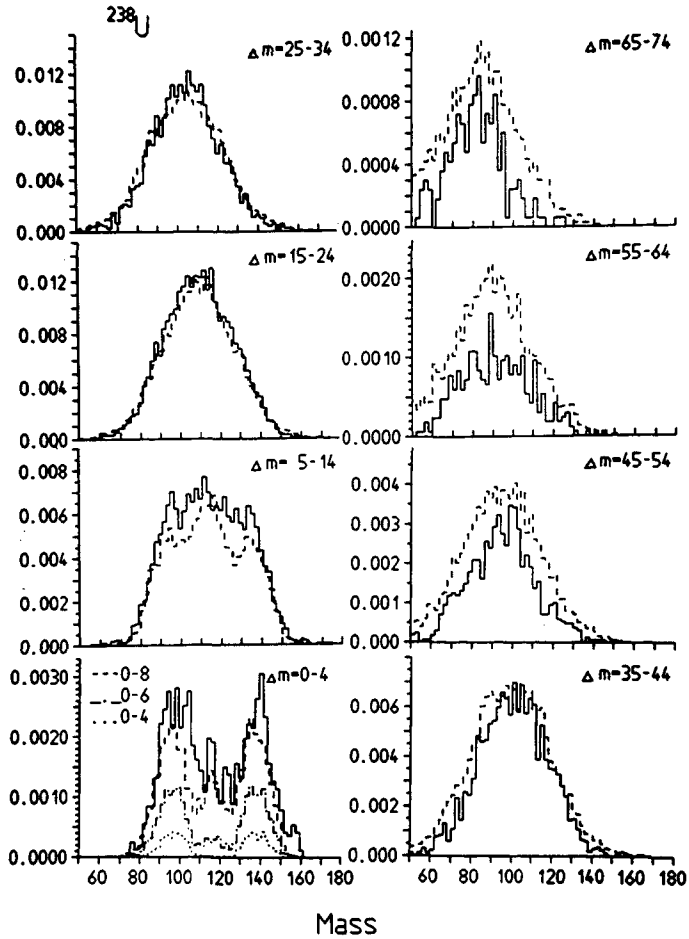

FIGURE 21. The mass distribution for fission of U nuclei by antiprotons, corresponding to different intervals of the mass loss Δm. The total surface area of histograms is equal to unity for all intervals. The rest of the notation is the same as in Figure 19.

the case of fission of hot C-nuclei. It is also interesting to consider, in detail, the distribution over the total kinetic energy for the bin $\Delta m = 0 - 4$, for which the low-energy fission is predominant. It follows from Figure 21 that, for $\Delta m = 0 - 4$, fission is purely asymmetric, whereas an admixture of symmetric fission appears for $\Delta m = 0 - 6$ and $\Delta m = 0 - 8$. The case of asymmetric fission is characterized by a higher value of the average kinetic energy of fragments than that of symmetric fission (see Section IB.2). Therefore, the peak of the distribution is shifted to smaller values of the total kinetic energy with increasing mass loss, and there can even appear the second peak in the distribution for the bins $\Delta m = 0 - 6$ and $\Delta m = 0 - 8$ (Figure 23).

The momentum of a C-nucleus before fission can be determined by measuring the angle of divergence of two fragments. Figure 24 shows the experimental and

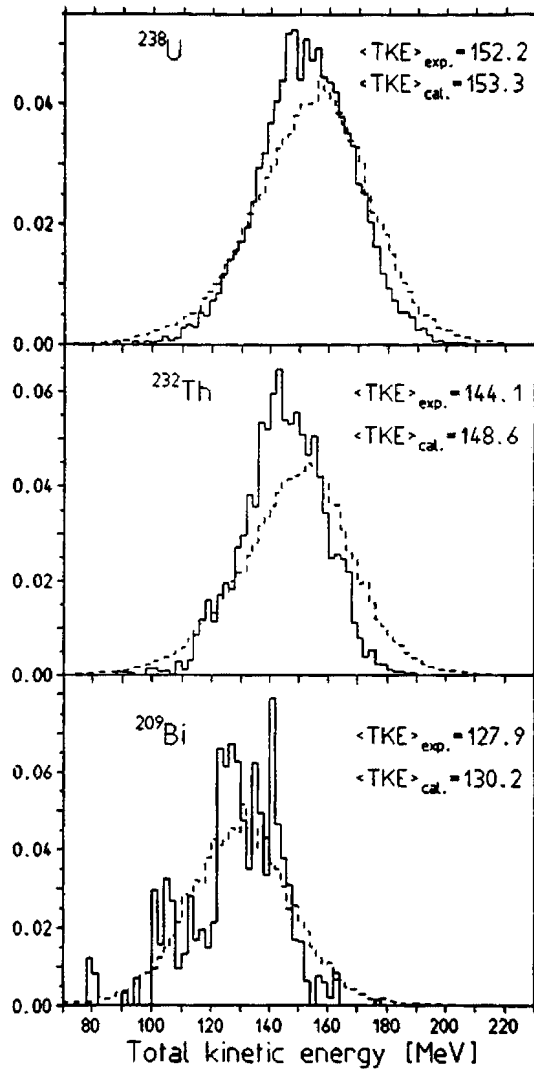

FIGURE 22. The distribution of fragments of fission of heavy nuclei by antiprotons over the total kinetic energy. The notation coincides with that used in Figure 19.

the calculated distribution over the momentum of C-nuclei. The reason behind the discrepancy between experimental data and theory at small values of momentum for U and Th targets lies in an insufficiently sharp resolution with respect to momentum, which was 500 MeV/s in the experiment reported in Reference 37 (the experimental distribution was not corrected with regard to this resolution). In the case of the Bi target, C-nuclei with low excitation energies (which have small momenta) do not undergo fission nor do they give any contribution to this distribution. Therefore, the calculated average momentum for the Bi target is larger

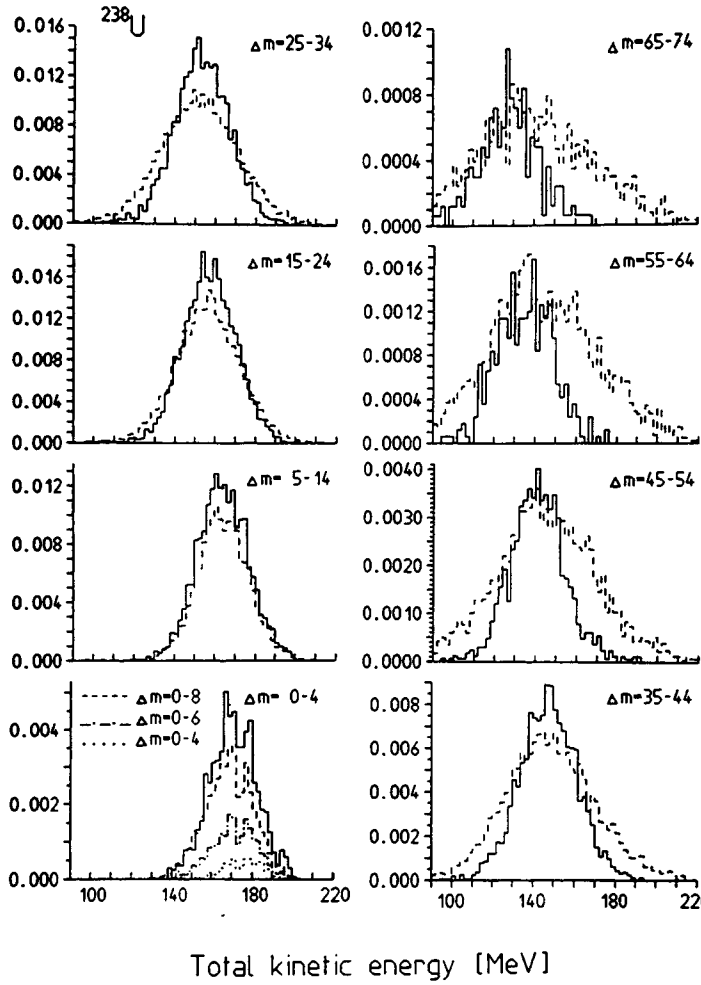

FIGURE 23. The distribution of fragments of fission of U nuclei by antiprotons over the total kinetic energy for different intervals of the mass loss Δm. The notation coincides with that used in Figure 21.

than that for the Th and U targets, and the agreement between the theory and the experimenal data in the domain of small momenta is reasonably well for Bi.

Thus, the cascade-evaporation model sufficiently well describes the experimental data on the inclusive distributions of fragments over the mass, the total mass, the total kinetic energy, and on the momentum distribution of C-nuclei before fission, correctly reproducing even such find details as small admixture of asymmetric mode in the fission of nuclei by antiprotons. Therefore, this model can be applied in the future for detailed and systematic analysis of new data (including the exclusive data) on fission of nuclei by various intermediate-energy particles.

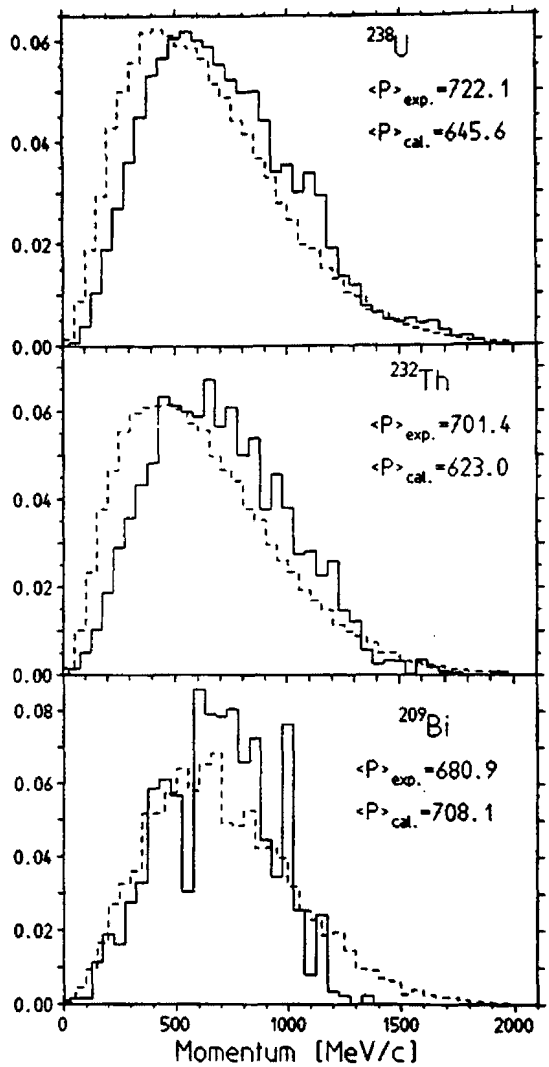

FIGURE 24. The momentum distribution of nuclei undergoing fission, plotted for the case when they are produced in the annihilation of antiprotons on heavy T-nuclei. The notation coincides with that used in Figure 19.

II. MULTIFRAGMENTATION

Formation of several fragments (multifragmentation) was discovered for the first time more than 25 years ago in NRs initiated by intermediate-energy protons.[38] At that time, however, the discovery did not attract any attention. Recently, a considerable interest in the study of this phenomenon was aroused by the fact that multifragmentation can be one of the manifestations of the first order phase transition

in hot nuclear matter (see Chapter 3). A great diversity of proposed models of multifragmentation[39,40] (see Section VB, Chapter 3) reflects the absence of a deep insight into the mechanism of this process. In such a situation, a detailed and systematic comparison of predictions of different models with experimental data is of paramount importance.

It has been shown in preceding chapters that highly-excited R-nuclei which can undergo multifragment breakup are produced in deep inelastic interactions of hadrons and heavy ions of intermediate energies with nuclei. Up to now a considerable body of information, primarily on inclusive characteristics of fragments,[39,40] has been accumulated in such NRs. These data were analyzed, as a rule, on the basis of the assumption that a hot thermalized R-nucleus with fixed values of the excitation energy E* and of the number of nucleons A and protons Z is produced in an NR.[41] However, investigations of deep inelastic interactions demonstrate (see preceding chapters) that this approximation is too crude. It seems reasonable to consider the multifragmentation as a complicated process proceeding in several stages: 1) formation of an intermediate highly excited nuclear system, 2) production of fragments and breakup of the system, and 3) divergence and de-excitation of hot fragments. It has been mentioned above that the process of "preparation" of an intermediate nuclear system creates an ensemble of R-nuclei which is characterized by a broad distribution over the excitation energy E*, the momentum $\mathbf{p}_r$, and the nucleonic composition A and Z. Any realistic model of multifragmentation must take into account this fact in analysis of experimental data.

A. CASCADE-FRAGMENTATION-EVAPORATION MODEL

A realistic model of the multifragment breakup of nuclei by intermediate-energy particles has been formulated.[42] It uses the INC-model (see Section II, Chapter 2) to describe the first stage of the process and the microscopic statistical model of multifragmentation to describe the second and the third stages (see Section VB, Chapter 3). Unification of these models, called the cascade-fragmentation-evaporation (CFE) model, allows us to simulate the entire process of hadron-nucleus interaction from the initial to the final stage and to calculate all observable characteristics of secondary particles and fragments including exclusive characteristics.

The basic assumption of the CFE-model on the existence of the fast stage of the INC which prepares an excited R-nucleus and of slower stages of the subsequent decay of this nucleus is well substantiated for relatively low excitation energy $E^* \lesssim 2$ MeV/nucleon, where the evaporation mechanism of the de-excitation of C-nuclei is dominant. In this case, a large distinction (by several orders of magnitude) between characteristic time of the INC and of the evaporation leads to a clear separation of the fast (INC) and the slow (evaporation) stages. For the excitation energy $E^* \gtrsim 5$ MeV/nucleon comparable with the total binding energy of a nucleus, an R-nucleus undergoes fast (as compared to the evaporation) explosive breakup into a large number of parts (multifragmentation), and division of the process into a fast and a slow stage becomes dubious. The model,[42] nevertheless, assumes that explosive breakup of a highly-excited R-nucleus takes place after the establishment of statistical equilibrium. The time $\tau_{fr} \sim 10^{-21}$s of the formation of fragments (see

Section VB4, Chapter 3) exceeds several times the characteristic time $\tau_{cas} \sim 10^{-22}$s of the fast stage. This can serve as a certain substantiation of this assumption. However, more convincing arguments can be obtained only through the comparison of predictions of the model with experimental data.

B. ENSEMBLE OF HOT R-NUCLEI

The INC-model, and hence the CFE-model,[42] takes into account a broad distribution of the ensemble of R-nuclei, formed after the completion of the cascade stage, over the excitation energy E*, the momentum $\mathbf{p}_r$, and the nucleonic composition A and Z. Such a form of these distributions is caused by the fluctuations of particle fluxes in the cascade shower. However, there are a number of uncertainties and unresolved problems in the description of the dissipation of energy within the framework of the INC-model. One must keep this in mind while analyzing the data on multifragmentation. It has been shown in Section VB, Chapter 3, that multifragment decay of nuclei begins to manifest itself starting from a certain threshold excitation energy $E^*_{thr} \approx$ 2-3 MeV/nucleon. Therefore, the multifragmentation, unlike other channels of deep inelastic interaction, is sensitive to the high-energy part of the distribution of R-nuclei over E*. It is clear that the calculation of the high-energy "tail" carried out within the framework of the INC-model is more uncertain than that of the other part of the distribution over E*. To estimate the scale of uncertainties associated with the description of the fast stage of an NR calculation were carried out according to the standard INC-model and according to the INCT-model (see Section II, Chapter 2). Moreover, in each version of the INC-model, the effects associated with the pre-equilibrium emission of particles in the process of the establishment of the equilibrium in an R-nucleus arising after the completion of the INC were estimated with the help of the exciton model (see Section IE, Chapter 2). It should be kept in mind that, in the vicinity of the excitation energy E* $\sim$ 10 MeV/nucleon, the exciton model may pretend to an ability of giving only a qualitative estimate of effects of preequilibrium emission.

Let us note the general properties of the ensemble of R-nuclei which do not depend on the version of the model used in the calculations. The spectrum of the excitation energy of R-nuclei extends from minimum values of E* to the limiting value E* $\sim$ 10 MeV for which it is still possible to consider a nucleus as a whole (see Figure 25). Therefore, there are the products of both mechanisms of de-excitation, evaporation and multifragmentation, in NRs. About several scores of nucleons can be knocked out of a T-nucleus, and an R-nucleus can acquire a large value of momentum. As the initial energy increases in the domain $\epsilon_p < 5° \div 10$ GeV, a T-nucleus loses a larger number of nucleons and acquires a larger momentum. For larger energies, the characteristics of the pA-interactions, including the characteristics of R-nuclei, do not depend practically on the incident energy (see Section IV, Chapter 4).

One more regularity of a deep inelastic NR which is important for the analysis of the mechanism of decay of hot R-nuclei should be noted. The more branched the INC, i.e., the larger is the number of the NN- and πN-collisions initiated by a primary particle in the T-nucleus, the larger are the values of E* and $\mathbf{p}_r$ acquired

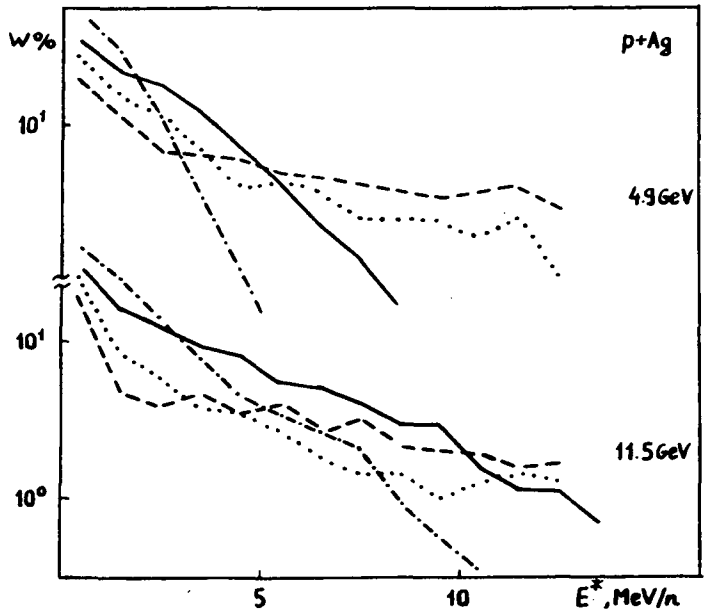

FIGURE 25. Distribution of the ensemble of R-nuclei over the excitation energy E* (in % over the energy interval of 1 MeV/nucleon) after the INC is indicated here, along with the target and the proton energies. The solid curve is calculated[42] on the basis of the INC-model with trawling, the dashed curve without trawling, the dash-dotted curve with trawling and subsequent pre-equilibrium emission of particles, and the dotted curve without trawling, but with pre-equilibrium emission.

by an R-nucleus, and the smaller number of nucleons remains in it. Therefore, hot R-nuclei, undergoing multifragment breakup, have smaller masses and larger momenta than C-nuclei, emitting particles (see Figure 26).

Figures 25 and 26 also demonstrate the sensitivity of characteristics of the ensemble of R-nuclei to the method of description of the fast cascade stage of the reaction. Calculations carried out with the help of different versions of the INC-model demonstrate that uncertainties in the prediction of the yield of hot ($E^* \sim 5$-10 MeV/nucleon) R-nuclei, which are of principal interest from the viewpoint of the multifragment breakup, are especially large. The standard version of the INC-model gives reliable results only in the domain of not very high energies of protons $\epsilon_p \lesssim 3$ GeV (see Section IV, Chapter 4). At higher energies, it overestimates significantly the yield of hot R-nuclei.

In the INCT-model, the number of collisions of cascade particles with nucleons of a T-nucleus, and hence, the yield of highly excited R-nuclei is significantly smaller. However, this version apparently overestimates the yield of hot nuclei with $E^* \gtrsim 10$ MeV/nucleon as well (see Figure 25), since it does not take into account the production of pionic and baryonic resonances and the effects associated with a finite length of hadron formation in the INC. Pre-equilibrium emission of particles reduces significantly the values of the excitation energy and of the mass number of thermalized R-nuclei (see Figures 25 and 26). However, the exciton model used

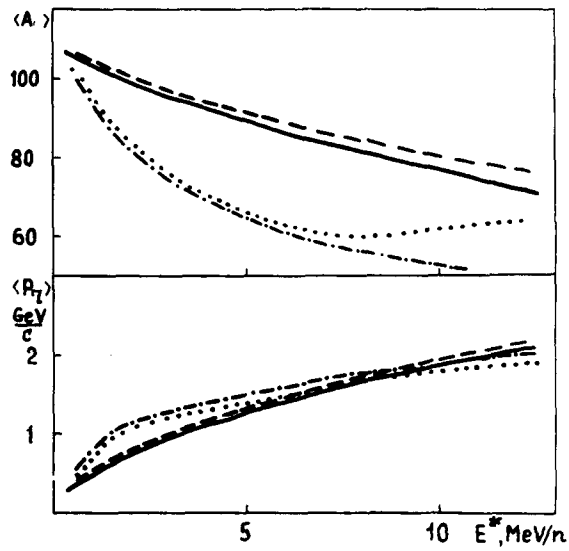

FIGURE 26. Average masses ⟨A⟩ and average momenta ⟨p_r⟩ of R-nuclei after the INC are given as functions of their excitation energy E*. The calculation[42] is given for the p(11.5 GeV) + Ag reaction. Correspondence of different curves to specific cases is the same as in Figure 25.

for the description of this process apparently overestimates this effect. Thus, uncertainties in the description of the distribution of R-nuclei at high excitation energies close to the total binding energy of a nucleus call for a serious improvement of the INC-model and for a special study of this problem within the framework of kinetic theory.

Another problem is associated with the fact that the INC-model considers the dissipation of the initial energy only over single-particle degrees of freedom. The collective effects in NRs with intermediate energy particles are sure to be less important and can be disregarded in the first approximation with more confidence than in the case of nucleus-nucleus collisions. However, the contribution of the collective effects can be noticeable in the NRs under consideration as well. As an example, we shall consider one of such effects which follows from the calculations carried out within the framework of the INCT-model. After the completion of the cascade stage, the spatial distribution of nucleons in R-nuclei turns out to be non-uniform and spherically asymmetric. Figure 27 shows the distribution of the nuclear density after the completion of the INC initiated by the central collision between a proton of the energy 11.5 GeV and an ^{108}Ag nucleus. It is seen that the proton creates the channel in a T-nucleus in which the nucleon density is reduced by a factor of two. Relaxation of such a nonequilibrium nuclear system may result in collective vibrations of the system. Moreover, the destruction of internucleon bonds may result in the breakup of a nucleus into fragments up to the attainment of statistical equilibrium.

While analyzing experimental data one must bear in mind these uncertainties and unresolved problems of the INC-model.

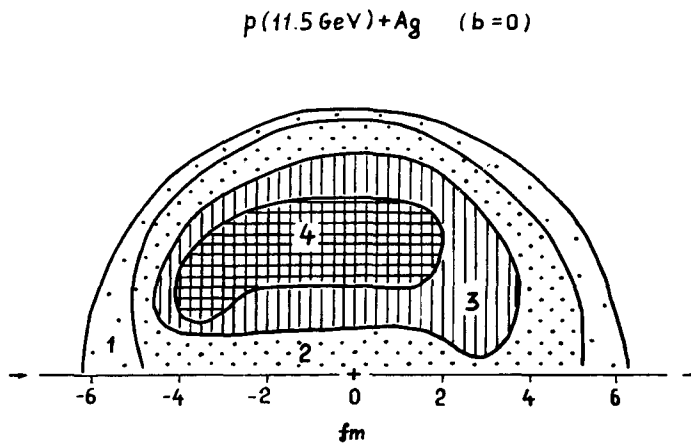

FIGURE 27. The distribution of nuclear density in R-nuclei after the INC initiated in the collision p(11.5 GeV) + Ag for the impact parameters b = 0 is represented here. The INCT-model was used for the calculation.[42] The figure is plotted in the polar coordinates with the center of a nucleus shown by a cross. The arrow shows the direction of motion of an incident proton. The density bins are given by figures: 1 - 0.011 ÷ 0.040 fm^{-3}, 2 - 0. 041 ÷ 0,070 fm^{-3}; 3 - 0.071 ÷ 0.100 fm^{-3}; 4 - 0.101 ÷ 0.130 fm^{-3} (the density in the center of a nucleus before the interaction is 0.17 fm^{-3}).

C. ANALYSIS OF EXPERIMENTAL DATA ON THE PRODUCTION OF NUCLEAR FRAGMENTS BY INTERMEDIATE-ENERGY PARTICLES

Let us consider experimental data on the formation of nuclear fragments produced as a result of bombardment of nuclei by intermediate- and high-energy protons on the basis of the CFE-model.[42] While carrying out this analysis we shall invoke the data obtained on medium-weight T-nuclei (with A $\sim$ 100) in order to reduce to a minimum the contribution both of the fission and of the products of the Fermi breakup to observable quantities (see Section I). Taking into account the fact that most of the data were obtained for $\epsilon_p \gtrsim 5$ GeV, we shall use the INCT-model as a principal version of the calculation. The inclusive characteristics of the fragmentation constitute the main part of experimental data. Since only one fragment is registered in this case, this characteristic contains contributions of all mechanisms of production of nuclear fragments.

Figure 28 shows the mass spectrum of fragments produced as a result of bombardment of Ag by protons with energies ϵ_p = 1-11.5 GeV. Measurements were carried out over a wide interval of mass number from lightest fragments to fragments close to a T-nucleus. The yield of fragments with A = 10-50 is small for $\epsilon_p \lesssim 1$ GeV, increases rapidly with the energy in the domain ϵ_p = 1-5 GeV, and varies only slightly with a further increase in ϵ_p. The same figure shows the results of calculations carried out within the framework of the cascade-evaporation model. Although nuclides with masses differing from the mass of a target by 50 or more mass units are produced in this model as a result of strong spallation of a T-nucleus, the model cannot, nevertheless, reproduce the yield of fragments with A = 50-

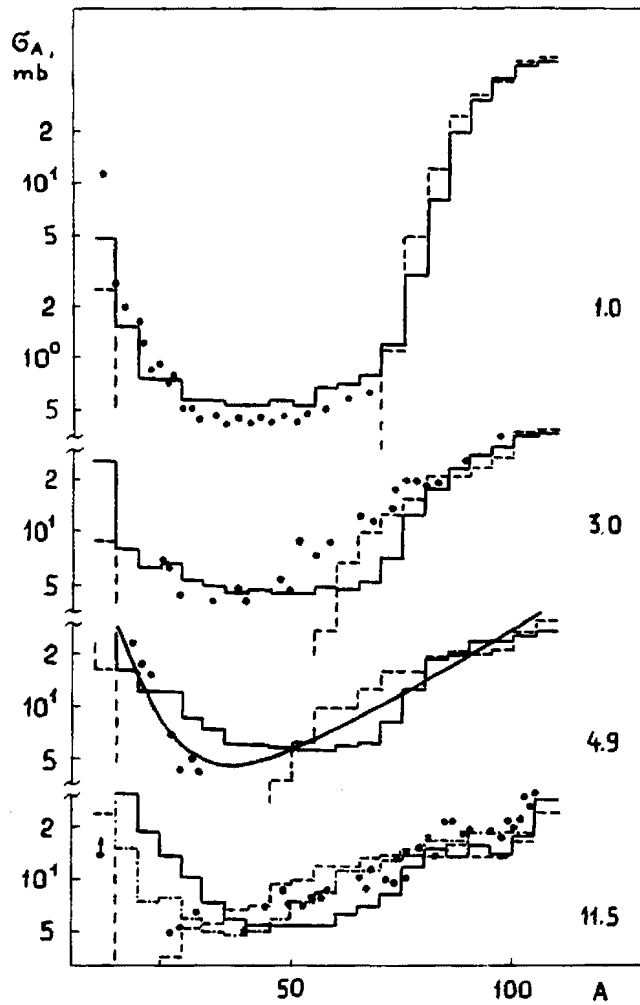

FIGURE 28. Fragment mass yields in the p + Ag reaction for different incident energies (in GeV) are shown by the figures. The solid curve is the fit of the experimental data at 4.9 GeV.[43] The dots present the experimental data: at 1 GeV,[44] 3 GeV,[45] at 4.9 GeV,[46] and at 11.5 GeV.[47] The histograms show the results of the calculations.[42] The solid lines correspond to the CFE-model, the dashed lines to the cascade-evaporation model, and the dash-dotted line to the CFE-model with intermediate distribution for R-nuclei over excitation energy (see text).

150. Only taking into account the multifragment breakup, we can eliminate this discrepancy. The CFE-model agrees qualitatively with experimental mass yields over the entire range of masses of fragments.

On the other hand, the shape of the distribution over A is not reproduced very well by the CFE-model (see Figure 28). Analysis has shown[42] that the fragments with A = 40-70 are produced, mainly, in events with a small multiplicity of fragments, whereas fragments with A = 10-40 are associated with multifragmen-

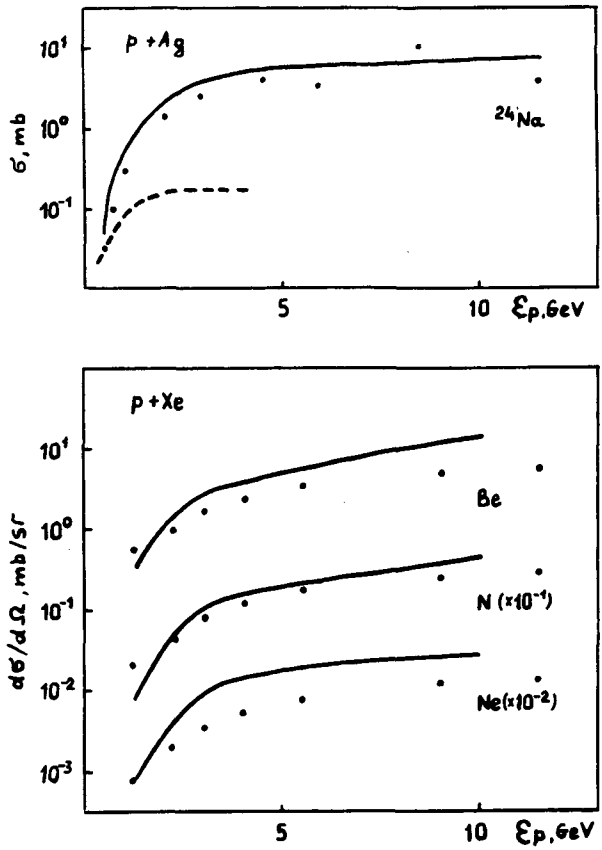

FIGURE 29. Here are excitation functions of different fragments. The reactions and fragments are shown in the figure. The dots present the experimental data: the upper figure shows the data of Reference 48, and the lower figure the data of Reference 49 (at the angle ϑ = 48.5°). The solid curves correspond to the calculation[42] by the CFE model and the dashed curve to the calculation by the cascade-evaporation model.

tation of hot R-nuclei. The CFE-model distorts slightly the relative yield of these two groups of fragments. This discrepancy is caused by an inaccuracy in the characteristics of the ensemble of thermalized nuclei predicted by the INC-model. It should be noted that this discrepancy is eliminated (see Figure 28), if for this ensemble we take an intermediate distribution over the excitation energy and mass lying in the middle of the interval of uncertainty in the predictions of the INC-model (shown in Figures 25 and 26).

Figure 29 shows the excitation functions for certain fragments produced as a result of bombardment of Ag and Xe nuclei by protons. The CFE-model agrees satisfactorily with experimental data. The model reflects correctly the threshold nature of the multifragmentation, i.e., a rapid increase in the yield of fragments in the energy range ϵ_p = 0.5-3 GeV. Such a behavior is explained by an increase in

the fraction of R-nuclei whose excitation energies are higher than the "threshold" of multifragmentation E^*_{thr} = 2-3 MeV/nucleon. It has been mentioned above that this increase is terminated as the initial energy increases further. As a result the excitation functions flatten out in this domain (see Figure 29).

In the domain of proton energies $\epsilon_p > 10$ GeV, the characteristics of the ensemble of R-nuclei do not depend practically on ϵ_p (see Section IV, Chapter 4). This saturation property can be used in analysis of data on the yield of fragments for ϵ_p = 80-350 GeV. The same ensemble of thermalized nuclei as in the case of ϵ_p = 10 GeV was taken for the calculations[42-43] in this energy range. Such an approximate calculation describes satisfactorily experimental data on the isotope yield (see Figure 30).

Angular distributions of fragments produced in the pA-interaction are anisotropic (see Figure 31). This may be associated with the translational motion of R-nuclei forward. It is seen from Figure 31 that this effect can account for an angular anisotropy of the yield of fragments for sufficiently high ϵ_p. For $\epsilon_p < 1$ GeV, the experimental anisotropy is higher than the calculated one (see Figure 31). This may be indicative of the contribution coming from other mechanisms of production of a single fragment, e.g., from a direct knockout of a cluster.

Energy spectra of fragments are shown in Figure 32. The CFE-model reproduces the magnitude, the position of the peak, and the shape of spectra reasonably well. On the contrary, the cascade-evaporation model leads to the results which are qualitatively incorrect, namely, the magnitude of the cross-section is underestimated by several orders of magnitude and the spectrum falls too quickly both at low and high energies. This is explained by large distinctions in the energy spectra of fragments emitted through evaporation and produced as a result of multifragmentation. These distinctions are caused, in particular, by the fact that the Coulomb barrier is significantly smaller in the many-body multifragment breakup than in the two-body evaporation (see Section VB4, Chapter 3). Such a reduction of the Coulomb barrier relative to its value corresponding to evaporation was observed long ago,[51] but a satisfactory physical explanation of it was lacking. A concept of a many-body breakup of nuclei offers a natural explanation of this effect.

Unfortunately, only fragmentary correlation measurements have been carried out for the fragmentation reaction up to now. The multiplicities of fast particle emitted at the cascade stage (these multiplicities characterize the degree of the cascade branching and hence the excitation energy of R-nuclei) were measured[52] in the coincidence with characteristics of products of decay of R-nuclei. It is seen from Figure 33 that the CFE-model describes such a correlation satisfactorily. This is indicative of the self-consistency of the model adequately reflecting the linkage between various stages of the process. Another class of the coincidence experiments reposes on the analysis of individual events, namely, measuring the characteristics of the fragments produced in a given event, we can obtain a more direct information on the mechanism of multifragmentation. It has been shown in Section VB4, Chapter 3 that the multiplicity of not too light ($Z \geqslant 3$) fragments is the simplest correlation of such a type which allows one to effectively separate the evaporation and the multifragmentation mechanism of decay. Figure 34 shows the available experimental

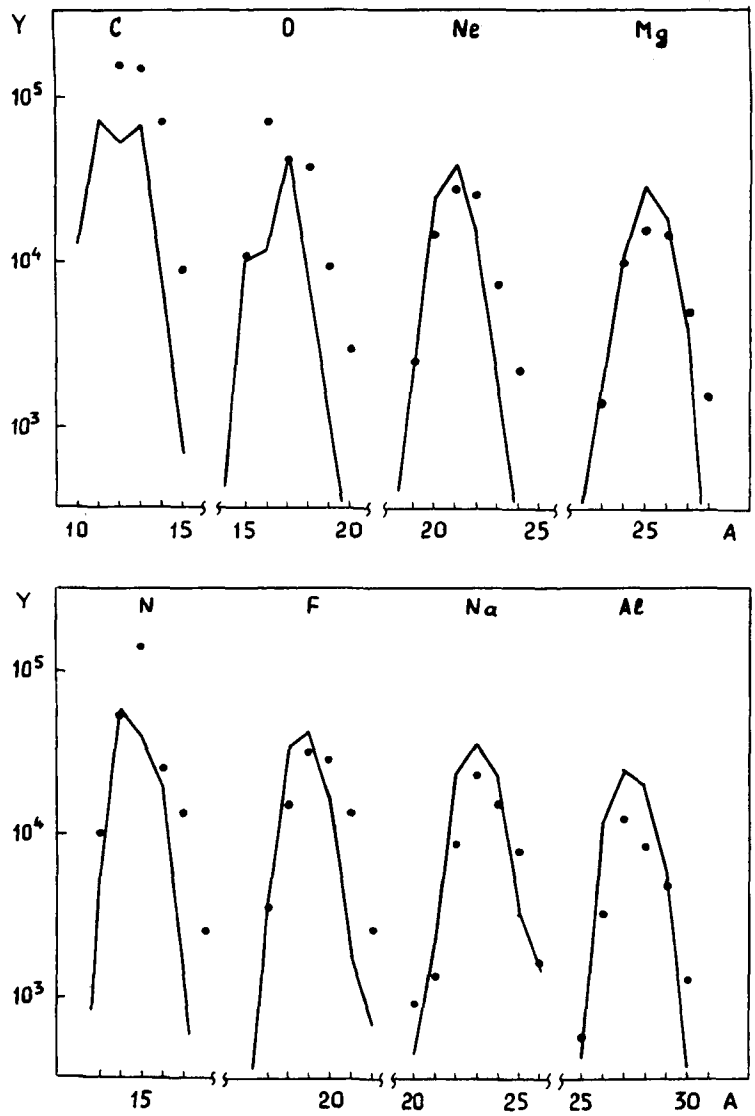

FIGURE 30. The isotope yield Y (in relative units) is portrayed in the p(80 ÷ 350 GeV) + Kr reaction. The dots are the experimental data.[50] The curves present the calculation[42] by the CFE-model.

data on the multiple production of such fragments. It is seen that the CFE-model describes this correlation satisfactorily without invoking any additional assumptions. Exclusion of the many-body breakup leads to a significant discrepancy with experimental data. This is explained by the fact that multiple emission of fragments is practically impossible in the evaporation cascade, since the probability of the evaporation of even one fragment decreases exponentially as its mass number and/or charge increase (see Section VB4, Chapter 3).

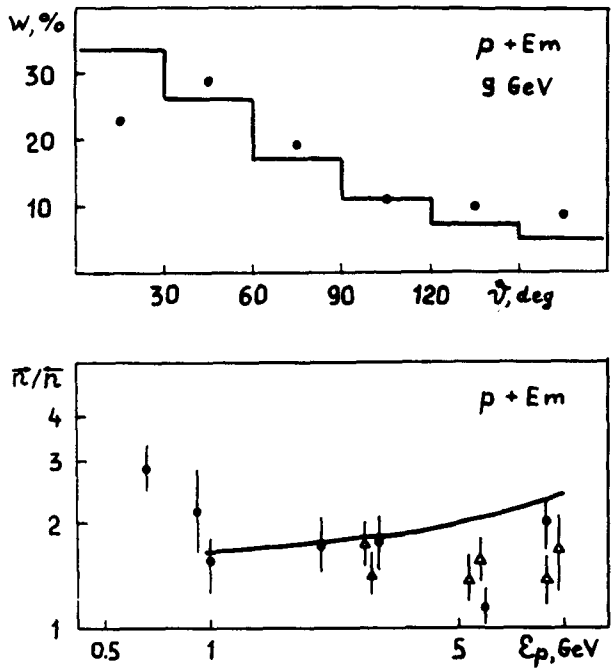

FIGURE 31. The angular distribution of fragments (the upper figure) and the energy dependence of the ratio of the fragment yield in the forward hemisphere to that in the backward hemisphere (the lower figure) for the interaction of protons with nuclei of photoemulsion. The full circles (fragments with $4 \leqslant Z \leqslant 9$) and triangles (the ^{8}Li nuclei) show experimental data.[38,48] The histogram and the curve show the results of the calculation[42] carried out within the framework of CFE-model for fragments with $4 \leqslant Z \leqslant 9$.

Thus, the CFE-model[42] is capable of describing a wide range of data on the production of nuclear fragments by intermediate- and high-energy protons. On the basis of the analysis performed we can conclude that the multifragment breakup of highly-excited R-nuclei is an inevitable element of a deep inelastic hadron-nucleus interaction. A good agreement of the CFE-model with experimental data, in particular, with the data on the correlation between the multiplicities of fast particles and yields of fragments, shows that basic tenets of this model, such as the separation of the deep inelastic interaction into the stage of formation of a thermalized R-nucleus after the completion of the INC and the stage of the multifragment breakup of a hot nucleus, are quite reasonable.

The conclusion that the multifragmentation is a universal phenomenon is a natural corollary of the CFE-model. This statement implies that this phenomenon must be observed in NRs initiated by different particles of intermediate and high energies (photons, pions, antinucleons, etc.). This is confirmed by the comparison of its predictions[39] with still fragmentary experimental data which include the charge distribution of fragments produced in the interaction of pions of the energy 7.5 GeV with nuclei of photoemulsion[53] (Figure 35), the data[54] on the multiple pro-

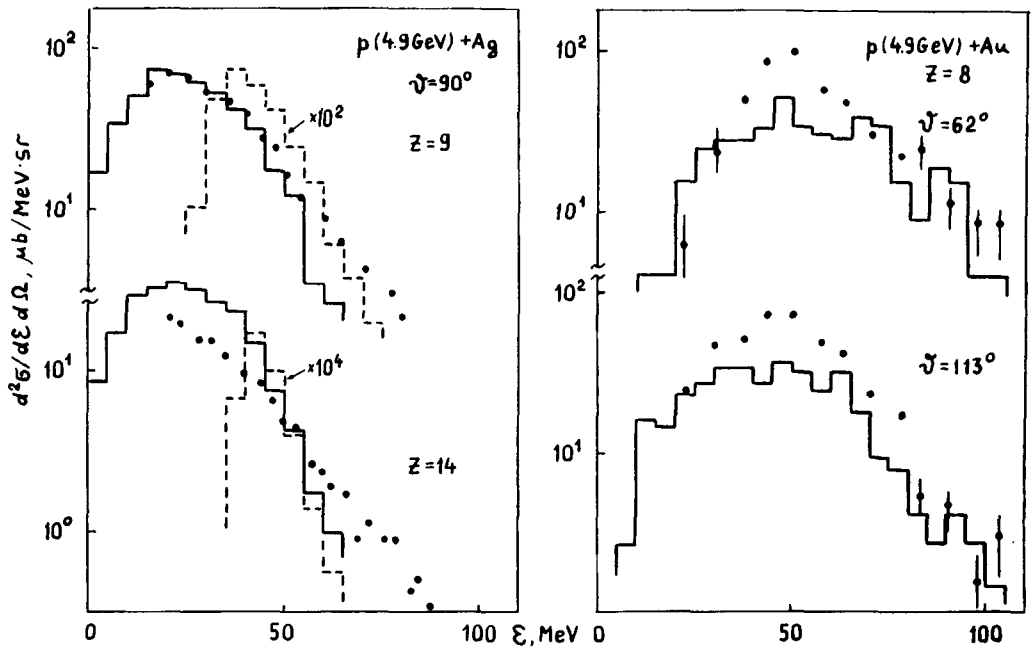

FIGURE 32. Energy spectra of fragments are represented here at different angles. Reactions, fragments and angles are shown. The dots present experimental data borrowed from Reference 46 (the left-hand figure) and from Reference 52 (the right-hand figure). The histograms show the results of the calculation.[42] The solid line corresponds to the results obtained with the help of the CFE-model, and the dashed line to the use of the cascade-evaporation model.

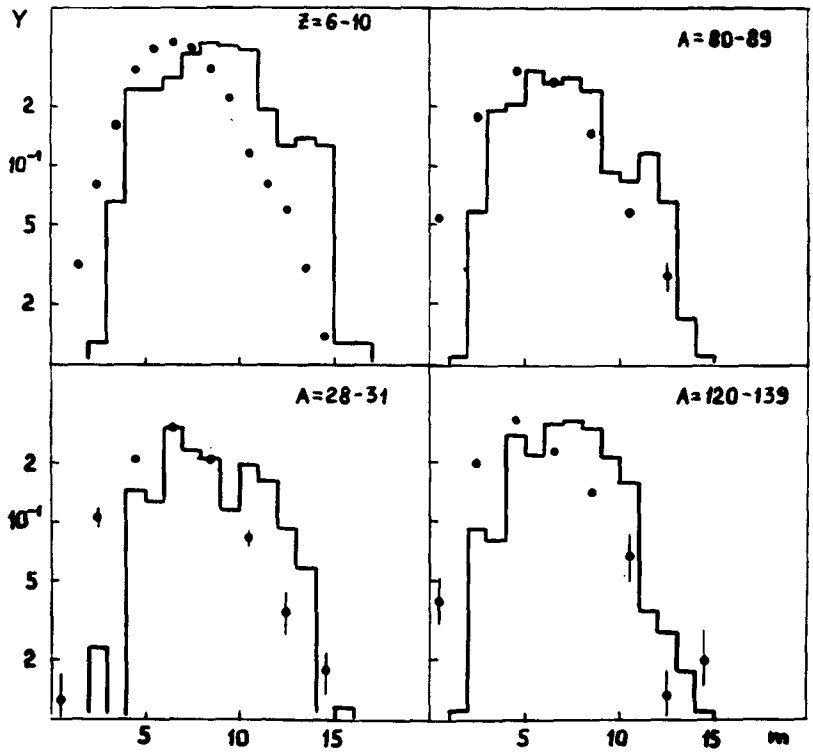

FIGURE 33. Here is the relative yield Y of intermediate and heavy fragments vs. the multiplicity m of fast particles in the p(4.9 GeV) + Au reaction. The dots present experimental data.[52] The histograms show the calculation[42] by the CFE-model normalized to the maximum of experimental distributions.

duction of fragments in the interaction of antiprotons of the energy 2.9 GeV with nuclei of photoemulsion (Figure 36), and the data[55] on the production of fragments in the interaction of ^{3}He nuclei with medium-weight nuclei (Figures 37 and 38), and other nuclear interactions as well.

Therefore, one can hope that predictions obtained on the basis of the CFE-model are sufficiently reliable. Figures 39 and 40 show examples of such predictions for the mass yield of fragments in the annihilation of stopped antiprotons on nuclei[56] and in the interaction of photons of the energy $\epsilon\gamma = 1$ GeV with a heavy nucleus.[18] It should be noted that the processes presented in these figures are characterized by different spatial domains of production of a multipion system in the initial elementary interaction, namely, Figure 39 corresponds to the surface $\bar{p}$A-annihilation, and Figure 40 to the volume γA-reaction. Calculated data presented in Figures 37 and 38 illustrate the dependence of the process of formation of hot R-nuclei on the number of nucleons interacting with a T-nucleus.

In conclusion, let us note one more facet of the studies associated with production of R-nuclei in the deep inelastic pA-interaction. It has been shown above that a broad spectrum of nuclides belonging to different domains of the nuclide

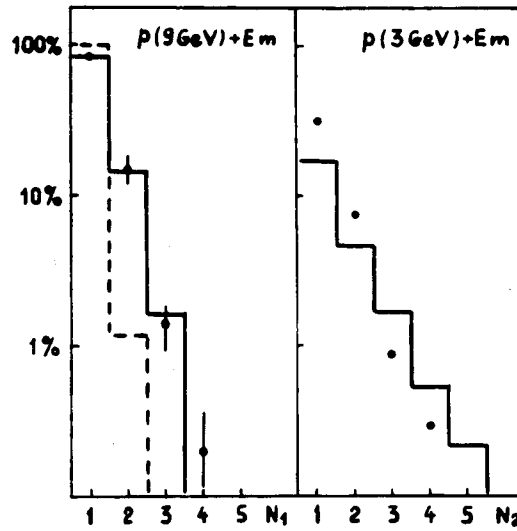

FIGURE 34. The multiplicity distribution of "heavy" fragments produced in the reactions are given in the figure. The dots correspond to experimental data borrowed from Reference 38 (the left-hand figure, in which N_1 is the number of fragments with $4 \leqslant Z \leqslant 9$ in events, where they are present), and from Reference 53 (the right-hand figure, in which N_2 is the number of fragments with $3 \leqslant Z \leqslant 6$ in events with production of α-particles). The solid-line histogram is calculated[42] by using the CFE model and the dashed-line histogram by using the cascade-evaporation model.

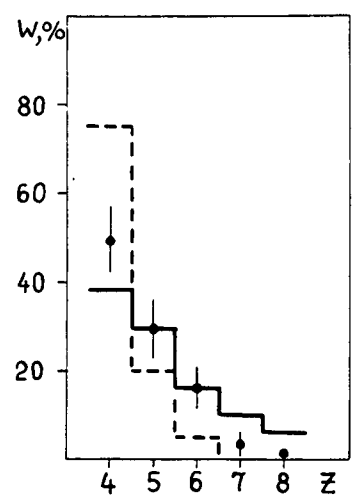

FIGURE 35. The relative yield of fragments with the charge Z in the interaction of 7.5 GeV π^--mesons with nuclei of photoemulsion. The points show experimental data.[53] The rest of notation is the same as in Figure 34.

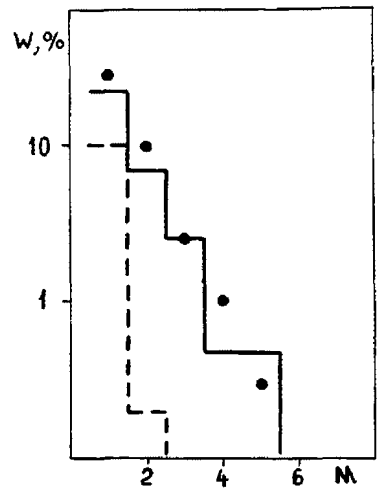

FIGURE 36. This shows the distribution of events over the multiplicity M of fragments with $3 \leqslant Z \leqslant 6$ produced in these events as a result of the interaction of 2.9 GeV antiprotons with nuclei of photoemulsion. Those events are chosen in which at least one α-particle is emitted. The points show experimental data.[54] The rest of notation is the same as in Figure 34.

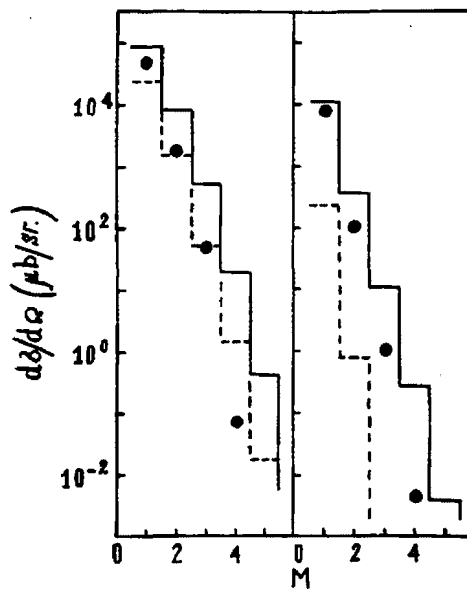

FIGURE 37. Here is the distribution of events over the multiplicity M of fragments with the charge Z lying in the interval $3 \leqslant Z \leqslant 12$. These fragments are emitted in the interaction of ^{3}He of the energy 0.9 GeV (the left-hand figure) and 3.6 GeV (the right-hand figure) with Ag nuclei in a solid angle close to 1 steradians. The points show experimental data.[55] The solid and the dashed histogram correspond to the calculations carried out within the framework of the CFE-model without and with regard for pre-equilibrium emission, respectively.

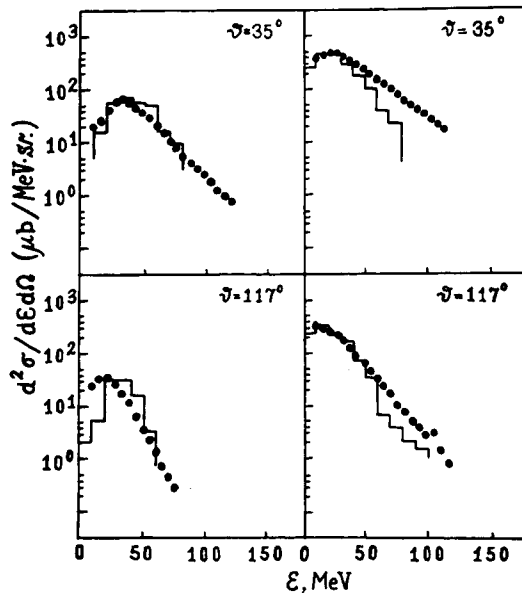

FIGURE 38. This charts the energy spectra of carbon fragments emitted in the interactions of ^{3}He of the energy 0.9 GeV (the left-hand figure) and 3.6 GeV (the right-hand figure) with Ag nuclei at different angles ϑ. The rest of notation is the same as in Figure 37.

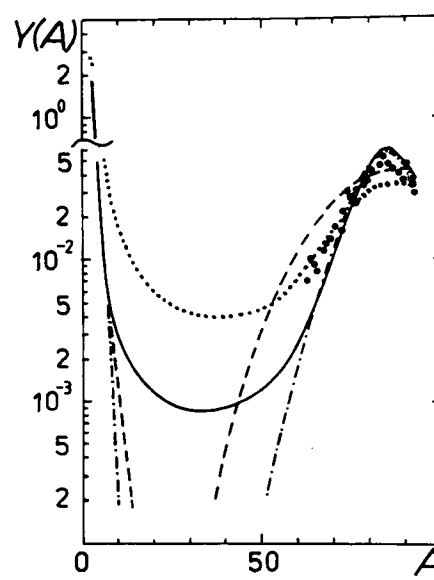

FIGURE 39. Here is the mass yield of R-nuclei (per one antiproton) produced in the annihilation of stopped antiprotons on a ^{95}Mo nucleus. The dots show experimental values.[57] The curves correspond to the calculations[56] by the following model: the dashed and the dash-dotted curve represent the calculations with and without trawling effect, respectively (evaporation), and the dotted and the solid curves correspond to the calculations without and with the trawling effect (the multifragmentation of thermalized R-nuclei), respectively.

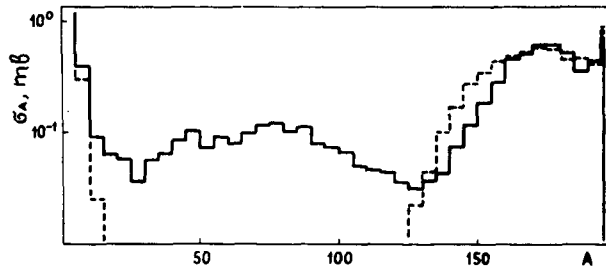

FIGURE 40. This shows the mass yield for the interaction of 1 GeV photons with ^{197}Au nuclei. The solid curve represents the calculations by the CFE-model and the dashed curve the calculations by the cascade-evaporation model.[18]

chart is formed in this interaction. For instance, neutron-deficient isotopes are predominantly created as a result of the deep spallation, light neutron-rich nuclides in the case of fragmentation and medium-weight neutron-rich nuclides in the case of fission. Cross-sections for production of radionuclides in the pA-interaction are large.[58] They are produced in large amounts in targets bombarded by a primary proton beam of a meson (or kaon) facility. Therefore, modern accelerators of intermediate energies can be applied for the production of high-intensity secondary beams of radionuclides along with their use for the production of high-intensity secondary beams of pions, kaons, and other elementary particles. There exist effective methods nowadays for extraction of radionuclides from a target, their separation and subsequent acceleration. These methods allow one to obtain, in principle, radioactive nuclear beams with intensities which are higher by several orders of magnitude than those obtained on modern heavy-ion accelerator complexes of intermediate energies (up to 10^{12} nuclei per second).[59]

Putting at the disposal of scientists unique possibilities of synthesizing nuclei lying far apart both from the β-stability line and from the domain of known nuclei, and of study of properties of such nuclei, the use of radioactive nuclear beams gives a new impetus to the development of modern nuclear physics. As an example of problems that can be apparently solved with the help of this method, we would like to cite the problem of the existence of superheavy double magic nuclei with $Z = 110\text{-}112$ and $N = 184$. With the help of beams of neutron-rich nuclei one can hope to bridge a broad gap between the domain of known heavy nuclides ($N \leqslant 162$) and the closed neutron shell $N = 184$. C-nuclei with low-excitation energy $E^* \lesssim 20$ MeV can be produced in a cold fusion of neutron-rich nuclei with a heavy T-nucleus.[60] This allows one to avoid adverse consequences of thermal damping of shell effects and to synthesize superheavy elements whose increased stability is caused exclusively by these effects. As another example, we would like to cite the problem of the synthesis of nuclides in the Universe. Nuclear reactions which proceed on radioactive T-nuclei play a pivotal role in the powering of many astrophysical objects from the sun to the supernova explosions. So, data obtained in experiments with radioactive nuclear beams are very important for nuclear astrophysics as a major keystone in modern physics. To develop new promising trends

in nuclear physics the projects aimed at production of high-intensity radioactive nuclear beams on proton accelerators of intermediate energies have been worked out.[59,61,62]

III. CONCLUSIONS

Fission as a process slow in comparison with the emission of particles can be used as a natural indication of the establishment of statistical equilibrium in R-nuclei. In the domain of T-nuclei whose fission barrier heights are well known, one can extract reliable information on the process of thermalization of an R-nucleus produced in deep inelastic interaction from the study of fission of nuclei by particles of relatively low energies ($\epsilon_0 \lesssim$ 100-200 MeV). On achieving the detailed comprehension of thermalization in such studies, we can go over to the domain of higher energies ($\epsilon_0 \approx$ 500-1000 MeV) in order to quantitatively investigate macroscopic thermal effects to which the height of the fission barrier and, hence, the fissility of a nucleus are especially sensitive. The use of correlations between the excitation energy E* and the value of the mass loss ΔA measurable in experiments seems very promising in the problem of determination of E*, which is one of the most important characteristics of a C-nucleus.

The investigation of multifragmentation of nuclei is a natural development and a complement for the study of nuclear fission in the domain of high energies ($\epsilon_0 \sim$ 1-10 GeV) of incident particles. Nuclei with the excitation energy from the threshold ($E^*_{thr} \approx$ 2-3 MeV/nucleon) up to the limiting value ($\sim$ 7-10 MeV/nucleon), that a nucleus as a whole can take on, can undergo multifragment breakup. Therefore, in such investigations, one can obtain, in principle, information not only on the evolution of the evaporation mechanisms of decay of highly-excited nuclei to the mechanism of explosive many-body breakup, but also on the high-energy part of the distribution over E* of the ensemble of thermalized R-nuclei.

A specific feature of NRs with intermediate-energy particles is that, unlike heavy ions, such particles bring relatively low values of the angular momentum and momentum in a nucleus and excite, mainly, single-particle degrees of freedom of a nucleus. This allows one to study thermal effects in nuclei in purer forms. Therefore, the study of properties and mechanism of decay of highly-excited nuclei produced in reactions with intermediate-energy particles supplement and enrich analogous investigations with heavy ions.

A broad spectrum of nuclides is produced in the deep spallation, fragmentation, and fission channels of deep inelastic pA-interaction. Making use of this phenomenon, we can obtain high-intensity radioactive nuclear beams on meson facilities (and in the future, on kaon ones as well).

REFERENCES

1. **Vandenbosch, R. and Huizenga, J.R.,** *Nuclear Fission,* Academic Press, New York, 1973.
2. **Swiatecki, W. J.,** Three lectures on macroscopic aspect of nuclear dynamics, in *Progress in Particles and Nuclear Physics,* Wilkinson, D., Ed., Vol. 4, Pergamon Press, Oxford, 1980, 383.
3. **Specht, H. J.,** Nucleus-nucleus collisions: Observations and expectations, *Nucl. Phys. A,* 400, 43c, 1983.
4. **Ngo, C., Gregoire, C., Remaud, B., and Tomasi, E.,** Fast fission: A dissipative mechanism following sometimes fusion, *Nucl. Phys. A,* 400, 259c, 1983.
5. **Iljinov, A. S., Cherepanov, E. A., and Chigrinov, S. E.,** Probability of nuclear fission induced by intermediate-energy particles, *Sov. J. Nucl. Phys.,* 32, 166, 1980.
6. **Barashenkov, V. S., Gereghi, F. G., Iljinov, A. S., and Toneev, V. D.,** Inelastic interactions of high energy nucleons with heavy nuclei, *Nucl. Phys. A,* 222, 204, 1974.
7. **Ivanova, N. S. and Pyanov, I. I.** Fission of uranium nuclei by high-energy protons, *Eksp. Teor. Fiz.,* 31, 416, 1956.
8. **Sugarman, N., Munzel, H., Panontin, J. A., et al.,** High-energy fission of U^{238}, *Phys. Rev.,* 143, 952, 1966.
9. **Lindner, M. and Osborn, R. N.,** Nonfission inelastic events in uranium and thorium induced by high-energy protons, *Phys. Rev.,* 103, 378, 1956.
10. **Pate, B. D. and Poskanzer, A. M.,** Spallation of uranium and thorium nuclei with BeV-energy protons, *Phys. Rev.,* 123, 647, 1961.
11. **Myers, W. D. and Swiatecki, W. J.,** Anomalies in nuclear masses, *Ark. Fysik,* 36, 343, 1967.
12. **Krappe, H. J., Nix, J. R., and Sierk, A. J.,** Unified nuclear potential for heavy ion elastic scattering, fusion, fission and ground state masses and deformations, *Phys. Rev. C,* 20, 992, 1979.
13. **Hasse, R. W.,** Studies in the shape dependence of the droplet model of nuclei, *Ann. Phys.,* 68, 377, 1971.
14. **Plasil, F., Awes, T. C., Cheynis, B., et al.,** Angular-momentum-dependent fission barriers in the rare-earth region, *Phys. Rev. C,* 29, 1145, 1984.
15. **Golubeva, Ye. S., Iljinov, A. S., and Mebel, M. V.,** Fission of nuclei as a result of stopped antiproton capture, *Nuovo Cimento A,* 103, 781, 1990.
16. **Iljinov, A. S., Mebel, M. V., Guaraldo, C., et al.,** Comparison of fission of heavy nuclei induced by different probes, *Phys. Rev. C,* 39, 1420, 1989.
17. **Polikanov, S.,** Meson, hyperon, and antiproton induced fission, *Nucl. Phys. A,* 502, 195c, 1989.
18. **Lucherini, V., Bianchi, N., De Sanctis, E., et al.,** Proposal of measuring the mechanism of nuclear excitation leading to fission with the ADONE jet-target photon beam, Preprint *LNF*-90/019 (R), Frascati, 1990.
19. **Fong, P.,** *Statistical Theory of Fission,* Gordon and Breach, New York, 1969.
20. **Nix, J. R. and Swiatecki, W. J.,** Studies in the liquid-drop theory of nuclear fission, *Nucl. Phys.,* 71, 1, 1965.
21. **Adeev, G. D., Gonchar, I. I., Pashkevich, V. V., et al.,** Diffusion model of formation of fission-fragment distributions, *Part. Nucl.,* 19, 529, 1988.
22. **Oganessian, Yu. Ts. and Lazarev, Yu. A.,** Heavy ions and nuclear fission, in *Treatise in Heavy Ion Sciences,* Bromley, D. A., Ed., Plenum Press, New York, 1985, Vol. 4, 1.
23. **Grange, P., Lu Jim-Qing, and Weidenmuller, H. A.,** Induced nuclear fission viewed as a diffusion process: Transitions, *Phys. Rev. C,* 27, 2063, 1983.
24. **Wada, T., Carjan, N., and Abe, Y.,** Multi-dimensional Langevin approach to fission dynamics, *Nucl. Phys. A,* 538, 283c, 1992.
25. **Frobrich, P. and Xu, S. Y.,** The treatment of heavy-ion collisions by Langevin equations, *Nucl. Phys. A,* 477, 143, 1988.

26. **Brack, M., Damgaard, J., Jensen, A. S., et al.,** Funny hills: The shell-correction approach to nuclear shell effects and its applications to the fission process, *Rev. Mod. Phys.*, 44, 320, 1972.
27. **Davies, K. T. R., Managan, R. A., Nix, J. R., and Sierk, A. J.,** Rupture of the neck in nuclear fission, *Phys. Rev. C*, 16, 1890, 1977.
28. **Randrup, J. and Swiatecki, W. J.,** One-body dissipation and nuclear dynamics, *Ann. Phys.*, 125, 193, 1980.
29. **Bohr, N. and Wheeler, J. A.,** The mechanism of nuclear fission, *Phys. Rev.*, 56, 426, 1939.
30. **Viola, V. E., Kwiatkowski, K., and Walker, M.,** Systematics of fission fragment total kinetic energy release, *Phys. Rev. C*, 31, 1550, 1985.
31. **Itkis, M. G., Okolovich, V. N., Rusanov, A. Ya., and Smirenkin, G. N.,** Symmetric and asymmetric fission of nuclei lighter than thorium, *Part. Nucl.*, 19, 301, 1988.
32. **Adeev, G. D., Botvina, A. S., Iljinov, A. S., Mebel, M. V., et al.,** Method of calculation of mass-energy distributions of fragments of fission of nuclei by intermediate energy particles, Preprint INR 816/93, Moscow, 1993.
33. **Adeev, G. D.,** Influence of dynamic characteristics of fission on formation of charge distribution of fragments, *Part. Nucl.*, 23, 1572, 1992.
34. **Wang Fu-cheng and Hu Ji-min,** A study of the multimode fission model, *J. Phys. G: Nucl. Part. Phys.*, 15, 829, 1989.
35. **Brosa, U., Grossmann, S., and Muller, A.,** Fission channels in ^{258}Fm, *Z. Phys. A*, 325, 241, 198.
36. **Cuninghame, J. G.,** Present status of data on fission fragment yields, in *Nuclear Data on Fission Products*, Vol. 2, Atomizdat, Moscow, 1979, 87 (in Russian).
37. **Hofmann, P., Iljinov, A. S., Mebel, M. V. et al.,** Fission of heavy nuclei induced by stopped antiprotons. I. Inclusive characteristics of fission fragments, *Phys. Rev. C*, 1993 (to be published).
38. **Perfilov, N. A., Lozhkin, O. V., and Ostroumov, V. I.,** *Nuclear Reactions Induced by High-Energy particles*, USSR Academy of Sciences Press, Moscow, 1962.
39. **Bondorf, J. P., Botvina, A. S., Ilyinov, A. S., et al.,** Statistical multifragmentation of nuclei, *Phys. Rep.*, to be published.
40. **Lynch, W. G.,** Nuclear fragmentation in proton- and heavy-ion-induced reactions, *Annu. Rev. Nucl. Part. Sci.*, 37, 493, 1987.
41. **Gross, D. H. E.,** Nuclear physics with heavy ions — Many body systems with specific flavour, *Nucl. Phys. A.*, 428, 313c, 1984.
42. **Botvina, A. S., Iljinov, A. S., and Mishustin, I. N.,** Multifragment breakup of nuclei by intermediate-energy protons, *Nucl. Phys. A*, 507, 649, 1990.
43. **Campi, X., et al.,** Sum rules study and scaling property of fragmentation mass yield curves, *Phys. Lett.* B, 138, 353, 1984.
44. **Andronenko, L. N., et al.,** Mass-yield distribution for 1 GeV proton induced nuclear reactions on Ni and Ag, *Phys. Lett. B*, 174, 18, 1986.
45. **Katcoff, S., Fickel, H. R., and Wyttenbach, A.,** Distribution of radionuclides from interaction of 3- and 29 GeV protons with silver, *Phys. Rev.*, 166, 1147, 1978.
46. **Westfall, G. D., Sextro, G. R., Poskanzer, A. M., et al.,** Energy spectra of nuclear fragments produced by high energy protons, *Phys. Rev. C*, 17, 1368, 1978.
47. **English, G., Porile, N. T., and Steinberg, E. P.,** Nuclear reactions of silver with 11.5-GeV protons, *Phys. Rev. C*, 10, 2268, 1974.
48. **Barashenkov, V. S. and Toneev, V. D.,** *Interaction of High Energy Particles and Nuclei with Atomic Nuclei*, [in Russian] Atomizdat, Moscow, 1972.
49. **Sangster, T. C., Bajak, A. T., Carmony, D. D., et al.,** Light-fragment production in proton-xenon interactions between 1 and 19 GeV, *Phys. Lett. B*, 188, 29, 1987.
50. **Hirsch, A. S., Bujak, A. T., Finn, J. E., et al.,** Experimental results from high energy proton nucleus interactions, critical phenomena and the thermal liquid drop model of fragment production, *Phys. Rev. C*, 29, 508, 1984.
51. **Poskanzer, A. M., Butler, G. W., and Hyde, E. K.,** Fragment production in the interaction of 5.5-GeV protons with uranium, *Phys. Rev. C*, 3, 882, 1971.

52. **Warwick, A. I., Wieman, H. H., and Gutbrod, H. H.,** Break-up of spectator residues in relativistic nuclear collisions, *Phys. Rev. C,* 27, 1083, 1983.
53. **Gagarin, Yu. F. and Ivanova, N. S.,** Fragment production on emulsion nuclei induces by 7.5 BeV π-mesons, *Eksp. Teor. Fiz.,* 45, 1793, 1963.
54. **Katcoff, S.,** Interactions of 3.7 GeV/c antiprotons with Ag and Br, *Phys. Rev.,* 157, 1126, 1967.
55. **Pollacco, E. C., Volant, C., Dayras, R., et al.,** Search for the onset of multifragmentation in the reaction ^{3}He + ^{nat}Ag, *Nucl. Phys. A,* 519, 197c, 1990.
56. **Golubea, Ye. S., Iljinov, A. S., Botwina, A. S., and Sobolevsky, N. M.,** Inelastic interactions of intermediate-energy antinucleons with nuclei, *Nucl. Phys. A,* 483, 539, 1988.
57. **Moser, E. F., Daniel, H., von Egidy, T., et al.,** Residual nuclei after antiproton annihilation in Mo and Ho, *Z. Phys. A,* 333, 89, 1989.
58. **Iljinov, A. S., Semenov, V. G., Semenova, M. P., Sobolevsky, N. M., and Udovenko, L. V.,** *Production of Radionuclides at Intermediate Energies,* Landolt-Bornstein, Vol. 13, Springer-Verlag, Berlin, 1991.
59. **Iljinov, A. S., Lobashev, V. M., and Oganessian, Yu. Ts.,** Prospects for studies with radioactive nuclear beams from the Moscow meson factory, in *Proc. 1st Int. Conf. Radioactive Nucl. Beams,* Myers, W. D., Nitschke, J. M., and Norman, E. B., Eds., World Scientific, Singapore, 1990, 23.
60. **Iljinov, A. S., Mebel, M. V., and Cherepanov, E. A.,** The possibilities of synthesizing heavy elements with radioactive nuclear beams, in *Proc. 1st Int. Conf. Radioactive Nucl. Beams,* Myers, W. D., Nitschke, J. M., and Norman, E. B., Eds., World Scientific, Singapore, 1990, 289.
61. **Nomura, T.,** Exotic nuclei arena in Japanese hadron project, in *Proc. 1st Int. Conf. Radioactive Nucl. Beams,* Myers, W. D., Nitschke, J. M., and Norman, E. B., Eds., World Scientific, Singapore, 1990, 13.
62. **Buchmann, L., Vincent, J. S., D'Auria, J. M., et al.,** Proposals and estimates for an experimental program at ISAC, in *Proc. 1st Int. Conf. Radioactive Nucl. Beams,* Myers, W. D., Nitschke, J. M., and Norman, E. B., Eds., World Scientific, Singapore, 1990, 46.

Taylor & Francis
Taylor & Francis Group
http://taylorandfrancis.com

INDEX

A

Absorption probability, radial distribution of, 256
Accelerators, high-current proton type, 173, 183
Actinides, double-humped structure of fission barrier in, 124–126
Additive quark model, 95
(α,γ) reaction, data on level spacing obtained in, 122
(α,n) reaction, data on level spacing obtained in, 122
α-type particle, probability of emission of, 81
Aluminum-27, parameters Q and n of nuclei of, 74
Analyzing power, 179
  derivation of, 171–173
Angle of incidence, angle of refraction relation to, 87
Angular momentum
  dependence of fission barrier on, 118
  high
    decay of C-nucleus with, 115–118
    effect on nuclear properties, 117–118
  for production of C-nucleus, 129
  of R-nuclei, 44, 92, 232–237
  of zero, decay of C-nucleus with, 99–114
Annihilation, in $\bar{p}$p-interaction, 260
Antinucleons
  annihilation on nuclei, 255–295
  potentials of interaction between other particles and, 12
  production of, 173
  refraction and reflection of, 263
Antiprotons
  absorption by nuclei, 198
    cascade model for, 259–263
    at nuclear periphery, 256
    OC-model for, 255–263
  charge exchange reaction of, 265
  production of, 173
    cross-sections for, 197–198
    inclusive cross-section for, 197
    in proton-nucleus interactions, 195–199
    subthreshold, 196, 198
Astrophysics, radioactive nuclear beam experiment importance in, 349
π–Atom, de-excitation of, 216
$\bar{p}$–Atom, formation of, 255
Atomic electromagnetic cascade, in absorption of π^--mesons, 216
Auger-electrons, 216, 218
  emission by antiprotons, 255
Auger transitions, 218

B

Baryonic resonances
  cross-sections for production of, 91
  use as dynamical sources for P-, D-, and S-wave interactions, 280
Baryons, single-particle phase functions of, 197
BBGKY-hierarchy, use in quantum statistical mechanics, 48
b (black)-particles
  classification and properties of, 199–201
  production and multiplicity of, 5
Bessel function(s), 73, 77, 179
  spherical, 117
Bethe-Weizsacker formula, 138
Binding energy
  of inverse reaction for emitted particles, 83
  of a nucleus, 22
  of particles, 100
  total, 132
Boltzmann equation, 35, 52, 146, 248–249
  generalization of, 36
Boltzmann statistics, fragments assumed to obey, 138
Boltzmann-Uehling-Uhlenbeck equation, 180–181
  linearization of, 37–39
  use to describe INC, 35–37, 52
Breakup, probability of, statistical weight and, 137
Breakup channel, description of, 132
Breakup volume, decay of nucleus in, 132

C

Calcium-41, level density of, energy dependence, 108
Canonical approximation, statistical model of multifragmentation based on, 139, 142
Canonical equations

for dynamical many-particle systems, 15–16
solution of, use in phase-density expression, 25
Carbon-12 nucleus, pion production by protons on, 180
Cascade component, of cross-section, 173
calculation, 71
Cascade-evaporation model, 307
Cascade-exciton model, 92, 160
Cascade-fragmentation-evaporation model, use to describe multifragmentation, 334–335, 338–339, 341–343
Cascade model, of deep inelastic interactions of antinucleons with nuclei, 259–263
Cascade nucleons
coalescence of, 266
cross-section for production at low energies, 75–80
definition of, 55
distribution functions of, 71
solution of equations for, 168–171
Center-of-mass system of coordinates, anisotropy of NN-scattering in, 58
Channels, deep inelastic, in interaction between high-energy particle and nucleus, 87
Channel temperature, determination by energy balance equation, 137–138
Charge distribution, of fragments, calculation, 316
Charge exchange, as channel of $\bar{N}N$-interaction, 261
Charge exchange reactions
of antiprotons on nucleus, 265
involving pions, 176–177, 181, 240, 242, 245
in πN-channel, 89
Chemical potential, 102
Closed shell, fission barrier increase and, 124
C-nucleus
decay of
with angular momentum, 115–118
in heavy-ion-induced reactions, 128–130
probability per unit time of, 100
statistical model, 99–101
total probability of, 100
emission of heavy clusters from, 127–128
excited, properties and decay of, 122–130
fission of, fragment distributions in, 319–324
formation of, 2
cross-section for, 100, 128
limiting angular momentum for, 129
lifetime of, 122, 130
with zero angular momentum, decay of, 99–114
Coalescence model, 161
Cold fusion, of neutron-rich nuclei, 349
Collective effects, in nuclei, 124
Collision problem, quantum formulation of, 5–14
Collisions
of heavy ions, 50
subsequent, mean time interval between, 22, 47, 50
Collision term
for collisions inside nucleus, 48, 50–51
derivation of, 24–25, 47, 49
Pauli blocking factor introduction into, 49
Pauli exclusion principle incorporation into, 27–29
Combinatorial method, use in calculation of ρ, 101
Complex particle, probability of formation of, 83
Compound nucleus, see C-nucleus
Continuous spectrum, single-particle state of, 81
Copper-64, parameters Q and n of nuclei of, 74
Coulomb barriers
for emitted particles, 100–101, 113–114
inverse reaction, 83
in many-body multifragment breakup, 341
Coulomb component, of liquid-drop energy of nucleus, 112
Coulomb energy, redistribution of, between fragments at stage of divergence, 149
Coulomb field, 87, 171–172
Coulomb interaction, between charged pion and nucleus, 183
Coulomb potential, 75
Coulomb term, in expression of free energy of a fragment, 138
Coupled-channel isobar model, πN-, ηN-, and πNN-systems, 280
Coupling, absence of, between vectors **I** and l, 116
"Cracking" phase transition, in finite nuclear system, 143
Cross-section(s)
of absorption and reaction, as function of pion energy, 245
definition of, 2
for elastic scattering, 240
expressions for, 39–40
inclusive, 43, 55
for production of secondary nucleons, 155–163

of inelastic interaction, 55–60
partial, of channels, 88
of quasifree nucleons, 55–60
topological and exclusive, 42–43
Cut-off energy, definition of, 91–92

D

de Broglie wavelength
of incident particle, 11, 91, 93, 129
of j-particle, 115
mean free path of pion and, 51
Decay
of C-nucleus with high angular momentum, 115–118
of excited C-nuclei, 122–130
explosive, of hot nuclei, 130–150
of highly excited nuclei, 99–154
Decay width, of ρ-mesons, 278
De-excitation, of primary fragments, 145
Deformed nuclei, rotation enhancement of level density of, 109
Density
of final states, 82
of nucleus, 256
of single-particle states, 103, 105
Density matrix
definition for, 17
Liouville-von Neumann equation in determination of, quantum effects, 44–45
role in quantum theory, 18
use in statistical description of dynamical many-particle systems, 14, 16
Density operator, definition for, 17
Depolarization tensor, 167
Detailed balance, principle of, 115
Differential elastic scattering cross-section
definition of, 3
of elastic NN-scattering, 13
Diffuse layer, of nucleus, thickness of, 256
Diffusion model, of formation of fragments by fission of C-nuclei, 310
Dipole E1-transitions, role in γ-quanta emission, 119
Dipole isovector vibrations, role in charge distribution of fragments, 316–317
Dipole matrix elements, of hydrogen-like atom, 218
Direct process, nuclear reactions as, 2
Discrete single-particle spectrum, 103
Distorted wave impulse approximation (DWIA), 62, 68, 240
calculation of matrix elements by, 13
quasifree component of cross-section calculated in, 160
Doppler effect, use to measure recoil momentum, 237
Double differential cross-sections
expression for, 73
for production of π^+-mesons, 178
for production of α-nucleons, 174
for production of secondary protons, 158–163
Double-humped structure, of fission barrier in actinides, 124–127
(d,p) reaction, data on level spacing obtained in, 122
Dual parton model, 95
Dynamical many-particle systems, statistical description of, 14–19
delta(1232) dynamics, 287

E

Effective field(s), 47
of a nucleon, 24
Effective nuclear potential, for pions, 179
Effective nuclear potential field, 56
Effective potential, 174
Eikonal (diffraction) approximation, 13, 63, 241
definition of, 12
validity of, 11
Elastic channel, number of particles in, 11
Elastic collision, probability of, 26
Elastic scattering, 2
as channel of NN-interaction, 261
cross-section of, 11, 89
differential cross-section of, 12
in πN-channel, 89
of nucleon on nucleus, 60
in pp-interaction, 260
Electromagnetic interaction, 245
Electron scattering, charge distribution obtained in experiments on, 86
Elements, superheavy, synthesis of, 349
Emitted particles, lifetime of, 100
Energy, intermediate, polarization effects in inclusive nucleon-nucleus reactions at, 163–173
Energy balance equation, 133
use to determine channel temperature, 137–138
Energy-momentum conservation law, 221
Energy spectra, of secondary nucleons, 155–158, 160

Entrance channel
  cross-section of reaction proceeding from, 99–100
  transmission coefficient for, 116
Entropy, 102, 104, 107
  for system of noninteracting fermions, 103
Equidistant scheme, of single-particle levels, 105
Equidistant single-particle spectrum, 82
Equilibrium deformations, of nuclei, 110, 118
Equilibrium statistical model, validity of, 132
Ericson fluctuations, data from measurements of, 122
Ericson's standard optical πA-potential, 216–217
η value, as ratio of probability of annihilation on neutron to that on proton, 259
Evaporation, particle emission resembling, 22
Evaporation cascade
  in absorption of π^--mesons, 216
  calculation methods for, 118–122
    Monte Carlo technique, 121
  fluctuations in, 122
  multifragment decay compared to, 146–150
Evaporation model, 130, 222
  INC-model supplemented with, 75, 81
  statistical properties of nuclei and, 122
  use to describe de-excitation of light nucleus, 134–135
Excitation, of discrete nuclear levels, 158
Excitation energy, 81
  effects on macroscopic properties of nucleus, 111–114
  of fragments, 318
  of a nucleus, 22, 92
  R-nuclei distribution and, 44
  threshold, for multifragment decay of nuclei, 335
Excited particles, 81
Exciton model
  characteristics of, 81, 222
  master equations of, 92
Exciton number, 81
Excitons, coalescence of, 267
Exclusive cross-sections
  for escape of nucleons, 42–43
  of reaction, 3
Exit channel
  cross-section of reaction ending at, 99–100
  highly-excited C-nucleus decay in, 118
Expansion time
  collective, 150
  derivation of, 137
Explosive breakup, of highly excited R-nucleus, 334–335

F

Fermi breakup
  calculation by Monte Carlo technique, 133–134
  of light nuclei, 132–135, 226
  of R-nucleus, 267
Fermi energy, 221, 230
  enhanced, model of three-zone nucleus with, 157
  notation for, 28, 104
  of α-nucleons, 87
  nucleons with energy lower than, 85
  of protons and neutrons, 57, 86
Fermi gas
  consisting of two particle types, 106
  with constant density, 105
  of nucleons, 165–166
    relaxation, 80
  nucleus behavior as, 62, 86, 108
  strongly degenerate, 105
Fermi gas distribution, 181
Fermi gas model, 44, 115, 158
  of degenerate nucleons, 28
Fermi liquid, nucleus considered as, 106
Fermi model, for multiple production of particles, 257
Fermi momentum, 168
  notation for, 28
Fermi momentum distribution, of intranuclear nucleons, 93
Fermi motion
  effect on distributions of nucleons, 66, 68
  effect on indicatrix of elastic scattering of excited nucleons, 76
  of intranuclear nucleons, 168, 173–174, 181, 284, 288
  of a partner, 88
  in quasifree pN-collision, 172
Fermions, thermodynamic potential of, 102–103
Fermi statistical model, use in calculation of nucleon momenta, 221
Fermi surface, 103
Fermi systems
  open finite type, quantum kinetic equations for, 83
  theory of finite, 106, 114
Fission

asymmetric, 319
cross-section of, 247
fast, time of, 297
multimode nature of, 319
of nuclei by intermediate-energy particles, 297–353
Fission barrier, dependence on angular momentum, 118
Fission barrier height, 119
decrease in, 113, 118
of heavy transuranium nuclei, 124
Fission fragments
incorporation in intranuclear cascade model, 4
mass-energy distribution of, 309–333
Fission saddle point
density of levels of nucleus at, 123
rotational energy of nucleus at, 118
Fission valley, 311
Fission width
of double-humped barrier, 127
expression for, 119
Fluctuation mechanism, of nuclear twisting, 236–237
Flux, of primary nucleons, 55
Fokker-Planck equation, 310
Fourier transformation, 66–67, 169
Fragments, formation from explosive breakup of highly excited R-nucleus, 334–335
Free energy
expression for, 110
of f channel, 138
solution of equations for, 113
Free volume, accessible to translational motion of fragments, 139

G

Gamma function, 133
γN-collisions, characteristics of secondaries produced by, 91
(γ,n) reaction, data on level spacing obtained in, 122
Gaussian distribution, of nucleon density, 70
Gaussian form, for optical potential of incident and quasifree nucleons, 63
Gaussian nuclear density, 190–191
Geometrical cross-section, 101
g (grey)-particles, classification and properties of, 199–201, 208, 249
Giant dipole resonance, parameters of, 119
Gibbs potential, 112
Glauber-Sitenko approximation, 12, 48
Gluons, transition to hadrons, 95
Grand canonical ensemble, 102
Green functions, 25, 175
for pions, 176–177
single-particle, 249

H

Hadronization length, 95
Hadron-nucleus interaction, 4, 95, 122, 191–192
elastic scattering and total cross-section of, 12
results of, 204
Half-density radius, 219
Hamiltonian
for dynamical many-particle systems, 15, 18
of INC-model, 23–24
Hamiltonian formalism, problems associated with, 16
Harmonic-oscillator model, 63
Harp-Miller-Berne model, INC-model and, 80
Hartree-Fock equation, 111
Hartree-Fock method, use in studies of thermal effects on nuclei surfaces, 111–112, 114, 136
Hartree-Fock model, time-dependent, 26
Heavy-ion-induced reactions, decay of C-nuclei produced in, 128–130
(^{3}He,d) reaction, data on level spacing obtained in, 122
Heisenberg S-matrix, 7
Heisenberg uncertainty principle, 8, 19
(^{3}He,α) reaction, data on level spacing obtained in, 122
h (heavy)-particles, classification and properties of, 199–201, 208, 249, 268
High-momentum component, 198
High-spin isomeric states, excitation of, 232–237
Hilbert space, 6
Holes
exciton number and, 81
formation of, 21
Hot nuclear matter, first-order phase transition in,
multifragmentation as sign of, 333–334
Hot nuclei, explosive decay of, 130–150
Hydrogen-like atom, wave functions of, 218
Hypercharges, production and form of, 278
Y-Hyperon, rest masses of, 187
Hyperons
production of, 173
rest masses of, 185

I

INC, see also INC-model; INCT-model
calculation of, 94
exclusive description of, 23–35
general scheme for calculation of, 85
inclusive description of, 35–39
initial conditions of, 240
at low energies, 75–83
macroapproximation use in calculation of, 33
models of antinucleon-nucleus annihilation based on, 255–263, 271
quantum-mechanical effects at initial stage of, 68
trawling effect in, 93–95
Inclusive cross-section(s)
definition of, 5
for escape of nucleons, 43
of nucleon-nuclear reactions, 39, 163
for production of secondary nucleons, 55
quasifree component of, 60–64
Inclusive differential cross-section(s)
definition of, 4
for quasifree knockout of nucleons, 14
Inclusive invariant cross-section, definition of, 4–5
INC-model, 16, 21–54, 163, 222, 245, 334
basic assumptions of, 21–23
calculations for, 49
as description of collision between particle and nucleus, 21, 51–52
formulation of problem in, 21–22
kinetic equations for, 163
analytic methods, 55–60
solution, 55–99
with mesonic resonances, 282–283, 287
nucleon-nuclei interaction analysis based on, 155–214
phase density and Hamiltonian of, 23–24
quantum effects in, 44–51
use of Wigner probability function for substantiation of, 19
validity conditions of, 48, 51, 240
Walecka version (model) of, 50
INCT-model, 93–95, 206, 249, 271, 336
Inelastic interaction
average cross-section of, 73
between nucleon and nucleus, cross-section of, 79
total cross-section of, 41–42
Initial nonequilibirum state, of excited nucleus, 81
Interaction
elementary, calculation of, 88–91
strong, time duration of, 95
Interaction point, particle search for, 88
Intranuclear cascade, see INC
Intranuclear cascade model, see INC-model
with trawling, see INCT-model
Intranuclear nucleonic cascade, in absorption of π^--mesons, 216
Intranuclear nucleons, high-momentum component of, 181, 193
Invariant inclusive cross-sections, for production of various fast secondaries, 161
Inverse reaction
cross-section of, 100–101, 119
of emitted particle, 83
Iron-56, level density of, energy dependence, 108
Isobar model, elementary interaction described by, 91
Δ-Isobars
incorporation in development of INC, 248–249
pion creation through production of, 91
production in nuclear matter, 50, 181
Isomeric ratios, 235
dependence on number of emitted neutrons, 236
Isomers, population of high-spin type, 272
Isospin effects, role in pion absorption, 220
Isotopes, yield of, excitation energy of R-nuclei and, 230–232
Isotopic invariance, cross-section derivation from, 89
Isotopic invariance hypothesis, 181
Isotopic spins, 278

K

Kaon facilities, construction of, 173, 183
Kaons
potentials of interaction between other particles and, 12
production of, 173, 187–188
by intermediate pions, 193
transport in nucleus, 189
two-nucleon absorption of, 285
Kinetic equations
for absorption of pion by nucleus, 220
for INC-model, 163
for cascade nucleons in P_1-approximation, 70–75

small-angle approximation, 64–70, 76
solution, 55–99
for intranuclear nucleonic-mesonic cascade, 174–175
general scheme of solution, 175–179
linear system of, 37
for open finite Fermi systems, 83
for quasifree nucleons, 165–168
use to describe nuclear relaxation, 81
Kisslinger potential, 218
Klein-Gordon equation, 217, 241
Knocked-out nucleons
distortion of wave function of, 63
total number of, 79
Knockout process, 227
K^+p (K^+n)-interaction, total free cross section of, 190
Kronecker δ-symbols, 6, 15

L

Landau-Vlasov equation, 35
Langevin equations, 310
Legendre polynomial, 73, 116
Level density
collective enhancement of, 109
dependence on angular momentum of nucleus, 115
extrapolation of, 110
in fission saddle point, 119–120, 123–124
of highly excited nuclei, 101–106
parameter a of, 106–107
Fermi-gas value, 106–107
rotation enhancement of, 109
Level spacings, in particle emission, 22
Light fragments, emission of, 22
Light nuclei, 118
Fermi breakup of, 132–135
incorporation in intranuclear cascade model, 4
Limiting temperature, 132
Liouville equation, 15, 28
analysis of collision term in, 93
applications of, 18
classical, 47
formulations of, 16, 24, 28, 51
integral forms of, 29–32
solution in form of von Neumann series, 32–33
phase density and, 14–16, 19
problems associated with, 16
specific forms of, 23
Liouville-von Neumann equation
in determination of density matrix, quantum effects, 44–45
transformation to classical form, 45–48
Liquid-drop fission barrier, temperature dependence of, 307
Liquid-drop model, potential energy surface in, 311
Liquid-drop properties, of nucleus, 106–107, 109–110, 112, 124–125
Liquid-gas phase transition
critical temperature of, 138
in hot nuclear matter, 136
Local density approximation, 223, 244
Lorentz-Lorenz effect, 245
Low-density approximation, 242, 247–248
Low-energy particles, C-nuclei produced in reactions with, 122
Low-lying bound states, data obtained from analysis of, 122

M

Macroapproximation, 166
definition of, 33–35
in linearization of Boltzmann-Uehling-Uhlenbeck equation, 37
use in calculation of INC, 33–35, 39, 43, 84, 93
Macrocanonical approximation, statistical model of multifragmentation based on, 139, 144
Macroscopic properties
of highly excited nuclei, 101
of nucleus, changes caused by excitation energy, 111–114
Macroscopic thermal effects, on nucleus, 111
Magic nuclei
existence of superheavy double type, 349
level density in vicinity of, 106–107
Manganese-55, level density of, energy dependence, 108
Marshak condition, 72
Master equation(s)
of exciton model, 92
use to describe nuclear relaxation, 81
Matrix element, 82
Mean free path, of nucleons in nucleus, 47, 50
Medium-weight nuclei, multifragment breakup of, 136–150
Mellin transformation, 66–67, 71, 77, 169
Meson facilities, 173, 215, 239–240
Mesons
heavy, two-nucleon absorption of, 285

interaction of resonances of, with nuclei, 277–292
production of
cross-sections for, 91
heavy type, 277
in NN-collisions, 165, 174
resonances of, production in NN-annihilation, 278–279
η-Mesons
bound states in nuclei, 287–292
energy spectrum of, 290
interaction with nucleons, 279–282
near threshold production of, 287–292
production by secondary pions, 290
production in NA-annihilation, 283–287
subthreshold production of, 193–194
two-nucleon absorption of, 280
K^+-Mesons
production of, 173
in pA-collisions, 183–192
in proton-nucleus interactions at various energies, 187–195
rest masses of, 185
ω-Mesons
decay mean free path of, 279
interaction with nucleons, 279–282
near threshold production of, 287–292
in nonet of vector mesons, 287
production in NA-annihilation, 283–287
ρ-Mesons, decay width of, 278–279
Microcanonical approximation, statistical model of multifragmentation based on, 139–142, 144
Moment of inertia, of a nucleus, 109
at saddle point, 118
Momentum, of R-nucleus, 92
Momentum distribution
of intranuclear nucleons, 157, 160, 244
high-momentum component in, 161, 163
of nuclear nucleons, derivation, 64
of nucleons in incident nucleus, 206
Monte Carlo technique, 49, 257
Fermi breakup simulation by, 133–134
solution of kinetic equations of INC-model using, 83–95
use in calculation of double differential cross-sections of secondary protons, 160
use in calculation of evaporation cascade, 121
use in simulation of particle in cascade, 33, 35, 52, 93
use in solving hadron-nucleus interactions, 191–192
use in studies of multifragmentation, 139, 143
mπA-interaction, multiplicity of, 271–272
Multifragmentation
basic properties of, 139–143
definition of, 136
evaporation cascade compared to, 146–150
fragment formation time in, 150
mass spectrum studies of, 147–148
of nuclei by intermediate-energy particles, 297–353
simulation of, 143–146
statistical model of, 136
threshold of, 140, 341
Multifragment breakup, of medium-weight nuclei, 136–150
Multinucleon associations
momentum of, 237
role in pion absorption, 220–221, 225, 228
Multipion-nucleus interaction, 255
incoherent, 263–277
emitted particle characteristics, 263–271
Multiplicity
average, of cascade nucleons, 78, 80
of type b particles, 5

N

NA-annihilation, production of η- and ω-mesons in, 283–287
NA-interaction, 11
profile function of, 12
NA-reactions
inclusion polarization characteristics of, 164–165
inelastic, 163
Neutron halo, 259, 264
Neutron resonances
data on spacings between, 122
level density from data on, 106
Neutrons, emission of, 222
Neutrons N, distributions of R-nuclei over, 43–44
Nickel-60, level density of, energy dependence, 108
$\bar{N}N$-annihilation
complex particle emission in, 266
description of, 261
mesonless, 271
production of mesonic resonances in, 278–279
single-meson, 271
statistical model with SU(3)-symmetry of, 278–279

NN-collision(s)
antiproton production in, 196
characteristics of secondaries produced by, 90–91
elementary subprocesses for, 89
first, quantum-mechanical description of, 160
inelastic, expansion in number of, 175–176
meson production in, 23, 174
Monte Carlo generators of, 95
pion production in, 173, 177
threshold, 179
polarization effects in, 163, 167, 171
tensor of transfer of polarization in, 167
NN-interaction
in INC-model, 260
long-range part of, 50
parameters of, 171
polarization characteristics of, 173
separation of, 24
short-range parts of, 47
spin dependence of, 163
n-$\bar{n}$ oscillations, registration in vacuum, 292
NN-scattering
in c.m.s., 58, 65, 178
elastic, 168
differential cross-section of, 13
within a nucleus, 13
nn-scattering, description of, 167
Nonlocal processes, role in antiproton production, 198
Notation, 1
np-scattering, description of, 167
Nuclear density
derivation of, 112
distribution of, 219
Gaussian representation of, 190–191
Nuclear fission
liquid-drop barrier for, thermal decrease in height of, 113
surface of potential energy in, 110
Nuclear levels
density of, 100
widths of, 99
Nuclear mass, shell correction in formula for, 107
Nuclear matter, effect on collisions of nucleons in nucleus, 49
Nuclear potential, effect on projectile momentum, 84
Nuclear reaction(s)
cascade stage of, 39–40
characteristics of, 39–44
collective effects in, with intermediate energy particles, 337
cross-sections of, classification, 2–5
as direct processes, 2
evaporation stage of, 39
exclusive description of, 3
as independent binary collisions, 75
pre-equilibrium emission stage of, 39
process of, 21
quantum-mechanical models of, 10
Nuclear scaling, in nuclear reactions, 161
Nuclear shells
effects of
disappearance, 106–110
influence, 107
knockout of, 106
Nuclear surface
diffuseness of, 48
structure of, 157, 173
Nuclear viscosity, two-body nature of, 312
Nuclei, see Nucleus (nuclei)
Nucleon(s)
cascade-type, definition, 55
collisions of, in nuclear matter, 27
density of, 24
distribution in first generation, 55
elastic collision of, 26
elastic scattering of pions on, 176
emission of, 118
excited
approximation of Liouville equation and, 33
definition of, 21
free quiescent, indicatrix of scattering on, 58
frozen, approximation of, 93
Gaussian distribution of density of, 70
interaction with nuclei, 155–214
intranuclear
density of, 60, 169
distribution of, 86
momentum distribution of, 157, 160, 244
particle collision with, 21
pion scattering by, 240
unexcited, 175
wave function of, 14
last, energy required for separation of, 87
mean density of, 57
mean energy of separation of, 58
momenta of pairs of, 221
in nuclear matter, mean free path, 60
numbers of, in R-nucleus, 92
potential acting on, 87
primary

flux of, 68
single-particle phase density of, 167
quasifree, definition of, 55
quasifree knockout of, 5, 12
inclusive differential cross-section of, 14
radius of core of, 93
secondary, see Secondary nucleons
energy distribution, 73
energy spectra and average multiplicities of, 155–158
inclusive cross-sections for production of, 155–163
secondary and higher, distributions, 68
unexcited, phase density of, 33
uniform distribution of density of, 69
unpolarized
elastic scattering, 167
interaction with nucleus, 170
Nucleonic cascade, 175
Nucleonic-mesonic cascade, intranuclear, kinetic equations for, 174–179
Nucleon-nucleon collisions, polarization effects in, 62
Nucleon-nucleus absorption
of one nucleon, 261
of two nucleons, 261
Nucleon-nucleus reactions, at intermediate energies, polarization effects in, 163–173
α-Nucleons
double differential cross-section for production of, 55, 62, 69, 80, 165, 174
flux density of, 174
single-particle phase-space distribution function of, 27
Nucleus (nuclei)
annihilation of antinucleons on, 255–295
models of, 255–263
boundary of
definition, 21
particle departure from, 21
complete fusion of, formation of C-nucleus from, 128
with diffuse boundary, 60
diffuse layer of
pion interaction in, 247
thickness of, 112
distribution of, production in INC, 43–44
equilibrium deformations of, 110
fission by intermediate-energy particles, 297–353
parametrization of nuclear shape in, 311
probability of, 298–309
global properties of, temperature dependence of, 111
hadron interaction with, elastic scattering and total cross-section of, 12
high angular momentum effects on properties of, 117–118
highly excited
decay and properties of, 99–154
effects on structure, 106–114
general pattern of decay, 118–122
level density, 101–106
macroscopic properties, 101
shell knockout in, 106
statistical equilibrium in, 80
statistical properties, 103
interaction of mesonic resonances with, 277–292
lightest, nucleon interaction with, 155–214
liquid-drop energy of, components of, 112
liquid-drop properties of, 106–107
as a local Fermi gas of nucleons, 62
multifragmentation by intermediate-energy particles, 297–353
neutron-rich, cold fusion of, 349
potentials of interaction between other particles and, 12
quantization of energy levels of, 60
single-particle degrees of freedom of, 101
superheavy double magic type, 349
surface area of, 109
surface layer of, 218, 234
thermal effects on, 109
surface tension of, 113
thermodynamic properties of, 114
Nucleus-nucleus optical potential, 129
Nuclides, synthesis in Universe, 349

O

Occupation numbers, of single-particle nuclear states, 80, 112
OC-model, 245
for absorption of antiprotons by nuclei, 255–263
analysis of interference effects in INC using, 48–49
comparison with other methods of calculation, 247–248
for inelastic πA-interaction, 240–245
of pion absorption, 215–222
use for first collision of incident particle in nucleus, 49–51

Open channels, c.m.s. of, 9
Optical πA-potential, of second order, 241
Optical + cascade model, see OC-model
Optical model, 12–13, 24
  use in calculations of inverse cross-sections, 100–101
  use to describe elastic scatter of particles, 10
Optical p̄A-potential, 262
  form of, 256
Optical potential
  definition of, 10–11
  energy of primary nucleon related to depth of, 13
  of incident and quasifree nucleons, Gaussian form, 63
  parameter of diffuseness in, 48
Optical theorem, 11
Orbital momentum
  of a particle, 115
  of a pion, 232
Overlap integral, of wave functions of independent nucleons and complex particle, 83

P

pA-interactions
  particle production in, 173
  trawling effect in, 199–204
Pairing energy, expression for, 109
P_1-approximation, 155
  kinetic equations for cascade nucleons in, 70–75
  small-angle approximation compared to, 155, 159
(p,α) reaction, data on level spacing obtained in, 122
Partial decay widths, effects on exit channels, 118
Partial widths, energy dependence of ratio of, 123
Partial widths of absorption, 218
Particle(s)
  correlations of emission of, 5
  elastic and inelastic interaction of, amplitudes, 9
  energy spectra of, 222–227
  intermediate-energy type, nuclear fragment production by, 338–350
  mean free path of, 22, 88
  multiple production of, statistical model, 91
  production in proton-nucleus collisions, 173–179
  range of strong interaction of, 93
  refraction and reflection of, 87
  search for a partner and interaction point, 88
  subthreshold production of, 196
α-Particle mechanism of absorption, 221, 232
Partition function, of grand canonical ensemble, 102
Parton phenomenology, 95
Pauli blocking factor(s), 27, 28, 241
  introduction into collision term, 49
  for scattering cross-sections in nuclear medium, 58
  use for approximation of Liouville equation, 33
Pauli exclusion principle, 58, 82, 221, 244
  Boltzmann equation and, 36, 52
  constraints imposed on INC by, 85
  effect on interaction of excited nucleons, 158
  effect on secondary nucleons, 180
  incorporation into collision term, 27–29, 44
Pauli matrices, 167
p̄-capture, nuclear, principal mechanism, 257
Perturbation theory, residual two-body interaction and, 82
(p,γ) reaction, data on level spacing obtained in, 122
Phase density
  of INC-model, 23–24, 29
  Liouville equation and, 14–16
  role in classical physics, 18
  single-particle, 164, 167
Phase space, 23
  Fermi breakup and, 133
  occupation number of single-particle nuclear states in, 81
Phase volume
  of a channel, 132
  Lorentz-invariant, 278
Photoabsorption, of a nucleus, cross-section of, 119
Photons
  emission of, 218
  intermediate-energy type, absorption by nuclei, 89
Photonuclear reactions, use of INC-model for analysis of, 90
Pickup process, 227
πA-interaction
  deep inelastic type, 246
  OC-model for, 240–245
π-Mesons, absorption by nuclei, 234
π^+-Mesons

energy spectrum of, 183
production of
in inelastic pp-collision, 178
in proton-nucleus interactions, 183–194
π^--Mesons, stopped, absorption by nuclei, 215–239
πN-collisions
characteristics of secondaries produced by, 91
elementary subprocesses for, 89
πN-interaction, 176
total and partial cross-sections of, 89
πN-scattering, cross-sections of, 242
Pion(s)
absorption of
correlations between emitted particles in, 227–230
mechanism, 220–221
multinucleon, 225, 228
OC-model of, 215–222
per one nucleon, 175
probability, 216–220
by two-nucleon associations, 160–161, 240
captured by Coulomb field of nucelus, initial distribution of, 218
charge exchange reactions involving, cross-section for, 177
decay width of, 218
double differential distributions of, 181
elastic scattering of, 176, 240
Green functions for, 176–177
incorporation in INC-model, 4
interaction with intranuclear nucleons, 198
mean free path of, de Broglie wavelength and, 51
multiple charge exchange of, 275
near threshold production of mesons by, 287–292
nonannihilation production of, 261–262
in nuclear matter
mean free path of, 241–243
potential energy of, 243–244
orbital momentum of, 232
potentials of interaction between other particles and, 12
production of, 173–183
inclusive cross-sections for, 179–183
in nuclear matter, 50–51, 89
single-particle phase functions of, 197
two-nucleon absorption of, 89–90, 285
Pionic atom, formation of, 216
Pion-nucleus interactions, 215–254
absorption of stopped π^--mesons by nuclei, 215–239
at energies lower than 300 MeV, 239–249
j-Pions
flux density of, 174
production of, cross-section of, 179
pN-annihilations, experimental data on, 257
pn-interactions, 173
total and partial cross-sections of, 89
pNN-system, relativistic phase volume of, 197
pn-scattering, anisotropy of, 58
pn-scattering lengths, 256
Poisson brackets, 15
Polarization effects, in inclusive nucleon-nucleus reactions
at intermediate energies, 163–173
Polarization vector, 165
pp-collisions, π^+-meson production in, 178, 184–185
double differential cross-sections for, 187
inclusive cross-sections for, 185–187
πp-interaction, total cross-section of, 175
pp-interactions, total and partial cross-sections of, 89
p,pn reaction, cross-sections of, 63
pp(pn)-interaction, inelastic, free cross-section of, 190
(p,p′) reaction, data on level spacing obtained in, 122
p,2p reactions, cross-sections of, 63
pp-scattering, in center-of-mass system of coordinates, 58
$\bar{p}$p-scattering lengths, 256
Pre-equilibrium effects, 125
Pre-equilibrium emission, 225
coalescence of excitons as, 267
description of, 22
Pre-equilibrium Harp-Miller-Berne model, INC-model and, 80
Pre-equilibrium models, for description of nuclear reactions at low energies, 75, 80–83
Pre-equilibrium particle, partial width of emission of, 82
Prefragments, formation of, 137
Prescission kinetic energy, 313
Probabilities, of transitions, 81
Propagators, of a system, 25, 30
Proton, rest masses of, 185
Proton-nucleus collisions, particle production in, 173–179
Proton-nucleus interactions, antiproton production in, 195–199
Protons

energy spectra of, 160
near threshold production of mesons by, 287–292
numbers of, in R-nucleus, 92
quasifree scattering of, 168
secondary, double differential cross-sections for production of, 158–163
total cross-section of pion production by, 180
Protons Z, distributions of R-nuclei over, 43–44

Q

Quadrupole γ-transitions, removal of angular momentum by, 121
γ-Quanta
absorption of, 235
emission of, 22
from highly excited nuclei, 119
from transitions of all products of nuclear reaction, 3
Quantum Liouville-von Neumann equation, density matrix and, 16–18
Quantum-mechanical calculation, of quasifree component of inclusive cross-section, 60–64
Quantum-mechanical effects
affecting nucleon wave functions, 75
at initial stage of INC, 68
Quark-gluon string model, 91, 95, 191
Quarks, transition to hadrons, 95
Quasideuteron model, use to describe pion absorption, 89–90, 232, 261
Quasielastic scattering, coupling between channels of absorption and, 245
Quasievaporation, effect on breakup, 140
Quasifission, effect on breakup, 140
Quasifree component
of cross-section, disregard of quantum-mechanical effects in, 160
of inclusive cross-section
in domain of low energy, 76
quantum-mechanical calculation, 60–64
Quasifree knockout, of fast nucleons from nucleus, 48
Quasifree nucleons
cross-section for production of, 167
at low energies, 75–80
definition of, 55
double differential distributions of, 60, 68
Quasifree peak, 171
quasifree scattering of protons on nuclei over, 168
Quasifree scattering
of nucleons, 56, 60, 168
cross-section, 58
of protons, 168
quantum-mechanical effects on, 173
Quasiparticles
formation and activity of, 21
number of, 92
Quasiparticle states, densities of, 83

R

Radiation width, of C-nucleus, 122–123
Radioactive nuclear beams, production of, 349
Reaction channels, in collision of particles, 5, 10
Recoil momentum, R-nuclei distribution and, 44
Rectangular potential well, with infinitely high walls, 105
Reduced mass
of inverse reaction for emitted particle, 83
of particles, 100
Relativistic effects, influence of, 66
Residual interactions
correlation type, 103
effects of, 109
short-range, 24
two-body, perturbation theory and, 82
Residual nucleus, see R-nuclei
(3,3)-Resonance, pion production through, 176–177, 242, 265, 270–271
Resonances
effect of production of, 204–206
mesonic, INC-model with, 282–283
nucleon, contribution to cross-section, 198
R-nucleus (nuclei)
angular momentum of, 232–237
characteristics of, 92, 271–277
distributions of, 23, 43
excitation energy of, 22, 92
isotope yield and, 230–232
explosive breakup of, 334
Fermi breakup of, 267
hot, ensemble of, 335–337
incorporation in intranuclear cascade model, 4
momentum of, 237–239

S

Saddle point, descent to scission point, 312
Scattering amplitude, 8–10
determination of, 11
Scattering matrix, definition of, 8

Schrödinger equation, 7–10, 18, 256
solution of, 10–11
Scission line, definition of, 312
Scission point, nuclear deformation at, 124, 311
Scission time, 297
Secondary nucleons
angular distributions of, 76
differential cross-section of, 78
energy distributions of, 76
Secondary particles, fast, 190
Secondary protons, analyzing power and polarization of, 163, 165
Self-consistent field, potential field as, 26
Series in number of collisions, expansion of phase density in, 32–33
Series in the generations, expansion of phase density in, 32–33
Shell-correction values, 110
Shell effects
damping of, 307, 349
in nuclei, 124
damping with excitation energy, 124
Shell model
of a nucleus, 103
use in calculations of INCs in light T-nuclei, 87
Shells, of nuclei, see Nuclear shells
Single-particle distribution functions
as descriptive of nucleonic cascade, 38, 55
of α-nucleons, 27
Single-particle fermionic states, 101
Single-particle phase functions, of pions and baryons, 197
Single-particle shell model, for wave functions of bound nucleon states, 62–63
Single-particle state(s)
of continuous spectrum, 81
density of, 103–104
energies and average occupation numbers of, 103
equidistant scheme for, 105
of nucleus, distance fluctuation in, 106
Six-quark configuration, heavy meson absorption by, 287
Skyrme-type potential, 24, 112
Small-angle approximation, 155, 169
P_1-approximation compared to, 155, 159
S-matrix, transition probabilities and, 6–8
Space-time development, of multiple production process, 255
Spallation
of nucleus, after π^- capture, 231
of R-nucleus, 267–268
of T-nucleus, 272
Spherical harmonic, 63
Spin
of inverse reaction for emitted particle, 83
of particles, 100
Spin-orbital interaction, calculation of radial wave functions and, 63
$\bar{s}s$-component, contribution of, for omega-meson, 287
s (shower)-particles, classification and properties of, 199–201, 208, 268
Statistical description, of dynamical many-particle systems, 14–19
Statistical equilibrium
equilibrium number of excitons in, 81
in highly excited nucleus, 80
Statistical model, of multifragmentation, 136–139
Statistical properties, of C-nuclei produced in reactions with low-energy particles, 122–128
Steepest descent method, 102
Streaming term, 136
derivation of, 24–25
Strong-coupling limit, 117
Superdeformed strongly rotating nuclei, fragment emission from, 118
Superheavy elements, synthesis of, 349
Superheavy nuclei
double magic type, existence of, 349
shell effects in, 127
Surface component, of liquid-drop energy of nucleus, 112
Surface tension
effect on nuclear reactions, 136
of nucleus, 113
Surface term, in expression of free energy of a fragment, 138
Symmetry term, in expression of free energy of a fragment, 138

T

Target nucleus, see T-nucleus
Temperatures, limiting, nuclear macroscopic properties and, 114
Thermal energy, of nucleus in saddle point, 120
Thermal expansion, nuclear density and, 112
Thermodynamical equilibrium
at breakup, 137

establishment of, 130
Thermodynamical potential, for system of noninteracting fermions, 102–103
Thermodynamical stability, of hot nuclear matter, 136
Thomas-Fermi model, 114
use in approximation of Liouville equation, 33
use in studies of thermal effects on nuclei surfaces, 111
use in studies of thermodynamical stability of hot nuclear matter, 136
Threshold energy, 198
of antiproton production in NN-collisions, 196
role in breakup, 134
T-nucleus
analyzing power in reaction on, 163
characteristics of incident particle inside, 87
incident nucleon and number of neutrons and protons in, 43
model of, 86–87
momentum distribution of nucleons in, 190
strong spallation of, 272
Topological cross-section(s)
definition of, 4
for escape of nucleons, 42–43
Total binding energy, 132
Total elastic scattering cross-section, definition of, 3
Transfer of polarization, tensor of, 167
Transition probabilities, S-matrix and, 6–8
Translational term, in expression of free energy of a fragment, 138
Transmission coefficient, 116, 129
Transverse momentum, 187
Trawling effect, 199–207, 249, 268, 270–271
in INC, 93–95
macroapproximation and, 33
in $\bar{N}A$ reaction, 263
in pA-interaction, 199–204
in reactions initiated by lightest nuclei, 206–207
Two-body interaction, residual, 81

U

Uniform nucleus, model of, 168
Unitary relation, 11
Unstable fragments, formation and secondary decay of, 134

V

Vacuum-scattering amplitude, matrix element expression by, 13
Velocity of sound, in nuclear matter, 137
Vibrational enhancement, coefficient of, 109
Vlasov-Uehling-Uhlenbeck equation, 35
Volume term, in expression of free energy of a fragment, 138
von Neumann series, 35, 55, 84, 167
solution of integral Liouville equation in form of, 32–33

W

Walecka model, as version of INC-model, 50
Wave functions
of bound nucleon states, single-particle shell model for, 62
distortions of, 63
Wave packet, use to describe a system, 6
Weak-coupling limit, 117
Weight functions method, 288
use for calculation of inclusive cross-sections for subthreshold pion production, 180
Wigner probability function
definition and properties of, 18–19
use in solving problems of quantum statistical mechanics, 19
use in statistical description of dynamical many-particle systems, 14
use in transformation of Liouville-von Neumann equation, 45–46, 52
Wigner representation, 249
Wigner-Seitz approximation, 133, 138
Woods-Saxon potential, 105, 108, 172
WPF, equation for, 49

X

X-ray emission
by antiprotons, 255
in de-excitation of π-atom, 216